ISSN 0021-9673

VOL. 484 DECEMBER 22, 1989
COMPLETE IN ONE ISSUE

Preparative Chromatography

including

6th Int. Symp. on Preparative Chromatography, Washington, DC, May 8–10, 1989

JOURNAL OF CHROMATOGRAPHY

INTERNATIONAL JOURNAL ON CHROMATOGRAPHY, ELECTROPHORESIS AND RELATED METHODS

ELSEVIER

JOURNAL OF CHROMATOGRAPHY

Scope. The *Journal of Chromatography* publishes papers on all aspects of chromatography, electrophoresis and related methods. Contributions consist mainly of research papers dealing with chromatographic theory, instrumental development and their applications. The section *Biomedical Applications*, which is under separate editorship, deals with the following aspects: developments in and applications of chromatographic and electrophoretic techniques related to clinical diagnosis or alterations during medical treatment; screening and profiling of body fluids or tissues with special reference to metabolic disorders; results from basic medical research with direct consequences in clinical practice; drug level monitoring and pharmacokinetic studies; clinical toxicology; analytical studies in occupational medicine.

Submission of Papers. Papers in English, French and German may be submitted, in three copies. Manuscripts should be submitted to: The Editor of *Journal of Chromatography*, P.O. Box 681, 1000 AR Amsterdam, The Netherlands, or to: The Editor of *Journal of Chromatography, Biomedical Applications*, P.O. Box 681, 1000 AR Amsterdam, The Netherlands. Review articles are invited or proposed by letter to the Editors. An outline of the proposed review should first be forwarded to the Editors for preliminary discussion prior to preparation. Submission of an article is understood to imply that the article is original and unpublished and is not being considered for publication elsewhere. For copyright regulations, see below.

Subscription Orders. Subscription orders should be sent to: Elsevier Science Publishers B.V., P.O. Box 211, 1000 AE Amsterdam, The Netherlands, Tel. 5803 911, Telex 18582 ESPA NL. The *Journal of Chromatography* and the *Biomedical Applications* section can be subscribed to separately.

Publication. The *Journal of Chromatography* (incl. *Biomedical Applications*) has 37 volumes in 1989. The subscription prices for 1989 are:

J. Chromatogr. + *Biomed. Appl.* (Vols. 461–497):
Dfl. 6475.00 plus Dfl. 999.00 (p.p.h.) (total *ca.* US$ 3428,50)

J. Chromatogr. only (Vols. 461–486):
Dfl. 5200.00 plus Dfl. 702.00 (p.p.h.) (total *ca.* US$ 2707.25)

Biomed. Appl. only (Vols. 487–497):
Dfl. 2200.00 plus Dfl. 297.00 (p.p.h.) (total *ca.* US$ 1145.50).

Our p.p.h. (postage, package and handling) charge includes surface delivery of all issues, except to subscribers in Argentina, Australia, Brasil, Canada, China, Hong Kong, India, Israel, Malaysia, Mexico, New Zealand, Pakistan, Singapore, South Africa, South Korea, Taiwan, Thailand and the U.S.A. who receive all issues by air delivery (S.A.L. — Surface Air Lifted) at no extra cost. For Japan, air delivery requires 50% additional charge; for all other countries airmail and S.A.L. charges are available upon request. Back volumes of the *Journal of Chromatography* (Vols. 1–460) are available at Dfl. 195.00 (plus postage). Claims for missing issues will be honoured, free of charge, within three months after publication of the issue. Customers in the U.S.A. and Canada wishing information on this and other Elsevier journals, please contact Journal Information Center, Elsevier Science Publishing Co. Inc., 655 Avenue of the Americas, New York, NY 10010. Tel. (212) 633-3750.

Abstracts/Contents Lists published in Analytical Abstracts, ASCA, Biochemical Abstracts, Biological Abstracts, Chemical Abstracts, Chemical Titles, Chromatography Abstracts, Clinical Chemistry Lookout, Current Contents/Physical, Chemical & Earth Sciences, Current Contents/Life Sciences, Deep-Sea Research/Part B: Oceanographic Literature Review, Excerpta Medica, Index Medicus, Mass Spectrometry Bulletin, PASCAL-CNRS, Pharmaceutical Abstracts, Referativnyi Zhurnal, Science Citation Index and Trends in Biotechnology.

See inside back cover for Publication Schedule, Information for Authors and information on Advertisements.

0021-9673/89/$03.50

Printed in The Netherlands

For Contents see p. VII

JOURNAL OF CHROMATOGRAPHY

VOL. 484 (1989)

JOURNAL *of* CHROMATOGRAPHY

INTERNATIONAL JOURNAL ON CHROMATOGRAPHY,
ELECTROPHORESIS AND RELATED METHODS

ELSEVIER
AMSTERDAM — OXFORD — NEW YORK — TOKYO

0021-9673/89/$03.50

Printed in The Netherlands

For Contents see p. VII

SPECIAL VOLUME

PREPARATIVE CHROMATOGRAPHY

including

SIXTH INTERNATIONAL SYMPOSIUM ON PREPARATIVE CHROMATOGRAPHY

Washington, DC (U.S.A.), May 8–10, 1989

Editors

G. GUIOCHON
(Knoxville and Oak Ridge, TN, U.S.A.)

L. R. SNYDER
(Orinda, CA, U.S.A.)

CONTENTS

PREPARATIVE CHROMATOGRAPHY (INCLUDING 6TH INTERNATIONAL SYMPOSIUM ON PREPARATIVE CHROMATOGRAPHY; WASHINGTON, DC, MAY 8–10, 1989)

In articles with more than one author, the name of the author to whom correspondence should be addressed is indicated in the article heading by a 6-pointed asterisk (*)

Journal of Chromatography, 484 (1989) IX
Elsevier Science Publishers B.V., Amsterdam — Printed in The Netherlands

FOREWORD

The *Sixth International Symposium on Preparative Chromatography* (PREP'89) took place in Washington, DC, May 8–10, 1989 at the Washington Sheraton Hotel. The renewed vigor of the research in this area of chromatography, the importance of newly developed applications of preparative chromatography and the impact of recent advances in the understanding of the non-linear aspects of chromatography were demonstrated by the scope of the program and the enthusiasm of the participants. The meeting was attended by over 250 registered delegates from over 12 countries. 30 lectures and oral contributions were presented, while 35 poster contributions were exhibited and discussed. Three active discussion sessions contributed to important clarification of ideas on (i) the importance of efficiency in preparative-scale liquid chromatography, (ii) the strategies for optimization of purifications and (iii) the costs of preparative liquid chromatography purifications.

It is a pleasure to thank Drs. E. Dose and S. Golshan-Shirazi and Ms. A. M. Katti who actively contributed to the smooth conduct of the meeting. Special thanks are due to Mrs. Janet Cunningham, Symposium Manager, for lending her organizational skills before and during the meeting and allowing its successful operation. The support of the Washington Chromatography Discussion Group is gratefully acknowledged.

The success of the meeting was largely due to the high quality of its scientific program. The help of the members of the scientific committee in the review of the abstracts submitted and in the selection of the program was critically important.

The present volume of the *Journal of Chromatography* was organized around the symposium. It contains the text of most of the papers presented during the symposium and submitted by their authors for inclusion in the proceedings. It was supplemented by invited contributions dealing with preparative chromatography. This has permitted the presentation of a substantial sample of the experimental and theoretical work currently carried out in this area. We hope that this volume will be of broad interest to the chromatographic community. Once again, we are grateful to the editorial staff of the *Journal of Chromatography* for their skill in producing this volume and their efforts in doing so in such a timely fashion.

GEORGES GUIOCHON
LLOYD R. SNYDER

Journal of Chromatography, 484 (1989) 1–27
Elsevier Science Publishers B.V., Amsterdam — Printed in The Netherlands

CHROM. 22 047

GRADIENT ELUTION IN NON-LINEAR PREPARATIVE LIQUID CHROMATOGRAPHY

FIROZ D. ANTIA and CSABA HORVÁTH*
Department of Chemical Engineering, Yale University, P.O. Box 2159 Yale Station, New Haven, CT 06520 (U.S.A.)

SUMMARY

The effect of column overload in gradient elution is studied theoretically using a model based on a differential mass balance equation that is solved numerically by an orthogonal collocation method. First elution profiles of a single component and then the separation of binary mixtures having both constant and non-constant separation factors with changing modulator concentration are examined and contrasted with results obtained by isocratic elution under comparable conditions. In overloaded chromatography of binary mixtures with constant separation factor gradient elution is shown to be superior to isocratic elution for the cases studied on the basis of production rate, yield and enrichment factor. For the examination of the results obtained by gradient elution with binary mixtures having non-constant separation factors, a logarithmic mean separation factor, which offers a simple means for comparison and indicates whether or not separation will occur in overloaded conditions, is introduced. The effect of selectivity inversion due to changes in eluent strength and the role played by the logarithmic mean separation factor are illustrated.

INTRODUCTION

In elution chromatography, also called wave or zonal chromatography, a pulse of a mixture is fed into the column and its components are eluted by a continuous stream of an eluent that binds less strongly to the stationary phase than any of the eluites. Elution is isocratic when the eluent strength is kept constant throughout the separation. In gradient elution, introduced almost four decades ago[1], the eluent strength is increased continuously during the chromatographic run by suitable manipulation of the mobile phase composition upon increasing or decreasing the concentration of an appropriate additive termed the mobile phase modulator. This facilitates the separation, in a single run, of all the components of the mixture, whether they are initially weakly or strongly bound to the stationary phase. For this reason, gradient elution is widely used for the separation of mixtures whose components display a broad range of retentivity. Furthermore, gradient elution is employed frequently in the separation of biopolymers in order to take advantage of the concomitant increase in the peak capacity[2].

0021-9673/89/$03.50

In most analytical applications, linear elution chromatography (where analytes are present at low concentrations and their adsorption is governed by Henry's law) is employed so that the migration of a component is not perturbed by the presence of other eluites. In preparative chromatography, however, feed concentrations can be high enough so that the migrating molecules interfere with each other's adsorption. As a result the adsorption isotherms are non-linear and, under these conditions, the process is termed non-linear, or overloaded, chromatography.

Gradient elution chromatography with linear adsorption isotherms has been studied theoretically since the introduction of the technique[3–10]. The most comprehensive treatment has been provided by Snyder[6]. Since the results of these theories do not apply directly in non-linear conditions, attempts have been made recently to model overloaded gradient elution with the help of Craig simulations[11–14]. The goal of our work is to compare gradient and isocratic elution chromatography under overloaded conditions using a mathematical description based on a differential mass balance[15]. We first outline our model and test it under linear conditions to verify that it matches the extant theory for this case. The model is then used to compute elution profiles of single components and of binary mixtures in non-linear gradient elution chromatography. Next, a comparison of performance in gradient and isocratic elution for a binary mixture having a constant separation factor is presented. Finally, the phenomenon of selectivity reversal with changing eluent strength and its effects on the separation of binary mixtures by gradient elution under overloaded conditions are discussed.

MODEL

The adsorption isotherm

In chromatography, the migration rate of the components of a mixture, and thus their separation, depends on how they distribute between the stationary and mobile phases. In overloaded chromatography, the concentration of an eluite i in the stationary phase, q_i, depends on its own local concentration, c_i, as well as on the local concentrations of all the other eluites and of the mobile phase modulator, φ. Thus the adsorption isotherm, which formally describes the equilibrium concentrations of the components in the two phases, must account for the interdependence of the sorption behavior of the eluites and the modulator. The simplest multicomponent adsorption isotherm is the Langmuir isotherm, given by[16,17]

$$q_i = \frac{a_i c_i}{1 + \sum_{j=1}^{n} b_j c_j} \qquad i = 1, 2, \ldots, n \tag{1}$$

where a_i and b_i are the parameters of the respective single component isotherms and n is the total number of eluites. The parameter a_i is dimensionless and represents the initial slope of the isotherm, b_i has the dimension of reciprocal concentration and the ratio a_i/b_i is equal to λ_i, the saturation capacity per unit volume of the sorbent for species i. In the limit of infinite dilution the isotherm is linear and the retention factor, k'_i, is equal to Φa_i, where Φ is the ratio of stationary to mobile phase volumes (the phase ratio) which, for simplicity, is set to unity in this study. The isotherm in eqn. 1 predicts that the

separation factor for two components, i and j, defined as $q_j c_i / q_i c_j$, is constant. For this reason, when the saturation capacities of the various components are unequal, eqn. 1 does not satisfy the surface analogue of the Gibbs–Duhem equation (the so-called Gibbs' isotherm) and is therefore thermodynamically inconsistent[18,19]. Nevertheless, use of the Langmuir isotherm has been found to give results that are in reasonable concord with experimental data obtained under various conditions when there are no drastic changes in separation factor with eluite concentration[20–22].

In view of eqn. 1, the modulator could be treated as one of the n species so that at low eluite concentrations, the dependence of the retention factor on the modulator concentration, φ, would be given by

$$k'_i = \frac{\Phi a_i}{1 + b_\varphi \varphi} \tag{2}$$

where b_φ is the pertinent isotherm parameter for the modulator. However, the data in the literature of analytical chromatography for the retention factor *versus* modulator concentration do not support eqn. 2. For example in reversed-phase chromatography the data appear to conform to a relationship of the type[6]

$$\kappa_i = \kappa_{0,i} - S_i \varphi / 2.3 \tag{3}$$

Here κ is $\log_{10} k'_i$, κ_0 is $\log_{10}(\Phi a_{0,i})$ where $a_{0,i}$ is the value of a_i in the absence of modulator and $-S_i/2.3$ is the slope of the $\kappa - \varphi$ plot. Assuming that the saturation capacity for a component is constant and independent of the modulator concentration, substituting eqn. 3 into eqn. 1 yields the isotherm

$$q_i = \frac{a_{0,i} \exp(-S_i \varphi) c_i}{1 + \sum_{j=1}^{n} \frac{a_{0,j}}{\lambda_j} \exp(-S_j \varphi) c_j} \qquad i = 1, 2, \ldots, n \tag{4}$$

Similarly, in ion-exchange (electrostatic interaction) chromatography with a salt as the modulator, retention is related to the salt molality in the mobile phase, φ_s, via[23]

$$\kappa_i = \log_{10}(\Phi a_{1,i}) - Z \log \varphi_s \qquad i = 1, 2, \ldots, n \tag{5}$$

where $a_{1,i}$ is the projected value of a_i at $\varphi_s = 1$ and Z is a constant representing the ratio of the apparent valence of the eluite to the valence of the salt counterion. Substitution of eqn. 5 in eqn. 1 yields the isotherm

$$q_i = \frac{a_{1,i} \varphi_s^{-Z} c_i}{1 + \sum_{j=1}^{n} \frac{a_{1,j}}{\lambda_j} \varphi_s^{-Z} c_j} \qquad i = 1, 2, \ldots, n \tag{6}$$

A shortcoming of eqn. 6 is that it becomes indeterminate at $\varphi_s = 0$. Alternatively, the rigorous isotherm for ion-exchange could be employed[24,25], but it has the disadvantage of being implicit in q_i.

In this study we use only the isotherm in eqn. 4 which is expected to hold under conditions where eqn. 3 is valid, *i.e.*, in reversed-phase chromatography with organic solvent as the modulator, and, with appropriate changes of sign, in reversed-phase or hydrophobic interaction chromatography with salt as the modulator. The groups $a_{0,i} \exp(-S_i\varphi)$ and $a_{0,i} \exp(-S_i\varphi)/\lambda_i$ can be viewed as modified Langmuir parameters a_i and b_i, respectively. Although the assumption of constant λ is not expected to hold over a wide range of modulator concentration, there is some experimental support for eqn. 4 from data on the variation of single component Langmuir isotherm parameters with modulator concentration[20,22]. More information is needed to ascertain the true nature of multicomponent adsorption isotherms of various species, particularly of biopolymers at large and the effect of modulators in particular.

Dispersive effects

In chromatography, band spreading occurs due to various factors, including diffusion in the mobile phase, flow maldistribution arising from non-uniformities in the column packing structure, mass transfer to, from and within the sorbent beads, slow sorption kinetics, and non-linearities in the adsorption isotherms. It is assumed that the effect of all dispersive processes, with the exception of those due to slow sorption kinetics and isotherm non-linearities, can be lumped into an effective dispersion coefficient, $\mathscr{D}$, whose value is estimated from chromatograms of the eluites in linear chromatography[26]. The value for $\mathscr{D}$ can be determined theoretically from the sorbent particle size, the column packing structure, the flow velocity of the mobile phase and the diffusivity and retention factor of the migrating components[27]. Although in non-linear systems $\mathscr{D}$ is likely to depend on the eluite concentrations, in the present study it is assumed to be concentration independent. Moreover, a single value of $\mathscr{D}$ is used to describe the dispersion of all the eluites. This appears to be acceptable for closely related components under some circumstances[26], but needs more support under conditions when diffusivities are strongly concentration dependent. Bandspreading due to slow sorption is neglected in the model since kinetic limitations are assumed to be absent.

Governing equations

With these assumptions, the chromatographic process can be described by an isothermal one-dimensional differential mass balance as[15,26]

$$\frac{\partial c_i}{\partial t} + \Phi\frac{\partial q_i(c_1, c_2, \ldots, c_n, \varphi)}{\partial t} + u_0\frac{\partial c_i}{\partial z} = \mathscr{D}\frac{\partial^2 c_i}{\partial z^2} \qquad i = 1, 2, \ldots, n \quad (7)$$

with the initial and boundary conditions for elution of the feed components being[28]

$$c_i(0,z) = 0 \qquad 0 \leq z \leq L$$

$$c_i(t,0) = c_{0,i} \qquad 0 < t \leq t_{\text{inj}} \qquad i = 1, 2, \ldots, n \quad (8)$$

$$\left(\frac{\partial c_i}{\partial z}\right)_{z=L} = 0 \qquad t \geq 0$$

Here $q_i(c_1, c_2, \ldots, c_n, \varphi)$ indicates that the stationary phase concentration is a function of the eluite and modulator concentrations as given by an adsorption isotherm such as those in eqns. 4 or 6, u_0 is the mean velocity of the bulk mobile phase which is considered not to be bound to the stationary phase[26], t is time, z is the distance in the direction of bulk flow, L is the column length, t_{inj} is the time of feed introduction, and $c_{0,i}$ is the concentration of component i in the feed.

The progress of the eluent modulator proper through the system ought to be described by an equation similar to eqn. 7 with appropriate boundary conditions. However, for simplicity, adsorption of the modulator onto the stationary phase is assumed to be negligible compared to that of the eluites. Furthermore, the modulator molecule is often smaller than the eluites and therefore is expected to disperse to a much lesser extent. With these approximations the mass balance for the modulator is

$$\frac{\partial \varphi}{\partial t} + u_0 \frac{\partial \varphi}{\partial z} = 0 \tag{9}$$

and the initial and boundary conditions are

$$\begin{aligned} &\varphi(t_{inj},z) = 0 \quad 0 \leq z \leq L \\ &\varphi(t,0) = g(t - t_{inj}) \quad t > t_{inj} \end{aligned} \tag{10}$$

where g is an arbitrary function that represents the gradient profile, given by the modulator concentration as a function of time at the column inlet. Here the gradient is assumed to begin immediately after the feed is introduced, *i.e.*, at time t_{inj}. Any appropriate delay time to account for system dwell volume between the gradient former and column can be readily introduced by adding this to t_{inj}, but this is neglected here . The solution to eqns. 9 and 10 at any axial location z is simply $\varphi = g(t - z/u_0 - t_{inj})$. We will consider only linear forms for the gradient profile, *i.e.*, the rate of change of modulator concentration is a constant, β, so that

$$\varphi(t,z) = \varphi_0 + \beta\left(t - \frac{z}{u_0} - t_{inj}\right) \tag{11}$$

where φ_0 is the modulator concentration in the eluent at the start of the gradient.

Our model for overloaded gradient elution chromatography is completely specified by eqns. 4, 7, 8 and 11 that must be solved numerically. To facilitate the calculations we introduce the dimensionless independent variables $\theta\,(= tu_0/L)$ for time and $X\,(= z/L)$ for distance. In terms of the dimensionless variables the model for gradient elution chromatography is written as

$$\begin{aligned} &\frac{\partial c_i}{\partial \theta} + \Phi \frac{\partial q_i}{\partial \theta} + \frac{\partial c_i}{\partial X} = \frac{1\partial^2 c_i}{2N\partial X^2} \\ &c_i(0,X) = 0 \qquad 0 \leq X \leq 1 \end{aligned} \tag{12}$$

$$c_i(\theta,0) = c_{0,i} \quad 0 < \theta \leq \tau \quad i = 1, 2, \ldots, n \tag{12}$$

$$\left(\frac{\partial c_i}{\partial X}\right)_{X=1} = 0 \qquad \theta \geq 0$$

$$q_i = q_i(c_1, c_2, \ldots, c_n, \varphi)$$

$$\varphi = \varphi_0 + \beta t_0(\theta - X - \tau)$$

Here t_0 is L/u_0, τ is t_{inj}/t_0 and the expression for q_i is given by eqn. 4.

The parameter N is a Peclet number given by $u_0 L/2\mathscr{D}$ that equals the plate number under conditions of linear isocratic chromatography. The effective dispersion coefficient, $\mathscr{D}$, in eqn. 7 is defined so as if all dispersive process would occur in the time that the eluite molecules spend in the mobile phase. Thus when relating N and $\mathscr{D}$, only the time spent by the eluite in the mobile phase, and not the total retention time, must be considered.

Presentation of results

It is convenient to introduce a dimensionless gradient steepness parameter, G[6] given by

$$G \equiv \frac{S_{ref}\beta t_0}{2.3} \tag{13}$$

where S_{ref} is the S value (see eqn. 3) for one of the eluting components chosen as a reference. Similarly a dimensionless load parameter, $\mathscr{L}$ is defined by the mass of the reference feed component normalized to the saturation capacity of the column for that component under conditions prevalent at the start of the run.

$$\mathscr{L} \equiv \frac{\tau c_{0,ref}}{\Phi \lambda_{ref}} \tag{14}$$

In general any feed components may be chosen as reference for G and $\mathscr{L}$; when the S and λ values and feed concentrations are the same for each eluite G and $\mathscr{L}$ are independent of the choice of reference. Selection of the reference component in other cases is discussed later.

For a given feed mixture, results calculated from eqn. 12 are illustrated as "chromatograms" showing the outlet concentration of the components *versus* column volumes of mobile phase passed through the system (numerically the same as the dimensionless time, θ) for specified values of the parameters φ_0, N, G and $\mathscr{L}$. Other attributes of the chromatogram may be calculated from these results, as discussed later. When $a_{0,i}\exp(-S_i\varphi_0)$, *i.e.*, the "$a$" parameters at the start of the run, G and the ratio of S values of each component to the reference component are specified, the results are independent of the particular S values.

Calculations

The model for gradient elution is given by a set of partial differential equations, one for each component, which must be integrated numerically. When substituting eqn. 4 into eqn. 12, use of the chain rule yields a set of equations of the form

$$\boldsymbol{A}y = \boldsymbol{B} \tag{15}$$

where y is a vector of temporal derivatives with elements $\partial c_i/\partial\theta$, $\boldsymbol{B}$ is a vector whose elements contain spatial derivatives and the terms $(\partial q_i/\partial\varphi)$ $(\partial\varphi/\partial\theta)$, and $\boldsymbol{A}$ is a matrix of coefficients that depend on $\partial q_i/\partial c_j$. Orthogonal collocation on finite elements is used to estimate the spatial derivatives (subroutine DSS046 in the software package DSS/2 supplied by Prof. W. E. Schiesser at Lehigh University, Bethlehem, PA, U.S.A.), and eqn. 15 is then solved for the temporal derivatives using a standard linear algebraic equation solver (routine SGEFCS, written at Argonne National Labs., and available in the Numerical Analysis Program Library at the Yale Computer Center). The resulting set of ordinary differential equations, n for each collocation point, are integrated using a standard ODE solver (routine LSODE, available in the DSS/2 library and elsewhere). Sharp transitions at the beginning of the gradient profile are smoothened by the arc of a circle so as to ensure that the time derivative of the modulator concentration is defined at every point. Similar orthogonal collocation schemes have been used to simulate fixed-bed absorption column performance[29].

All calculations were performed on either a MicroVAX computer in the Yale Chemical Engineering Department or on a VAX 8600 computer in the Yale Computer Center. Results were plotted using software from Passage Software (Ft. Collins, CO, U.S.A.) on a Macintosh computer. A fourth order collocation scheme with the column divided into about 80 identical elements was used. The time required for the simulation of a single chromatographic run on the VAX 8600 computer varied from 2 to 10 min for a single component and from 7 to 45 min for a binary mixture, depending on the values of the parameters.

RESULTS AND DISCUSSION

Validation of numerical procedure for linear chromatography

The accuracy of the numerical procedure *per se* was confirmed in both isocratic and gradient elution with linear isotherms ($\lambda_j \to \infty$ in eqn. 4) for $100 < N < 2000$ and k' values up to 10. In isocratic elution at very low loads, plate numbers measured by standard methods[30] from simulated chromatograms matched within 5% the plate number used in our calculations. In gradient linear elution with low loads, bandwidths predicted by our model under linear conditions tallied closely with those calculated using Snyder's linear solvent strength (LSS) theory of gradient elution[6,31]. Details of these calculations are provided in the Appendix. A comparison of the results obtained by the two approaches is shown in Fig. 1, where the ratio of the peak variance in isocratic elution to that in gradient elution, $\sigma^2_{is}/\sigma^2_{gr}$, is plotted against gradient steepness for different values of the apparent retention factor, k'_{app}. Linear adsorption isotherms were used and, for the comparison, retention times were taken to be the same in both isocratic and gradient elution. It was found that in agreement with the LSS theory the predictions of the method did not depend on the plate number.

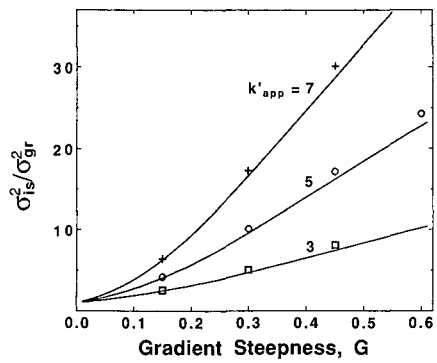

Fig. 1. The ratio of peak variances in isocratic and gradient elution for components having linear isotherms ($\lambda_j \rightarrow \infty$ in eqn. 4) as a function of the gradient steepness with the apparent retention factor, k_{app}, as the parameter. Solid lines were calculated according to eqn. A6 whereas symbols represent values calculated using eqn. 12 at very low loads.

In calculating the results in Fig. 1 by the LSS theory the correction factor for "anomalous" band broadening[6] was not used. The close match between the band variances calculated from our model and those from the linear theory in the absence of excessive broadening suggests that the origins of the anomaly lie in processes such as slow sorption kinetics that are not accounted for explicitly in either model. Since the anomalous broadening is not universally observed[32], and axial dispersion is overshadowed by band spreading due to isotherm non-linearity[33], correction for anomalous band broadening may not be necessary in overloaded elution.

Concentration profiles of single components

Although the behavior of a single component yields little information on the separation proper in non-linear chromatography, it is instructive to examine the concentration profiles of single components under overloaded conditions. In Fig. 2 single peaks obtained in isocratic elution are compared to those in gradient elution for three values of the gradient steepness parameter, G, and five values of the load parameter, $\mathscr{L}$. The value of a_0 is adjusted such that all peaks have a common end point, keeping τ constant so that load is varied only by changing the concentration (overload at constant volume). Therefore the peaks at different loads have coincident tails.

In Fig. 2, there is a regular progression from the concave upward rear envelope of the isocratic bands to the accentuated concave downward rear profile at high values of G. In gradient elution the strength of the eluent is greater at the rear of the peak than at its front: when the isotherm is linear, this causes molecules at the rear to move faster than those at the front, giving rise to a peak compression that counteracts dispersion. Although under overloaded conditions the velocity of the molecules depends not only on the local concentration of the modulator, but also on that of the eluite, the compressive effect tends to oppose band broadening arising from isotherm non-linearity and gives the rear of the band its characteristic concave downward shape.

For a given value of $\mathscr{L}$, the maximum concentration of the bands in Fig. 2 first decreases and later increases with increasing G, as indicated in Table I. This occurs

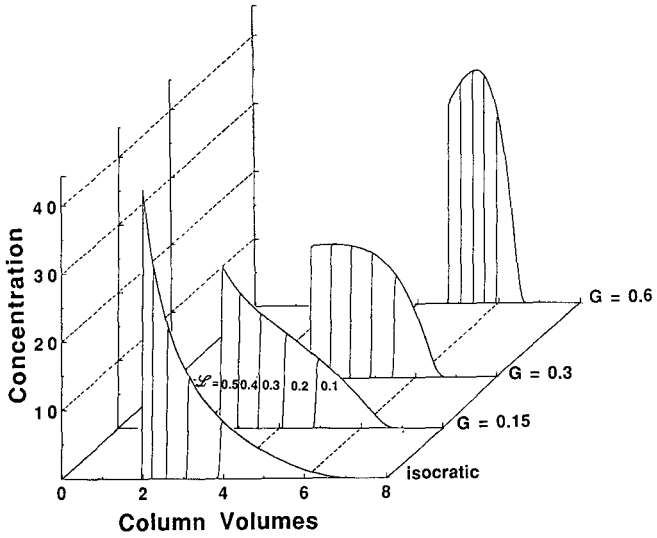

Fig. 2. Effect of elution conditions and column overloading on the peak profile of a single component. Peaks obtained for different loads under otherwise identical conditions are superposed in each case. Conditions: $N = 500$, $\Phi = 1$, $\tau = 0.5$, $\lambda = 100$; in isocratic elution, $a = 5$; in gradient elution $\varphi_0 = 0$, a_0 adjusted such that $k'_{app} = 5$. Concentration units are arbitrary.

because, in order to ensure a common elution time for all the peaks, conditions have been adjusted so that the binding strength at the start of the process is larger for runs with higher gradient steepness. Thus the progress of the band immediately following injection is arrested more strongly with increasing G, with a concommitant decrease in the concentration of the peak front. The concentration at the peak front is the maximum band concentration until at higher G band compression becomes significant and the maximum concentration increases. Unlike the maximum concentration the mean peak concentration always increases with increasing G, as summarized in Table I.

TABLE I

COMPARISON OF SINGLE COMPONENT PEAKS IN ISOCRATIC AND GRADIENT ELUTION[a] AS MEASURED BY THE MAXIMUM CONCENTRATION, c_{max}, THE MEAN CONCENTRATION, $\bar{c}$, THE FIRST MOMENT AT $\mathscr{L} = 0.5$ RELATIVE TO THAT AT $\mathscr{L} = 0.1$, $\mu_1(0.5)/\mu_1(0.1)$, THE SECOND CENTRAL MOMENT, μ_2^*, THE APPARENT PLATE NUMBER, μ_1^2/μ_2^*, AND THE SKEWNESS[b], μ_3^*/μ_2^{*3}

G	c_{max}	$\bar{c}$	$\frac{\mu_1(0.5)}{\mu_1(0.1)}$	μ_2^*	μ_1^2/μ_2^*	μ_3^*/μ_2^{*3}
0.0[c]	42.4	10.3	0.652	0.988	9.86	1.081
0.15	23.8	12.1	0.721	0.978	16.02	0.509
0.3	19.9	15.4	0.805	0.612	36.48	0.231
0.6	34.5	26.7	0.897	0.198	155.1	0.144

[a] $\mathscr{L} = 0.5$. Conditions as in Fig. 2.
[b] *cf.* ref. 30.
[c] Isocratic elution.

Quasi-linearization due to the gradient. When gradient elution produces bands of reduced asymmetry as compared with corresponding isocratic band profiles, the effect may be termed as a quasi-linearization due to the gradient. Several characteristics of the overloaded isocratic and gradient elution peaks for $\mathscr{L} = 0.5$ are summarized in Table I. The trends for peaks at other loads are similar. In overloaded chromatography, unlike under linear conditions, the first moments of the peaks do vary with load, as indicated by values of the first moments of peaks at $\mathscr{L} = 0.5$ normalized to those at $\mathscr{L} = 0.1$, but the variation decreases with increasing gradient steepness. The apparent efficiency of the column may be expressed by the ratio of the square of the first moment to the second central moment (μ_1^2/μ_2^*), which follows from the definition of the plate number under analytical isocratic conditions. The results in Table I show that this ratio increases fifteen-fold as G is increased from 0 to 0.6 and the skewness of the peaks, larger positive values of which indicate a greater extent of tailing[30], decreases significantly with increasing G. Thus, at higher gradient steepness, peak shapes approach more closely the symmetrical peaks encountered in analytical chromatography and this is an indication of the quasi-linearization due to the gradient. In turn, slight column overloading in analytical chromatography is less likely to lead to asymmetrical peaks with gradient elution than with isocratic elution. However, quasi-linearization is meaningful only at low levels of overload, since in multicomponent separations at higher loads interference between eluites is important and distorts peak shapes considerably, as discussed later.

Concentration and volume overload in gradient elution. In preparative chromatography with isocratic elution two limiting cases are distinguished: concentration overload, when the feed is introduced as an impulse of infinitesimal volume, and volume overload, when the feed is introduced in a finite volume at sufficiently low concentrations such that the adsorption isotherms are linear. In practice, conditions lie somewhere in between these two extremes. In non-linear isocratic elution, the effect of large sample volume becomes noticeable when τ exceeds more than half the bandwidth of a concentration overloaded peak having the same mass load[33,34]. However, in gradient elution, when the initial loading step is carried out under strong binding conditions ($a_0 > 100$) the adsorption isotherm is almost rectangular[25]. Therefore, immediately following feed introduction, the sample, regardless of its input concentration, is confined to a very narrow band in the column. Consequently, the band shape observed when the peak is eluted under gradually weaker binding conditions is practically independent of the load volume. Thus, in gradient elution with initially strong binding conditions, only the magnitude of the mass load counts and the concept of volume overloading is not pertinent.

Concentration profiles for binary mixtures with constant separation factor

Because of interference between migrating species, peak profiles in multicomponent chromatography have little resemblance to the corresponding single component peak shapes until they are completely separated and interference ceases, as evidenced by theoretical and experimental examples of non-linear isocratic elution[22,35,36]. Representative peak profiles of a 1:1 binary mixture calculated for non-linear gradient elution at increasing values of $\mathscr{L}$ for fixed values of the gradient steepness and initial modulator concentration, φ_0, are shown in Fig. 3. For both components the value of S is the same and thus the separation factor, $q_B c_A/q_A c_B$, *i.e.*, the selectivity, is

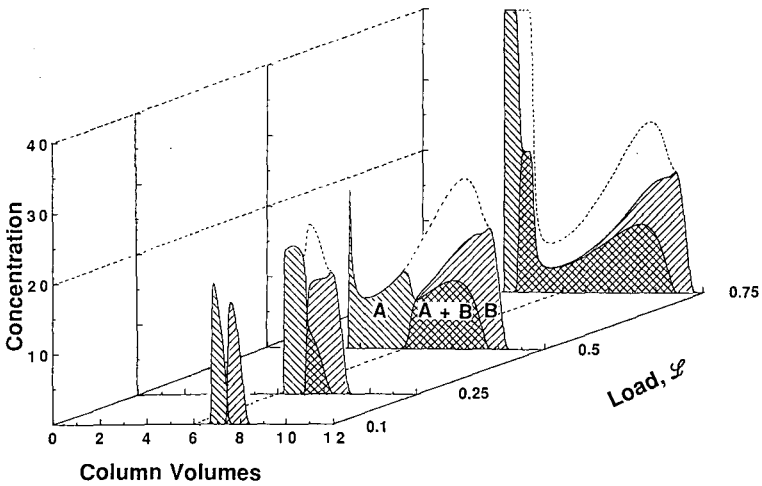

Fig. 3. Elution profiles of a 1:1 binary mixture in non-linear gradient elution at different loads. An envelope representing the response of a non-specific detector, *i.e.*, the total concentration, is shown in addition to the concentration profiles of the two components. Conditions: $\varphi_0 = 0, G = 0.45, N = 250, \Phi = 1; \lambda_A = \lambda_B = 100, a_{0,A} = 600, a_{0,B} = 1000, S_A = S_B$. Component A elutes first.

independent of modulator concentration. Separations with non-constant selectivity are discussed later. In the calculated chromatograms shown in Fig. 3, at a loading of approximately 50% of the total stationary phase capacity for each component, peak splitting occurs. Note that no split portion of the peak appears at $\theta = 1$, as it would in split-peaks arising from slow adsorption kinetics[37] where the early eluting split fraction moves with the mobile phase velocity. In our case it is a result of interference during the feed step, which is essentially foreshortened frontal chromatography: a fraction of the first component is pushed ahead by the second one, and, due to the concave downward shapes of the isotherms, is concentrated to a level greater than its concentration in the feed[38,39]. Furthermore, at high load the feed time and consequently the value of the gradient delay is large, and the first component front travels a significant distance (more than halfway through the column in this case) before the gradient is introduced at the column inlet. As a result, the front of the first component traverses the column by isocratic elution leaving behind a long tail. The compressive effect of the gradient later acts to concentrate the trailing portion of the first component peak. The trailing portion of component A forms two distinct humps as a result of the abrupt change in its isotherm parameters across the second component front. Such complex peak shapes, which are the result of interfering adsorption behavior of the components, are of course not observed with single components. At even higher loads, the fronts of both the first and second component may pass through the column under isocratic conditions during the long feed time and the process increasingly exhibits the features of frontal chromatography followed by gradient elution.

Design parameters in preparative chromatography

The goal of a preparative separation is to recover from a mixture the largest

quantities of a set of desired substances at a specified purity and concentration in the shortest possible time. These aims can be quantified in terms of three design parameters[28,40]:

(i) The production rate, P_i, defined as the mass of the desired substance i produced per run at a specified purity divided by the cycle time, θ_c, that includes any wash and regeneration steps. In dimensionless terms

$$P_i = \frac{\int_{\theta_{1,i}}^{\theta_{2,i}} c_i(\theta,1)\mathrm{d}\theta}{\Phi\lambda_{\mathrm{ref}}\theta_c} \tag{16}$$

where $c_i(\theta,1)$ is the outlet concentration of the product i, and $\theta_{1,i}$ and $\theta_{2,i}$ are "cut" points between which it is collected. The cut points are chosen such that the product is of the specified purity. For P_i to be a meaningful parameter for scaling purposes, normalization is done in the same manner as for the load parameter in eqn. 14. For simplicity, results reported here for both isocratic and gradient elution are based on a cycle time that extends from the start of the run to the point where the last traces of the last component elute. Actual dimensional production rates would depend upon the value of the flow-rate: detailed analysis of flow-rate effects can be found in the literature[41].

(ii) The yield, Y_i, which is the fraction of the desired substance i fed into the column that is recovered as product.

(iii) The enrichment factor, E_i, given by concentration of product i normalized to its concentration in the feed.

Separation of a binary mixture with constant separation factor

Optimization of isocratic elution. Our aim here is to compare preparative separations of a given binary mixture in isocratic and gradient elution on the basis of the three design parameters. For this purpose the separation must first be optimized under isocratic conditions. We will examine the separation of a 1:1 binary mixture with a constant separation factor of 1.67 on a column having 250 plates. In order that the separation factor remains constant, the κ–φ plots for the two components must be parallel, *i.e.*, they must have the same slope: this is often true of closely related compounds[6]. In non-linear elution, when $\mathscr{L}$ is greater than 0.1, the bandwidth is essentially independent of plate number for N greater than 200[33]; hence the low value used for the plate number to facilitate the numerical calculations is justified. On such a column under linear isocratic conditions at analytical loads the resolution between the components, R_s[30], would lie between 1.1 and 1.4, depending on the value of a_B.

There are two independent variables in the optimization: the load, $\mathscr{L}$, and the modulator concentration, or, equivalently, the Langmuir parameter, a_B, which may be manipulated by changing the modulator concentration. In Fig. 4, the production rates, yields and enrichment factors in isocratic elution for 98% pure A and B are plotted against load for different values of a_B. For each a_B value the production rates for both components as functions of load go through maximas, yields fall monotonically with increasing load, and enrichment factors reach a plateau at high load, as has been

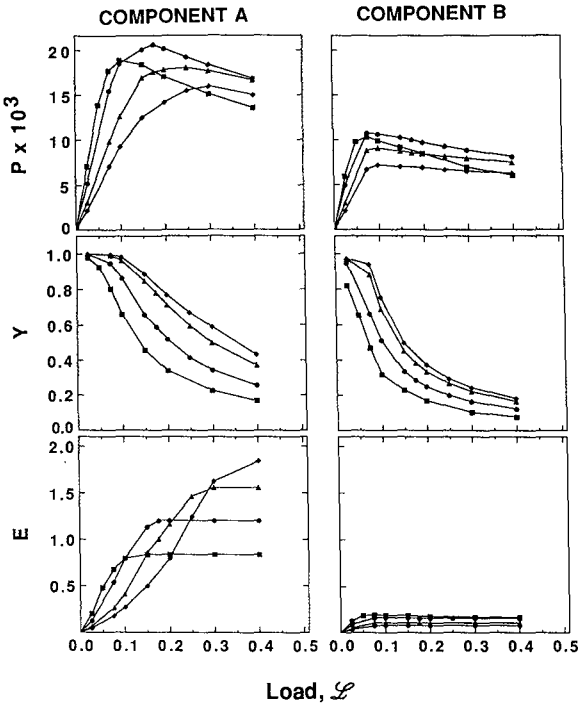

Fig. 4. Production rate, P (see eqn. 17), yield, Y, and enrichment factor, E, for the components of a 1:1 binary mixture in overloaded isocratic elution as functions of load, $\mathscr{L}$. Conditions not indicated here are as in Fig. 3; $a_{0,B}/a_{0,A} = 1.67$. ◆ = $a_B = 7.5$; ▲ = $a_B = 5.0$; ● = $a_B = 2.5$; ■ = $a_B = 1.5$.

reported elsewhere[15,40,42]. Values of a_B and $\mathscr{L}$ can be found such that the production rate is maximized. In the example shown, maximal production for component A is achieved with $a_B = 2.5$ and $\mathscr{L} = 0.175$, and for component B at the same value for a_B but at $\mathscr{L} = 0.075$. Production rates are significantly higher for the first component as compared with the second. This is because component A tails into the most concentrated region of peak B. Since the isotherm of A is suppressed in the presence of B due to competition for adsorption sites on the stationary phase (*vide* eqn. 4), A is desorbed and consequently displaced by B, resulting in enrichment factors which are higher for the first than for the second component. The tailing is reduced and the displacement enhanced when B is present in higher concentrations than A in the feedstock[42] and also if $\lambda_A < \lambda_B$, as discussed later.

In general, choice of optimal conditions depends on the relative importance of the three design parameters for the application at hand, and on the component designated as the product. In many cases production rate and enrichment factor are the most significant parameters. The yield is often of minor importance, since it is always possible, in principle, to recycle impure fractions. However, in such circumstances, the feedstock composition would change from run to run, and a careful analysis of viable recycle schemes is warranted.

Optimization of gradient elution and comparison with isocratic elution. For

a binary mixture with constant separation factor under analytical conditions, the resolution in gradient elution is lower than in a corresponding isocratic separation (see Appendix). Thus in linear chromatography of such binary mixtures, gradient elution can actually be detrimental to the separation. On the other hand, in preparative chromatography, resolution has little significance, and comparison of the two techniques should be based on the three design parameters discussed earlier.

In Fig. 5, production rates normalized with respect to the corresponding maximum production rate in isocratic elution ($P_{gr}/P_{max,is}$), yields and enrichment factors for components A and B in gradient elution are plotted against load for different values of G with fixed initial gradient conditions (*i.e.*, fixed $a_{0,B}$). The general trends followed in gradient elution mirror those in isocratic elution: production rates and enrichment factors are higher for the first component as compared with the second. Enrichment factors are significantly larger for both components in gradient elution as compared with isocratic elution. This is a result of band compression, and is also partly due to the increased displacement of A by B since the latter is maintained at higher concentrations in gradient as compared with isocratic elution. The enrichment factor for component A goes through a minima as a result of the peak splitting illustrated in Fig. 3. At high loads, component A is essentially recovered by frontal chromatography and the plateau value of the enrichment factor reflects the concentration reached in a frontal process.

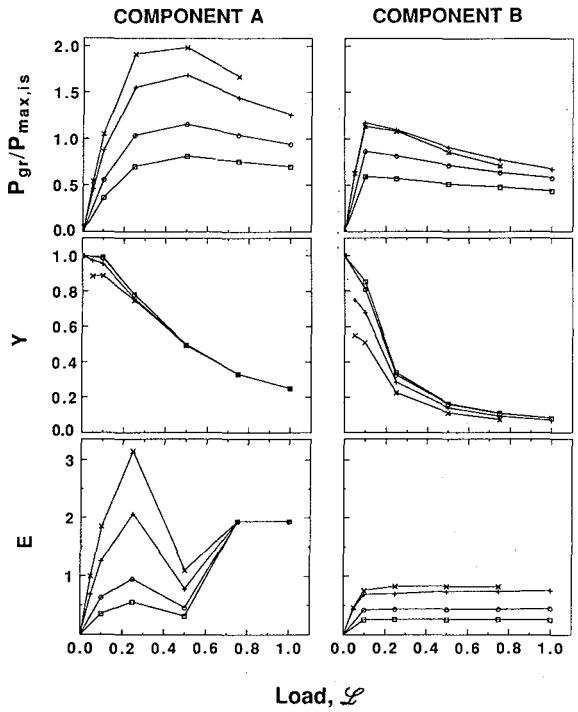

Fig. 5. Production rate normalized to the maximum production rate under isocratic conditions ($P_g/P_{max,is}$), yield, Y, and enrichment factor, E, for the components of a 1:1 binary mixture in overloaded gradient elution as functions of load, $\mathscr{L}$. Conditions not indicated here are as in Fig. 3. × = G = 1.50; + = G = 0.95; ○ = G = 0.45; □ = G = 0.25.

As shown in Fig. 5, production rates in gradient elution can be considerably higher than in isocratic elution for the first component whereas there appears to be no significant advantage for the second component. In gradient elution, the production rate for the second component can be improved by appropriately changing the initial gradient conditions by changing the initial modulator concentration. For a binary mixture with constant separation factor of 1.67, the highest production rate for B is achieved with $G = 0.6$ and $a_{0,B}\exp(-S\varphi_0) = 50$ at $\mathscr{L} = 0.1$ and is approximately 40% higher than the maximum isocratic production rate shown in Fig. 4. This gain may be important in certain large scale industrial applications. However, the advantages may well be vitiated if gradient formation and column regeneration in the gradient elution cycle are significant economic factors. Since the production rate is far less for B than for A in both gradient and isocratic elution, when the purification of component B is the goal, displacement chromatography[28,39,43] may be the method of choice.

After gradient elution, the column must be re-equilibrated with the initial mobile phase before subsequent runs, and this adds to the cycle time. Furthermore in isocratic elution it is possible to introduce the next feed batch before the components of the previous one exit the column and this reduces the cycle time somewhat. However, since it is a good practice to wash the column to remove contaminants after every run, isocratic or gradient, re-equilibration considerations depend largely on the particular application and must be addressed independently in each case.

The results shown in Figs. 4 and 5 are for a case in which the stationary phase has equal saturation capacities, λ, for both components of the binary mixture. If the capacity for the early eluting component A is less than that for component B, simulations with either our or other[14] models show a considerably enhanced displacement effect in both gradient and isocratic elution, with concomitantly higher production rates and yields, for both components, than those reported in this study. Although for such conditions the Langmuir isotherm is thermodynamically inconsistent, its employment has some experimental support[44]. In the opposite case, however, when $\lambda_A > \lambda_B$, models based on the Langmuir isotherm fail to provide adequate descriptions of observed phenomena[21,45].

Separation of binary mixtures with non-constant separation factor

Thus far we have been concerned with the special case of binary mixtures where the separation factor between the components is assumed to be constant, regardless of their concentrations or that of the modulator. In practice, however, the separation factor may vary with the concentration of the components in the feed (concentration dependent selectivity), or the modulator (modulator dependent selectivity), or both (concentration and modulator dependent selectivity). Our model for non-linear gradient elution is based on the isotherm relationship in eqn. 4, which predicts constant separation factors at a given modulator concentration and thus does not account for concentration dependent selectivity. However, it allows us to treat modulator dependent selectivity: here we examine those cases where values of the slope of the κ–φ plots are different for the individual components and thus selectivity varies with modulator concentration.

Perusal of the literature (*cf.* refs. 32, 46 and 47) shows that the κ–φ plots for a pair of eluites with fundamentally different molecular structures may converge or diverge

from their initial value at $\varphi = 0$, as shown in the insets in Fig. 6, and we may call them convergent or divergent eluite pairs, respectively. The κ–φ plots for a convergent pair always cross, leading to selectivity reversal over a defined modulator concentration range, although this range may or may not be significant in practice. For convenience, in the following study of binary mixtures only the parameters of component A are altered, whereas those of component B are left unchanged. With fixed values of the parameters for B ($a_{0,B} = 1000$, $\lambda_B = 100$) the retention behavior of the pair in gradient elution is completely specified by a value for the selectivity in the absence of modulator, α_0 ($=a_{0,B}/a_{0,A}$), the ratio of slopes S_B/S_A, and a value for λ_A, if different from λ_B. With $\varphi_0 = 0$ and given values of G the results as calculated from eqn. 12 are independent of the particular value of S_B. For illustration, however, κ–φ plots are drawn with $S_B = 20$.

Comparison of convergent, divergent and parallel eluite pairs. A comparison of the behavior of convergent, divergent and parallel pairs having the same value of α_0 in overloaded gradient elution is shown in Fig. 6. The chromatograms indicate that at a given load, initial modulator concentration (fixed at zero in this study) and gradient steepness, separation appears to be inferior for a convergent and superior for a divergent pair as compared with that for the parallel pair. This behavior is intuitively reasonable, and has been observed in a broad range of α_0.

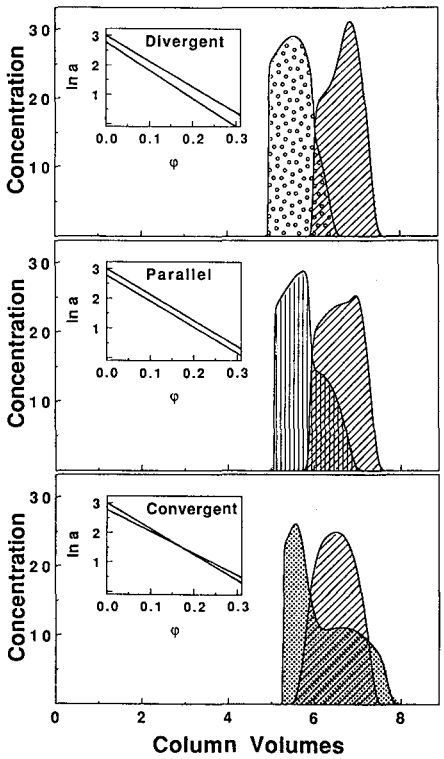

Fig. 6. Elution profiles of a 1:1 binary mixture with convergent, parallel and divergent κ–φ plots with $\alpha_0 = 1.67$ as shown in the insets. Conditions: $\varphi_0 = 0$, $G = 0.45$, $\mathscr{L} = 0.325$; convergent plot, $S_B/S_A = 1.176$; divergent plot, $S_B/S_A = 0.91$. Other conditions as in Fig. 3. Elution profiles are independent of S_B but $S_B = 20$ is shown in insets for illustration.

In order to compare such systems with modifier dependent selectivity, we introduce on the basis of the κ–φ plot a logarithmic mean separation factor, $\bar{\alpha}_{ln}$, defined by

$$\bar{\alpha}_{ln} \equiv \frac{\alpha_{\varphi_0} - \alpha_{\varphi^*}}{\ln\left(\frac{\alpha_{\varphi_0}}{\alpha_{\varphi^*}}\right)} \tag{17}$$

where α_{φ_0} is the separation factor at the initial modulator concentration and α_{φ^*} is evaluated at the modulator concentration, φ^*, at which Φa for the less retained component is unity. The concentration φ^* is chosen because in gradient linear chromatography when the isocratic retention factor, k', *i.e.* the value of Φa, is initially high (> 100), the components elute when Φa is $1/2.3G$, the value of which is approximately unity in practice[6]; thus, the modulator concentration is near φ^* at the end of the separation. For a pair of components with given α_{φ_0} and ratio of slopes S_B/S_A, $\bar{\alpha}_{ln}$ is independent of the value chosen for S_B, as may be verified by substituting into eqn. 17 the pertinent relationships for κ *versus* φ given by eqn. 3.

A comparison of the behavior of convergent, divergent and parallel eluite pairs having the same $\bar{\alpha}_{ln}$ is shown in Fig. 7. For a given load, initial modulator

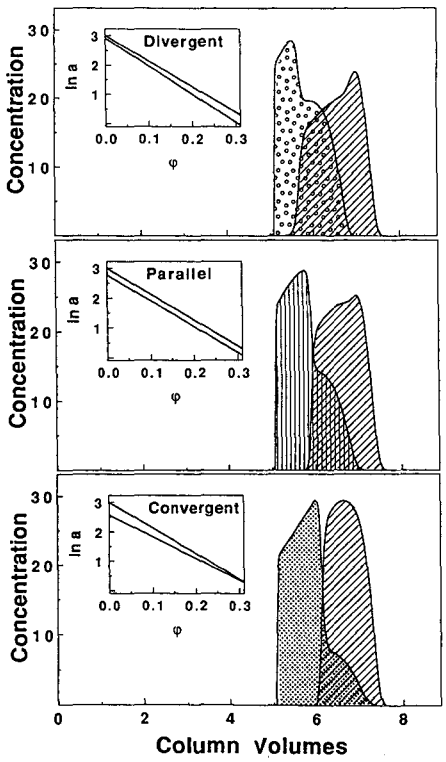

Fig. 7. Elution profiles of a 1:1 binary mixture with convergent, parallel and divergent κ–φ plots with $\bar{\alpha}_{ln} = 1.67$ as shown in the insets. Conditions: convergent plot, $\alpha_0 = 2.682$; divergent plot, $\alpha_0 = 1.212$. Other conditions as in Fig. 6.

concentration and gradient steepness, the extent of separation is approximately the same although the three chromatograms show somewhat different elution profiles. Indeed, given the necessarily *ad hoc* nature of eqn. 17, separations of different pairs of components having different S_B/S_A ratios but the same $\bar{\alpha}_{ln}$, exhibit remarkably similar separation characteristics. The similarities tend to break down at low loads and for very large or very small S_B/S_A ratios. By and large, however, under overloaded gradient conditions, different eluite pairs with the same logarithmic mean separation factor and reference component chromatographed under otherwise identical conditions show similar separation behavior. We conclude that the logarithmic mean separation factor is a useful parameter in such studies. Separations of components is expected to improve with increasing values of $\bar{\alpha}_{ln}$ as discussed below.

Modulator dependent selectivity reversal. Convergent pairs are most interesting since they may be subject to modulator dependent selectivity reversal. In the following we consider eluite pair I (A_I–B) and eluite pair II (A_{II}–B), with $\bar{\alpha}_{ln}$ of 1 and 2, respectively. Their convergent κ–φ plots that have the same ratio of slopes (1.5) are shown in Fig. 8: the two cross each other at different points and the k' (or "a" parameter, since we consider $\Phi = 1$) values at which the separation factor is unity are approximately 50 and 8 for pairs I and II, respectively.

Although the selectivity of both eluite pairs is reversed over a defined modulator range, in linear chromatography under practical operating conditions the reversal is evident only for pair II. In Fig. 9 resolution of eluite pair II by a 250-plate column is plotted against the apparent retention of component B, $k_{app,B}$, under linear conditions for different values of the gradient steepness, G. The resolution for pair I at $G = 0.3$ is also shown for comparison. Details of the necessary calculations are outlined in the Appendix. The low plate number is used only for consistency with the simulations under overloaded conditions: values in the plot may be scaled for any N by multiplying the ordinate by $\sqrt{N/250}$. Since chromatography with $k_{app,B}$ larger than 20 is not likely to be feasible due to excessively long run times, the $k_{app,B}$ span in the plot represents the practical working range for the separations. In this range eluite pair II shows selectivity

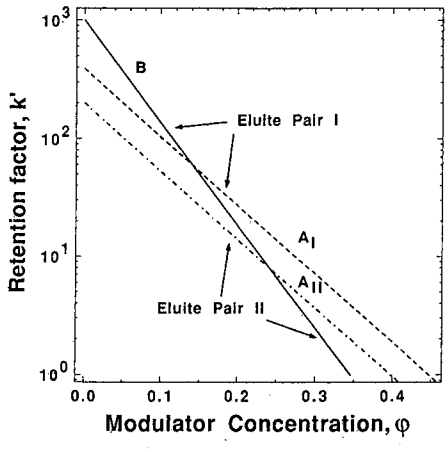

Fig. 8. Two pairs of convergent κ–φ plots both with $a_{0,B} = 1000$, $S_B = 20$ and $S_B/S_{AI} = S_B/S_{AII} = 1.5$; pair I, $a_{0,AI} = 400$; pair II, $a_{0,AII} = 200$.

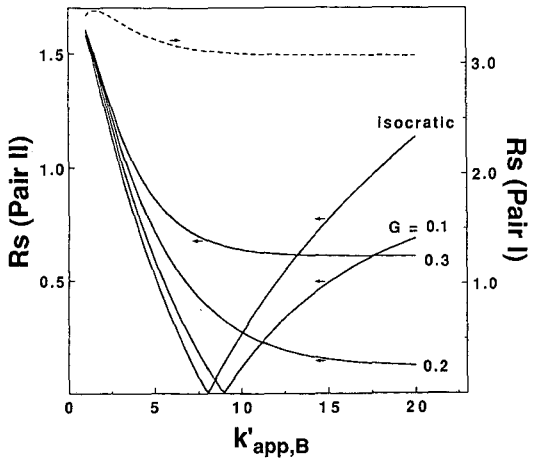

Fig. 9. Plots of the resolution, R_s, of the two eluite pairs whose κ–φ plots are shown in Fig. 8 *versus* $k'_{app,B}$, the apparent retention factor of component B, under analytical conditions. For eluite pair II, values of gradient steepness, G, based on component B (see eqn. 13) are shown on the plot. For eluite pair I, one curve with $G = 0.3$ is shown. Details of the calculations are given in the Appendix.

reversal for G values up to and slightly above 0.1, with increasing $k_{app,B}$ the resolution first decreases to zero and then increases). At $k_{app,B}$ values below the point of zero resolution, B elutes prior to A_{II} and *vice versa*. For all other values of G, and for all separations, whether isocratic or gradient, of eluite pair I in the range of interest, B is the early eluting component. Unlike the case of binaries with invariant selectivity, there is an operating range in which gradient is superior to isocratic elution under linear conditions.

Under overloaded conditions separations of both eluite pairs in gradient elution are greatly influenced by selectivity inversion. Chromatograms for eluite pairs I and II at increasing loads under fixed gradient conditions are shown in Figs. 10 and 11

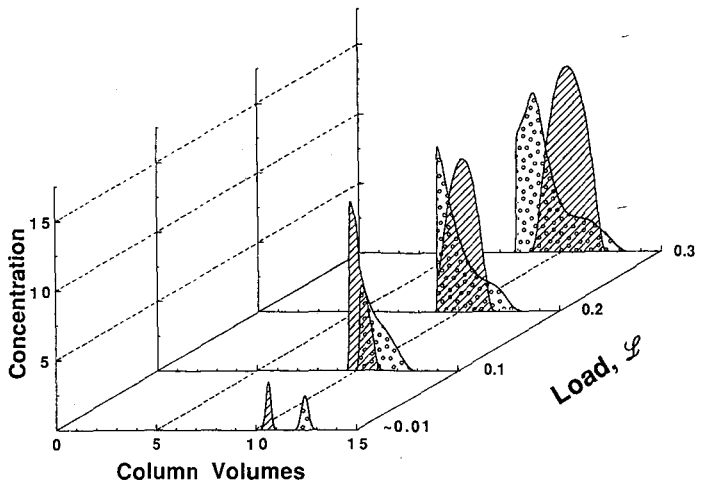

Fig. 10. Elution profiles of a 1:1 binary mixture of eluite pair I in Fig. 8 obtained with gradient elution at different loads. Conditions: $\varphi_0 = 0$, $G = 0.3$, $N = 250$, $\lambda_{AI} = 80$, $\lambda_B = 100$.

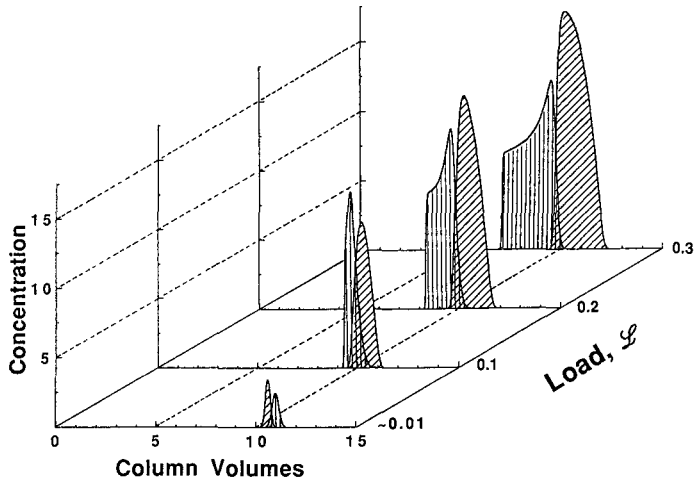

Fig. 11. Elution profiles of a 1:1 binary mixture of eluite pair II in Fig. 8 obtained with gradient elution at different loads. $\lambda_{AII} = 80$, other conditions as in Fig. 10.

respectively. At the low loads representative of linear chromatography pair I is well resolved but pair II is poorly resolved, as anticipated by the preceding analysis. The separation for pair I deteriorates drastically with increasing load, and eventually the "peak" of B is engulfed within that of A_I. On the other hand, the separation for pair II improves at higher loads, with A_{II} eluting prior to B and a sharp boundary between the bands. These observations are readily explained by phenomena that occur during the initial stages of the process. In both cases the feed step is essentially frontal chromatography under isocratic conditions with a separation factor greater than unity; under conditions of column overload, a pure fraction of component A_I or A_{II} is pushed ahead by component B to a greater extent than at low loads. Upon increasing the modulator concentration during the gradient, selectivity is reversed for both pairs, but the reversal occurs at lower modulator concentration, *i.e.*, earlier in the separation, for pair I than for pair II, as depicted in Fig. 8. In the case of pair I, the early separation between A_I and B is destroyed. In the case of pair II, however, the components have migrated a fair distance down the column before the inversion of selectivity occurs, and component B continues to displace component A_{II} throughout the separation process. As a result sharp boundaries form between the bands; this has also been observed by Snyder and co-workers[14,44].

We have found in other simulations that for eluite pair II, the sharpness of zone boundaries between A and B decreases with increasing initial modulator concentration, φ_0, *i.e.*, increases with the strength with which the components are bound to the stationary phase prior to the start of the gradient. This is in agreement with other observations from our laboratory that strong initial binding is often favorable in preparative chromatography at large. In the light of this, and the results shown in Figs. 10 and 11, we can draw the following conclusion about separations of binary mixtures with convergent κ–φ plots: for a given ratio of slopes and initial modulator concentration there is a critical value of the initial selectivity, $\alpha^*_{\varphi_0}$, above which separation by gradient elution improves with increasing load and below which the

opposite is true. The value of $\alpha^*_{\varphi_0}$ depends on those factors that determine the magnitude of the displacement effect. For instance, an increase in the proportion of component B or a decrease in the ratio of column adsorption capacities for the two components, λ_A/λ_B, would enhance the displacement of A by B and thus lower the value of $\alpha^*_{\varphi_0}$. Whether or not separation will improve with increasing load in such cases can roughly be estimated from the magnitude of the logarithmic mean separation factor, which is evaluated from the pertinent κ–φ plots. In the cases discussed above, eluite pair I, having a $\bar{\alpha}_{ln}$ of unity is not separated at high load, but pair II, with a $\bar{\alpha}_{ln}$ value of 2, is.

The κ–φ plots, *i.e.*, an examination of the separation factors at different φ values, also offer a means to predict whether isocratic or gradient elution is more suitable to bring about the separation of a given binary mixture under conditions of column overload. In practice the upper limit for k'_B in isocratic elution is about 15. Therefore in the cases shown by the plots in Fig. 8, isocratic elution is feasible for pair I but not for pair II because of the very small separation factor in the latter. Thus for the separation of pair I at high load, isocratic elution is likely to outperform gradient elution, whereas for the separation of pair II, gradient elution would be strongly favored over isocratic elution when the column is overloaded.

CONCLUSIONS

We have compared isocratic and gradient elution under overloaded conditions for single components and binary mixtures. The approach used here is rigorous and allows the investigation of the effect of gradient elution over a wide range of operating conditions and thermodynamic properties, which may not readily accessible in an experimental study. The insight gained on the separation of binary mixtures from this investigation can serve as a starting point for developing rational methods for the selection of conditions for the preparative separation of ternary and higher mixtures.

In the chromatography of a single component at high column load, simulated concentration profiles illustrate that gradient elution as compared with isocratic elution exhibits distinctly improved characteristics, in terms of apparent column efficiency. Whether or not this improvement is manifest in the separation of mixtures depends on a number of factors, the foremost being the separation factor and its dependence on the modulator concentration. Our results for binary mixtures with constant separation factor over the modulator concentration range of interest indicate that under overloaded conditions gradient elution gives better results in terms of production rates and enrichment factors for both components of the mixture with yields comparable with those in isocratic elution. These findings are in contradistinction to those in analytical chromatography where isocratic elution always gives superior results. For binary mixtures with separation factors that depend on the modulator concentration, the logarithmic mean separation factor, $\bar{\alpha}_{ln}$, provides a reasonable estimate of the extent of separation under overloaded conditions, regardless of whether the pertinent κ–φ plots of the components converge or diverge. In systems with convergent κ–φ plots where selectivity reversal occurs in the course of gradient elution over the modulator concentration range of interest, separation behavior changes dramatically with column load. The logarithmic mean separation factor can be used to predict whether or not separation will improve with increasing

load. The results suggest that isocratic elution is most useful when $\bar{\alpha}_{ln}$ is near unity, and that gradient elution is advantageous for higher values of $\bar{\alpha}_{ln}$.

ACKNOWLEDGEMENTS

This work was supported by Grants Nos. CA21948 and GM20993 from the National Institutes of Health, U.S. Department of Health and Human Resources, and by the National Foundation for Cancer Research.

APPENDIX

Here we briefly summarize the important relationships of the linear solvent strength (LSS) theory of gradient elution, which is applicable only to linear elution chromatography[6]. These expressions are then rearranged so that calculations for Figs. 1 and 9 can be made. With the help of the relationships it is shown for binary mixtures with constant selectivity over the modulator range of interest that resolution in isocratic elution is always greater than that in gradient elution.

Summary of results of the LSS theory

The LSS theory is developed for solutes that obey eqn. 3 (see text) and have linear isotherms, under gradient conditions such that eqn. 11 holds[6]. If there is no gradient delay, the retention time, t_R, of a component is given by

$$t_R = t_0 + \frac{t_0 \ln(2.3Gk'_0 + 1)}{2.3G} \tag{A1}$$

where k'_0 is the retention factor at the start of the gradient run, G is the gradient steepness (see eqn. 13) and t_0 is the column holdup time. The standard deviation in time units of a peak in gradient elution, σ_{gr} is given by

$$\sigma_{gr} = \frac{Ct_0}{\sqrt{N}}\left(1 + \frac{k'_0}{2.3k'_0G + 1}\right) \tag{A2}$$

where N is the plate number measured under isocratic conditions for a peak that elutes with a retention time of t_R, and C is a band compression factor given by

$$C = \frac{\left(1 + p + \frac{p^2}{3}\right)^{\frac{1}{2}}}{1 + p} \tag{A3}$$

where

$$p = \frac{2.3k'_0G}{1 + k'_0} \tag{A4}$$

In the above equations, the anomalous band broadening factor, J (ref. 6), is neglected as discussed in the text.

Comparison of the results in isocratic and gradient elution

An apparent retention, k'_{app}, in gradient elution is defined as

$$k'_{app} \equiv \frac{t_R - t_0}{t_0} = \frac{\ln(2.3Gk'_0 + 1)}{2.3G} \tag{A5}$$

The peak variance in isocratic elution, σ^2_{is}, is given by $t_0(1 + k')/\sqrt{N}$, where k' is the retention factor in isocratic linear elution. Combining this with eqn. A2, the ratio of peak variance in isocratic elution to that in gradient elution, $\sigma^2_{is}/\sigma^2_{gr}$, when k' and k'_{app} are the same, is given by

$$\frac{\sigma^2_{is}}{\sigma^2_{gr}} = \frac{(1 + k'_{app})^2}{C^2\left(1 + \dfrac{k'_0}{2.3Gk'_0 + 1}\right)^2} \tag{A6}$$

Here k'_0 is related to k'_{app} by the expression

$$k'_0 = \frac{\exp(2.3Gk'_{app}) - 1}{2.3G} \tag{A7}$$

and C is a function of k'_0 as indicated in eqns. A3 and A4. Equations A5–A7 are used in the calculations for Fig. 1.

The resolution, R_s, between two peaks A and B in linear chromatography is given by[30]

$$R_s = \frac{|t_{R,B} - t_{R,A}|}{2(\sigma_B + \sigma_A)} \tag{A8}$$

where subscripts A and B represent the corresponding peaks. For given values of G, based on component B (see eqn. 13), and $k'_{app,B}$, $k'_{0,B}$ can be calculated from eqn. A7, and $k'_{0,A}$ determined from the expression

$$k'_{0,A} = \Phi a_{0,A}\left(\frac{k'_{0,B}}{\Phi a_{0,B}}\right)^{S_A/S_B} \tag{A9}$$

where the Φa_0 are the retention factors of the respective components in the absence of the modifier and S_B/S_A is the ratio of slopes of their respective κ–φ plots. Eqn. A9 is derived by noting that $k'_{0,i} = \Phi a_{0,i}\exp(-S_i\varphi_0)$ (see eqns. 3, 4 and 11) and eliminating φ_0 between the respective expressions for $k'_{0,A}$ and $k'_{0,B}$. Using eqns. A1–A4, and A7 and A9, t_R and σ for the two components can be determined (for component A, S_AG/S_B must be used in place of G). Eqn. A8 can then be used to calculate the resolution as is done in Fig. 10.

For binary mixtures with constant selectivity, *i.e.*, with $S_B/S_A = 1$, resolution in isocratic elution, R_{is}, can be approximated as[30]

$$R_{is} = \frac{\sqrt{N}}{2}\left(\frac{\alpha - 1}{\alpha + 1}\right)\frac{\overline{k'}}{1 + \overline{k'}} \approx \frac{t_0\overline{k'}}{2\sigma_{is}}\left(\frac{\alpha - 1}{\alpha + 1}\right) \tag{A10}$$

where α is the selectivity ($=k'_B/k'_A$) and $\overline{k'}$ is the mean retention factor of the two components. An analogous approximation for resolution in gradient elution can be written as

$$R_{gr} = \frac{t_0\overline{k'_{app}}}{2\sigma_{gr}}\left(\frac{\alpha_{gr} - 1}{\alpha_{gr} + 1}\right) \tag{A11}$$

where α_{gr} is an observed relative retention ($= k'_{app,B}/k'_{app,A}$) which can be derived from eqn. A5 and is given by

$$\alpha_{gr} = \frac{\ln(2.3Gk_{0,B} + 1)}{\ln(2.3Gk_{0,B}/\alpha + 1)} \approx \frac{\ln(2.3G\overline{k'_{app}} + 1)}{\ln(2.3G\overline{k'_{app}}/\alpha + 1)} \tag{A12}$$

Therefore, when $\overline{k'} = \overline{k'_{app}}$ the ratio of the resolution in gradient to that in isocratic elution, R_{gr}/R_{is}, is expressed as

$$\frac{R_{gr}}{R_{is}} = \frac{\sigma_{is}}{\sigma_{gr}}\left(\frac{\alpha_{gr} - 1}{\alpha_{gr} + 1}\right)\left(\frac{\alpha + 1}{\alpha - 1}\right) \tag{A13}$$

For given values of $\overline{k'_{app}}$ and α, R_{gr}/R_{is} can be calculated as a function of G using eqns. A12 and A13. Although it cannot be readily shown algebraically, substitution of $1 < \overline{k'_{app}} < 10$ and $1.01 < \alpha < 1.7$ into the above expressions did confirm that for all finite values of G, $R_{gr}/R_{is} < 1$. This implies that for a given component pair with constant separation factor, assuming that N does not change with $\overline{k'_{app}}$, there exists at least one condition for an isocratic separation at which the resolution is larger than for any gradient separation with finite G.

SYMBOLS

a_i	initial slope of the Langmuir type multicomponent adsorption isotherm for component i when all $c_{j\neq i} = 0$.
$a_{0,i}$	value of a_i without modulator in the mobile phase
$a_{1,i}$	extrapolated value of a_i at $\varphi_s = 1.0$ M (eqns. 5 and 6)
b_i	parameter of the Langmuir type multicomponent isotherm: the reciprocal of mobile phase concentration, c_i, at half saturation of the stationary phase for component i when all $c_{j\neq i} = 0$
b_φ	b parameter for mobile phase modulator (eqn. 2)
c_i	concentration of eluite i in the mobile phase

$c_{0,i}$ inlet concentration of component i
$c_{0,\mathrm{ref}}$ inlet concentration of reference component (eqns. 13 and 14)
C band compression factor according to the LSS theory (eqn. A3); same as parameter G in ref. 6
$\mathscr{D}$ lumped effective dispersion coefficient, see discussion preceding eqn. 7
E_i enrichment factor, *i.e.* ratio of product to feed concentration, of component i
g function describing gradient profile (eqn. 10)
G gradient steepness parameter defined in eqn. 13; same as parameter b in ref. 6
k'_{app} apparent retention factor in gradient linear elution (eqn. A5)
$\overline{k'_{\mathrm{app}}}$ mean apparent retention factor of two components (eqn. A11)
k' retention factor in isocratic linear elution
$\overline{k'}$ mean retention factor of two components (eqn. A10)
k'_0 retention factor at start of gradient run (eqns. A4, A5 and A7)
L column length
$\mathscr{L}$ load parameter (eqn. 14)
n total number of eluites
N plate number under conditions of isocratic linear chromatography, $u_0 L/2\mathscr{D}$
p dimensionless group in the expression for C (eqn. A4)
P_i dimensionless production rate (eqn. 16)
q_i concentration of eluite i in the stationary phase
R_{gr} resolution in gradient linear elution (eqn. A11)
R_{is} resolution in isocratic linear elution (eqn. A10)
R_{s} resolution between two peaks (eqn. A8)
S_i 2.3 times the slope of the κ–φ plot for component i (eqn. 3); it is 2.3 times the value for the S used in ref. 6
t time
t_0 mean hold-up time of the mobile phase in the column, *i.e.*, the residence time of an unretained homomorph of the eluite
t_{R} retention time in linear elution
t_{inj} time of feed introduction
u_0 chromatographic velocity, L/t_0
X dimensionless axial distance, z/L
Y_i yield of component i, *i.e.*, the ratio of mass recovered in product to that in feed
z axial distance in the column
Z ratio of eluite to salt valence in electrostatic interaction chromatography (eqns. 5 and 6)

Greek

α selectivity or relative retention or separation factor for two components in isocratic linear elution (eqn. A10)
α_{gr} ostensible selectivity for two components, $k'_{\mathrm{app,B}}/k'_{\mathrm{app,A}}$, in gradient linear elution (eqn. A11)
$\bar{\alpha}_{\mathrm{ln}}$ logarithmic mean separation factor (eqn. 17)
α_{φ_0} separation factor at modulator concentration φ_0 (eqn. 17)
α_{φ^*} separation factor at modulator concentration φ^* (eqn. 17)

β linear rate of change of modulator concentration at the inlet, *i.e.*, the difference between final and initial modulator concentration divided by the gradient time

Φ phase ratio, *i.e.*, the ratio of stationary phase to mobile phase volumes within the column; set to unity in this study

φ modulator concentration in the mobile phase

φ_0 modulator concentration at the start of the gradient run

φ^* modulator concentration at which Φa_0 is unity for the least retained component of an eluite pair (eqn. 17)

κ_i $\log_{10} k'_i$ (eqn. 3)

$\kappa_{0,i}$ $\log_{10}(\Phi a_{0,i})$ (eqn. 3)

λ_i parameter of the Langmuir type multicomponent adsorption isotherm for component i, *i.e.*, the saturation value of stationary phase concentration for that component, a_i/b_i

$\lambda_{\text{ref.}}$ saturation value of stationary phase concentration for reference component (eqns. 14 and 16)

μ_1 first moment of peak (Table I)

μ_2^* second central moment of peak (Table I)

μ_3^* third central moment of peak (Table I)

θ dimensionless time, t/t_0

θ_c dimensionless cycle time (eqn. 16)

σ_{gr}^2 peak variance in gradient linear elution

σ_{is}^2 peak variance in isocratic linear elution

τ dimensionless time for feed introduction, t_{inj}/t_0

REFERENCES

1 R. S. Alm, R. J. P. Williams and A. Tiselius, *Acta Chem. Scand.*, 6 (1952) 826.
2 Cs. Horváth and S. R. Lipsky, *Anal. Chem.*, 39 (1967) 1893.
3 B. Drake, *Ark. Kemi*, 8 (1955) 1.
4 E. C. Freiling, *J. Am. Chem. Soc.*, 77 (1955) 2067.
5 P. J. Schoenmakers, H. A. H. Billiet, R. Tijssen and L. de Galan, *J. Chromatogr.*, 149 (1978) 519.
6 L. R. Snyder, in Cs. Horváth (Editor), *High-Performance Liquid Chromatography—Advances and Perspectives*, Vol. 1, Academic Press, New York, 1980, pp. 208–316.
7 S. Yamamoto, K. Nakanishi, R. Matsuno and T. Kamikubo, *Biotechnol. Bioeng.*, 25 (1983) 1465.
8 P. Jandera and J. Churacek, *Gradient Elution in Column Liquid Chromatography (Journal of Chromatography Library*, Vol. 31), Elsevier, Amsterdam, 1985.
9 S. J. Gibbs and E. N. Lightfoot, *Ind. Eng. Chem. Fundam.*, 25 (1986) 490.
10 K. Kang and B. J. McCoy, *Biotechnol. Bioeng.*, 33 (1989) 786.
11 J. E. Eble, R. L. Grob, P. E. Antle and L. R. Snyder, *J. Chromatogr.*, 405 (1987) 51.
12 L. R. Snyder, G. B. Cox and P. E. Antle, *J. Chromatogr.*, 444 (1988) 303.
13 G. B. Cox, P. E. Antle and L. R. Snyder, *J. Chromatogr.*, 444 (1988) 325.
14 L. R. Snyder, J. W. Dolan and G. B. Cox, presented at *6th International Symposium on Preparative Chromatography, Washington, DC, May 8–10, 1989.*
15 F. D. Antia and Cs. Horváth, *Ann. NY Acad. Sci.*, (1989) in press.
16 I. Langmuir, *J. Am. Chem. Soc.*, 38 (1916) 2221.
17 G. M. Schwab, *Ergebnisse der exacten Naturwissenschaften*, Vol. 7, Julius Springer, Berlin, 1928, p. 276.
18 D. B. Broughton, *Ind. Eng. Chem.*, 40 (1948) 1506.
19 C. Kemball, E. K. Rideal and E. A. Guggenheim, *Trans. Faraday Soc.*, 44 (1948) 948.
20 J. Jacobson, J. Frenz and Cs. Horváth, *J. Chromatogr.*, 316 (1984) 53.
21 A. Velayudhan, *Ph.D. Thesis*, Yale University, New Haven, CT, 1989.
22 A. L. Lee, *Ph.D. Thesis*, Yale University, New Haven, CT, 1989.

23 A. Velayudhan and Cs. Horváth, *J. Chromatogr.*, 367 (1986) 160.
24 F. Helfferich, *Ion Exchange*, McGraw-Hill, New York, 1962.
25 A. Velayudhan and Cs. Horváth, *J. Chromatogr.*, 443 (1988) 13.
26 G. Guiochon and A. Katti, *Chromatographia*, 24 (1987) 165.
27 Cs. Horváth and H.-J. Lin, *J. Chromatogr.*, 149 (1978) 43.
28 A. L. Lee, A. Velayudhan and Cs. Horváth, in G. Durand, L. Bobichon and J. Florent (Editors), *8th International Biotechnology Symposium*, Société Française de Microbiologie, Paris, 1989, pp. 593–610.
29 N. S. Raghavan and D. M. Ruthven, *AIChE J.*, 29 (1983) 922.
30 Cs. Horváth and W. R. Melander, in E. Heftmann (Editor), *Chromatography—Fundamentals and Applications of Chromatographic and Electrophoretic Methods*, Part A, Elsevier, Amsterdam, 1983, pp. A27–A135.
31 L. R. Snyder and M. A. Stadalius, in Cs. Horváth (Editor), *High-Performance Liquid Chromatography—Advances and Perspectives*, Vol. 4, Academic Press, New York, 1986, pp. 195–312.
32 M. T. W. Hearn and M. I. Aguilar, *J. Chromatogr.*, 392 (1987) 33.
33 L. R. Snyder, G. B. Cox and P. E. Antle, *Chromatographia*, 24 (1987) 82.
34 J. H. Knox and H. M. Pyper, *J. Chromatogr.*, 363 (1986) 1.
35 E. Glueckauf, *Discuss. Faraday Soc.*, 7 (1949) 12.
36 G. Guiochon and S. Ghodbane, *J. Phys. Chem.*, 92 (1988) 3682.
37 J. L. Wade and P. W. Carr, *J. Chromatogr.*, 449 (1988) 53.
38 P. C. Wankat, *Anal. Chem.*, 46 (1974) 1400.
39 F. D. Antia and Cs. Horváth, *Ber. Bunsenges. Phys. Chem.*, (1989) in press.
40 S. Ghodbane and G. Guiochon, *J. Chromatogr.*, 444 (1988) 275.
41 S. Ghodbane and G. Guiochon, *J. Chromatogr.*, 452 (1988) 209.
42 A. Katti and G. Guiochon, *Anal. Chem.*, 61 (1989) 982.
43 J. Frenz and Cs. Horváth, in Cs. Horváth (Editor), *High-Performance Liquid Chromatography—Advances and Perspectives*, Vol. 5, Academic Press, New York, 1988, pp. 211–314.
44 G. B. Cox, B. J. Permar and L. R. Snyder, presented at *6th International Symposium on Preparative Chromatography, Washington, DC, May 8–10, 1989.*
45 D. D. Frey, *J. Chromatogr.*, 409 (1987) 1.
46 L. R. Snyder, M. A. Quarry and J. L. Glajch, *Chromatographia*, 24 (1987) 33.
47 B. F. D. Ghrist and L. R. Snyder, *J. Chromatogr.*, 459 (1988) 43.

Journal of Chromatography, 484 (1989) 29–59
Elsevier Science Publishers B.V., Amsterdam — Printed in The Netherlands

CHROM. 22 015

MASS TRANSFER EFFECTS IN ISOCRATIC NON-LINEAR ELUTION CHROMATOGRAPHY

CASSIAN K. LEE, QIMING YU, SEUNG UN KIM and NIEN-HWA LINDA WANG*
School of Chemical Engineering, Purdue University, West Lafayette, IN 47907 (U.S.A.)

SUMMARY

In large-scale liquid chromatography, solute competition for sorbent sites (interference) coupled with mass transfer effects can result in complex solute distribution patterns and concentration dependent migration of solute bands. A rate equation model, which accounts for axial dispersion, film mass transfer, intraparticle diffusion, size exclusion and non-linear isotherms, was used to simulate the effluent histories of multicomponent ion-exchange systems. The method of orthogonal collocation on gradient-directed moving finite elements developed by Yu and Wang in 1989 was used to solve the model equations. The theory was verified by comparing the model predictions with data on amino acid and protein ion exchange and good agreement was obtained.

Dimensionless groups were used to identify the local equilibrium regime, in which the effects of axial dispersion, film mass transfer and intraparticle diffusion are negligible. Mass transfer effects were pronounced for systems with small pulse sizes and for solutes with long retention times. For a system with a pulse size about 20 pore volumes $\bar{C}/C_i = 10^3$, and α (separation factor of a solute against eluent) = 1.6, mass transfer effects were negligible at $N_p > 10^3$. For low affinity solutes ($\alpha < 0.1$) of a similar pulse size, local equilibrium was approached at a lower N_p.

The dimensionless groups were also useful for studying the combined effects of design and operating parameters. The effects of these parameters on band shape and band spreading were examined for non-linear systems with various solute affinities. The dimensionless groups were also used to establish simple scaling rules for non-linear chromatography. The scaling rules suggest that one can achieve the same degree of separation but significantly higher throughputs by using small particles, short columns and rapid cycles.

INTRODUCTION

In linear chromatography, solute bands have a simple shape and the mechanisms which cause band spreading during migration in a chromatography column are well understood[1–3]. In non-linear chromatography, however, peak shapes and spreading are affected by solute competition for sorbent sites (interference), axial dispersion, film mass transfer and intraparticle diffusion. As a result, peak shape and spreading are

0021-9673/89/$03.50

complex functions of equilibrium isotherms, mass transfer parameters (film mass transfer coefficients and intraparticle diffusivity), design parameters (particle size and column length), and operating parameters (pulse size, feed concentration and flow-rate). Understanding interference and mass transfer effects on band spreading in non-linear systems is crucial for designing and scaling large-scale chromatography, in which large pulses and concentrated feeds are usually used to increase throughputs.

Because of the complexity of non-linear systems, significant simplifications are usually introduced into chromatography models. In a local equilibrium model, the mass transfer resistances are assumed to be negligible. Therefore, local equilibrium models are useful for explaining thermodynamic effects on the separation and migration of solute bands. They are useful for predicting column dynamics (unsteady state concentration profiles and effluent histories) when mass transfer effects are insignificant. Among them, the interference theory[4–8] provides the most extensive analyses for isocratic systems. However, solutions of local equilibrium models are usually restricted to simple forms of equilibrium isotherms, simple step inputs, and isocratic operations. Only recently, the interference theory was extended to non-linear systems with gradients and two-way flow operations[8]. Also, computer simulations for general non-linear isotherms were carried out recently for isocratic single component gas chromatography (GC) and liquid chromatography (LC)[9], and two-component isocratic LC[10]. Despite the numerous local equilibrium theories, there have been no clear guidelines for judging whether the assumption of local equilibrium is valid for a given system.

For models in the literature that do include mass transfer effects, such as staged models and rate equation models, simplifications are made on equilibrium isotherms or the mass transfer processes. Table I shows a summary of selected theoretical studies that account for mass transfer effects in ion-exchange and adsorption systems. Because of mathematical complexity, detailed solutions are available only for linear isotherm systems, for which interference effect is absent. For non-linear systems, one or more of the following simplifications are used: no intraparticle diffusion, no axial dispersion, no film mass transfer resistance, single component, or special isotherm type. Certain assumptions also make it difficult to study the effects of design and operating parameters. For example, in the linear driving force approach[11], the effects of particle diameter and flow-rate are not explicit. For systems with non-linear isotherms, the lumped mass transfer coefficient estimated under one condition may not apply when solute concentration, particle size, or flow-rate changes. Moreover, a systematic study of axial dispersion, film mass transfer, intraparticle diffusion in non-linear chromatography has not been reported before.

In this article, a detailed rate equation model developed by Yu and Wang[12] is used to study interference and mass transfer effects in non-linear chromatography. The objectives are (1) to verify the rate equation model with experiments on amino acid elution and protein ion exchange; (2) to compare the results with a local equilibrium model in order to identify the regions where the mass transfer effects are negligible; and (3) to study the relative importance of interference, axial dispersion, film mass transfer, and intraparticle diffusion on peak shape and peak spreading under various design and operating conditions.

The model equations expressed in dimensionless form are solved by a gradient-directed moving finite element technique developed by Yu and Wang[12]. Using various

TABLE I

SUMMARY OF RATE EQUATION THEORY LITERATURE

Abbreviations: Adspt = adsorption process; diffusion = intraparticle diffusion; dispersion = axial dispersion; film = film mass transfer; IEX = ion exchange process; LDFA = linear driving force approach.

Ref.	*Feature*	*Isotherm*	*Component*	*Input*	*Method of solution*	*Adspt/ IEX*
24	Diffusion, film	Langmuir	Multi	Batch	Orthogonal collocation	Adspt
25	LDFA	Linear	–	All	Analytical, Laplace transform	Adspt
26	Dispersion, diffusion, film	Linear	–	Step	Analytical, Fast Fourier transform	Adspt
27	Dispersion, diffusion	Parabolic	Single	Step	Finite difference	IEX
28	Diffusion, film	Linear	–	Step	Parabolic & quadratic profiles	Adspt
29	Dispersion LDFA	Langmuir S-shaped	Single	Pulse	Finite difference	Adspt
30	Dispersion, diffusion, film	Linear	–	Pulse	Method of moments	Adspt
31	Dispersion, diffusion, film	Fritz & Schlunder type	Binary	Step	Orthogonal collocation	Adspt
32	Diffusion, film	Linear	–	Step	Parabolic profile	Adspt
33	Diffusion, film, LDFA	Freundlich	Multi	Step	Finite difference	Adspt
34	Dispersion, LDFA	Langmuir	Multi	Step	Finite difference	Adspt
35	Diffusion	Shrinking core	Single	Step	Finite difference	IEX
36	Diffusion	Langmuir	Single	Step	Method of moments	Adspt
37	Diffusion, film	Linear	–	Step	Analytical, Laplace transform	Adspt
38	Two pore diffusion, film	Langmuir	Single	Step	Finite difference	Adspt
39	LDFA	Langmuir, Freundlich	Multi	Step	Finite difference	Adspt
40	Diffusion, film	Langmuir	Single	Step	Numerical	Adspt
41	Dispersion, dual-pore diffusion	Freundlich	Single	Step	Finite difference	Adspt
42	LDFA, non-isothermal	Langmuir	Multi	Step	Method of line	Adspt

dimensionless groups allows us to study the combined effects of design and operating parameters. The magnitudes of these groups indicate the relative importance of film mass transfer, intraparticle diffusion and axial dispersion for a given system. Furthermore, they are useful for scaling of non-linear systems.

THEORY

In formulating this model, we assume uniform packing, uniform velocity distribution, pseudo-homogeneous spherical particles with uniform size distribution, isothermal behavior and constant physical properties. Convection and axial dispersion are considered the only mechanisms of mass transfer in the axial direction. The axial dispersion coefficient is estimated from a standard correlation[13]. The pressure and velocity variations along the axis are assumed to have no effects on equilibrium and column dynamics. The mass transfer coefficient between the bulk mobile phase and the stationary phase is estimated from a J factor correlation[14]. For each particle, its surroundings are assumed to be uniform. Surface diffusion within the particle is also neglected. Along the radial direction in a particle, local equilibrium is assumed between the stagnant fluid in the pores and the sorbent surface.

For each component j, the mass balance equations and initial and boundary conditions are given in eqns. 1 and 2, where subscripts b and p denote the bulk and particle phases, respectively.

Bulk phase

$$\frac{\partial c_{bj}}{\partial \tau} = \frac{1}{Pe_z}\frac{\partial^2 c_{bj}}{\partial x^2} - \frac{\partial c_{bj}}{\partial x} - N_{bj}(c_{bj} - c_{pj,\xi=1}) \tag{1a}$$

$$x = 0, \quad \frac{\partial c_{bj}}{\partial x} = Pe_z(c_{bj} - c_{fj}) \tag{1b}$$

$$x = 1, \quad \frac{\partial c_{bj}}{\partial x} = 0 \tag{1c}$$

$$\tau = 0, \quad c_{bj} = c_{bj}(0,x) \tag{1d}$$

where

$$\tau = t/(L/u_0), \quad x = z/L, \quad N_{bj} = \frac{L}{R}\frac{3(1-\varepsilon)}{\varepsilon}\frac{Bi_j}{Pe_{pj}}, \quad Bi_j = k_j R/E_{pj},$$
$$Pe_z = u_0 L/E_{bj}, \quad Pe_{pj} = u_o R/E_{pj}.$$

All concentration variables are normalized by their respective feed concentrations. Thus, c_{bj} is a dimensionless bulk phase concentration, c_{fj} is a dimensionless feed concentration, z is the axial distance, L is the column length, R is the particle radius, t is time, u_0 is the interstitial velocity, k_j is the film mass transfer coefficient of component

j, ε is the bed void fraction and E_{bj} and E_{pj} are the axial dispersion coefficient and effective diffusivity of component j, respectively.

Particle phase

$$Ke_j\left[\theta\frac{\partial c_{pj}}{\partial\tau}+(1-\theta)\frac{\partial c^*_{pj}}{\partial\tau}\right]=N_{pj}\frac{1}{\xi^2}\frac{\partial}{\partial\xi}\left[\xi^2\frac{\partial c_{pj}}{\partial\xi}\right] \tag{2a}$$

$$\xi=0,\quad \frac{\partial c_{pj}}{\partial\xi}=0 \tag{2b}$$

$$\xi=1,\quad \frac{\partial c_{pj}}{\partial\xi}=Bi\,(c_{bj}-c_{pj}) \tag{2c}$$

$$\tau=0,\quad c_{pj}=c_{pj}(0,\xi) \tag{2d}$$

where $\xi=r/R$, $N_{pj}=(L/R)\cdot(1/Pe_{pj})$, c_{pj} is the local dimensionless concentration of component j in the fluid phase within a particle, c^*_{pj} is the dimensionless concentration of component j in the solid phase within a particle and it is in equilibrium with the local concentrations of the fluid phase ($c_{p1}, c_{p2}, \ldots, c_{pn}$), n is the number of components, r is the radial coordinate of the particle, θ is intraparticle porosity, and Ke_j is the size exclusion factor of component j.

One of the objectives of this study is to compare the results of the rate equation model with those from a previous local equilibrium model based on the assumption of constant separation factors[7]. The comparison is needed to identify the conditions under which the local equilibrium model is applicable. For this reason, the equilibrium isotherms here are represented by constant separation factors. For a multicomponent system with constant separation factors, the non-linear equilibrium isotherm for component i can be written as follows

$$c^*_{pi}=\frac{c_i\bar{C}/C_i}{\alpha_{li}\sum_j\dfrac{c_j}{\alpha_{lj}}} \tag{3}$$

where α_{ij} is the separation factor of i against j, $\bar{C}$ is column capacity per bed volume, C_i is the feed concentration of the i^{th} component based on per bed volume, and $\bar{C}/C_i$ is an important dimensionless group. Although all simulations reported in this paper are for constant separation factor systems, this model can incorporate any complex isotherms. Simulations for systems with Langmuir isotherms have been reported in a previous paper[12].

The dimensionless group Pe_z in eqn. 1 is the axial Peclet number, which is proportional to the ratio of a characteristic convection rate to that of axial dispersion. The dimensionless group Pe_p in eqn. 2 is the particle Peclet number, which is proportional to the ratio of a characteristic convection rate to that of intraparticle diffusion. The Biot number (Bi) in eqn. 2 represents the ratio of a characteristic film mass transfer rate to that of intraparticle diffusion.

A correlation developed by Chung and Wen[13] is used to estimate E_b or Pe_z.

$$Pe_z = \frac{L}{2R\varepsilon}(0.2 + 0.011Re^{0.48}) \tag{4}$$

where the Reynolds number (Re) is defined as

$$Re = \frac{2R\rho u_0 \varepsilon}{\mu} \tag{5}$$

Since Re is typically in the order of 0.1 or less, Pe_z is essentially only a function of $L/(R\varepsilon)$.

The film mass transfer coefficient k can be estimated from a J factor correlation proposed by Wilson and Geankoplis[14]. This correlation is valid for liquid systems with low Reynolds numbers.

$$J = \left(\frac{k}{u_0\varepsilon}\right)\left(\frac{\mu}{\rho D^\infty}\right)^{2/3} = \frac{1.09}{\varepsilon} Re^{-2/3} \tag{6}$$

As shown in eqn. 6, the film mass transfer coefficient k is related to D^∞ (Brownian diffusivity) and u_0 (interstitial velocity). The effective intraparticle diffusivity (E_p) of a solute is also related to D^∞ for a given sorbent material (see eqn. 10). Because of this interdependence, one can rearrange eqn. 6 to give the following explicit relation:

$$\frac{u_0}{k} = \left[\frac{(2\varepsilon)^{2/3}}{1.09}\right]\left(\frac{E_p}{D^\infty}\right)^{2/3}\left(\frac{Ru_0}{E_p}\right)^{2/3} \tag{7}$$

which is equivalent to

$$Pe_p/Bi = \left[\frac{(2\varepsilon)^{2/3}}{1.09}\right]\left(\frac{E_p}{D^\infty}\right)^{2/3}(Pe_p)^{2/3} \tag{8a}$$

or

$$Pe_p = \left[\frac{(1.09)^{3/2}}{2\varepsilon}\right]\left(\frac{D^\infty}{E_p}\right)\left(\frac{Pe_p}{Bi}\right)^{3/2} \tag{8b}$$

Eqn. 8b can be rearranged to give an explicit relation between Pe_p and Bi.

$$Pe_p = \frac{4\varepsilon^2}{1.09^3}\left(\frac{E_p}{D^\infty}\right)^2 Bi^3 \tag{9}$$

Eqn. 9 suggests that as Pe_p increases with increasing particle size or flow-rate, Bi also increases. This implies that as Pe_p increases, intraparticle diffusion resistance becomes relatively more important than film resistance.

We are interested in comparing simulation results with data for amino acid and protein ion exchange here, but unfortunately, experimental data of E_p are usually unavailable. For small ions and particles with uniform pores, the following equation can be applied to estimate E_p from Brownian diffusivity D^∞[15,16].

$$E_p = \left(\frac{\theta}{2-\theta}\right)^2 D^\infty \tag{10}$$

If this equation is used, eqn. 9 becomes

$$Pe_p = \frac{4\varepsilon^2}{1.09^3}\left(\frac{\theta}{2-\theta}\right)^4 Bi^3 \tag{11}$$

Pulse size is another important scaling parameter for this system. A dimensionless pulse size $\Delta\tau$ is defined here as

$$\Delta\tau = \frac{V_p}{\varepsilon V_{bed}} = \frac{V_p u_0}{FL} \tag{12}$$

where F is volumetric flow-rate, V_p is the volume of a feed pulse and V_{bed} is bed volume. As shown in eqn. 12, $\Delta\tau$ represents a dimensionless pulse volume, where V_p is normalized by interparticle void volume (εV_{bed}) in a packed bed. This dimensionless pulse $\Delta\tau$ is related to the fractional loading ΔT_i, which was defined previously for local equilibrium studies[4,8].

$$\Delta T_i = \frac{C_i \Delta\tau}{\bar{C}} \tag{13}$$

This fractional loading also represents a dimensionless pulse size, in which the total amount of solute i input to the column during $\Delta\tau$ is normalized by total column capacity.

Eqn. 9 (or eqn. 11) can be substituted into eqns. 1 and 2 to eliminate Pe_p. Thus, we are left with Pe_z and Bi as the independent transport parameters, L/R, ε and θ (and E_p/D^∞, if eqn. 10 is used) are the system parameters, $\bar{C}/C_i$ and $\Delta\tau$ are the operating parameters. These dimensionless parameters are useful for scaling purposes and for studying the combined effects of L, R and u_0. They are especially convenient for estimating the relative importance of intraparticle diffusion, film mass transfer, and axial dispersion on band spreading for a given system. These results will be discussed later.

Since the systems being studied involve non-linear isotherms, eqns. 1 and 2 must be solved numerically. An efficient numerical method was developed by Yu and Wang[12] for solving non-linear boundary value problems. This method, being

especially useful for fixed-bed systems with steep gradients, was used to solve the model equations here. It employs orthogonal collocation on both bulk and particle phases as well as a gradient-directed moving finite elements scheme. Details of this technique and convergence behavior are available elsewhere[12]. A typical elution simulation requires two collocation points in the particle phase and four points in each element for the bulk phase. The number of elements varies from 16 initially to about 4 at the end of simulation.

RESULTS AND DISCUSSION

Before studying mass transfer effects and interference phenomena, we verified this model with data from ion exchange of amino acids and proteins. Previous data on isocratic elution of lysine and proline were considered first[17]. A 7.5 × 1 cm I.D. column was used. It was packed with Bio-Rad AG 50W-X8 cation-exchange resin, with a particle radius of about 25 μm. A 50-ml mixture of 0.01 *N* lysine and 0.01 *N* proline in 0.19 *N* of sodium citrate buffer at pH 4.4 was injected into the column at 2 ml/min, and eluted with 0.20 *N* of sodium citrate buffer at the same pH. Fig. 1a shows the effluent history of the column plotted in dimensionless concentration *versus* dimensionless time. The results from the rate equation model (solid lines) are compared with those from the local equilibrium model (dashed lines). As the figure shows, the local equilibrium model can predict the average retention time, but it cannot predict the exact product concentration and zone spreading behavior because it neglects mass transfer effects.

As mentioned before, both axial dispersion and film diffusion coefficients were estimated from standard correlations. Since E_p values were not readily available for this sytem, approximate values were obtained from eqn. 10. Except where indicated, eqn. 10 was used to estimate E_p from D^∞ for all simulations in this paper. An E_p of 3.5 $\cdot 10^{-5}$ cm^2/min was used for both lysine and proline for the simulations shown in Fig.

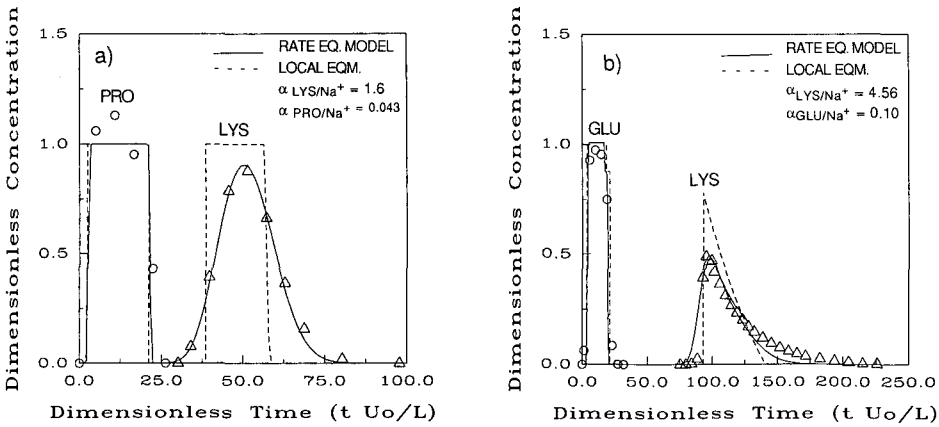

Fig. 1. (a) Experimental results and model predictions of the lysine–proline system. $Pe_z = 672$, $Pe_p = 337$, $Bi = 42$, $Pe_p/Bi = 8$, $\Delta\tau = 18.86$, $\alpha_{Lys/Na^+} = 1.6$, $\alpha_{Pro/Na^+} = 0.043$. Parameters used in simulations are listed in Table II. (b) Experimental results and model predictions of the lysine–glutamic acid system. $Pe_z = 653$, $Pe_p = 202$, $Bi = 36$, $Pe_p/Bi = 5.6$, $\Delta\tau = 15.50$, $\alpha_{Lys/Na^+} = 4.56$, $\alpha_{Glu/Na^+} = 0.10$.

1a. The value of D^{∞} was first estimated from the Wilke–Change correlation given in ref. 18 and eqn. 10 was then used to estimate E_p. This E_p value is similar to the values given for other amino acids in a similar exchanger[19]. The same separation factors from the local equilibrium simulation were used ($\alpha_{Lys/Na^+} = 1.6$ and $\alpha_{Pro/Na^+} = 0.043$). Both bed void fraction (ε) and particle porosity (θ) were 0.45. All the parameter values used for simulations are listed in Table II.

Because proline has a low affinity relative to Na^+, it elutes immediately without any peak broadening, and the concentration is the same as in the feed pulse. This behavior is closely predicted by both models. For the lysine peak, only the rate equation model can predict the experimental behavior in detail. Because the retention time of lysine is longer and mass transfer effects are more pronounced, the lysine peak becomes less concentrated than the feed and it spreads more than the proline peak. This example shows the validity and accuracy of the rate model for high affinity solutes.

Fig. 1b shows the results of elution of a glutamic acid and lysine mixture. A 7.3-cm column packed with the same resin was used, and a pulse of 40 ml with 0.02 *N* lysine, 0.01 *N* glutamic acid and 0.20 *N* sodium citrate was injected into the column at a flow-rate of 1 ml/min. It was then eluted with 0.20 *N* of sodium citrate buffer at pH 3.5[8]. At this pH, α_{Glu/Na^+} is 0.10, and α_{Lys/Na^+} is 4.56, which is much higher than in the previous case. The rate equation model again can predict the data closely by using the same E_p, θ and ε as in the previous system. For the same reason as in the previous case,

TABLE II

SUMMARY OF PARAMETER VALUES USED FOR SIMULATIONS

$\theta = \varepsilon = 0.45$, $E_p = 4.2 \cdot 10^{-5}$ cm²/min, $D^{\infty} = 5 \cdot 10^{-4}$ cm²/min, $\bar{C} = 2.3$ mequiv./ml packed volume.

Fig.	*L (cm)*	*V_p (ml)*	*F (ml/min)*	*R (μm)*	*α_{Lys/Na^+}*	*α_{Pro/Na^+}*	*[Lysine] (N)*	*[Proline] (N)*	*[Na^+] (N)*
1a[a]	7.5	50	2	25	1.6	0.043	0.01	0.01	0.19
1b[a]	7.3	40	1	25	4.56	0.10[b]	0.02	0.01[b]	0.20
4	7.5	50	0.1–40	25	1.6	0.043	0.01	0.01	0.18
7	7.5	50	0.5–40	25	4.0	0.5	0.01	0.01	0.18
8–10					1.6	0.043	0.01	0.01	0.18
13a	7.5	50	2	25–160	1.6	0.043	0.01	0.01	0.18
13b	7.5	50	2	10–100	4.0	0.5	0.01	0.01	0.18
14	1–15	50	2	25	1.6	0.043	0.01	0.01	0.18
15	7.5	10–250	2	25	1.6	0.043	0.01	0.01	0.18
16a	7.5	50	2	25	1.6	0.043	0.01–0.16	0.01–0.16	0.18
16b[c] (1)	7.5	50	2	25	1.6	0.043	0.01	0.01	0.18
(2)							0.031	0.031	0.139
(3)							0.047	0.047	0.106
(4)							0.064	0.064	0.072
16c	7.5	100	2	25	1.6	0.043	0.01–0.16	0.01–0.16	0.18
17a	7.5	100	2	25	1.6	0.043	0.04	0.04	0.04–0.34
17b	7.5	50	2	25	1.6	0.043	0.04	0.04	0.04–0.34

[a] $E_p = 3.5 \cdot 10^{-5}$ cm²/min, $D^{\infty} = 4.16 \cdot 10^{-4}$ cm²/min.

[b] $\alpha_{Glu/Na^+} = 0.10$, $c_{Glu} = 0.01$ *N*.

[c] The fractions of lysine, proline and Na^+ are the same as in Fig. 16a except the total concentration is kept at 0.2 *N*.

the glutamic acid passes through the column immediately without any zone spreading. For this low affinity solute, because mass transfer effects are insignificant, the local equilibrium model is adequate. Asymmetric lysine peak is predicted by both models. This is because solute migration speed is a function of solute concentration and α; the larger the α or the higher the solute concentration, the more does the migration speed vary with concentration, and the more pronounced is the tailing[8]. Again in this case, the rate equation model is needed to predict the lysine data accurately.

Experimental data obtained from protein ion exchange were also used to verify the model. An 11-cm column packed with DEAE Sepharose Fast Flow (Pharmacia) was presaturated with chloride ions initially. A 5-mg/ml myoglobin (Myo) solution in 0.1 *M* Tris buffer at pH 8 was injected into the column at a flow-rate of 0.5 ml/min. Bovine serum albumin (BSA) with the same concentration as myoglobin was introduced into the column to displace myoglobin after 111 min (τ = 18.36). The effluent history is shown in Fig. 2a. Because of the size of protein molecules, not the whole resin particle is accessible to the protein; therefore, size-exclusion factors of 0.72 and 0.6 (ref. 8) were used for myoglobin and BSA, respectively, to obtain the simulation results in Fig. 2a.

The E_p values for the proteins were estimated from the Brownian diffusivities using eqn. 10 (θ = 0.95). They were $5.55 \cdot 10^{-5}$ cm^2/min for myoglobin[20], $3.34 \cdot 10^{-5}$ cm^2/min for BSA[21] and $9.98 \cdot 10^{-4}$ for Cl^- (ref. 18). Values of $\alpha_{BSA/Cl^-} = 6.0$ and $\alpha_{Myo/Cl^-} = 1.5$ were used to obtain the curves in Fig. 2a. As the figure shows, this rate equation model gives close prediction for this system. It appears that under the experimental conditions, ion exchange of both BSA and myoglobin is reversible. If the proteins undergo slow adsorption or desorption, this model is not expected to give good predictions.

For the same system except with 20 mg/ml each of BSA and myoglobin, 5.5 cm column length and 0.25 ml/min flow-rate, the effluent history is shown in Fig. 2b. In this case, BSA was introduced after 102 min (τ = 16.87) to displace myoglobin. The same size-exclusion factors, separation factors and diffusion coefficients used in Fig. 2a were used to obtain the result here. Again, the model predicts closely the experimental data.

The results from a local equilibrium model are also included in Fig. 2a and b for comparison. Identical parameters as in the rate model were used. The definition of adjusted time T reported previously was modified here in order to take into account intraparticle porosity θ and size exclusion.

$$T_j = \frac{Cu_0}{Ke_j\bar{C}L}\left\{ t - \frac{L}{u_0}\left[1 + \frac{(1-\varepsilon)Ke_j\theta}{\varepsilon}\right]\right\} \tag{14}$$

For the cases with multiple step changes (Fig. 2a and b), the local equilibrium model gives good predictions of the average breakthrough times, but not the details of the breakthrough curves.

Mass transfer analysis by dimensionless groups

The dimensionless groups defined in this paper (Pe_z, Pe_p, Bi, L/R, $\bar{C}/C_i$ and $\Delta\tau$) are important scaling parameters. They are also helpful for identifying the local

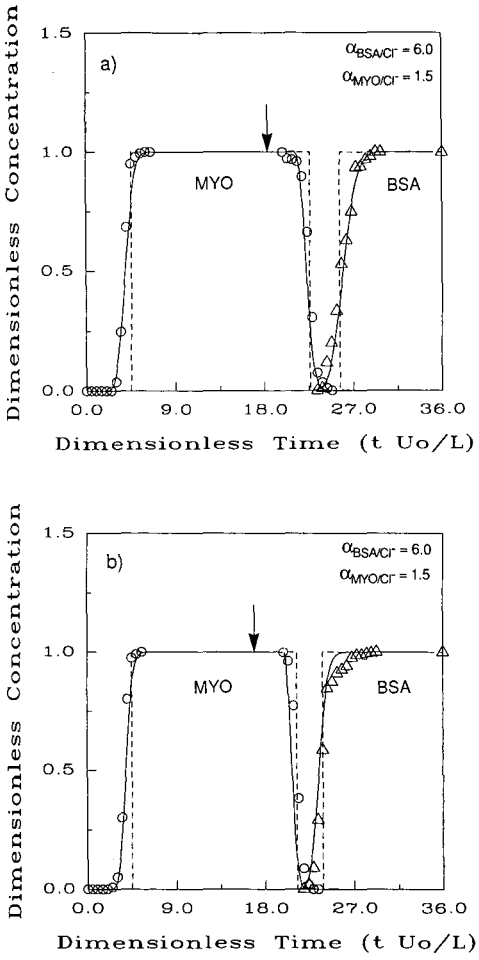

Fig. 2. (a) Experimental results and model predictions of the BSA–myoglobin system. Pe_z = 632, $Pe_{p,Myo}$ = 164, $Pe_{p,BSA}$ = 272, Pe_{p,Cl^-} = 9.11, Bi_{Myo} = 8.65, Bi_{BSA} = 10.24, Bi_{Cl^-} = 3.30. L = 11.0 cm, R = 50 μm, F = 0.5 ml/min, c_{BSA} = c_{Myo} = 5 mg/ml, c_{Cl^-} = 0.16 N. (b) Experimental results and model predictions of the BSA–myoglobin system. Pe_z = 316, $Pe_{p,Myo}$ = 81.9, $Pe_{p,BSA}$ = 136, Pe_{p,Cl^-} = 4.56, Bi_{Myo} = 6.86, Bi_{BSA} = 8.13, Bi_{Cl^-} = 2.62. L = 5.5 cm, R = 50 μm, F = 0.25 ml/min, c_{BSA} = c_{Myo} = 20 mg/ml, c_{Cl^-} = 0.16 N. Solid lines represent the predictions of the rate equation model; dashed lines represent predictions of the local equilibrium model; and arrows indicate the times of step input of BSA solution.

equilibrium regime and for understanding the relative importance of film mass transfer, intraparticle diffusion and axial dispersion for a given system.

Local equilibrium region. Since Bi gives the ratio of intraparticle diffusion resistance over film mass transfer resistance, the absolute magnitude of the two resistances are not clear from this parameter. In order to identify the region that has negligible mass transfer resistances (local equilibrium conditions), other dimensionless groups must be examined. The N_{bj} parameter in the film mass transfer term of eqn. 1a, which consists of L, R, ε, Pe_p and Bi, can be taken as a normalized film mass transfer

rate. The N_{pj} of eqn. 2a can be taken as a normalized intraparticle diffusion rate. For a given system, a plot of $1/N_{pj}$ against $1/N_{bj}$ shows how normalized intraparticle diffusion resistance changes with normalized film resistance (Fig. 3). At the lower left corner of the plot, both intraparticle diffusion and film resistances are negligible. If $1/Pe_z$ is plotted as the third axis, then the origin is the true local equilibrium point.

Eqn. 8b can be modified to give the following relationship between N_p and N_b.

$$N_p = \left(\frac{3(1-\varepsilon)}{\varepsilon}\right)^{3/2} \left(\frac{L}{R}\right)^{1/2} \left(\frac{1.09^{3/2}}{2\varepsilon}\right) \left(\frac{D^\infty}{E_p}\right) N_b^{3/2}$$

This implies that for a given set of ε, L/R, D^∞/E_p (or θ, if eqn. 10 is valid), all possible $1/N_p$ and $1/N_b$ values form a straight line with a slope of 1.5 in a log–log plot (Fig. 3). For example, at $\theta = \varepsilon = 0.45$, $\Delta\tau = 18.86$ and $L/R = 3000$, the seven triangle points represent the cases with seven different flow-rates shown in Fig. 4 (see Table II for values of other parameters) and indeed, they follow a straight line. It should be noted that Pe_z is the third parameter, and these seven points have slightly different Pe_z.

As the flow-rate decreases, both $1/N_p$ and $1/N_b$ decrease along the line. It has been found that there are no changes in the effluent history when the flow-rate is less than 0.1ml/min. Therefore, the elution peaks approach a limiting shape, which occurs at about $Bi = 16$ and $Pe_p = 17$. In order to approach local equilibrium conditions at this point, L/R needs to be increased to further reduce $1/N_b$ and $1/N_p$. Fig. 5 shows the results at various L/R values while all other dimensionless parameters are kept constant. Since $\Delta\tau$ (= 18.86) is fixed, increasing L requires increasing V_p in these cases. As L/R increases to 12000, the peak of high-affinity solute approaches the local equilibrium curve at $N_p = 7.1 \cdot 10^2$, $N_b = 4.1 \cdot 10^4$ and $Pe_z = 2.7 \cdot 10^3$.

When $\Delta\tau$ was decreased to 0.377 with all other parameters kept the same as in

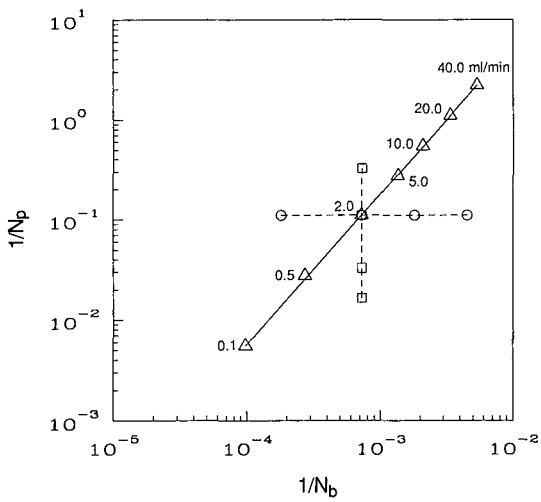

Fig. 3. Normalized intraparticle diffusion resistance ($1/N_p$) *versus* normalized film resistance ($1/N_b$). The same parameters as those in Fig. 1a except different flow-rates are used in calculating the seven triangles. The four circles represent the four cases shown in Fig. 9. The four squares represent the four cases shown in Fig. 10.

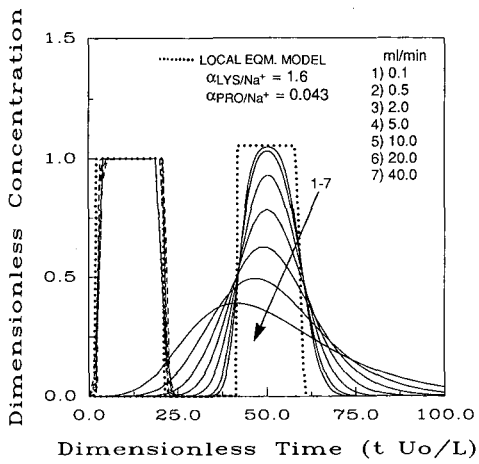

Fig. 4. Effect of flow-rate. Parameters correspond to the seven triangles in Fig. 3. Lysine and proline histories predicted from the rate equation model are shown in solid lines and dashed lines, respectively. Predictions from the local equilibrium model are shown in dotted lines.

Fig. 4, the effluent histories of the highly retained solute at four different flow-rates are shown in Fig. 6. Note the heights of the peaks are less than 0.05 in dimensionless concentration. At flow-rates below 0.01 ml/min, no changes were observed. Actually, the 0.1 ml/min curve is already very close to the limiting shape.

Attempts were made to increase L/R (to further decrease $1/N_b$ and $1/N_p$) to approach local equilibrium conditions. The dashed curves shown in Fig. 6 were simulated at 0.01 ml/min flow-rate, and $L/R = 15\,000$ ($Pe_z = 3340$) and $L/R = 60\,000$ ($Pe_z = 13\,360$). The peaks do become sharper, but they are still very far from reaching 1.0 (where the local equilibrium peak would reach). Further increase of L/R (and also Pe_z) would require substantially longer computation time because of numerical

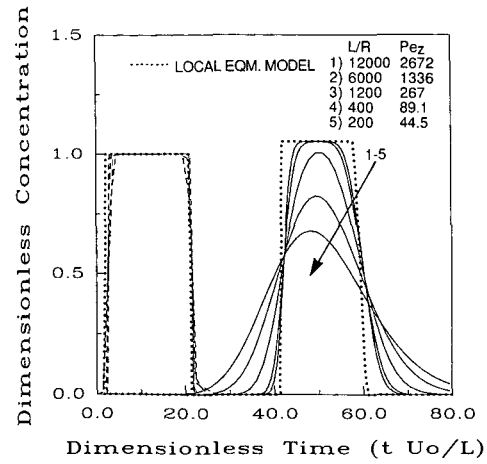

Fig. 5. Varying L/R for the case at 0.1 ml/min flow-rate in Fig. 4.

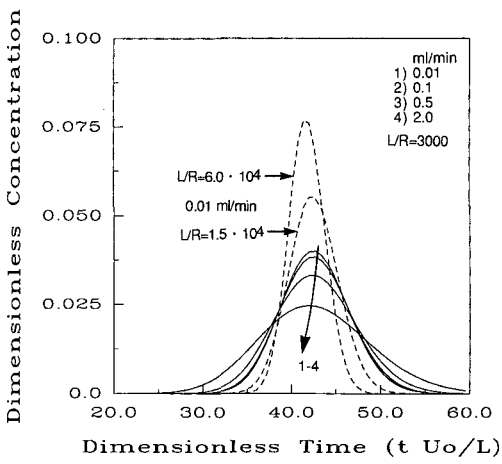

Fig. 6. Approaching local equilibrium conditions with $\Delta\tau = 0.377$. Unless noted otherwise, all the other parameters are the same as those for Fig. 5.

difficulties. This result shows that for a smaller $\Delta\tau$, it requires larger values of N_b and N_p to approach local equilibrium.

The affinity of the solute (α) is another factor that affects the region of local equilibrium. Fig. 7 shows the results for $\Delta\tau = 18.86$ but with a different set of α values ($\alpha_{Lys/Na^+} = 4.0$ and $\alpha_{Pro/Na^+} = 0.5$ in Fig. 7, compared to $\alpha_{Lys/Na^+} = 1.6$ and $\alpha_{Pro/Na^+} = 0.043$ in Fig. 4). All other parameters in these two figures are identical. For the solute with $\alpha = 0.043$ (Fig. 4), the peak at 40 ml/min flow-rate ($N_p \approx 0.5$) is very similar to the local equilibrium peak. For the solute with $\alpha = 0.5$ (Fig. 7), local equilibrium is approached at 0.5 ml/min ($N_p = 35.6$, $N_b = 3.5 \cdot 10^3$ and $Pe_z = 670$).

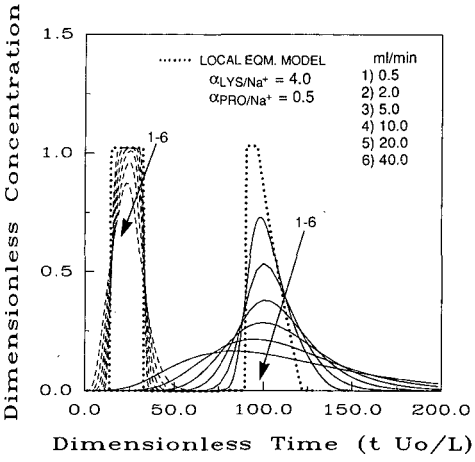

Fig. 7. Effect of flow-rate. The parameters are the same as those in Figs. 1a and 4 except $\alpha_{Lys/Na^+} = 4.0$ and $\alpha_{Pro/Na^+} = 0.5$.

For the solute with $\alpha = 1.6$ (Fig. 4), local equilibrium is approached at 0.1 ml/min ($N_p = 7.1 \cdot 10^2$, $N_b = 4.1 \cdot 10^4$ and $Pe_z = 2.7 \cdot 10^3$). For the solute with $\alpha = 4$ (Fig. 7), even the peak at the lowest flow-rate is still quite different from that at local equilibrium. Therefore, the larger the α, the larger the values of N_p, N_b and Pe_z required to approach local equilibrium.

Effect of Pe_z. Changing E_b changes only Pe_z, and all other parameters remain constant. This way, the isolated effect of the Pe_z term in eqn. 1a can be studied. Fig. 8a shows the effluent history of the same lysine–proline system discussed earlier. Assuming that Pe_z can be varied independently, one can plot the results for Pe_z at 1000, 500, 200, 100, 50 and 5. The other parameters are $Pe_p = 100$, $Bi = 28$, $\varepsilon = \theta = 0.45$ and $L/R = 3000$. The lysine peak ($\alpha = 1.6$) at $Pe_z = 500$ is very close to that at $Pe_z = 1000$, but it is still quite different from that at $Pe_z = 200$. Therefore, a Pe_z of 1000 is the limit for negligible axial dispersion for lysine. Axial dispersion broadens the bands and

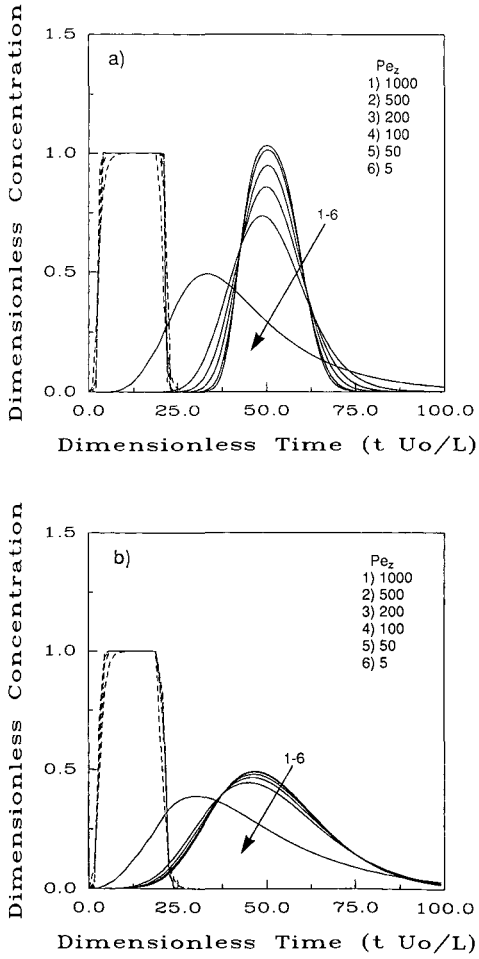

Fig. 8. (a) Effect of axial dispersion at $Pe_p = 100$, $Bi = 28.2$, $L/R = 3000$, $\Delta\tau = 18.86$. (b) Effect of axial dispersion at $Pe_p = 3370$, $Bi = 91.2$, $L/R = 3000$, $\Delta\tau = 18.86$.

eventually produces asymmetric peaks at small Pe_z. For the proline peak ($\alpha = 0.043$), axial dispersion and film and intraparticle diffusion have negligible effects on band spreading.

The effects of axial dispersion are relatively more pronounced when Pe_p and Pe_p/Bi are small (close to local equilibrium conditions). When intraparticle resistance or film resistance is large, axial dispersion has very minor effects. For example, for the same system shown in Fig. 8a except at $Pe_p = 3370$ and $Bi = 91.2$, the results for the same set of Pe_z numbers are shown in Fig. 8b. In this case, the lysine peak is broadened by large intraparticle diffusion resistance. Changing Pe_z from 1000 to 100 has almost no effect, and minor effect for $Pe_z = 50$. At $Pe_z = 5$, the lysine peak becomes noticeably more asymmetric and overlaps with the proline peak. Therefore for $Pe_p = 3370$ and $Bi = 91.2$, the limit for negligible axial dispersion is around Pe_z of 50, which is considerably smaller than the limit in Fig. 8a.

Effects of Pe_p/Bi and Pe_p. It is also worthwhile to study the isolated effects of the film mass transfer term (Pe_p/Bi) in eqn. 1a and intraparticle effective diffusion term (Pe_p) in eqn. 2a. Fig. 9 shows the results when keeping all dimensionless parameters constant and changing only k to vary Pe_p/Bi. The four curves shown here are represented by the four circles in Fig. 3: $Pe_p = 337$, $L/R = 3000$ and Pe_p/Bi ranging from 2 to 50. This gives Bi ranging from 169 to 6.7. As k decreases, Bi decreases, and the lysine peak ($\alpha = 1.6$) becomes broader and less concentrated, but relatively small changes are observed in this range of Bi. For the same reason mentioned before, because the low affinity of the proline peak ($\alpha = 0.043$), changing k or Pe_p/Bi has no effects at all. Moreover, as k increases (or Pe_p/Bi decreases), a limiting peak shape indicates negligible film resistance.

Fig. 10 shows the results when keeping $Pe/Bi = 8$, $L/R = 3000$ and changing Pe_p from 50 to 1000. This provides the effect of changing E_p (or Pe_p) alone. The four curves are also represented as squares in Fig. 3. As E_p decreases, both Pe_p and Bi increase. This leads to broadening of the lysine peak. A limiting peak shape is expected for large E_p values which correspond to negligible intraparticle diffusion resistance.

The results shown in Figs. 8–10 indicate that for the experimental systems tested,

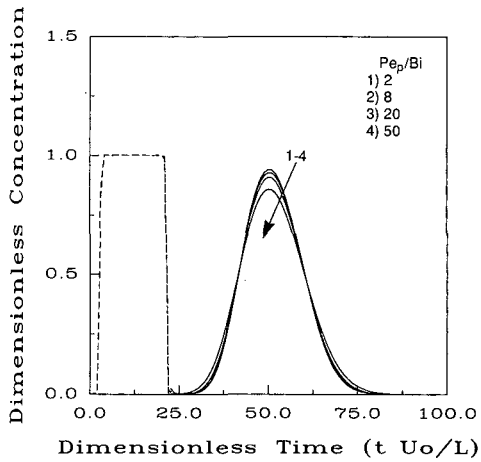

Fig. 9. Effect of Pe_p/Bi at $Pe_z = 672$, $Pe_p = 337$, $L/R = 3000$, $\Delta\tau = 18.86$.

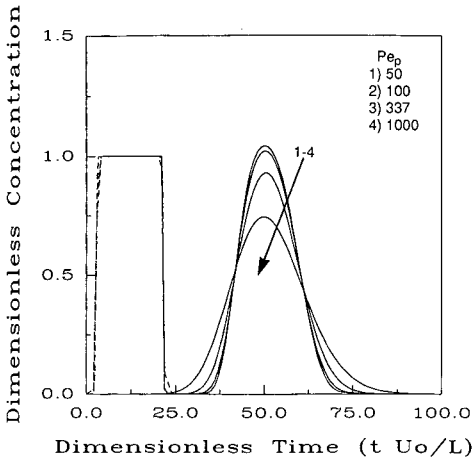

Fig. 10. Effect of Pe_p at $Pe_z = 782$, $Pe_p/Bi = 8$, $L/R = 3000$, $\Delta\tau = 18.86$.

axial dispersion and film resistance are unimportant; intraparticle diffusion resistance is the major cause for lysine band spreading (Fig. 1a and b) and the spreading of BSA and myoglobin breakthrough curves (Fig. 2a and b). Therefore, the good agreement between data and model predictions shown in Figs. 1 and 2 does not prove the accuracy of the correlations for axial disperision coefficient (eqn. 4) and film mass transfer coefficient (eqn. 6). Thorough testing of these correlations and others[22] requires further studies of systems for which axial dispersion and film resistance are dominating.

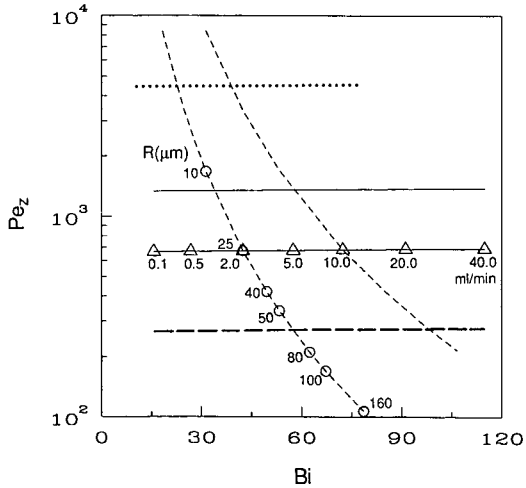

Fig. 11. *Pe_z versus Bi* at various operating conditions. The seven triangles from Fig. 3 are shown here. ---O---: R varies from 2 to 160 μm, while all other parameters are the same as those for the case with 2 ml/min flow-rate. ------: R varies from 2 to 160 μm, while all other parameters are the same as those for the case with 10 ml/min flow-rate. ———: $R = 25$ μm, $L = 15$ cm, flow-rate varies from 0.1 to 40 ml/min. – – – –: $R = 25$ μm, $L = 3$ cm, flow-rate varies from 0.1 to 40 ml/min. ·····: $R = 7.5$ μm, $L = 15$ cm, flow-rate varies from 0.1 to 40 ml/min.

Variation of dimensionless parameters with operating parameters. Since Pe_p is related to Bi, a plot of Pe_z *vs.* Bi would be sufficient to represent an entire fixed-bed system for a given set of L/R, $\Delta\tau$, $\bar{C}/C_i$, ε and θ (or E_p/D^∞). Fig. 11 shows the ranges of Pe_z and Bi that are encompassed by some typical operating conditions for a column of 1 cm I.D. The triangles shown in Fig. 3 are plotted here. These data are from a 7.5 cm $\times$ 1 cm I.D. column with 25-μm particles at different flow-rates (effects of flow-rate are shown in Fig. 4 and will be discussed later).

From the J factor correlation discussed earlier, the film mass transfer coefficient k increases with $u_0^{1/3}$. Because the normalized film resistance $1/N_b$ is proportional to u_0/k, it increases with $u_0^{2/3}$. The normalized intraparticle diffusion resistance $1/N_p$ increases linearly with u_0. As a result, as flow-rate increases, Bi increases and intraparticle diffusion resistance becomes more important relative to film resistance. The axial Peclet number Pe_z, on the other hand, has a very weak dependence on flow-rate because Re is typically 0.1 or less (see eqn. 4). As shown in Fig. 11, Bi ranges from 15.6 for 0.1 ml/min to 115 for 40 ml/min, while Pe_z only varies from 665 to 692. The ratio L/R has a major effect on Pe_z. When column length is increased from 7.5 cm to 15 cm, Pe_z increases proportionally (see solid line above). Pe_z values range from 1340 (0.1 ml/min) to 1385 (40 ml/min). On the other hand, when column length is decreased to 3 cm, Pe_z becomes much lower, ranging from 265 to 277 (see dashed line below).

The dotted line shown on the top of Fig. 11 is from a 15-cm column with 7.5 μm particle radius at different flow-rates. The flow-rate range is the same as the previous cases but for this smaller particle radius and longer column, the Bi ranges from 10.4 to 77 instead of 15.6 to 115 for $R = 25$ μm.

The circles in Fig. 11 are values for a 7.5-cm column at a flow-rate of 2 ml/min and different particle radii (which will be discussed later). It ranges from $Pe_z = 1676$ and $Bi = 31.2$ ($R = 10$ μm) to $Pe_z = 107$ and $Bi = 78.6$ ($R = 160$ μm). The dashed curve joining the circles is extended to $R = 2$ μm at a Pe_z over 8000. Therefore, increasing particle size not only decreases Pe_z, it also increases Bi at the same time.

When the flow-rate is increased from 2 ml/min to 10 ml/min, the whole curve for 2 ml/min just shifts to the right. It should be noticed that when these two curves intersect the varying flow-rate lines, it means two different sets of flow-rate, column length and particle size would give the same Pe_z and Bi. For example, if a large particle is used, one can operate at a lower flow-rate and use a longer column to achieve the same Pe_z and Bi. This scaling concept is useful for design and economic analysis and will be discussed later.

Overall, increasing interstitial velocity mainly increases the relative importance of intraparticle resistance but has little effect on axial dispersion. Increasing particle size increases both the relative importance of axial dispersion and intraparticle diffusion (Fig. 11). Increasing column length (or L/R ratio) increases Pe_z, N_b, and N_p. However, the longer the column, the smaller the dimensionless pulse size $\Delta\tau$. The effect of $\Delta\tau$ will be discussed later.

Effect of operating and design parameters

Flow-rate. In a chromatographic process, flow-rate is an important operating parameter. It influences resolution, product concentration and cycle time. The question concerning scaling-up chromatographic processes with the proper flow-rate,

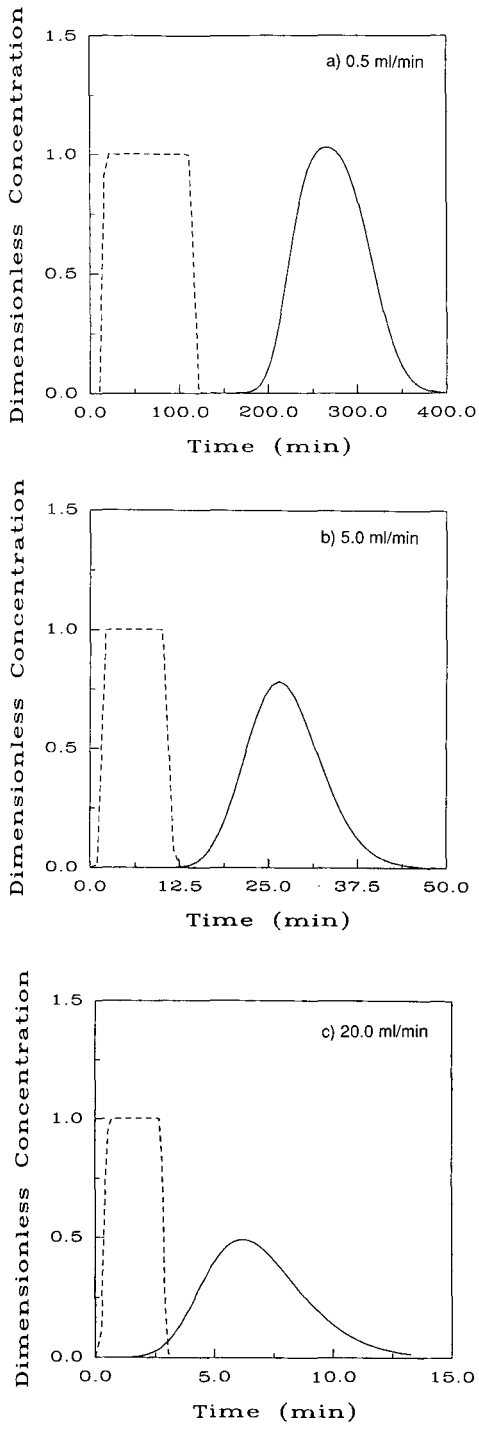

Fig. 12. Replot of effluent histories in real time (min) for the three cases in Fig. 4.

particle size, column length and pulse size will be addressed after the effects of each parameter is discussed.

Fig. 4 shows the simulation results of the lysine–proline system discussed earlier at various flow-rates. An E_p of $4.2 \cdot 10^{-5}$ cm^2/min and $\varepsilon = \theta = 0.45$ were used here. Effluent histories from seven flow-rates ranging from 0.1 ml/min to 40 ml/min are shown here. The pulse volumes are the same for these cases. Little or no change is observed for the proline peak at all flow-rates. This is because proline has a low affinity relative to Na^+. The proline peak passes through the column almost without being retained, and flow-rate has very little effect in this case. The lysine peak becomes broader and its concentration becomes lower as the flow-rate increases. At a flow-rate higher than 20 ml/min, the peak actually becomes asymmetric because of large intraparticle diffusion resistance.

Since the feed pulse concentration of lysine is only 0.01 N, and the α for lysine at this pH is only 1.6, these conditions are close to a linear system where asymmetric peaks are not normally observed. The asymmetry in the lysine peak observed at a flow-rate greater than 20 ml/min is due to mass transfer effect. In order to confirm this, simulations were conducted with a linear isotherm under identical conditions. Asymmetric peaks were also observed. Therefore, the peak asymmetry is largely due to intraparticle diffusion.

The results under the same conditions but with different separation factors are shown in Fig. 7. This case can be viewed as the lysine–proline system at another pH value. Values of $\alpha_{Lys/Na^+} = 4.0$ and $\alpha_{Pro/Na^+} = 0.5$ were used instead. Since both α values are higher, both solutes are retained in the column longer; as a result, both peaks are more spread than before. The effect of flow-rate in this case is similar to that in Fig. 4; as the flow-rate increases, solute band broadens and its concentration decreases. Because of the large α_{Lys/Na^+} value, even at 0.5 ml/min, the lysine peak is already slightly asymmetric. The explanation given for Fig. 1b is also valid here. The tailing of lysine peak at 40 ml/min is due to a combination of intraparticle diffusion resistance and interference effect, because the local equilibrium model also predicts tailing for this peak.

Although increasing flow-rate can decrease the product concentration, it also decreases the elution time, which in turn decreases the cycle time. For certain cases, it may be more economical to speed up the separation process and sacrifice the product concentration. Fig. 12 gives a better representation of the actual time scale involved for the results shown in Fig. 4. Fig. 12a–c are the effluent histories in real time (min) for 0.5, 5 and 20 ml/min, respectively. By increasing the flow-rate from 0.5 to 5 ml/min, the actual cycle time is decreased to about 1/8 of that at the slower flow-rate, whereas the product concentration is only decreased by about 20%.

Particle size. Another way to study the intraparticle diffusion effect is to change the particle size and keep other parameters constant. Increasing the particle size increases Pe_p and Bi, whereas decreases the L/R and Pe_z at the same time. Therefore increasing particle size increases intraparticle diffusion resistance, film resistance, and axial dispersion effects. Fig. 13a flows the simulation results at four different particle radii. These four cases are also represented by circles in Fig. 11. Other parameters are the same as for Fig. 1a.

Increasing particle size decreases product concentrations, and eventually results in asymmetric peaks. As discussed before, the feed pulse concentrations considered

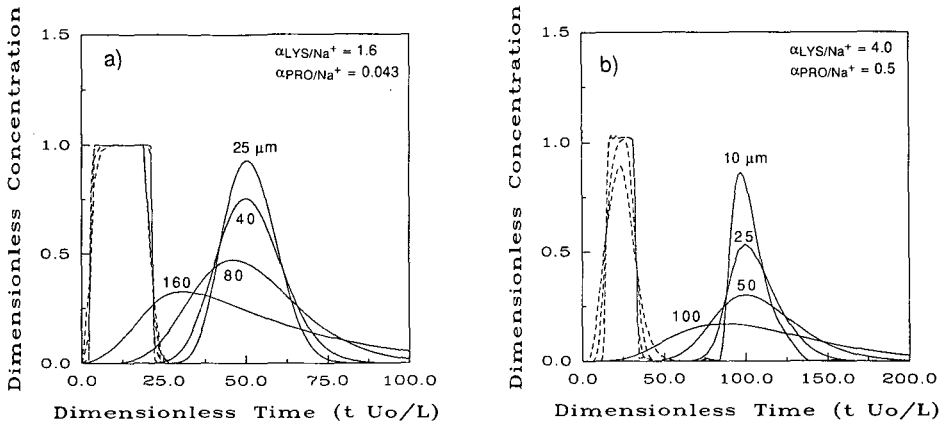

Fig. 13. (a) Effect of particle size. All the other parameters are the same as in Fig. 1a. (b) Effect of particle size at different separation factors. All other parameters are the same as in Fig. 13a.

here are close to those of linear systems. Therefore, the asymmetry of the lysine peak is mostly due to mass transfer effects. For the case at $R = 160\ \mu m$, Bi and Pe_z are 79.6 and 107, respectively. It indicates that intraparticle diffusion is dominating and the effect of axial dispersion is relatively small. Therefore, large intraparticle diffusion resistance can also produce asymmetric peaks.

Although Fig. 13a looks very similar to Fig. 4 in dimensionless time scale, if they were plotted in actual time (t), they would look quite different (see Fig. 12). Each curve in Fig. 4 has a different interstitial velocity (u_0), while all curves in Fig. 13a have the same interstitial velocity. Only a slight decrease in retention time is observed when particle size is increased.

Fig. 13b shows the results of the same system with different solute affinities. The four radii are also represented as circles in Fig. 11. Since $\alpha_{Lys/Na+}$ is 4.0 in this case, asymmetric peaks are observed for particle radius as small as 10 μm. For the proline peak, increasing the particle size does decrease the product concentration in this case, because the $\alpha_{Pro/Na+}$ is larger in this case. As expected, the average retention times for both solutes are longer than in the previous case.

When designing a chromatographic process, it is important to choose the right particle size and flow-rate. This rate equation model provides information on the effects of particle size and flow-rate on resolution and product concentration that local equilibrium models cannot provide. This is a major advantage of using this model for design and scale-up purposes.

Column length. When only the length of the column is increased, and all other parameters are kept constant, Pe_z, N_b and N_p would increase, but $\Delta\tau$ would decrease. In Fig. 14, four column lengths ranging from 1 to 15 cm were considered. For the 15-cm column, good resolution is achieved. However, for this pulse size, the whole column is not fully utilized; also the lysine peak has a lower concentration than the feed. Therefore this case has the problem of long cycle time and low product concentration. When the column is shortened to 7.5 cm, the cycle time is decreased,

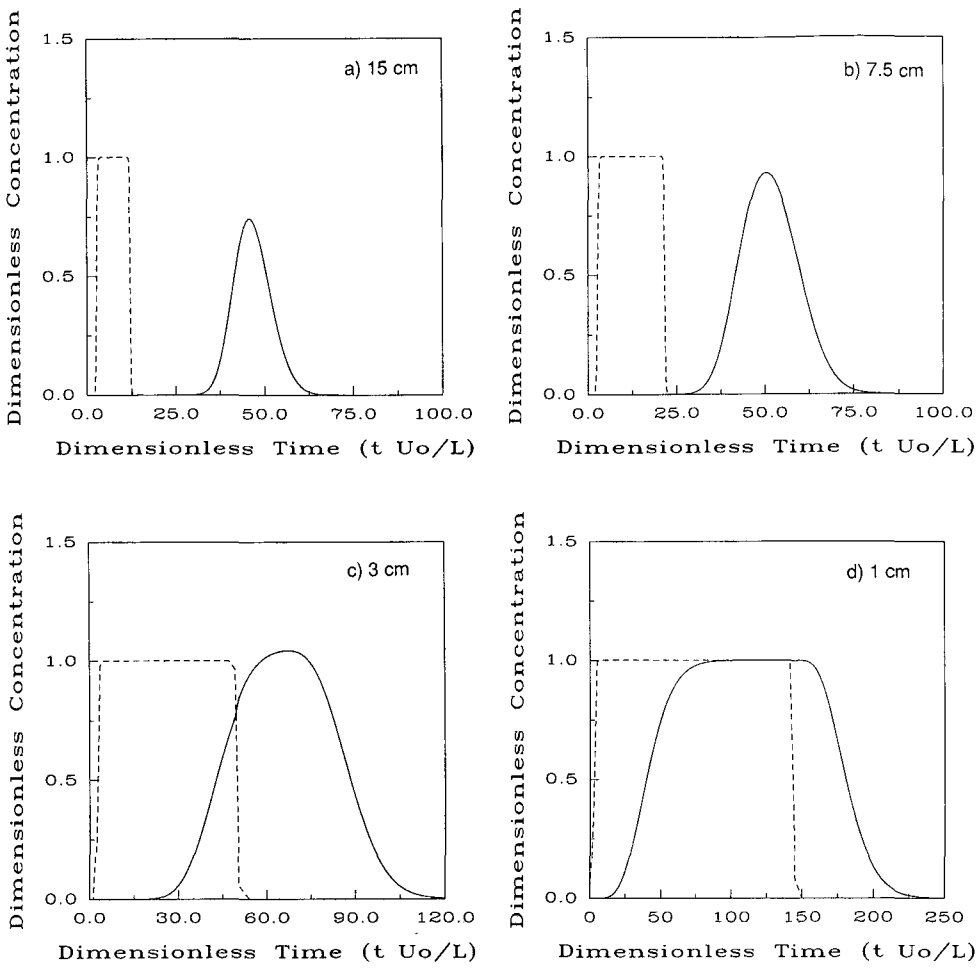

Fig. 14. Effect of column length at $Pe_p = 338$, $Bi = 42$. (a) $L/R = 6000$, $Pe_z = 1340$, $\Delta\tau = 9.43$; (b) $L/R = 3000$, $Pe_z = 670$, $\Delta\tau = 18.86$; (c) $L/R = 1200$, $Pe_z = 223$, $\Delta\tau = 47.15$; (d) $L/R = 400$, $Pe_z = 110$, $\Delta\tau = 141.5$.

and the eluted lysine peak has a higher concentration than for the 15-cm column. This is expected because $\Delta\tau$ is larger for a shorter column.

For the 3-cm column, the two peaks overlap, but part of the lysine peak has a concentration slightly higher than the feed pulse. Therefore, this is another example of trade offs among resolution, cycle time and product concentration. For this case a length between 3 and 7.5 cm would give the best resolution. For the 1-cm column, a large overlap occurs between the two peaks. This column is just too short to resolve the two solutes, even though their separation factors are far apart.

If $\Delta\tau$ is kept constant, a shorter bed has the advantages of a lower pressure drop and a shorter cycle time. If the aforementioned conditions for local equilibrium are met, this is definitely a good strategy. However, in a region far away from local

equilibrium, as L/R decreases, film and intraparticle resistances increase and axial dispersion also becomes more important. As a result, resolution will decrease. In order to achieve the same resolution in a shorter bed, certain scaling rules must be followed, and they will be discussed later.

Pulse size (V_p). Another important operating parameter is the feed pulse size (V_p). An increase in pulse size results in an increase in $\Delta\tau$ and produces similar effects as a decrease in column length. Fig. 15 shows the results of three different pulse sizes in a 7.5-cm column. Very good separation is achieved for the case with a pulse size of 10 ml ($\Delta\tau$ = 3.77), but because of mass transfer effects, the concentration of the lysine peak becomes much lower than the feed. When the pulse size is increased to 100 ml ($\Delta\tau$ = 37.7), the lysine concentration actually becomes higher than the feed value because of interference, but there is a slight overlap between the two peaks. For the 250-ml case ($\Delta\tau$ = 94.3), the pulse volume is 42.4 times the column volume and resolution is poor.

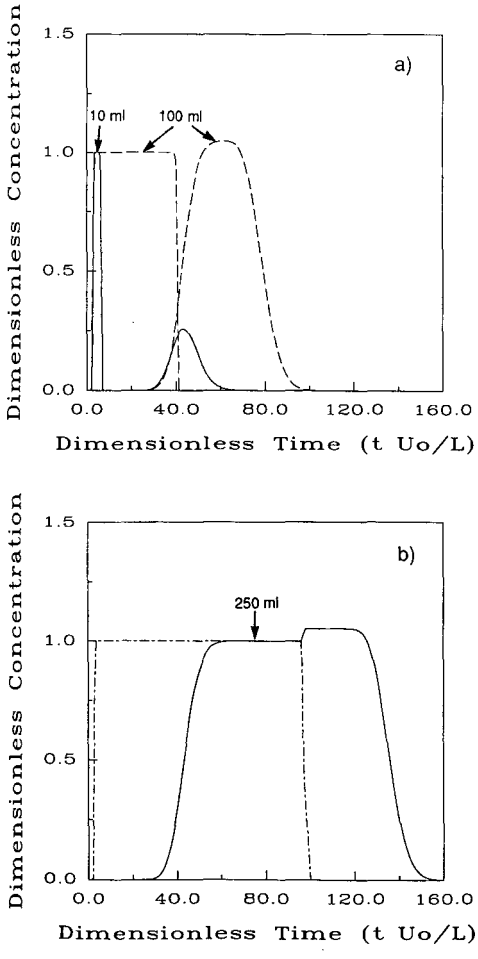

Fig. 15. Effect of pulse size at Pe_p = 338, Bi = 42, L/R = 3000, Pe_z = 670. (a) $\Delta\tau$ (10 ml) = 3.77, $\Delta\tau$ (100 ml) = 37.7; (b) $\Delta\tau$ (250 ml) = 94.3.

The effluent history is similar to a smaller pulse with a shorter column, shown in Fig. 14.

Regardless of the differences in pulse volume, solutes in all cases start to elute at about the same times. This is expected for systems with negligible interference effects. Since for a fixed column length and mass transfer resistances, the left flank of the product peak always exits at certain dimensionless time (τ), regardless of its feed pulse volume. Even though the qualitative effects of increasing V_p are similar to decreasing column length, the quantitative results are different because in the latter case, the ratio L/R is also decreased.

Solute concentration. Fig. 16a shows a series of simulations with different solute concentrations in the feed pulse. For all cases both lysine and proline have the same concentration, and the concentration of Na^+ in the feed pulse is 0.18 N; the

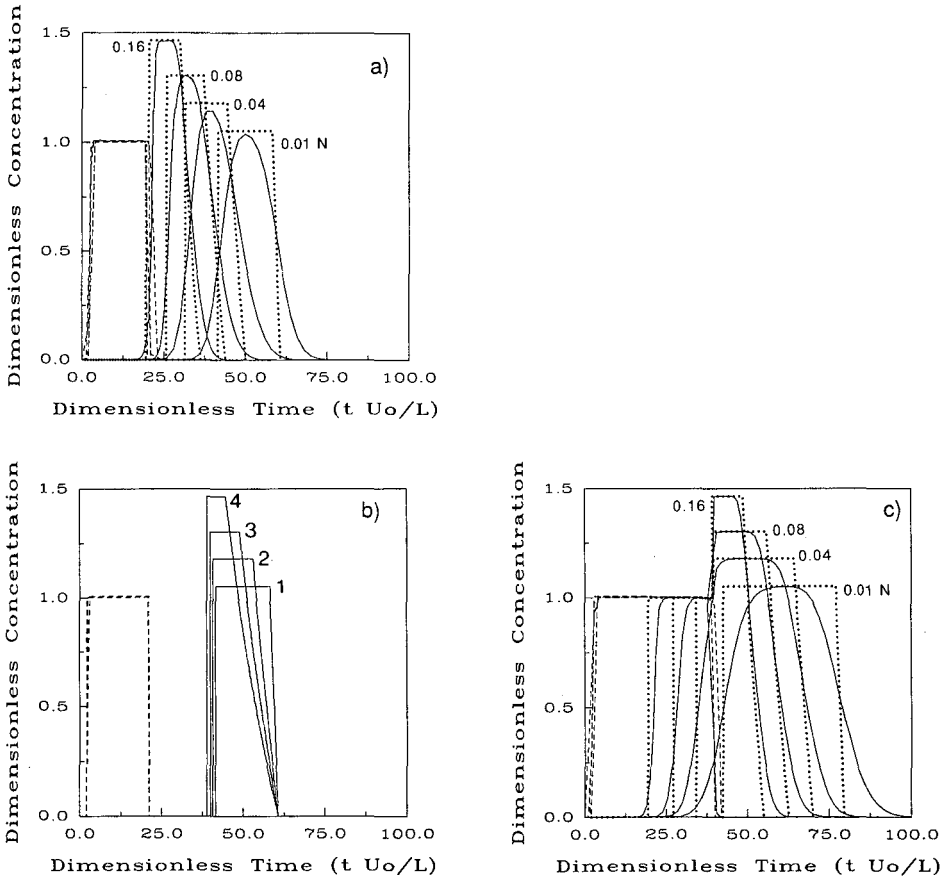

Fig. 16. (a) Effect of solute concentration at $Pe_p = 338$, $Bi = 42$, $Pe_z = 670$, $L/R = 3000$, $\Delta\tau = 18.86$. Lysine histories predicted from the local equilibrium model are shown in dotted lines (····). (b) Effluent histories predicted from the local equilibrium model. The feed fractions of lysine and proline and other parameters are the same as those in Fig. 16a except the total concentration is kept at 0.2 N. Lysine histories are shown in solid lines; proline histories are shown in dashed lines. Concentrations of lysine and proline for 1–4 are listed in Table II. (c) Effect of solute concentration under the same conditions as in Fig. 16a except $\Delta\tau = 37.72$.

concentration of the presaturant and eluent is always equal to the total concentration of solutes plus Na^+ in the feed pulse. All other parameters are kept constant.

As the concentration of proline increases, the eluted proline peak does not change significantly. This is because proline has a much lower affinity relative to lysine and Na^+ and it quickly separates from lysine. As a result, the proline band, despite its high fraction in the feed, is similar to that in a dilute system, in which the feed concentration doesn't affect its product concentration or retention time.

There is, however, a larger change in retention time and effluent concentration for lysine as its feed concentration increases. A higher lysine concentration gives a higher fraction of lysine in the feed as well as a higher total concentration. A higher lysine fraction in the feed results in stronger interference and a higher lysine peak concentration. A higher total concentration results in a shorter retention time. At a feed lysine fraction of 0.235 (0.08 *N*), the lysine peak becomes about 30% more concentrated than the feed. As the feed lysine fraction is increased to 0.32 (0.16 *N*), the lysine peak has a 45% higher concentration than the feed, with only a slight overlap with the proline peak. The results from the local equilibrium model also show more concentrated lysine peaks than the feed. Since the local equilibrium model accounts for only interference effects but not mass transfer effects, it indicates that interference effects dominate in this case. Furthermore, comparison of the predictions from the two models allows us to isolate mass transfer effects from interference effects.

As solute concentration in the feed increases, the significant decrease in lysine retention time is mainly due to the increase in total concentration from 0.2 to 0.5 *N*. This point is verified with the results shown in Fig. 16b, in which the fractions of lysine and proline in the feed are kept the same as in Fig. 16a, whereas the total concentration is kept at 0.2 *N*. The effluent histories predicted from the local equilibrium model are shown. Here the peak lysine concentrations are the same as the corresponding concentrations in Fig. 16a, whereas the retention times are only altered slightly. Comparison of Fig. 16a with Fig. 16b clearly shows the different effects of increasing total concentration from those of increasing solute fraction in the feed.

The results of doubling the pulse size to 100 ml for the system in Fig. 16a are shown in Fig. 16c. The general behavior is similar to that in Fig. 16a. The maximum concentrations of lysine are the same as those in Fig. 16a. This is expected because in the absence of mass transfer effects the maximum peak height due to interference is determined by the lysine fraction in the feed and relative affinities, which are the same in these two figures. However, because of a large pulse size, the lysine and proline peaks overlap for all cases, with the overlap being more severe at higher solute concentrations.

Sodium ion concentration. When the concentrations of the solutes are kept constant and only the concentration of Na^+ in the feed pulse is changed, interference phenomena are observed. The concentration of presaturant and eluent is kept the same as the total concentration of solutes plus Na^+ in the feed pulse. Fig. 17a shows the same lysine–proline system with a 100 ml feed pulse that contains 0.04 *N* each of lysine and proline and various Na^+ concentrations. The fractions of lysine in the feed are 0.333, 0.222 and 0.095 at Na^+ concentrations of 0.04, 0.10 and 0.34 *N*, respectively. The corresponding total concentrations are 0.12, 0.18 and 0.42 *N*. As shown in Fig. 16, the higher the lysine fraction in the feed, the higher the lysine peak concentration in the effluent. Similar results are also seen in Fig. 17a. At an Na^+ concentration of 0.04 *N*,

the lysine fraction in the feed is the highest (0.333). Therefore, the lysine concentration in the effluent is also the highest. However, because the total concentration is the lowest (0.12 *N*), the lysine peak has the longest retention time. In Fig. 16, on the other hand, as lysine concentration in the feed increases, both the lysine fraction and total concentration increase. Therefore, the lysine peak at 0.16 *N* has the highest effluent concentration and the shortest retention time.

Because the three cases shown in Fig. 17a have a large feed pulse ($\Delta\tau = 37.72$) and high solute concentrations, the effluent histories are similar to those predicted from the local equilibrium model. For clarity, only the predicted histories for lysine from the local equilibrium model are shown for comparison; proline histories predicted from the two models are too close to show any difference. This comparison shows that for a concentrated system with a large feed pulse, interference effects control the lysine peak height.

As we reduce the pulse size from 100 to 50 ml ($\Delta\tau = 18.86$) while keeping all other parameters the same, the results are shown in Fig. 17b. The local equilibrium model again predicts the highest lysine concentration in the effluent at $Na^+ = 0.04\ N$. However, because of a smaller pulse size ($\Delta\tau = 18.86$), mass transfer effects are more pronounced than in Fig. 17a. Furthermore, mass transfer effects are most significant for the lysine peak at $Na^+ = 0.04N$ because the retention time is the longest at the lowest total concentration (0.12 *N*). Because of the significant mass transfer effects, the lysine peak at $Na^+ = 0.04\ N$ has a lower concentration than those at $Na^+ = 0.10\ N$ and 0.34 *N*. For this case, mass transfer effects, not interference effects, control the lysine peak height. The comparison of Fig. 17a with Fig. 17b clearly shows the complexity of interference phenomena coupled with mass transfer effects.

Rate equation model vs. local equilibrium model

Local equilibrium model can generally predict the average breakthrough times of concentration waves, and it usually requires relatively short computation time (a

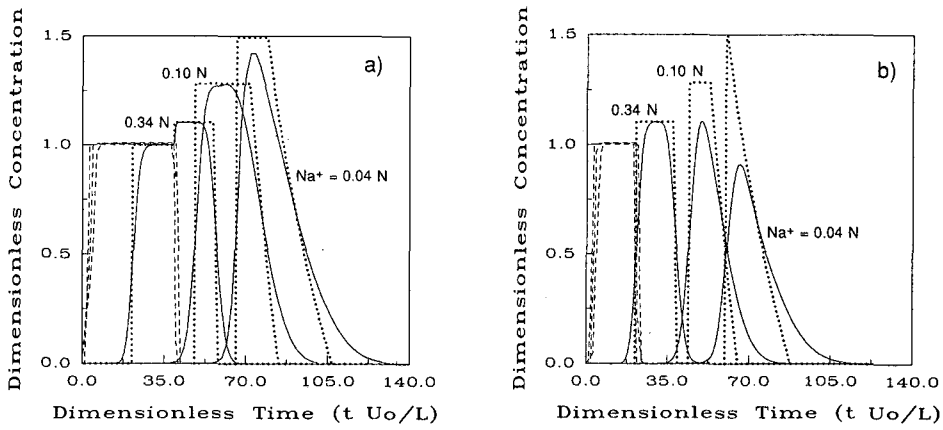

Fig. 17. (a) Effect of sodium ion concentration. The concentration of both lysine and proline is 0.04 *N*; the concentrations of Na^+ are 0.04, 0.10 and 0.34 *N*; $\Delta\tau = 37.72$; other conditions are the same as those for Fig. 16c. (b) Effect of sodium ion concentration under the same conditions as in Fig. 17a except $\Delta\tau = 18.86$.

few minutes on a Gould NP1 computer). It is also a simple model to use for studying interference in complicated operating modes, for example, gradients and two-way flow column operations[8]. It can be used for preliminary design and scale-up purposes when mass transfer effects are insignificant. However, the rate equation model developed here would be a better model to use if (1) mass transfer resistances are important, (2) effects of changing particle size or flow-rate are needed, or (3) isotherms are complex. The only drawback of this model is the long computation time that is required. A two-component elution process typically would take about 1 h on a Gould NP1 computer. The computation time depends on the equilibrium isotherm, the number of collocation points, number of elements used, and how often the elements are updated.

Scaling rules

Finally, we would like to address the question of scaling using dimensionless groups. As shown in our analysis, for a given set of Pe_z, Pe_p, Bi, L/R, $\Delta\tau$, θ, ε, $\bar{C}/C_i$ and feed concentration, this model predicts a unique column profile and effluent history in dimensionless time. As discussed earlier, more than one set of operating and design parameters (F, D, R, L, V_p, E_p, θ and ε) can give an identical set of dimensionless parameters. This means that one can use this model to design and scale up a process for various conditions and scales; as long as the dimensionless parameters are the same, the results in dimensionless variables are identical.

Provided θ, ε and E_p are constant for a given system, the Chung and Wen[13] correlation suggests Pe_z to be a function of L/R and Re. Using the correlation of Wilson and Geankoplis[14] leads to an explicit relation between Pe_p and Bi (eqn. 9). Therefore, only Re, Pe_p, L/R and $\Delta\tau$ have to be kept constant for all other dimensionless parameters to be constant. In order to achieve this, the following three conditions must be satisfied:

$$\frac{FR}{D^2} = \sigma \tag{16a}$$

$$L/R = \beta \tag{16b}$$

$$\frac{V_p}{D^2 L} = \gamma \tag{16c}$$

where σ, β and γ are constants. Eqn. 16a alone is sufficient to keep both Re and Pe_p constant, and eqn. 16c is needed to keep $\Delta\tau$ constant. Thus, we are left with three equations and five variables (F, D, L, R and V_p). Any two variables can be fixed arbitrarily and the other three can be solved from the above equations.

For example, we can consider a standard case: $D = 1$ cm, $R = 25$ μm, $L = 2.5$ cm, $V_p = 50$ ml and $F = 2$ ml/min. This case has the following constants: $\sigma = 5 \cdot 10^{-3}$ ml/(min cm), $\beta = 3000$ and $\gamma = 6.666$. Keeping D the same and scaling R to 2.5 μm would require a 0.75-cm column, 5 ml pulse and 20 ml/min flow-rate. Scaling R to 250 μm, on the other hand, would require a 75-cm column, 500 ml pulse and 0.2 ml/min flow-rate (Table III). All three cases have the same dimensionless parameters, and hence, identical column profiles and effluent history in terms of dimensionless time. However, cycle time, throughput, pressure drop, and amount of packing for these

TABLE III
SCALING USING DIMENSIONLESS GROUPS

	Case 1	*Case 2*	*Case 3*	*Case 4*
D (cm)	1.0	1.0	1.0	10.0
R (μm)	25	2.5	250	2.5
L (cm)	7.5	0.75	75	0.75
F (ml/min)	2	20	0.2	2000
V_p (ml)	50	5	500	500
Relative[a] V_{bed}	1.0	0.1	10	100
Relative cycle time	1.0	0.01	100	0.01
Relative throughput[b]	1.0	10	0.1	1000
Δp[c]	1.0	100	0.01	100
Relative productivity[d]	1.0	100	0.01	100

[a] Relative to the values in case 1.
[b] Throughput $\equiv V_p$/cycle time.
[c] $\Delta P \propto (u_0 L)/R^2$ (Blake–Kozeny equation) 43.
[d] Productivity $\equiv$ throughput/V_{bed}.

three cases are quite different. As shown in Table III, reducing the particle size by ten fold (compare cases 2 and 3 with case 1) can result in a ten-fold reduction in column length, ten-fold increase in flow-rate, and 100-fold reduction in cycle time; it, however, requires a ten-fold reduction in feed pulse and a 100-fold increase in pressure drop. Overall, a ten-fold reduction in particle size can result in a ten-fold increase in throughput (defined here as volume of feed processed per unit cycle time) and a 100-fold increase in productivity (defined here as throughput per unit bed volume).

The throughput for case 2 can be further increased by increasing the column diameter. As shown in case 4 in Table III, a ten-fold increase in diameter can increase the throughput by 100-fold. However, because column volume is also increased 100-fold, the productivity remains the same. The pressure drop for case 4 is the same as for case 2, because column length is kept the same in order to keep L/R constant (eqn. 16b).

In general, the scaling rules of eqn. 16 lead to the following: cycle time is proportional to R^2, throughput is proportional to $1/R$ and D^2, and productivity is proportional to $1/R^2$. Therefore using smaller particles and more rapid cycles can achieve the same resolution but with higher throughputs and higher productivities. Similar conclusions were also reached from a different analysis[23].

CONCLUSIONS

A general rate equation model was used to study the mass transfer effects in isocratic, non-linear elution chromatography. Axial dispersion, intraparticle diffusion, and film mass transfer were considered. This model took into account non-linear isotherms, interference, and size-exclusion effects. Experimental data from ion exchange of amino acids and proteins were in good agreement with the model predictions.

When N_b, N_p and Pe_z become very large, the solution of this rate equation model approaches that of the local equilibrium model. The criteria for approaching local equilibrium conditions depend mainly on α, $\bar{C}/C_i$ and $\Delta\tau$. For example, for $\alpha = 1.6$, $\bar{C}/C_i = 10^3$ and $\Delta\tau = 18.86$, the requirements are $N_b > 4.1 \cdot 10^4$, $N_p > 7.1 \cdot 10^2$ and $Pe_z > 2.7 \cdot 10^3$, whereas for $\alpha = 0.5$ and at the same $\bar{C}/C_i$ and $\Delta\tau$, $N_b > 3.5 \cdot 10^3$, $N_p > 35.6$ and $Pe_z > 670$. For a smaller pulse, $\Delta\tau = 0.377$, a much larger N_b, N_p and Pe_z are required to approach local equilibrium.

The effects of various design and operating parameters on resolution, retention time, peak shape and peak spreading were examined. As flow-rate or particle size increases, Bi increases, which means intraparticle diffusion resistance becomes increasingly more important relative to film resistance. Band spreading due to axial dispersion becomes more pronounced as particle size increases, but it does not increase significantly with increasing flow-rate. Axial dispersion, film diffusion and intraparticle diffusion can all cause peak spreading, peak asymmetry and decrease in retention time. Their effects are more pronounced for systems with small pulses and for solutes with long retention times.

When solute concentration or eluent concentration is increased, retention time is shortened as a result of increasing total concentration. For concentrated feed pulses, interference results in asymmetric peaks and product concentrations which are much higher than their feed concentrations. In general, in the absence of mass transfer effects, the higher the solute fraction in the feed, the higher the solute affinity, the higher the product peak concentration due to interference. However, mass transfer effects tend to reduce peak heights and can have a major influence on the peak concentrations.

Results from a local equilibrium model, which neglects all mass transfer resistances, were compared with those from the rate equation model. The local equilibrium model is easier to use and requires much less computation time, but it can only predict the average breakthrough times of concentration waves. For systems with large pulses and solutes with short retention times, it can give close predictions of dynamics under complicated operating conditions. The rate equation model is much more versatile because it takes into account mass transfer resistances, complex isotherms and size exclusion. However, computation time is much longer. But, if detailed column dynamics are desired for systems with small pulses and solutes of high affinities, the rate equation model should be used.

The dimensionless groups are useful for scaling of nonlinear liquid chromatography. If θ, ε, E_p, $\bar{C}/C_i$ and feed concentration are fixed, as long as Re, L/R and $\Delta\tau$ are kept the same, identical effluent histories in terms of dimensionless variables can be obtained. Applying this scaling rule, one can show that the smaller the particle size, the shorter the cycle time, the higher the throughput and productivity.

SYMBOLS

Bi_j k_jR/E_{pj}, Biot number of the j^{th} component
C mobile phase total concentration based on per bed volume (N)
$\bar{C}$ stationary phase total concentration based on per bed volume (N)
C_i concentration of i in feed on the basis of per bed volume

c_i dimensionless solution phase concentration
c_b dimensionless bulk mobile phase concentration
c_f dimensionless feed concentration
c_p dimensionless solution phase concentration in sorbent particles
c_p^* dimensionless solid phase concentration in sorbent particles
D column diameter
D^∞ Brownian diffusivity (cm^2/min)
E_b axial dispersion coefficient (cm^2/min)
E_p effective diffusivity in the particle phase (cm^2/min)
F flow-rate (ml/min)
J J factor
k mass transfer coefficient (cm/min)
Ke size-exclusion factor
L column length (cm)
n number of species
Pe_z $u_0 L/E_b$, axial Peclet number
Pe_p $u_0 R/E_p$, particle Peclet number
r particle radial axis
R particle radius (cm)
Re $2R\rho u_0 \varepsilon/\mu$, Reynolds number
t time (min)
T adjusted dimensionless time, eqn. 14
ΔT dimensionless pulse size, eqn. 13
u_0 interstitial velocity (cm/min)
V_p pulse volume (ml)
V_{bed} column volume (ml)
x dimensionless axial axis
z axial axis (cm)

α_{ij} separation factor of species i against j
ξ dimensionless particle radial axis
$\Delta\tau$ dimensionless time for the pulse
ε void fraction
θ intraparticle porosity
ρ fluid density
μ fluid viscosity
τ dimensionless time ($\tau = tu_0/L$)

ACKNOWLEDGEMENTS

This research was supported by NSF Grants CBT-8412013, CBT-8604906, CBT-8620221 and ECE-8613167. A fellowship from Korea Explosives Company in support of S.U.K. is also acknowledged.

REFERENCES

1 J. J. van Deemter, F. J. Zuiderweg and A. Klinkenberg, *Chem. Eng. Sci.*, 5 (1956) 271.
2 J. C. Giddings, *Dynamics of Chromatography*, Marcel Dekker, New York, 1965.
3 J. A. Jönsson in J. A. Jönsson (Editor), *Chromatographic Theory and Basic Principles (Chromatographic Science Series*, Vol. 38), Marcel Dekker, New York, 1987, p. 27.
4 F. G. Helfferich and G. Klein, *Multicomponent Chromatography Theory of Interference*, Marcel Dekker, New York, 1970.
5 H.-K. Rhee, R. Aris and N. R. Amundson, *Philos. Trans. R. Soc. London, Ser. A*, 267 (1970) 419.
6 H.-K. Rhee and N. R. Amundson, *AIChE J.*, 28 (1982) 423.
7 Q. Yu and N.-H. L. Wang, *Sep. Purif. Methods*, 15 (1986) 127–158.
8 Q. Yu, *Ph.D. Thesis*, Purdue University West Lafayette, IN, 1988.
9 P. Rouchon, M. Schonauer, P. Valentin and G. Guiochon, *Sep. Sci. Technol.*, 22 (1987) 1793–1833.
10 G. Guiochon and S. Ghodbane, *J. Phys. Chem.*, 92 (1988) 3682.
11 D. M. Ruthven, *Principles of Adsorption and Adsorption Processes*, Wiley, New York, 1984.
12 Q. Yu and N.-H. L. Wang, *Comput. Chem. Eng.*, 13 (1989) 915–926.
13 S. F. Chung and C. Y. Wen, *AIChE J.*, 14 (1968) 857.
14 E. J. Wilson and J. Geankoplis, *Ind. Eng. Chem. Fundam.*, 5 (1966) 9–14.
15 J. S. Mackie and P. Meares, *Proc. R. Soc. London, Ser. A*, 232 (1955) 498.
16 F. G. Helfferich, in L. Liberti and F. G. Helfferich (Editors), *Mass Transfer and Kinetics of Ion Exchange (NATO ASI Series E: Applied Sciences*, No. 71), Martinus Nijhoff, The Hague, 1983, p. 162.
17 Q. Yu, J. Yang and N.-H. L. Wang, *React. Polym.*, 6 (1987) 33–44.
18 R. E. Treybal, *Mass-Transfer Operations*, McGraw-Hill, New York, 1980.
19 P. B. Hamilton, D. C. Bogue and R. A. Anderson, *Anal. Chem.*, 32 (1960) 1782.
20 *CRC Handbook of Biochemistry*, CRC Press, Boca Raton, FL, 2nd ed., 1970.
21 P. A. Charlwood, *Biochem. J.*, 57 (1953) 125.
22 N. Wakao and T. Funazkri, *Chem. Eng. Sci.*, 33 (1978) 1375–1384.
23 P. C. Wankat and Y. M. Koo, *AIChE J.*, 34 (1988) 1006–1019.
24 B. H. Arve and A. I. Liapis, *AIChE J.*, 33 (1987) 179.
25 G. Carta and R. L. Pigford, *Chem. Eng. Sci.*, 42 (1986) 511–517.
26 T. L. Chen and J. T. Hsu, *AIChE J.*, 33 (1987) 1387.
27 C. J. Colwell and J. S. Dranoff, *I&EC Fundam.*, 8 (1969) 193.
28 D. D. Do and R. G. Rice, *AIChE J.*, 32 (1986) 149.
29 G. Guiochon, S. Golshan-Shirazi and A. Jaulmes, *Anal. Chem.*, 60 (1988) 1856.
30 E. Kucera, *J. Chromatogr.*, 19 (1965) 237–248.
31 A. I. Liapis and D. W. T. Rippin, *Chem. Eng. Sci.*, 33 (1978) 593–600.
32 C. H. Liaw, J. S. P. Wang, R. A. Greenkorn and K. C. Chao, *AIChE J.*, 25 (1979) 376–382.
33 H. Moon and W. K. Lee, *Chem. Eng. Sci.*, 41 (1986) 1995–2004.
34 M. Morbidelli, G. Storti and S. Carra, *Ind. Eng. Chem. Fundam.*, 21 (1985) 123–131.
35 N. G. Pinto and E. E. Graham, *React. Polym.*, 5 (1985) 49–53.
36 K.-H. Radeke, H.-J. Ortlieb and D. Gelbin, *Chem. Eng. Sci.*, 36 (1981) 11–17.
37 J. B. Rosen, *J. Chem. Phys.*, 20 (1952) 387–394.
38 A. Seidel and D. Gelbin, *Chem. Eng. Sci.*, 41 (1986) 541–548.
39 S.-C. Wang and Chi Tien, *AIChE J.*, 28 (1982) 565–573.
40 T. W. Weber and R. K. Chakravorti, *AIChE J.*, 20 (1974) 228.
41 W. J. Weber and S. Liang, *Environmental Progress*, 2 (1983) 167.
42 Y. W. Wong and J. L. Niedzwiecki, *AIChE Symp. Ser.*, 78 (1982) 120–127.
43 R. B. Bird, W. E. Stewart and E. N. Lightfoot, *Transport Phenomena*, Wiley, New York, 1960.

Journal of Chromatography, 484 (1989) 61–82
Elsevier Science Publishers B.V., Amsterdam — Printed in The Netherlands

CHROM. 22 063

STUDY OF PREPARATIVE REVERSED-PHASE CHROMATOGRAPHY BY APPLICATION OF KINETIC AND EQUILIBRIUM MODELS OF COLUMN OVERLOAD

CHARLES A. LUCY[a], JAMES L. WADE[b] and PETER W. CARR*
Department of Chemistry and Institute for Advanced Studies in Biological Process Technology, Kolthoff and Smith Halls, University of Minnesota, 207 Pleasant Street SE, Minneapolis, MN 55455 (U.S.A.)

SUMMARY

Currently, there are three fundamental models of column overload which lead to closed-form equations for the peak profile. All use some simplifying assumption(s) to make the mathematics tractable, while at the same time retaining important features of the non-linear chromatographic behavior. In this work, the kinetic model based on the work of Thomas and the equilibrium models of Houghton, and Haarhoff–Van der Linde are used to study overload processes in reversed-phase chromatography. By adjustment of the parameters, all three models can be made to closely match the experimental peak shapes under conditions of moderate overload (up to 2.5% of the column capacity), but for higher overloads the Haarhoff–Van der Linde model fails to reproduce the experimental peak shape.

All of the models involve a set of three physico-chemical parameters. These parameters are related to retention (capacity factor, k') and peak width under dilute conditions, and to the degree of isotherm overload. Experimental results show that only the parameter related to k' is essentially independent of the solute concentration and flow-rate. In principle, for all three models the peak width parameter should be independent of solute concentration, but in all cases this parameter was found to vary such that the intrinsic peak width increased with concentration. Given that all three models display this same trend, even at moderately low overloads where we feel the mathematical approximations are reasonable, we believe that the change in the peak width parameters shows an as yet unknown additional band broadening phenomenon which is related to the degree of overload and independent of flow-rate.

The solute loading capcity, in terms of the adsorption site density, can be calculated from the isotherm overload parameter. The capacity is independent of flow-rate for all three models, but only that from the kinetic model is also independent of the amount of sample loaded onto the column. The adsorption site density derived from the kinetic model for a number of different mobile phases and solutes is

[a] Present address: General Chemistry Branch, Chalk River Nuclear Laboratories, Chalk River, Ontario K0J 1J0 Canada.
[b] Present address: Hercules Research Center, Wilmington, DE 19894, U.S.A.

0021-9673/89/$03.50

consistent with results from more traditional isotherm studies. For chemically simple solutes such as the benzyl alkanols, a site density of about 3–4 μmol/m^2 was obtained.

INTRODUCTION

Interest in preparative liquid chromatography (LC) has increased rapidly over the past few years, primarily driven by the emergence of biotechnology. Together with electrophoresis, chromatography is one of the major separation methods for chemical analysis in biochemistry, but as a preparative method it stands alone due to its ability to produce a high degree of purification, coupled with little denaturation of the native molecule.

In analytical chromatography, the sample size is maintained low enough to be on the linear portion of the adsorption isotherm; consequently, retention times and band profiles are independent of concentration. In preparative chromatography, this is neither true nor desired, since sample capacity and through-put are the important figures-of-merit. Large concentrations of sample "overload" the column so that peaks become highly asymmetric, and in the case of Langmuir isotherm the peaks become tailed.

While there is a great deal of interest in preparative chromatography, there is a dearth of fundamental information. In principle, the chromatographic peaks produced under overloaded conditions contain a wealth of information about the nature of the adsorption isotherm and the band broadening processes in the column. Recently, it was shown that the ideal model of chromatography (*i.e.*, negligible axial dispersion and infinitely fast mass transfer kinetics) is very useful for the rapid determination of the adsorption isotherm[1]. However, the ideal model obviously can say nothing about the band broadening characteristics of the column. Currently there are three *closed-form* equations which can be used to generate elution profiles under non-linear chromatographic conditions: the kinetic model[2] based on the work of Thomas[3], and the equilibrium models of Houghton[4], Jaulmes *et al.*[5] and Haarhoff and Van der Linde[6]. Since it is not clear which of these three approaches is physically most realistic for the study of reversed-phase chromatography, all three models were examined.

While it is a necessary condition for the validity of a model of non-linear chromatography to accurately reproduce the skewed elution profiles, this by itself is not sufficient to "prove" that the model is valid, as has been implied by Cretier and Rocca[7]. We have shown that the Houghton model and the kinetic model can generate experimentally indistinguishable peak profiles, even under conditions such that the former does not conserve mass and yields biased values for its parameters[8]. Thus a high quality fit does not by any means indicate that a model is valid, or that the parameters are meaningful[5,8]. Rather the validity of a model can only be determined by establishing that its physico-chemical parameters have physical significance. In this work, the applicability of the kinetic, Houghton and Haarhoff–Van der Linde models to reversed-phase chromatography will be assessed by comparing the physical significance of the parameters. In addition, we hope to gain a greater understanding of the processes involved in reversed-phase chromatography by examining this mode of chromatography from the perspective of all three models.

THEORY

Giddings[9] has shown that under linear chromatographic conditions, it is possible to represent the effects of slow interphase transfer in terms of a longitudinal dispersion factor and *vice versa*. It has never been demonstrated that this equivalency holds under *non-linear chromatographic* conditions, even when the system is nearly at equilibrium. Thus there is a need to be cautious about the model used to interpret the results obtained in comparing various models of non-linear chromatography.

The differential equation that describes the mass balance in a chromatographic column is

$$\frac{\partial C}{\partial t} + u\frac{\partial C}{\partial x} + \varepsilon\frac{\partial q}{\partial t} - E\frac{\partial^2 C}{\partial x^2} = 0 \tag{1}$$

where C is the concentration of solute in the mobile phase (M), u is the chromatographic velocity (cm/s, the velocity of an unsorbed solute which explores the pores and elutes at t_0), ε is the porosity ratio which equals $(1 - \varepsilon_T)/\varepsilon_T$, where ε_T is the total porosity of the column, q is the concentration of solute in the stationary phase (M), E is the axial dispersion coefficient, x is distance (cm), and t is time (s).

A closed-form mathematicl solution of the complete non-linear chromatographic problem, as expressed in eqn. 1, is very likely impossible. A number of closed-form solutions have been obtained by neglecting one or more processes which contribute to eqn. 1, to achieve a mathematically tractable solution which preserves some of the important features of the problem.

In the *kinetic model* of column overload[2,3], axial dispersion (axial diffusion and eddy dispersion) is assumed to be negligible; that is, E is set to zero. The chromatographic mass balance under these conditions reduces to

$$\frac{\partial C}{dt} + u\frac{\partial C}{\partial x} + \varepsilon\frac{\partial q}{\partial t} = 0 \tag{2}$$

and the associated kinetic equation is

$$\frac{\partial q}{\partial t} = k_a(S_0 - q)C - k_d q \tag{3}$$

where S_0 is the concentration of binding sites (M, same units as q). Eqn. 3 is posited based on the concept that the solute forms a 1:1 complex with a fixed number of non-interacting adsorption sites on the surface of an adsorbent. At equilibrium, eqn. 3 is fully consistent with Langmuir adsorption. In contrast to the situation that prevails in affinity chromatography, in reversed-phase LC it is not clear that a solute binds to a fixed set of non-interacting sites.

The rate constants k_a and k_d are "lumped" rate parameters corresponding to solute adsorption ($M^{-1}\,s^{-1}$) and solute desorption (s^{-1}). These parameters are termed "lumped" since both chemical kinetics and solute mass transfer can contribute to them. Hiester and Vermeulen[10] have shown that the resistances to mass transfer can be

combined with the kinetic resistance of chemical adsorption under non-linear conditions when either the chemical kinetics or mass transfer clearly dominates the broadening process, or when the constant pattern condition is satisfied[10]. [In this work a large k' (*ca.* 10) was always used, which we believe justifies the constant pattern assumption[11–15].]

The solution to eqns. 2 and 3 for an impulse input has been presented previously[2] and the resultant peak profile, in dimensionless form, is

$$\frac{C}{C_0} = \left\{\frac{1 - \exp(-\gamma K C_0)}{\gamma K C_0}\right\} \left\{\frac{[\gamma(k'/y)^{\frac{1}{2}} I_1(2\gamma(k'y)^{\frac{1}{2}}) + \delta(y)]\exp[-\gamma(y + k')]}{1 - \mathrm{T}(\gamma k', \gamma y)[1 - \exp(-\gamma K C_0)]}\right\} \quad (4)$$

where $y \equiv t/t_0 - 1$; $\gamma \equiv k_d t_0$ (dimensionless rate parameter); $k' \equiv (k_a/k_d)S_0\varepsilon$ (thermodynamic k'); $K \equiv k_a/k_d$; $C_0 \equiv$ (mol of solute injected)/(column dead volume).

In the above definitions, $S_0\varepsilon$ is the maximum adsorption capacity of the column. In eqn. 4, I_1 is a first order modified Bessel function of the first kind, and the T-function is a related Bessel function integral:

$$\mathrm{T}(u,v) = \mathrm{e}^{-v} \int_0^u \mathrm{e}^{-t} I_0(\sqrt{vt})\mathrm{d}t$$

where I_0 is a zeroth order Bessel function of the first kind. The T-function acts as a switching function and produces the skew in the peak profile as the column is overloaded.

The dimensionless parameters which describe an overload peak are k', γ and KC_0. Solute retention is governed by k'; the peak width under linear chromatographic conditions is inversely related to the dimensionless rate parameter γ, and the peak skew and retention time shift due to isotherm non-linearity are reflected in the overload parameter, KC_0.

In the *equilibrium-dispersive* model of column overload based on the work of Houghton[4], it is assumed that equilibrium exists between the mobile and stationary phase at each point along the column and that axial dispersion is the dominant band broadening process. The corresponding chromatographic mass balance equation under linear conditions is

$$(1 + \varepsilon K_1)\frac{\partial C}{\partial t} + u\frac{\partial C}{\partial x} - E\frac{\partial^2 C}{\partial x^2} = 0 \quad (5)$$

In order to make eqn. 1 mathematically tractable, the isotherm is *approximated* via a parabolic relationship between q and C, and equilibrium is assumed

$$q = K_1 C + K_2 C^2 \quad (6)$$

The derivative of q with respect to t in eqn. 1 is replaced via the time derivative in eqn. 6. Note that K_1 is identical in meaning to KS_0 in the kinetic model. This type of isotherm has the advantage of being able to simulate either a convex (Langmuir) or a concave

isotherm, and so it can model either the tailing or fronting peaks resulting from column overload[5]. However, one can expect this approximation to be valid for only a small deviation from a linear isotherm[5].

Substituting the parabolic isotherm, eqn. 6, into the chromatographic mass balance, eqn. 5, and redefining variables yields the mass balance expression

$$\frac{\partial C}{\partial t} - \frac{\lambda UC}{1 + \lambda C}\frac{\partial C}{\partial \psi} - \frac{E_z}{1 + \lambda C}\frac{\partial^2 C}{\partial \psi^2} = 0 \tag{7}$$

where $U = u/(1 + K_1)$; $E_z = E/(1 + K_1)$; $\lambda = 2K_2/(1 + K_1)$; $\psi = x - Ut$.

In eqn. 7, U is the velocity that a solute band would have under linear chromatographic conditions. The parameter λ is proportional to the K_2 factor in eqn. 6. It is a measure of the non-linearity of the isotherm, and is positive for a concave and negative for a convex isotherm. The variable ψ represents the axial coordinate, z, in a reference frame moving with velocity U. The effects of axial dispersion are represented by E_z.

Eqn. 7 is a complicated non-linear partial differential equation due to the term $\lambda UC/(1 + \lambda C)$. However, if it is assumed that $|\lambda C| \ll 1$ in both denominator terms, then eqn. 7 can be solved. The resultant peak profile, written in dimensionless form, is:

$$\frac{C}{C_0} = \frac{1}{\lambda C_0}\left[\frac{4P(1 + k')}{\pi \bar{t}}\right]^{\frac{1}{2}} \frac{\exp\left[\dfrac{-(1 + k' - \bar{t})^2}{4P\bar{t}(1 + k')}\right]}{\coth\left[\dfrac{\lambda C_0}{4P(1 + k')}\right] + \operatorname{erf}\left[\dfrac{1 + k' - \bar{t}}{(4P\bar{t}[1 + k'])^{\frac{1}{2}}}\right]} \tag{8}$$

where $\bar{t} = t/t_0$ (dimensionless time); $P = E_z t_0/L^2$ (dimensionless dispersion coefficient), in which L is the length of the column. A ramification of the assumption that $|\lambda C| \ll 1$ is that the equation is restricted to very dilute solutions, or what amounts to the same thing, small non-linearities in the isotherm. Beyond this limit eqn. 8 will still closely fit experimental elution profiles, but the resultant physico-chemical parameters are biased[5,8]. The manner in which the assumption of low overload affects the peak parameters under moderate overload conditions has been discussed recently[8]. It was found that under overload conditions on a convex (Langmuir) isotherm, the peak profiles generated by eqn. 8 have a smaller area than the actual normalized peaks, and so the model is said to "lose mass". This loss of mass necessitates the inclusion of a fourth fitting parameter, a weighting factor, W, to compensate for this artifact. The mass loss has the added effect of perturbing both the effective dispersion coefficient, P, and the overload parameter, λC_0. These effects are clearly evident in the data discussed below.

An alternative equilibrium model, derived by Haarhoff and Van der Linde[6], builds on the work of Houghton, taking into account the column overload (again using a parabolic isotherm) as well as the effects of axial dispersion and lateral non-equilibrium. However, this model is not *mathematically* equivalent to the Houghton model, in contrast to what has been stated previously[16]. Based on extensive computations over a wide range in parameters, particularly at high overload, the Haarhoff–Van der Linde approach appears to conserve mass. In this work, any observed deviation of the model

was within experimental error or could be attributed to numerical inaccuracy of the computer system and algorithms employed.

In the Haarhoff–Van der Linde model, the effects of axial dispersion and lateral non-equilibrium are incorporated into a single term, the standard deviation (σ). The chromatographic mass balance is

$$\frac{\partial Q}{\partial T} - Q\frac{\partial Q}{\partial \Gamma} - \frac{1}{2}\frac{\partial^2 Q}{\partial \Gamma^2} = 0 \tag{9}$$

where Q, T and Γ are dimensionless terms related to the solute concentration, time and axial distance, respectively.

$$Q = \frac{k' Y C_0}{\sigma}$$

$$T = t/t_R$$

$$\Gamma = \frac{t_R}{t_0 \sigma L}\left(x - \frac{ut}{1 + k'}\right)$$

In these expressions, σ is the dimensionless standard deviation for a dilute sample and Y is the isotherm parameter:

$$\sigma = \sigma_{t,C=0}/t_0 = \sigma_{v,C=0}/V_0$$

$$Y = -1/k'(\mathrm{d}^2 q/\mathrm{d}C^2)_{C=0}$$

Using this treatment, the resultant dimensionless expression for the peak profile is

$$\frac{C}{C_0} = \frac{\sigma}{\sqrt{2\pi k' Y C_0}} \frac{\exp(-\tau^2/2)}{\left[\dfrac{1}{\exp(k' Y C_0/\sigma^2) - 1}\right] + 0.5[1 + \mathrm{erf}(\tau/\sqrt{2})]} \tag{10}$$

here $\tau = (t - t_{r,C=0})/\sigma_t$ (reduced time); $k' = k'_{C=0}$ (thermodynamic k'); C_0 = (mol of solute injected)/(dead volume). The dimensionless parameters which describe the overloaded peak are k', σ and YC_0. As before, k' describes the retention of the solute under linear conditions; σ is a measure of the broadening of the peak under linear conditions, and the skewing of the peak due to column overload is governed by YC_0.

It must be understood that the above three models do not reduce to the same equation under infinitely dilute conditions. The kinetic model, with KC_0 set to zero, becomes

$$\frac{C}{C_0} = \{[\gamma(k'/y)^{\frac{1}{2}}]I_1[2\gamma(k'y)^{\frac{1}{2}}] + \delta(y)\} \exp -\gamma(y + k') \tag{11}$$

which is identical to the Giddings–Eyring kinetic-stochastic model of chromato-

graphy[17]. This equation produces assymetric peak profiles unless γ is rather large. The variance corresponding to this peak can easily be shown to be

$$\sigma^2 = 2k't_0/k_d$$

Under linear isotherm conditions, that is, λC_0 equal to zero, the Houghton equation reduces to

$$\frac{C}{C_0} = \frac{1}{2\sqrt{\pi\bar{t}P(1+k')}} \exp\left[-\frac{(1+k'-\bar{t})^2}{4P\bar{t}(1+k')}\right] \tag{12}$$

This result also exhibits peak assymetry under infinitely dilute conditions unless P is very small.

The Haarhoff–Van der Linde equation reduces to the form:

$$\frac{C}{C_0} = \frac{1}{\sqrt{2\pi}\sigma} \exp\left[\frac{-(t-t_R)^2}{2\sigma^2}\right] \tag{13}$$

This is obviously a Gaussian form.

EXPERIMENTAL

Materials and equipment

3-Phenyl-1-propanol, 4-phenyl-1-butanol, 5-phenyl-1-pentanol, *o*-cresol, 4-ethylaniline and 9-anthracenecarboxylic acid were from Aldrich (Milwaukee, WI, U.S.A.) and were used as received. 2-Phenylethanol was obtained from Sigma (St. Louis, MO, U.S.A.) and was also used as received. Triethylamine was from Aldrich and was fractionally distilled and dried before use. HPLC-grade water was obtained from a Barnstead System, HPLC-grade methanol was purchased from EM Science and HPLC-grade tetrahydrofuran was from Fisher.

The apparatus consisted of an Altex Model 110 pump (Beckman Instruments, Altex Div., San Ramon, CA, U.S.A.), a Rheodyne 7125 sampling valve (Berkeley, CA, U.S.A.) with a 100-μl loop, and a Hitatchi Model 110A UV–VIS spectrometer fit with a 20-μl high-pressure flow cell. Preliminary experiments showed that a volume of 100 μl caused no additional increase in peak width under linear isotherm conditions relative to a 10 μl injection. The linearity of the solute absorbance at the eluent concentrations was verified independently on a Varian DMS 200 UV–VIS spectrophotometer. Vydak 201THP (Sep A Ra Tions Group, Hesperia, CA, U.S.A.) (10 μm particle size; 300 Å pore size; specific surface area of the ODS material of 56 m^2/g by BET) was slurry packed into a 150 × 4.6 mm I.D. column from isopropyl alcohol at 4500 p.s.i. A long column was chosen to minimize the effects of extra column dispersion on the peak shape and width. Packing density was measured as 790 g/l. The column was thermostatted to 30.0°C using a water jacket connected to a Haake water bath. The dead time was measured using uracil [mobile phase: methanol–water (25:75)]. The corresponding dead volume was 1.92 ml.

Data were digitized and stored using an IBM Instruments Model 9000 Lab

Computer with the Chromatography Applications Program (Version 4.0, IBM Instruments). Acquisition rates were 4–40 points/s for uracil at flow-rates from 0.5 to 5.0 ml/min and from 0.25 to 2.5 points/s for retained compounds under the same conditions. All injections were made in duplicate. Raw data files for each injection were transferred to a Heath H-386 microcomputer (with a 80387 coprocessor) for subsequent analysis and fitting to eqns. 4, 8 and 10.

Prior to data fitting, the baseline (as determined by linear least-squares) was subtracted from the raw data and the time axis was normalized to the dead time of the system. The normalized data were then stored on disk for later access by the fitting programs. Each peak was represented by at least 200 points.

A randomized simplex algorithm[18] was used to fit eqns. 4, 8 and 10 to 50 data points evenly spaced across the breadth of the peak. Three parameters were used in the fitting procedure for the kinetic model (γ, k' and KC_0) and the Haarhoff–Van der Linde model (k', σ and YC_0). Four parameters were used in the fits to the Houghton model (P, k', λC_0 and a weighting factor, W). The fitting procedure was repeated at least three times on each peak, with different initial guesses, to assure that false minima were not obtained. Goodness-of-fit is reflected by the sum of the residuals, χ^2.

RESULTS AND DISCUSSION

Experimental conditions were adjusted to insure large k' values in order to minimize extra-column effects and validate the constant pattern assumption implicit in the kinetic model. Initial studies were performed with 3-phenyl-1-propanol at solute loadings ranging from those sufficiently low to be on the linear portion of the isotherm up to moderate column overload conditions (2.5% of the total capacity of the column). Fig. 1 illustrates the types of peaks observed over this range. The dots represent the experimental data points. All three models fit these peaks equally well based on χ^2, as shown in Table I, so only a single theoretical curve is shown for each peak.

There is some systematic lack of fit evident in these plots, especially at high solute loads near the leading edge of the peak. The lack of fit was not as serious, nor was it of

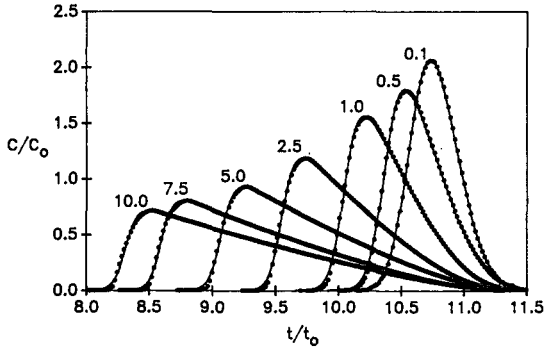

Fig. 1. Experimental elution peaks of 3-phenyl-1-propanol for various loadings. The points are the experimental data and a single curve is given for the best fit of the kinetic model. The elution profiles for the Houghton and Haarhoff–Van der Linde models are indistinguishable from the kinetic model. Experimental conditions: flow-rate, 1.0 ml/min; mobile phase, methanol–water (25:75); temperature, 30.0°C; injection volume, 100 μl. The number above each curve is the amount of solute injected in μmoles.

the same type, as previously observed in modeling high-performance affinity chromatography[2]. At this point, it does not concern us nearly so much as other complexities described below. We hypothesize that it is due to the effect of extra-column dispersion acting to broaden the nearly vertical rise in concentration from the baseline. Nevertheless, all three models can effectively match the experimental peak profiles. However, the quality of the fitting does not "prove" that the models are valid, or that the physico-chemical parameters derived from the fits are meaningful[5,8]. Rather, as stated above, the models must be judged on the basis of the physical significance of physico-chemical parameters determined in the fitting of the models to the experimental peaks. In this work, the physical significance of the parameters was probed by varying the amount of solute injected and the flow-rate. Table I shows the physico-chemical parameters extracted from chromatographic peaks resulting from trace to moderate overloads of a reversed-phase column using 3-phenyl-1-propanol as the test solute. Table II shows the physico-chemical parameters determined for a linear chromatographic peak (0.1 μmol injected) and a moderately overloaded peak (10 μmol) at flow-rates ranging from 0.5 to 5.0 ml/min.

Thermodynamic k'

In all models, the thermodynamic k' refers to the extent of solute retention expected under linear chromatographic conditions; it should be independent of concentration. Under all conditions studied, the k' extracted from each peak by all three models are comparable. Replicate injections under a variety of circumstances showed that k' is reproducible to ± 0.01. The k' did not remain absolutely constant as the solute loading increased (Table I); rather it decreased slightly. Nevertheless, no assumptions as to the significance of this trend will be made since in previous studies of preparative reversed-phase chromatography using the Houghton equilibrium-dispersive model, k' was observed to increase, decrease or remain constant depending on the chromatographic conditions[5,19].

Changes in the flow-rate had no significant effect on k', as can be seen in Table II. (The shift in k' between the 1.0 and 4.0 ml/min studies in Table I is a result of a minor change in the mobile phase composition.)

We conclude that all three models recover the k' accurately; it is not dependent on either the amount of solute injected or flow-rate.

Peak width parameters

The dimensionless rate parameter γ of the kinetic model, the dimensionless dispersion coefficient P of the equilibrium-dispersive model and the dimensionless standard deviation σ of the Haarhoff–Van der Linde model all reflect the peak width resulting from a broadening process other than overloading, in essence, the broadening of the solute band under linear chromatographic conditions. The peak width is inversely related to γ, and linearly related to P and to the square of σ.

Effect of sample loading. Table I shows the three peak width parameters obtained from the peak profiles with 0.049–9.87 μmol of 3-phenyl-1-propanol. All of the chromatographic peak width parameters change significantly as the solute loading increases. At 1.0 ml/min, γ decreased 3.8-fold, P increased 4.8-fold and σ^2 increased 2.9-fold. Similar, although smaller, trends are evident for the 4.0 ml/min data also presented in Table I. Analogous results were obtained in earlier studies of preparative

TABLE I

INFLUENCE OF SAMPLE LOADING ON THE PARAMETERS OF THE KINETIC, HOUGHTON EQUILIBRIUM-DISPERSIVE AND HAARHOFF–VAN DER LINDE MODELS FOR COLUMN OVERLOAD

Conditions: column, 150 × 4.6 mm I.D. C_{18} Vydak 201TPB; mobile phase, methanol–water (25:75); sample, 3-phenyl-1-propanol; injection volume, 100 μl and column temperature, 30.0°C.

Flow-rate (ml/min)	*μmol injected*	*Kinetic model*				*Equilibrium-dispersive model*					*Haarhoff–Van der Linde model*			
		k'	*γ*	*K* (M^{-1})	χ^2 ($\times 10^3$)	*k'*	*P* ($\times 10^4$)	*λ* (M^{-1})	*W*	χ^2 ($\times 10^3$)	*k'*	*σ*	*Y*	χ^2 ($\times 10^3$)
1.0[a]	0.049	9.94	520	82.6	7.5	9.92	1.61	−137	1.004	7.2	9.93	0.193	165	8.7
	0.099	9.88	535	61.1	4.1	9.86	1.58	−103	1.006	4.3	9.89	0.191	142	7.3
	0.49	9.90	450	40.7	11.8	9.90	1.88	−77.0	1.018	8.8	9.92	0.202	84	9.9
	0.99	9.83	385	39.2	9.7	9.82	2.30	−73.2	1.027	9.5	9.84	0.216	76	9.3
	2.47	9.80	275	37.2	7.2	9.78	3.38	−70.5	1.044	8.4	9.78	0.250	69	7.1
	4.94	9.80	200	36.4	5.1	9.79	4.90	−71.3	1.066	5.7	9.77	0.286	64	5.2
	7.40	9.72	165	36.3	4.2	9.70	6.10	−72.4	1.082	6.1	9.68	0.301	61	4.7
	9.87	9.76	135	36.0	4.3	9.74	7.70	−73.2	1.096	5.3	9.68	0.328	59	3.7
4.0[b]	0.049	9.66	310	78.8	13.0	9.65	2.74	−140	0.996	11.6	9.67	0.249	187	15.2
	0.099	9.65	305	55.2	4.6	9.65	2.80	−104	1.006	2.8	9.66	0.250	135	3.8
	0.49	9.62	300	42.9	5.9	9.63	2.86	−78.6	1.006	3.8	9.66	0.245	92	7.2
	0.99	9.70	285	42.0	4.3	9.68	3.10	−75.8	1.015	3.4	9.70	0.252	81	7.5
	2.47	9.62	235	39.5	3.8	9.62	3.90	−74.1	1.036	3.1	9.62	0.268	73	7.7
	4.94	9.59	180	38.2	3.8	9.56	5.65	−73.3	1.061	4.2	9.56	0.300	67	5.1
	7.40	9.57	165	37.1	0.8	9.55	6.10	−73.4	1.076	1.2	9.50	0.305	62	4.6
	9.87	9.58	134	37.1	2.6	9.55	8.00	−74.9	1.093	2.1	9.48	0.332	60	4.5

[a] t_0 = 108.9 s.
[b] t_0 = 27.45 s.

TABLE II

INFLUENCE OF FLOW-RATE ON THE PARAMETERS OF THE KINETIC, THE HOUGHTON EQUILIBRIUM-DISPERSIVE MODELS AND THE HAARHOFF–VAN DER LINDE MODELS

Conditions: column, 150 × 4.6 mm I.D. C_{18} Vydak 201TPB; mobile phase, methanol–water (25:75); sample, 3-phenyl-1-propanol; injection volume, 100 μl and column temperature, 30.0°C.

μmol injected	*Flow-rate (ml/min)*	*Kinetic model*				*Equilibrium-dispersive model*					*Haarhoff–Van der Linde model*			
		k'	γ	$K\ (M^{-1})$	$\chi^2\ (\times 10^3)$	k'	$P\ (\times 10^4)$	$\lambda\ (M^{-1})$	W	$\chi^2\ (\times 10^3)$	k'	σ	$Y\ (M^{-1})$	$\chi^2\ (\times 10^3)$
0.099	0.50	9.90	415	62	6.4	9.89	2.00	−98	0.997	4.7	9.91	0.217	130	7.4
	1.0	10.01	365	83	8.2	10.01	2.25	−143	0.998	6.1	10.03	0.232	180	9.3
	2.0	9.95	305	88	9.5	9.94	2.70	−159	0.995	6.8	9.97	0.253	210	10.0
	3.0	9.96	265	98	10.0	9.92	3.10	−125	0.991	7.0	9.96	0.271	200	10.0
	4.0	9.94	240	109	9.1	9.93	3.50	−178	0.995	5.6	9.95	0.286	230	8.4
	5.0	9.85	225	114	11.7	9.84	3.70	−199	0.993	7.8	9.85	0.293	250	12.5
9.87	0.50	9.73	110	37.1	2.8	9.70	9.45	−75.0	1.091	3.5	9.65	0.362	61.1	4.7
	1.0	9.78	100	38.4	3.2	9.75	10.30	−76.9	1.087	3.5	9.72	0.387	63.3	4.8
	2.0	9.85	105	39.7	1.1	9.82	9.60	−80.2	1.090	1.5	9.76	0.378	64.9	3.7
	3.0	9.74	105	38.5	1.0	9.71	9.75	−77.4	1.087	1.5	9.67	0.374	63.3	3.0
	4.0	9.85	95	39.7	1.5	9.82	10.90	−80.3	1.091	2.3	9.78	0.401	65.3	1.7
	5.0	9.70	90	38.8	2.4	9.66	11.55	−77.8	1.086	3.0	9.63	0.409	64.3	3.7

reversed-phase chromatography using the Houghton equilibrium-dispersive model[5,19]. Thus, regardless of the model adopted, the peak width parameter for all three models changes in a manner indicative of an increase in the intrinsic peak width as the solute loading increases.

However, all of the models were derived such that the peak width parameters should be independent of the degree of column overload, and so in essence, all three models have failed. However, the cause of this failure, whether it is due to flawed initial assumptions or rather due to the incompleteness of our fundamental understanding of non-linear chromatography, is unclear.

It is obvious that at the higher levels of column overload studied herein, the Houghton and Haarhoff–Van der Linde models are invalid. Both models utilize a parabolic approximation for the isotherm which is only reasonable under linear or low overload conditions. In addition, the Houghton model makes a further explicit assumption of low overload conditions ($1 + \lambda C \approx 1$). Thus, it could be argued that the results of these models, under high overload conditions, should be ignored. We are then left solely with the results for the kinetic model where γ decreases with increasing overload, which theoretically it ought not do. Based on this line of argument, the only reasonable conclusion is that the kinetic model fails to predict the details of band broadening in preparative reversed-phase chromatography.

This failure most likely results from the widely held concept that mechanical dispersion (axial diffusion and eddy dispersion) is the dominant form of band broadening in reversed-phase chromatography, as can be seen in the plot of *H vs. u* under analytical conditions, open circles in Fig. 2. At 1.0 ml/min, almost 80% of the band broadening is due to dispersion. Although Giddings has shown that dispersion effects can be represented in terms of slow interphase transfer under linear conditions, it is not known whether this equivalency is valid under non-linear conditions. If it is accepted that the kinetic model has failed, this indicates that the equivalency between dispersion and slow interphase kinetics has also failed under non-linear chromatographic conditions.

However, one point which we neglected in the above argument is that the

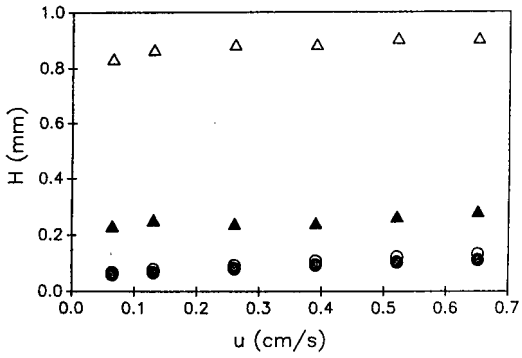

Fig. 2. *H–u* curves for analytical (○, ●) and overloaded (△, ▲) conditions. Open symbols are the observed plate heights and filled symbols represent H_{linear} calculated using eqn. 15 based on the kinetic model. Experimental conditions: flow-rate, 0.5–5.0 ml/min; mobile phase, methanol–water (25:75); temperature, 30.0°C; injection volume, 100 μl; sample, 3-phenyl-1-propanol; loading 0.099 (analytical) and 9.87 (overloaded) μmoles.

Houghton and Haarhoff–Van der Linde models *are* valid under linear and low overload conditions. Therefore, under these conditions, the peak width parameters of these models should not vary with solute loading. However, Jaulmes *et al.*[5], using the Houghton model, found that their dispersion parameter increased over two-fold under overload conditions for which they predicted the model to be valid (*i.e.*, $\lambda C_{max} < 0.05$). We observe variations in P and σ and λC_{max} values which are smaller than the range of validity of the parabolic isotherm approximation. Thus, the variation in the peak width parameter may not be solely an artifact of mathematical failure of the models.

Fig. 3 shows the relationship between the peak width parameters from the three models over the full range of overload studied. The terms $1/\gamma$, P and σ^2 are all directly related to the peak width. What is seen in this figure is that in comparing the kinetic with either the Haarhoff–Van der Linde or Houghton models, the linear relationship established between the terms of the two models under the low overload conditions (see the lines in Fig. 3) is continued throughout the concentration range studied. The deviation at higher overload conditions for P *vs.* $1/\gamma$ results from the "loss of mass" of the Houghton model[8], and is in any case minor compared to the change in P already predicted from the low overload conditions. Furthermore, it would be expected that the relationship between γ *vs.* P and σ would change as the degree of overload was increased since the Houghton and Haarhoff–Van der Linde models fail for mathematical reasons, whereas, using the argument above, the kinetic model should fail as a result of fundamental physical flaws in the model. However, no such break in the relationship between the peak width parameters of the kinetic model and the equilibrium-dispersive models is evident, even at the higher concentrations where the parabolic isotherm assumption perturbs the overload parameters (Fig. 4).

Thus, since all three models display the same trend of increasing intrinsic peak width as the overload increases, we believe that there must be an underlying physical cause, separate from the assumptions of each individual model, which is responsible. That is, the models are believed to fail, not due to invalid assumptions, but rather due to *incompleteness*. We have a number of speculations as to the origin of this "additional" band broadening process, but at this time we are not able to devise a definitive experiment.

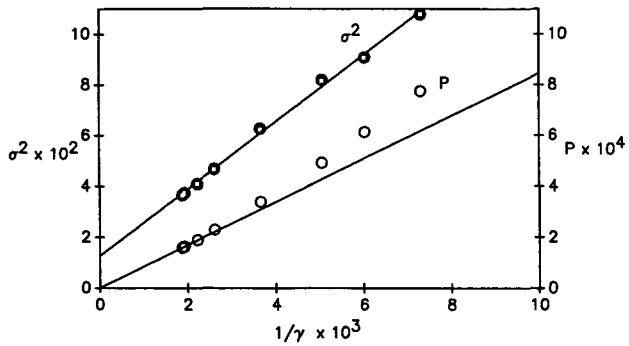

Fig. 3. Relationship between peak width parameters for injections of 0.049 (linear conditions) to 9.87 (moderate overload) μmol of 3-phenyl-1-propanol. Open circles indicate P plotted *versus* $1/\gamma$ and solid circles are σ^2 *vs.* $1/\gamma$. Lines are the extrapolation of the relationship between the peak width parameters under load overload conditions (*i.e.*, lowest values of $1/\gamma$). Conditions are as stated in Table I.

TABLE III

MODEL PARAMETERS FOR INJECTIONS OF 9-ANTHRACENECARBOXYLIC ACID

Conditions: column, 150 × 4.6 mm I.D. C_{18} Vydak 201TPB; mobile phase, methanol–0.01 *M* phosphate buffer, pH 6.8 (20:80); flow-rate, 1.0 ml/min; injection volume, 100 μl and column temperature, 30.0°C.

μmol injected	*Kinetic model*				*Equilibrium-dispersive model*					*Haarhoff–Van der Linde model*			
	k'	γ	$K\ (M^{-1})$	$\chi^2\ (\times 10^3)$	k'	$P\ (\times 10^4)$	$\lambda\ (M^{-1})$	W	$\chi^2\ (\times 10^3)$	k'	σ	$Y\ (M^{-1})$	$\chi^2\ (\times 10^3)$
0.02	12.30	340	820	8.4	12.29	2.1	−1480	1.008	10.2	12.31	0.264	1700	10.0
0.20	12.21	160	850	2.6	12.19	4.8	−1670	1.050	2.7	12.10	0.358	1540	3.8
2.01	11.70	43	690	1.4	11.66	24.0	−1570	1.178	1.0	–	–	–	7.7[a]

[a] Haarhoff–Van der Linde model could not satisfactorally fit this peak, as evidenced by χ^2 being 6–7 times that of the other models.

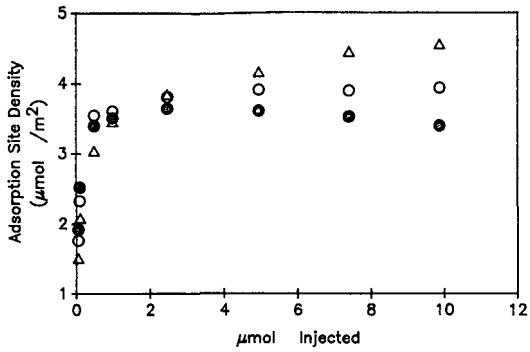

Fig. 4. Adsorption site densities for 3-phenyl-1-propanol as determined by the kinetic model using eqn. 16 (○), the Houghton equilibrium-dispersive model using eqn. 17a (●) and the Haarhoff–Van der Linde model using eqn. 18 (△). Experimental conditions are: flow-rate, 1.0 ml/min; mobile phase, methanol–water (25:75); temperature, 30.0°C; injection volume, 100 μl.

However, one interesting and potentially relevant observation which can be made is illustrated in Table III. In this table the physico-chemical parameters obtained upon injection of 0.02–2 μmol of 9-anthracenecarboxylic acid, under conditions for which it is completely ionized, are shown. The first point is that the same trend of peak width parameter *versus* loading is present for 9-anthracenecarboxylate as was observed for 3-phenyl-1-propanol in Table I. This indicates that this behavior is not limited to benzyl alcohol and its homologues. More significantly, however, the peak width is greater (*i.e.*, γ is lower; P and σ are higher) for 9-anthracenecarboxylate than for 3-phenyl-1-propanol (Table I) when compared on the basis of equal amounts injected. Jacobson *et al.*[20] observed that ionized solutes have column capacities nominally only a tenth that of comparable neutral solutes. In this work the carboxylate was observed to have only a fifteenth of the capacity of 3-phenyl-1-propanol (Table III). When 9-anthracenecarboxylate and 3-phenyl-1-propanol injections are compared on the basis of the degree of overload (*i.e.*, multiply 9-anthracenecarboxylate concentration by 15 for sake of comparison), it can be seen that the absolute value of the peak width parameters are approximately the same for the two solutes. Some discrepancy is to be expected due to the differences in k'. Thus, if it is assumed that the band broadening processes for the two solutes are the same, even though the factors controlling their isotherms are different, then the change in the peak width parameters is a function of the degree of column overload rather than the mobile phase solute concentration.

Obviously, more work needs to be done to elucidate the origin of this additional "overload induced" band broadening effect. Knowledge of the manner in which the overload increases the peak width parameters is an absolute prerequisite if any of the non-linear chromatography models are to be used to predict scale-up effects from linear chromatographic behavior.

An additional important observation from Table III is that the Haarhoff–Van der Linde model did not fit the experimental peak shape of the 2-μmol injection of 9-anthracenecarboxylate, as can be seen by the six-fold difference in the χ^2 between this model and the other two. Thus the Haarhoff–Van der Linde model can match experimental peak shapes under low or moderately overloaded peaks, whereas the

TABLE IV

EFFECT OF SOLUTE ON THE ADSORPTION SITE DENSITY ON A REVERSED-PHASE COLUMN

Conditions: injection volume, 100 μl; column temperature, 30.0°C; sample concentration, 0.05 *M* (except 9-anthracenecarboxylic acid); column, 150 × 4.6 mm I.D. C_{18} Vydak 201TPB (different column from Table V); flow-rate, 1.0 ml/min.

Solute	k'	γ	KC_0	Λ_0 ($\mu mol/m^2$)
2-Phenylethanol[a]	8.85	130	0.112	3.1
3-Phenyl-1-propanol[b]	10.46	190	0.108	3.7
4-Phenyl-1-butanol[c]	11.24	130	0.117	3.8
5-Phenyl-1-pentanol[d]	10.58	130	0.111	3.7
o-Cresol[a]	11.93	120	0.211	2.1
4-Ethylaniline[e]	10.96	270	0.058	6.5
9-Anthracenecarboxylic acid[f]	11.71	43	0.709	0.25

[a] Mobile phase methanol–water (10:90).
[b] Mobile phase methanol–water (25:75).
[c] Mobile phase methanol–water (31.5:68.5).
[d] Mobile phase methanol–water (40:60).
[e] Mobile phase methanol–phosphate buffer, pH 6.8 (25:75), with 0.010 *M* triethylamine.
[f] Sample concentration, 0.02 *M*; mobile phase methanol–phosphate buffer, pH 6.8 (20:80).

kinetic and Houghton equilibrium-dispersive models can match even severely overloaded chromatographic peaks.

Effect of flow-rate. The influence of flow-rate on the physico-chemical parameters of the three models is given in Table II for injections of 0.099 and 9.87 μmol of 3-phenyl-1-propanol. Overloading the column has the effect of shifting the *H versus u* plot upwards to higher plate heights, as observed previously[21,22], and shown in Fig. 2, where the open circles and open triangles correspond to the plate heights observed for injections of 0.099 and 9.87 μmol, respectively.

In essence, the band broadening due to overload of the isotherm can be separated from that of the linear chromatographic broadening processes:

$$H = H_{\text{linear}} + H_{\text{overload}} \tag{14}$$

This additivity of plate heights was first described by Haarhoff and Van der Linde[6] as a consequence of their model. A similar approximation can be made based on the kinetic model[23].

For injections of 0.099 μmol shown in Table II, the peak width parameters vary in the expected manner based on an *H–u* plot, since the loading is sufficiently low as to be on the linear portion of the isotherm. One can use the theory of linear chromatography to show that

$$H_{\text{linear}} = \frac{2k'}{(1+k')^2}\frac{L}{\gamma} \tag{15}$$

A plot of H_{linear} computed via the measured γ values for the 0.099 μmol injections is shown as the filled circles in Fig. 2. H_{linear} is slightly lower that the observed H since some of the band broadening was ascribed to the isotherm overload parameter (*i.e.*, KC_0 was not zero).

For the higher loading, 9.9 μmol, the chromatographic parameters are almost independent of flow-rate. The band broadening processes operative under trace conditions are still taking place; however, their effect on the peak width parameters is overwhelmed by the "solute overload effect" discussed in the last section. We also show the H_{linear} computed based on eqn. 15 and the measured value of γ (see Fig. 2, filled triangles). It is clear that we are now recovering a poorer value of γ since the peak width is dominated by the overload process. The observation that this "effect" is flow-rate independent is consistent with the assumption that it is related to the column overload, and not simply an enhancement of the traditional band broadening processes.

Similar results can be obtained using the peak width parameters of the Houghton and Haarhoff–Van der Linde models.

Overload parameters

In Table I, the effect of solute concentration on the overload parameters, KC_0, λC_0 and YC_0, is factored out, to yield K, λ and Y, which characterize the curvature of the isotherm at the origin. These isotherm parameters should be independent of concentration. For the 20-fold change in solute loading from 0.5 to 9.9 μmol: K decreases 12%, λ decreases 5% and Y decreases 30%. For lower amounts of solute, the system is essentially on the linear portion of the isotherm, and the isotherm parameters (K, λ, Y) respond to the minor peak asymmetry arising from effects other than isotherm overload (i.e., extra-column or dispersion effects). It is very difficult to measure the peak asymmetry at low overload. For instance the K observed for a 0.049-μmol injection of 3-phenyl-1-propanol was 82.6 M^{-1} (Table I, 1.0 ml/min). Generating a peak using the same k' and γ values but decreasing K to 36 M^{-1} (the value observed for a highly overloaded peak), resulted in only a 1% change in peak width and the peak asymmetry, as measured by the third statistical moment, varied from 0.0014 to 0.0008. The difference in χ^2 was insignificant.

The isotherm curvature at the origin is a rather esoteric parameter. The capacity of the column is a more useful and practical parameter. Jacobson *et al.*[20] found that the isotherms for a wide variety of solutes in reversed-phase chromatography were of the Langmuir form. Using this as the assumed isotherm form, the capacity of the column can be calculated using the isotherm parameters determined by each model. An expression for the column capacity, in terms of an adsorption site density. Λ_0 (μmol/m^2), has been derived[2]:

$$\Lambda_0 = \left(\frac{\varepsilon_T}{\rho a_S}\right)\left(\frac{k'}{K}\right) \tag{16}$$

where $\varepsilon_T = \varepsilon_e + \varepsilon_i(1 - \varepsilon_e)$. The interstitial ($\varepsilon_e$) and intraparticle ($\varepsilon_i$) porosities were both taken to be 0.4[24]; hence $\varepsilon_T = 0.64$. ρ is the density of the adsorbent in the packed tube, which was measured as 790 g/l. a_S is the specific surface area, which was measured

as 56 m^2/g by BET. C_0 is the concentration injected (in μM) times the fraction of the column dead volume represented by the 100-μl loop.

Using the same assumptions, the Houghton equilibrium-dispersive model yields the expression[19]:

$$\Lambda_0 = -\left[\frac{\varepsilon_T}{\rho a_S}\right]\left[\frac{2k'^2}{\lambda(1+k')}\right] \tag{17a}$$

where

$$\lambda = \frac{-2k'K}{1+k'} \tag{17b}$$

For the Haarhoff–Van der Linde model, the relevant expression is:

$$\Lambda_0 = \left(\frac{\varepsilon_T}{\rho a_S}\right)\left(\frac{2k'}{Y}\right) \tag{18}$$

Fig. 4 shows the adsorption site densities computed from each model for the data in Table I. All three models show essentially the same general trend. At low concentrations, where the peak skew results predominantly from factors other than isotherm overload, the adsorption site density appears to be low, since all of the models incorrectly attribute the other sources of peak asymmetry to the isotherm overload parameter. Once the isotherm overload effects become large enough to control the peak skew, the site densities approach a limiting value for the kinetic model, and drift downwards and upwards for the Houghton equilibrium-dispersive and the Haarhoff–Van der Linde models, respectively.

It is not correct to say that since the kinetic model gives reasonable results for the adsorption site density under high overload conditions, that overall the model is valid. At high sample loadings, the band is controlled mainly by the thermodynamic effect of overloading the column, not by kinetic effects. In fact, at moderate to high loadings, the ideal model[1] gives comparable results to the kinetic model for the adsorption site density. Thus the success of the kinetic model herein results solely from the asssumption of the correct form of the adsorption isotherm; the Langmuir isotherm.

The upward tendency of the site density calculated using the Haarhoff–Van der Linde model is not surprising, since the deviation between the parabolic isotherm used in the model and the Langmuir isotherm assumed in the derivation of eqn. 18 increases with increasing column overload. However, it is interesting that this deviation increases so rapidly after overload asymmetry becomes significant. This illustrates a shortcoming of both the Houghton and Haarhoff–Van der Linde equations. That is, their assumption that a parabolic isotherm is a reasonable approximation of the Langmuir isotherm is only valid at low overloads where the models are numerically not very sensitive to the value of the overload parameter.

With the Houghton equilibrium-dispersive model, the same deviation between the parabolic and Langmuir isotherms occurs, but the observed behavior is further

complicated by the lack of mass conservation inherent in this model. In a comparison of the kinetic and equilibrium-dispersive models, we observed that as the overload increased, λ deviated positively from its true value due to the mass loss[8]. Thus for the equilibrium-dispersive model, the deviation of its parabolic isotherm from the Langmuir is overwhelmed by the opposite effects arising from non-conservation of mass.

The adsorption site density for all three models is independent of flow-rate provided that the column is significantly overloaded. When 9.87 μmol of solute are injected (Table II), Λ_0 is 3.67 with a standard deviation of 0.08 μmol/m^2 for the kinetic model, 3.28 (0.07) for the Houghton equilibrium-dispersive model and 4.40 (0.09) for the Haarhoff–Van der Linde model.

The adsorption site densities determined for loadings greater than 1.0 μmol, 3.7 μmol/m^2, are in good agreement with the 4.3 μmol/m^2 observed for benzyl alcohol in methanol–water (30:70) determined using the Craig distribution model of non-linear chromatography[25], and it is also in reasonable agreement with the value expected for monolayer adsorption of the solute molecule (*ca.* 3 μmol/m^2) onto a collapsed ODS surface[26]. The fact that Λ_0 is close to the value expected based on an adsorption model of reversed-phase LC regardless of the model chosen is most interesting. It is not evident how a partition model of reversed-phase LC could lead to such a coincidence.

Effect of mobile phase on adsorption site density. As shown above, only the adsorption site density derived from the kinetic model is independent of both the amount of solute and flow-rate. While this behavior and the value of Λ_0 for 3-phenyl-1-propanol are consistent with expectations, it still remains to be shown that this parameter has any physical significance. Shown in Table V are the physico-chemical parameters obtained from fits of the kinetic model to additional experiments in which 5 μmol of 3-phenyl-1-propanol were injected under various mobile phase conditions. Using mobile phases of between 15 and 35% methanol, the adsorption site density, as calculated from eqn. 16, is constant; at methanol–water (10:90), Λ_0 drops by 20%. Previously, Jaulmes *et al.*[19] studied a similar system (benzyl alcohol) in 10–30% methanol using the Houghton equilibrium-dispersive model; but uncertainties in their measurements obscured any such trend. Eble *et al.*[26], using the Craig distribution model, observed a constant (within experimental error) capacity for benzyl alcohol over the range of 20 to 40% methanol, although they did comment that there may be a small increase associated with increasing modifier concentration in the mobile phase[25].

The behavior of Λ_0 observed for methanol–water mobile phase can be rationalized in terms of the wetting characteristics of reversed-phase bonded phases. McCormick and Karger[27] observed that the amount of methanol sorbed by an octyl stationary phase increased for mobile phase concentrations of methanol up to 20% and was constant for higher concentrations of methanol. The sorption of methanol into the collapsed bonded phase will solvate the octyl chains, allowing them to adopt more of a "brush" orientation[28]. We believe that the "brush" orientation exposes a larger surface of the octyl chains than does a collapsed chain, which then becomes available to interact with the solute, and thus producing a higher effective site density.

In Table V, the data for the tetrahydrofuran (THF)–water system indicate a capacity comparable to the well methanol-wetted stationary phase, and increasing the percentage of THF makes a small, but significant, change in the adsorption site

TABLE V

EFFECT OF MOBILE PHASE ON ADSORPTION SITE DENSITY FOR 3-PHENYLPROPANOL

Conditions: injection volume, 100 μl; column temperature, 30.0°C; sample concentration, 0.05 M; column, 150 × 4.6 mm I.D. C_{18} Vydak 201TPB; flow-rate, 1 ml/min. All experiments, except methanol–water (10:90), were run successively.

Mobile phase	k'	γ	KC_0	Λ_0 ($\mu mol/m^2$)
Methanol–water (10:90)[a]	25.35	48	0.334	2.9
Methanol–water (15:85)	21.86	59	0.232	3.6
Methanol–water (25:75)	10.06	160	0.102	3.7
Methanol–water (35:65)	4.45	300	0.045	3.7
THF–water (10:90)	8.66	180	0.089	3.7
THF–water (15:85)	5.40	280	0.052	3.9

[a] Column was a second 150 × 4.6 mm I.D. C_{18} Vydak 201TPB column.

density. This result is consistent with the THF isotherm behavior on octyl bonded phases[27], where it was observed that the isotherm did not level off until 40–60% THF. However it is surprising that the use of the much stronger modifier, THF, had such a small effect on the capacity. This indicates that the major capacity effect of the modifier is to solvate the bonded phase such that it can adopt the "brush" form. Once the bonded phase is in the brush form, further increases in mobile phase do not significantly alter its form, and thereby its capacity.

Effect of solute type on adsorption site density. The physico-chemical parameters obtained by fitting the kinetic model to injections of a number of chemically distinct solutes are shown in Table IV. It should be noted that a different column, but packed with the same stationary phase, was used in this experiment than in Table V. Nevertheless, Λ_0 for 3-phenyl-1-propanol is still the same as for the column used in the previous studies (Table V). The larger benzyl alcohol homologues show similar adsorption site densities to 3-phenyl-1-propanol, but 2-phenylethanol was significantly lower. However, this lower value of Λ_0 is probably a result of wetting the stationary phase, as is evident by comparing Λ_0 for 2-phenylethanol with 3-phenyl-1-propanol in methanol–water (10:90) (Table V).

Other types of solutes show strikingly different adsorption site densities from that of the benzyl alcohol homologues. *o*-Cresol shows a lower capacity than 3-phenyl-1-propanol under the same mobile phase conditions [2.1 *vs.* 2.9 μmol/m^2 for methanol–water (10:90)]. This is comparable to the relationship observed recently by Golshan-Shirazi and Guiochon[1] for phenol and benzyl alcohol. In contrast 4-ethylaniline has a capacity 1.75 times greater than that of 3-phenyl-1-propanol. This is consistent with the results of Jacobson *et al.*[20], in which the capacity of *p*-toluidine (4-methylaniline) was 2.74 times that of phenol on ODS using pure water as the mobile phase. It should be noted that 4-ethylaniline is silanophilic, but if it had been strongly retained by the silanols, the peak would have been more tailed and the model would then have predicted a low capacity rather than the higher capacity observed. Finally, 9-anthracenecarboxylate has an adsorption site density of only 0.25 μmol/m^2. Such low capacities are typical of ionized solutes[20].

Thus, the behavior of the adsorption site density, and therefore K, derived from the kinetic model, is consistent with previous observations and rational expectations.

CONCLUSIONS

A good fit between a non-linear chromatographic model and experimental overloaded peaks cannot be used as the sole criterion of a model's validity. The kinetic, Houghton equilibrium-dispersive and Haarhoff–Van der Linde models all precisely reproduce the peak shapes observed under low to moderate overload conditions. However for all of the models the parameter which describes the peak width under linear chromatographic conditions, and thus should be independent of solute concentration, was found to vary several fold as the extent of column overload was increased. Since the models were derived using distinctly different assumptions, it is believed that this parameter variation results from a physical band broadening process intrinsic to the overloading of the column. The origin of this additional band broadening process is as yet unknown, but is a question which warrants further investigation.

Another conclusion from this work is that the isotherm parameter of the equilibrium-dispersive and Haarhoff–Van der Linde model lacks physical significance as the result of the intrinsic assumption of an unrealistic isotherm. The former model also is affected by the effects of a mathematic failure to conserve mass. The isotherm parameter of the kinetic model, and the associated adsorption site density, do appear to have physical significance. The adsorption site density derived from this model does not vary with solute concentration, when the skew due to column overload is significant. Also, the variation of the site density with mobile phase and solute is consistent with results from traditional breakthrough studies. These results indicate that the kinetic model may be a convenient method of studying factors affecting the capacity of high-performance liquid chromatography packings. Studies such as those described here are much faster than breakthrough curve studies and provide more detailed information at the cost of some computational complexity.

Finally, we believe that the data indicate there is, at present, no model which incorporates all of the important events involved in retention in reversed-phase LC.

ACKNOWLEDGEMENTS

This work was supported in part by grants from the Institute for Advanced Studies in Biological Process Technology, University of Minnesota, and the 3M Company. Charles Lucy was supported by a fellowship from the Natural Science and Engineering Research Council of Canada. We also would like to thank Professor Abraham Lenhoff for his comments during the course of this work.

REFERENCES

1 S. Golshan-Shirazi and G. Guiochon, *Anal. Chem.*, 61 (1989) 462.
2 J. L. Wade, A. F. Bergold and P. W. Carr, *Anal. Chem.*, 59 (1987) 1286.
3 H. C. Thomas, *J. Am. Chem. Soc.*, 66 (1944) 1664.
4 G. Houghton, *J. Phys. Chem.*, 67 (1963) 84.
5 A. Jaulmes, C. Vidal-Madjar, H. Colin and G. Guiochon, *J. Phys. Chem.*, 90 (1986) 207.
6 P. C. Haarhoff and H. J. van der Linde, *Anal. Chem.*, 38 (1966) 573.

7 G. Cretier and J. L. Rocca, *Chromatographia*, 18 (1984) 623.
8 J. L. Wade and P. W. Carr, *J. Phys. Chem.*, submitted for publication.
9 J. C. Giddings, *Dynamics of Chromatography*, Part I, Marcel Dekker, New York, 1965.
10 N. K. Hiester and T. Vermeulen, *Chem. Eng. Prog.*, 48 (1952) 505.
11 M.-S. Razavi, B. J. McCoy and R. G. Carbonell, *Chem. Eng. J.*, 16 (1978) 211.
12 J. B. Rosen, *J. Phys. Chem.*, 20 (1952) 387.
13 R. S. Cooper and D. A. Liberman, *Ind. Eng. Chem. Fundam.*, 9 (1970) 620.
14 R. S. Cooper, *Ind. Eng. Chem. Fundam.*, 4 (1965) 308.
15 K. R. Hall, A. Acrivos, L. C. Eagleton an T. Vermeulen, *Ind. Eng. Chem. Fundam.*, 5 (1966) 212.
16 H. Poppe and J. C. Kraak, *J. Chromatogr.*, 255 (1983) 395.
17 J. C. Giddings and H. Eyring, *J. Phys. Chem.*, 59 (1955) 416.
18 J. L. Wade, *Ph.D. Thesis*, University of Minnesota, Minneapolis, MN, 1988.
19 A. Jaulmes, M. J. Gonzalez, C. Vidal-Madjar and G. Guiochon, *J. Chromatogr.*, 387 (1987) 41.
20 J. Jacobson, J. Frenz and Cs. Horváth, *J. Chromatogr.*, 316 (1984) 53.
21 A. W. J. de Jong, J. C. Kraak, H. Poppe and F. Nooitgedacht, *J. Chromatogr.*, 193 (1980) 181.
22 C. Dewaele, M. de Coninck and M. Verzele, *Sep. Sci. Technol.*, 22 (1987) 1919.
23 C. A. Lucy and P. W. Carr, in preparation.
24 K. K. Unger, J. N. Kinkel, B. Anspach and H. Giesche, *J. Chromatogr.*, 296 (1984) 3.
25 J. E. Eble, R. L. Grob, P. E. Antle and L. R. Snyder, *J. Chromatogr.*, 405 (1987) 31.
26 J. E. Eble, R. L. Grob, P. E. Antle and L. R. Snyder, *J. Chromatogr.*, 384 (1987) 45.
27 R. M. McCormick and B. L. Karger, *Anal. Chem.*, 52 (1980) 2249.
28 R. K. Gilpin, *J. Chromatogr. Sci.*, 22 (1984) 371.

Journal of Chromatography, 484 (1989) 83–102
Elsevier Science Publishers B.V., Amsterdam — Printed in The Netherlands

CHROM. 21 519

INFLUENCE OF CALCULATION ERRORS IN THE NUMERICAL SIMULATION OF CHROMATOGRAPHIC ELUTION BAND PROFILES USING AN IDEAL OR SEMI-IDEAL MODEL

BINGCHANG LIN, ZIDU MA and GEORGES GUIOCHON*

**Department of Chemistry, University of Tennessee, Knoxville, TN 37996-1600, and Division of Analytical Chemistry, Oak Ridge National Laboratory, Oak Ridge, TN 37831-6120 (U.S.A.)*

SUMMARY

The theoretical models of chromatography, whether they assume or not quasi-equilibrium between the phases of the chromatographic system, lead to a set of partial differential equations that cannot be integrated but must be solved by numerical calculations. This procedure leads to computational errors. An analysis of the origin and importance of these errors is presented. A comparison is made between the errors introduced by different calculation procedures (mainly the characteristic and the Lax–Wendroff methods). The concentration dependence of the artificial diffusion introduced by the characteristic algorithm is discussed.

INTRODUCTION

Much attention has been given recently to the numerical solution of the set of mass balance equations of chromatography. Preparative chromatography has become a separation and purification method of considerable importance in the pharmaceutical industries. The operation of preparative chromatographs must be carried out at high feed concentrations in order to achieve economical production. The prediction of the column performance and the optimization of the experimental conditions require a knowledge of the breakthrough curves for different injection conditions, corresponding to elution, frontal analysis or displacement, for samples of various composition.

The only possibility for calculating these band profiles is by solving one of the relevant models of chromatography. The main feature of these models is the set of mass balance equations for the various compounds involved in the problem, the components of either the feed or the mobile phase. We can eliminate only the weakest solvent mass balance, by assuming that this solvent does not interact with the stationary phase, which sets a reference convention. The set of these mass balance equations must be completed by equations relating the concentrations of each component in the two phases of the chromatographic system at each time.

In most instances, we can assume that we are near equilibrium, *i.e.*, that the column efficiency is high, and we can replace the diffusive term of the mass balance

0021-9673/89/$03.50

equations by a term that accounts for the rapid kinetics of radial mass transfer in modern columns[1–3]. In some rare instances, kinetic equations must be used[4–6]. These equations relate the time differential of the concentration of each compound involved in the stationary phase to the concentration of this component in the stationary phase and to the concentrations of all the compounds involved in the mobile phase, in a given slice of column. The former models are called equilibrium or ideal models (if the column efficiency is infinite and equilibrium between both phases of the chromatographic system always takes place) or semi-ideal models (if equilibrium is not achieved but the deviation from equilibrium remains small, *e.g.*, the column efficiency exceeds a few hundred theoretical plates). The latter models are called kinetic models. This paper is mainly concerned with semi-ideal models.

The mass balance equation obtained for a pure compound is a partial differential equation that cannot be solved analytically and for which numerical solutions must be calculated. The numerical integration of a partial differential equation always introduces truncation errors because finite increments of the variable must be considered. As a huge number of loops must be circled during the integration, the errors made during the numerical calculation propagate and accumulate from one stage to the next. In some instances these errors have most undesirable consequences, as they lead to numerical instability of the solution, and must be avoided. In other instances they may be used to advantage. In this paper, we present an analysis of the nature and extent of these errors, with emphasis on those resulting from the characteristic and the Lax–Wendroff algorithms.

In a previous paper[7] we showed that, for a linear equilibrium isotherm between the two phases of a chromatographic system, the truncation error introduced by using the first-order characteristic type calculation scheme for the numerical integration of the partial differential equation has the same effect as a dispersion term on the band profile. If proper values are chosen for the space and time increments, this artificial dispersion term permits a successful account of the effect on the band profile of a finite column efficiency. With a non-linear isotherm, however, the artificial dispersion effect is different from that with a linear isotherm and the consequences are analyzed below.

The investigation of the elution band profile of a pure compound is interesting as a necessary step in the study of the chromatographic separation of complex mixtures. In itself, however, it does not provide much useful information. As chromatography is a separation method, the elution of a binary mixture should be investigated. For the more practical and relevant discussion of the calculation of elution profiles of multicomponent samples, the use of the artificial dispersion introduced by the finite difference method and the characteristic algorithm is not suitable, in principle. In practice, it is acceptable only when the relative retention of the compounds considered is close to unity. The basic reason for the method being unsuitable is that the artificial dispersion it introduces depends on the slope of the isotherm. The simulation of the elution profiles of different compounds for which the column has the same efficiency requires different values of the space and time increments for the different compounds, a procedure which is at best complicated and impractical.

For this reason, considerable difficulties are encountered when trying to extend our previous results to the simulation of non-linear chromatography in the gradient elution mode. In this particular case, a numerical procedure that is easy to implement and is accurate would be very attractive for simulating the separation of multi-

component systems. A satisfactory approach is in the use of a higher order method, *i.e.*, a method with which the truncation errors introduced by replacing the exact partial differential equation by an approximate difference algebraic equation are of second order with respect to the time and length increments.

ERROR ANALYSIS IN THE CASE OF THE CHARACTERISTIC TYPE DIFFERENCE METHOD

The ideal model of chromatography assumes constant equilibrium between the two phases and a column of infinite efficiency. Hence the diffusion term of the mass balance equation written for a pure compound in a slice of column is zero and the concentration in the stationary phase (C_s) which appears in this mass balance is replaced by the value given by the equilibrium isotherm. The mathematical model of ideal chromatography for a pure compound is

$$\left(1 + F \cdot \frac{\partial q}{\partial C}\right)\frac{\partial C}{\partial t} + u \cdot \frac{\partial C}{\partial z} = 0 \tag{1}$$

The isotherm is an equation [$C_s = q = f(C_m)$] which relates the concentrations at equilibrium in the mobile (C_m) and the stationary phases. In eqn. 1, F is the phase ratio of the chromatographic column, u the cross-section average velocity of the mobile phase, t the time and z the abscissa along the column.

The boundary and initial conditions for the integration in the case of a rectangular pulse injection, with a concentration C_0 and a time τ, are

$$C(z = 0, t) = C_0, \qquad 0 \leqslant t \leqslant \tau \tag{2}$$

and

$$C(z = 0, t) = 0, \qquad t > \tau$$

with

$$C(z, t = 0) = 0 \tag{3}$$

Eqn. 1 is not the canonical form of this type of partial differential eqn. 2 (ref. 8). It is frequently encountered in aerodynamics and hydraulics, where it is discussed by mechanical engineers in the form

$$\frac{\partial C}{\partial z} + B \cdot \frac{\partial H}{\partial t} = 0 \tag{4}$$

where

$$B = \frac{1}{u} \tag{5}$$

and

$$H = C + Fq \tag{6}$$

In the general case, there is no analytical solution known for eqn. 1. When solutions are needed, they must be calculated.

The principle of the calculation of numerical solutions of eqn. 1 is to replace the continuous (z, t) plane by a grid and to calculate the numerical values of the concentration C of the compound studied in the mobile phase at each point (n, j) of this grid. The space and time increments of the grid are h and τ, respectively. The injection profile is discretized. Then, for each time $t = j\tau$, the concentration at each point in the column, $z = nh$, $0 < n < L/h$, is calculated from the similar profile, $C(n, j)$, obtained at the previous instant, $t = (j - 1)\tau$ and from the initial and boundary conditions. The set of values of the concentration for $z = L$ (L = length of the column) for each time frame constitutes the elution chromatogram. In this paper, we discuss two numerical schemes for the numerical calculation of profiles which are solutions of eqn. 1. The first type has been used for writing the computer program we have developed and used for the calculation of the elution band profiles of pure compounds[3,7,8], binary mixtures[9] or system peaks[10] and of the profiles of displacement bands[11].

First difference type

In the calculation procedure described above, eqn. 1 is replaced by the following algebraic equation, which is its finite difference equivalent:

$$\frac{C_j^{n+1} - C_j^n}{h} + \frac{1}{u} \cdot \frac{C_j^n - C_{j-1}^n}{\tau} + \frac{F}{u} \cdot \frac{q_j^n - q_{j-1}^n}{\tau} = 0 \tag{7}$$

Eqns. 1 and 7 would be entirely equivalent only if the increments, h and τ, could be made zero, which, in turn, would require an infinite computation time, not a realistic proposition. As the increments must be finite, a numerical error results from the replacement of eqn. 1 by eqn. 7. During the calculation process, these errors propagate and build up. If the values of the space and time increments are not properly chosen, divergence and oscillations may occur and the numerical solution does not bear any resemblance to the exact solution of the partial differential equation studied. The stability condition for this method, in the ideal approximation, is

$$\frac{h}{u_z \tau} < 1 \tag{8}$$

where u_z is given by eqn. 16b (see below)[2,7]. This condition is called the Courant condition of the problem and $u_z\tau/h$ is its Courant number. It has been demonstrated that, when h and τ satisfy it, the numerical solution obtained converges towards the exact solution of the partial differential equation with decreasing increment values[2].

In order to calculate the error made by replacing eqn. 1 by eqn. 7 in the calculation of the elution band profile, we may replace the different concentration terms by their three-term expansion:

$$C_j^{n+1} = C_j^n + h\left(\frac{\partial C}{\partial z}\right)_j^n + \frac{h^2}{2}\left(\frac{\partial^2 C}{\partial z^2}\right)_j^n \tag{9}$$

and

$$C_{j-1}^n = C_j^n - \tau\left(\frac{\partial C}{\partial t}\right)_j^n + \frac{\tau^2}{2}\left(\frac{\partial^2 C}{\partial t^2}\right)_j^n \tag{10}$$

We shall assume here that the equilibrium isotherm is given by the classical Langmuir equation, although most of the conclusions are valid with other equilibrium equations. With a Langmuir isotherm we have

$$q_j^n = f(C_j^n) = \frac{GC_j^n}{1 + bC_j^n} \tag{11}$$

where G and b are constants. Therefore,

$$q_{j-1}^n = \frac{GC_{j-1}^n}{1 + bC_{j-1}^n} \tag{12}$$

The three difference terms in eqn. 7 become

$$\frac{C_j^{n+1} - C_j^n}{h} = \left(\frac{\partial C}{\partial z}\right)_j^n + \frac{h}{2}\left(\frac{\partial^2 C}{\partial z^2}\right)_j^n \tag{13}$$

$$\frac{C_j^n - C_{j-1}^n}{\tau} = \left(\frac{\partial C}{\partial t}\right)_j^n - \frac{\tau}{2}\left(\frac{\partial^2 C}{\partial t^2}\right)_j^n \tag{14}$$

and

$$F \cdot \frac{q_j^n - q_{j-1}^n}{\tau} = \frac{FG(C_j^n - C_{j-1}^n)}{(1 + bC_{j-1}^n)(1 + bC_j^n)\tau} \tag{15a}$$

which is equivalent to

$$F \cdot \frac{q_j^n - q_{j-1}^n}{\tau} \approx \frac{FG(C_j^n - C_{j-1}^n)}{(1 + bC_j^n)^2\tau} = F\left(\frac{\partial f}{\partial C}\right)_j^n\left[\left(\frac{\partial C}{\partial t}\right)_j^n - \frac{\tau}{2}\left(\frac{\partial^2 C}{\partial t^2}\right)_j^n\right] \tag{15b}$$

Combining eqn. 7 with eqns. 9–15 gives

$$\left(1 + F \cdot \frac{\partial f}{\partial C}\right)\frac{\partial C}{\partial t} + u \cdot \frac{\partial C}{\partial z} = \frac{\tau}{2}\left(1 + F \cdot \frac{\partial f}{\partial C}\right)\frac{\partial^2 C}{\partial t^2} - \frac{hu}{2}\left(\frac{\partial^2 C}{\partial z^2}\right) \tag{16}$$

From eqn. 1 we can derive a relationship giving the velocity, u_z. associated with a concentration[8]:

$$\frac{\partial C}{\partial t} = -u_z \cdot \frac{\partial C}{\partial z} \tag{17a}$$

with

$$u_z = \frac{u}{1 + F \cdot \dfrac{\partial f}{\partial C}} \tag{17b}$$

From eqns. 17a and 17b we obtain

$$\frac{\partial^2 C}{\partial t^2} = \frac{\partial}{\partial t}\left(-u_z \frac{\partial C}{\partial z}\right) = -\frac{F u_z^2}{1 + F \cdot \dfrac{\partial f}{\partial C}} \cdot \frac{\partial^2 f}{\partial C^2}\left(\frac{\partial C}{\partial z}\right)^2 + u_z^2 \cdot \frac{\partial^2 C}{\partial z^2} \tag{18}$$

Substituting eqn. 18 into eqn. 16 permits the determination of the error made in the calculation of the profile when using eqn. 7. We have

$$\left(1 + F \cdot \frac{\partial f}{\partial C}\right)\frac{\partial C}{\partial t} + u \cdot \frac{\partial C}{\partial z} = \frac{hu}{2}(a - 1)\frac{\partial^2 C}{\partial z^2} - \frac{\tau}{2} \cdot u^2 F \cdot \frac{\partial^2 f}{\partial C^2}\left(\frac{\partial C}{\partial z}\right)^2 \Bigg/ \left(1 + F \cdot \frac{\partial f}{\partial C}\right)^2 \tag{19}$$

where a is the Courant number $[u_z\tau/h = u\tau/(1 + k'_0)h]$, which we have taken as equal to 2, by selecting properly the time increment, τ, as a function of the space increment[3,7,9]. The choice of a Courant number of 2 ensures numerical stability of the calculated solution (eqn. 16), *i.e.*, avoids widely oscillating profiles with negative values of the concentration, results which have no physical sense.

The right-hand side of eqn. 19 represents the error made. This error is of first order with respect to h and τ [*i.e.*, $O(h + \tau)$]. It is the sum of two terms, the first being a dispersion term, proportional to the space increment, h, and the second, proportional to the time increment, τ, being non-linear. It vanishes when $\tau \to 0$ or when $\partial^2 f/\partial C^2 \to 0$. In the case of a Langmuir isotherm, $\partial^2 f/\partial C^2 = -2Gb/(1 + bC)^3$, and is never zero. $\partial^2 f/\partial C^2$ can be zero only for a linear isotherm. The sign of this second term is determined by the curvature of the isotherm.

In the case of a Langmuir isotherm, or of an isotherm convex towards the axis of stationary phase concentrations, the profile predicted by the ideal model exhibits a front shock[2,3,8]. The second differential of the isotherm is negative and the two terms add to each other. The effect of the error is in the appearance of a dispersion term, the replacement of the concentration discontinuity by a shock layer, with a finite thickness and a decrease in the shock amplitude. If the isotherm is concave, in contrast, the shock appears on the rear of the profile, but the qualitative influence of the numerical errors remains the same.

Second difference type

An alternative form of the general equation of the ideal (equilibrium) model of chromatography, equivalent to eqn. 1, is the following:

$$\frac{\partial C}{\partial t} + F \cdot \frac{\partial q}{\partial t} + u \cdot \frac{\partial C}{\partial z} = 0 \tag{20}$$

In this case, the equivalent finite difference equation is written as

$$\frac{C_j^{n+1} - C_j^n}{\tau} + F \cdot \frac{q_j^{n+1} - q_j^n}{\tau} + u \cdot \frac{C_j^{n+1} - C_{j-1}^{n+1}}{h} = 0 \tag{21}$$

In eqn. 20, n is the time index and j is the space index. For this type of finite difference equation, the Courant condition (see above), in the ideal approximation, is $u_z\tau/h > 0$. It is, of course, always satisfied. Expansion of the different terms gives

$$C_j^{n+1} = C_j^n + \tau\left(\frac{\partial C}{\partial t}\right)_j^n + \frac{\tau^2}{2}\left(\frac{\partial^2 C}{\partial t^2}\right)_j^n \tag{22}$$

and

$$C_{j-1}^{n+1} = C_j^n + \tau\left(\frac{\partial C}{\partial t}\right)_j^n - h\left(\frac{\partial C}{\partial z}\right)_j^n + \frac{\tau^2}{2}\left(\frac{\partial^2 C}{\partial t^2}\right)_j^n + \frac{h^2}{2}\left(\frac{\partial^2 C}{\partial z^2}\right)_j^n - \tau h\left(\frac{\partial^2 C}{\partial z \partial t}\right)_j^n \tag{23}$$

The equilibrium isotherm is again given by eqn. 12 (Langmuir isotherm). In a practical calculation, we could use the following approximation:

$$q_j^{n+1} \approx \frac{GC_j^{n+1}}{1 + bC_j^n} \tag{24}$$

Combining eqns. 22–24 gives the second term of eqn. 21:

$$\frac{q_j^{n+1} - q_j^n}{\tau} = \frac{1}{\tau} \cdot \frac{G(C_j^{n+1} - C_j^n)}{1 + bC_j^n} = \frac{1}{\tau} \cdot \frac{G(C_j^{n+1} - C_j^n)}{(1 + bC_j^n)^2}(1 + bC_j^n)$$

$$= \left[\left(\frac{\partial f}{\partial C}\right)\left(\frac{\partial C}{\partial t} + \frac{\tau}{2} \cdot \frac{\partial^2 C}{\partial t^2}\right)(1 + bC)\right]_j^n \tag{25}$$

By combining eqns. 21 with eqns. 22–25, we obtain

$$\left(1 + F \cdot \frac{\partial f}{\partial C}\right)\frac{\partial C}{\partial t} + u \cdot \frac{\partial C}{\partial z} =$$

$$-\frac{\tau}{2}\left(1 + F \cdot \frac{\partial f}{\partial C}\right)\frac{\partial^2 C}{\partial t^2} + \frac{hu}{2} \cdot \frac{\partial^2 C}{\partial z^2} - \tau u \cdot \frac{\partial^2 C}{\partial z \partial t} - FbC \cdot \frac{\partial f}{\partial C}\left(\frac{\partial C}{\partial t} + \frac{\tau}{2} \cdot \frac{\partial^2 C}{\partial t^2}\right) \tag{26}$$

From eqn. 17, we can derive that

$$\frac{\partial^2 C}{\partial z \partial t} = \frac{u_z}{1 + F \cdot \dfrac{\partial f}{\partial C}} \cdot F \cdot \frac{\partial^2 f}{\partial C^2}\left(\frac{\partial C}{\partial z}\right)^2 - u_z \cdot \frac{\partial^2 C}{\partial z^2} \tag{27}$$

Combination of eqns. 18, 26 and 27 gives

$$\left(1 + F\cdot\frac{\partial f}{\partial C}\right)\frac{\partial C}{\partial t} + u\cdot\frac{\partial C}{\partial z} = -FbC\cdot\frac{\partial f}{\partial C}\cdot\frac{\partial C}{\partial t} + \frac{hu}{2}(a+1)\frac{\partial^2 C}{\partial z^2} -$$

$$\frac{\tau}{2}\left\{Fu_z^2\cdot\frac{\partial^2 f}{\partial C^2}\left(\frac{\partial C}{\partial z}\right)^2 - FbC\cdot\frac{\partial f}{\partial C}\left[u_z\cdot\frac{\partial^2 C}{\partial z^2} - \frac{Fu_z^2}{1 + F\cdot\dfrac{\partial f}{\partial C}}\left(\frac{\partial^2 f}{\partial C^2}\right)\left(\frac{\partial C}{\partial z}\right)^2\right]\right\} \qquad (28)$$

The essential difference between the equation derived in the case of a linear isotherm and eqn. 28 is in the first term of the right-hand side, equal to $-FbC\partial f/\partial C\cdot\partial C/\partial t$, *i.e.*, to $k'bC\partial C/\partial t$. This term is independent of the value of the integration increments. The error cannot be made infinitely small by increasing the computer time: the solution converges towards a solution of the top part of eqn. 28, *i.e.*, without the lower term, proportional to τ, which is not eqn. 20. Actually, the term which contains FbC comes from the approximation made above (see eqn. 24). The error is complex and the numerical solution obtained by this method cannot be trusted entirely. Of course, in the linear case the coefficient b is zero.

If an approximation other than eqn. 24 is taken for q_j^{n+1}, *e.g.*, $q_j^{n+1} \approx GC_{j-1}^{n+1}/(1 + bC_{j-1}^{n+1})$, the term which contains FbC can also be eliminated, and the results may be better.

This analysis illustrates the difficulties and pitfalls which may be encountered in non-linear chromatography when a numerical algorithm is not very carefully studied before it is implemented.

Comparison between the two difference types

If the non-linear contribution can be ignored (small deviation from the linear isotherm), the apparent dispersion coefficient in the case of the first difference type studied becomes

$$D_a = \frac{hu}{2}\left[\frac{\tau u}{(1 + k')h} + 1\right] \qquad (29)$$

and in the case of the second difference type

$$D_a = \frac{hu}{2}\left[\frac{\tau u}{(1 + k')h} - 1\right] \qquad (30)$$

In practice, we want to use the apparent diffusion coefficient, D_a, to account for the diffusion term, D, which we neglected when we replaced the exact mass balance equation by the equation of the ideal model (eqns. 1 and 20). In fact, D_a could be used to simulate the finite column efficiency. Then it is necessary to keep the apparent dispersion coefficient constant during the entire calculation. The Courant number will be kept constant, hence we must have

$$\frac{\tau u}{\left(1 + F\cdot\dfrac{\partial f}{\partial C}\right)h} = \text{constant} \qquad (31)$$

If one takes, for the sake of simplicity and clarity, the space increment to be equal to the column height equivalent to a theoretical plate ($h = H$), the time increment is given by

$$\tau = \text{constant} \cdot (1 + k')\frac{H}{u} \tag{32}$$

In all our calculations[3,7–10], we have taken the Courant number as equal to 2, hence

$$\tau = \frac{2\left(1 + F \cdot \frac{\partial f}{\partial C}\right)H}{u} \tag{33}$$

Our first requirement is the numerical stability of the solution. This does not require that we keep the Courant number constant, but merely that we make sure that it exceeds unity[7]. One simple way to satisfy this condition, in the case of a Langmuir-type isotherm, would be to take τ equal to $2(1 + k'_0)h/u$, where k'_0 is the limit value of $\partial f/\partial C$ for an infinitely small sample. However, then the apparent diffusion coefficient increases during the elution of the band (see eqn. 29). If we adopt a variable time increment, $\tau = \tau(C)$, the error term introduced will have certain effects on the results of the simulation of the migration of the chromatographic band. Comparison between the exact analytical solution of eqn. 1 in the case of a Langmuir isotherm and the numerical solution obtained with the first difference type shows, however, that the difference between the two profiles, *i.e.*, the error introduced by the numerical calculation and accounted for by eqn. 19, is small and cannot be very different from that predicted by eqn. 29 with a constant value of the Courant number[12].

In the case of the first difference type, the error contains two terms (eqn. 19). The first one is the artificial dispersion term just discussed. The second one is smaller but, in the case of a Langmuir type isotherm, it tends to enhance the self-sharpening effect of the band due to the non-linear behavior of the equilibrium isotherm and to the strong concentration dependence of the velocity associated with a concentration u_z.

The second difference method should be avoided because of the presence of a constant term in its error function, a term which is independent of the integration increments.

ERROR ANALYSIS IN THE CASE OF THE LAX–WENDROFF TYPE DIFFERENCE METHOD

The kinetic model for non-linear chromatography is more general than either the ideal or the semi-ideal models, which postulate near equilibrium between the two phases at any time and any location in the column. The only assumption made in this model is in the choice of the kinetic equation which relates the rate of change of the concentration in the stationary phase to the concentrations of the compound under study in both phases. In one of its simplest forms, the kinetic model can be written as

$$\frac{\partial C}{\partial t} + F \cdot \frac{\partial q}{\partial t} + u \cdot \frac{\partial C}{\partial z} = D \cdot \frac{\partial^2 C}{\partial z^2} \tag{34}$$

$$\frac{\partial q}{\partial t} = K[f(C) - q] \tag{35}$$

Eqn. 34 is the general mass balance of chromatography. Eqn. 35 is the kinetic model. In this equation, K is the rate constant or mass transfer coefficient and q is the concentration of the compound of interest in the stationary phase. First-order kinetics have been selected here. The classical initial and boundary conditions are written as

$$\begin{aligned} &C(z = 0, t) = C_0, \qquad 0 \leqslant t \leqslant \tau \\ &C(z = 0, t) = 0, \qquad t > \tau \\ &C(z, t = 0) = 0 \qquad q(z, t = 0) = 0 \end{aligned} \tag{36}$$

There is no analytical solution for this system of equations, although Goldstein[13] and Wade *et al.*[14] derived an analytical solution in the closely related case when the kinetic equation is that of the classical Langmuir adsorption–desorption kinetics. Numerical solutions must be calculated, and the best approach seems to be the Lax–Wendroff method[15,16]. Two cases can be distinguished, depending whether the problem discussed involves a near-equilibrium model (*i.e.*, fast kinetics of mass transfer between phases, so the number of transfer stages in the column is large[6]) or a true kinetic problem, in which case the mass transfers between phases are slow.

NEAR EQUILIBRIUM PROBLEM

Under the equilibrium approximation, the system of eqns. 33 and 34 can be replaced by a single partial differential equation[17], which is written as

$$\frac{\partial C}{\partial t} + u_z \cdot \frac{\partial C}{\partial z} = D_z \cdot \frac{\partial^2 C}{\partial x^2} \tag{37}$$

where D_z stands for $D/(1 + F \cdot \partial f/\partial C)$. The corresponding finite difference equation is

$$\frac{C_j^{n+1} - C_j^n}{\tau} + u_z \cdot \frac{C_{j+1}^n - C_{j-1}^n}{2h} - \left(\frac{u_z^2 \tau}{2h^2} + \frac{D_z}{h^2}\right)(C_{j+1}^n - 2C_j^n + C_{j-1}^n) = 0 \tag{38}$$

where n is the time index and j the space index. For this method, the stability condition is $(u_z\tau/h)^2 + 2D_z\tau/h^2 < 1$ (ref. 16).

In order to calculate the truncation error introduced by the Lax–Wendroff procedure in the near equilibrium case, we write as follows the four-term expansion of the higher order terms in eqns. 34 and 35, at the index values n and j:

$$C_j^{n+1} = C_j^n + \tau\left(\frac{\partial C}{\partial t}\right)_j^n + \frac{\tau^2}{2}\left(\frac{\partial^2 C}{\partial t^2}\right)_j^n + \frac{\tau^3}{6}\left(\frac{\partial^3 C}{\partial t^3}\right)_j^n \tag{39}$$

$$C_{j+1}^n = C_j^n + h\left(\frac{\partial C}{\partial z}\right)_j^n + \frac{h^2}{2}\left(\frac{\partial^2 C}{\partial z^2}\right)_j^n + \frac{h^3}{6}\left(\frac{\partial^3 C}{\partial z^3}\right)_j^n \tag{40}$$

and

$$C_{j-1}^n = C_j^n - h\left(\frac{\partial C}{\partial z}\right)_j^n + \frac{h^2}{2}\left(\frac{\partial^2 C}{\partial z^2}\right)_j^n - \frac{h^3}{6}\left(\frac{\partial^3 C}{\partial z^3}\right)_j^n \tag{41}$$

In the ideal approximation, we have (see above)

$$\frac{\partial}{\partial t} = -u_z \cdot \frac{\partial}{\partial z} \tag{42}$$

and

$$\frac{\partial^2}{\partial t^2} = u_z^2 \cdot \frac{\partial^2}{\partial z^2} \tag{43}$$

Combining eqns. 38–43 gives

$$\left(\frac{\partial C}{\partial t}\right)_j^n + u_z\left(\frac{\partial C}{\partial z}\right)_j^n - D\left(\frac{\partial^2 C}{\partial z^2}\right)_j^n = \frac{u_z}{6}\left[(u_z\tau)^2 - h^2\right]\left(\frac{\partial^3 C}{\partial z^3}\right)_j^n \tag{44}$$

an equation which is equivalent to

$$\left(1 + F \cdot \frac{\partial f}{\partial C}\right)\left(\frac{\partial C}{\partial t}\right)_j^n + u\left(\frac{\partial C}{\partial z}\right)_j^n - D\left(\frac{\partial^2 C}{\partial z^2}\right)_j^n = \frac{u}{6}\left[(u_z\tau)^2 - h^2\right]\left(\frac{\partial^3 C}{\partial z^3}\right)_j^n \tag{44a}$$

This relationship shows that the truncation error caused by the use of the Lax–Wendroff calculation procedure under equilibrium conditions, in the linear approximation, and by the replacement of eqn. 34 by eqn. 36 for the numerical calculation is equal to

$$\frac{u}{6}[(u_z\tau)^2 - h^2]\frac{\partial^3 C}{\partial z^3} \tag{45}$$

The truncation error introduced by the Lax–Wendroff method is of second order, *i.e.*, $O(h^2 + \tau^2)$. Furthermore, no artificial dispersion term is introduced in the calculation.

If we assume the elution band to be a near Gaussian profile, we can fit the upper part of the peak (most of the portion above the inflection points) on a polynomial, *i.e.*, $C(z, t) = \sum_i a_i C^i$. If the profile is Gaussian, a parabola would suffice[18] and the term in eqn. 44 is zero. If the profile is unsymmetrical, a third-degree polynomial, or a polynomial with a very small fourth-degree term, gives satisfactory results, hence, $\partial^3 C/\partial z^3 \approx a_3 + a_4 z \approx a_3$. The last term in eqn. 44 contains a constant, whose effect is to change the position of the solution, that is, to change the solution from $C(z, t)$ to $C(z, z - \alpha t)$, where α is the product of the coefficient of eqn. 44 and a_3.

If we compare eqns. 28 and 44, we see that, whereas the truncation error introduced by the characteristic scheme is of second order with respect to h and τ, with

the Lax–Wendroff scheme the truncation error is only of the third order. The main effect of the former is to disperse the band, and in most instances to act mainly as an apparent diffusion term. In the latter instance, the effect is essentially a shift in the peak position.

Non-equilibrium problem

In this instance, the system of partial differential eqns. 34 and 35 is replaced by the following system of algebraic, finite difference equations:

$$\frac{C_j^{n+1}-C_j^n}{\tau}+F\cdot\frac{q_j^{n+1}-q_j^n}{\tau}+u\cdot\frac{C_{j+1}^n-C_{j-1}^n}{2h}-\left(\frac{u_z^2\tau}{2h^2}+\frac{D_z}{h^2}\right)(C_{j+1}^n-2C_j^n+C_{j-1}^n)=0 \tag{46}$$

and

$$\frac{q_j^{n+1}-q_j^n}{\tau}=-K(q_j^n-f_j^n) \tag{47}$$

We combine now these equations with eqns. 39–41 and the equation similar to eqn. 39 which can be written for q_j^{n+1}:

$$\left(\frac{\partial C}{\partial t}\right)_j^n+F\left(\frac{\partial q}{\partial t}\right)_j^n+u\left(\frac{\partial C}{\partial z}\right)_j^n-D\left(\frac{\partial^2 C}{\partial z^2}\right)_j^n=\frac{\tau^2}{6}\left(\frac{\partial^3 C}{\partial z^3}+F\cdot\frac{\partial^3 C}{\partial t^3}\right)_j^n+$$
$$+\frac{uh^2}{6}\left(\frac{\partial^3 C}{\partial z^3}\right)_j^n+\frac{\tau}{2}\left[\left(\frac{\partial^2 C}{\partial t^2}+F\cdot\frac{\partial^2 q}{\partial t^2}\right)-u^2\cdot\frac{\partial^2 C}{\partial z^2}\right]_j^n \tag{48}$$

The numerical error contains two parts. The first part contains the first two terms of the right-hand side of eqn. 48 and is of second order $[O(h^2+\tau^2)]$. The last term of eqn. 48 is of first order in τ. Hence, in the non-equilibrium case, the Lax–Wendroff procedure introduces a first-order error. The third term of eqn. 48 is equal to

$$\frac{\tau}{2}\cdot\frac{\partial}{\partial z}[K(q-f)] \tag{49}$$

It is obvious that when the system approaches equilibrium, this last term becomes zero. An apparent diffusion term appears, much as with the characteristic procedure. There is an important difference, however. With the characteristic procedure, the apparent diffusion coefficient depends only on the integration increments and on the differential of the isotherm (eqn. 29). If a proper set of values is chosen for these increments, in order to simulate the elution profile of a band with a column having a certain finite efficiency, the apparent column efficiency for other compounds having a different retention will be fixed. This efficiency varies rapidly with the retention (*i.e.*, with k'_0). Thus, although it is possible to simulate properly the elution of a binary mixture with a relative retention close to unity, the procedure cannot be applied to multicomponent

mixtures or to gradient elution. In contrast, the use of a kinetic model and of the Lax–Wendroff calculation procedure permits the simulation of the migration of a multicomponent band in gradient elution, while keeping the column efficiency of each component constant and equal to the required value, or varying it as needed, during an experiment.

RESULTS AND DISCUSSION

Numerical simulations were performed for the different cases discussed above, varying the values of the space and time increments of the integration, in order to test the validity of our theoretical analysis of the error problem. The results of these calculations are reported in Figs. 1–12. In Fig. 1, two chromatograms are shown, calculated by integration of eqn. 1, performed using the characteristic method and two different values of the space increment, for the same value of the time increment. A linear isotherm was used. A Gaussian band profile should be obtained. This is the result given by the calculation. The effect of doubling the space increment is important and corresponds to a two-fold reduction of the apparent column efficiency. This phenomenon has been used to advantage in our recent work[3,9–12]. Fig. 2 shows the effect of the same change in the space increment when a non-linear isotherm is used,

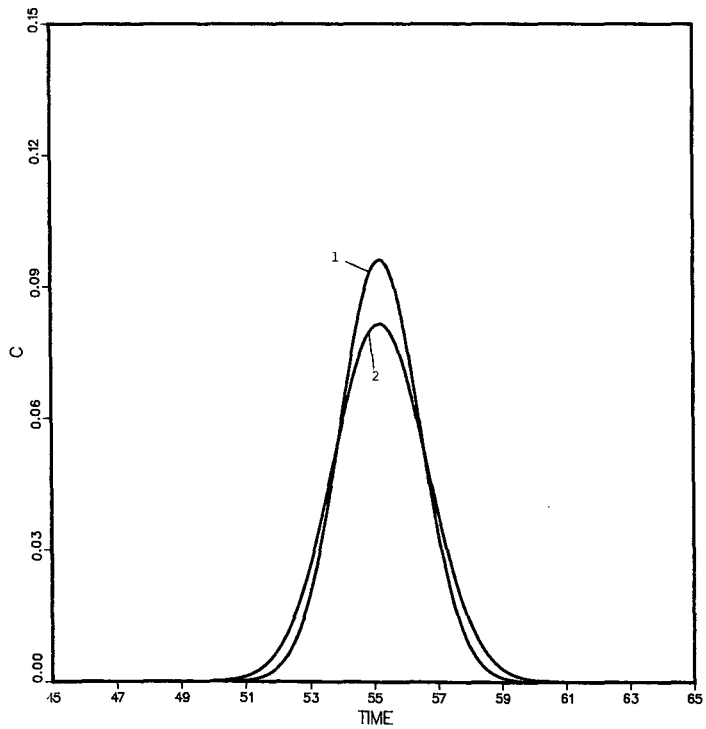

Fig. 1. Profiles obtained as solution of eqn. 1 using the characteristic method and the first type difference equation. Linear isotherm; column length, 5 cm; linear flow velocity, 0.25 cm/s; constant time increment, $\tau = 0.05$ s. Profile 1, $h = 0.0005$ cm; profile 2, $h = 0.001$ cm.

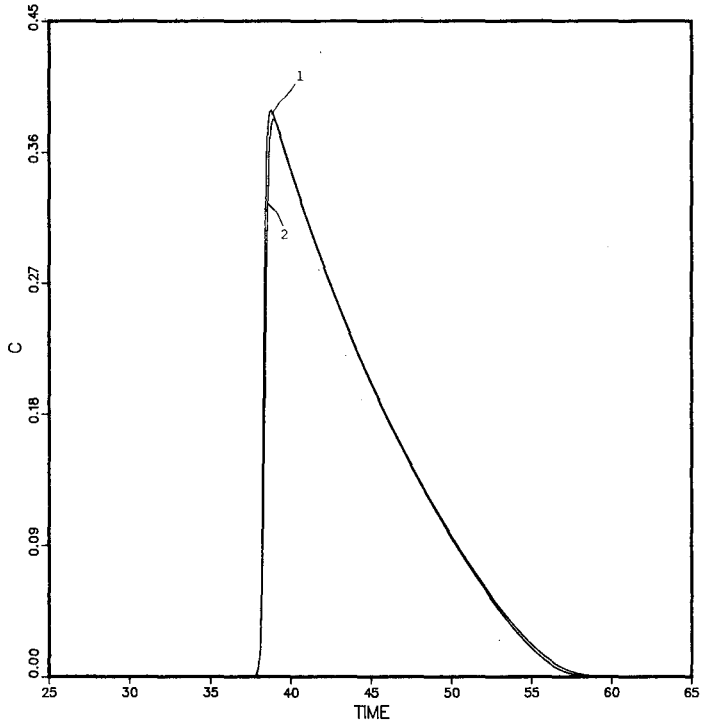

Fig. 2. Same as Fig. 1, except non-linear isotherm and sample size 100 times larger.

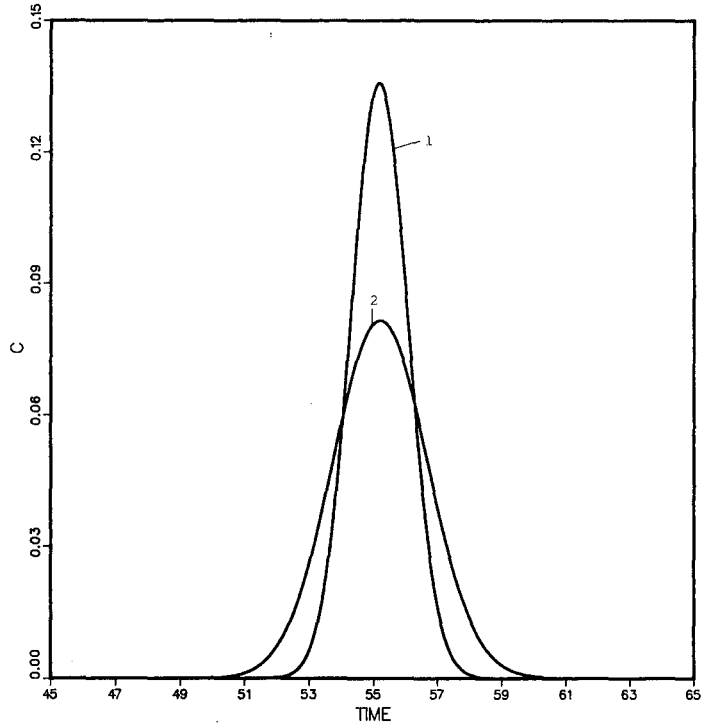

Fig. 3. Same as Fig. 1, except constant space increment, $h = 0.001$ cm. Profile 1, $\tau = 0.025$ s; profile 2, $\tau = 0.05$ s.

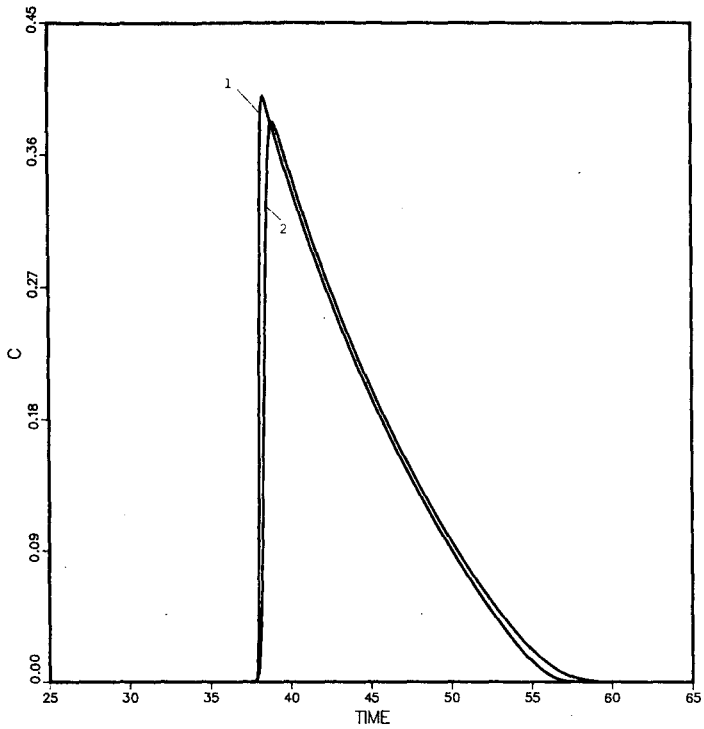

Fig. 4. Same as Fig. 3, except non-linear isotherm and sample size 100 times larger.

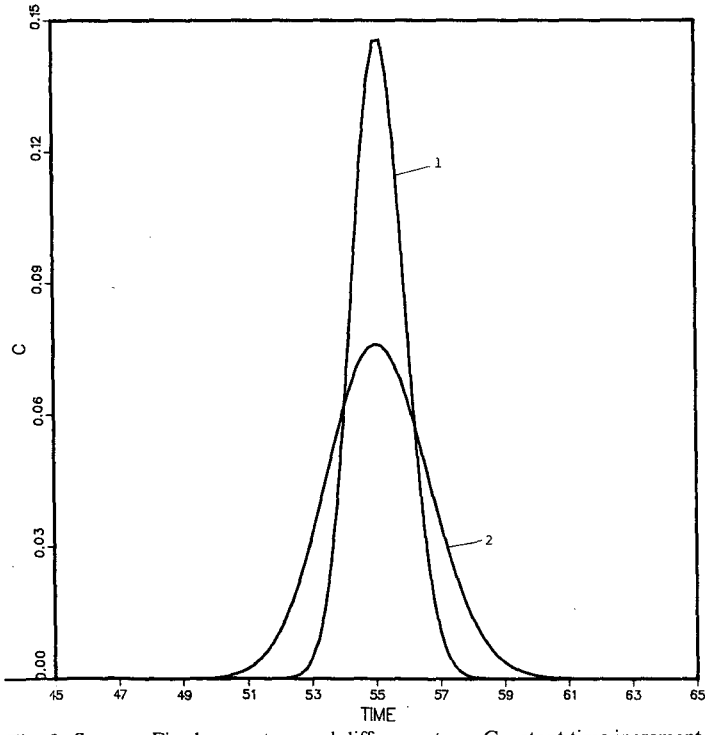

Fig. 5. Same as Fig. 1, except second difference type. Constant time increment, $\tau = 0.01$ s. Profile 1, $h = 0.0025$ cm; profile 2, $h = 0.005$ cm.

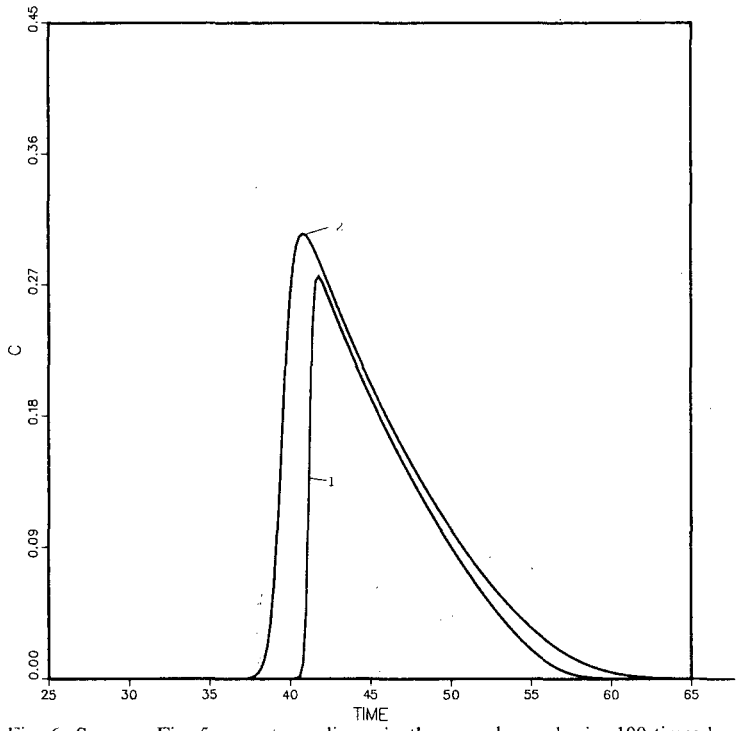

Fig. 6. Same as Fig. 5, except non-linear isotherm and sample size 100 times larger.

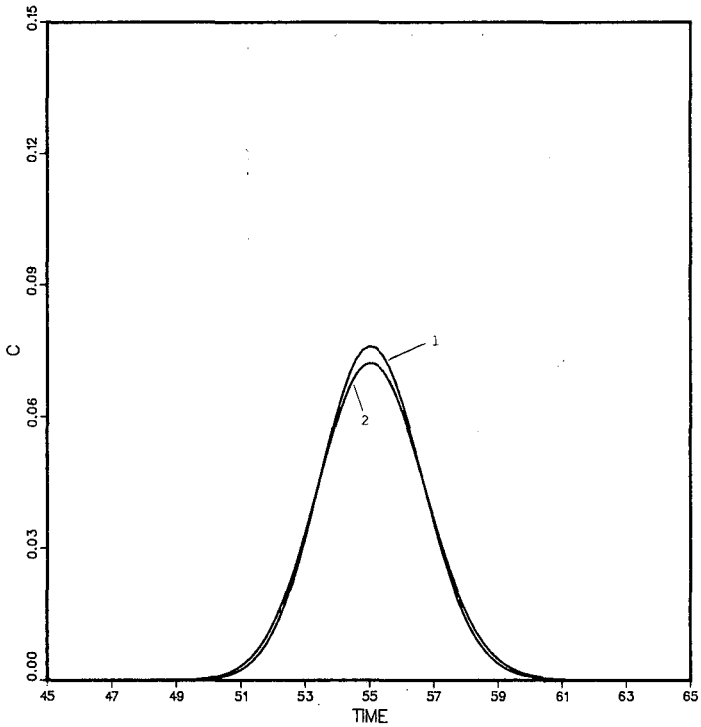

Fig. 7. Same as Fig. 5, except constant space increment, $h = 0.005$ cm. Profile 1, $\tau = 0.005$ s; profile 2, $\tau = 0.01$ s.

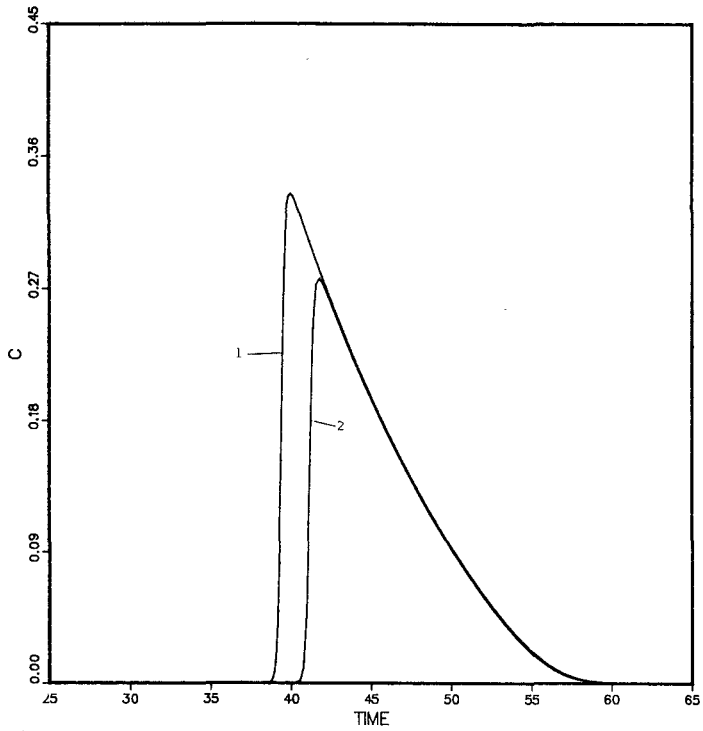

Fig. 8. Same as Fig. 7, except non-linear isotherm and sample size 100 times larger.

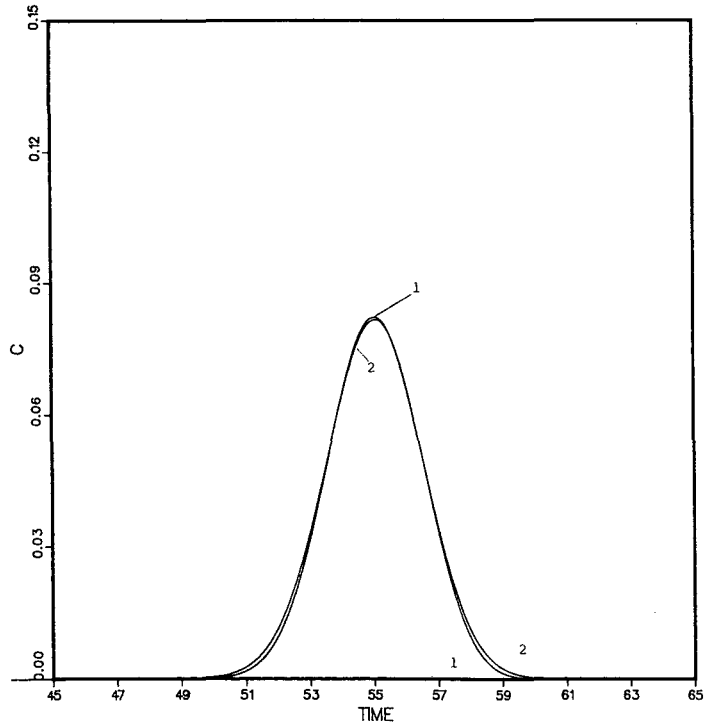

Fig. 9. Profiles obtained as solutions of eqn. 33, using the Lax–Wendroff procedure. Linear isotherm. Column length, 5 cm; linear flow velocity, 0.25 cm/s; mass transfer coefficient, $K = 60\ s^{-1}$; axial dispersion coefficient, $D = 0.00011\ cm^2\ s^{-1}$; constant time increment, $\tau = 0.005$ s. Space increment: profile 1, $h = 0.0025$ cm; profile 2, $h = 0.005$ cm.

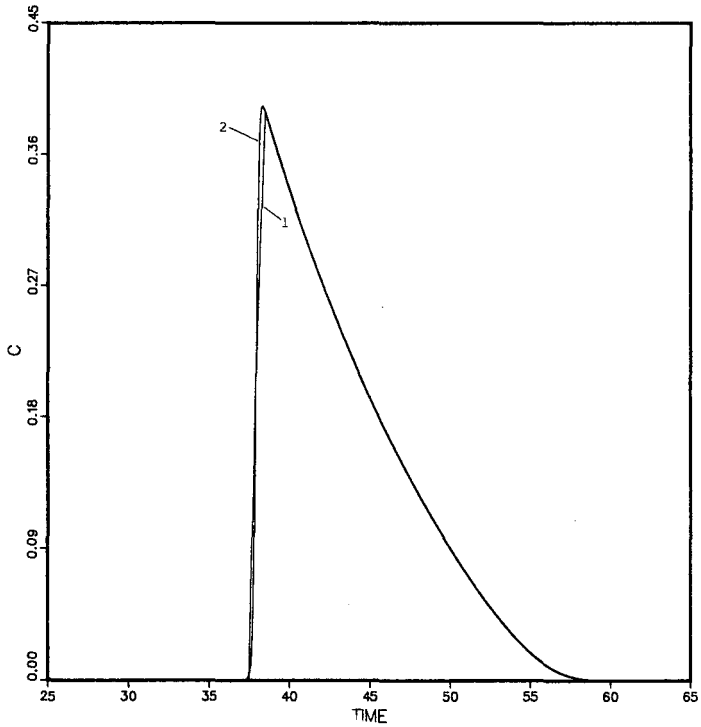

Fig. 10. Same as Fig. 9, except non-linear isotherm and sample size 100 times larger.

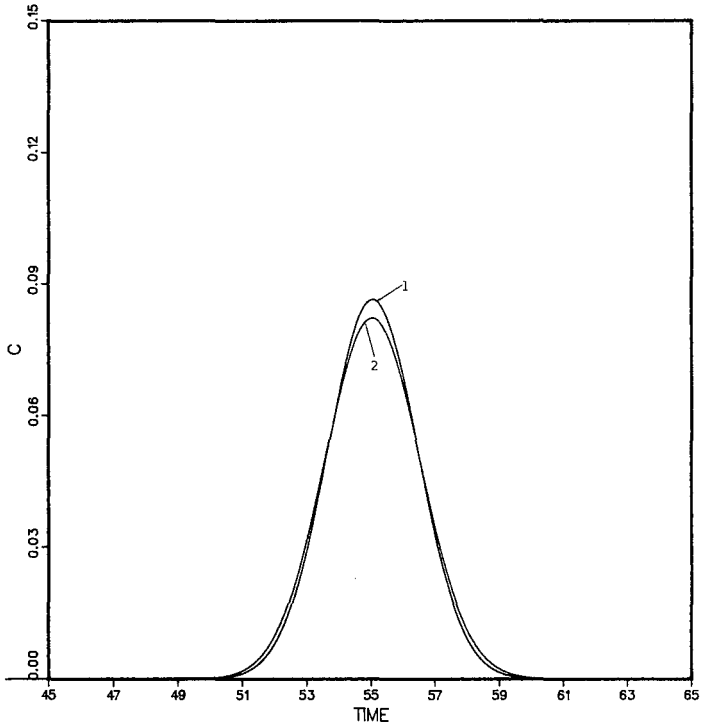

Fig. 11. Same as Fig. 9, except constant space increment, $h = 0.005$. Time increment: profile 1, $\tau = 0.0025$ s; profile 2, $\tau = 0.005$ s.

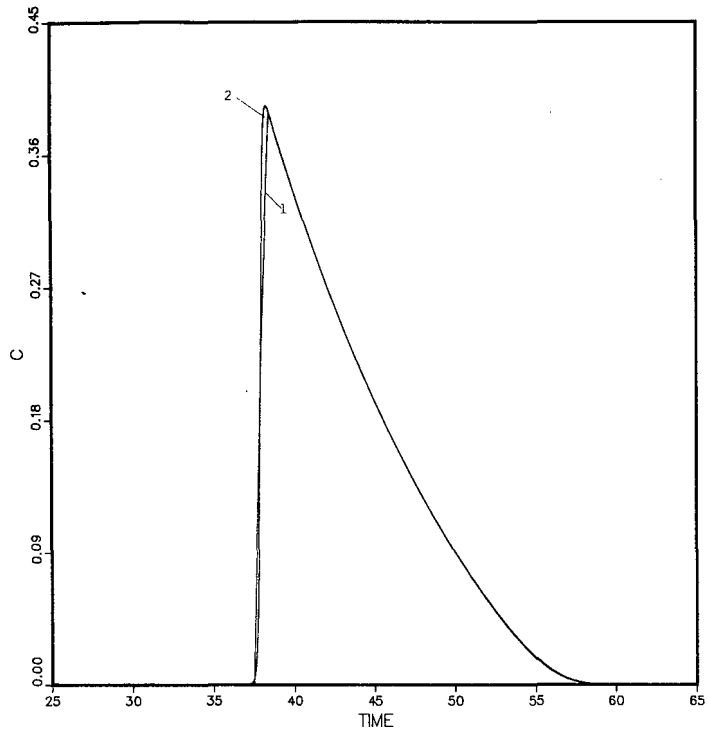

Fig. 12. Same as Fig. 11, except non-linear isotherm and sample size 100 times larger.

with a large sample size. Then the effect is small, which is in agreement with the fact that the influence of the column efficiency on the band profile is small at high loading factors[12].

Figs. 3 and 4 show similar chromatograms, obtained by changing the time increment, while keeping the space increment constant, which is the reverse of what was done in Figs. 1 and 2. The results obtained are very similar to those obtained in the previous case, as predicted by our discussion of eqn. 19.

Figs. 5–8 show chromatograms obtained under nearly the same conditions as those in Figs. 1–4, but with the second difference method described here. The results obtained under linear conditions are satisfactory, and are as predicted by eqn. 27. The effect of the choice of the space increment on the efficiency of the peak obtained is important (Fig. 5), while the effect of the choice of the time increment is nearly negligible (Fig. 7). In contrast, the results obtained under non-linear conditions are poor: it is seen in Figs. 6 and 8 that the mass is not even conserved! This method should certainly be avoided, although it gives profiles that look realistic.

Figs. 9–12 show chromatograms obtained by solving eqn. 34 using the Lax–Wendroff method. The equilibrium isotherm is again linear in Figs. 9 and 11, and two different values of the space increment were used with the same value of the time increment for Fig. 9, the opposite, two different values of the time increment with the same space increment for Fig. 11. In both instances the two profiles are extremely close, almost impossible to differentiate in most of the concentration range. Finally,

Figs. 10 and 12 show the solutions obtained under non-linear conditions, with two different values of the space increment (Fig. 10) for the same time increment, or two different values of the time increment for the same space increment. The differences between the two profiles on either Fig. 10 or Fig. 12 are very small, comparable to the differences between the two profiles shown in Figs. 2 and 4.

There are differences between the two basic approaches studied here, the characteristic and the Lax–Wendroff methods, regarding the stability of the numerical solutions. Oscillations easily take place, especially with the Lax–Wendroff scheme, if the integration increments are not properly chosen. Hence a direct comparison between the results obtained by the two methods is difficult and must be limited to a narrow range of values of τ and h. Depending on the nature of the problem studied, the first type difference method[2,3,7,9–12] or the Lax–Wendroff method[6,15] will be chosen.

ACKNOWLEDGEMENTS

This work was supported in part by Grant CHE-8715211 from the National Science Foundation and by the cooperative agreement between the University of Tennessee and Oak Ridge National Laboratory.

REFERENCES

1 P. C. Haarhoff and H. J. Van der Linde, *Anal. Chem.*, 38 (1966) 573.
2 P. Rouchon, M. Schonauer, P. Valentin and G. Guiochon, *Sep. Sci. Technol.*, 22 (1987) 1793.
3 G. Guiochon, S. Golshan-Shirazi and A. Jaulmes, *Anal. Chem.*, 60 (1988) 1856.
4 H. C. Thomas, *J. Am. Chem. Soc.*, 66 (1944) 1664.
5 L. Lapidus and N. L. Amundson, *J. Phys. Chem.*, 56 (1952) 984.
6 B. C. Lin, S. Golshan-Shirazi and G. Guiochon, *J. Phys. Chem.*, 93 (1989) 3343.
7 B. C. Lin and G. Guiochon, *Sep. Sci. Technol.*, 24 (1988) 31.
8 B. C. Lin, S. Golshan-Shirazi, Z. Ma and G. Guiochon, *Anal. Chem.*, 60 (1988) 2647.
9 G. Guiochon and S. Ghodbane, *J. Phys. Chem.*, 92 (1988) 3682.
10 S. Golshan-Shirazi and G. Guiochon, *J. Chromatogr.*, 461 (1989) 1.
11 A. Katti and G. Guiochon, *J. Chromatogr.*, 449 (1988) 25.
12 S. Golshan-Shirazi and G. Guiochon, *Anal. Chem.*, 60 (1988) 2364.
13 S. Goldstein, *Proc. R. Soc. London, Ser. A*, 219 (1953) 151.
14 J. L. Wade, A. Bergold and P. W. Carr, *Anal. Chem.*, 59 (1987) 1286.
15 B. C. Lin, Z. Ma and G. Guiochon, *Sep. Sci. Technol.*, in press.
16 R. D. Richtmyer and K. W. Morton, *Difference Methods for Initial-Value Problems*, Interscience, New York, 2nd ed., 1967.
17 P. C. Haarhof and H. J. Van der Linde, *Anal. Chem.*, 38 (1966) 573.
18 M. Goedert and G. Guiochon, *J. Chromatogr. Sci.*, 11 (1973) 326.

Journal of Chromatography, 484 (1989) 103–124
Elsevier Science Publishers B.V., Amsterdam — Printed in The Netherlands

CHROM. 21 814

THEORETICAL STUDY OF MULTI-COMPONENT INTERFERENCES IN NON-LINEAR CHROMATOGRAPHY

STEPHEN JACOBSON, SADRODDIN GOLSHAN-SHIRAZI, A. M. KATTI, MARTIN CZOK, ZIDU MA and GEORGES GUIOCHON*

**Department of Chemistry, University of Tennessee, Knoxville, TN 37996-1600 (U.S.A.) and Division of Analytical Chemistry, Oak Ridge National Laboratory, Oak Ridge, TN 37831-6120 (U.S.A.)*

SUMMARY

The semi-ideal model of non-linear chromatography is used to calculate the elution band profiles of each component of various ternary mixtures. It is assumed that these compounds compete for interaction with the stationary phase following the competitive ternary Langmuir isotherm model. Calculated profiles are generated for a series of mixtures of variable relative compositions, using different sample sizes. The patterns obtained are discussed.

The calculated results are easily predicted in most instances from the combination of the displacement effect, the compression of an early eluting band by a later eluting band, and the "tag-along" effect, *i.e.*, the spreading of a band by the band which is eluted just before it. When the concentration of the second component of the ternary mixture is low, and those of the first and third components are high, the second component band is squeezed between the other two and its profile is most unusual.

INTRODUCTION

In previous papers we discussed on a theoretical basis the progressive separation between the two bands of a binary mixture during elution[1–6] and during displacement[7] chromatography. These investigations permitted a better understanding of band interference in chromatographic columns under non-linear conditions, *i.e.*, when the concentrations of the sample components are large enough for their equilibrium isotherms between the two phases to be non-linear. The importance of the displacement of the first component band by the second band has been illustrated[1]. This effect permits a considerable improvement in the production rate and recovery yield of the first-eluted component of a feed in preparative chromatography[6]. This theoretical prediction has been confirmed by various experimental results[8–10]. The displacement effect depends greatly on the relative concentrations of the two components of the binary mixture. It is especially strong when the first component is at a lower or much lower concentration than the second[10,11].

When the reverse is true, the displacement effect is small or negligible, but another effect, the "tag-along" effect, has been found[1,2]. Because of the competition

0021-9673/89/$03.50

for access to the stationary phase, the molecules of the first component crowd out those of the second component. The second component band tags along with the first and is spread over a wide volume of mobile phase. The result is a low production rate and a poor recovery yield at high column loadings[6,12].

Experimental results have confirmed the validity of both predictions, and observations of both effects have been reported[8–10,13,14]. It has been noted in several instances[9,14] that the displacement effect is stronger than predicted and, conversely, the tag-along effect weaker. In one instance at least, the opposite has been found[13]. This is not surprising, as the theoretical investigations were made using the simplest general equation for competitive isotherms, the Langmuir isotherm. This model assumes that the adsorbent surface is homogeneous, that the column saturation capacities of the two components are the same and that both the mobile phase solution of the sample components and the stationary phase are ideal, *i.e.*, that there are no molecular interactions between the retained components, which is a simplistic assumption. Compared with the assumption of linear chromatography, where there is no interaction between bands, *i.e.*, no competition for retention, the Langmuir competitive isotherm is a considerable improvement. It gives a good first approximation of the competitive isotherm behavior. Molecular interactions must be taken into account, however, to achieve a quantitative prediction of the band profiles of a multi-component mixture. Depending on the comparative strengths of the interactions of the molecules of each compound with those of the same compound and those of the other, deviations from the prediction of the Langmuir isotherm in one or the other direction may be expected.

In summary, the predictions of the ideal and semi-ideal models of chromatography for the elution profiles of the bands of a pure compound pulse[15,16] or of a binary mixture[1,17] are sufficiently accurate to predict the phenomena associated with band interference and progressive band separation in chromatography. However, they cannot give accurate elution profiles unless, of course, the exact isotherms are known.

All the previous work referred to here relates to pure compound band profiles or to the separation of binary mixtures. In most practical situations, however, real mixtures are not binary but contain a larger number of components. It is useful at this stage to investigate the separation of multi-component mixtures on a purely theoretical basis, in order to search for possible new effects that could not be accounted for on a straightforward basis by simple combinations of the displacement and tag-along effects taking place between each pair of the components involved.

This paper discusses results obtained using the semi-ideal model[1,16] applied to a ternary mixture. Ternary Langmuir competitive isotherms have been used, assuming the same column capacity for the three components. The relative retentions of the two successive pairs of components (1–2 and 2–3) have been varied, in addition to the total sample size, expressed as the loading factor, *i.e.*, the fraction of the column saturation capacity. The compositon of the mixtures investigated covers a wide range of relative compositions, including all the possible combinations where a component is either major or minor.

THEORY

The model used for the simulation of the elution and separation of the

components of a ternary mixture is the semi-ideal model applied previously to the simulation of the band profiles for a pure compound[16] and for a binary mixture[1–6] on an overloaded column. It is based on the ideal model of chromatography[18–22]. The ideal model assumes the column efficiency to be infinite and focuses attention on the phenomena that arise because of the non-linear behavior of the equilibrium isotherms at high concentrations and on the competitive interactions between the components of a mixture. This model stems from the properties of the equation system of chromatography.

The differential mass balance equation for a single compound in a slice of a chromatographic column can be written as

$$\frac{\partial C_m}{\partial t} + F \cdot \frac{\partial C_s}{\partial t} + \frac{\partial (uC_m)}{\partial z} = D \cdot \frac{\partial^2 C_m}{\partial z^2} \tag{1}$$

where C_m and C_s are the concentrations of the compound considered in the mobile and stationary phases, respectively, at time t and abscissa along the column, F is the phase ratio of the column packing, with $F=(1-\varepsilon)/\varepsilon$, ε being the column packing porosity, u is the mobile phase velocity and D is the coefficient of axial dispersion.

In liquid chromatography, the compressibility of the mobile phase is negligible and the partial molar volumes of the compounds investigated in the mobile and the stationary phases are nearly the same. Accordingly, the mobile phase velocity, u, is constant and can be taken out of the differential operator.

Integration of eqn. 1 requires a relationship between C_m and C_s. Giddings[23] has shown that, provided the column efficiency exceeds a few hundred theoretical plates, which is the general case in modern liquid chromatography, we can take for C_s the value corresponding to thermodynamic equilibrium between the two phases, *i.e.*, the value given by the isotherm:

$$C_s = \partial(C_m) \tag{2}$$

Having made this simplifying assumption, the axial dispersion coefficient in eqn. 1 is replaced by an apparent dispersion coefficient that accounts for the finite column efficiency, *i.e.*, for the deviation from the thermodynamic equilibrium resulting from the finite rate of the radial mass transfer[23]. However, it is not possible to find an exact analytical solution following this replacement and it is extremely difficult to write the appropriate computer programs for its calculation.

The task becomes much easier if we assume that the column has an infinite efficiency, making the apparent dispersion coefficient zero. Further, it can then be shown that the computation process itself introduces errors that are equivalent to the addition of a dispersion term (*i.e.*, $k\partial^2 C/\partial z^2$)[24,25].

Thus, we obtain the following equation, which constitutes the ideal model for the ternary mixture:

$$\left(1 + F \cdot \frac{dC_{s,i}}{dC_{m,i}}\right) \frac{\partial C_{m,i}}{\partial t} + u \cdot \frac{\partial C_{m,i}}{\partial z} = 0 \tag{3}$$

where dC_s/dC_m is the differential of the equilibrium isotherm and $i = 1$, 2 and 3 represents the three components of the ternary mixture. Numerical solutions of eqn. 3 can easily be calculated if the numerical value of each parameter is previously known[16]. As already described[26], a finite difference method, using the Godunov algorithm, is especially suitable for this calculation[27,28]. We take the column efficiency into account by chosing the following values for the space and time integration increments:

$$dz = H \tag{4}$$

and

$$dt = 2H/u_{z,0} \tag{5}$$

where $u_{z,0}$ is the velocity associated with an infinitely small concentration of the compound considered [$u_{z,0} = u_0/(1 + k'_0)$, where k'_0 is the column capacity factor of the compound under analytical, *i.e.*, linear, conditions]. We also need a set of ternary competitive isotherms and a value for $u_{z,0}$, in order to select these integration increments (see the next section).

EXPERIMENTAL

The computations were carried out using ternary competitive Langmuir isotherms:

$$C_{s,i} = \frac{a_i C_{m,i}}{1 + b_1 C_{m,1} + b_2 C_{m,2} + b_3 C_{m,3}} \tag{6}$$

with $i = 1$–3. The numerical values of the six coefficients selected for most of the calculations are given in Table I. The parameters of the three individual isotherms were selected so that the column saturation capacity was the same for the three compounds ($q_i = a_i/b_i = 1.60$ for all values of i). The k' value for the third component at infinite dilution was $a_3F = 4.0$. In most instances, the two values of the selectivity of the stationary phase (*i.e.*, $\alpha_{1,2} = a_2/a_1$ and $\alpha_{2,3} = a_3/a_2$) were equal to 1.10. In a few cases, a value of 1.4 was used instead.

TABLE I
COEFFICIENTS OF THE TERNARY COMPETITIVE ISOTHERMS

Selectivity	*Parameter (i=1, 2, 3)*	*Component 1*	*Component 2*	*Component 3*
$\alpha_{1,2} = \alpha_{2,3} = 1.10$	k'_i	3.31	3.64	4.00
	aa_i	13.24	14.56	16.00
	b_i (l/mol)	2.07	2.27	2.50
$\alpha_{1,2} = \alpha_{2,3} = 1.40$	k'_i	1.97	2.85	4.00
	a_i	7.88	11.40	16.00
	b_i (l/mol)	1.27	1.78	2.50

The column calculated is 25 cm long, its phase ratio is 0.25 and the flow velocity (u_0 = 0.125 cm/s) corresponds to a dead time of 200 s. The column efficiency is 12 500 theoretical plates for the second component (*i.e.*, height equivalent to a theoretical plate = 0.0020 cm), except when the influence of the column efficiency on the separation between the three bands is considered. The values of the integration increments were calculated from the data selected for this component. Accordingly, the column efficiencies for the other two compounds are 11 250 and 13 750 theoretical plates, respectively[28]. Eqns. 4 and 5 show that, as dt and dz are constant during the integration, the simulated column efficiency is different for the three components[24,28].

The sample size is given as the total loading factor, calculated for the whole sample, as the column saturation capacity is the same for all components. In most instances the loading factor used was either 10% or 40%. Values of 5%, 20% and 60% have also been used, and some results are reported. The relative composition is given in fraction of the sample size. An x–y–z mixture means that the concentrations of the three components in that mixture are as x to y to z, *e.g.*, the relative concentration of the second component in the sample is $y/(x+y+z)$.

RESULTS AND DISCUSSION

The results reported were obtained exclusively with the parameters of the ternary isotherms given in Table I. Therefore, only two values of the selectivity are discussed here, 1.10 and 1.40. The value of 1.10 provides strong band interactions for low sample loadings. Compared with the larger selectivity value of 1.40, which requires higher loadings to induce similar band interactions, it permits the investigation of the non-linear effects associated with strong band interactions when using relatively small sample sizes. The use of a low selectivity reduces the relative importance of the displacement effect and increases that of the tag-along effect[4].

Other calculations, not reported here, were performed using values of the selectivity for either pair of components or for both equal to 1.15, 1.30 and 1.50. No qualitative differences were observed for the chromatograms generated. The degree of column overload and the band interference pattern obtained with a selectivity of 1.15 and a total sample size of 20% of the column saturation capacity were nearly identical with those observed with a selectivity of 1.10 and a loading factor of 10% on the chromatograms presented here. When the selectivities were unsymmetrical (*e.g.*, $a_{1,2}$ = 1.10 and $a_{2,3}$ = 1.30), the result was the coupling of a strong interaction between one pair of bands, a weak interaction between the other pair and nearly none between the first and the third compounds. In other words, the degree and type of band interaction can be simply predicted from what we know about binary mixtures whether the selectivities are symmetrical or unsymmetrical.

Changes in the sample size provide an easy adjustment of the degree of interference between bands. Compared with a single component band or even a binary mixture, the sample band system of a ternary mixture is spread over a longer section of the column, resulting in a less stationary phase overloading. At a loading of 5% for a mixture of three components, typically used in preparative liquid chromatographic applications, adjacent compounds competed only minimally. Much more interesting results were obtained for loadings of 10%, the most often discussed in this work, or 20%. Under the grossly overloaded conditions corresponding to loading factors of 40% or 60%, even the first component interacted with the third.

The main parameter investigated, that having the strongest influence on the profiles of the three component bands, was the relative composition of the mixture. From this point of view, we can separate our results into three categories: (i) those corresponding to mixtures where the three components are present in equal amounts, (ii) those corresponding to mixtures where one of the three components dominates in the presence of the other two and (iii) those obtained for mixtures where the second component is at low concentration compared with the other two and its band is squeezed between two major component bands. The last series of results are the only ones which were really unexpected.

The displacement effect and the tag-along effect are illustrated in Figs. 1 and 2, respectively. They will be referred to often in the following discussion, as most band systems for ternary mixtures exhibit features which are combinations of displacement (Fig. 1) and tag-along (Fig. 2) effects.

Mixtures with equivalent concentrations of the three components

Chromatograms calculated for samples of increasing size from 5% to 40% are shown in Figs. 3–6. Fig. 7 shows, for comparison, the chromatogram obtained for a 10% loading factor, assuming that there is no competition between the three components. This is the superimposition of the three bands obtained by successively injecting samples of each of the three compounds pure, with a loading factor of 3.33%. The band profiles in Fig. 7 are typical of those associated with a Langmuir isotherm under that degree of overloading.

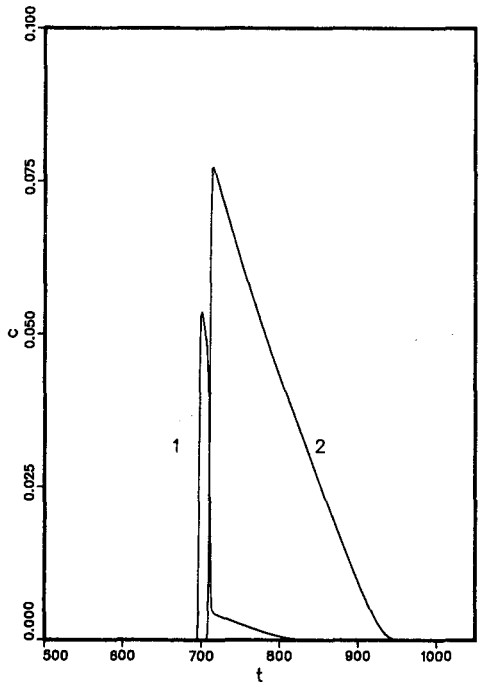

Fig. 1. Chromatogram calculated for a 1:9 binary mixture (concentration, c, in M *versus*, time, t, in s). Total loading factor: 10%. Isotherms, see eqn. 6. For isotherm coefficients, see Table I with $\alpha = 1.10$. First and second components only.

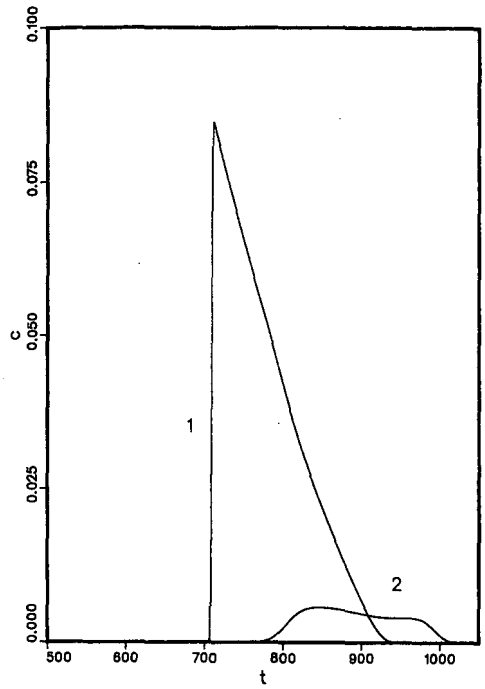

Fig. 2. As in Fig. 1, but for a 9:1 mixture. Total loading factor: 10%. Second and third components only.

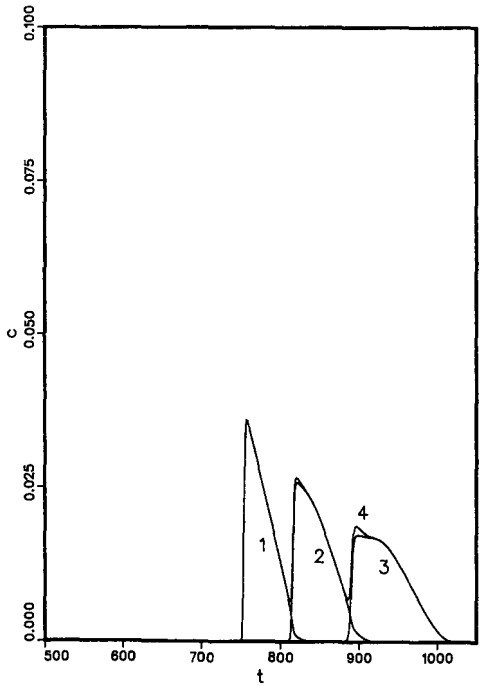

Fig. 3. Chromatogram calculated for a 1:1:1 mixture. Total loading factor: 5%. Isotherms, see eqn. 6. For isotherm coefficients, see Table I with $\alpha = 1.10$. Column characteristics, see Experimental. The number on each profile is the rank of the component; 4 is for the total concentration profile, as recorded by an ideal, non-selective detector.

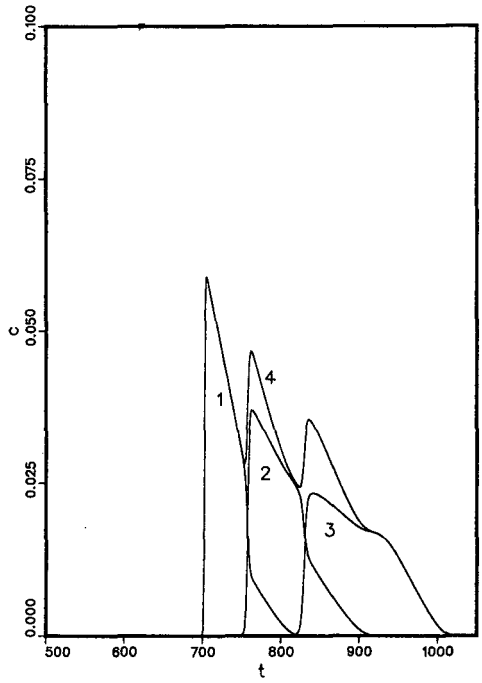

Fig. 4. Chromatogram calculated for a 1:1:1 mixture as in Fig. 3, except total loading factor: 10%.

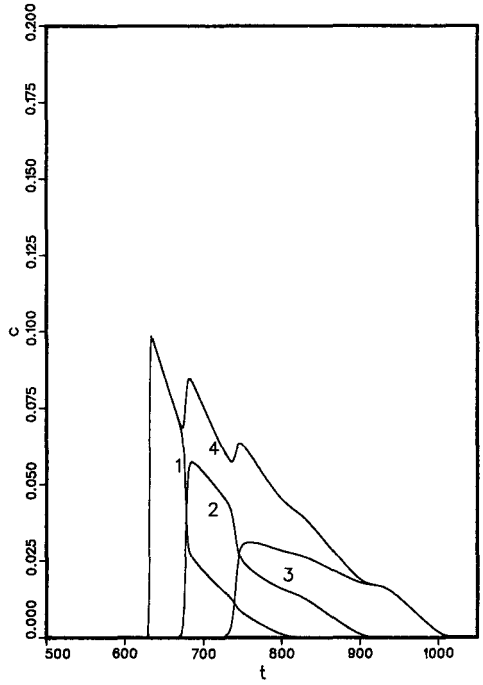

Fig. 5. Chromatogram calculated for a 1:1:1 mixture as in Fig. 3, except total loading factor: 20%.

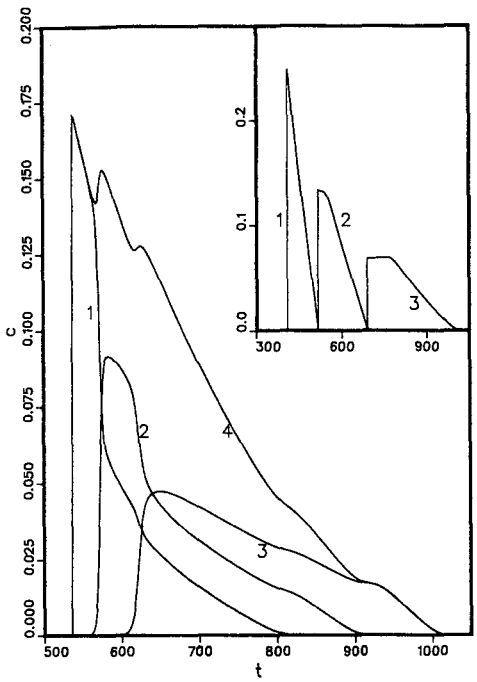

Fig. 6. Chromatogram calculated for a 1:1:1 mixture as in Fig. 3, except total loading factor: 40%. Inset: chromatogram calculated for a 1:1:1 mixture with total loading factor: 40%. Isotherm coefficients as in Table I with $\alpha = 1.40$. Column characteristics, see Experimental.

Compared with Fig. 7, where no interaction takes place between the compounds (because pure compound adsorption isotherms are used), the chromatograms in Figs. 3–6 show moderate to considerable band interaction, depending on the sample size. In Fig. 3, there is a slight displacement effect of the first component band by the second and of the second component band by the third. This is demonstrated essentially by the earlier time at which the elution of these bands is completed and by the inflection points on the back of their profiles, although the rear shock layers are barely discernible. Similarly, a modest tag-along effect is exhibited by the second band and a slightly stronger one by the third band.

In Fig. 4, corresponding to a 10% loading factor, the two effects are stronger. The front shock layers of the three bands are eluted much earlier than in Fig. 7, obtained with the same sample size for each component. The time gain decreases, however, from the first to the second and to the third component. A shock layer is clearly noticed on the rear of the first two bands. These shock layers are followed by slight tails, as the bands are not completely separated. This demonstrates the presence of the displacement effect. The tag-along effect is shown by the wider profiles of the second and third bands, the marked inflection point on the rear of these last two band profiles, with a nearly horizontal tangent for the third band. While the band of the second component simultaneously experiences a displacement by the third band and tags along with the first band, the other two bands are affected only by one effect each, displacement for the first one and tag-along for the third.

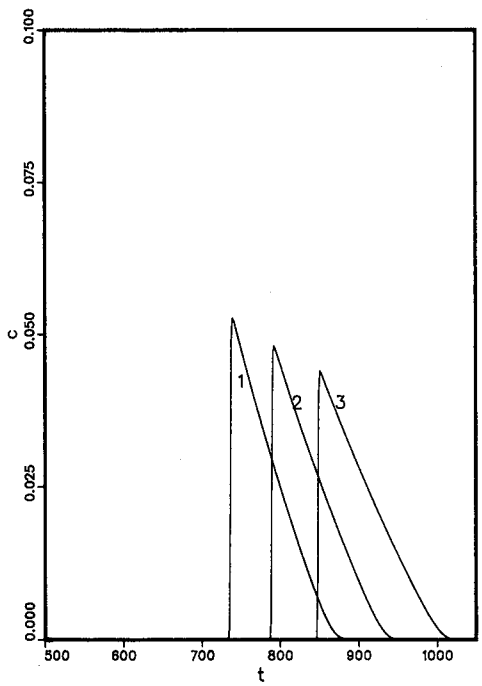

Fig. 7. Chromatogram calculated for a 1:1:1 mixture as in Fig. 4, except the components are not supposed to interact. Alternatively, superimposition of the chromatograms obtained successively for the three pure compounds, with a loading factor of 3.33% each.

In Figs. 5 and 6, which correspond to larger values of the loading factors, the band of the first component experiences a double displacement effect, while the third component band exhibits a double tag-along effect, the column being so overloaded that the first and third component bands interfere. This phenomenon becomes even stronger in Fig. 6, where the width of the third band profile reaches 400 s.

In the inset in Fig. 6, $a_{1,2} = a_{2,3} = 1.40$ (instead of 1.10, Fig. 6) and a column loading of 40% (instead of 10%, Fig. 6) were used. The three bands are resolved, but the second and third bands still show the effects of previous interactions with adjacent components. The third band plateau would shrink and disappear if it were allowed to migrate further. The profile of the second band can be considered as an intermediate stage in the recovery of the third band to its typical triangular shape.

If we compare Figs. 3–6, we see that the first part of the first band, that corresponding to the elution of the pure first component, becomes narrower with increasing sample size, while the recovery yield of the pure product decreases. The width of the third component band increases considerably, but the size corresponding to the last zone of the chromatogram, when the last component is eluted pure, does not change significantly. This confirms earlier results[6] that, because of the displacement effect, the production rate of the first component increases with increasing sample size until well into the range of severe band interference. In contrast, the production rate for the last component increases with increasing sample size only until its band begins to interfere with the previous band. Above that sample size, the production rate

remains constant, while the recovery yield decreases[29]. A similar conclusion is reached for the second component[12]. The production rate of the second component is certainly lower under the conditions in Fig. 4 than under those in Fig. 3. It seems to be maximum for a sample load of about 5%, corresponding to Fig. 3.

Mixtures in which one component predominates

In this group, we examined five mixtures, three for which one compound is in large excess, corresponding to concentration distributions of 9:1:1, 1:9:1 and 1:1:9, and two mixtures for which the first or third component is minor, 9:9:1 and 1:9:9. The profile of the last possible mixture in this series, 9:1:9, is discussed in the next section.

Fig. 8 shows the chromatogram calculated for a mixture containing a large excess of the first component (9:1:1). The strong tag-along effect of the first component band on the last two is obvious. It is expectedly stronger on the second band than on the third as the degree of interaction is lower and the time during which the two bands interact in the column is shorter. In fact, the third component band is in the process of recovering from the deformation caused by the tag-along effect that it underwent during the first part of its elution. Simultaneously, there is a very weak displacement of the second band by the third, which can be recognized by the slightly shorter elution time of the band end in Fig. 8 compared with Fig. 7 (note that for a pure compound with a Langmuir isotherm, the time at which the band ends does not depend on the sample size).

In the inset in Fig. 8 (calculated under the same conditions as the inset in Fig. 6),

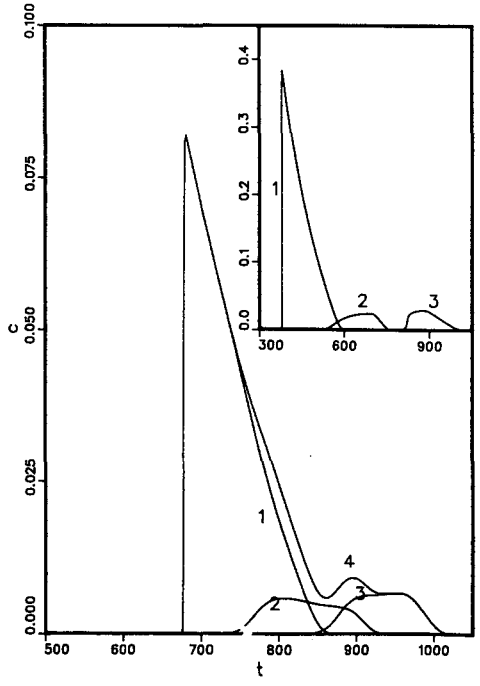

Fig. 8. Chromatogram calculated for a 9:1:1 mixture. Total loading factor: 10%. Conditions as in Fig. 3. Inset: chromatogram calculated for a 9:1:1 mixture with conditions as in Fig. 6, inset.

the second band tags along with the first and the third band, although separated, has not fully recovered from the tag-along effect. The shock front is slowly reforming as the tag-along plateau decays. Eventually, this third band profile will regain its typical triangular shape expected for a pure compound, under overloaded conditions.

Fig. 9 shows the chromatogram corresponding to the mixture having a large excess of the second component (1:9:1). The second component band displaces the first band strongly, while forcing the third to tag along. The first and third component bands do not interact significantly. Nevertheless, it would not be possible to prepare much pure second component under the conditions selected for Fig. 9. The first part of the second band contains about 40% of the amount of the first component injected, while the second part contains nearly 60% of the amount of the third component contained in the sample.

In the inset in Fig. 9 (calculated under the same conditions as for the inset in Fig. 6), no interaction takes place between the first and the third components, which are effectively shielded by the second. We observe merely the sum of two two-component problems. Comparing Fig. 9 and its inset, we see a stronger displacement effect and a weaker tag-along effect in the inset, as expected because of larger values of the selectivity and the loading factor[4].

Fig. 10a shows the chromatogram calculated with a mixture containing an excess of the third component (1:1:9). In this instance, two strong displacement effects are observed. The third component band displaces the second and in so doing forces it to displace the first component band. Under the conditions selected, with a small loading

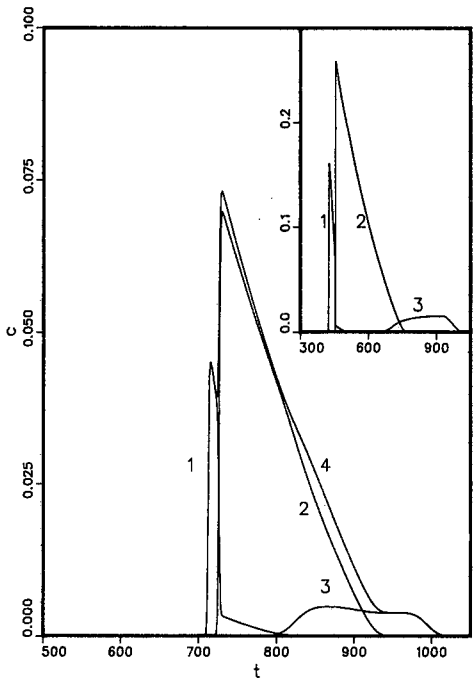

Fig. 9. Chromatogram calculated for a 1:9:1 mixture. Total loading factor: 10%. Conditions as in Fig. 3. Inset: chromatogram calculated for a 1:9:1 mixture with conditions as in Fig. 6, inset.

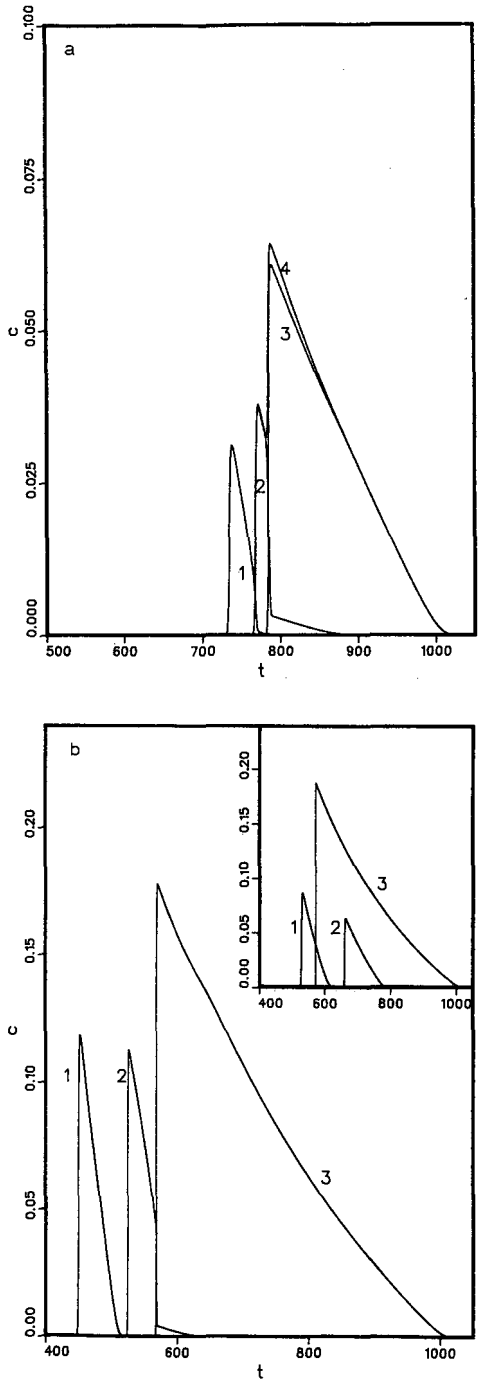

Fig. 10. Chromatograms calculated for a 1:1:9 mixture. (a) Total loading factor: 10%. Conditions as in Fig. 3. (b) Same conditions as in Fig. 6, inset (selectivity: 1.4). Inset: same conditions, except without component–component interaction (similar to Fig. 7).

factor for the first two components (0.9%), there would be no displacement of the first band by the second in the absence of a large excess of the third component (see Fig. 3). The second component has the classical L-shape profile of a band strongly displaced by a more retained compound, when the selectivity of the column is low or moderate. The displacement of the first band, however, is easier to observe by comparing the retention time of that band and its width in Figs. 3 and 10 than by visually comparing its profiles in the two figures.

In Fig. 10b, the selectivity has been increased (a_{ij} = 1.4) together with the total loading factor (40%). Comparing this figure with its inset under the same conditions except that the calculation was carried out assuming there are no component–component interactions, the displacement effect of the first two bands by the last is markedly evident. Although the first component appears unaffected in its profile, it is both narrower and eluted earlier after having been displaced strongly by the third component and mildly by the second component. The second component also suffers from the displacement effect, but although present in the same amount as the first component, no tag-along is seen between the first and second components. The displacement effect, therefore, overpowers the tag-along effect under these conditions.

The double displacement effect is illustrated for a very strong column overload in Figs. 11 and 12. Fig. 11 shows the chromatogram calculated for a 40% loading factor with a 1:1:18 mixture and Fig. 12 shows an enlargement of the front parts of the elution profiles of the two minor compounds. These chromatograms are striking. The chromatogram exhibits some similarity to those obtained in displacement chromatography during the formation of the isotachic displacement train[7]. They show that

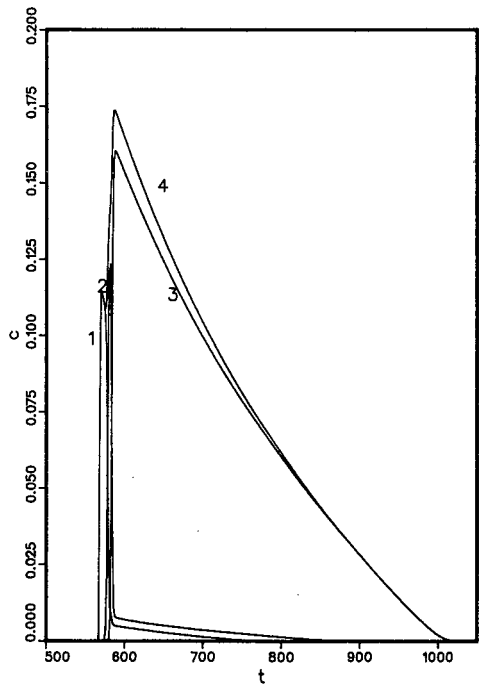

Fig. 11. Chromatogram calculated for a 1:1:18 mixture. Total loading factor: 40%. Conditions as in Fig. 3.

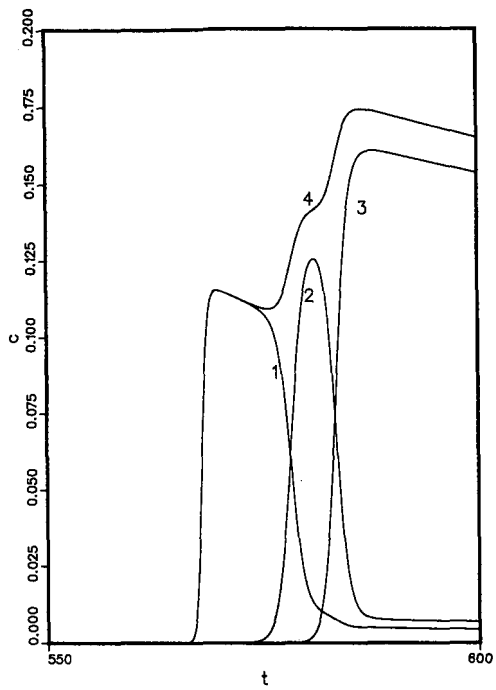

Fig. 12. Chromatogram calculated for a 1:1:18 mixture. Total loading factor: 40%. Enlargement of the front of the chromatogram in Fig. 11.

a large fraction of the impurities of a pure compound can be recovered at the front of the main component band (see Fig. 12). Unfortunately, the recovery yields would not exceed about 70% for the first component and 60% for the second. The maximum concentration of these impurity bands, however, is of the order of that of the main component. This phenomenon can be used in combined liquid chromatography–mass spectrometry for the easier identification of impurities or for the extraction of small amounts of them for further experiments[30]. It cannot be used for the purification of the main component, as we have already said, or for the total recovery of these compounds.

In Figs. 8–12, as in Figs. 1 and 2, the major component causes a total change in the shape of the elution band of the minor component(s), but its band profile is essentially unaffected. Next, we shall consider the opposite situation where the interference between the bands of the major compounds controls the shape of the chromatogram.

Fig. 13 shows the chromatogram calculated for a mixture where the third component is minor (9:9:1). The chromatogram for the first two components is very much like that corresponding to an overloaded band of a 1:1 binary mixture. The second band displaces the first and at the same time tags along with it. These two effects are easily recognized. The third band tags along with the other two and is spread over a wide retention time range (nearly 200 s). The elution profiles of the first two bands of the 9:9:1 mixture in Fig. 13 are very similar to the elution profiles of the last

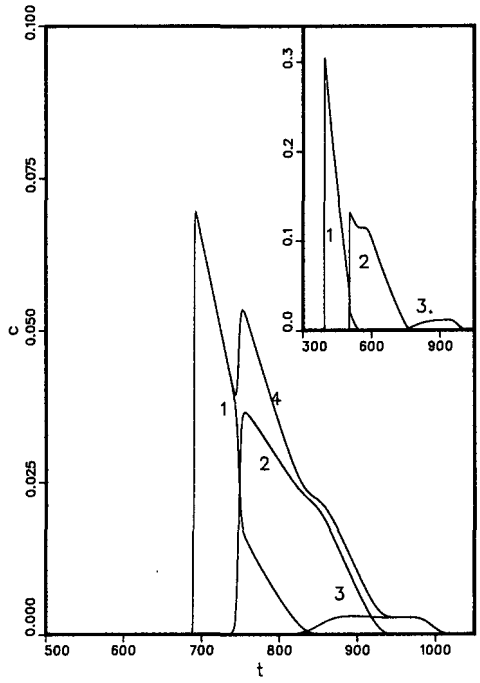

Fig. 13. Chromatogram calculated for a 9:9:1 mixture. Total loading factor: 10%. Conditions as in Fig. 3. Inset: chromatogram calculated for a 9:9:1 mixture with conditions as in Fig. 6, inset.

two bands of the 1:9:9 mixture in Fig. 14. These two bands interact in exactly the same way, the third band displacing the second and tagging along with it at the same time. The difference between the chromatograms in Figs. 13 and 14 is that in the former instance the third band tags along with the other two, whereas in the latter instance the first band is displaced by the system of the other two. However, the displacement effect in Fig. 14 is not as strong as with the 1:9:1 mixture (Fig. 9). In part this is because the actual amount of the second component injected with the sample is markedly smaller in Fig. 14 than in Fig. 9.

Similarly,the same phenomena are observed in the insets in Figs. 13 and 14 as for the respective main figures, except that they take place with larger values of the selectivity and the loading factor in the insets. The interferences between bands are much reduced in the insets, in spite of the higher loading factors. This confirms that both the recovery yield and the production rate of purified individual components are greatly enhanced by an increase in the selectivity[12,31].

Mixtures in which the second component is minor

With a ternary mixture in which the intermediate component is a minor one, it simultaneously undergoes a strong displacement effect from the third component band which pushes it forward, and a strong tag-along effect from the first band which pulls it ahead. The combination of these two effects results in very strong squeezing of the band, which acquires an unexpected elution profile (see Figs. 15–18). The squeezing effect results from the superimposition of strong displacement and tag-along effects.

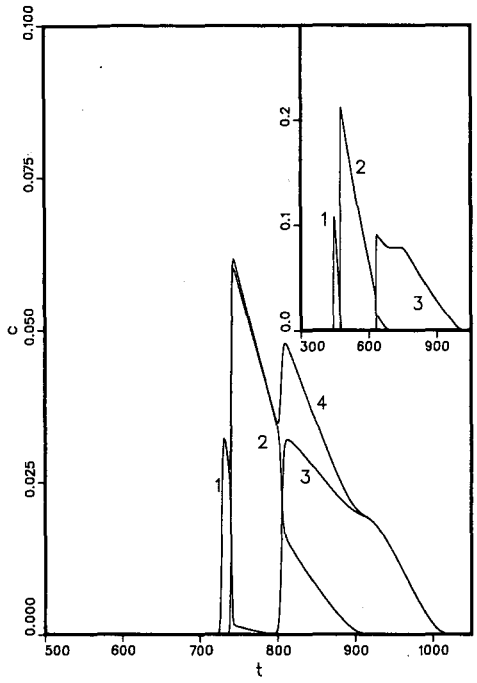

Fig. 14. Chromatogram calculated for a 1:9:9 mixture. Total loading factor: 10%. Conditions as in Fig. 3. Inset: chromatogram calculated for a 1:9:9 mixture with conditions as in Fig. 6, inset.

This causes a much greater change in the band profiles than any other effect or combination of effects observed so far in the investigation of multi-component mixtures.

In Fig. 15a, the column loading factor (10%) is moderate and the first and third bands are well resolved. The second component band is sandwiched between them. If Fig. 15 is compared with Fig. 7, however, it is clear that the first band has been displaced (the retention time of the front is reduced by about 40 s) and the third component band has undergone a slight tag-along effect from which it is beginning to recover. This perturbation is caused by the elution of the second, minor band squeezed between these two major bands.

This squeezing is maximized with increasing efficiency in Fig. 15b (column loading factor 5%). Whereas no pure second component can be recovered with an efficiency of only 1500 theoretical plates as the efficiency improves the second band undergoes a stronger displacement effect from the third component and a weaker tag-along effect from the first component. With an efficiency of 12 500 plates very pure fractions of the individual components can be collected with a high recovery yield. In this instance at least, increasing the column efficiency certainly increases markedly the production rate of fractions of constant purity.

In Fig. 15c, the column loading factor (60%) is high and $a_{1,2} = a_{2,3} = 1.4$. The high loadings were necessary in order to force competitive interactions between adjacent components. The inset in Fig. 15c has a column loading factor (40%) under

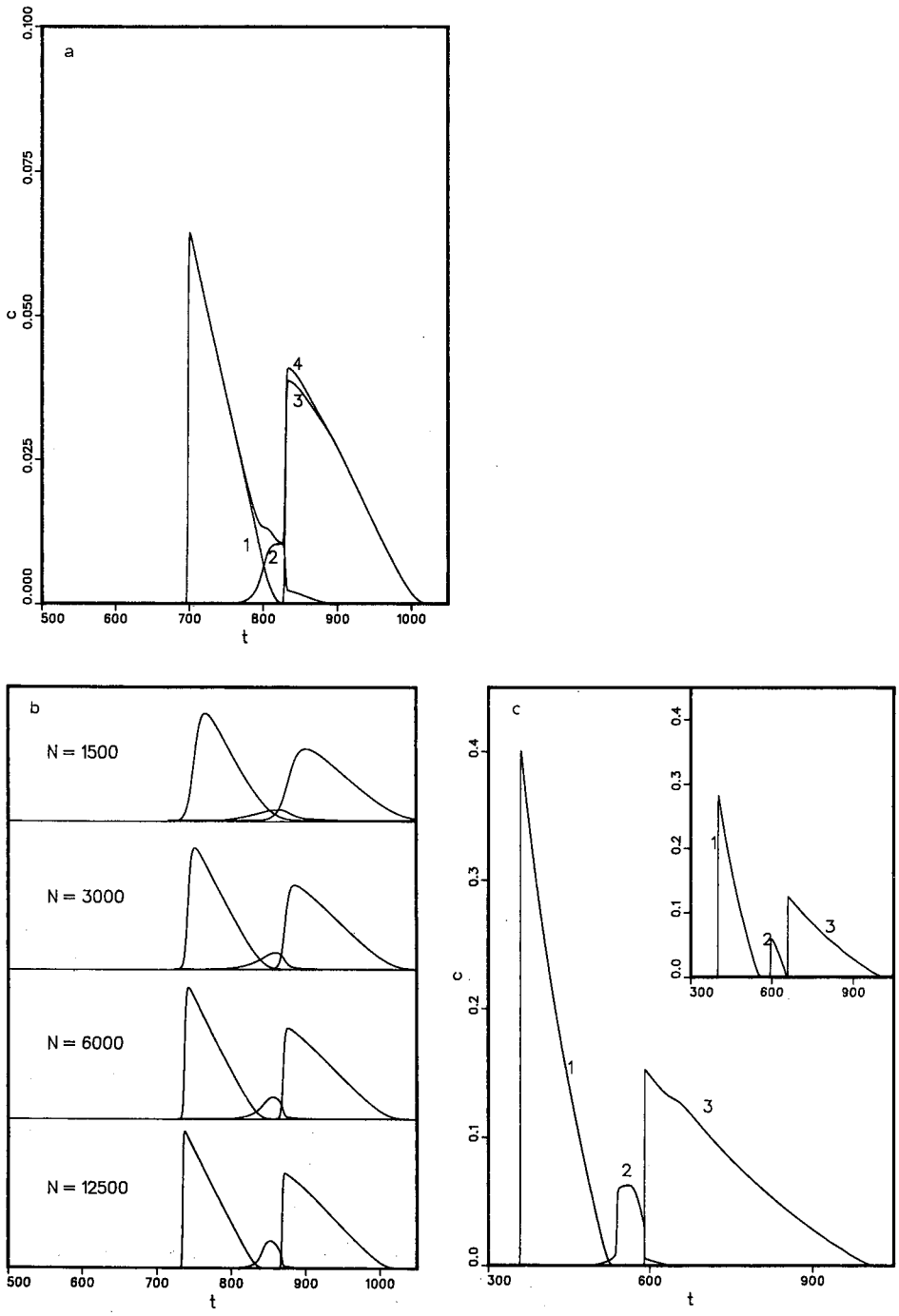

Fig. 15. Chromatograms calculated for a 9:1:9 mixture. (a) Total loading factor: 10%. Conditions as in Fig. 3. (b) Total loading factor: 5%. Conditions as in Fig. 3, except number of theoretical plates, N. (c) Total loading factor: 60%. Conditions as in Fig. 6, inset. Inset: same except total loading factor: 40%.

the same conditions as in Fig. 15c. Only subtle effects are seen in the inset under heavily overloaded conditions. The second profile shows a slight bowing of its rear side. In Fig. 15c under more overloaded conditions, the profiles are very similar to those in Fig. 15a. In fact, the separation is better in Fig. 15c than in Fig. 15a even though in Fig. 15c the column loading factor is six times that in Fig. 15a, 60% *vs.* 10%. The significant difference comes from the selectivity, 1.4 in Fig. 15c and 1.1 in Fig. 15a.

Clearly, if the sample size is increased from 10%to 20% (with a selectivity of 1.1) (Fig. 16), the first and last bands of the chromatogram will interfere strongly. The first is displaced by the second, which in turn tags along with the first. The second band is squeezed between the other two bands and has a small, but not entirely negligible, effect on the overall profile. The second band causes a very slight displacement of the first band and a weak tag-along effect, seen as a very small hump on the rear of its profile.

Schematically, the second component band looks like a half-Gaussian profile with a rear shock followed by a very long tail. This tail, in turn, looks also like a half-Gaussian profile, but one that is much shorter than the first and much wider. Figs. 17 and 18 show the progressive changes in the profile of the second component band when samples of constant size of an equimolar binary mixture of the first and third components are injected and the mixture contains decreasing concentrations of an impurity eluted between the two main components. The separation of samples whose sizes amount to 10% (Fig. 17) and 20% (Fig. 18) of the column saturation capacity, respectively, and relative compositions of 9:1:9, 25:1:25, 50:1:50 and 100:1:100 were calculated. For the sake of clarity, only the profiles of the second band are shown.

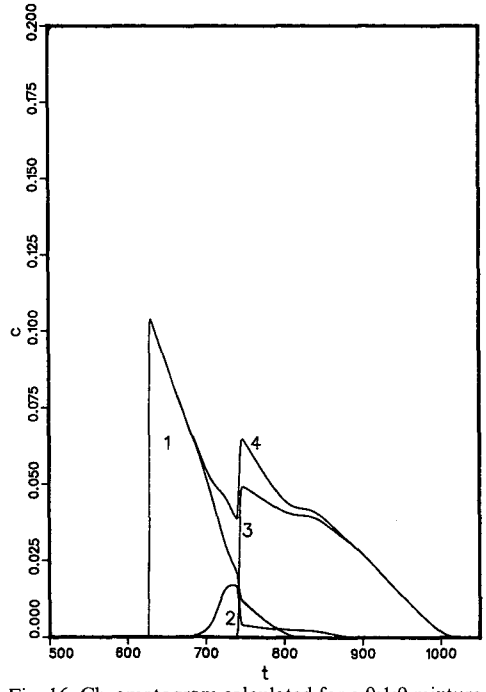

Fig. 16. Chromatogram calculated for a 9:1:9 mixture. Total loading factor: 20%. Conditions as in Fig. 3.

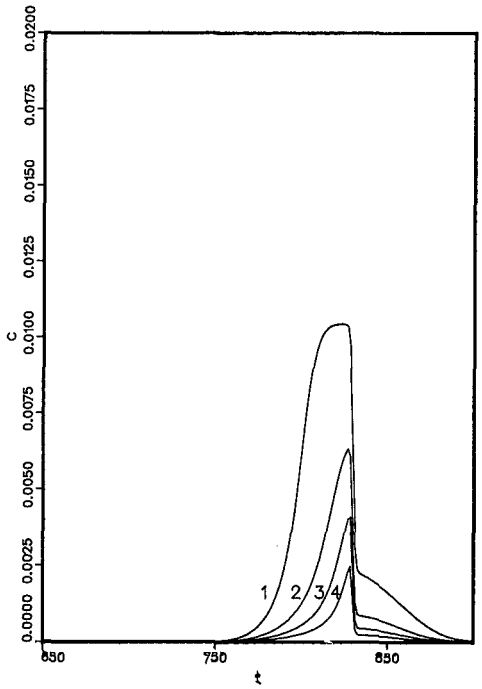

Fig. 17. Chromatogram calculated for the minor second component of a ternary mixture. Conditions as in Fig. 3, except total loading factor: 10%, and mixture composition: (1) 9:1:9; (2) 25:1:25; (3) 50:1:50; (4) 100:1:100.

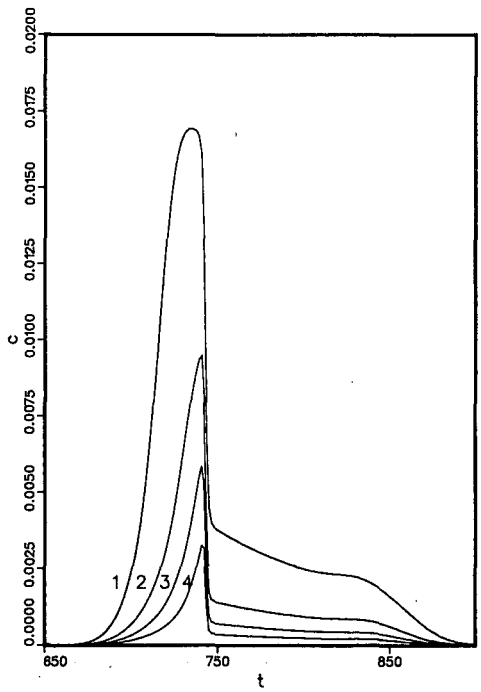

Fig. 18. Same as Fig. 17, except total loading factor: 20%.

The top part of the second component profile (Figs. 17 and 18) becomes sharper with decreasing amount of this component in the sample, but the relative importance of the tail does not change much.

CONCLUSION

This theoretical investigation has shown few unexpected results. On a qualitative basis, almost all the results obtained could have been understood in terms of combinations between the displacement and tag-along effects already discussed. Only with a minor component squeezed between two major components is the band profile intricate enough to be nearly impossible to predict or explain without the help of computer calculations based on the use of the semi-ideal model.

Experimental verifications of computer-predicted profiles for binary mixtures have already shown that both displacement and tag-along effects are observed[13]. Significant deviations from the predictions made on the basis of a competitive Langmuir isotherm model take place, however. Depending on the system studied, these deviations result from one of the effects, displacement or tag-along, being stronger and the other being weaker than predicted[13,14]. The competitive Langmuir isotherms derived by introducing in eqn. 6 the numerical values of the coefficients measured for the single compound isotherms of the mixture components remains an excellent first-order approximation for the calculation of individual band profiles.

Accordingly, the chromatograms presented give a good description of the type of band interference patterns that can be expected in practical preparative chromatography when columns are overloaded with large samples of multi-component mixtures for the achievement of high production rates.

ACKNOWLEDGEMENTS

This work was supported in part by grant CHE-8901382 from the National Science Foundation and by the cooperative agreement between the University of Tennessee and the Oak Ridge National Laboratory.

REFERENCES

1 G. Guiochon and S. Ghodbane, *J. Phys. Chem.*, 92 (1988) 3682.
2 S. Ghodbane and G. Guiochon, *J. Chromatogr.*, 440 (1988) 9.
3 S. Ghodbane and G. Guiochon, *J. Chromatogr.*, 444 (1988) 275.
4 S. Ghodbane and G. Guiochon, *J. Chromatogr.*, 450 (1988) 27.
5 S. Ghodbane and G. Guiochon, *J. Chromatogr.*, 452 (1988) 209.
6 S. Ghodbane and G. Guiochon, *Chromatographia*, 24 (1989) 53.
7 A. M. Katti and G. Guiochon, *J. Chromatogr.*, 449 (1988) 25.
8 J. Newburger, L. Liebes, H. Colin and G. Guiochon, *Sep. Sci. Technol.*, 22 (1987) 19.
9 J. Newburger and G. Guiochon, *J. Chromatogr.*, 484 (1989) 153.
10 J. Perry, presented at *the 6th Symposium on Preparative Chromatography, Washington, DC, May 8–10, 1989.*
11 G. Guiochon, S. Ghodbane, S. Golshan-Shirazi, J. X. Huang, A. Katti, B. C. Lin and Z. Ma, *Talanta*, 36 (1989) 19.
12 S. Golshan-Shirazi and G. Guiochon, *Anal. Chem.*, 61 (1989) 1368.
13 A. M. Katti and G. Guiochon, *J. Chromatogr.*, 499 (1990) 21.
14 S. Golshan-Shirazi and G. Guiochon, in preparation.

15 S. Golshan-Shirazi and G. Guiochon, *Anal. Chem.*, 60 (1988) 2364.
16 G. Guiochon, S. Golshan-Shirazi and A. Jaulmes, *Anal. Chem.*, 60 (1988) 1856.
17 S. Golshan-Shirazi and G. Guiochon, *J. Phys. Chem.*, 93 (1989) 4341.
18 J. N. Wilson, *J. Am. Chem. Soc.*, 62 (1940) 1583.
19 E. Glueckauf, *Proc. R. Soc. London, Ser. A*, 186 (1946) 35.
20 D. DeVault, *J. Am. Chem. Soc.*, 65 (1943) 532.
21 H. K. Rhee, R. Aris and N. R. Amundson, *Philos. Trans. R. Soc. London, Ser. A*, 267 (1970) 419.
22 G. Guiochon and L. Jacob, *Chromatogr. Rev.*, 14 (1971) 77.
23 J. C. Giddings, *Dynamics of Chromatography*, Marcel Dekker, New York, 1965.
24 B. C. Lin and G. Guiochon, *Sep. Sci. Technol.*, 24 (1989) 32.
25 B. C. Lin, Z. Ma and G. Guiochon, *J. Chromatogr.*, 484 (1989) 83.
26 P. Rouchon, M. Schonauer, P. Valentin and G. Guiochon, *Sep. Sci. Technol.*, 22 (1987) 1793.
27 S. K. Godunov, *Mat. Sb.*, 47 (1959) 271.
28 M. Czok and G. Guiochon, *Anal. Chem.*, submitted for publication.
29 A. M. Katti and G. Guiocon, *Anal. Chem.*, 61 (1989) 982.
30 A. M. Katti, R. Ramsey and G. Guiochon, *J. Chromatogr.*, 477 (1989) 119.
31 S. Golshan-Shirazi and G. Guiochon, *Anal. Chem.*, 61 (1989) 1276.

Journal of Chromatography, 484 (1989) 125–151
Elsevier Science Publishers B.V., Amsterdam — Printed in The Netherlands

CHROM. 21 819

ANALYTICAL SOLUTION OF THE IDEAL MODEL OF ELUTION CHROMATOGRAPHY IN THE CASE OF A BINARY MIXTURE WITH COMPETITIVE LANGMUIR ISOTHERMS

II. SOLUTION USING THE *h*-TRANSFORM

SADRODDIN GOLSHAN-SHIRAZI and GEORGES GUIOCHON*

**Department of Chemistry, University of Tennessee, Knoxville, TN 37996-1600 (U.S.A.) and Division of Analytical Chemistry, Oak Ridge National Laboratory, Oak Ridge, TN 37831–6120 (U.S.A.)*

SUMMARY

Using the results published by Helfferich and Klein, an exact solution of the ideal model of chromatography (infinite column efficiency) is derived, giving the band profiles for the two-component elution problem in the case when the equilibrium isotherms are given by the classical competitive Langmuir equations. The variations of the band profile of each component during elution is analyzed and the interactions between the two profiles are investigated. Two concentration shocks appear, one at the front of each component elution profile. The chromatogram is separated into three zones. The first zone, between the two concentration shocks, contains only the first component. The second zone, immediately after the second shock, contains a mixture of the two components. The third zone, at the rear, contains only the second component. The profiles of the two components in the three zones and their concentrations on both sides of the second shock are given by simple analytical equations. If the sample is injected as a rectangular pulse, it takes some time to erode the corresponding concentration plateaux of each component. On both sides of the mixed zone, a second concentration plateau appears for each component. The heights of these plateaux remain constant as long as they are present. The first component plateau disappears rapidly, but the second component plateau, whose formation explains the "tag-along" effect, remains stable as long as the second zone has not vanished and decreases progressively after the two bands are resolved.

Comparison between the profiles obtained as solutions of the ideal model and those calculated using the program of the semi-ideal model, which accounts for the finite efficiency of actual columns, shows very good agreement when the column efficiency exceeds a few hundreds to 1000 plates. The extent of the agreement depends on both the sample size and the column efficiency. The concentration shocks are replaced by shock layers whose thickness is proportional to the column plate height, but depends also on the shock height. The thickness of the second shock, which separates the first and second zones, seems to depend much more than the thickness of the first shock on the actual column efficiency.

0021-9673/89/$03.50

INTRODUCTION

In a previous paper[1], we discussed the derivation of an analytical solution of the ideal model of chromatography in the case of a two-component problem and for the injection of a rectangular pulse of mixture (elution). This solution further assumes that the equilibrium isotherms of the two components in the chromatographic phase system is Langmuirian. We used classical results of the theory of systems of non-linear, quasi-hyperbolic partial differential equations applied to the case of hyperbolic systems such as those encountered in the classical model of ideal chromatography[2,3]. The most important concepts used in this first derivation were the association of a velocity to each value of the concentration and the possibility for the system to propagate concentration shocks or discontinuities[4–6]. Accordingly, the analytical solution obtained is composed of two concentration discontinuities, the first affecting the first component only and the second one affecting both, and of four continuous concentrations profiles that have relatively simple equations[1].

The purpose of this paper is to show that the same results can be derived using the general theory of the ideal model of chromatography constructed by Helfferich and Klein[7] and based on the use of the concept of coherence and of the *h*-transform. The advantage of this second solution is that it makes use of a theoretical tool specifically developed for handling problems of application of the ideal model of chromatography and, accordingly, the analytical solution of a two-component problem appears simpler to derive in that way. A first drawback, however, is that the approach derived by Helfferich and Klein[7] has received modest attention from chromatographers who are not familiar with its distance–time diagrams or with the concepts of coherence and of composition trajectories. A second drawback, which may in part explain that first, is that Helfferich and Klein essentially used their approach to investigate displacement chromatography[7]. This mode of chromatography is claimed by some[7,8] to be the most efficient one for preparative applications. Most users have not yet accepted this last point and, in practice, elution remains the mode of choice for most of the chromatographic purifications carried out in biotechnology laboratories. In addition to the experimental difficulties associated with the need to find a suitable displacer for each separation, this resistance appears to be due to the requirement of a close to total recovery yield by workers who have spent much time and energy in the preparation of minute amounts of rare and valuable biochemicals.

More important, the approach of Helfferich and Klein is closely related to the ideal model and suffers from its unrealistic assumption of an infinitely efficient column. The shock theory suffered originally from the same difficulties, but is has been completed later by the concept of the shock layer, also derived from aeronautical research[9], which gives it a much deeper physical relevance and permits, in chromatography, the convenient handling of columns of finite efficiency. A shock layer propagates at the same velocity as the shock but has a thickness proportional to the column height equivalent to a theoretical plate[10]. In contrast, it has not been possible yet to correct the results derived using the approach of Helfferich and Klein for the finite column efficiency, which is responsible, in both the displacement and elution modes, for a considerable decrease in the recovery yield[11].

THEORY

The theory developed by Helfferich and Klein[7] is based on the use of the concept of coherence, on the determination of distance–time diagrams to represent the migration of band profiles and their progressive transformation and on the use of the *h*-transform to calculate the composition trajectories in these diagrams.

Helfferich and Klein called "coherent" those boundaries which migrate in a way such that "a given concentration of one species [then] remains accompanied by the same set of concentrations of all other species"[12]. This concept of coherent boundaries, first developed for breakthrough curves, has been extended to the migration of concentration pulses.

In principle, the theory of Helfferich and Klein, and especially the *h*-transform itself, should be valid only for stoichiometric retention mechanisms, such as ion exchange. Its extension to other retention mechanisms such as adsorption is straightforward, however, by assuming a fictitious component guaranteeing stoichiometric exchanges between the mobile and stationary phases.

Helfferich and Klein[13] published distance–time diagrams that describe the process of migration, dilution and progressive separation of the bands of the two components of a binary mixture injected as a rectangular pulse[13]. These diagrams have been calculated in the case when the equilibrium isotherm of the two components studied between the phases of the chromatographic system are given by the classical Langmuir isotherms. Hence these diagrams apply to the case we are investigating. However, they calculated only the trajectories of a given concentration, not the elution profiles of the two bands. This derivation is carried out here. We do not report the derivation of the trajectories, for which the interested reader is referred to the original work[7]. In the second part of this paper, the equations obtained for the different parts of the double band elution profile are compared with the results of the semi-ideal model[14].

Preliminary calculations

The principle of the *h*-transform is to replace the concentrations of the three compounds present in the band (the two components of the mixture and the fictitious compound required as explained above) by the two roots of an equation in h, where h is a dummy variable.

In the case of Langmuir competitive isotherms for the two components of a binary mixture eluted by a pure mobile phase, the *h*-transform is written as

$$\sum_{i=1,2}\left[\frac{b_i C_i}{(ha_i/a_1)-1}-1\right]=0 \tag{1}$$

where the coefficients a_i and b_i are those of the Langmuir isotherms (see Table I, eqn. I.1) and C_i is the local concentration of component i in the mobile phase.

This equation has two roots, h_1 and h_2. In contrast to the notation used by Helfferich and Klein, we interchange the subscripts 1 and 2, using the subscripts 1 for the first eluted component and the subscript 2 for the second one. The subscript

3 represents the dummy component, as in ref. 7. As chromatographers classically use $\alpha = a_2/a_1$ for the selectivity of the phase system, we use β where they use α, for

$$\beta = \alpha_{22}\,\alpha_{21}\,\alpha_{23} = \frac{a_2}{a_2}\cdot\frac{a_2}{a_1}\cdot\frac{a_2}{R} = \frac{a_2^2}{a_1 R} \tag{2}$$

since for the fictitious solute $\alpha_{23} = a_2/R$, with $R = \Sigma_i q_i/\Sigma_i C_i$ = constant. The value of that constant can be chosen arbitrarily in the interval $(0, a_1)$. q_i and C_i are the concentrations of the compound i in the stationary and the mobile phases, respectively, at equilibrium.

The solutions of eqn. 1 are:

$$h_1 = \frac{S + \sqrt{(S^2 - 4P)}}{2} \tag{3}$$

and

$$h_2 = \frac{S - \sqrt{(S^2 - 4P)}}{2} \tag{4}$$

where S and P are the sum and the product of the roots h_1 and h_2, respectively. S and P are derived by reducing eqn. 1 to its canonical form:

$$S = h_1 + h_2 = \alpha + 1 + b_2 C_2 + \alpha b_1 C_1 \tag{5}$$

and

$$P = h_1\,h_2 = \alpha(1 + b_2 C_2 + b_1 C_1) \tag{6}$$

Particular values of h_i used later are those corresponding to the pure eluent ($C_1 = C_2 = 0$):

$$h_2' = 1; \qquad h_1' = a_2/a_1 = \alpha \tag{7}$$

and the values, h_1° *and* h_2°, which correspond to the injected sample, and which are obtained by inserting the initial concentrations C_1° and C_2° in eqns. 5 and 6.

In order to compare the results derived in this paper with those calculated in our previous work, we need to derive a relationship between the roots of eqn. 1, h_1° and h_2°, and the roots, r_1 and r_2, of the Offord equation, *i.e.*, the equation which gives the characteristics of the Clairaut differential equation associated with the system of partial differential equations of the ideal model (eqn. 22 in ref. 1). This equation establishes a relationship between the concentrations of the two components which is valid as long as they coexist in the column. The Offord equation is written as

$$\alpha b_1 C_2^\circ r^2 - (\alpha - 1 + \alpha b_1 C_1^\circ - b_2 C_2^\circ) r - b_2 C_1^\circ = 0 \tag{8}$$

Comparison between the roots of eqn. 1, at $C_i = C_i^\circ$, and those of eqn. 8 gives

$$h_2^\circ = 1 + (b_2 + \alpha b_1 r_2)C_2^\circ = 1 + b_2(C_2^\circ - C_1^\circ/r_1) = 1 + b_2 C_2^B = \frac{\alpha}{\gamma} \tag{9}$$

where γ is defined in ref. 1 as $(\alpha b_1 r_1 + b_2)/(b_2 + b_1 r_1)$ and r_1 is the positive root of eqn. 8. C_2^B is the concentration of the plateau of the second component which appears immediately after the end of the second zone of the chromatogram[1] and is equal to $C_2^\circ - C_1^\circ/r_1$.

Finally, the adjustable time, τ, considered in the equations derived by Helfferich and Klein[7] is

$$\tau = \frac{u}{FR}\left(t - \frac{z}{u}\right) \tag{10}$$

and the pulse time ($\Delta\tau$) is

$$\Delta\tau = \frac{ut_p}{FR} \tag{11}$$

where F is the phase ratio, t_p the width of the rectangular pulse of sample injected in the column and R is defined in eqn. 2.

TABLE I

DEFINITIONS

(1) *Equilibrium isotherms:*

$$q_i = a_i C_i/(1 + b_1 C_1 + b_2 C_2) \tag{I.1}$$

where q_i and C_i are the concentration of component i at equilibrium in the stationary and mobile phases, respectively

(2) *Relative retention:*

$$\alpha = a_2/a_1 \tag{I.2}$$

(3) *Constant γ:*

$$\gamma = \frac{\alpha b_1 r_1 + b_2}{b_1 r_1 + b_2} \tag{I.3}$$

(4) *Roots of the Clairaut differential equation:*
They are the roots ($r_1 > 0$, $r_2 < 0$), of the following equation:

$$\alpha b_1 C_2^\circ r^2 - (\alpha - 1 + \alpha b_1 C_1^\circ - b_2 C_2^\circ)r - b_2 C_1^\circ = 0 \tag{I.4}$$

(5) *Loading factor:*

$$L_f = \left(1 + \frac{b_1 r_1}{b_2}\right)L_{f,2} \tag{I.5}$$

$$L_{f,2} = \frac{b_2 C_2^\circ t_p}{t_{R,2}^\circ - t_0} = \frac{b_2 N_2}{F_v(t_{R,2}^\circ - t_0)} = \frac{b_2 N_2}{\varepsilon S L k'_{o,2}} \tag{I.6}$$

Table I gives some useful definitions and equations used in the following sections.

Trajectory of the second component shock and time of certain events

When a rectangular pulse of the binary mixture is injected, and the two components have competitive Langmuir isotherms, the front of each concentration profile is sharp (discontinuity) and the rear is diffuse, or continuous[10]. Consider the plateau at the top of this rectangular injected pulse. The front part moves as the shock, *i.e.*, more slowly than the rear which migrates as a continuous profile[1], so the width of this plateau narrows progressively.

In a distance–time diagram, the coordinates of the intersection between the trajectory of the sharp front (shock) of the second component and the beginning of the continuous part of the first component profile (point I in ref. 1) is given by eqn. A.77 in ref. 7:

$$z_0 = \frac{h_2' h_2^\circ h_1^{\circ 2}}{(h_1^\circ - h_2')\beta} \cdot \Delta\tau \tag{12}$$

and

$$\tau_0 = \frac{h_1^\circ}{h_1^\circ - h_2'} \cdot \Delta\tau \tag{13}$$

Inserting eqns. 2, 6, 7, 10, 11 in eqns. 12 and 13 gives

$$z_0 = ut_p \cdot \frac{(1 + b_1 C_1^\circ + b_2 C_2^\circ)^2}{Fa_2(1 + b_1 C_1^\circ + b_2 C_2^\circ - h_2^\circ/\alpha)} \tag{14}$$

and

$$t_0 = \frac{z_0}{u}\left(1 + \frac{Fa_2}{1 + b_1 C_1^\circ + b_2 C_2^\circ}\right) \tag{15}$$

Eqns. 14 and 15 are identical with eqns. 33 and 34 in ref. 1 if h_2° is replaced by its value given by eqn. 9.

The trajectory of the front of the slower band beyond I is given by eqn A.85 in ref. 7:

$$z_{\Delta_2(\tau)} = \frac{h_2' h_2^\circ}{\beta}[\sqrt{h_2'(t - \Delta\tau)} + \sqrt{(h_1^\circ - h_2')\Delta\tau}]^2 \tag{16}$$

Combining eqns. 2, 6, 7 and 9–11 with eqn. 16 and solving for t gives

$$t = t_p + \frac{z}{u} + \gamma\left[\sqrt{Fa_2 \cdot \frac{z}{u}} - \sqrt{\left(b_1 C_1^\circ + b_2 C_2^\circ + 1 - \frac{1}{\gamma}\right)t_p}\right]^2 \tag{17}$$

which is identical with eqn. 38 in ref. 1. Replacing z by L and z/u by t_0 (dead time) in this equation gives the retention time of the second component, *i.e.*, the elution time of the

second discontinuity of the chromatogram (eqn. 40 of ref. 1). Eqn. 17 remains to represent the trajectory of the second component shock as long as there is a mixed band, *i.e.*, until the separation is complete. The separation between the two bands is just complete at the "crossover point", the coordinates of which are given by eqns. A.88 in ref. 7:

$$z_{1/2} = \frac{h_2^\circ h_2' h_1'^2 (h_1^\circ - h_2') \Delta\tau}{(h_1' - h_2')^2 \beta} \tag{18}$$

and

$$\tau_{1/2} = \left[1 + \frac{h_2'(h_1^\circ - h_2')}{(h_1' - h_2')^2} \right] \Delta\tau \tag{19}$$

Combining eqns. 2, 6, 7 and 9–11 with eqns. 18 and 19 gives

$$z_{1/2} = u \left(\frac{\alpha}{\alpha - 1} \right)^2 \cdot \frac{t_p(b_1 C_1^\circ + b_2 C_2^\circ + 1 - 1/\gamma)}{Fa_2} \tag{20}$$

and

$$t_{1/2} = t_p + \frac{z_{1/2}}{u} \left(1 + \frac{\gamma Fa_2}{\alpha^2} \right) \tag{21}$$

which are identical with eqns. 69 and 70 in ref. 1, giving the trajectory of the point where the resolution between the two bands is just complete. Beyond that point, the slow component band begins to migrate alone but, first, the plateau which has appeared during the progressive separation between the bands of the two components shrinks and disappears. During that time, the trajectory of the front shock of its band is given by the relationship A.93 in ref. 7:

$$z_{\Delta_2(\tau)} = \frac{h_2' h_1' h_2^\circ}{\beta} \left(\tau + \frac{h_1^\circ - h_2'}{h_1' - h_2'} \cdot \Delta\tau \right) \tag{22}$$

Combining this equation with eqns. 2–11 gives

$$t = t_p + \frac{z}{u} + \gamma \left[Fa_1 \cdot \frac{z}{u} - \frac{t_p(1 + b_1 C_1^\circ + b_2 C_2^\circ - 1/\gamma)}{\alpha - 1} \right] \tag{23}$$

This equation is equivalent to eqn. 72 in ref. 1. While the second band front migrates on this trajectory, the concentration plateau of component 2 shrinks. It disappears at point L (see ref. 1) of coordinates given by eqn. A.56 in ref. 7:

$$z_2 = \frac{h_2^{\circ 2} h_2' h_1' (h_1^\circ - h_2') \Delta\tau}{(h_1' - h_2')\,(h_2^\circ - h_2')\beta} \tag{24}$$

and

$$\tau_2 = \left[1 + \frac{h'_2(h^\circ_1 - h'_2)}{(h'_1 - h'_2)(h^\circ_2 - h'_2)}\right]\Delta\tau \tag{25}$$

These equations may be rearranged as the previous ones into

$$z_2 = \frac{\alpha - 1}{\alpha - \gamma} \cdot z_{1/2} \tag{26}$$

and

$$t_2 = t_p + \frac{z_2}{u}\left(1 + \frac{Fa_2\gamma^2}{\alpha^2}\right) \tag{27}$$

which are identical with eqns. 73 and 74 in ref. 1.

Finally, eqn. A.93 in ref. 7 gives the trajectory of the second component front after the separation has been completed. After rearrangement, this equation becomes

$$t = t_p + \frac{z}{u} + \left(\sqrt{Fa_2 \cdot \frac{z}{u}} - \sqrt{b_2 C^\circ_2 t_p}\right)^2 \tag{28}$$

which is equivalent to eqn. 75 in ref. 1, with $z = L$.

The main equations in this section, which give the position of the most important events on the chromatogram, are summarized in Table II. The corresponding points are shown in Fig. 1.

Equations for the continuous parts of the profiles

As the continuous parts of the concentration profiles of the first and second components were given by Helfferich and Klein[7] as the H-function roots, we have to transform the h roots into concentrations. This can be done using the general equation

$$C_j = \frac{\pi_{i=1}^{n}(h_i a_j/a_1 - 1)}{b_j \pi_{i=1, i\neq j}^{n}(a_j/a_i - 1)} \tag{29}$$

In the case of two solutes we have

$$C_1 = \frac{(h_1/\alpha - 1)(h_2/\alpha - 1)}{b_1(1 - \alpha)/\alpha} \tag{30}$$

$$C_2 = \frac{(h_1 - 1)(h_2 - 1)}{b_2(\alpha - 1)} \tag{31}$$

In order to obtain the equations for the continuous parts of the profiles in the different zones of the chromatogram, we need to find first the roots h_1 and h_2 of the H-function in these zones.

TABLE II

RETENTION TIMES OF THE CHARACTERISTIC FEATURES OF THE CHROMATOGRAM IN FIG. 1

(1) *Second shock:*

$$t_{R,2} = t_p + t_0 + \gamma(t^\circ_{R,2} - t_0)(1 - \sqrt{L_f})^2 \qquad \text{(II.1)}$$

(2) *End of the first component band:*

$$t_B = t_p + t_0 + \frac{\gamma}{\alpha}(t^\circ_{R,1} - t_0) \qquad \text{(II.2)}$$

(3) *End of the second component concentration plateau:*

$$t_{B'} = t_B + \frac{\gamma(\gamma - 1)}{\alpha^2}(t_{R,0,2} - t_0) \qquad \text{(II.3)}$$

(4) *End of the second component band:*

$$t_e = t_p + t^\circ_{R,2} \qquad \text{(II.4)}$$

(5) *First shock:*
The retention time of the first shock cannot be calculated analytically. It is derived by calculating the lower boundary of the finite integral of the profiles of the first component (eqns. III.1 and III.2, Table III). This integral is the mass of first component injected[1].

For the diffuse rear part of the slower band profile, the trajectory in a distance–time diagram associated with a certain concentration can be derived from eqns. A.80 and A.81 in ref. 7:

$$z''_2(\tau) = h^{\circ 2}_2 h'_1 \cdot \frac{\tau - \Delta\tau}{\beta} \qquad \text{for } z \leqslant z_2 \qquad (32)$$

and

$$z(h_2,\tau) = h^2_2 h'_1 \cdot \frac{\tau - \Delta\tau}{\beta} \qquad \text{for } z \leqslant z_{\Delta_2(\tau)} \qquad (33)$$

Accordingly, at the column exit ($z = L$), where we have $h'_1 = \alpha$ and $a_2 = (t^\circ_{R,2} - t_0)/Ft_0$, the h_2 root of the H-function in the different zones of the chromatogram is obtained by combining eqns. 2, 10, 11, 32 and 33:

$$h_2 = \sqrt{\frac{t^\circ_{R,2} - t_0}{t - t_p - t_0}} \qquad \text{for } t'_B < t \qquad (34)$$

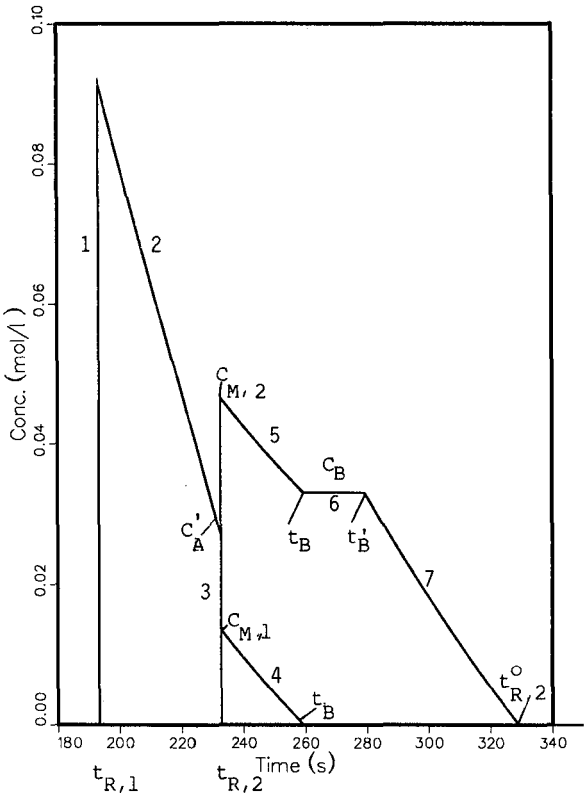

Fig. 1. Example of the solution of the ideal model for a two-component mixture when the two bands are not completely resolved at the end of the column. 1 = Front shock of the first component; 2 = first arc of the first component band; 3 = rear shock of the first component and front shock of the second component; 4 = second arc of the first component band; 5 = first arc of the second component band; 6 = concentration plateau of the second component band; 7 = second arc of the second component band. The retention times of the second concentration shock (3), the end of the first component band and of the mixed zone, the end of the concentration plateau (6) of the second component and the end of the second component zone are given in Table II. The equations for the continuous parts of the concentration profiles of the first component [between the two shocks (2) and after the second shock (4)] and of the second component (between the second concentration shock (5) and the beginning of the plateau and after the end of the plateau (7)] are given in Table III. Experimental conditions: relative retention, $\alpha = 1.20$; relative composition, 1:1; feed concentrations, $C_1^\circ = C_2^\circ = 2.5$ M; column length, 25 cm; phase ratio, $F = 0.25$; $k'_{0,1} = 6.0$; injection duration, 1 s. Retention times of the fronts: 193.3 and 232.7 s. Retention times of the rear plateau of the second component profile: 259.4 and 279.3 s. Retention time of the second component at infinite dilution: 328 s. Concentrations of the first component: at the top of the first shock, 0.091 M; at the front of the second shock, 0.0027 M; at the rear of the second shock, 0.014 M. Concentration of the second component: at the top of the second shock, 0.046 M; at the rear plateau, 0.033 M.

$$h_2 = h_2^\circ = \alpha/\gamma \qquad \text{for } t_{R,2} \leqslant t \leqslant t'_B \tag{35}$$

$$h_2 = h'_2 = 1 \qquad \text{for } t \leqslant t_{R,2} \tag{36}$$

(see Tables II and III and Fig. 1 for the definition of t'_B and similar parameters).

TABLE III

EQUATIONS FOR THE CONTINUOUS PARTS OF THE CHROMATOGRAM SHOWN IN FIG. 1

(1) *First arc of the first component band:*

$$t = t_p + t_0 + (t_{R,1,0} - t_0)\left\{\frac{1}{(1 + b_1C_1)^2} - L_{f,2}\cdot\frac{\alpha - 1}{\alpha}\cdot\frac{1}{[(\alpha - 1)/\alpha + b_1C_1]^2}\right\} \qquad \text{(III.1)}$$

(2) *Second arc of the first component band:*

$$C_1 = \frac{1}{b_1 + b_2/\alpha r_1}\left[\sqrt{\left(\frac{\gamma}{\alpha}\cdot\frac{t^\circ_{R,1} - t_0}{t - t_p - t_0}\right)} - 1\right] \qquad \text{(III.2)}$$

(3) *First arc of the second component band:*

$$C_2 = \frac{1}{b_2 + \alpha b_1 r_1}\left[\sqrt{\left(\gamma\cdot\frac{t^\circ_{R,2} - t_0}{t - t_p - t_0}\right)} - 1\right] \qquad \text{(III.3)}$$

(4) *Second arc of the second component band:*

$$C_2 = \frac{1}{b_2}\left[\sqrt{\left(\frac{t^\circ_{R,2} - t_0}{t - t_p - t_0}\right)} - 1\right] \qquad \text{(III.4)}$$

Similarly, for the diffuse rear part of the faster pulse, the trajectories associated with a certain concentration (*i.e.*, value of h_1) in a distance–time diagram can be derived from eqns. A.84 and A.90 in ref. 7:

$$z(h_1,\tau) = h_1^2h_2^\circ\cdot\frac{\tau - \Delta\tau}{\beta} \qquad \text{for } z \leqslant z_{\Delta_2(\tau)} \qquad (37)$$

and

$$z(h_1,\tau) = \frac{h_1^2h_2'}{\beta}\left\{\tau - \left[1 - \frac{(h_1^\circ - h_2')(h_2^\circ - h_2')}{(h_1 - h_2')^2}\right]\Delta\tau\right\} \qquad \text{for } z_{\Delta_2(\tau)} \leqslant z \leqslant z_{\Delta_1(\tau)} \quad (38)$$

Accordingly, at the column exit, the values of h_1 in the different zones of the chromatogram are given by

$$h_1 = \sqrt{\gamma\cdot\frac{t^\circ_{R,2} - t_0}{t - t_p - t_0}} \qquad \text{for } t_{R,2} \leqslant t \leqslant t_B \qquad (39)$$

$$h_1 = h_1' = \alpha \qquad \text{for } t_B < t \qquad (40)$$

and

$$t = t_p + t_0 + \frac{\alpha(t^\circ_{R,2} - t_0)}{h_1^2} - (\alpha - 1)b_2C_2^\circ t_p\cdot\frac{1}{(h_1 - 1)^2} \qquad \text{for } t_{R,1} \leqslant t \leqslant t_{R,2} \quad (41)$$

Combining equations 9, 34–36 and 39–41 with eqns. 30 and 31 gives eqns. 43, 28 and 47 in ref. 1 (the two slanted parts of the rear profile of the second component band, before and after the intermediate plateau and the concentration of this plateau) and eqns. 63 and 44 in ref. 1 (the two parts of the rear profile of the first component band, before and after the second shock of the chromatogram).

The concentrations of the first and second components at the second shock are obtained as follows. In all instances, h_1 is obtained by solving eqn. 41 with $t = t_{R,2}$. On the front side of the second shock, h_2 is equal to 1; on the rear side of the second shock, h_2 is equal to α/γ (eqn. 35). The concentrations are obtained by substituting appropriate values of h_1 and h_2 in eqns. 30 and 31. The results are identical with eqns. 51, 52 and 55 in ref. 1 (see Table IV).

The equations giving the continuous parts of the profile are summarized in Table III. The position of the corresponding arcs are indicated on Fig. 1. The values of the concentrations in the most important points of the chromatograms are summarized in Table IV.

TABLE IV

EQUATIONS FOR SOME SPECIFIC CONCENTRATIONS

(1) *Maximum concentration of the second component:*

$$C_{2,M} = \frac{1}{b_2 + \alpha b_1 r_1} \cdot \frac{\sqrt{L_f}}{1 - \sqrt{L_f}} \tag{IV.1}$$

(2) *Concentration of the first component on the front side of the second shock:*

$$C_{1,A'} = \frac{[(1-\alpha)/\alpha] + \sqrt{L_f}}{1 - \sqrt{L_f}} \tag{IV.2}$$

(3) *Concentration of the first component on the rear side of the second shock:*

$$C_{1,M} = \frac{r_1}{b_2 + \alpha b_1 r_1} \cdot \frac{(1-\alpha) + \alpha\sqrt{L_f}}{1 - \sqrt{L_f}} \tag{IV.3}$$

(4) *Concentration of the second component plateau:*

$$C_{2,B} = \frac{\alpha - 1}{b_2 + \alpha b_1 r_1} \tag{IV.4}$$

(5) *Concentration of the first component plateau:*

$$C_{1,A} = C_1^{\circ}\left(1 + \frac{b_2}{\alpha b_1 r_1}\right) \tag{IV.5}$$

(6) *Maximum concentration of the first component:*
As the retention time of the first shock, the maximum concentration of the first component (*i.e.*, the front shock height) cannot be calculated analytically. This concentration is obtained by placing the retention time of the first component shock in eqn. III.1.

RESULTS AND DISCUSSION

In this section we first discuss the mechanism of the progressive separation of the bands of a binary mixture, as it can be derived from the profiles given by the analytical solution of the ideal model. Then we compare the profiles obtained by the analytical solution of the ideal model and by numerical solution of the semi-ideal model. In a separate publication[15], we shall show that there is excellent agreement between these theoretical profiles and those determined experimentally in the case when the components of a binary mixture equilibrate between the two phases of the chromatographic system as predicted by the competitive Langmuir isotherms.

Progressive separation of the bands of the two components

We have calculated the band profiles predicted by the equations in Tables II–IV for two binary mixtures of relative compositions 1:3 and 3:1. In the following illustrations, Figs. 2a–6a correspond to the 3:1 muxture and Figs. 2b–6b to the 1:3 mixture. The numerical values used for the parameters of the isotherms (eqn. I-1, Table I) are given in Table V. The feed concentrations of the two components are 1.25 and 3.75 M, respectively. The duration of the injection pulse, t_p, is 1 s. The value of the relative retention, α, is 1.30. The mobile phase velocity is 0.6 cm/s. The different chromatograms shown in Figs. 2–7 correspond to columns of increasing length. In all these figures, curves 1 and 2 are the elution profiles of the first and second components, respectively, predicted by the analytical solution of the ideal model derived from the equation in Tables II–IV. The profiles 3 and 4 are their elution profiles calculated using the numerical solution of the semi-ideal model. These profiles are discussed in the next section. Insets in the figures illustrate some particular features of the chromatogram.

Fig. 2a and b show the elution profiles of a binary mixture with a relative retention equal to 1.30 at the exit of a 1-cm long column. This length is less than z_0 (eqn. 12) and the plateaux of the two compounds corresponding to the injection pulse are not completely eroded yet. However, two plateaux at the concentrations $C_{1,A}$ and $C_{2,B}$ (Table IV) have formed. The first corresponds to an increase in the concentration of the first component, due to the displacement effect caused by the second component. The second plateau, on the tail of the second component, can be seen in the data file used to draw the plot but it is not visible on the figure. It can be distinguished on the inset in Fig. 2a, between 12 and 14 s. There is a distinct separation between the fronts of the two bands in Fig. 2a. This separation exists also in Fig. 2b, but it is smaller and is

TABLE V

NUMERICAL VALUES OF THE COEFFICIENTS OF THE COMPETITIVE LANGMUIR ISOTHERMS USED FOR THE TWO COMPOUNDS STUDIED

The column saturation capacity for the first component is 1.59 mmol/cm (4.6 mm I.D.).

Coefficient	*Value*
a_1	24
a_2	31.2 ($\alpha = 1.30$)
b_1 (l/mol)	2.5
b_2 (l/mol)	3.25

barely visible. The band of the minor, first component (Fig. 2b) begins with a very thin spike which is easily explained by the mathematical properties of the solution[1] but has no chance of being seen in the experimental profiles because of the intense diffusion flux close to a shock layer.

Fig. 3a and b show chromatograms obtained under conditions such that the injection pulse plateau has just disappeared ($L = z_0$, see eqn. 12). The corresponding column lengths at which this phenomenon takes place are different with the 3:1 and the 1:3 mixtures, being 1.20 and 1.35 cm, respectively. The plateau of the first component, at $C_{1,A}$, begins immediately to erode away and disappears rapidly. On the other hand, the plateau of the second component at $C_{2,B}$ becomes longer and longer, while the two shocks becomes further apart. As the column length is barely longer for Fig. 3a and b than for Fig. 2, the separation between the two bands is hardly improved.

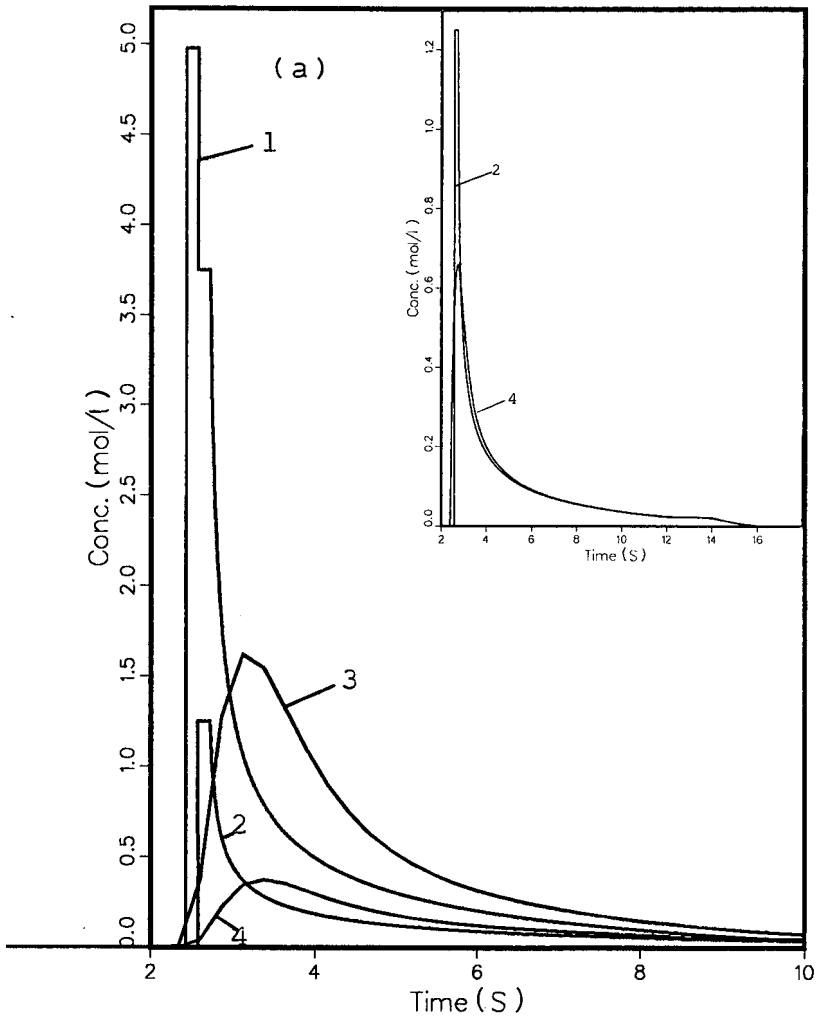

Fig. 2.

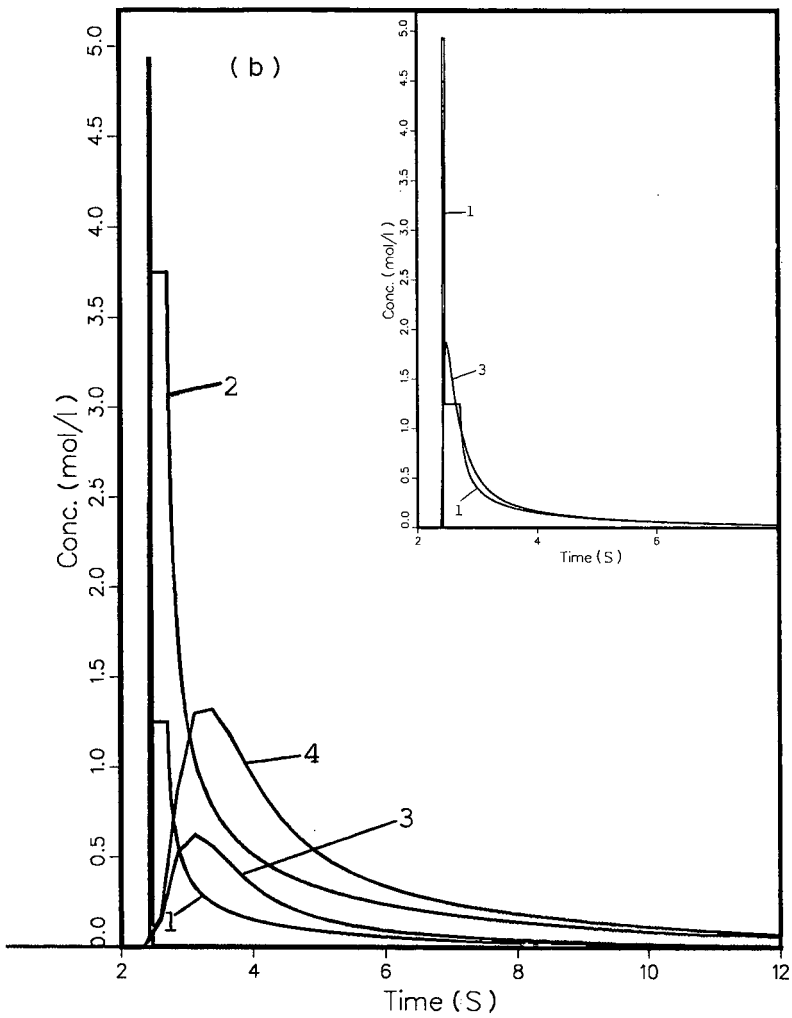

Fig. 2. Band profiles of the components of a binary mixture at the end of a 1-cm long column. Mobile phase flow velocity, 0.6 cm/s; flow-rate for a 4.6 mm I.D. column, 4.8 ml/min; $\alpha = 1.30$; $k'_{0,1} = 6.0$; phase ratio, 0.25; porosity, 0.80. Solution of the ideal model: curves 1 (first component) and 2 (second component). Numerical solution of the semi-ideal model with $H = 0.01$ cm: curves 3 (first component) and 4 (second component). Insets: numerical solution of the semi-ideal model with $H = 0.001$ cm. (a) Relative feed composition: 3:1. Concentrations of the components in the feed: $C_1^\circ = 1.25$ M, $C_2^\circ = 3.75$ M. $L_{f.2} = 31.25\%$. Inset: solution of the ideal model for the second component (curve 2) and solution of the semi-ideal model with $H = 0.001$ cm (curve 4). (b) Same as (a), including total sample size, except relative feed composition = 1:3. $C_1^\circ = 3.75$ M, $C_2^\circ = 1.25$ M. $L_{f.2} = 93.75\%$. Inset: solution of the ideal model for the first component (curve 1) and solution of the semi-ideal model with $H = 0.001$ cm (curve 3).

An intermediate chromatogram, on which a partial separation takes place between the two bands, is shown in Fig. 4a and b, both of which correspond to a column length of 10 cm. In the first instance (Fig. 4a), the first component has a small shock on its rear profile, at the time as the front shock of the second component takes place. The displacement effect of the first component by the second is weak. The rear

shock of the first component profile corresponds to an abrupt decrease in the amount of that component associated with the surge of the second component concentration which takes place at its front shock. The plateau at the end of the second component profile is long and this profile is spread over a period that considerably exceeds the width of the profile of the same amount of that compound when injected pure, under the same conditions. In Fig. 4b, the concentration discontinuities at the second shock are much more important that in Fig. 4a. The displacement effect of the first component by the second is very significant, because now the surge of concentration of the second component is very strong. The first component band has a very narrow, tall first part, followed by a small tail which lasts about twice as long as the first part of the band. On the other hand, the plateau on the rear part of the second component profile is narrow and its concentration is high. It will not result in a marked "tag-along" effect.

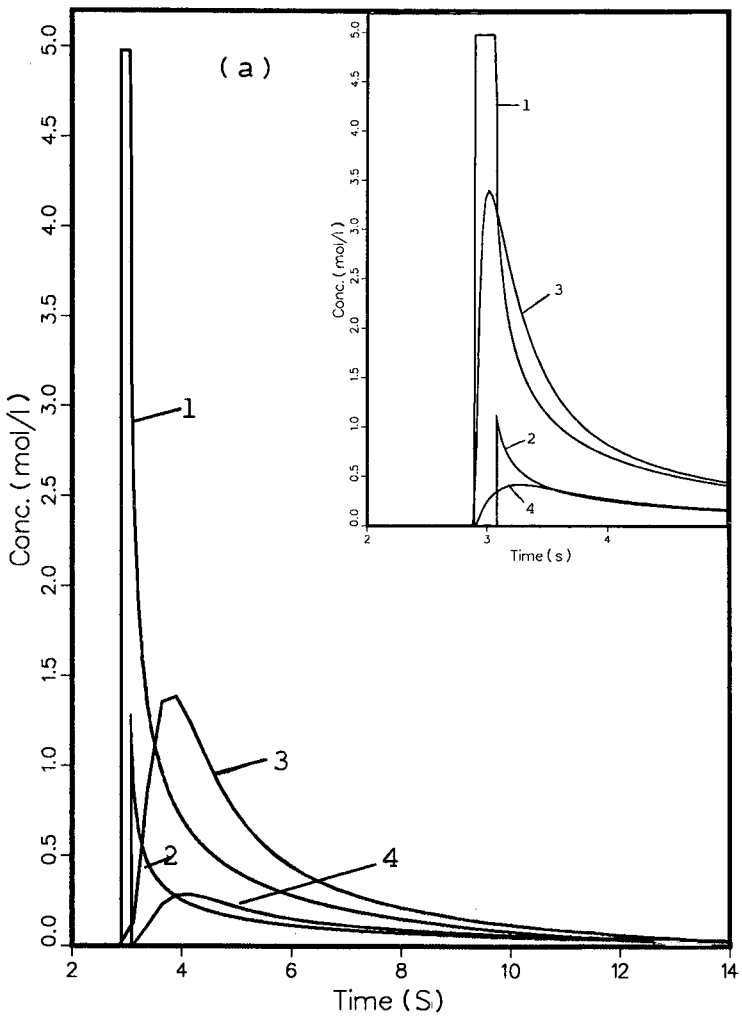

Fig. 3.

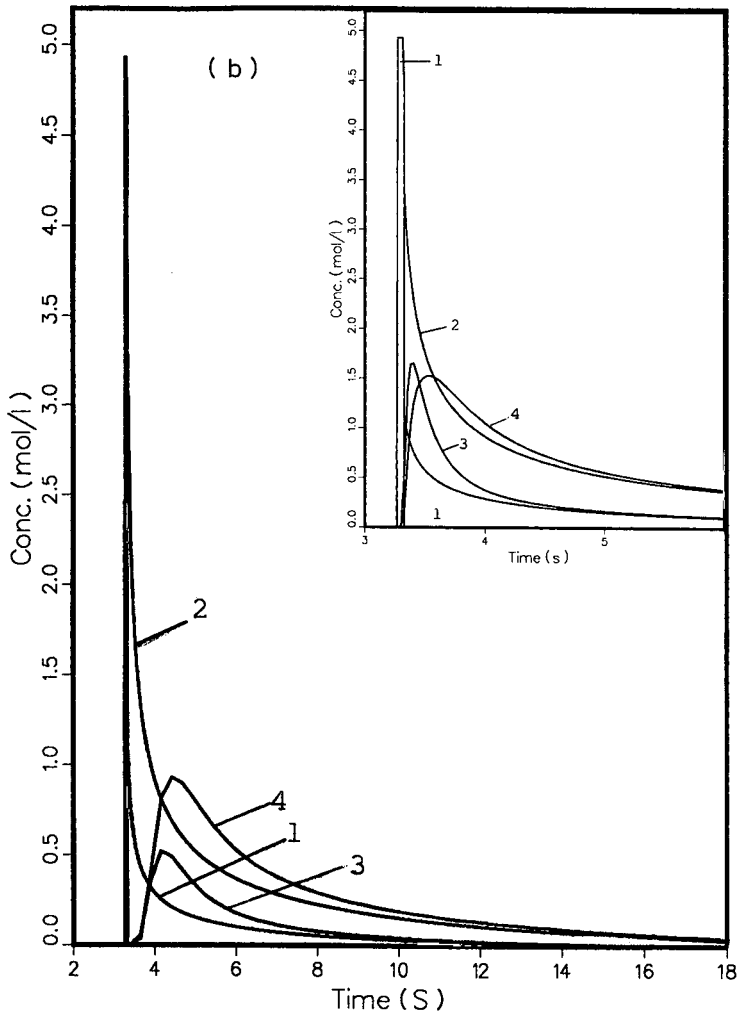

Fig. 3. Same as Fig. 2, but profiles at the end of a column such that the injection pulse plateau has just been eroded. (a) Same as Fig. 2a, but column length = 1.20 cm. $L_{f,2}$ = 26%. Inset: same as main figure, but H = 0.001 cm for the solution of the semi-ideal model. (b) Same as Fig. 2b, but column length = 1.35 cm. $L_{f,2}$ = 69.4%. Inset: same as main figure, but H = 0.001 cm for the solution of the semi-ideal model.

It is obvious in Fig. 4b that under the conditions selected, the first component can be recovered in a reasonable yield, with a high degree of purity, but that the same is not true for the second component.

The chromatograms in Fig. 5a and b correspond to the column length for which the mixed band or zone II of the chromatogram just disappears. The two bands are totally resolved for the first time. The shock of the second component is eluted just when the concentration of the first component becomes zero, the rear profile shock of this first component has just vanished, but there is still a plateau at the top of the second component profile. This phenomenon takes place for column lengths that

depend on the composition of the feed. The column length is equal to $z_{1/2}$ (see eqn. 20). In Fig. 5a and b, they are 19.7 and 22.2 cm for the 3:1 and the 1:3 mixtures, respectively.

Beyond the point where the two bands are resolved, they continue their migration. The plateau at the top of the second band erodes progressively because the velocity associated with a concentration on a continuous profile is higher than the velocity of a shock from the baseline to that same concentration[1]. The point at the back of the plateau of the second component moves faster than the point at its front, so the plateau narrows down and eventually disappears. Fig. 6a and b show the chromatograms at the column lengths for which this happens. The phenomenon takes place faster when the concentration of the second component is higher, because the plateau is much narrower (compare Fig. 5a and b). The corresponding column length is given by eqn. 26. It is much shorter in Fig. 6b (L = 28 cm) than in Fig. 6a (L = 65.9

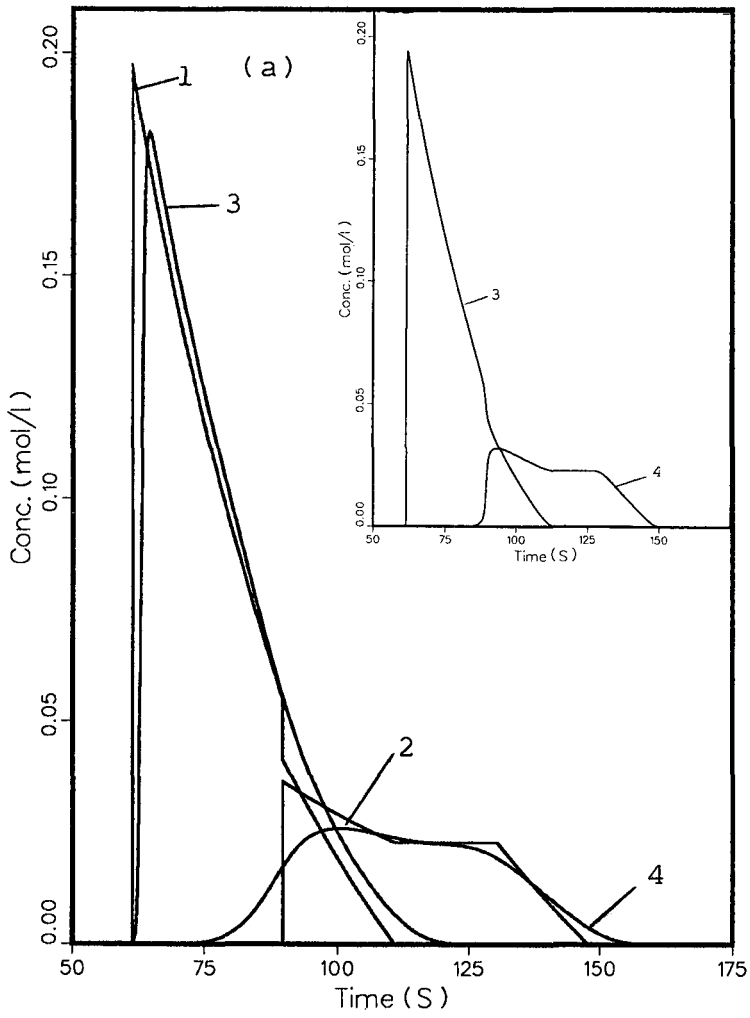

Fig. 4.

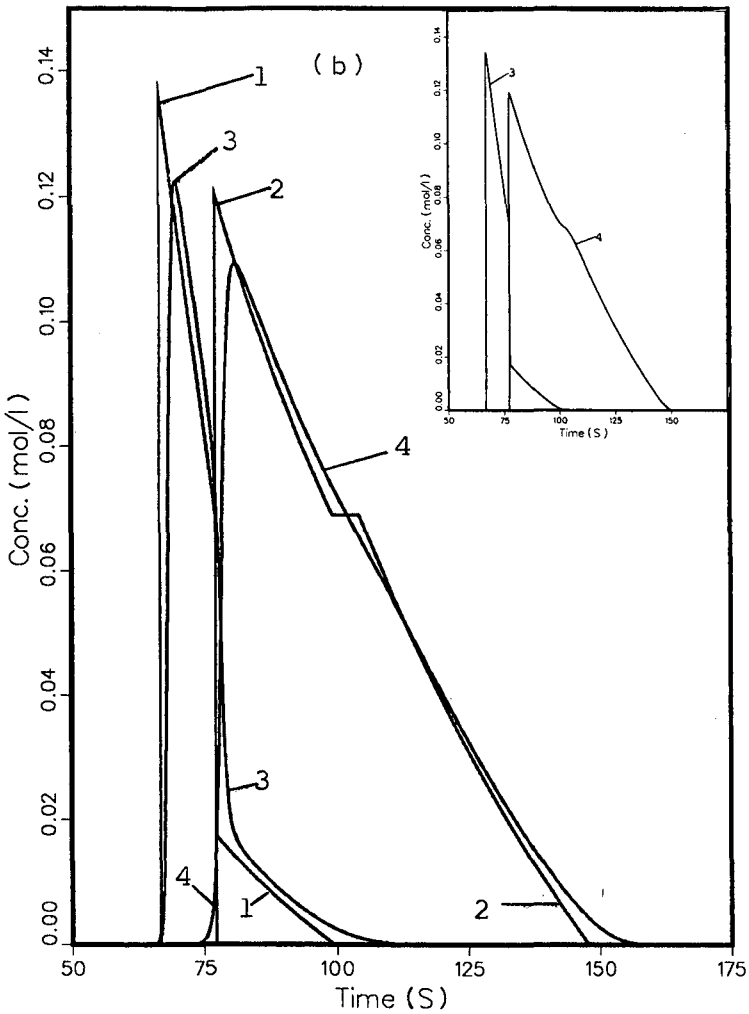

Fig. 4. Same as Fig. 2, except column length = 10 cm. (a) Same as Fig. 2a, 3:1 mixture. $L_{f,2}$ = 3.1%. Inset: concentration profiles of the two components obtained as solution of the semi-ideal model, with H = 0.001 cm (N = 10 000 theoretical plates). (b) Same as Fig. 2b, 1:3 mixture. $L_{f,2}$ = 9.3%. Inset: as for inset in (a).

cm), and the resolution between the two bands when the plateau disappears is much better in Fig. 6a.

When the plateau at the top of the second component band has disappeared, this band continues its migration as if it had never interacted with the first component band[1]. The band profile is identical with that for a band of the same amount of that compound injected pure (see Fig. 7). This is not true for the band of the first compound, which always remains narrower and taller than if no interaction had taken place. Fig. 8 illustrates this phenomenon. It shows a comparison between the band profiles of the same amount of the same 1:3 mixture derived from the single compound and from the two-component ideal model solutions. In the case of the two-component

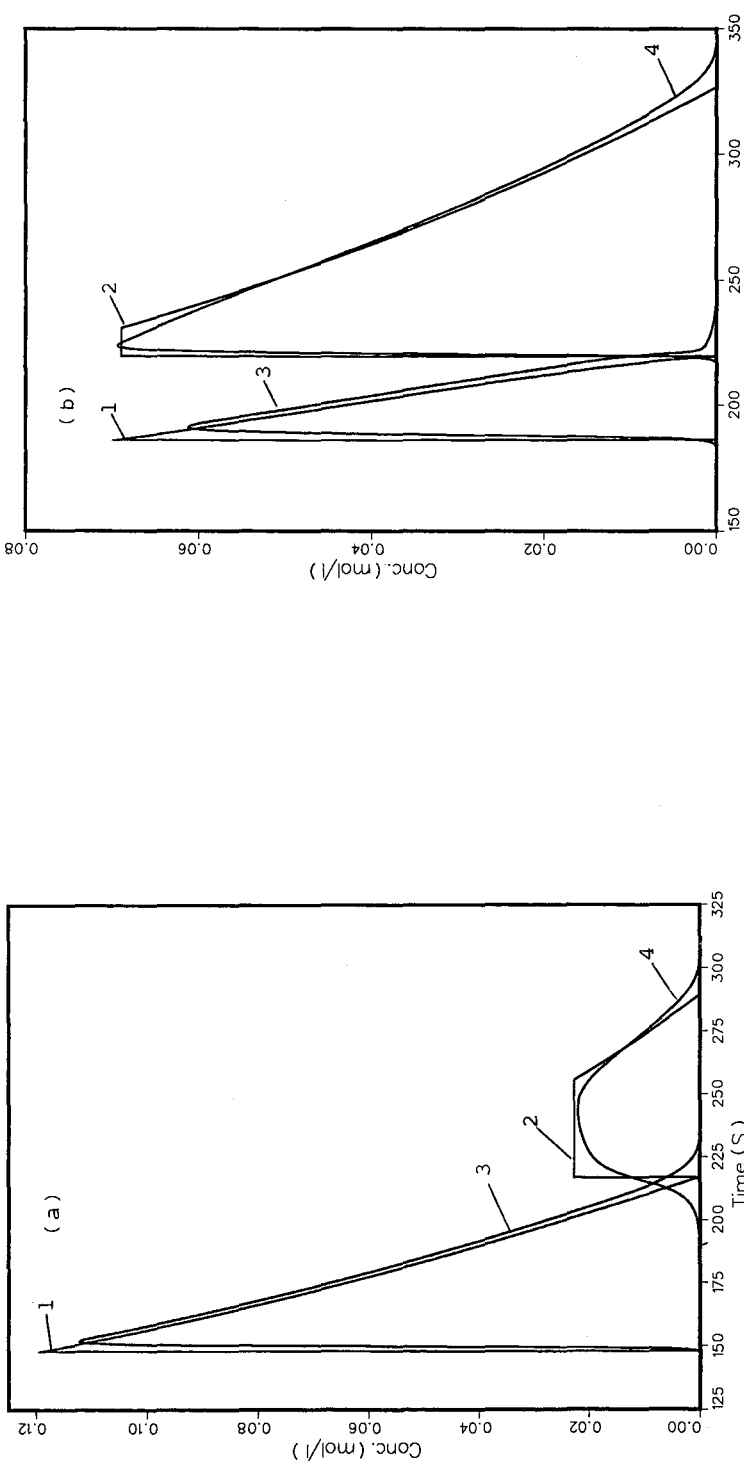

Fig. 5. Same as Fig. 2, but profiles at the end of a column such that the two bands are just resolved. (a) Same as Fig. 2a, 3:1 mixture, but column length = 19.7 cm. $L_{f,2}$ = 1.59%. (b) Same as Fig. 2b, 1:3 mixture, but column length = 22.2 cm. $L_{f,2}$ = 4.22%.

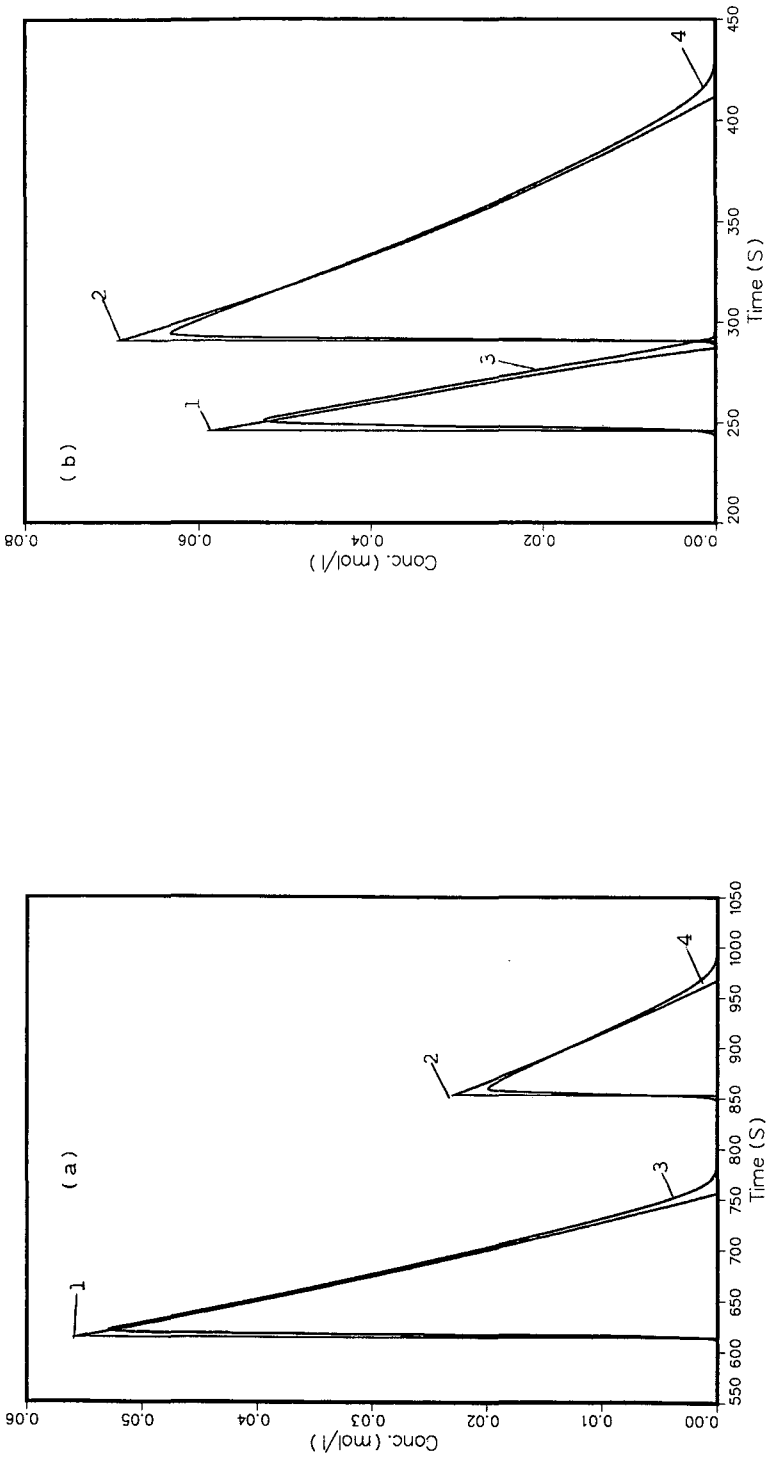

Fig. 6. Same as Fig. 2, but profiles at the end of a column such that the plateau at the top of the second component band is just totally eroded. (a) Same as Fig. 2a, 3:1 mixture, but column length = 65.9 cm. $L_{f,2}$ = 0.47%. (b) Same as Fig. 2b, 1:3 mixture, but column length = 28.0 cm. $L_{f,2}$ = 3.35%.

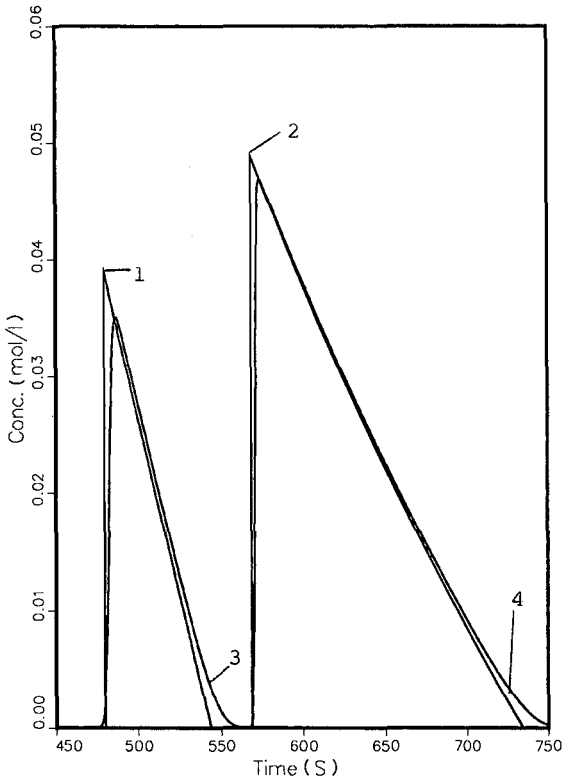

Fig. 7. Same as Fig. 2b, but at the end of a 50-cm long column. $L_{f,2} = 1.87\%$.

model, the solution obtained is that already shown in Fig. 7; this model takes the band interaction due to the competitive adsorption isotherms into account. The single compound model gives the band profiles which would be observed for compounds that do not interact. The profiles obtained for the second component are identical. In contrast, the profiles obtained for the first component are markedly different. The displacement of the first component by the second increases the resolution between the bands and also increases the maximum concentration of the fist component.

Comparison between the profiles predicted by the ideal and semi-ideal models

In order to achieve as realistic a simulation as possible, we have assumed that the column height equivalent to a theoretical plate, H, is constant along the whole column. In Figs. 2–7, profiles 3 and 4 are those calculated using the semi-ideal model and selecting the integration increments in order to simulate a column with an HETP of 0.01 cm. This is a low efficiency for a high-performance liquid chromatographic column, but the simulated column is operated at a very high velocity of 0.6 cm/s because it has been shown that maximum production rate in preparative chromatography is achieved at high mobile phase flow velocities[16]. Under these conditions, this HETP value would correspond to a well packed column ($A = 1$ in the classical Knox plate-height equation[17]) filled with 15-μm particles and operated at a reduced

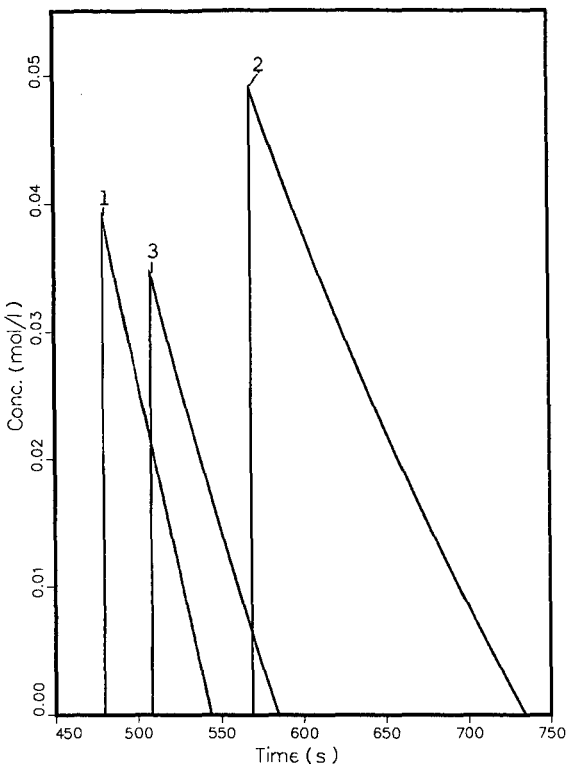

Fig. 8. Influence of the interaction term in the isotherm equation on the band profile of two well resolved compounds. Comparison between the solutions of the single-compound and the two-component ideal models for the same amount of the same sample as in Fig. 7. Profile 1, first component in a binary mixture; profile 2, second component in a binary mixture or alone (the two profiles cannot be distinguished); profile 3, first component alone.

flow-rate of approximately 90. As a term of comparison, profiles 3 and 4 in the insets in Figs. 2, 3 and 4 were calculated with a ten times lower HETP value. In practice, most experimental conditions correspond to intermediate values of the HETP.

The consequence of the choice of the HETP value is that, for very short columns (Fig. 2a–3b) which have a very low efficiency, the agreement between the profiles derived from the analytical solution of the ideal model and the profiles calculated numerically is poor. The apparent axial diffusion, which includes the consequences of a finite rate of mass transfer between the two phases, explains the shallow profiles 3 and 4 in Figs. 2 and 3. The concentration shocks have been considerably relaxed. Note, however, that the time scale is in seconds and that the front parts of these profiles last about 0.5 s (Fig. 2) to 1 s (Fig. 3). As predicted by the ideal model, however, the two fronts are nearly coincidental in Figs. 2b and 3b, whereas they are separated in Figs. 2a and 3a.

If we compare profiles 3 and 4 in Figs. 2a, 2b, 3a, 3b, 4a and 4b and the profiles in the insets in these figures, we see how the column efficiency is critical in determining how closely the band profile follows the prediction of the ideal model. The agreement,

which is poor when the efficiency is low, improves rapidly with increasing column efficiency and becomes very good at high plate numbers (see insets).

For Figs. 4–7, the column efficiency is higher and the agreement between the profiles derived from the ideal and semi-ideal models becomes good. Although the front shocks are much softened and the plateaux totally eroded, the characteristic features of the profiles predicted by the ideal model can still be found on the profiles calculated with the semi-ideal model. In Fig. 4a, however, the second shock has disappeared from the rear of the first component profile and, correspondingly, there is not much of a shock layer at the front of the second component profile (curve 4). As shown by the inset in Fig. 4a, the slope of this front and, accordingly, the recovery yields and production rates for both components depend very much on the column efficiency. With an extremely efficient column, the band profiles obtained will be very close to those predicted by the ideal model. In Fig. 4b, in contrast, the second shock predicted by the ideal model becomes a thin shock layer on the calculated profiles. The tail of the first component (profile 3) is slightly larger than predicted. The plateau on the rear of the second component profile has disappeared. The tail of that profile

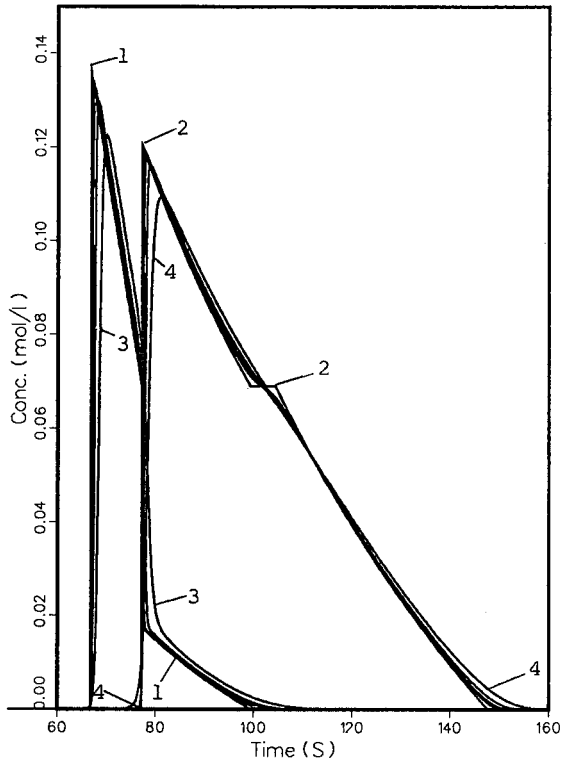

Fig. 9. Comparison between the profiles derived from the analytical solution of the ideal model (profiles 1 and 2) and the profiles calculated as solutions of the semi-ideal model of chromatography, at the outlet of a 10-cm column. Loading factor, $L_{f,2}$ = 9.4%. Relative feed composition: 1:3. Other conditions as in Fig. 2, except column efficiency. Profiles 3 and 4 correspond to 1000 theoretical plates. The three intermediate profiles correspond to 2500, 5000 and 10 000 theoretical plates.

(curve 4) has no inflection point. The chromatogram in the inset shows, however, that with an extremely efficient column a hump is observed, which is the residual of the plateau.

In Fig. 5a and b, the plateaux at the top of the second band profile have disappeared, but the bands are wider than normal chromatographic bands. The calculated profiles of the first component in Fig. 5a and b and all the calculated profiles in Figs. 6 and 7 are very similar to those predicted by the ideal model. They are only slightly rounded at the top, with shock layers at the front and slightly tailing rears.

Fig. 9 compares the profiles calculated with column efficiencies of 1000, 2500, 5000 and 10 000 theoretical plates with the profiles derived from the analytical solution of the ideal model. Only the first profile (N = 1000 plates) is significantly different from the others. For the three larger plate numbers, the rear of the second component profile exhibits an inflection point at the concentration predicted by the ideal model for the plateau.

CONCLUSION

The approach developed by Helfferich and Klein[7] permits the derivation of the elution profiles of the two components of a binary mixture in the case of an infinitely efficient column when the isotherms of the two components are given by the classical competitive Langmuir equations. Although tedious and lengthy, the derivation is simple and straightforward. It results in very simple algebraic equations which are easy to calculate. Although the profiles obtained are unrealistic, because real columns have a finite efficiency, they give an excellent first approximation of the actual band profiles obtained with columns having an efficiency larger than 1500–2000 theoretical plates, at values of the loading factor in excess of 1% of the column saturation capacity. Accordingly, these results can serve as a basis for a theory of the optimization of the experimental conditions in preparative liquid chromatography. More accurate results could then be obtained, when needed, by proceeding to numerical calculations[14]. On the other hand, the results derived from the analytical solution of the ideal model have the major advantage of showing the trends and permitting the rapid determination of the experimental conditions which are worthy of further detailed investigation, either by simulation or by carrying out actual experiments.

Unfortunately, it is difficult to extend the analytical solution of the ideal model to the case of a three-component mixture. The third-degree algebraic equations obtained cannot be solved simply (the Cantor formulae appear to be too difficult to handle). Numerical solutions of these equations could be possible in any practical situation. It is not obvious then whether the advantage of this rapid numerical calculation of the shock retention times and of the different arcs of continuous profiles of the three components in the case of the ideal model solved by the Helfferich and Klein equations would compensate for the much higher accuracy of the numerical solution of the semi-ideal model, which correctly takes the finite column efficiency into account.

SYMBOLS[a]

a_1, a_2	coefficients (origin slope) in the Langmuir isotherm (eqn. I.1)
b_1, b_2	coefficients in the Langmuir isotherm (eqn. I.1)
C_1, C_2	concentrations of the first and second solutes (components of the mixture) in the mobile phase, respectively (eqn. I.1)
q_1, q_2	concentrations of the first and second solutes in the stationary phase at equilibrium with the mobile phase, respectively (eqn. I.1)
C_1°, C_2°	concentrations of the two components in the sample plug introduced in the column
$C_{1,A}$	concentration of the first component plateau (eqn. IV.5)
$C_{2,B}$	concentration of the second component plateau (eqn. IV.4)
$C_{1,A'}$	concentration of the first component on the front side of the second shock (eqn. IV.2)
$C_{1,M}$, $C_{2,M}$	concentrations of the two components at the rear of the second shock (eqns. IV.1 and IV.3)
F	phase ratio (eqn. 10)
h	dummy variable (eqn. 1)
h_1, h_2	roots of eqn. 1
k_0'	column capacity factor at infinite solute dilution ($k_0' = Fa$)
L_f	loading factor for the mixed zone (eqn. I.5)
$L_{f,2}$	loading factor for the second component (eqn. I.6)
N_2	amount of the first component in the injected pulse, mole (eqn. I.6)
r_1, r_2	roots of eqn. 8
u	linear velocity of the mobile phase (eqn. 10)
t	time (eqn. 10)
t_B	elution time of a concentration $C_{2,B}$ on the band tail (eqn. II.2); this is also the time when ends the elution of the first component zone
t_B'	time when ends the elution of the plateau of the second component zone, at concentration $C_{2,B}$ (eqn. II.3)
$t_{R,1}$, $t_{R,2}$	retention times of the two concentration shocks (eqn. II.1)
t_0, z_0	coordinates of the point I, where the top width of the injected sample pulse of the second component shrinks to zero (eqns. 14 and 15)
$t_{1/2}$, $z_{1/2}$	coordinates of the point K, where the zones of the two components are just resolved (eqns. 20 and 21)
t_2, z_2	coordinates of the point L, where the concentration plateau on the tail of the second component at $C_{2,B}$ just disappears (eqns. 26 and 27)
t_0	hold-up time of the column (L/u)
t_p	width of the injected pulse (eqn. 11)
$t_{R,1}^\circ$, $t_{R,2}^\circ$	retention time of the two components under linear conditions
S	cross-sectional area of the column (eqn. I.6)
z	abscissa along the column (eqn. 10)

[a] The Roman numbers refer to equations in the corresponding Tables (*e.g.*, eqn. IV.5 is the fifth equation in Table IV).

α	relative retention of the two components at infinite dilution (eqn. I.2)
β	product of the separation factors (eqn. 2)
γ	convenient combination of parameters (eqn. I.3)
ε	column total porosity (eqn. I.6)
τ	adjusted time (eqn. 10)
$\Delta\tau$	duration of injection pulse, in units of adjusted time (eqn. 11)

Subscripts

1, 2	lesser and the more retained components of the sample, respectively.

ACKNOWLEDGEMENTS

This work was supported in part by grant CHE-8715211 of the National Science Foundation and by the cooperative agreement between the University of Tennessee and the Oak Ridge National Laboratory.

REFERENCES

1 S. Golshan-Shirazi and G. Guiochon, *J. Phys. Chem.*, 93 (1989) 4143.
2 J. N. Wilson, *J. Am. Chem. Soc.*, 62 (1940) 1583.
3 D. DeVault, *J. Am. Chem. Soc.*, 65 (1943) 532.
4 R. Courant and K. O. Friedrichs, *Supersonic Flow and Shock Waves*, Wiley, New York, 1948.
5 P. D. Lax, *Commun. Pure Appl. Math.*, 10 (1957) 537.
6 R. Aris and N. R. Amundson, *Mathematical Methods in Chemical Engineering*, Vol. 2, Prentice-Hall, Englewood Cliffs, NJ, 1973.
7 F. Helfferich and G. Klein, *Multicomponent Chromatography—Theory of Interference*, Marcel Dekker, New York, 1970.
8 Cs. Horváth, A. Nahum and J. H. Frenz, *J. Chromatogr.*, 218 (1981) 365.
9 G. B. Whitham, *Linear and Non-Linear Waves*, Wiley, New York, 1974.
10 B. Lin, S. Golshan-Shirazi, Z. Ma and G. Guiochon, *Anal. Chem.*, 60 (1988) 2647.
11 F. G. Helfferich, *J. Chromatogr.*, 373 (1986) 45.
12 F. Helfferich and G. Klein, *Multicomponent Chromatography—Theory of Interference*, Marcel Dekker, New York, 1970,p. 53.
13 F. Helfferich and G. Klein, *Multicomponent Chromatography—Theory of Interference*, Marcel Dekker, New York, 1970, pp. 384–388 and Fig. A.5.
14 G. Guiochon and S. Ghodbane, *J. Phys. Chem.*, 92 (1988) 3682.
15 A. M. Katti and G. Guiochon, *J. Chromatogr.*, 499 (1990) 21.
16 S. Golshan-Shirazi and G. Guiochon, *Anal. Chem.*, 61 (1989) 1368.
17 J. H. Knox, *J. Chromatogr. Sci.*, 15 (1977) 352.

Journal of Chromatography, 484 (1989) 153–166
Elsevier Science Publishers B.V., Amsterdam — Printed in The Netherlands

CHROM. 21 931

EXPERIMENTAL UTILIZATION OF A DISPLACEMENT EFFECT FOR THE OPTIMIZATION OF THE SEPARATION OF A TWO-COMPONENT MIXTURE

JOAN NEWBURGER[a]
Wyeth-Ayerst Research, Inc., Princeton, NJ 08540 (U.S.A.)
and
GEORGES GUIOCHON*
**Department of Chemistry, University of Tennessee, Knoxville, TN 37996-1600, and Division of Analytical Chemistry, Oak Ridge National Laboratory, Oak Ridge, TN 37831-6120 (U.S.A.)*

SUMMARY

Using a mixture of two substituted cyclohexanone epimers, sample loading, binary mixture composition and column efficiency were investigated for their influence on the displacement effect observed between the first and the second eluted components ("sample self-displacement effect"). This effect occurs and can enhance production for loads as high as 1 g on a 250 × 21.4 mm I.D. column. Separations over a broad range of epimer mixture compositions, from 10:90 to 75:25, show a displacement effect on the first-eluting component by the second. In loading and composition studies, interference between the tailing portion of the first component and the front of the second component is the predominant factor influencing recovery loss for both components. A high column efficiency is essential for sharpening band zone boundaries and maximizing yields. There is a very good correlation between experimental results and reported computer simulations of the band profiles of binary mixture components.

INTRODUCTION

It has long been recognized that preparative chromatography must be carried out under conditions such that the column is at least somewhat overloaded[1]. Until recently, however, the origin, nature and consequences of the band broadening and component interference phenomena that take place under such conditions were elusive. It was difficult to control or use to advantage effects that were poorly understood and few detailed investigations of these band interactions were reported.

In 1987, three papers were published independently on this topic[2–5] and interest in this area has been growing steadily since. In a previous contribution[2,3], we demon-

[a] Present address: Squibb Institute for Medical Research, P.O. Box 4000, Princeton, NJ 08543-4000, U.S.A.

0021-9673/89/$03.50

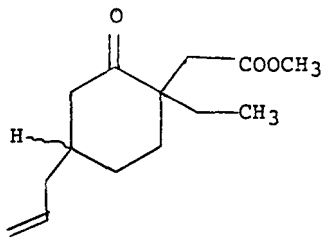

Fig. 1. Structure of the two 1,1,4-trisubstituted cyclohexanone epimers investigated.

strated that column overloading is accompanied not only by the elution of broader, unsymmetrical bands, but also by a high degree of interaction between the bands of closely eluting components. This interaction is not necessarily detrimental. While exploring the relationship between particle size, loading capacity and production rate of a pair of epimers (Fig. 1), the recovery of pure material was found to increase well past the load at which fronting of the second-eluting epimer was expected to reduce production because of overlap with the first component. Fraction collection during the elution of the bands followed by analysis of these fractions revealed that the second epimer was displacing the first, literally pushing this first epimer ahead of itself through the column[2]. Very similar experimental results were described by Parker *et al.*[4] in gradient elution and by Eble *et al.*[5] in isocratic analysis. However, in a companion paper[6], the latter group proposed a new model, termed the "blockage effect", to account for what can be readily explained as a displacement effect[7,8].

Displacement of mixture components by a solution of a more strongly adsorbed compound, called the displacer, is a well known mode of preparative liquid chromatography[7], recently revived by Horváth *et al.*[8]. The fundamental origin of this phenomenon is in the competition between the more strongly adsorbed displacer and the sample components or, more precisely, the last-eluted, most strongly adsorbed component of the mixture. In turn, this component competes with the second most strongly adsorbed component and displaces it. Eventually, if proper experimental conditions are selected (sufficiently long column, displacer concentration sufficiently high and mobile phase velocity sufficiently great), an isotachic train of bands is formed, where each band displaces the previous one and is displaced itself by the next one[8,9].

Although the displacement effect cannot lead to the formation of an isotachic train in the case of the elution of a binary mixture under column overloading conditions, the competition between the two components of the mixture for access to the stationary phase is governed by the same mechanism and follows the same law. Therefore, when the degree of column overload is high enough and the two bands interfere, usually because the front of the second tends to be eluted before the tail of the first, a displacement effect on the first band by the second takes place. This phenomenon has been termed the "sample self-displacement effect"[2]. The major advantage of a generalized use of this effect over the standard elution practice of using slightly overloaded columns is the much larger sample size afforded, especially for the purification of the first component of a closely eluting pair. Compared with the classical "touching band" approach[10], the gain is approximately one order of magnitude[11,12]. The major advantages over conventional displacement with a displacer are

the ability to perform repetitive injections without the need for lengthy column re-equilibration steps in between, and a much faster method development procedure as a search for a suitable displacer is not needed.

The original data[2] were limited to injections of 100–500 mg, on a 21.4 mm I.D. column, for a 25:75 mixture of two epimers, where the more retained epimer was in excess. The range of experimental conditions under which sample self-displacement takes place, especially in terms of sample composition and column loading, remained unexplored. The dependence of the effect on column efficiency also needed further investigation.

In the meantime, computer modelling methods were developed that were able to simulate the observed data[13,14]. Theoretical calculations further predicted the occurrence of sample self-displacement over a broad range of mixture compositions and loadings[14,15] and a dependence on efficiency[16,17]. These theoretical results are based on the assumption of competitive Langmuir isotherms for the components of a binary mixture, a fair approximation in most instances[18]. A detailed theoretical explanation of the mechanism of the displacement effect in the elution of a binary mixture in chromatography has been published[19,20].

In order both to confirm empirically the simulated data and to explore the practical utility of this displacement effect, further work was indicated. The experiments reported here were designed to examine the circumstances under which sample self-displacement occurs, with emphasis on factors integral to production optimization.

EXPERIMENTAL

Apparatus

Preparative experiments were carried out on a Varex (Rockville, MD, U.S.A.) PSLC 100 preparative liquid chromatograph, equipped with a UV detector and a Houston Instruments (Austin, TX, U.S.A.) Model 5000 strip-chart recorder. The mobile phase fluid path of the chromatograph had to be modified to meet specifications for minimum dead volume.

Isomer ratios were determined on an analytical high-performance liquid chromatographic (HPLC) system consisting of a Waters Assoc. (Milford, MA, U.S.A.) Model M6000 pump, a Waters Assoc. Model 710B sample processor, a Kratos (Ramsey, NJ, U.S.A.) Spectroflow 773 variable-wavelength detector and a Spectra-Physics (San Jose, CA, U.S.A.) SP4200 integrator.

The preparative columns were 250 × 21.4 mm I.D. Dynamax HPLC columns packed with 8-μm, 60-Å silica, 12-μm, 150-Å silica (Rainin Instruments, Woburn, MA, U.S.A.) or 40-μm, 150-Å silica (PQ, Valley Forge, PA, U.S.A.). With the exception of the efficiency study, all injections were made on 8-μm particle columns.

Reagents

Solvents were of HPLC grade from J. T. Baker (Phillipsburg, NJ, U.S.A.). The substituted cyclohexanone mixture was synthesized at Wyeth-Ayerst (Princeton, NJ, U.S.A.).

Procedures

A mixture of two epimeric compounds, methyl *cis*- and *trans*-1-methyl-2-oxo-4-(2-propenyl)cyclohexaneacetate (Fig. 1), was chromatographed using ethyl acetate–*n*-hexane (2.5:97.5) as the mobile phase. For the loading and efficiency studies, an isomer ratio of 1:3 was used, with the minor isomer eluting first. The isomer mixture was dissolved in the mobile phase and injections of 60, 100, 200, 300, 500, 700 or 1000 mg were made. The flow-rate was 40 ml/min and elution was monitored at 300 nm. For the composition study, pure amounts of each isomer were recovered from the loading study, and the mixture ratios were adjusted as needed.

For each injection, the total sample was recycled twice. Fractionation began with the third elution as soon as a slope change was noted. Fraction volumes were monitored indirectly by counting chart-paper units. The first one or two and the last two or three fractions collected were 26 ml in volume. Intermediate fractions were 13 ml in volume. The width of the intermediate band being of the order of 5 min (see below), ten to twelve fractions were collected. This number proved sufficient to sketch the individual band profiles in the mixed zone. Quantitative comparison between the experimental results and the prediction of the model would require the determination of a much larger number of experimental data points. However, such a treatment was not the aim of this work.

It is very important in these experiments to keep negligibly small the contributions of the recycling system and the fraction collection system to minimize band broadening. This is not very difficult with a 20 mm I.D. column.

The fractions were analyzed to determine isomer ratios using a 5-μm ODS-2 (Phase Separations, Norwalk, CT, U.S.A.) silica column (250 mm × 4.5 mm I.D.) and ethyl acetate–*n*-hexane (5:95) as the mobile phase at a flow-rate of 1.7 ml/min. Elution was monitored at 276 nm. Fractions having a purity of 92% or greater were included in the recovery determinations to yield a combined purity of at least 95% A or B epimer. The area under each preparative chromatographic peak was determined by counting the number of chart-paper units. The procedure was repeated and found to be reproducible to within several per cent. The amount of isomer present in each fraction was then determined using the isomer ratio.

Calculations

Theoretical plate numbers were calculated using the conventional equation, $N = 5.54\ (t_R/w_{1/2})^2$. This equation was chosen specifically to elucidate particular aspects of peak shape resulting from the self-displacement effect.

RESULTS AND DISCUSSION

Sample self-displacement, or the displacement of the first component band of a mixture by the second, is a phenomenon that occurs for certain relative compositions of a mixture when a sufficiently large sample is injected. The sharp front of the second component desorbs the molecules of the first (less adsorbed) component from the stationary phase and forces their earlier elution. The consequence of sample self-displacement is a concentration and a compression of the first component band. This effect occurs when the relative concentration of the second to the first component is high enough and when the equilibrium isotherms are convex upwards. It takes place

because the amount of each component adsorbed in the stationary phase at equilibrium is a function of the concentration of *both* components in the mobile phase. Initial recognition of this phenomenon was based on the following observations.

The elution behavior of the two epimers injected as a mixture is compared with the chromatograms of these compounds injected alone in Fig. 2a and b. Each of the three chromatograms shows the detector response after the sample has migrated one, two and three times through the column (recycling). The chromatograms obtained for the successive injections of 72 mg of the lesser retained epimer and 228 mg of the more retained are overlaid in Fig. 2a. The column is seriously overloaded in both instances, but obviously it is more so with the second epimer than with the first. The

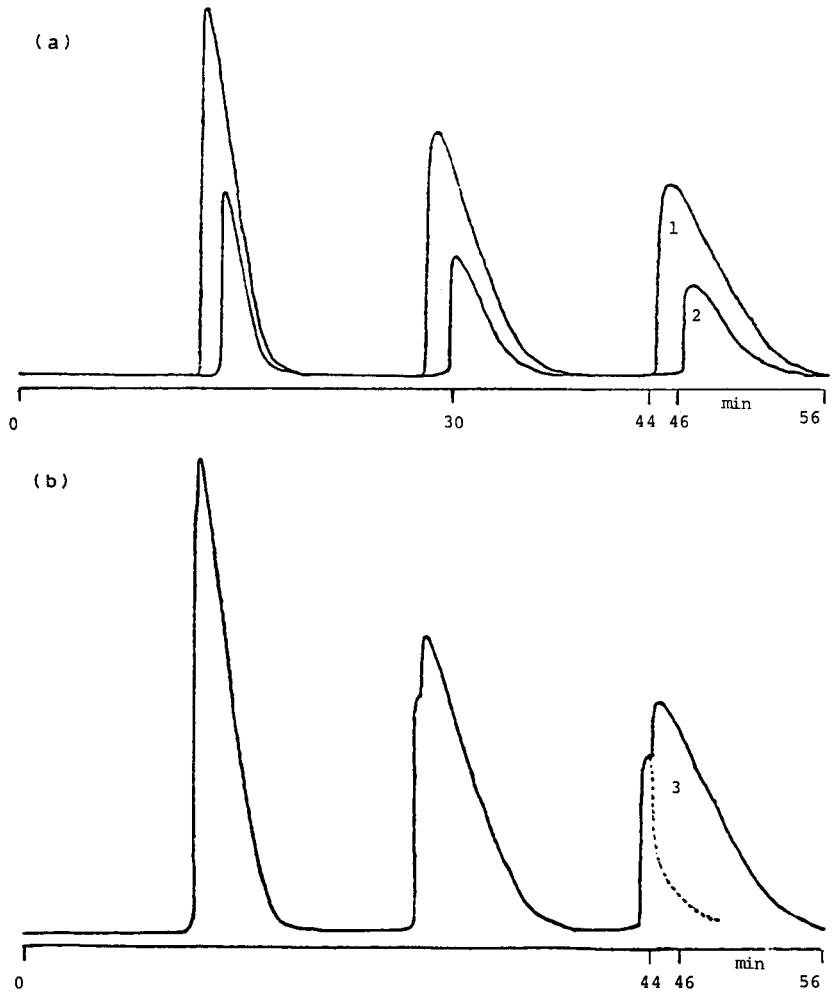

Fig. 2. Elution behavior of the two epimers when injected singly or as a mixture. Chromatograms recorded after each of three cycles (one initial elution, two recycles). For experimental conditions, see text. Column packed with 12-μm particles. Samples sizes: line 1 (a), 228 mg of epimer B; line 2 (a), 72 mg of epimer A; line 3 (b), 300 mg of a 1:3 mixture.

column overloading for these pure compound samples results in the classical band shape associated with the elution of compounds experiencing single-compound Langmuir equilibrium isotherms between the mobile and stationary phases[21]. The bands have a very steep front and a diffuse, smooth rear profile which extends to the retention time of an extremely small pulse, *i.e.*, to the analytical retention time. Owing to the greater degree of overloading for the second epimer, its band has fronted to such an extent that its retention time is now shorter than the retention time of the band of the first, less concentrated epimer.

Based on the individual band profiles of the epimers in Fig. 2a, successful purification of large samples of a mixture of the two epimers (with $\alpha = 1.04$) would have been hard to predict, but rather coelution would be expected. However, the chromatogram of a 300-mg sample of the mixture, shown in Fig. 2b, reveals that a substantial recovery of pure material is possible. The band profile of the smaller component can be interpolated from the analyses of the fractions collected during the elution of the third band in Fig. 2b. The dotted line shows that the first band is strongly compressed, that most of the first epimer elutes prior to the second component and that a sharp boundary separates the top of the two elution zones. Total band separation is not achieved as the first component trails into the second, but the mixed zone in between the zones of pure components is not very wide. The discrepancy between the chromatograms in Fig. 2a and b occurs because the second epimer significantly influences the behavior of the first as they migrate down the column, displacing it as predicted[13–20].

A series of experiments were performed to investigate the influence of sample size and composition and also of column efficiency on this effect.

Influence of column loading

Loading experiments were conducted and analyzed to give both gross data on production and yield and a more specific evaluation of displacement effects. Table I presents the overall variation in production and yield for injections from 60 to 1000 mg. In the following discussion, the first eluting epimer is designated the A epimer and the second the B epimer. The increase in sample load is accompanied by a substantial decrease in yield, a 58% relative loss for the A epimer and 72% for the B epimer. Neither the production of A nor that of B, however, actually declines. It appears to peak between the 500- and 700-mg injections, but then rises again with the

TABLE I

RECOVERY AS A FUNCTION OF LOAD

Load (mg)	*Yield (%)*		*Amount recovered (mg)*		*Total production (mg)*
	A	*B*	*A*	*B*	
60	89	92	13	42	55
100	82	92	20	70	90
300	67	64	48	135	183
500	49	44	59	167	226
700	36	29	60	154	214
1000	37	26	89	198	287

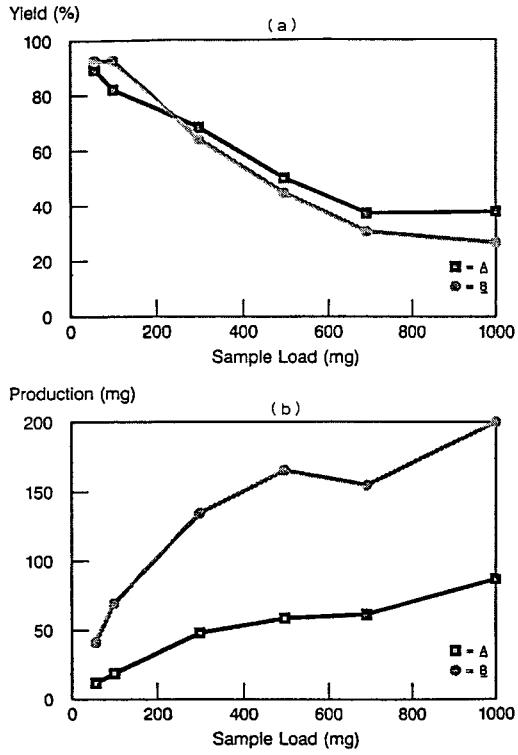

Fig. 3. Plot of (a) yield and (b) production for the two trisubstituted cyclohexanone epimers *versus* sample size. ■, epimer A; ●, epimer B. Conditions as in Fig. 2.

1000-mg injection. The data show a certain spread, due to the potential inaccuracy of these determinations inherent in the manual fraction collection procedure. A plot of the data (Fig. 3) shows that further increases in production with a possible leveling off in yield are predicted. Injection problems related to increasing sample viscosity with increasing feed concentration prevented continuation of the experiment.

The features of sample self-displacement that control the production of pure components are the sharpness of the boundary between the two component bands and the tailing of the first component into the second. Increasing the load from 200 to 1000 mg does not substantially alter the profile of the elution front of the second component as measured by the analysis of the collected fractions. This front remains nearly vertical and merely moves towards shorter retention times with increasing sample size. On the other hand, increasing the sample load does cause greater tailing of the first component, as seen in Fig. 4. Note that, in contrast to the tail of the second component which always ends at the k'_0 value, the tail of the first component is not anchored; it ends at a time that depends on the sample size, the relative concentration of the two components and the isotherm coefficients[19,20]. These experimental results are in excellent agreement with the theoretical predictions of the ideal[18–20] and the semi-ideal models[13–17] of non-linear chromatography.

The anatomy of loading effects on the displacement mechanism can be studied

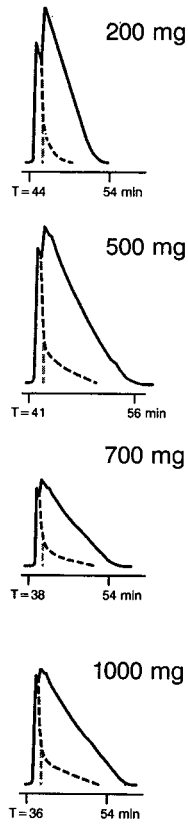

Fig. 4. Effect of increasing sample size on the elution profile of the A epimer. The third pass only of three cycles is shown for injections of (a) 200, (b) 500, (c) 700 and (d) 1000 mg. Conditions as in Fig. 2.

by determining the individual elution profiles of the A epimer under various experimental conditions. Values of the apparent plate number, N (ref. 2), the apparent column capacity factor, k', and the apparent relative retention, α, were derived, using classical relationships, from the retention times of the two band maxima and the band width of the first peak at half-height. The results are reported in Table II. As the

TABLE II

LOAD DEPENDENCE OF THE SEPARATION PARAMETERS

Load (mg)	k_A'	k_B'	α	N	A_v/A_t
1	6.50	6.80	1.045		N/A[a]
200	6.25	6.47	1.035	4889	4.07
500	5.75	5.93	1.03	6410	1.64
700	5.29	5.42	1.03	6843	1.30
1000	4.90	5.03	1.03	7300	0.95

[a] N/A = Not available.

column is loaded, k' decreases by 22%, whereas α remains virtually constant. Because of the difficulty in acquiring highly precise experimental data, the observed variation of $1 - \alpha$, which is of more fundamental importance, is probably not significant. Fronting is due to the thermodynamic properties of the equilibrium isotherms and the existence of a finite value of the column saturation capacity. The larger second component band, however, does not overlap into the less overloaded first component. In fact, as we have shown above, the upper part of the band of the first component is narrow and even seems to narrow down as the sample size is increased, again in agreement with theoretical results[10]. This is confirmed by the positive trend observed for the number of theoretical plates measured for the A band.

The values of the parameters N, k' and α are not diagnostic of the actual loss in recovery yield. The tailing of the A epimer into the B one accounts for all the decrease in the production of both epimers. An arbitrary parameter was defined, in an effort to determine the relative importance of the tailing of the first component under the second component and to study the influence of various parameters. The definition of this parameter is based on the L-shaped profile of the A band, reported previously[13–19]. A vertical line is dropped to the baseline from the point at which the band slope of the A band begins to change. This is shown as the dashed lines in Fig. 4. These lines divide the A band into a vertical front part containing pure material and a triangular portion which represents the amount of A in the mixed zone of the chromatogram[18]. The areas of each portion, denoted A_v and A_t respectively, are measured. The value of the ratio A_v/A_t is indicative of the extent of tailing and consequently of the decrease in recovery.

The data in Table II show that for a 200-mg injection, 80% of the material is accounted for by A_v and is recoverable. In contrast, for a 1000-mg injection, only 50% of the A epimer is in the front part of the band. Plotting $\ln(A_v/A_t)$ *versus* the logarithm of the amount of A epimer injected gives a straight line (Fig. 5). Although the validity of this relationship remains questionable at this stage because it has not yet been tested on any other mixture, it might prove useful in predicting optimum loads should it apply for other mixtures.

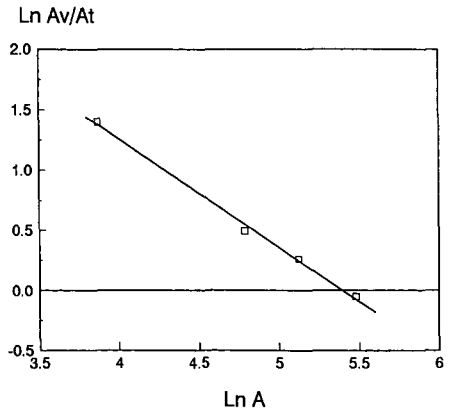

Fig. 5. Plot of $\ln(A_v/A_t)$ *versus* $\ln m$ (mg), where m is the amount of the A epimer injected. Data shown in Fig. 4. A_v is defined as the area under the A band to the left of the dashed line in Fig. 4 and A_t as the area under the A band to the right of the dashed line. Regression line: $y = 4.88 - 0.904x$, $R^2 = 0.996$.

Influence of sample composition

The loading experiments reported here and also the previously published results show sample self-displacement for a mixture ratio of 25:75. The elution profiles of 200-mg samples of mixtures of various compositions (see Fig. 6a) indicate that the phenomenon can occur over a wide range of sample composition. Tailing of the A epimer becomes more pronounced as its concentration increases from 10% to 75%. Some displacement of the A by the B epimer remains significant for an A concentration of 50% (Fig. 6a). Even with a mixture containing 75% of the A epimer, the profile of the B epimer begins with a very sharp front. The concentration jump is insufficient, however, to cause a noticeable drop in the A concentration and a significant displacement effect.

Material that elutes prior to the break in the slope of the rear profile of the A band can be collected as pure product. As found in the column loading study, loss of production is due to the tailing of the A band, not to the fronting of the B band. The displacement effect vanishes completely when the mixture composition becomes 90:10 and the second-eluting component trails along through the entire elution band, demonstrating a "tag-along" effect[13,15]. In the latter instance, no pure material is obtained.

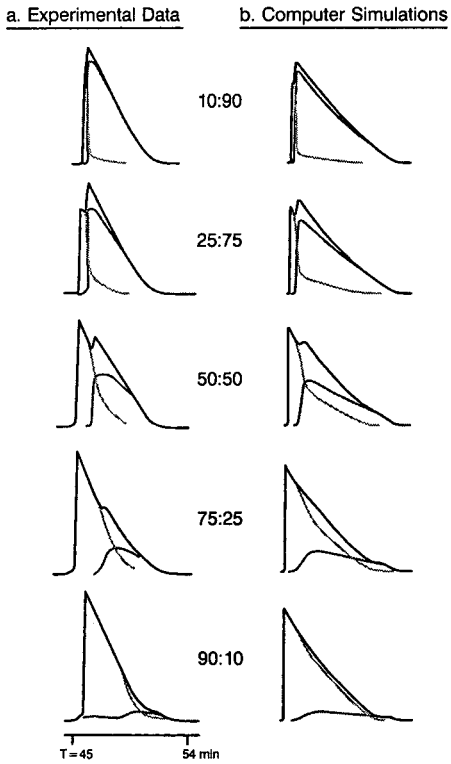

Fig. 6. Self-displacement effect on different mixture compositions of the two epimers. Conditions as in Fig. 2. (a) Experimental results, third pass only of three cycles; 200-mg injections at A:B mixture ratios of 10:90, 25:75, 50:50, 75:25 and 90:10. (b) Computer simulations for a 300-mg injection of two components in the same mixture ratios as in (a) (note: the time scale is different).

The mixture band profiles shown in Fig. 6b are computer simulations generated following the method previously described[5]. Their pattern is strikingly similar to that of the profiles derived from experimental determinations. The data constitute an experimental validation of these theoretical results, on a qualitative basis. An investigation of the degree of quantitative agreement would require the determination of the competitive equilibrium isotherms of the two epimers in the chromatographic system used here, which was beyond the scope of this work.

To explore the origin of the loss of the displacement effect with a 90:10 mixture, and whether it is due to the amount of the B epimer (too low) or to the composition of the mixture (too large a relative concentration of A), injections of both the 90:10 and the 75:25 mixtures were made at lower loads. The band profiles are shown in Fig. 7. Comparing chromatograms corresponding to the same amount of the B epimer, *e.g.*, a 200-mg injection of the 90:10 mixture and a 100-mg injection of the 75:25 mixture containing 20 and 25 mg of B, respectively, a much sharper boundary is observed with the latter mixture. A similar result is seen on comparing the profiles of a 100-mg injection of the 90:10 mixture and a 40-mg injection of the 75:25 mixture, where 10 mg

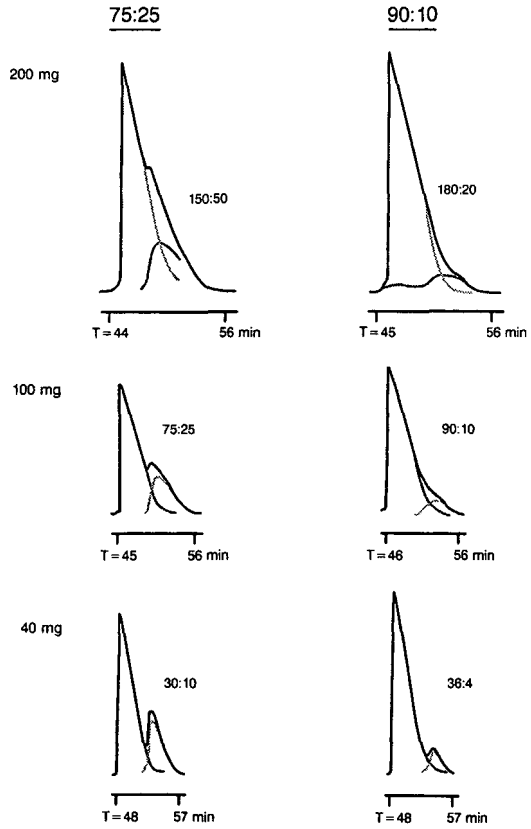

Fig. 7. Relative importance of mixture ratio and amount of the second-eluting component in causing a displacement effect. Third Pass of three cycles. Left: A:B mixture ratio of 75:25 for 200-, 100- and 40-mg samples. Right: A:B mixture ratio of 90:10 for 200-, 100- and 40-mg samples.

of B are present. Therefore, the relative composition of the sample, not the amount of second component injected, affects the relative intensity of the displacement and the tag-along effect.

It is important to emphasize that the two individual band profiles and the interaction between the two bands depend on two parameters, the total loading factor and the concentration ratio of the two components in the feed[13–20]. The first parameter determines the intensity of the non-linear effects and the second the relative importance of the displacement and the tag-along effects. Admittedly, the values of the loading factors for each component are important, as the total sample load decreases when the bands separate, but these factors, which are included in the definition of the effective sample loading factor[19,20], have to be taken into account only for quantitative predictions of the band profiles.

Influence of column efficiency

The phenomenon of sample self-displacement was first observed during a study of the relationship between production, sample size and the average particle size of the packing material used. In this work, we investigated this relationship again by

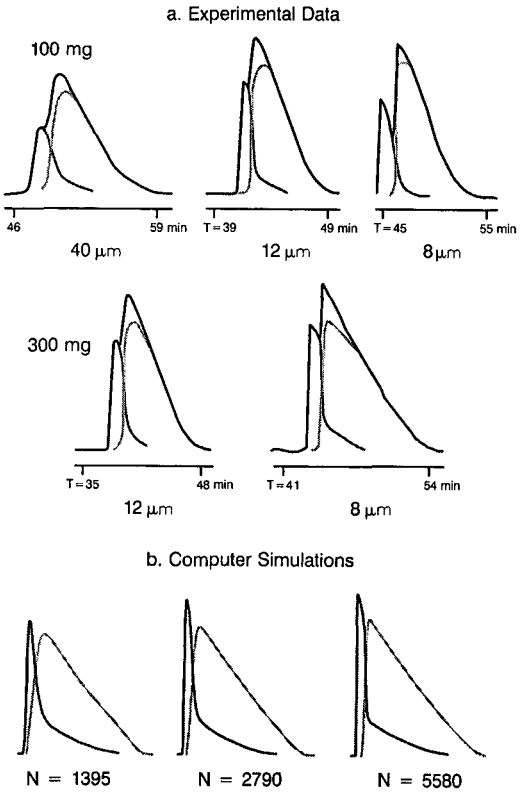

Fig. 8. Effect of column efficiency on elution profiles. (a) Experimental results. Third pass of three cycles. Injections of 100- and 300-mg samples of the epimer mixture at an A:B ratio of 1:3. Conditions as in Fig. 2, except packing material (40, 12 and 8 μm). (b) Computer simulations of 300-mg injections on columns having efficiencies of 1395, 2790 and 5580 theoretical plates.

determining the individual band profiles for each component of the eluting mixtures. The dependence of the displacement effect on column efficiency is illustrated in Fig. 8a.

The comparison between the production rates and the recoveries obtained with these three columns should take into account the difference between the values of the column saturation capacities that are likely to result from the different silica batches used and, with the 8- and 12-μm particles, the difference in average pore sizes and hence in specific surface area. The relative retentions with small sample sizes were nearly the same, however. Similarly to single-compound band fronts[21], the slope of the two individual bands in the mixed region depend little on the loading factor, but essentially on the column efficiency, provided that the latter exceeds a few thousand plates[19,20]. As is recognized, the proper prediction of any of the characteristic phenomena arising in non-linear chromatography depends on the possibility of simulating columns having at least several thousand plates[11–21].

Proceeding from a 40- to a 12- and an 8-μm packing material, we found increasingly sharp band interfaces, for both a 100-mg and a 300-mg sample size. The use of more efficient columns results in very similar chromatograms, with a single, but major, difference, *i.e.*, the sharpness of the boundary between the two components. This factor has the important effect of reducing the number of mixed, impure fractions that have to be collected between the two pure fractions, decreasing their total volume. Higher recoveries can be achieved.

The experimental results shown in Fig. 8a are again in excellent agreement with the predictions of the semi-ideal model of non-linear chromatography[5]. This similarity confirms the ability of computer modeling to predict experimental results correctly. The accuracy of these predictions is discussed independently[18].

CONCLUSIONS

This work confirms our previous results regarding the separation of binary mixtures of closely eluting compounds[2,3,13–20]. The interaction between the two epimers considered here gives rise to an important displacement effect of the first-eluted epimer by the second. Production of important amounts of pure material, especially of the first-eluted component, can be achieved under a high degree of column overloading. The production is greater than could be predicted by a direct extrapolation from the individual band profiles. The loading factor, the mixture composition and the column efficiency together determine the production per cycle.

Efficient columns are essential for maximizing the recovery, because column efficiency has been shown to determine the sharpness of the demarcation of band boundaries. In studies of loading factor and mixture composition, the loss of yield has been ascribed to the tailing of the first band into the second. This feature clearly distinguished the band profiles obtained in overloaded elution chromatography from the more rectangular zones found in actual displacement chromatography. The tailing is due to the decrease in concentration of the second component on the rear part of its zone, contrasting with the constant concentration of a displacer throughout the whole run. An awareness of the first-component band profile is critical for an accurate prediction of the optimum sample load for maximum production of a pure fraction from a feed having a given composition.

There are a number of instances where optimum conditions are achieved by first collecting a significant amount of the first-eluting component to attain a more desirable relative composition of the mixture used as the feed. In practice, this first collection step is easy to accomplish as pure material can be identified as that portion eluting prior to the obvious onset of the second component, eliminating the need for fraction cutting and purity determinations of mixed zone fractions.

The close similarities between the experimental and calculated chromatograms emphasize the usefulness of modeling in prediction and optimization. Moreover, as the equations used to generate the calculated band profiles rely on very general principles and on a fundamental model of chromatography, the ability to predict accurately these particular experimental data implies that the phenomenon of sample self-displacement is not limited to the pair of epimers studied so far. Further experiments are in progress to show that these results are valid for other compound mixtures and that they can be used as a routine model of separation[22].

Finally, we wish to emphasize the importance of selecting the chromatographic system that gives the optimum elution order for the mixture investigated.

ACKNOWLEDGEMENTS

We thank Dr. David Cochran (Wyeth-Ayerst Research, Princeton, NJ, U.S.A.) for his support of this project and S. Golshan-Shirazi and A. M. Katti for fruitful discussions. This work was supported in part by grant CHE-8715211 of the National Science Foundation and by the cooperative agreement between the University of Tennessee and the Oak Ridge National Laboratory.

REFERENCES

1 L. R. Snyder and J. J. Kirkland, *Introduction to Modern Liquid Chromatography*, Wiley-Interscience, New York, 2nd ed., 1979, Ch. 6.
2 J. Newburger, L. Liebes, H. Colin and G. Guiochon, *Sep. Sci. Technol.*, 22 (1987) 1933.
3 J. Newburger and G. Guiochon, presented at the *9th International Symposium on Column Liquid Chromatography, Edinburgh, July 1985.*
4 J. M. R. Parker, C. T. Mant and R. S. Hodges, *Chromatographia*, 24 (1987) 832.
5 J. E. Eble, R. L. Grob, P. E. Antle and L. R. Snyder, *J. Chromatogr.*, 405 (1987) 1.
6 J. E. Eble, R. L. Grob, P. E. Antle, G. B. Cox and L. R. Snyder, *J. Chromatogr.*, 405 (1987) 31.
7 A. Tiselius and S. Claesson, *Ark. Kemi Mineral. Geol.*, 16A (1943) 18.
8 Cs. Horváth, J. Frenz and Z. El Rassi, *J. Chromatogr.*, 255 (1983) 273.
9 A. M. Katti and G. Guiochon, *J. Chromatogr.*, 449 (1988) 25.
10 J. H. Knox and H. M. Pyper, *J. Chromatogr.*, 363 (1986) 1.
11 S. Ghodbane and G. Guiochon, *Chromatographia*, 26 (1988) 53.
12 S. Golshan-Shirazi and G. Guiochon, *Anal. Chem.*, 61 (1989) 1368.
13 G. Guiochon and S. Ghodbane, *J. Phys. Chem.*, 92 (1988) 3682.
14 S. Ghodbane and G. Guiochon, *J. Chromatogr.*, 440 (1988) 9.
15 S. Ghodbane and G. Guiochon, *J. Chromatogr.*, 444 (1988) 275.
16 S. Ghodbane and G. Guiochon, *J. Chromatogr.*, 450 (1988) 27.
17 S. Ghodbane and G. Guiochon, *J. Chromatogr.*, 452 (1988) 209.
18 A. M. Katti and G. Guiochon, *J. Chromatogr.*, 499 (1990) in press.
19 S. Golshan-Shirazi and G. Guiochon, *J. Phys. Chem.*, 93 (1989) 4143.
20 S. Golshan-Shirazi and G. Guiochon, *J. Chromatogr.*, 484 (1989) 125.
21 G. Guiochon, S. Golshan-Shirazi and A. Jaulmes, *Anal. Chem.*, 60 (1988) 1856.
22 J. Newburger and G. Guiochon, presented at the *6th International Symposium on Preparative Chromatography, Washington, DC, May 1989.*

Journal of Chromatography, 484 (1989) 167–185
Elsevier Science Publishers B.V., Amsterdam — Printed in The Netherlands

CHROM. 22 041

RAPID METHOD FOR DETERMINING MULTICOMPONENT LANGMUIR PARAMETERS FOR DISPLACEMENT CHROMATOGRAPHY

TEN-WEN CHEN and NEVILLE G. PINTO*
Department of Chemical Engineering, 697 Rhodes Hall, University of Cincinnati, Cincinnati, OH 45221-0171 (U.S.A.)
and
LESTER VAN BROCKLIN
The Procter and Gamble Company, Winton Hill Technical Center, Cincinnati, OH 45224-1703 (U.S.A.)

SUMMARY

A new method, based on the coherence theory of chromatography, has been presented for determining Langmuir equilibrium coefficients in multicomponent systems. The method provides a quick and simple technique for obtaining equilibrium data for the simulation of displacement chromatography, and is applicable to mixtures involving any number of components. In essence, the method uses a combination of elution and frontal chromatography experiments to characterize the equilibrium behavior. Pure component samples are not necessary, and sample preparation involves simple dilution or concentration steps with the process mixture and displacer. Furthermore, if the equilibrium behavior of the displacer in the Henry's law region is known, the characterization can be achieved, in most cases, with a single elution and single frontal chromatogram. Explicit equations relating the Langmuir coefficients to characteristics of the elution and frontal chromatograms have been derived. These equations have been successfully applied to a four-component adsorption system.

INTRODUCTION

It has been recognized for sometime that liquid chromatography (LC) has considerable potential as a large-scale purification and separation process in the production of biological and specialty chemical products. The strengths of this technique are its ability to achieve very high degrees of product purity, and its potential for achieving two operations, concentration and purification, in a single step. This reduction in the number of steps in the purification scheme can result in a significant economic advantage, as has been demonstrated in the production of streptomycin and cephalosporin[1].

Currently, the quickest and most commonly used approach for developing large-scale chromatographic processes is the direct scale-up of analytical systems[2]. Consequently, an overwhelming number of preparative processes are based on elution development, both linear and non-linear. Though elution chromatography is commonly used for large-scale purifications, this development technique can result in

0021-9673/89/$03.50

a chromatographic process that is economically less favorable than one using displacement development[3]. This fact has been recognized for sometime, but elution chromatography continues to be the technique of choice, because it is based on the wealth of knowledge accumulated from analytical chromatography. Correspondingly, the lack of bench-scale experience with displacement chromatography has hindered its acceptance in large-scale chromatographic processes.

The paucity of experimental data with regard to displacement chromatography can be compensated for, to a degree, by appropriate computer simulations of the process. These simulations allow the determination of optimal operating conditions for the desired separation. Essential to this approach is the availability of a suitable model for non-linear, multicomponent chromatography. Such a model is available[4], but the use of this model requires that multicomponent equilibrium behavior be known *a priori*; since equilibrium behavior establishes the primary response characteristics of the chromatographic process.

Multicomponent equilibrium data for liquid–solid systems have been traditionally obtained by batch methods. Briefly, the method involves generating the isotherm by equilibrating solution of known composition with a known weight of the adsorbent. Once equilibrated, the liquid solution is analyzed usually by chromatography, and its change in composition is used to locate a point on the isotherm. The disadvantage of this approach is that it is time consuming and tedious. Consequently, it is generally not suitable for the industrial environment, especially when only a preliminary analysis of competing separation techniques is being conducted.

An alternative method for obtaining equilibrium data is based on chromatography. Advantages of this method are speed and accuracy. The chromatographic approach was first used by Glueckauf[5] to study solid–liquid equilibria. Since then, various other chromatographic procedures have been proposed[6]. For multicomponent systems specifically, two chromatographic methods are commonly used. In the tracer pulse (TP) method proposed by Helfferich and Peterson[7], the column is initially equilibrated with a carrier fluid of constant, known composition. After equilibration, a small sample with the same composition as the carrier but containing a detectable isotope of the species of interest is injected into the fluid stream. The retention time of the isotope is measured, and this is used to calculate one point on the isotherm. The experiment is repeated at a number of carrier compositions to generate the required portion of the multicomponent isotherm. Though the TP method is applicable to any number of components and any equilibrium behavior, its major disadvantages are the need for a separate measurement for each point on the isotherm, and the need to have a detectable isotope of each species being studied.

The second chromatographic method is the elution on a plateau (EP) method (also called perturbation chromatography) introduced by Reilley *et al.*[8]. In this method, the column is first equilibrated with a fluid of known composition. It is then perturbed slightly from this state, and the response is observed. This experiment is repeated over a suitable composition grid, and the data are used with a non-linear parameter estimation method developed by Glover and co-workers[9,10] to determine the adsorption isotherm. While the EP method does not use isotopes, like the TP method it requires substantial chromatographic data. Furthermore, the method involves a complex parameter estimation method.

Despite the potential of the chromatographic approach for measuring equilib-

rium data, the use of this approach has been almost exclusively limited to gas chromatography (GC). This is due to the fact that, until recently, LC was used primarily for analytical purposes. In this case, the process is restricted to the linear portion of the isotherm, and a detailed knowledge of the adsorption behavior at high concentrations is not necessary. However, with the increasing use of LC in large-scale separations and purifications there is a need for a simple and quick procedure for measuring multicomponent isotherms. Both the TP and EP methods used in GC are directly applicable to LC. However, for reasons outlined earlier, neither one of these serves as a simple and quick method for determining multicomponent isotherms. Consequently, other, more suitable methods have to be developed.

Jacobson *et al.*[11,12] have used LC to successfully study adsorption behavior. In one study[11], they measured the adsorption of single solutes on silica-bound hydrocarbonaceous sorbents by frontal chromatography. More recently[12], they have presented two methods, both based on frontal chromatography, for the measurement of competitive adsorption isotherms. In one method, the method of mass balance (MMB), the effluent composition history is used in conjunction with the column mass balance to generate a point on the adsorption isotherm. The advantage of this method is that it is applicable to any type of adsorption behavior. However, MMB requires detailed effluent composition histories, and a substantial amount of frontal chromatography data; since a single frontal chromatogram generates only one point on the isotherm. The second method, the method of composition velocities (MCV), is based on the coherence theory of chromatography[4]. In this method, migration velocities of concentration waves generated by frontal chromatography are regressed to yield parameters of the complex Langmuir isotherm. The advantage of MCV over MMB is that it requires only retention volumes and not composition histories. It is, however, restricted to systems obeying the complex Langmuir isotherm. A further disadvantage of MCV is that, though the method is in principle applicable to any number of components, the regression procedure becomes increasingly complex, and the regression parameters more uncertain, as the number of components increases.

In this paper, a new method, called the *h*-root method (HRM), will be presented. This new method is geared toward obtaining equilibrium data for displacement chromatography. Like MCV, it is restricted to systems obeying the compound Langmuir isotherm. The new method uses a combination of elution and frontal chromatography. It is based on propagation velocities of the composition fronts and compositions of the effluent plateaus, but requires no parameter estimation. Furthermore, if equilibrium data for the displacer are known in the linear region, the multicomponent isotherm can be established with a single elution and single frontal experiment, regardless of the number of components present. Also, samples required for both experiments can be obtained directly from process solutions, without extensive sample preparation.

THEORY

Equilibrium isotherm

The equilibrium distribution of species between the stationary and mobile phases in chromatography establishes the primary characteristics of the effluent composition history. For LC with a single solute, a commonly used isotherm is the Langmuir isotherm[13]:

$$q_i = \frac{a_i c_i}{1 + b_i c_i} \tag{1}$$

For multicomponent systems eqn. 1 is readily extended to give:

$$q_i = \frac{a_i c_i}{1 + \sum_{j=1}^{n} b_j c_j} \tag{2}$$

With $b_j > 0$, eqn. 2 allows for competitive behavior between species. Eqn. 2 is the only multicomponent isotherm for which a comprehensive theory of chromatography exists[4]. Consequently, this isotherm is frequently used for modeling large-scale chromatographic separation processes[3].

Summary of coherence theory

The coherence theory of chromatography[4] is a useful equilibrium theory that has been applied successfully to a variety of chromatographic processes[14–20]. No attempt will be made in this article to outline the theory in detail; only features essential to the current development will be given.

Fundamental to the coherence theory is the recognition of the phenomenon of coherence. A chromatographic column subject to a disturbance will, after a period, settle into a "resolved" state, which consists of a series of composition waves each subject to the coherence condition:

$$v_{c_i} = v_{c_j} \tag{3}$$

for all i and j. Using DeVault's[21] equation for concentration velocity,

$$v_{c_i} = \frac{v_0}{1 + \frac{\rho}{\varepsilon}\left(\frac{\partial q_i}{\partial c_i}\right)_z} \tag{4}$$

and the compound Langmuir isotherm, eqn. 2, it can be shown that the coherence condition defines a grid of coherent composition paths to which the system is restricted once the coherence condition, eqn. 3, is satisfied. Thus, given the feed history, this grid can be used to find the composition route for the column, and, therefore, the column effluent history can be predicted.

In order to allow the use of this approach to any number of components, Helfferich and Klein[4] have orthogonalized the composition path grid by defining the h-composition space with the non-linear transformation:

$$\sum_{i=1}^{n} \left(\frac{b_i c_i}{h a_i/a_1 - 1}\right) - 1 = 0 \tag{5a}$$

and

$$h_{j-1} = a_1/a_j \text{ or } h_j = a_1/a_j \text{ if } c_j = 0 \quad (1<j\leq n) \tag{5b}$$

$$h_1 = 1 \qquad \text{if } c_1 = 0 \tag{5c}$$

In the h-space, the velocity of the composition front with kth h-root as the variable root is given by:

$$u_k = h_k \prod_{i=1}^{n} h_i \prod_{i=1}^{n+1} \alpha_{i1} \tag{6}$$

for a diffuse wave, and

$$u_k = h_k' h_k'' \prod_{\substack{i=1 \\ i\neq k}}^{n} h_i \prod_{i=1}^{n+1} \alpha_{i1} \tag{7}$$

for a sharp wave. Eqns. 6 and 7 are written for an n-component non-stoichiometric system obeying eqn. 2, that has been converted to an equivalent $n+1$ component stoichiometric system[4]. The velocities in eqns. 6 and 7 are adjusted velocities and are related to real velocities by the equation:

$$v_k = \frac{v_0}{1 + \dfrac{R\rho}{u_k \varepsilon}} \tag{8}$$

where R is an adjustable parameter used in the conversion of the n-component non-stoichiometric system to an $n+1$ component stoichiometric system[4]. The separation factors α_{i1} in eqns. 6 and 7 are related to the Langmuir equilibrium constants as follows:

$$\begin{aligned} \alpha_{i1} &= a_i/a_1 \quad i\neq p \\ \alpha_{p1} &= R/a_1 \end{aligned} \tag{9}$$

where p is the dummy species in the $n+1$ component stoichiometric system. In this development, the R value will be selected in the range $0<R<a_n$, to ensure that the dummy species is the least retained species ($p = n+1$).

Tracer pulse elution

Tracer pulse elution is a special case of elution chromatography in which the injected pulse contains trace concentrations of all components except the eluent. In this case, the response pulses will travel at the trace-species velocities, and it can be shown that the pulse containing the species j on a background of the eluent, k, will have an adjusted velocity[4]:

$$u_j = \alpha_{kj} \tag{10}$$

Using eqn. 8, the adjusted velocity in eqn. 10 can be replaced with the real velocity:

$$\alpha_{kj} = \frac{R\rho}{\varepsilon}\left(\frac{1}{\frac{v_o}{v_j} - 1}\right) \tag{11}$$

Applying eqn. 11 to species 1, the most strongly retained species, and dividing the resultant equation by eqn. 11, we obtain:

$$\alpha_{j1} = \frac{\frac{v_0}{v_j} - 1}{\frac{v_0}{v_1} - 1} \tag{12}$$

Frontal chromatography

In frontal chromatography, a column initially equilibrated with a solution containing no solutes is subject to a step change in the influent fluid composition. If the step change involves n solutes, n sharp composition waves will be generated in the column. Fig. 1 is a convenient, schematic representation of the column profile during frontal development. The horizontal lines represent sharp waves generated by the development, and the fastest wave, wave n, is furthest downstream. Also shown in Fig. 1 are the plateau compositions, defined in the h-composition space. These h-root values establish the velocities of the concentration fronts, as can be seen from eqn. 7.

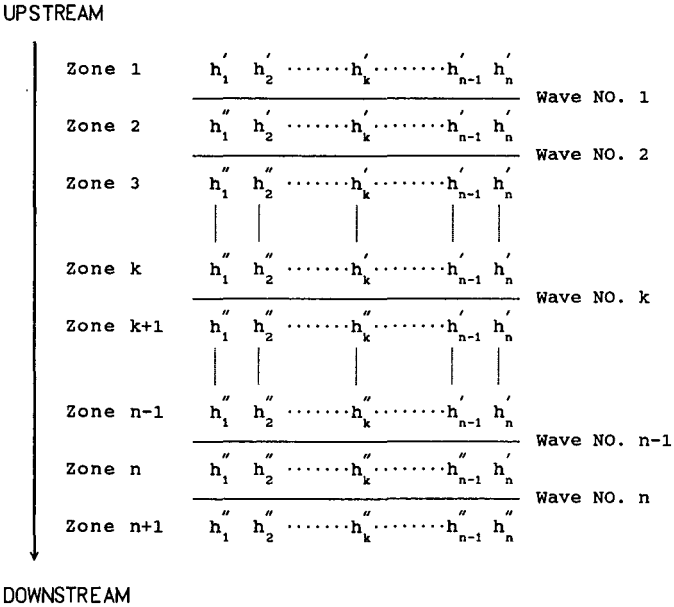

Fig. 1. Schematic representation of frontal development.

For the nth wave, the fastest wave,

$$u_n = h_n' h_n'' \prod_{i=1}^{n-1} h_i'' \prod_{i=1}^{n+1} \alpha_{i1} \tag{13}$$

Since the column does not contain any solutes initially, we have from eqn. 5b and c,

$$h_j'' = a_1/a_j \quad j = 1, \ldots, n \tag{14}$$

With the dummy species as the $(n+1)$th species, eqns. 9 and 14 give:

$$h_j'' = \alpha_{1j} \quad j = 1, \ldots, n \tag{15}$$

Substituting eqn. 15 in eqn. 13, and solving for h_n':

$$h_n' = u_n \alpha_{1n+1} \tag{16}$$

Finally, eqn. 9, applied to the dummy species, can be substituted in eqn. 16 to give:

$$h_n' = \frac{u_n a_1}{R} \tag{17}$$

From eqn. 7, the wave velocity of the $(n-1)$th wave is:

$$u_{n-1} = h_n' h_{n-1}' \prod_{i=1}^{n-1} h_i'' \prod_{i=1}^{n+1} \alpha_{i1} \tag{18}$$

Substituting eqns. 15 and 17 in eqn. 18 and solving for h_{n-1}', we obtain:

$$h_{n-1}' = \frac{a_1 u_{n-1}}{a_n u_n} \tag{19}$$

This procedure can be repeated for all slower waves, and it can be shown that

$$h_k' = \frac{a_1 u_k}{a_{k+1} u_{k+1}} \qquad k = 1, \ldots, (n-1) \tag{20}$$

DETERMINATION OF LANGMUIR CONSTANTS

HRM determines the Langmuir constants, a and b in eqn. 2, through a combination of tracer elution and frontal chromatography experiments. Tracer pulse elution is used to estimate dilute solution equilibrium behavior, and frontal chromatography establishes equilibrium behavior in the high-concentration region. The method will be described for the situation where the equilibrium behavior of the displacer in the dilute concentration region (Henry's law region) is known. If the dilute

solution behavior of the displacer is not known, it can be obtained from simple frontal chromatography experiments, and these will be described in more detail later.

Dilute solution behavior

The elution experiments involve the following sequence of steps: (1) equilibration of the column with a suitable eluent; (2) injection of a short pulse of a mixture of the multicomponent process solution, the displacer, and the eluent; and (3) development of the chromatogram with the eluent.

The preparation of injection samples for the elution experiments is straightforward. The selected displacer is mixed with a sample of the process solution to give a product that has a displacer concentration that is no greater than that of the most concentrated components in the process solution; this will ensure that the displacer does not dominate over process components. This mixture is then diluted appropriately with the eluent. The degree of dilution depends on the total concentration of the solutes, the maximum concentration of any one solute, and the competitive adsorption behavior between solutes. The degree of dilution necessary cannot be established *a priori*, but can be determined quickly through a simple procedure.

The objective of the dilution process is to ensure that the elution occurs in the linear portion of the isotherm. From eqn. 2, this requires that

$$\sum_{j=1}^{n} b_j c_j \ll 1 \tag{21}$$

In order to identify dilution conditions that satisfy eqn. 21, the elution experiment is first performed with a sample diluted to a known but arbitrary degree. For an n-component process solution, this experiment will give $n+1$ concentration pulses. The first pulse eluting, pulse $n+1$, will correspond to the least retained component in the process solution. The most highly retained component will be the displacer, which will elute last (pulse 1). Between pulse $n+1$ and pulse 1, the other components in the process solution will elute, with retention times increasing with increasing affinity. As

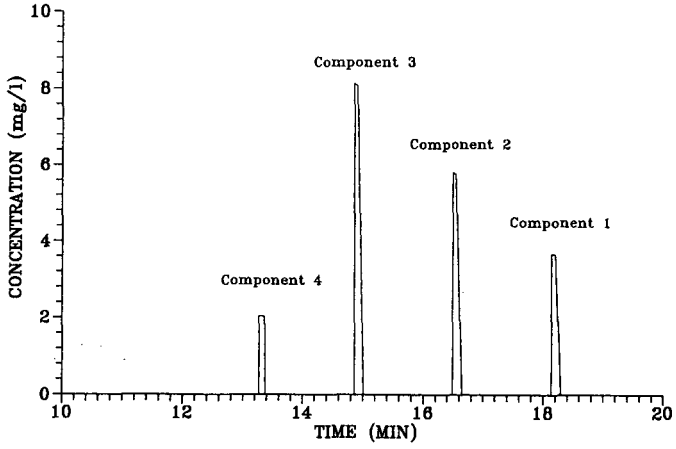

Fig. 2. Elution chromatogram for sample No. 3.

TABLE I
LANGMUIR CONSTANTS FOR CHROMATOGRAPHIC SIMULATIONS

Component No.	*a (l/g)*	*b (l/mg)*
1	5	0.25
2	4	0.25
3	3	0.25
4	2	0.25
5	1	0.25

an example, an ideal elution chromatogram for a three-component process solution is shown in Fig. 2. The peak retention times for each of the pulses is recorded. The elution experiment is now repeated with a sample that is ten times more dilute than the sample used in the first experiment. The new peak retention times are noted, and compared to the set obtained earlier. If the degree of dilution first selected is adequate, the retention times obtained from the two experiments will be essentially the same. If they are not, the process has to be repeated until a degree of dilution consistent with the requirements of tracer elution chromatography is established.

The procedure for identifying adequate dilution is illustrated for the five-component system shown in Table I. Component 1 is the displacer, and component 5 is the eluent. Components 2–4 are solutes in the process solution for which the displacement scheme is being developed. For this system, the coherence theory of chromatography[4] was used in conjunction with the operating conditions given in Table II, to simulate the column response during the isocratic elution of various samples, each diluted to a different degree. The results of these simulations are summarized in Table III. Sample 1 corresponds to the initial sample prepared with an arbitrarily selected degree of dilution. Sample 2 corresponds to a ten-fold increase in the dilution, relative to sample 1. It is clear from a comparison of the retention times obtained with these two samples, that the initial degree of dilution is insufficient for linear elution chromatography. Sample 3 corresponds to a further ten-fold increase in the degree of dilution. Once again, the change in retention times exhibited between samples 2 and 3 indicate that the degree of dilution represented by sample 2 is insufficient. In contrast, a comparison of retention times obtained with samples 3 and 4 indicates that the dilution represented by sample 3 is sufficient to satisfy eqn. 21.

Once an adequate degree of sample dilution has been identified, the corres-

TABLE II
OPERATING CONDITIONS FOR ELUTION SIMULATIONS

Column length	100 cm
Packing density	20 g/l of column
Column porosity	0.97
Interstitial fluid velocity	10 cm/min
Injection time	0.1 min
Eluent	500 mg/l component 5 in inert carrier

TABLE III
EFFECT OF DEGREE OF DILUTION ON RETENTION TIME

Sample No.[a]	*Relative degree of dilution*	*Retention time (min) for peak No.*			
		1	*2*	*3*	*4*
1[b]	1	16.7	15.0	13.5	12.6
2	10	17.8	16.2	14.5	13.2
3	100	18.1	16.5	14.9	13.3
4	1000	18.2	16.5	14.9	13.3

[a] All samples prepared in a solution containing 500 mg/l of eluent in an inert carrier.
[b] 400 mg/l component 1; 600 mg/l component 2; 800 mg/l component 3; 200 mg/l component 4; 500 mg/l component 5.

ponding elution chromatogram can be used to calculate the séparation factors, α_{j1}, of all components except the eluent. For example, for sample 3 in Table III, the elution chromatogram is shown in Fig. 2. From the retention times of each of the peaks in this chromatogram, the propagation velocities of the peaks are calculated. These velocities are reported in Table IV. Once peak velocities are known, eqn. 12 is used to calculate the separation factors. For the case being considered, the separation factors calculated in this manner are given in Table IV. The dilute solution constants, a_j, for the process solution components ($1 < j \leq n$), can now be calculated from eqn. 14 and the value of a_1, which is assumed to be known. As shown in Table IV, the values of a_j used in the simulation are recovered.

From this development, it is clear that tracer elution allows the explicit determination of the dilute solution Langmuir constants from a single chromatogram, once an appropriate degree of dilution has been identified. Notice that the method works regardless of the number of components present in the process solution. Furthermore, injection samples are obtained directly from the process solution, and the sample preparation process involves only dilution.

Characterization of competitive behavior

The characterization of competitive behavior between adsorbing species can be

TABLE IV
DILUTE SOLUTION LANGMUIR CONSTANTS FROM ELUTION CHROMATOGRAM OF SAMPLE No. 3

Species No., j	*Peak velocity, v_j (cm/min)*	*Separation factor, α_{j1}*	*Calculated constant a_j (l/g)*
1	5.52	1.0	–
2	6.06	0.8	4.0
3	6.71	0.6	3.0
4	7.52	0.4	2.0

achieved with frontal chromatography. The frontal chromatogram should be obtained for an appropriate mixture of the process solution and the displacer; the concentration of displacer in the injected mixture should, for the reason outlined earlier, be no greater than that of the most concentrated components in the process solution. Before performing the frontal experiment, it is necessary to ensure that the chromatographic process will occur in the non-linear regime. This can be established with the elution experiments described earlier. If it is found that the adsorbate content in the process solution is low, concentration of this solution will be necessary.

As was stated earlier, frontal chromatography with n components will produce n sharp concentration boundaries in the column, each travelling with a different, but constant, velocity (Fig. 1). Since for frontal chromatography the resolution from non-coherence to coherence is instantaneous, the waves maintain their positions in the sequence from the start of the operation to the time they exit the column; *i.e.*, there will be no interference between the migrating waves. Thus, the plateau regions between the waves will be conserved.

From the frontal chromatography experiment, the retention time for each of the boundaries can be obtained. These retention times can then be used to calculate the velocities of the corresponding boundaries. From the real velocities, adjusted velocities are calculated with eqn. 8. At this point, it is necessary to obtain the value of the nth h-root in the injected solution (the h_n' value in Fig. 1). This is achieved with eqn. 17, using an R value that is arbitrarily selected in the range $0 < R < a_n$. Helfferich and Klein[4] have shown that the value of R selected does not affect the computation. However, selecting a value in the range specified will ensure that the concentrations of all physically existing species will be positive.

The frontal chromatography experiment will also provide the compositions of each of the plateau regions between the migrating boundaries. These compositins can be used in eqn. 5a with the calculated value of h_n' to systematically determine the values of the competitive binding coefficients b_i. Eqn. 5a is first applied to plateau zone n in Fig. 1. For this zone, the concentrations of all components except component n, the least retained component in the process solution, are zero. Thus, eqn. 5a simplifies to:

$$\frac{b_n c_n}{h a_n/a_1 - 1} - 1 = 0 \tag{22}$$

Since h_n' is a non-trivial root in zone n, it will satisfy eqn. 22. Therefore, the only unknown in eqn. 22 is b_n;

$$b_n = \frac{h_n' a_n/a_1 - 1}{c_n} \tag{23}$$

Eqn. 5a is now applied to zone $n-1$. In this case, all concentrations except those of components n and $n-1$ are zero. Therefore, eqn. 5a simplifies to:

$$\sum_{i=n-1}^{n} \left(\frac{b_i c_i}{h a_i/a_1 - 1} \right) - 1 = 0 \tag{24}$$

Since h'_n is also a non-trivial root in zone $n-1$, it will satisfy eqn. 24. Thus, b_{n-1} can be calculated from the equation:

$$b_{n-1} = \frac{h'_n a_{n-1}/a_1 - 1}{c_{n-1}} \left(1 - \frac{b_n c_n}{h'_n a_n/a_1 - 1}\right) \tag{25}$$

In this manner, successive zones from the downstream end to the upstream end can be used to calculate the remaining b constants. For the kth component ($k \neq n$), b_k will be given by:

$$b_k = \frac{h'_n a_k/a_1 - 1}{c_k} \left(1 - \sum_{i=k+1}^{n} \frac{b_i c_i}{h'_n a_i/a_1 - 1}\right) \tag{26}$$

This approach has been applied to the four-component system of Table I. For this system, with the operating conditions of Table V, the coherence theory predicts the chromatogram shown in Fig. 3. As expected, four sharp boundaries are obtained. The retention time for each of these boundaries, and the compositions of the plateaus between the boundaries are given in Table VI. Using the retention time for the fastest wave with eqn. 17, h'_4 in Table VII was calculated. This h-root and the composition of the zone upstream of wave 4 were used in eqn. 23 to calculate b_4. The computation was repeated with the other plateau compositions, using eqn. 26 instead of eqn. 23. The values of b thus obtained are reported in Table VII. Comparing these values with the values used for the simulation (Table I), it can be seen that the Langmuir b parameters are recovered.

In the calculation method described, only h'_n was used. It is also possible to calculate the b values by using the other h-roots in the injected solution (h' roots in Fig. 1). In this case, the retention time data are used in conjunction with eqn. 20 to obtain the desired h-roots. These non-trivial h-roots are then used in eqn. 26, with appropriate plateau compositions, to calculate the b parameters.

Two characteristics of the Langmuir coefficients used in the sample simulation need to be highlighted. First, the a_i/b_i ratio for each of the components in the mixture is different. This usually represents the situation when Langmuir coefficients for multicomponent systems cannot be obtained from single-component adsorption

TABLE V
OPERATING CONDITIONS FOR FRONTAL SIMULATIONS

Column length	30 cm
Packing density	400 g/l of column
Column porosity	0.4
Interstitial fluid velocity	10 cm/min
Injected fluid composition	
Component 1	400 mg/l
Component 2	600 mg/l
Component 3	800 mg/l
Component 4 (inert carrier)	200 mg/l

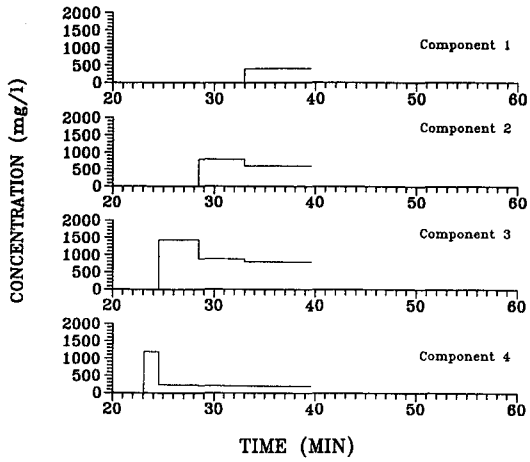

Fig. 3. Frontal chromatogram of four-component mixture with diverging isotherms.

data[12]. Secondly, the values of the constants selected give divergent isotherms. However, HRM is not restricted to divergent isotherms. Shown in Fig. 4 is the frontal chromatogram predicted with the coherence theory for the equilibrium conditions in Table VIII and the operating conditions in Table V; the parameters of Table VIII allow for crossing of the isotherms of components 2 and 3. Using the retention times and plateau compositions of this chromatogram with the procedure described earlier, the *b* parameters in Table IX were obtained. Once again, the calculated values coincide with the values used in the simulation.

TABLE VI
DATA FROM FRONTAL CHROMATOGRAM

Wave No.	*Retention time (min)*	*Component*	*Concentration (mg/l)*	
			Downstream	*Upstream*
4	23.1	1	0.0	0.0
		2	0.0	0.0
		3	0.0	0.0
		4	0.0	1190
3	24.5	1	0.0	0.0
		2	0.0	0.0
		3	0.0	1429
		4	1190	239
2	28.5	1	0.0	0.0
		2	0.0	794
		3	1429	880
		4	239	208
1	33.0	1	0.0	400
		2	794	600
		3	880	800
		4	208	200

TABLE VII
COMPETITIVE BINDING PARAMETERS FROM FRONTAL DATA
$h'_4 = 747.126$.

Component No.	*Calculated b_i (l/mg)*
2	0.25
3	0.25
4	0.25

It can be seen that HRM provides an explicit method for characterizing competitive binding coefficients in systems obeying the Langmuir isotherm. Regardless of the number of components present in the process solution, only one complete frontal chromatogram is necessary for the computation. Also, the injected sample is obtained directly from the process solution.

Dilute solution behavior of displacer

HRM, as described, is dependent on a knowledge of the dilute solution parameter, a_1, for the displacer. When a_1 is not known, it can be obtained with the existing method of single component frontal analysis (FA)[11], applied to the displacer in the dilute solution region; the dilute solution region can be established with elution experiments of the type described earlier. FA is appropriate because the displacer will in general be available as a pure component, separate from the components in the process solution. Furthermore, only a_1 is being determined with the single-component experiments, while competitive behavior is characterized with high concentration, multicomponent experiments. In principle, the retention time of the single, sharp concentration front obtained from a single FA experiment in the dilute solution region will give the value of a_1.

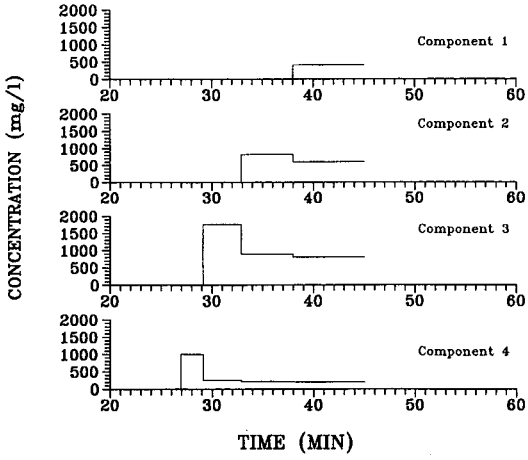

Fig. 4. Frontal chromatogram of four-component mixture with crossing isotherms.

TABLE VIII
LANGMUIR CONSTANTS FOR SYSTEM WITH CROSSING ISOTHERMS

Component No.	*a (l/g)*	*b (l/mg)*
1	5	0.25
2	4	0.25
3	3	0.16
4	2	0.25

TABLE IX
COMPETITIVE BINDING PARAMETERS FROM FRONTAL CHROMATOGRAM FOR CROSSING ISOTHERMS CASE
$h_4' = 624.297$.

Component No.	*Calculated b_i (l/mg)*
2	0.25
3	0.16
4	0.25

Trace components

In some applications of displacement chromatography, the concentrations of some components in the process solution may be at trace levels. In such cases, it may be difficult to establish the effluent concentration history of the more dilute components during frontal chromatography. For example, for the operating conditions of Table V, if the concentration of component 3 is dropped from 800 to 20 mg/l, the coherence

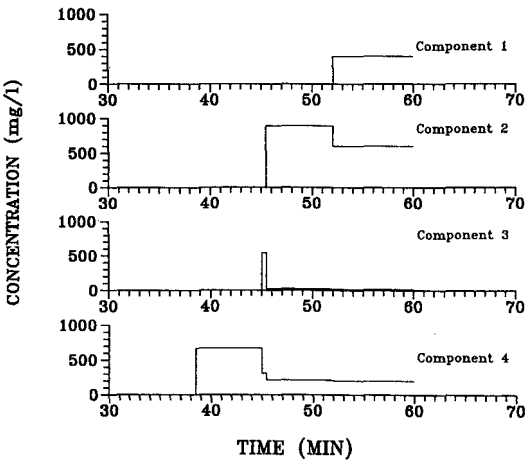

Fig. 5. Frontal chromatogram of four-component system with one trace component.

TABLE X
OPERATING CONDITIONS FOR DISPLACEMENT CHROMATOGRAPHY
Column length, 122 cm; packing density, 400 g/l of column; column porosity, 0.4; interstitial fluid velocity, 10 cm/min.

	Time (min)	*Component No.*	*Concentration (mg/l)*
Presaturant	–	1	0.0
		2	0.0
		3	0.0
		4	0.0
Sample	0.0	1	0.0
		2	600
		3	20
		4	200
Displacer	2.0	1	2000
		2	0.0
		3	0.0
		4	0.0

theory predicts the frontal chromatogram shown in Fig. 5. Depending on the sensitivity of the detection technique, the very short plateau region corresponding to the first appearance of component 3 may not be detected at all. Thus, it may not be possible to determine the coefficients b_i for trace components.

Fortunately, the determination of b values of trace components is not essential for simulation major features of the displacement chromatogram. As an example, consider the displacement experiment described in Table X. In this case, component 3 is the trace component. For the equilibrium constants of Table I, the coherence theory predicts the displacement chromatogram shown in Fig. 6. Repeating the

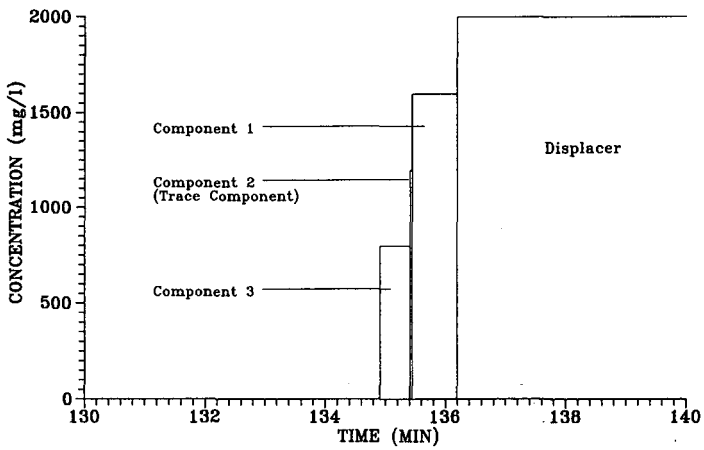

Fig. 6. Displacement chromatogram of three-component system with one trace component.

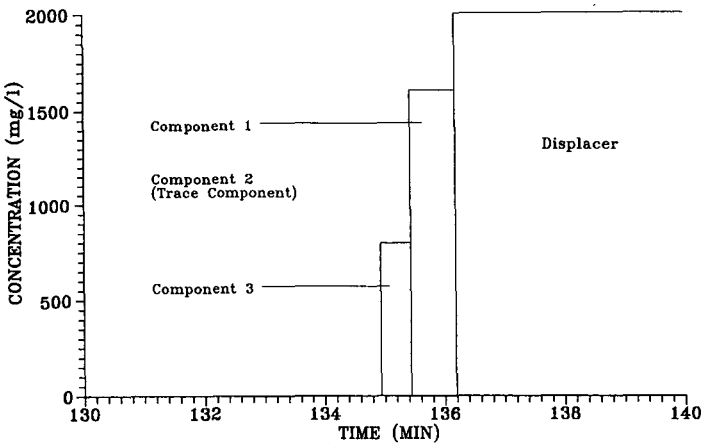

Fig. 7. Displacement chromatogram of three-component system neglecting trace component.

simulation with the same equilibrium and operating conditions, but assuming the absence of component 3, the chromatogram in Fig. 7 is obtained. Comparing Fig. 6 and 7 it is clear that the trace component has essentially no effect on the major features of the effluent composition history. If the location of the trace component zones in the chromatogram is desired, it is simply necessary to simulate the system with $b_i c_i \cong 0$, where i represents all trace components in the system; the values of a_i for the trace components will be available, since these can be determined from elution experiments using appropriate degrees of dilution.

CONCLUSION

In this paper, only theoretical aspects of HRM have been addressed. However, it must be noted that, in the practical application of this method, some difficulties may be encountered in obtaining the required experimental data. For the elution experiments, the theory has been presented for the isocratic case. The experimental difficulty with isocratic elution is that suitable eluents may not always be available to ensure efficient chromatographic development. Though the method can be extended to gradient elution, the computations are considerably more involved. For the frontal chromatography experiments, the determination of the concentrations of the fronts may require tedious analyses. Automated chromatographic analysis is likely to be useful in this case. These and other experimental aspects of HRM are currently being investigated in our laboratory.

A limitation of the coherence theory is that it is an equilibrium theory. In practice, secondary effects such as axial dispersion, mass transfer, and mixing will result in some degree of band spreading. This will affect the determination of the retention times of the concentration waves in the frontal chromatogram. Thus, care must be taken in establishing operating conditions, such as column packing, flow distribution, and support size, that minimize secondary effects during the frontal experiments. Under any circumstances some degree of spreading of the sharp concentration fronts will occur. In this case, the inflection points on the fronts can be used to approximate the retention times[12].

The coherence theory provides a potent framework for the rapid determination of equilibrium adsorption data. With a minimal number of experiments, the equilibrium behavior of multicomponent Langmuirian systems can be established. The theory gives a direct relationship between retention times and compositions and the coefficients of the multicomponent isotherm. Thus, the accuracy with which the equilibrium behavior can be characterized is dependent only on the accuracy of the experimental data. This is in contrast to other approaches, where parameter estimation techniques form an integral part of the method[10,12]. Another advantage of HRM relates to the determination of equilibrium characteristics of high-value products. Tracer elution experiments required by the method inherently use small quantities of solute, while frontal chromatograms can potentially be obtained by using automated, miniaturized chromatographic systems, similar to the one developed by Jacobson *et al.*[11]. Furthermore, pure samples of the solutes are not required, and equilibrium data are obtained from a minimal number of chromatographic experiments.

SYMBOLS

a_i Langmuir coefficient of species i (l/g)
b_i Langmuir coefficient of species i (l/mg)
c_i concentration of species i in external fluid (mg/l)
h_i the ith h-root
q_i concentration of species i in adsorbent (mg/g)
R conversion parameter (l/g)
u_i adjusted wave velocity of ith wave
v_{ci} concentration velocity (cm/min)
v_i real velocity of ith wave (cm/min)
v_0 interstitial fluid velocity (cm/min)
z distance coordinate (cm)

Greek symbols
α_{ij} separation factor
ε column porosity
ρ packing density (g/l of column)

Superscripts
$'$ upstream
$''$ downstream

Subscripts
i species i
n species n or number of component
p dummy spcies

ACKNOWLEDGEMENTS

This work was supported in part by Grant No. CTS-8909742 from the National Science Foundation and Grant No. CDO/R-86-14 from the Ohio Department of Development. This support is gratefully acknowledged.

REFERENCES

1 A. J. Hacking, *Economic Aspects of Biotechnology*, Cambridge University Press, Cambridge, 1986, p. 127.
2 M. R. Ladisch, in H. R. Bungay and G. Belfort (Editors), *Advanced Biochemical Engineering*, Wiley, New York, 1987, Ch. 9, p. 219.
3 J. Frenz and Cs. Horváth, in Cs. Horváth (Editor), *High-Performance Liquid Chromatography*, Vol. 5, Academic Press, New York, 1988, Ch. 3, p. 211.
4 F. Helfferich and G. Klein, *Multicomponent Chromatography*, Marcel Dekker, New York, 1970.
5 E. Glueckauf, *J. Chem. Soc.*, (1947) 1302.
6 J. R. Conder and C. L. Young, *Physicochemical Measurements by Gas Chromatography*, Wiley, New York, 1979, p. 353.
7 F. Helfferich and D. L. Peterson, *Science (Washington, D.C.)*, 142 (1963) 661.
8 C. N. Reilley, G. P. Hildebrand and J. W. Ashley, *Anal. Chem.*, 34 (1962) 1198.
9 C. J. Glover and W. R. Lau, *AIChE J.*, 29 (1983) 73.
10 W. A. Ruff, C. J. Glover and A. T. Watson, *AIChE J.*, 32 (1986) 1948.
11 J. Jacobson, J. Frenz and Cs. Horváth, *J. Chromatogr.*, 316 (1984) 53.
12 J. M. Jacobson, J. H. Frenz and Cs. Horváth, *Ind. Eng. Chem. Res.*, 26 (1987) 43.
13 I. Langmuir, *J. Am. Chem. Soc.*, 38 (1916) 2221.
14 F. Helfferich and D. B. James, *J. Chromatogr.*, 46 (1970) 1.
15 C. Tien, J. S. Hsieh and R. M. Turian, *AIChE J.*, 22 (1976) 498.
16 M. Bailly and D. Tondeur, *Chem. Eng. Sci.*, 36 (1981) 455.
17 D. Clifford, *Ind. Eng. Chem. Fundam.*, 21 (1982) 141.
18 J. Frenz and Cs. Horváth, *AIChE J.*, 31 (1985) 400.
19 M. M. Davis and M. D. LeVan, *AIChE J.*, 33 (1987) 470.
20 C. B. Bailey and N. G. Pinto, *Sep. Sci. Technol.*, 23 (1988) 1853.
21 D. DeVault, *J. Am. Chem. Soc.*, 65 (1943) 532.

Journal of Chromatography, 484 (1989) 187–210
Elsevier Science Publishers B.V., Amsterdam — Printed in The Netherlands

CHROM. 21 924

MODELLING METHODS TO AID THE DESIGN AND OPTIMISATION OF BATCH STIRRED-TANK AND PACKED-BED COLUMN ADSORPTION AND CHROMATOGRAPHY UNITS

G. H. COWAN*, I. S. GOSLING and W. P. SWEETENHAM
BIOSEP, Biotechnology Group, B353, Harwell Laboratory, Oxon OX11 0RA (U.K.)

SUMMARY

In this paper, work is described which has led to the development of a suite of computer programs for the prediction of adsorption and chromatographic processes to aid the design and optimisation of batch stirred-tank and packed-bed column units. Brief descriptions are given of the mathematical models incorporated within the codes, and the complementary small-scale experiments to provide the necessary physical parameter information on adsorption isotherms and mass transfer kinetics.

The models are formulated for single- and multi-component adsorption and for packed-column separation dealing with both frontal analysis and elution chromatography. Two types of predictive method are outlined. The first is based on simple kinetic type rate expressions for mass transfer, the second is a more complex model taking into account liquid film and pore diffusion resistances to mass transfer. For adsorption the models imply a favourable Langmuir type isotherm but they may be adapted for use with linear and irreversible isotherms.

Some details of the mathematics involved in the models and the methods of solution of the resulting equations are presented. In specific cases simplifying assumptions allow analytical solutions to be obtained, whereas in other instances numerical solutions derived by using the Harwell FACSIMILE code are required.

Typical results are given from small-scale and pilot-scale experiments to provide data to validate the codes. These experiments involved studies of the adsorption, washing and elution of single- and multi-component amino acids using Duolite A-162 resin spheres as adsorbent covering a range of conditions. Comparisons are given between code simulations and experimental data, and applications of the codes are discussed.

INTRODUCTION

The development of computer simulation programs to aid the design and optimisation of industrial batch stirred-tank and packed-bed column adsorption and chromatography units continues to attract major attention. In previous work the modelling of adsorption rate processes has been reviewed by Cowan *et al.*[1], and examples of the application of modelling to the design and optimisation of industrial adsorption units has been discussed by Cowan *et al.*[2].

In the present paper, recent publications relevant to the modelling of adsorption and chromatographic processes are reviewed and work is described which has led to the development of computer programs for the simulation of batch stirred-tank and packed-bed column adsorption units to aid in process optimisation and design, given specific information on equilibrium and kinetics derived from small-scale experiments. Brief details are also given of complementary programs which are used for the derivation of the appropriate equilibrium and kinetic parameters from the small-scale experiments. Such parameter fitting codes may be applied to data from small- or preparative-scale operations or from industrial plants to derive physical parameters for modelling and optimisation purposes.

Typical results are presented from small-scale and pilot-scale experiments to provide data to validate the codes. These experiments involved studies of the adsorption, washing and elution of single- and multi-component amino acids using Duolite A-162 resin spheres as adsorbent covering a range of conditions. Comparisons are given between code simulations and experimental data, and applications of the codes are discussed.

RECENT PUBLICATIONS RELEVANT TO MODELLING

Knowledge of capacity and equilibrium relationships and mass transport parameters are required in modelling work. Jacobsen *et al.*[3] have developed a fast, accurate and precise method of isotherm measurement by using a high-performance liquid chromatography (HPLC) technique requiring only milligram quantities of material with frontal development. Kirby *et al.*[4] have also described an HPLC technique suitable for isotherm determination where it is required to contact small quantities of adsorbate with an adsorbent for a short time. A micro-scale system for estimation of isotherm and kinetic parameters used in the modelling of fixed-bed adsorbers is detailed by Weber and Wang[5]. The application of the data from such measurements to the design or analysis of industrial packed-bed columns is of interest. From micro-scale column experiments using carbon particles of different size ranges Weber and Wang[5] concluded that adsorbent particle size did not affect capacity. Similarly Kirby *et al.*[4] found reasonable agreement between isotherm data by using the HPLC technique with 40–50-μm Amberlite XAD-2 particles and larger-scale packed-bed experiments with 700-μm XAD-2 particles. In comparing HPLC data with results from batch cell experiments Kirby *et al.*[4] showed isotherm data to be in sensible agreement, whereas Weber and Wang[5] indicated that batch cell results gave a higher value for adsorbent capacity than obtained from the microcolumn work. Weber and Wang[5] discussed application of the microcolumn data to system scale-up.

A new method of predicting adsorption equilibria for multicomponent liquid solutions on solids which combines the thermodynamic and kinetic treatments of liquid adsorption has been developed by Price and Danner[6]. The method requires the determination of liquid phase and adsorbed phase activity coefficients but provides a simpler computational technique than previous similar treatments. The potential advantage of the method is that complex experimental multi-component equilibrium studies can be replaced by more relatively straightforward experimental studies of binary mixtures. The determination of binding equilibrium constants by numerical simulation in zonal high-performance affinity chromatography has been reported by

Vidal-Madjar *et al.*[7]. The method was applied to the measurement of ligand–protein interactions in zonal elution chromatography to determine the amount of active immobilised protein and the equilibrium constant characterising the affinity interaction. These parameters are of use to compare different methods of protein immobilisation and for determining the contribution of the matrix to the retention.

Arve and Liapis[8] present general equations to describe single- and multicomponent biospecific as well as non-specific adsorption from a finite bath onto porous adsorbent particles whose internal surface is covered by immobilised ligands. The model accounts for the external film resistance and diffusional resistance within the particles and rate expressions for the interaction between the adsorbate and ligand are included. The adsorbate may be monovalent or multivalent and predictions are given for both adsorption and washing stages. Such models are most useful to indicate the effects of changing different parameters on adsorption and washing in complex batch systems, but more extensive comparisons against experimental data are required to validate the model over a wide range.

A mathematical model has been developed by Nigam and Wang[9] to study bioproduct adsorption for small-affinity adsorbent particles immobilised in hydrogel beads for whole-broth processing. The model accounts for diffusion in the hydrogel beads, adsorbent particles and binding within the immobilised adsorbent particles. Code predictions based on the model show that the performance of finely ground immobilised adsorbent particles within the hydrogel can be better than for freely suspended adsorbent. McConvey[10] describes a two-step model for the adsorption of the macromolecule Vitamin B_{12} onto a porous polymeric adsorbent from an aqueous solution in a batch reactor, and the model is used to determine the external film mass transfer and intraparticle surface diffusion coefficients for the process.

Mansour *et al.*[11] give a parametric study of multicomponent adsorption in stirred tanks. A mathematical model was developed by Mansour which takes into account internal and external diffusional resistances and liquid film resistance. A non-linear Fritz–Schlunder[12] type isotherm was used to describe the equilibrium between liquid and solid phases. Predicted transient bath concentration profiles were obtained for the cases of adsorption of single, binary and ternary systems. Predictions for the binary adsorption of 2-butanol and *tert.*-amyl alcohol onto activated carbon showed good agreement with the experimental data of Balzli[13]. Using a simplified model in which it was assumed that internal diffusion is a very rapid process, Mansour *et al.*[14] have also presented a study of the prediction of the effect of parameters influencing the performance of multicomponent adsorption in packed-bed columns. Predictions from the mathematical model satisfactorily agreed with previously published data.

Numerical methods relevant to the solution of adsorption models are discussed by Costa and Rodrigues[15] in the book edited by Rodrigues *et al.*[16], which gives several useful papers relevant to the kinetics of adsorption and fixed-bed processes and modelling. Details of the numerical simulation of fixed-bed adsorption dynamics using the method of lines and accounting for both axial dispersion and intraparticle diffusion are given by Brian *et al.*[17].

An overview of simulation and design for adsorption processes has been given by Weber and Smith[18], including discussion of Freundlich and ideal adsorbed-solution theory equilibrium models, a two-resistance, homogeneous-surface-diffusion dynamic

model, and parameter estimation. Important guidelines given are that continuing research is needed to improve the reliability of parameter estimation techniques, and to validate and enhance the capability of existing models to deal with the complexities encountered in field applications. Comments on possible future directions for process modelling are presented. A comparative study of two models to predict protein adsorption on packed beds of resins has been made by Graham *et al.*[19]. The models are a two-phase resistance model and a shrinking core model. The main difference between the models is the method used to account for diffusion of the protein within the resin particles. In the two-phase resistance model the resin particle is treated as a quasi-homogeneous media through which the protein molecules diffuse. The diffusional process is approximated by a linear driving force using a mass transfer coefficient, related to an effective particle diffusion coefficient which is determined from separate batch experiments. In the shrinking core model, it is assumed that once the protein reaches the resin particle it binds with the active sites and becomes immobilised producing a reacted core, and the concentration of protein diffusing is taken as only that in the pores of the resin. The diffusion equation is solved in the reacted resin region and the pore diffusivity is determined from the free solution diffusivity taking into account the tortuosity of the pores in the resin. Comparison of predictions from the two models with breakthrough curves derived from fixed-bed column experiments for bovine serum albumin (BSA) on Sephadex A-50, and BSA on DEAE-Sepharose indicated that the two-phase resistance model gave the better agreement with experimental data. The shrinking core model predicted broader breakthrough curves possibly because of the more imprecise determination of the pore diffusion coefficient. The optimisation of the process chromatography of proteins has been discussed by Janson and Hedman[20] and a simplified treatment for optimisation of production rate is presented. For such processes these authors conclude that it is more profitable to increase throughput by increasing selectivity rather than column efficiency.

A simplified model for multi-component fixed-bed adsorption is described by Moon and Lee[21] based on the assumption that a linear driving force approximation is valid in describing the intraparticle surface diffusion. The Freundlich-type multi-component isotherm (taken as suitable for highly heterogeneous adsorbents such as activated carbon) and the ideal adsorbed-solution theory were incorporated with the model to deal with competitive adsorption. Model parameters were estimated from correlations and obtained from single-component batch experiments. The model was satisfactorily used in predicting breakthrough curves for two-component simultaneous and counter-current adsorptions of phenols on activated carbon in fixed beds. An advantage claimed for the method is that computational times are small compared to those for diffusion models.

In studies of the uptake of various amino acids by two ion-exchange resins Carta *et al.*[22] found that a model for ion-exchange equilibrium which takes into account heterogeneity of functional groups on the resins gave an excellent correlation of binary data. By using parameters determined only from binary measurements the model was successfully extended to the prediction of multi-component equilibria. An equilibrium stage model which incorporates solution and ion-exchange equilibria is also presented for the prediction of packed-bed separation processes. The model which requires only equilibrium data was found to provide an approximate representation of multi-component packed-bed concentration profiles. Ching and Ruthven[23] report results

for the sorption and diffusion of some amino acids in ZX zeolite crystals of 50 μm size. The intercrystalline diffusivities were determined to be in the range of 10^{-7} to 10^{-9} cm^2s^{-1} showing a regular decrease with increasing molecular weight of amino acid. The research showed that it should be possible to obtain an efficient separation of smaller from larger amino acids based on size-selective exclusion.

Adsorption of pollutants onto activated carbon in fixed beds has been studied by McKay and Bino[24], who present a model based on external mass transport and internal pore diffusion for irreversible adsorption to predict breakthrough curves. Effective pore diffusion coefficients were determined for each sorbate carbon system by comparison of the predicted curves with experimental data by using a best-fit method. Reasonable agreement was achieved between predicted and measured breakthrough curves for phenol, *p*-chlorophenol and mercury, but the measured curves for sodium dodecyl sulphate (SDS) were broader than could be fitted. This was explained as due to the assumption of an irreversible isotherm not being applicable to SDS.

The influence of pore and particle size on the frontal uptake of proteins for silica-based anion-exchange packings is discussed by Kopaciewicz *et al.*[25]. Results from a mathematical model used to compute radial adsorption profiles across the adsorbent particles for frontal uptake showed that restricted intraparticle diffusion due to insufficient pore size leads to incomplete use of the internal surface area giving a reduced loading of the packing.

Moon and Tien[26] give details of the use of pseudo-species representation in the modelling of fixed-bed adsorption involving solutions containing unknown adsorbates of favourable adsorption behaviour. To demonstrate the validity of the method experimental data for the fixed-bed adsorption of humic substances from aqueous solutions by activated carbon were compared with model predictions with good agreement. A mathematical model of a fixed-bed ligand-exchange column is described by Bolden and Groves[27]. The model based on a Langmuir isotherm, liquid-phase film resistance and a single-resin phase effective diffusivity gave satisfactory prediction of experimental breakthrough curves for butylamine and diglycolamine on a Cu(II)-loaded carboxylic acid resin. Ching *et al.*[28] discuss the modelling of a counter-current adsorption process for separation of a fructose–glucose mixture at high concentrations where the equilibrium isotherms deviate from linear. It is shown that an equilibrium stage model with due correction for the concentration dependence of the apparent distribution coefficients, provide a good representation of the system behaviour.

A model to simulate the separation of a two-component mixture in preparative-scale non-linear liquid chromatography is presented by Guiochon and Ghodbane[29] with boundary conditions corresponding to the elution of large-concentration profiles, neglecting axial diffusion and assuming that the kinetics of radial mass transfer is infinitely fast. The model consists of two mass balance equations, one for each component, and the equations are solved numerically by a finite difference method. The predicted elution profiles compare reasonably well with experimental data from the literature. Wade *et al.*[30] present the impulse input solution to the equations describing non-linear chromatography and discuss applications to physicochemical measurements in affinity chromatography and the implications for optimisation of preparative-scale separations. The model is used to characterise the retention

behaviour of *p*-nitrophenyl-α-D-mannopyranoside on silica-bound Concanavilin-A affinity columns. The analysis gives information on adsorption–desorption rate constants and the binding site density for the more populous binding site in immobilized Concanavilin-A.

In a comprehensive study Knox and Pyper[31] present details of a framework for maximising throughput in preparative liquid chromatography. The work shows that concentration overload rather than volume overload provides the greatest throughput, and that the plate height concept can be used in optimisation computations. The use of computer simulation to optimise HPLC gradients for the separation of either small or large molecules is discussed in a series of papers by Ghrist *et al.*[32], and Ghrist and Snyder[33,34]. The method is to use a small number of experimental runs to measure sample characteristics which can be related to retention in gradient elution, and then to use computer simulation to predict retention as a function of any gradient conditions. The papers present information on minimising errors in computer simulations, the use of such simulations to determine the effects of different variables, and give recommendations for an efficient approach to the design of optimised gradients for complex samples by using computer simulations. In further papers Snyder *et al.*[35] and Cox *et al.*[36] report the use of the Craig model as a basis for computer simulations for mass-overloaded gradient elution for Langmuir and non-Langmuir isotherms related to the preparative separation of peptide and protein samples by HPLC. It seems possible to quantitatively predict bandwidth and resolution as a function of small-sample retention data, experimental conditions and sample size. The work leads to a proposed systematic approach for designing the preparative- or process-scale separation of protein mixtures by reversed-phase gradient elution. In a complementary development, Hodges *et al.*[37] give details of the use of a computer program to assist workers in devising methods of size-exclusion, cation-exchange, and reversed-phase HPLC for the analytical separation and purification of biologically active peptides and peptide fragments from enzymatic and chemical digests of proteins. It is stated that the program has the ability to examine the effects of flow-rate, gradient rate and sample size on the separation, and that use of the program to simulate experiments eliminates the time consuming trial-and-error methods used to determine suitable separation or purification methods.

The review illustrates the current wide range of applications of modelling to assist the design and optimisation of adsorption and chromatographic separation processes. It is seen that a general approach to modelling involves solution of mass balance and rate relationships for given boundary conditions and with knowledge of equilibrium and kinetic parameters. Models have different degrees of complexity depending on the simplifying assumptions made to achieve the required prediction with a reasonable degree of accuracy and computation time. It is desirable that a model should have as wide an application as possible and yet be of sufficient simplicity that the parameters needed to implement the model can be obtained with accuracy from small-scale experiments or from the literature. Details are now presented of complementary work in our laboratories to meet a general requirement for computer programs to predict the performance of batch stirred-tank and packed-bed column adsorption and chromatography units, whilst also determining equilibrium and kinetic parameters (for input to the simulation programs) by using fitting techniques to experimental data.

MATHEMATICAL MODELLING OF BATCH STIRRED-TANK AND PACKED-BED COLUMN ADSORPTION AND CHROMATOGRAPHIC UNITS

The models are formulated for single- and multi-component adsorption, and for packed-bed column operation deal with both frontal analysis and elution chromatography. In frontal analysis the sample is fed continuously to the column until breakthrough occurs. Loading is stopped at an appropriate time after breakthrough, and is generally followed by a washing stage to remove excess sample from the intersticies of the packed bed. Elution is then commenced to desorb and separate or recover desired components. In elution chromatography a small amount of sample is fed to the column, then the eluent, which has no affinity for the adsorbent and may be the same as the sample solvent, is introduced and separation of the components is achieved in the form of bands. In this paper isocratic elution in which the same eluent is used throughout is dealt with.

Two types of predictive method are described. The first is based on simple kinetic type rate expressions for mass transfer, the second is a more complex model taking into account liquid film and pore diffusion resistances to mass transfer, which may be suitable for cases where the simple kinetic type model is inadequate.

Batch stirred-tank, simple kinetic model

The adsorption process is formulated in terms of a reaction law which leads to a Langmuir type isotherm at equilibrium. The model is one used earlier by Chase[38], and is similar to models described by Thomas[39,40] as applied to ion exchange and chromatography.

The Langmuir isotherm is given by

$$q^* = \frac{Q_m c^*}{c^* + K_d} \tag{1}$$

where c^* and q^* are the values of c and q at equilibrium, Q_m is the maximum adsorption capacity of the adsorbent, and K_d is the dissociation constant. Thus Q_m can be evaluated from isotherm measurements as the value q^* tends to asymptotically as c^* tends to a high value, and K_d is the value of c^* when $q^* = Q_m/2$. The dissociation constant K_d is equal to the ratio of backward and forward rate constants K_2/K_1 for the process.

The forward rate constant K_1 can be evaluated from small-scale experiments to determine the rate of uptake of adsorbate, which then allows K_2 to be computed as $K_d K_1$.

For mono-component adsorption, or for multi-component adsorption without competition between species for adsorption sites, the mass balance and rate equations can be solved to give analytical solutions. For multi-component adsorption with competition between species for adsorption sites the rate equations are modified to comply with a model given by Chase[41], and it is then necessary to solve the equations numerically. This is facilitated by writing the computer programs in conjunction with the Harwell code FACSIMILE (Curtis and Sweetenham[42]) which is a program for solving initially valued ordinary differential equations.

Packed-bed column, simple kinetic model

For column simulation two processes within the column have been considered, adsorption and flow of adsorbate down the column. At each point along the column, the system is described by two values, the total concentration of adsorbate in the mobile phase, c, and the local concentration of adsorbate in the stationary phase, q. It is assumed that the system is well mixed across the column so c and q only vary with distance along the column. Transport along the column is governed by the fluid, the solute is assumed to flow with the fluid and to diffuse through it, whereas the adsorbed adsorbate is unaffected by the fluid. The height of the packed bed in the column is taken to be L, and the adsorbate in solution flows down the column with speed V, where V is the interstitial velocity expressed as

$$V = \frac{F}{a\varepsilon_e} \tag{2}$$

where F is the fluid volume entering the column in unit time, a the cross-sectional area of the column, and ε_e the interstitial porosity of the packed bed.

Under these conditions the equations governing the process are

$$\frac{\partial c}{\partial t} = D_a \frac{\partial^2 c}{\partial z^2} - \frac{V\partial c}{\partial z} - K_1 c\,(Q_m - q) + K_2 q \tag{3}$$

$$\frac{\partial q}{\partial t} = K_1 c\,(Q_m - q) - K_2 q \tag{4}$$

where D_a is the axial dispersion coefficient, t the time, z the distance along the column, Q_m the maximum capacity of the adsorbent, and q the concentration of the adsorbed material in consistent units.

For mono-component adsorption for the case where the axial dispersion is negligible eqns. 3 and 4 become

$$\frac{\partial c}{\partial t} = -V\frac{\partial c}{\partial z} - K_1 c\,(Q_m - q) + K_2 q \tag{5}$$

$$\frac{\partial q}{\partial t} = K_1 c\,(Q_m - q) - K_2 q \tag{6}$$

Eqns. 5 and 6 can be solved analytically (Thomas[39], Chase[38] and Cowan *et al.*[1]) the form of the analytical solution depending on the boundary conditions, given by the amount of adsorbate flowing into the column and the amount of adsorbate bound to the bed when the adsorption process starts. In further work analytical solutions have been given to eqns. 5 and 6 for loading, washing and elution conditions (Sweetenham[43]).

When axial dispersion is of importance for given boundary conditions with a single solute eqns. 3 and 4 are solved numerically by use of the FACSIMILE code. Numerical solutions to the equations can be found by assuming the column to be an

array of well mixed cells and then solving ordinary differential equations for the value of c and q in each cell, so that the equations can be solved for a wide range of mathematical models. For multi-component adsorption with competition between species the appropriate forms of eqns. 3 and 4 with axial diffusion, or eqns. 5 and 6 without axial dispersion are solved numerically by use of the FACSIMILE code.

The liquid film plus pore diffusion model

To give an alternative method of calculation when the simple kinetic model proves inadequate (Cowan[44]), particularly where the mass transfer is dependent on diffusion within the porous structure of the adsorbent, equations are presented applicable to a model (Horstmann and Chase[45,46]) taking into account the liquid film and pore diffusion resistances to mass transfer.

From the Horstmann and Chase[45,46] model the material balance in the particle is taken as

$$\varepsilon_i \frac{\partial c_i}{\partial t} = \varepsilon_i D_e \left(\frac{\partial^2 c_i}{\partial r^2} + \frac{2}{r} \frac{\partial c_i}{\partial r} \right) - (1 - \varepsilon_i) \frac{\partial \hat{q}_i}{\partial t} \tag{7}$$

where c_i is the solute concentration in the pore fluid, D_e the effective pore diffusivity of the adsorbate in the particle phase, ε_i the intraparticle porosity, and $\hat{q}_i$ the local solid phase concentration of adsorbed material in mass of adsorbate per unit adsorbent solid volume.

Eqn. 7 is subject to boundary conditions at the centre and radius of the particle as follows

$$\frac{\partial c_i}{\partial r} = 0 \text{ at } r = 0 \tag{8}$$

and, at the surface of the particle, the flux of solute is constant so

$$\frac{\partial c_i}{\partial r} = \frac{k_f}{D_e \varepsilon_i} (c_b - c_i) \text{ at } r = R \tag{9}$$

where c_b is the concentration of the solute in the bulk fluid, k_f the liquid film mass transfer coefficient, and R the radius of the particle.

For adsorption in a stirred tank, Horstmann and Chase[45,46] give the relation at the surface of the particle as

$$\frac{dc_b}{dt} = -3 \frac{V_s k_f}{R V_L} (c_b - c_i)_{r=R} \tag{10}$$

where V_s is the total volume of the adsorbent particles assumed to be spheres, and V_L the volume of external fluid.

Eqns. 7–10 are solved numerically by again implementing the FACSIMILE code.

Measurement of physical parameters

To use the models knowledge of the mono-component equilibrium adsorption isotherms and process kinetics is required. From the adsorption isotherms values of the maximum capacity and dissociation constant can be derived, and from the kinetics curves values of the forward rate constant (for the simple kinetic model), or the liquid film mass transfer coefficient and effective pore diffusion coefficient can be computed (for the liquid film plus pore diffusion model).

A common method (Chase[38], Fowell and Chase[47], and Cowan *et al.*[1,2,44]) of generating adsorption isotherms from small-scale experiments is to shake known amounts of adsorbent with various concentrations of adosrbate solution of known volume, until equilibrium is attained, allowing equilibrium parameters to be determined.

An alternative method for measurement of adsorption isotherms is to use a small packed-bed recirculation system (Horstmann *et al.*[48]) in which aliquots of adsorbate are successively added to a reservoir whose contents are recirculated by being pumped through a fixed bed of adsorbent. The level of adsorbate is continuously monitored at the column outlet by flow spectrophotometry and when the system is in equilibrium as evidenced by the lack of change of the level of adsorbate in the liquid phase, a further aliquot of adsorbate is added. An advantage of the technique is that the adsorbent is kept within the packed bed at all times, removing the possibility of adsorbent disintegration which may occur as the result of the mixing process in stirred-cell systems.

To provide data for the prediction of the elution stage it is desirable to check the isotherms for adsorption in the presence of eluent (Cowan *et al.*[2]), in parallel with the equilibrium measurements without eluent.

To measure kinetic parameters several workers (Chase[38], Horstmann *et al.*[48], and Cowan *et al.*[1,2]) have used a small stirred-cell apparatus to contact adsorbent and adsorbate solution of known concentration and monitored concentration changes of adsorbate by UV spectrophotometry to determine the rate of uptake of adsorbate by the adsorbent. In circumstances where it is not possible to use UV spectrophotometry the same investigators have used discrete sampling techniques with off-line assay to determine solution concentration changes with time. Many adsorption processes are performed in columns and, although small stirred-cell experiments provide useful information, small-scale column experiments may be required to provide appropriate kinetic data particularly if the liquid film mass transfer resistance is of importance (Cowan *et al.*[1], Cowan[44]). By measuring the breakthrough curve for a system it is possible to derive isotherm and kinetic parameters for the adsorption stage, and from the elution curve it is possible to derive data related to the elution kinetics.

Particle and pore size can have a significant effect on adsorption parameters (Horstmann *et al.*[48], Kopaciewicz *et al.*[25]) so it is desirable that experiments be performed on the same size particles as would be used in the actual process. In addition, it is required to simulate the appropriate process physical conditions particularly pH, ionic strength, temperature, and concentrations of other components if these compete or modify the adsorption process.

Codes for physical parameter derivation and simulation of adsorption and chromatographic processes

The modelling work described in this paper has led to the development within the BIOSEP project at Harwell of a suite of computer programs for application to the prediction of adsorption and chromatographic processes. The codes are of two types, those for the prediction of the performance of batch stirred-tank and packed-bed column units, and those for fitting parameters to batch stirred-cell or packed-bed column experimental results to derive requisite physical parameter data. The codes are written for use on appropriate IBM PC AT or compatible microcomputers, or for use on mainframe machines. Brief details of the codes are given in this section.

Derivation of physical parameters from isotherm measurements

The code used for analysis of isotherm data to determine whether a Langmuir isotherm can be fitted is called LANGFIT. The program takes the data and, if a Langmuir isotherm is applicable, fits the parameters K_d, the dissociation constant, and Q_m, the maximum capacity of the adsorbent, to the data. In doing this the code takes into account errors estimated or measured from the experimental protocol. The program gives the 5.0 and 95.0% confidence limits within which the actual values of Q_m and K_d are expected to lie.

Programs for fitting parameters to batch stirred-tank adsorption data

Three computer programs have been written to derive physical parameters by fitting to batch stirred-tank mono-component data. These codes are given the names KIFIT, TANFITK and TANFITP. The KIFIT and TANFIT codes are based on the simple kinetic model. KIFIT allows values of the forward rate constant K_1 to be determined, whereas TANFITK enables values of Q_m, K_d and K_1 to be fitted depending on available data. The TANFITP code is based on the liquid film plus pore diffusion model, and may be used to fit values of the liquid film mass transfer coefficient, k_f, and the effective pore diffusivity, D_e.

Simulation of batch stirred-tank adsorption units

The codes which have been developed for predicting the performance of batch stirred-tank adsorption units are designated as TANSIMK, TANSIMA and TANSIMP. The TANSIMK and TANSIMA programs both incorporate the simple kinetic model. For the prediction of multi-component adsorption TANSIMK assumes that there is no competition between components for sites on the adsorbent, whereas TANSIMA takes into account competition between components for sites on the adsorbent. TANSIMP is based on the liquid film plus pore diffusion model and currently is used for mono-component adsorption in stirred tank adsorbers when pore diffusion is of significance.

Program for fitting parameters to packed-bed column adsorption data

The COLOFITK program utilising the simple kinetic model is used to fit Q_m, K_1 and the backward rate constant K_2 to packed-bed column mono-component adsorption data, and may be applied to experimental results from loading, washing and elution stages.

Simulation of packed-bed column adsorption and chromatographic units

The programs which have been written to predict the performance of packed-bed adsorption columns are COLOSIMK, COLOSIMA and COLOSIMP. The COLOSIMK and COLOSIMA codes include the simple kinetic model and predict the loading, washing and elution stages of packed-bed operation. The COLOSIMK code may be used to predict multi-component adsorption when there is no competition between components for sites on the adsorbent, whereas COLOSIMA predicts multi-component adsorption with competition between adsorbate components for sites on the adsorbent. In addition, COLOSIMA may be used to compute the effect of axial dispersion. The COLOSIMP code which incorporates the liquid film plus pore diffusion model is used to predict the loading, washing and elution stages of packed-bed operation for mono-component adsorption when pore diffusion is of significance.

PARAMETER FITTING

The BIOSEP parameter fitting codes, such as TANFITK and COLOFITK, are written to allow the user to specify the values of some of the parameters governing adsorption and for the code to fit the remaining parameters to the supplied data. The data supplied by the user can come from one or more different experiments which involve the same set of adsorbate species with different initial concentrations for the species in the different experiments.

This provides the user with a lot of flexibility, but means that the user can easily provide insufficient data to fix all the parameter values. For example, suppose that a user uses TANFITK to fit Q_m, K_d and K_1 to data from several kinetics experiments where the data values were only measured at large times when the system had reached equilibrium. In that case, the fitting code may be able to determine values for Q_m, and K_d, which depend only on the isotherm. However, the code would not be able to determine a value for K_1 and the code's output would give values for Q_m and K_d and would state that the value of K_1 could not be determined by the data.

In all the fitting codes, the program first finds the best fit that it can. It then determines whether the fit to the experimental data is within the error estimates provided by the user. Finally, the code determines whether the parameter values are uniquely determined, and if not the code finds how the parameters can be altered without making the fit significantly worse.

EXAMPLES OF CODE VALIDATION WORK

Work to validate and apply the codes is ongoing and typical examples are given here of results from such work for both batch stirred-tank and packed-bed adsorption and chromatographic units. The experimental work associated with this research has involved studies of the adsorption of mono- and multi-component amino acids by the anion exchanger Duolite A-162, and several of the examples are taken from these studies. Duolite A-162 is a macroporous cross-linked polystyrene matrix with $-N^+(CH_3)_2C_2H_4OH$ functional groups to provide ion-exchange capacity, available as rigid beads resistant to attrition and osmotic shocks.

Batch stirred-tank examples

The LANGFIT code has been used extensively to analyse results from small-scale stirred-cell contactor experiments to derive physical parameters from Langmuir isotherms taking into account error estimates in experimental quantities. Fig. 1 illustrates the graphical output from the program showing the fit obtained by using LANGFIT to isotherm results for the adsorption of glutamic acid by Duolite A-162. The values of the maximum adsorbent capacity and dissociation constant were well determined, LANGFIT fitting values of Q_m equal to 295 mg/g (with 5 and 95% confidence limits of 270–321 mg/g) and K_d as 0.015 mg/ml (with confidence limits of 0.0093–0.024 mg/ml), respectively. Computation time for the example using an IBM PC AT microcomputer was 2.7 min.

Results have also been obtained from small-scale batch stirred-cell experiments for the mono-component adsorption of amino acids to Duolite A-162 to determine the rate of loss of the amino acids from solution for various conditions. The TANFITK code has been applied to the analysis of such results to derive in particular values of the forward rate constant K_1. A typical fit obtained by using the TANFITK code to analyse data for the adsorption of glutamine by Duolite A-162 is shown in Fig. 2. From the analysis a value of K_1 was derived as 0.099 ml min/mg with 5 and 95% confidence limits of 0.09–0.109 ml min/mg. Analysis of isotherm data for the adsorption of glutamine by Duolite A-162 yielded a value of the dissociation constant K_d as 0.018 mg/ml. Hence the value of the backward rate constant K_2 for the adsorption of glutamine by Duolite A-162 for the conditions studied can be derived as $K_2 = K_d K_1$

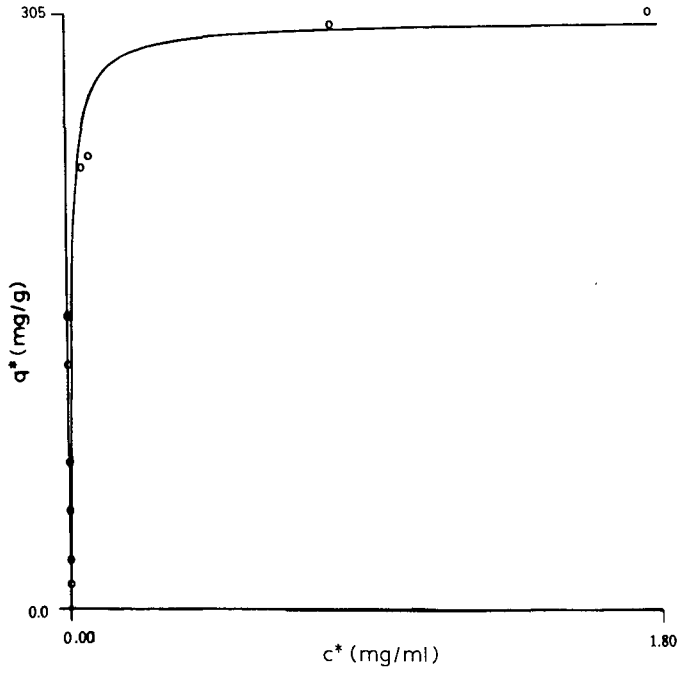

Fig. 1. LANGFIT analysis of isotherm results for the adsorption of glutamic acid by Duolite A-162. ○ = Observed q^*; ——— = calculated q^*.

giving $K_2 = 0.0018\ \text{min}^{-1}$. The computation time for this example was 3.2 min using the IBM PC AT microcomputer.

In further research, a pilot-scale batch stirred-tank rig has been used to study mono- and multi-component adsorption, washing and elution of amino acids by Duolite A-162. The main features and dimensions of the batch stirred tank and the apparatus to monitor adsorbate concentration changes during experiments are shown in Figs. 3 and 4. A 10-l volume of the appropriate amino acid solution was used with 50 g dry mass of Duolite A-162, which had been previously regenerated by using 1 *M* sodium hydroxide solution. To achieve a reasonably uniform suspension of the adsorbent and adequate mixing, the stirred tank was fitted with four stainless-steel baffles and a stirrer operating at a speed of 198 r.p.m. The baffles were sealed to the tank walls to prevent attrition of the Duolite A-162 in any gaps which could otherwise have formed between the baffle and vessel wall. In addition to the on-line monitoring of the experiments using the apparatus shown in Fig. 4, a fraction collector was used to take small samples at predetermined times, and solution concentration changes through the experiments were ascertained from analysis of the samples using HPLC.

The type of analysis which can be applied to results from the pilot-scale batch stirred-tank multi-component amino acid adsorption experiments is illustrated with reference to data for the adsorption of the three-component mixture asparagine, glutamine and serine, each with an initial concentration of 0.6 g/l, by Duolite A-162. The pH of the amino acid solution was not measured in the experiment but was estimated to be between pH 5 and 6. A complimentary code to TANSIMA known as TANFITA was used in the analysis. TANFITA has the ability to fit to multi-component data to derive physical parameters when either there is no competition

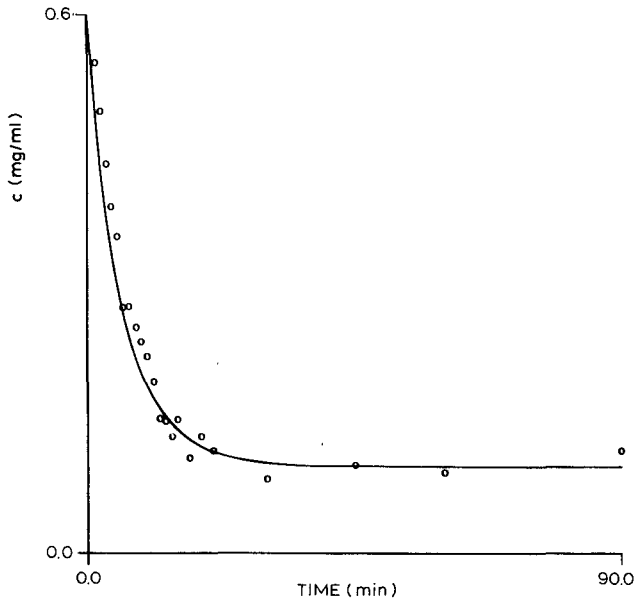

Fig. 2. TANFITK analysis of kinetic results for the adsorption of glutamine by Duolite A-162. O = Observed c; ——— = calculated c.

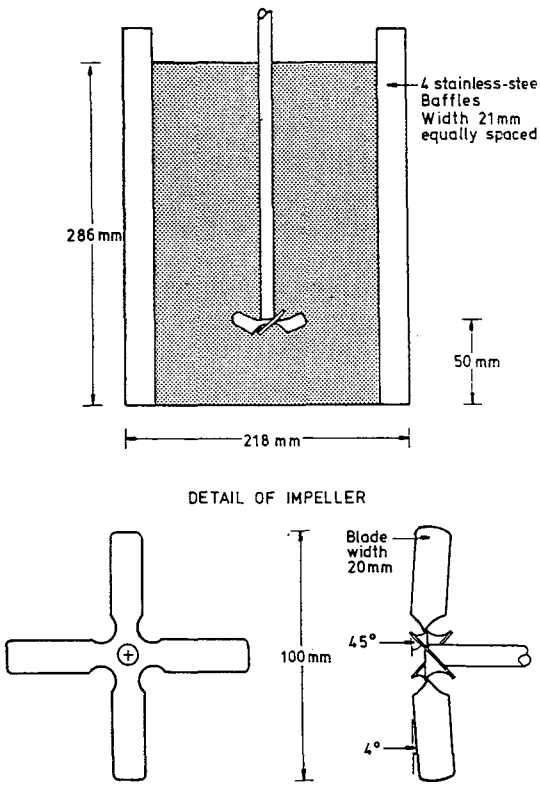

Fig. 3. Detail of pilot-scale stirred-tank adsorption unit.

between components for adsorption sites on the adsorbent, or when there is competition between components for adsorption sites on the adsorbent.

Initially, the TANFITA code was used to try to derive values of the maximum capacity Q_m, and the forward and backward rate constants K_1 and K_2 from

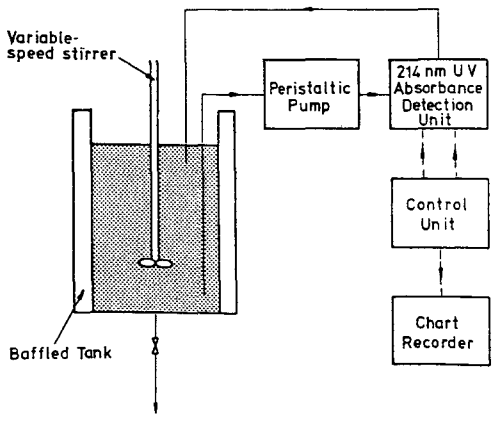

Fig. 4. Pilot-scale batch adsorption rig instrumentation.

mono-component equilibrium and kinetic results for serine, asparagine and glutamine and from the multi-component pilot-scale experiment for the simultaneous adsorption of serine, asparagine and glutamine assuming no competition between the components for adsorption sites. No fits could be obtained for the physical parameters. The exercise was repeated but with the assumption that in the multi-component experiment there was competition between components for adsorption sites. In this case well determined values of the physical parameters were derived. These values of Q_m, K_1 and K_2 were then used with the TANSIMA code to simulate the three-component adsorption of serine, asparagine and glutamine by Duolite A-162. Fig. 5 presents a compari-

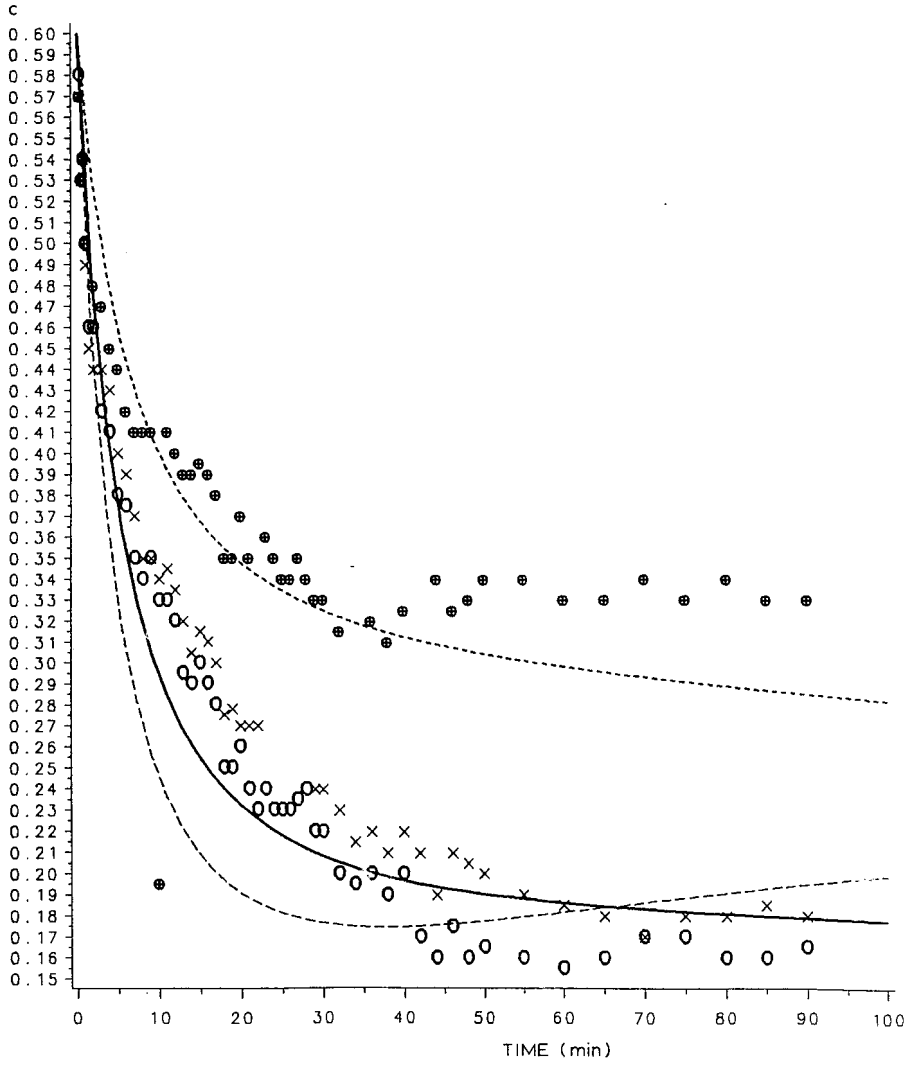

Fig. 5. TANSIMA simulation of the adsorption of serine, asparagine and glutamine by Duolite A-162. Asparagine: O = experimental, ——— = predicted; glutamine: ⊕ = experimental; ---- = predicted; serine: × = experimental; --- = predicted. c in mg/ml.

son between the experimental data and the predicted adsorption characteristics. It is seen from Fig. 5 that the change in concentration of asparagine is well predicted through the experiment. The rate of fall in the concentrations of serine and glutamine are also well predicted over the initial stage of the adsorption process. Subsequently, the model overpredicts the uptake of glutamine and underpredicts the uptake of serine, indicating that in this case the model may require a further degree of refinement.

Packed-bed column examples

The programme of experimental work for code validation is being extended to studies of multi-component amino acid adsorption by Duolite A-162 in packed-bed columns. An example of the use of the modelling codes to support this work has been the use of the COLOSIMA code to predict the adsorption of the binary component mixture tryptophan and aspartic acid by Duolite A-162 in a small-scale packed-bed column. In this exercise the values of the maximum capacity of the adsorbent Q_m, and the dissociation constant K_d were obtained from mono-component isotherm experiments, and the forward and backward rate constants K_1 and K_2 for each component were derived from binary component small-scale batch stirred-cell adsorption experiments. Using this data Fig. 6 shows a prediction from the COLOSIMA code for

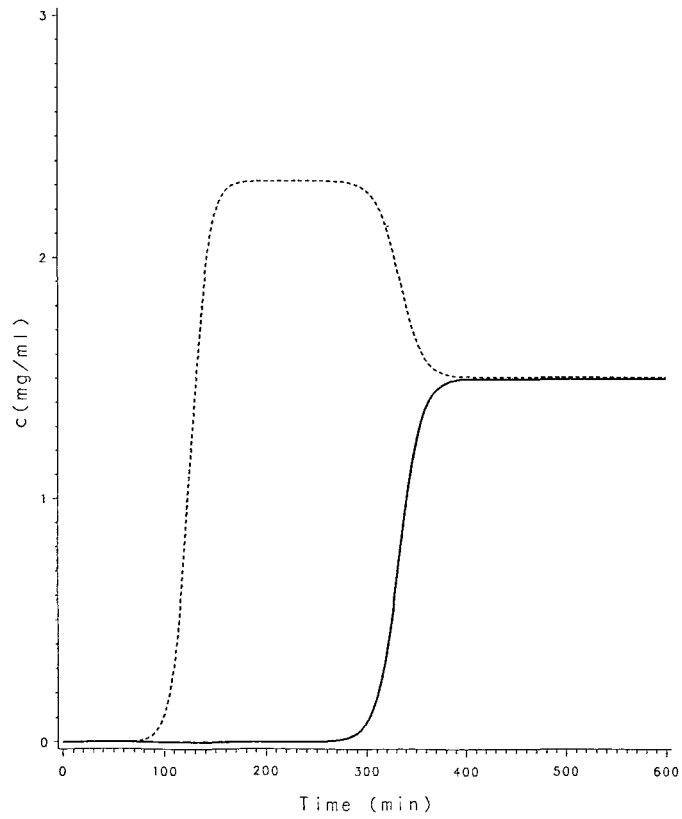

Fig. 6. COLOSIMA simulation of the adsorption of tryptophan (- - - -) and aspartic acid (———) by Duolite A-162.

the adsorption of tryptophan and aspartic acid by Duolite A-162 in a small-scale column operating in frontal analysis mode. It was assumed that both the tryptophan and aspartic acid were fed to the column in solution each at a concentration of 1.5 mg/ml. The predicted breakthrough curves shown in Fig. 6 are typical of competitive adsorption. Fig. 6 indicates that tryptophan will be displaced from the adsorbent by the aspartic acid such that after about 120 min the concentration of tryptophan at outlet becomes greater than at inlet to the column. The tryptophan concentration at column outlet is predicted to reach a maximum and ultimately becomes equal to the inlet concentration when the amount of tryptophan on the column has fallen from its maximum level to its equilibrium level. At this stage the breakthrough curve for aspartic acid is completed and the concentration of aspartic acid at the column outlet becomes equal to the inlet concentration to the column.

To obtain experimental results to compare with predictions from the COLO-SIMP code both small- and pilot-scale packed-bed column experiments have been completed for the loading, washing and elution of aspartic acid onto and from Duolite A-162. The small-scale packed-bed column apparatus is shown diagrammatically in Fig. 7. Aspartic acid solution was pumped downwards through the column which is 1.6 cm in diameter with a packed-bed height of 12.7 cm. The outlet concentration of aspartic acid from the column was monitored on-line by using a UV flow cell, but small samples were also taken from the outlet stream for off-line analysis. This is necessary since care is required with on-line UV measurements at 214 nm to check that correct concentrations are being measured and that there is no interfering absorption from

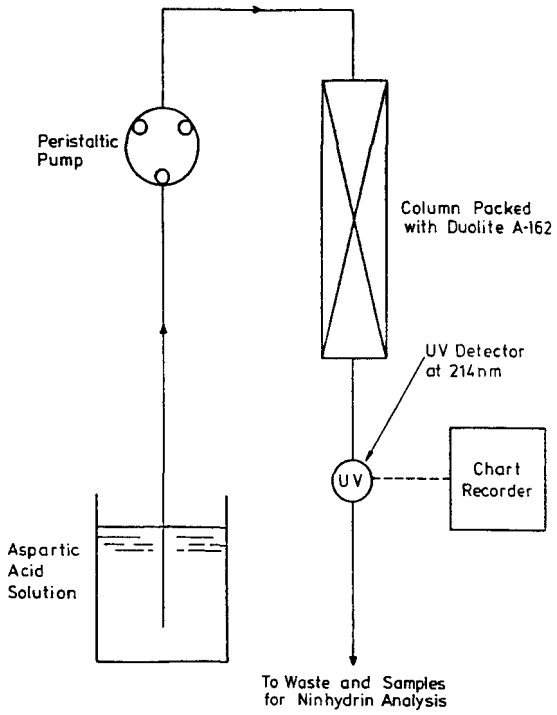

Fig. 7. Diagram of small-scale packed-bed column apparatus.

hydroxyl ions at low aspartic acid concentrations. The flowsheet for the pilot-scale packed-bed column rig is given in Fig. 8. The pilot-scale column was constructed of perspex with a column diameter of 8.8 cm and a packed-bed height of 11.5 cm. The column was normally operated in the downflow mode. As can be seen from Fig. 8 liquid was pumped in sequence from each of the holding tanks to the column to allow regeneration, loading, washing and elution to proceed in turn. The column outlet has a liquid sampling port which is used as a take-off point for liquid to be analysed by an on-line UV absorption detector or to allow samples to be taken for off-line analysis, for example, by HPLC.

Examples are presented in Figs. 9 and 10 of predictions from the COLOSIMP code with experimental data from the small- and pilot-scale columns respectively for both columns operating under similar conditions. In using the COLOSIMP code an estimate of the liquid film mass transfer coefficient was obtained from a correlation given by Wilson and Geankoplis[49] as

$$Sh = \frac{1.09}{\varepsilon_e} Re^{1/3} Sc^{1/3} \text{ for } 0.0015 < Re < 55 \tag{11}$$

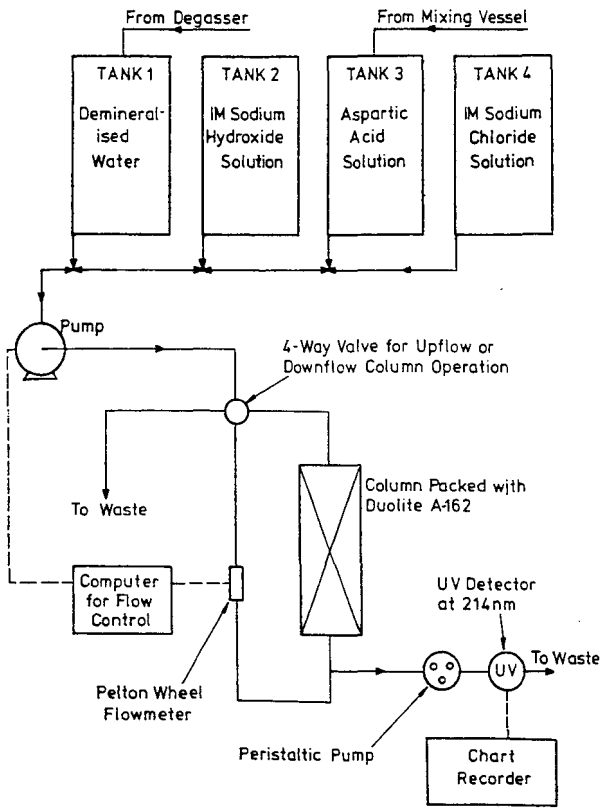

Fig. 8. Diagram of the BIOSEP mass transfer rig.

where Sh is the Sherwood number ($k_f d_p/D_L$), Re the Reynolds number based on the mean particle diameter in the packed bed, Sc the Schmidt number, ε_e the interstitial porosity, d_p the mean particle diameter, and D_L the diffusivity of solute in bulk solution.

An estimate of the diffusivity for aspartic acid in bulk liquid was obtained from an empirical correlation given as

$$D_L = \frac{7.7 \cdot 10^{-16} T}{\mu (V^{1/3} - V_0^{1/3})} \tag{12}$$

where V, the molar volume of aspartic acid, was determined from Kopp's law of additive volumes (Coulson and Richardson[50]), $V_0 = 0.008$ for diffusion in dilute water solutions, T is the absolute temperature of the liquid and μ is the liquid viscosity. The values of the maximum capacity of the adsorbent Q_m and the dissociation constant K_d for use with COLOSIMP for the loading and washing stages were obtained from LANGFIT analysis of equilibrium data for the adsorption of aspartic acid by Duolite A-162, taking into account the 5 and 95% confidence limits. For the elution stage K_d was set to the relatively high finite value of 30 mg/ml as $K_1 \to 0$ for 1 M sodium chloride as eluent.

The mass of resin per unit volume of packed bed was higher in the pilot-scale column than in the small-scale column probably caused by different wall and particle packing effects. The difference was compensated for in the computer analysis by specifying different interstitial porosity values. The value of the interstitial porosity was taken as 0.36 for the small-column experiment and 0.3 for the pilot-scale column experiment.

Consideration of Figs. 9 and 10 indicates (for the cases given) reasonable agreement between the small- and pilot-scale experimental data. Simulations were achieved by using COLOSIMP taking a value of k_f computed from eqn. 11 and varying the effective pore diffusivity, D_e, until a good fit was obtained to the experimental results. It is seen from Figs. 9 and 10, that by using COLOSIMP with values of $k_f = 0.116$ cm/min, and $D_e = 5 \cdot 10^{-4}$ cm^2/min for both the small- and pilot-scale columns acceptable prediction of the breakthrough and washing curves are obtained for both columns. Prediction of the elution stage with K_d taken equal to 30 mg/ml is more approximate. The computation time for examples of the type given in Figs. 9 and 10 was 2.5 h on a COMPAQ 386 microcomputer, for calculations with 20 computational cells along the column and 10 particle segments.

The fixed-bed codes may also be used to simulate the separation of components for isocratic elution chromatography conditions, and to determine the effect of changing different operational parameters. An example to illustrate the use of the COLOSIMK code to simulate the separation of a two-component mixture is shown in Fig. 11. A further example is given in Fig. 12 of the use of the COLOSIMA code to determine the effect of packed-bed length on the resolution of two components in elution chromatography. From Fig. 12 it is seen that as the bed length is increased it is predicted that the resolution of the two components will be increased. However, although resolution is improved, the peaks are broader (and hence the eluted material is more dilute) in the simulations with longer beds.

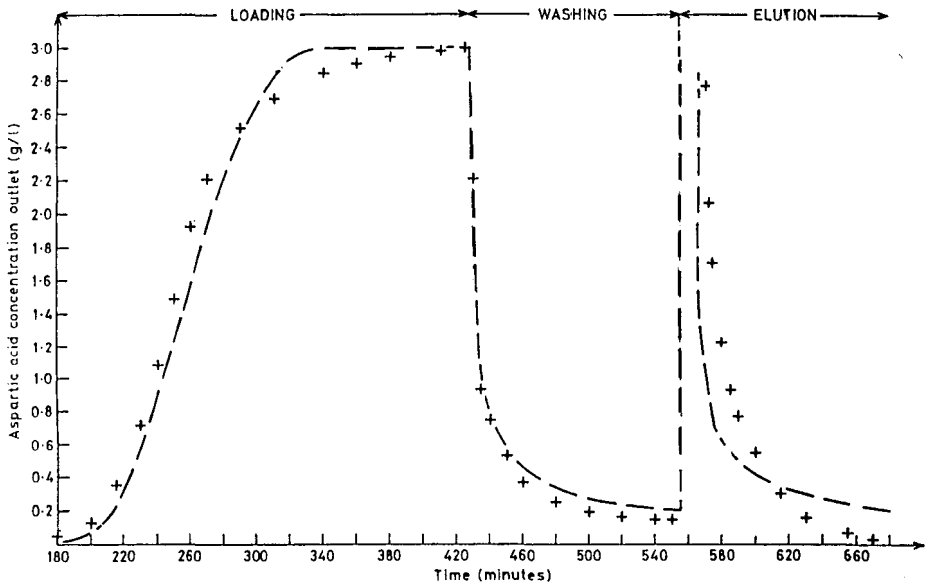

Fig. 9. COLOSIMP simulation of the loading, washing and elution in a small-scale packed-bed column for the aspartic acid–Duolite A-162 system. Column type, small-scale Pharmacia, packed-bed height 12.5 cm, column diameter 1.6 cm; superficial velocity, 1.79 cm/min; bead size range, 710–850 μm. COLOSIMP parameters: Q_m = 270 mg/g, k_f = 0.116 cm/min, $D_e = 5 \cdot 10^{-4}$ cm^2/min, K_d = 0.01 mg/ml, interstitial porosity = 0.36, intraparticle porosity = 0.45.

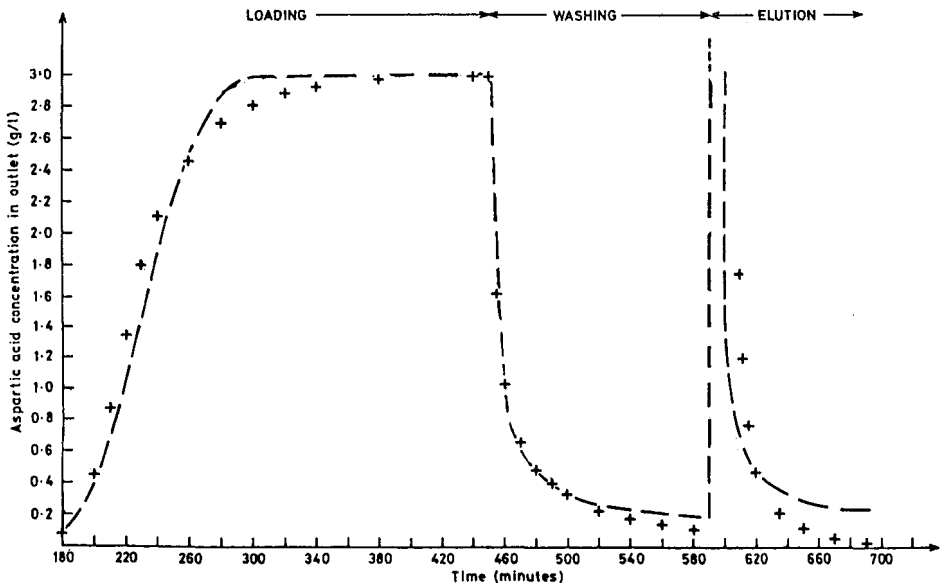

Fig. 10. COLOSIMP simulation of the loading, washing and elution in a pilot-scale packed-bed column for the aspartic acid–Duolite A-162 system. Column type, pilot-scale Perspex, packed-bed height 11.5 cm, column diameter 8.8 cm; superficial velocity, 1.79 cm/min; bead size range, 710–850 μm. COLOSIMP parameters: Q_m = 245 mg/g, k_f = 0.116 cm/min, $D_e = 5 \cdot 10^{-4}$ cm^2/min, K_d = 0.01 mg/ml, interstitial porosity = 0.30, intraparticle porosity = 0.45.

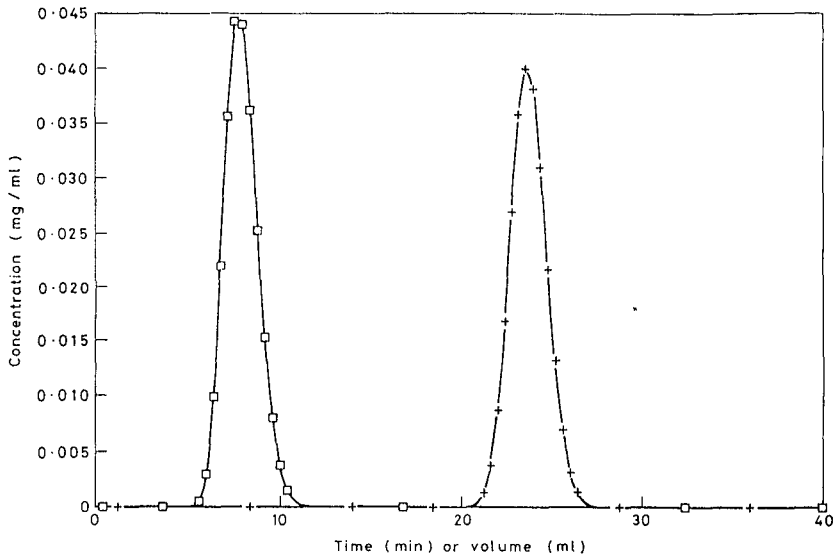

Fig. 11. Separation of components 1 (□) and 2 (+) by elution chromatography.

APPLICATION OF THE CODES

The simulation codes can be used to assist design. In design the requirements of the separation process are specified and it is desired to determine the adsorption equipment options which will meet the process specification. Ideally a design code

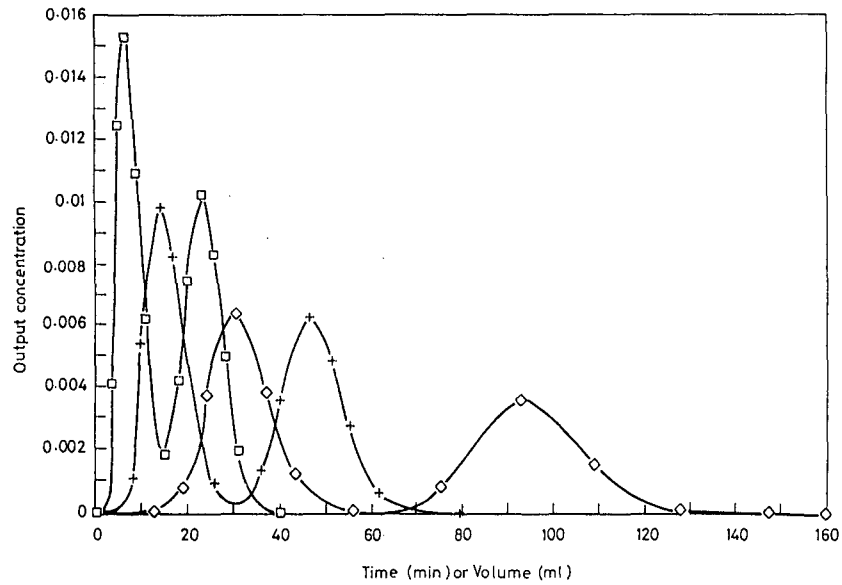

Fig. 12. Effect of column bed length on resolution of two components, column bed length 5 (□), 10 (+) or 20 (◇) cm.

would allow the major options to be computed, and with the incorporation of simple cost formulae would allow the alternative designs to be evaluated on a relative cost basis. Thus, design is concerned with evaluating the geometry of the contacting equipment for given operating conditions. To assist with design, the initial conditions for a separation would be specified to the appropriate simulation codes together with possible stirred-tank or packed-bed geometries for the process, and the codes would be used to predict the performance of the equipment to allow the evaluation of possible designs.

The simulation codes may also be used to assist with process optimisation. In process optimisation it is assumed that the scale and geometry of the batch stirred-tank or packed-bed column adsorption equipment is fixed, and it is necessary to consider the effect of changing operating variables on performance. Such variables may include the initial feed concentration or composition in a batch stirred tank or volumetric flow-rate in a packed-bed column, the physical characteristics of the solution and the operating protocol. Optimisation is necessary to ensure that the plant is running at its most effective, which usually means highest productivity or yield at acceptable purity. Increasing productivity means increasing the amount of material which is processed per unit time, which can be achieved by reducing the overall process time or by increasing the amount of material for a set process time. For optimisation purposes the conditions for the separation would be specified to the simulation code together with the adsorption plant geometry, for example, packed-bed height, column diameter. The simulation code would then be used to predict systematically the performance of the plant for different operating conditions, to allow the optimum conditions to be evaluated.

CONCLUSION

A suite of computer programs has been developed for application to adsorption and chromatographic processes. The programs are of two types, those for simulation of adsorption, washing and elution in batch stirred-tanks and packed-bed columns and to simulate elution chromatography in packed-bed columns, and those which may be used for the derivation of physical parameters relevant to equilibrium or kinetics in terms of adsorbent maximum capacity, dissociation constant, forward and backward rate constants, liquid film mass transfer coefficients and effective pore diffusion coefficients. The programs provide aids to the design and optimisation of adsorption processes.

ACKNOWLEDGEMENTS

The contributions of Dr. H. A. Chase and Miss B. J. Horstmann of the Department of Chemical Engineering, University of Cambridge, Mrs. A. Malleson of Tessella and Mr. A. Rodway, Mr. A. Reading and Miss H. M. Kellett of the Harwell Laboratory, to the work outlined in this paper, are acknowledged. Acknowledgement is also made to BIOSEP, Harwell Laboratory, Harwell, Oxfordshire OX11 0RA, U.K., for permission to publish the work presented in this paper.

REFERENCES

1 G. H. Cowan, I. S. Gosling, J. F. Laws and W. P. Sweetenham, *J. Chromatogr.*, 363 (1986) 37.
2 G. H. Cowan, I. S. Gosling and W. P. Sweetenham, in M. S. Verrall and M. J. Hudson (Editors), *Separations for Biotechnology*, Ellis Horwood, Chichester, 1987, p. 152.
3 J. Jacobsen, J. Frenz and Cs. Horváth, *J. Chromatogr.*, 316 (1984) 53.
4 N. F. Kirby, N. K. H. Slater, K. H. Weisenberger, F. Addo-Yobo and D. Doula, *Chem. Eng. Sci.*, 41 (1986) 2005.
5 W. J. Weber and C. K. Wang, *Environ. Sci. Technol.*, 21 (1987) 1096.
6 P. E. Price, Jr. and R. P. Danner, *AIChE J.*, 33 (1987) 551.
7 C. Vidal-Madjar, A. Jaulmes, M. Racine and B. Sébille, *J. Chromatogr.*, 458 (1988) 13.
8 B. H. Arve and A. I. Liapis, *AIChE J.*, 33 (1987) 179.
9 S. C. Nigam and H. Y. Wang, in J. A. Asenjo and J. Hong (Editors), *Separation, Recovery and Purification in Biotechnology*, American Chemical Society, Washington, DC, 1986, p. 153.
10 L. F. McConvey, *Chem. Eng. Res. Des.*, 65 (1987) 231.
11 A. R. Mansour, A. B. Shahalam and M. A. Sotari, *Sep. Sci. Technol.*, 20 (1985) 1.
12 W. Fritz and E. V. Schlunder, *Chem. Eng. Sci.*, 29 (1974) 1279.
13 M. W. Balzli, *Ph.D. Thesis*, Eidgenossiche Technische Hochschule, Zürich, 1977.
14 A. R. Mansour, A. B. Shahalam and N. Darwish, *Sep. Sci. Technol.*, 19 (1984–85) 1087.
15 C. Costa and A. E. Rodrigues, in A. E. Rodrigues, M. D. LeVan and D. Tondeur (Editors), *Adsorption: Science and Technology* (*NATO ASI Series E: Applied Sciences*, Vol. 158), Kluwer, Dordrecht, 1989, p. 257.
16 A. E. Rodrigues, M. D. LeVan and D. Tondeur (Editors), *Adsorption: Science and Technology* (*NATO ASI Series E: Applied Sciences*, Vol. 158), Kluwer, Dordrecht, 1989.
17 B. F. Brian, I. Zwiebel and R. S. Artigue, *AIChE Symp. Ser.*, 83 (259) (1988) 80.
18 W. J. Weber, Jr. and E. H. Smith, *Environ. Sci. Technol.*, 21 (1987) 1040.
19 E. E. Graham, A. Pucciani and N. G. Pinto, *Biotechnol. Prog.*, 3 (1987) 141.
20 J. C. Janson and P. Hedman, *Biotechnol. Prog.*, 3 (1987) 9.
21 H. Moon and W. K. Lee, *Chem. Eng. Sci.*, 41 (1986) 1995.
22 G. Carta, M. S. Saunders, J. P. DeCarli and J. B. Vierow, *AIChE Symp. Ser.*, 84 (264) (1988) 54.
23 C. B. Ching and D. M. Ruthven, *Chem. Eng. J.*, 40 (1989) B1.
24 G. McKay and M. J. Bino, *J. Chem. Technol. Biotechnol.*, 37 (1987) 81.
25 W. Kopaciewicz, S. Fulton and S. Y. Lee, *J. Chromatogr.*, 409 (1987) 111.
26 H. Moon and C. Tien, *AIChE Symp. Ser.*, 84 (264) (1988) 23.
27 W. B. Bolden and F. R. Groves, Jr., *AIChE Symp. Ser.*, 84 (264) (1988) 62.
28 C. B. Ching, C. Ho, K. Hidajat and D. M. Ruthven, *Chem. Eng. Sci.*, 42 (1987) 2547.
29 G. Guiochon and S. Ghodbane, *J. Phys. Chem.*, 92 (1988) 3682.
30 J. L. Wade, A. F. Bergold and P. W. Carr, *Anal. Chem.*, 59 (1987) 1286.
31 J. H. Knox and H. M. Pyper, *J. Chromatogr.*, 363 (1986) 1.
32 B. F. D. Ghrist, B. S. Cooperman and L. R. Snyder, *J. Chromatogr.*, 459 (1988) 1.
33 B. F. D. Ghrist and L. R. Snyder, *J. Chromatogr.*, 459 (1988) 25.
34 B. F. D. Ghrist and L. R. Snyder, *J. Chromatogr.*, 459 (1988) 43.
35 L. R. Snyder, G. B. Cox and P. E. Antle, *J. Chromatogr.*, 444 (1988) 303.
36 G. B. Cox, P. E. Antle and L. R. Snyder, *J. Chromatogr.*, 444 (1988) 325.
37 R. S. Hodges, J. M. R. Parker, C. T. Mant and R. R. Sharma, *J. Chromatogr.*, 458 (1988) 147.
38 H. A. Chase, *J. Chromatogr.*, 297 (1984) 179.
39 H. C. Thomas, *J. Am. Chem. Soc.*, 66 (1944) 1644.
40 H. C. Thomas, *Ann. N.Y. Acad. Sci.*, 49 (1948) 161.
41 H. A. Chase, personal communication, 1986.
42 A. R. Curtis and W. P. Sweetenham, *FACSIMILE Release H User's Manual, AERE-R11771*, Harwell Laboratory, Harwell, 1985.
43 W. P. Sweetenham, personal communication, 1986.
44 G. H. Cowan, in A. E. Rodrigues, M. D. LeVan and D. Tondeur (Editors), *Adsorption: Science and Technology* (*NATO ASI Series E: Applied Sciences*, Vol. 158), Kluwer, Dordrecht, 1989, p. 517.
45 B. J. Horstmann and H. A. Chase, presented at the *SCI Meeting on Separations for Biotechnology, Reading, 1987.*
46 B. J. Horstmann and H. A. Chase, *Chem. Eng. Res. Des.*, 67 (1989) 243.
47 S. L. Fowell and H. A. Chase, *J. Biotechnol.*, 4 (1986) 1.
48 B. J. Horstmann, C. W. Kenney and H. A. Chase, *J. Chromatogr.*, 361 (1986) 179.
49 E. J. Wilson and C. J. Geankoplis, *Ind. Eng. Chem. Fundam.*, 5 (1966) 9.
50 J. M. Coulson and J. F. Richardson (Editors), *Chemical Engineering*, Vol. 1, 3rd ed., 1977, p. 278.

Journal of Chromatography, 484 (1989) 211–223
Elsevier Science Publishers B.V., Amsterdam — Printed in The Netherlands

CHROM. 21 959

SCALE-UP AND OPTIMIZATION IN PRODUCTION LIQUID CHROMATOGRAPHY

A. M. WILHELM and J. P. RIBA*
U.R.A. CNRS 192, ENSIGC, Chemin de la Loge, 31078 Toulouse (France)

SUMMARY

A strategy is presented for the scale-up and optimization of a separation in liquid chromatography. It requires first a complete representation of the system (a mathematical model), but also an experimental evaluation of its parameters. The model presented takes into account the axial dispersion in the mobile phase and both internal and external resistances to mass transfer in the stationary phase. Small-scale and pilot-plant experiments that yield the equilibrium isotherms, the kinetics of mass transfer and the flow-pattern of the mobile phase are described. These techniques are illustrated with the example of the separation of sugars with an ion-exchange resin.

With the aid of the mathematical model, it becomes possible to approach the optimization of the process. The cost of the separation was found to be a good criterion for production chromatography. The aim of the optimization program was to provide a series of geometric and operating variables minimizing the criterion, taking into account the process purposes: production rate, purity and the characteristics of the apparatus.

INTRODUCTION

This paper describes the modelling and optimization of the separation of the sugars D-xylose and D-mannose using an ion-exchange resin in the lead form with water as eluent. The aim is to show through this example a technique for scaling-up, *i.e.*, how to predict the size and operating variables of a production apparatus from the results of small-scale[1] experiments. This requires a mathematical model of the chromatographic separation, then the experimental determination of the predominant phenomena with the evaluation of their characteristic parameters and finally the definition of the purposes and constraints of the separation in order to find the optimum design parameters.

MATHEMATICAL MODEL

A gas or liquid chromatographic column is usually treated as a packed bed of porous spheres submitted to a pulse of solute[2–7]. The transient mass balance will take into account the following phenomena: dispersed plug flow in the mobile phase;

0021-9673/89/$03.50

external resistance to mass transfer around the particles; internal diffusion inside the particles; and adsorption on the solid[3] or exchange and diffusion in another phase[8] (*e.g.*, a liquid grafted on the solid). The basic equations are as follows:

For the mobile phase:

$$\frac{\partial C}{\partial t} = D \cdot \frac{\partial^2 C}{\partial z^2} - u \cdot \frac{\partial C}{\partial z} - 3 \cdot \frac{1-\varepsilon}{\varepsilon R} \cdot \alpha D_i \left(\frac{\partial q}{\partial r}\right)_{r=R} \tag{1}$$

accumulation dispersion convection transfer to stationary phase

The column inlet and outlet conditions are described by Danckwerts'[9] equations for a "closed–closed" system.

For the stationary phase:

$$\frac{\partial q}{\partial t} = D_i \left(\frac{\partial^2 q}{\partial r^2} + \frac{2}{r} \cdot \frac{\partial q}{\partial r}\right) \tag{2}$$

accumulation internal diffusion

with the boundary conditions

$$D_i \left(\frac{\partial q}{\partial r}\right)_{r=R} = k_L (C - C^*) \tag{3}$$

diffusion external mass transfer

and

$$\left(\frac{\partial q}{\partial r}\right)_{r=0} = 0 \tag{4}$$

If other interactions are added, eqn. 2 becomes more complex and the number of parameters greater.

In eqns. 1 and 2, dimensionless parameters can be introduced:

Peclet number:

$$Pe = uL/D$$

Number of transfer units:

$$NUT = k_L \, 3(1-\varepsilon)\alpha\tau/\varepsilon R$$

Time ratio:

$$R_t = D_i\tau/R^2$$

These parameters represent dispersion in the liquid, external mass transfer and diffusion in the particles, respectively.

If the equilibrium isotherm linking the concentrations C^* (in the liquid) and q (in the particles) is linear:

$$q = kC^* \tag{5}$$

and

$$k' = k\alpha(1 - \varepsilon)/\varepsilon$$

This condition is often satisfied in the case of the separation of sugars on ion-exchange resins[10,11].

Eqns. 1 and 2 can then be integrated by means of the Laplace transform. The Laplace transform of the exit concentration is:

$$\bar{C}_s = \bar{C}_e Pe \cdot \frac{V - W}{V^2 \exp(-W) - W^2 \exp(-V)}$$

$$V = \frac{Pe}{2}\left\{1 + \sqrt{1 + \frac{4}{Pe}[s - G(s)]}\right\}$$

$$W = Pe - V \tag{6}$$

where the function $G(s)$ represents the phenomena occurring in the stationary phase:

$$G(s) = \frac{-F(s)}{1 + \frac{F(s)}{NUT}}; \quad F(s) = 3R_t\left(\sqrt{\frac{s}{R_t}}\coth\sqrt{\frac{s}{R_t}} - 1\right) \tag{7}$$

By derivation of the Laplace transform, $\bar{C}_s$, it is also possible to calculate the first two moments of the exit curve:

$$m_1 = \tau(1 + k') \tag{8}$$

$$m_2 = \tau^2\left[\frac{2}{Pe}(1 + k')^2 + \frac{2}{NUT} \cdot k'^2 + \frac{2}{15} \cdot \frac{k'}{R_t}\right] \tag{9}$$

It can be seen from eqn. 9 that the width of a peak (related to m_2) depends on three factors, flow pattern and external and internal mass transfer, and that these phenomena act independently and in a similar manner. Hence it is impossible to identify simultaneously, from a concentration peak, the parameters corresponding to these phenomena.

As the separation mechanism of our system is based on the difference between the strengths of sugar–ion complexes[12,13], adsorption can be neglected. In order to reduce the number of parameters in our model, we tried to determine with small-scale experiments which phenomenon is predominant.

EXPERIMENTAL

Materials

The separation of D-xylose and D-mannose[14] was achieved on an ion-exchange resin Duolite C-204/2078 (Rohm & Haas). The resin had a cross-linkage of 6.4% of divinylbenzene and was in the lead form; the particle diameters ranged between 0.15 and 0.30 mm. A temperature of 50°C was chosen. The sugar concentrations in the feed ranged between 100 and 500 kg/m^3.

Equilibrium isotherms

Equilibrium isotherms were plotted by contacting 90 cm^3 of sugar solutions of different concentrations C_0 with 10 cm^3 of wet resin in a well stirred reactor at constant temperature. Samples of sugar solution were withdrawn and the concentration C_{eq} was evaluated by refractometry when equilibrium had been reached. The concentration q_{eq} inside the resin was deduced from a mass balance on sugar. The isotherm at 50°C was plotted (Fig. 1). For both sugars, the isotherms are linear in the working range with values of the slopes of $k_{xylose} = 0.33$ and $k_{mannose} = 0.42$. This linearity was a necessary condition for a simple integration of the differential eqns. 1 and 2.

Internal diffusion

The kinetics of internal diffusion were studied in a stirred reactor, where dispersion and external mass transfer could be neglected. The experimental apparatus and conditions were the same as above, but the time dependence of the sugar concentration in the liquid phase was studied.

For both sugars, equilibrium was reached by the first withdrawal (30 s); it was therefore impossible to evaluate the diffusion coefficient, D_i. However, we could conclude that the diffusion inside the particles was very fast and consequently that this phenomenon could be neglected, and that the concentration could be assumed to be uniform in a particle.

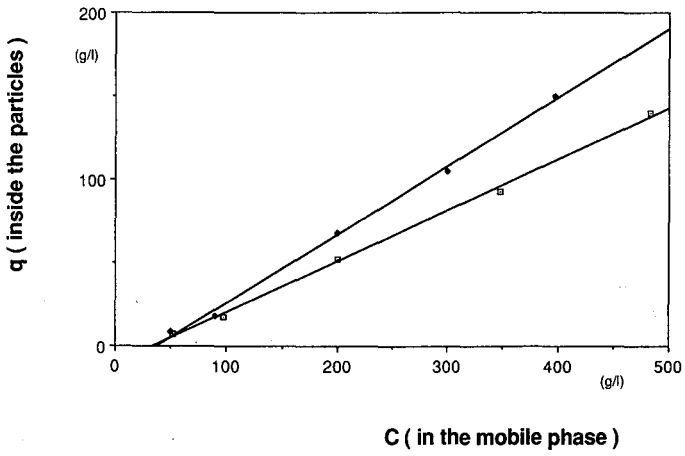

Fig. 1. Equilibrium isotherms of (□) D-xylose and (◆) D-mannose at 50°C.

External resistance to mass transfer

External resistance to mass transfer depends on the hydrodynamic conditions around the particles, so it has to be studied in a packed bed; we chose a thin bed where dispersion could be neglected. The reactor used is shown in Fig. 2; it was adapted from the differential reactor described by Ford *et al.*[15]. A thin packed bed (2.5 cm in diameter, 1.5 cm high) of particles was prepared between two stainless-steel grids. A section of glass beads (1 mm in diameter) placed at the reactor entrance allowed a good distribution of liquid over the whole section of the reactor. A peristaltic pump (Masterflex) ensured the recirculation of the liquid between the reactor and the reservoir. The flow-rates ranged between 0.6 and 7 cm^3/min in order to have the same velocities as in the column. The reactor and tubing were immersed in a constant-temperature water-bath.

The reservoir was initially charged with a sugar solution of concentration C_0 and samples of concentration C_L were withdrawn from the resevoir and analysed by refractometry.

If the bed of resin is thin enough, we may assume that the amount of sugar fixed in the reactor is very small and the concentration, C, in the reactor is uniform, and it is possible to derive an expression for C_L from the following mass balance:

in the reservoir:

$$V_R \cdot \frac{dC_L}{dt} = Q(C - C_L)$$

in the reactor:

$$V_L \cdot \frac{dC}{dt} = k_L A(C^* - C) = V_s \cdot \frac{dq}{dt} \tag{10}$$

$$C_L = \frac{C_0}{1+\beta} + \frac{\beta C_0}{1+\beta}\exp\left(-\frac{k_L A}{V_L} \cdot \frac{1+\beta}{\beta} \cdot t\right) \tag{11}$$

where $\beta = k(V_s/V_L)$ and $q = kC^*$.

The experimental concentration C_L/C_0 is plotted in Fig. 3 for D-xylose and the mass transfer coefficient k_L was obtained from eqn. 11. The values obtained for different conditions of flow-rate and initial concentration are given on Table I,

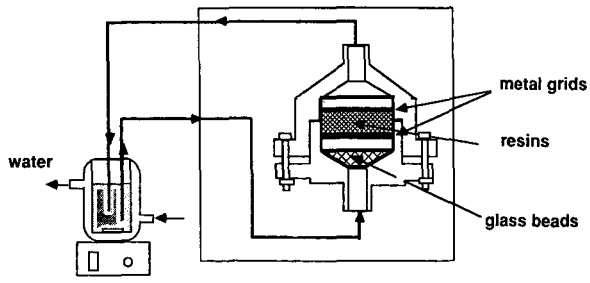

Fig. 2. Schematic diagram of differential reactor.

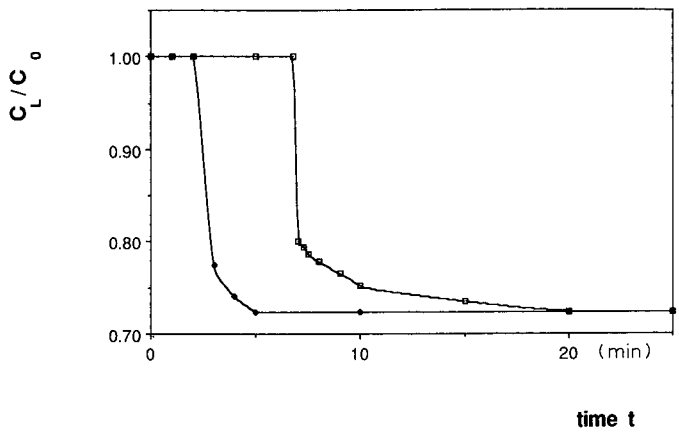

Fig. 3. Time dependence of xylose concentration in the reservoir of the recirculation system. Experimental conditions: C_0 = 10 g/l; T = 50°C. Flow-rate: □ = 1.6; ◆ = 7 ml/min.

together with the corresponding values calculated using the correlation of Dwivedi and Upadhyay[16]. It can be seen from Table I that our experimental k_L values are consistent with those calculated using the correlation and yield high values for *NUT*. The Peclet numbers that would produce the same contribution to m_2 range between 30 000 and 100 000; it seems improbable that our Peclet numbers reached such values. Consequently, dispersion in the mobile phase can be considered as the limiting step in the column.

Dispersion phenomenon

The column[14] was a glass tube (200 cm × 1.7 cm I.D.) packed by sedimentation of the resin particles. The temperature was kept constant (50°C) with water circulated through a jacket around the column. Deionized water, used as the eluent, was fed downwards by a peristaltic pump at a flow-rate of 0.6 cm^3/min. The sugar solution was applied at the top of the column; generally the sample volume was 1.5 cm^3, and the sugar concentration ranged between 100 and 500 kg/m^3. The sugar solutions were synthetic, prepared with D-xylose (Prolabo) and D-mannose (Sigma or Extrasynthese) in equal proportions.

TABLE I

EXPERIMENTAL VALUES OF k_L AND *NUT* OBTAINED WITH DIFFERENT INITIAL CONCENTRATIONS AND FLOW-RATES, COMPARED WITH k_L VALUES ISSUED FROM CORRELATIONS

Superficial velocity (cm/min)	*Initial concentration (g/l)*	*k_L (experimental) (10^{-3} cm/s)*		*k_L (correlation) (10^{-3} cm/s)*	*NUT*	$\frac{2k'}{NUT}$
		Xylose	*Mannose*			
0.35	10	5.2		4.2	20 000	$6 \cdot 10^{-5}$
	20	4.8	5.0			
1.54	10	7		5.8	5000	$2 \cdot 10^{-4}$
	20	8.1	8.7			

Fractions of 1–10 cm^3 were collected automatically at the exit of the column with a fraction collector (Gilson). Sugars were then assayed by refractometry (Milton-Roy) after a separation by high-performance liquid chromatography using a Milton-Roy system equipped with an Aminex HPX 87P column (Bio-Rad Labs.).

The void fraction of the packed bed was estimated as

$$\varepsilon = \frac{\text{volume of interstitial liquid}}{\text{volume of packed bed}}$$

The interstitial liquid was collected by opening the outlet and stopping the feed; ε was found to be 0.40.

The dispersion in the mobile phase may be assumed to be the unique source of peak broadening. It therefore becomes possible to obtain Pe and k' from the response curve of the column from the injection of one sugar.

If X is the dimensionless injection volume, the Laplace transform of the exit concentration is given by eqn. 6, where

$$G(s) = -k'_s; \qquad \bar{C}_e(s) = [1 - \exp(-Xs)]/Xs \tag{12}$$

The identification technique involves the following steps: calculation of the Fourier transform (using an FFT algorithm[17]) of the experimental concentration $C_{exp}(t)$; calculation by means of eqns. 6 and 12 of the theoretical response curve, $\bar{C}_{theo}(j2\pi f)$ as a function of Pe and k'; and minimization of a criterion of the form

$$E = \sum_{i=0}^{N-1} \left[\bar{C}_{theo}(j2\pi f_i) - \bar{C}_{exp}(j2\pi f_i) \right]^2 \tag{13}$$

by a Gauss–Newton method.

As can be seen from Fig. 4, we obtained good agreement between the experimental and theoretical curves, indicating that the model accurately describes the behaviour of the column. The magnitude of the Peclet numbers (less than 4000) (Table II) confirms the assumption that the term accounted for mass transfer in eqn. 9, is much smaller than the hydrodynamic term.

OPTIMIZATION

We shall consider here that the column is fed with the sugar solution during time intervals Δt separated by a period T.

The first step is then to determine the purposes of the separation, the requirements with respect to yield and purity, the technical limitations and the different variables of the system. A number of workers[18–21] chose to maximize the throughput P_o (amount of product isolated per unit time), but this criterion seems better suited to an occasional preparative separation (on an apparatus that already exists). We preferred an economical criterion[22] to evaluate the performances of a production set, and adopted the total separation cost per unit mass of product. Our constraints are the purity of the product, the throughput (P_o) and a technical limitation, the maximum pressure drop over the column.

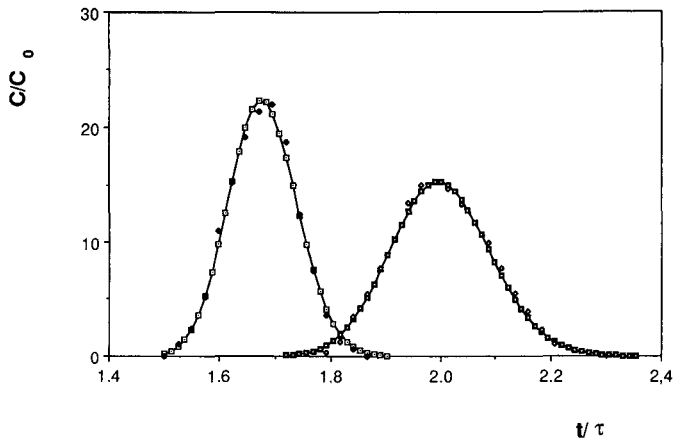

Fig. 4. Separation of xylose and mannose at 30°C (experimental and calculated elution curves). Experimental conditions: C_0 = 500 g/l (50:50 xylose–mannose); Q = 0.63 cm³/min; V_i = 1.5 cm³. □ = Xylose (theoretical); ◆ = xylose (experimental); ■ = mannose (theoretical); ◇ = mannose (experimental).

Derivation of optimization equations

Purity. We specified that the separation had to be complete between solutes A and B for one injection and for two following injections:

$$t_{2A} \leqslant t_{1B} \tag{14}$$

$$(t_{2B})_n \leqslant (t_{1A})_{n+1} \tag{15}$$

with[23]

$$t_{1i} = t_n + t_{Ri} - 2\sigma_i$$

$$t_{2i} = t_n + \Delta t + t_{Ri} + 3\sigma_i$$

TABLE II

Pe AND *k'* VALUES IDENTIFIED FROM EXPERIMENTS REALIZED WITH DIFFERENT SUGAR FEED CONCENTRATIONS AND DIFFERENT COLUMN TEMPERATURES

Temperature (°C)	*Injection concentration (g/l)*			*Injection concentration (g/l)*		
	100	*300*	*500*	*100*	*300*	*500*
30	Pe_X^a = 1430		Pe_X = 1442	k'_X = 0.66		k'_X = 0.66
	Pe_M = 1085		Pe_M = 955	k'_M = 0.96		k'_M = 0.98
50		Pe_X = 2684			k'_X = 0.65	
		Pe_M = 2310			k'_M = 0.95	
70	Pe_X = 4145		Pe_X = 2502	k'_X = 0.61		k'_X = 0.57
	Pe_M = 3634		Pe_M = 2108	k'_M = 0.77		k'_M = 0.76

[a] X = Xylose; M = mannose.

These conditions lead to the following equalities at the optimum:

$$\Delta t_{opt} = t_{RB} - t_{RA} - (2\sigma_B + 3\sigma_A) \tag{16}$$

$$T_{opt} = t_{RB} - t_{RA} + \Delta t_{opt} + (3\sigma_B + 2\sigma_A) \tag{17}$$

This condition with respect to purity may seem too drastic, and can be replaced by a maximum percentage superposition of the peaks.

Throughput: The throughput, P_o, can be expressed as

$$P_O = QC_0\Delta t/T = \varepsilon SuC_0\Delta t/T \tag{18}$$

Variables. Two types of variables are involved, geometric (S, L) and operating (u, T, Δt) variables. The particle diameter (d_p) cannot be considered as a continuous variable, and each value will be considered separately. The initial concentration C_0 will be the maximum concentration of the linear domain of the isotherms.

Criterion. The total separation cost involves[24] the costs of depreciation, operating labour, maintenance, utilities and packing renewals. For simplification, we consider here only the cost of the packing, G.

$$\text{crit} = G = SLg(d_p) \tag{19}$$

where g is the cost of packing per unit volume. Substituting eqns. 16, 17 and 18 into eqn. 19 yields

$$G = P_oTLg(d_p)/\varepsilon C_0u\Delta t \tag{20}$$

Without the constant term, it gives the following criterion:

$$\text{crit} = LT/u\Delta t \tag{21}$$

The optimization problem then consists in minimizing eqn. 21, together with eqns. 16 and 17, with respect to L and u, and with the constraint of maximum pressure drop:

$$\Delta P < \Delta P_{lim}$$

ΔP may be developed with the Blake–Kozeny equation[25]:

$$\Delta P = \eta Lu/K_0$$

The expressions for t_{Ri} and σ_i involved in eqns. 16 and 17 are given by eqns. 8 and 9, where Pe and NUT are written as functions of the variables u and L using the correlations of Chung and Wen[26] for Peclet numbers and Dwivedi and Upadhyay[16] for k_L.

Results

The first result is that the optimum conditions yield for ΔP the limit value, ΔP_{lim}, and that the optimum velocity is proportional to ΔP_{lim} (see Fig. 5). It can also be seen

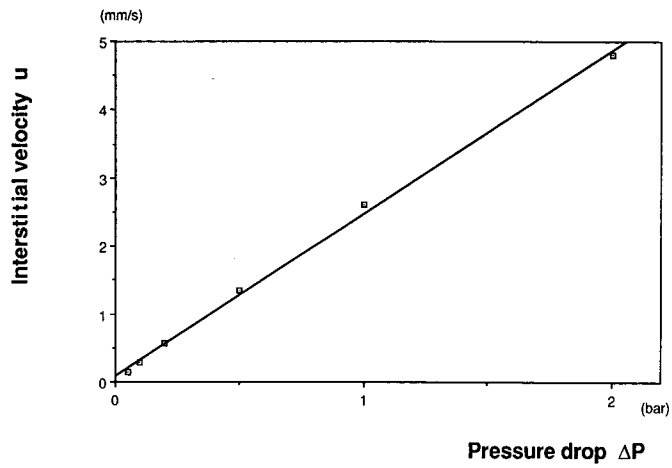

Fig. 5. Plot of interstitial velocity against pressure drop for optimum conditions.

from Fig. 6 that a higher ΔP_{lim} or a higher velocity will lead to a smaller criterion. It is then interesting to work with high liquid velocities.

From Fig. 7 it can be concluded that the column length does not vary greatly in this range of velocities; this is not the case for the column diameter, which is reduced by a higher velocity.

As can be seen in Table III, the values of the optimum variables (the values but not the trends) are very dependent of the value of the Peclet number, *i.e.*, the efficiency of the column. Hence it would be interesting to establish experimentally, on pilot plants, more precise correlations for Peclet numbers.

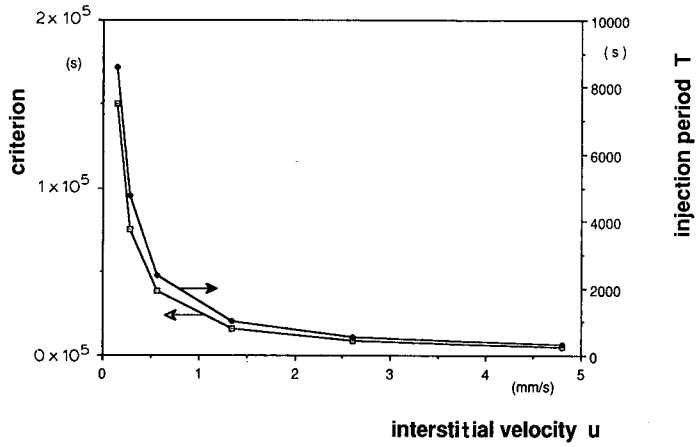

Fig. 6. Behaviour of the criterion and injection period with the velocity for optimum conditions.

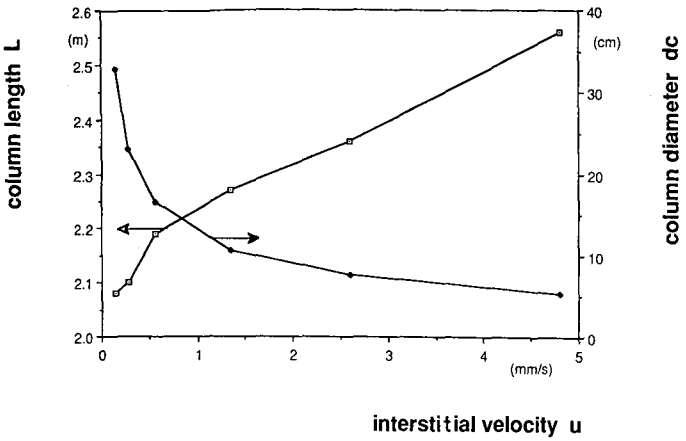

Fig. 7. Behaviour of column length and diameter with the velocity for optimum conditions.

TABLE III

INFLUENCE OF *Peg* NUMBER ON THE OPTIMIZATION RESULTS

Peg	*L (m)*	*u (mm/s)*	*Crit (s)*
0.11	2.56	4.8	4844
0.20	1.79	6.8	2260
0.40	1.37	8.9	1223

CONCLUSION

This work must be considered as a development of a strategy for scaling-up. It requires three steps: modelling of the column, experimental determination of the parameters and derivation of optimization equations. Each step has been simplified here, but the method is still valid for more complex systems. The model can be complicated if more phenomena are added (adsorption, etc.), but it will then require the corresponding experiments to evaluate the new parameters. The model may also be non-linear, and will then need a numerical integration. The optimization may also involve less restrictive conditions on purity, or a more detailed cost function. However, none of these factors will alter the principles of the method.

SYMBOLS

A Total area of particles in the reactor (m^2)
C solute concentration in the mobile phase (kg/m^3)
C^* concentration in the liquid in equilibrium with the solid phase
$\overline{C}(s)$ Laplace transform of $C(t)$
d_c column diameter (m)
d_p particle diameter (m)
D dispersion coefficient (m^2/s)

D_i internal diffusion coefficient (m^2/s)
f_i frequency (s^{-1})
g cost of packing (US$/$m^3$)
G separation cost (US$)
j complex number, $j^2 = -1$
k distribution coefficient
k_L mass transfer coefficient (cm/s)
k' capacity factor
K_0 permeability constant of the column
L column length (m)
ΔP pressure drop (Pa)
Pe Peclet number, uL/D
Peg Peclet number, udp/D
P_o throughput (kg/s)
Q flow-rate (cm^3/min)
q concentration inside the particles (kg/m^3)
r distance from the centre of the particle (m)
R particle radius (m)
s dimensionless Laplace variable
S column cross-section (m^2)
t time (s)
t_R retention time (s)
Δt injection time (s)
T injection period (s)
u interstitial velocity (m/s)
V volume (m^3)
X dimensionless injection volume
z distance in the column (m)

α internal particle porosity
ε external voidage of the packed-bed
τ ($= L/u$) mean residence time of the solute in the mobile phase
σ^2 variance (s^2)
η viscosity of the mobile phase

Subscripts
L in the liquid phase
R in the reservoir
S in the solid phase
0 at time zero
1 beginning of a peak
2 end of a peak
n nth period

REFERENCES

1 G. H. Cowan, I. S. Gosling, J. F. Laws and W. P. Sweetenham, *J. Chromatogr.*, 363 (1986) 37.
2 M. Kubin, *Collect. Czech. Chem. Commun.*, 30 (1965) 1104.
3 E. Kucera, *J. Chromatogr.*, 19 (1965) 237.
4 P. Schneider and J. M. Smith, *AIChE J.*, 14 (1968) 762.
5 M. Suzuki and J. M. Smith, *Chem. Eng. Sci.*, 26 (1971) 221.
6 P. A. Ramachandran and J. M. Smith, *Ind. Eng. Chem., Fundam.*, 17 (1978) 148.
7 R. V. Mehta, R. L. Merson and B. J. McCoy, *AIChE J.*, 19 (1973) 1068.
8 M. A. Alkharasani and B. J. McCoy, *Chem. Eng. J.*, 23 (1982) 81.
9 P. V. Danckwerts, *Chem. Eng. Sci.*, 2 (1953) 1.
10 Y. S. Ghim and H. N. Chang, *Ind. Eng. Chem., Fundam.*, 21 (1982) 369.
11 T. Sakiyama, K. Nakamura and T. Yano, *Agric. Biol. Chem.*, 49 (1985) 2619.
12 S. J. Angyal, G. S. Bethell and R. J. Beveridge, *Carbohydr. Res.*, 73 (1979) 9.
13 R. W. Goulding, *J. Chromatogr.*, 103 (1975) 229.
14 T. Carillon, *Thèse de Docteur-ingénieur*, Toulouse, 1987.
15 J. R. Ford, A. H. Lambert, W. Cohen and R. P. Chambers, *Biotechnol. Bioeng. Symp.*, 3 (1972) 267.
16 P. N. Dwivedi and S. N. Upadhyay, *Ind. Eng. Chem., Process Des. Dev.*, 16 (1977) 157.
17 P. W. Murill, R. W. Pike and C. L. Smith, *Chem. Eng.*, 76 (1969) 125.
18 A. W. J. De Jong, H. Poppe and J. C. Kraak, *J. Chromatogr.*, 148 (1978) 127.
19 J. R. Conder and M. K. Shingari, *J. Chromatogr. Sci.*, 11 (1973) 525.
20 G. Cretier and J. L. Rocca, *Chromatographia*, 16 (1982) 32.
21 K. P. Hupe and H. H. Lauer, *J. Chromatogr.*, 203 (1981) 41.
22 J. R. Conder, *Chromatographia*, 8 (1975) 60.
23 P. Gareil, *Thèse Doctorat ès Sciences*, Université Paris VI, Paris, 1981.
24 Abcor Inc., *Chem. Eng.*, February 12th (1968) 80.
25 R. B. Bird, W. E. Stewart and E. N. Lightfoot, *Transport Phenomena*, Wiley, New York, 1960, p. 199.
26 S. F. Chung and C. Y. Chen, *AIChE J.*, 14 (1968) 857.

Journal of Chromatography, 484 (1989) 225–236
Elsevier Science Publishers B.V., Amsterdam — Printed in The Netherlands

CHROM. 21 925

DISPLACEMENT CHROMATOGRAPHY OF BIOMOLECULES WITH LARGE PARTICLE DIAMETER SYSTEMS

GUHAN SUBRAMANIAN, MICHAEL W. PHILLIPS, GUHAN JAYARAMAN and STEVEN M. CRAMER*

Bioseparations Research Center, Department of Chemical Engineering, Rensselaer Polytechnic Institute, Troy, NY 12180-3590 (U.S.A.)

SUMMARY

Displacement chromatography was employed for the preparative-scale separation of peptides and proteins using large particle diameter chromatographic systems. Peptide displacements were successfully scaled-up with respect to particle and column diameter with no adverse effects on product recovery. Protein displacements on 30- and 90-μm agarose-based adsorbent systems resulted in well separated displacement zones of pure material. The present work extends the scope of biopolymer displacement chromatography to large particle diameter systems and is expected to further increase the distinct economic advantages associated with preparative-scale displacement chromatography.

INTRODUCTION

Displacement chromatography is rapidly emerging as a powerful preparative bioseparation technique due to the high throughput and purity associated with the process[1–3]. The operation of preparative elution systems at elevated concentrations has been shown to result in significant tailing of the peaks with the concomitant loss of separation efficiency[4]. In contrast, displacement chromatography offers distinct advantages in preparative chromatography as compared to the conventional elution mode[1,2]. The process takes advantage of the non-linearity of the isotherms such that a larger feed can be separated on a given column with the purified components recovered at significantly higher concentrations. Furthermore, the tailing observed in non-linear elution chromatography is greatly reduced in displacement chromatography due to the self-sharpening boundaries formed in the process. Whereas in elution chromatography the feed components are diluted during the separation, the feed components are often concentrated during displacement chromatography[1,5]. These advantages are particularly significant for the isolation of biopolymers from dilute solutions such as those encountered in biotechnology processes.

Although the physico-chemical basis of the displacement mode of chromatography was established by Tiselius in 1943[6], the potential of this technique for preparative bioseparations was not realized until the recent work on displacement chroma-

0021-9673/89/$03.50

tography employing high-performance liquid chromatography (HPLC) sorbents which exhibit rapid kinetics and mass transfer[1,3,5,7–25].

We have demonstrated that displacement chromatography can be successfully employed for the simultaneous concentration and purification of peptides, antibiotics, and proteins[1]. A mathematical model for the simulation of non-ideal displacement chromatography has also been developed to facilitate the optimization of these separations[26]. We have recently extended our work with biopolymer displacement to relatively complex mixtures and examined displacement behavior under elevated flow-rate and crossing isotherm conditions[8]. While the recent advances with displacement chromatography have been carried out with small particle diameter HPLC materials, there is a significant economic driving force for using larger particle diameter supports for preparative and process-scale liquid chromatography. The present work extends the scope of biopolymer displacement chromatography to large particle diameter systems and is expected to further increase the economic advantages associated with the elevated throughput and product purity of displacement chromatographic systems.

EXPERIMENTAL

Materials

μBondapak octadecylsilica (10 μm and 15–20 μm) columns in various column dimensions were gifts from Waters Chromatography Division (Millipore, Milford, MA, U.S.A.). 30-μm Sepharose S and 90-μm Sepharose S Fast-Flow bulk cation-exchange materials and a 50 × 5 mm I.D. column packed with 10-μm Mono-S cation-exchange material were donated by Pharmacia LKB Biotechnology (Piscataway, NJ, U.S.A.). Bulk Zorbax octadecylsilica and strong cation exchanger (SCX) chromatographic materials were gifts from DuPont (Wilmington, DE, U.S.A.). Methanol, 2-(2-butoxyethoxy) ethanol (BEE), sodium monophosphate and ammonium sulfate were purchased from Fisher Scientific (Rochester, NY, U.S.A.). N-Carbobenzoxy-L-alanyl-L-glycyl-L-glycine (Cbz-Ala-Gly-Gly), N-carbobenzoxy-L-alanyl-L-alanine (Cbz-Ala-Ala), N-benzoyl-L-arginine (Bz-Arg), cytochrome *c*, α-chymotrypsinogen and lysozyme were obtained from Sigma (St. Louis, MO, U.S.A.). Water-soluble coagulant, Nalcolyte 7105, was a gift from Nalco (Chicago, IL, U.S.A.).

Apparatus

The chromatograph employed for the peptide displacements consisted of a Model LC 2150 pump (Pharmacia LKB) connected to the chromatographic columns via a Model C10W 10-port valve (Valco, Houston, TX, U.S.A.). The column effluent was monitored by a Model 757 Spectroflow UV detector (Applied Biosystems, Ramsey, NJ, U.S.A.) and a Model L6512 strip chart recorder (Linseis, Princeton, NY, U.S.A.). Fractions of the column effluent were collected with an LKB Model 2212 Helirac fraction collector. The column temperature was controlled using a Model RM20 Lauda recirculating water bath (Brinkman, Westbury, NY, U.S.A.).

An FPLC chromatograph (Pharmacia LKB) was employed for the protein displacement experiments. This system consisted of a Model P-500 pump connected to the chromatographic column via a Model MV-7 valve. The column effluent was

monitored by a Model UV-M detector and a Pharmacia strip-chart recorder. Fractions of the column effluent were collected with a Model Frac-100 fraction collector. The system was controlled using a LCC-500-Plus controller.

Procedures

Operation of displacement chromatograph. A schematic of the displacement chromatograph system employed in this work is illustrated elsewhere[5]. In all displacement experiments, the columns were sequentially perfused with carrier, feed, displacer, and regenerant solutions. Fractions of the column effluent were collected throughout the displacement runs and were assayed by analytical chromatography.

Displacement of peptides. Feed mixtures containing Bz-Arg, Cbz-Ala-Gly-Gly, and Cbz-Ala-Ala were separated by displacement chromatography on μBondapak octadecylsilica columns of various column dimensions (Waters). The carrier solution was methanol–50 m*M* phosphate buffer, pH 2.2 (40:60, v/v). The displacer for these separations was 30 mg/ml BEE in the carrier. The column temperature was maintained at 45°C and flow-rates of 0.1, 0.4 and 2.5 ml/min were employed for the displacement experiments with columns of 3.9, 7.8 and 19 mm I.D., respectively.

Displacement chromatography of proteins on Mono-S 10-μm supports. Displacement experiments were carried out using 50 × 5 mm I.D. columns packed with 10-μm Mono-S cation exchange materials. The displacer was 30 mg/ml Nalcolyte 7105 in a carrier of 0.1 *M* ammonium sulfate in 25 m*M* phosphate buffer, pH 7.5. The regenerant contained 0.8 *M* ammonium sulfate in 50 m*M* phosphate buffer, pH 3.0. The feed mixture was a 0.5-ml solution containing α-chymotrypsinogen, cytochrome *c* and lysozyme at 1.67 mg/ml each. The protein displacement employed a flow-rate and temperature of 0.1 ml/min and 22°C, respectively.

Purification of proteins on 30-μm Sepharose S particles. Displacement experiments were carried out using 300 × 10 mm I.D. columns packed with 30-μm Sepharose S cation-exchange materials. The carrier contained 0.1 *M* ammonium sulfate in 25 m*M* phosphate buffer, pH 7.5. The displacer was 75 mg/ml Nalcolyte 7105 in the carrier. The regenerant solution and temperature employed were the same as described above. The flow-rate was 0.4 ml/min. The feed solution was 6 ml of 1.67 mg/ml each of α-chymotrypsinogen, cytochrome *c* and lysozyme.

A step-gradient experiment was carried out using the same conditions as described above, with the displacer replaced by a solution of 0.25 *M* ammonium sulfate in 25 m*M* phosphate buffer, pH 7.5.

The displacement experiment was repeated using a carrier of 25 m*M* phosphate buffer, pH 7.5, all other conditions as stated above.

Purification of proteins on 90-μm Sepharose S particles. Displacement experiments were carried out using 300 × 10 mm I.D. columns packed with 90-μm Sepharose S cation-exchange material. The displacer was 75 mg/ml Nalcolyte 7105 in a carrier of 0.1 *M* ammonium sulfate in 25 m*M* phosphate buffer, pH 7.5. The feed solution was a 6-ml solution containing 1.67 mg/ml each of α-chymotrypsinogen and lysozyme. All other conditions were the same as described above for the 30-μm displacement.

Preparative elution of the feed mixture was carried out in the absence of the displacer, all other conditions the same.

HPLC analysis. Fractions collected during the chromatographic runs were ana-

lyzed by HPLC. A Model LC 2150 pump (Pharmacia LKB), a Model 7125 sampling valve with a 20-μl sample loop (Rheodyne, Cotati, CA, U.S.A.), a Model 757 spectroflow UV detector (Applied Biosystems), and a Model C-R3A integrator (Shimadzu, Kyoto, Japan) were assembled to carry out HPLC analysis. Peptide analyses were carried out using a 100 × 4.6 mm I.D. Zorbax C_{18} column (DuPont). The eluent consisted of methanol–50 m*M* phosphate buffer, pH 2.2 (50:50, v/v). Protein analyses were performed with a 100 × 4.6 mm I.D. SCX column (DuPont). The eluent contained 0.15 *M* ammonium sulfate in 25 m*M* phosphate buffer, pH 7.5. Displacement fractions were diluted 50–500 fold with the eluent and 20-μl samples were injected. The flow-rate was 1.0 ml/min and column temperature was maintained at 22°C. The column effluents were monitored at 254 and 280 nm for the peptide and protein analyses, respectively. Quantitative analysis was carried out and the data was used to construct displacement chromatograms.

RESULTS AND DISCUSSION

Displacement chromatography has been established as a powerful technique for the simultaneous concentration and purification of biomolecules[1,3,5,7–25]. However, the biopolymer displacements performed to date have employed stationary phase materials with particle diameters of 10 μm or less. Clearly, for displacement chromatography to become a useful preparative separation tool in the biotechnology

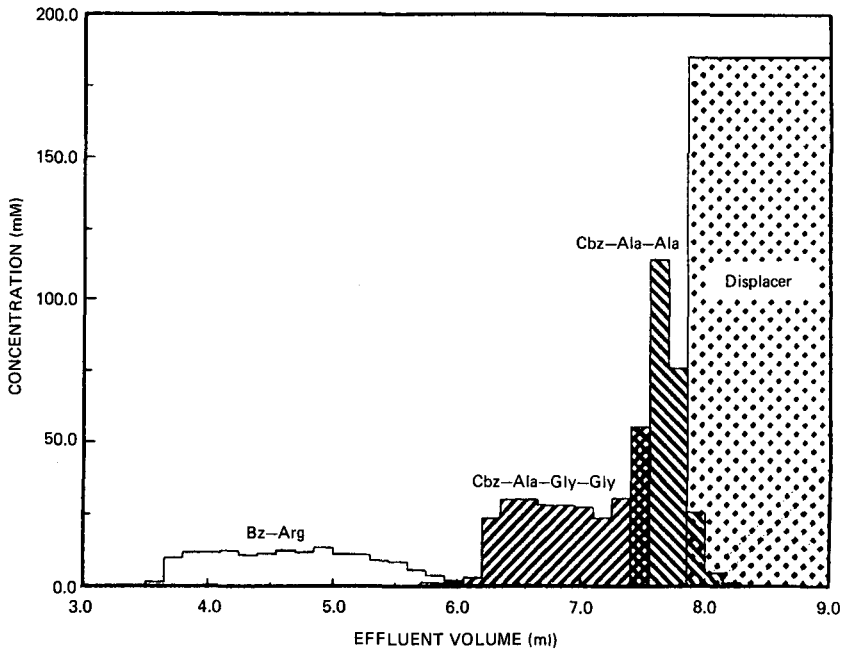

Fig. 1. Displacement chromatogram of a peptide mixture. Column, 300 × 3.9 mm I.D. μBondapak ODS (10 μm); carrier, methanol–50 m*M* phosphate buffer, pH 2.2 (40:60, v/v); displacer, 30 mg/ml BEE; feed, 7.2 mg Bz-Arg, 16.4 mg Cbz-Ala-Gly-Gly and 18.2 mg Cbz-Ala-Ala in 2 ml of carrier; flow-rate, 0.1 ml/min; temperature, 45°C; fraction volume, 150 μl.

industry, the economics of the process must be compelling. Since the cost of carrying out preparative chromatography decreases dramatically with increasing particle diameter, it is important to investigate the efficacy of displacement chromatography of biomolecules with large particle diameter systems. Accordingly, the present work examines the displacement chromatographic purification of peptides and proteins in such systems.

Scale-up of peptide displacement

In a previous report[1] we described the displacement purification of the peptides Bz-Arg, Cbz-Ala-Gly-Gly, and Cbz-Ala-Ala using BEE as the displacer on a reversed-phase analytical HPLC system. This model displacement was employed in this study to investigate the scale-up of displacement chromatography of peptides with respect to particle and column diameter.

The model displacement was first carried out on a 300 × 3.9 mm I.D. analytical column packed with 10-μm octadecylsilica material. The resulting displacement chromatogram is shown in Fig. 1. Under these conditions, Bz-Arg eluted ahead of the displacement train and Cbz-Ala-Gly-Gly and Cbz-Ala-Ala were well displaced as expected from the previously reported results.

The displacement separation was then scaled-up with respect to column diameter using two 150 × 19 mm I.D. columns in series packed with the same 10-μm stationary phase material. In this experiment, the feed volume and flow-rate were linearly scaled-up with respect to the cross-sectional area. The resulting displacement chromatogram, shown in Fig. 2, demonstrates that the same degree of separation was

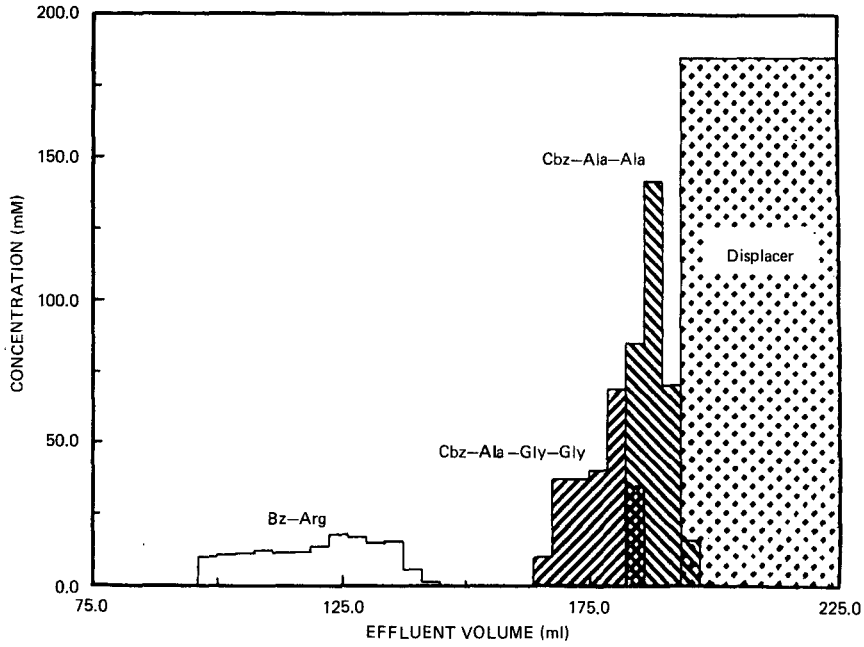

Fig. 2. Preparative-scale displacement of a peptide mixture. Chromatographic conditions as in Fig. 1 with the exception of: column, two 150 × 19 mm I.D. μBondapak ODS columns (10 μm) in series; feed, 161.9 mg Bz-Arg, 303.1 mg Cbz-Ala-Gly-Gly and 412.5 mg Cbz-Ala-Ala in 45.2 ml of carrier; flow-rate, 2.5 ml/min; fraction volume, 3.75 ml.

achieved as with the analytical column. In fact, the breakthrough time of the displacer in both experiments was identical, confirming the linear scale-up of the process. This separation corresponds to the purification of approximately one gram of peptide per displacement experiment. This result indicates that preparative HPLC columns can be readily employed for the displacement purification of peptides.

The displacement separation was also scaled-up with respect to particle diameter. Fig. 3 shows the displacement chromatogram of the model separation using a 300 × 7.8 mm I.D. column packed with 15–20-μm reversed-phase material. Under these conditions, the same degree of separation was obtained as with the 10-μm stationary phase.

We are presently extending this work to process-scale column systems and employing our model of non-ideal displacement chromatography[26] for the optimization of such systems. This work will be the subject of a future report.

Displacement chromatography of proteins

We have previously demonstrated that displacement chromatography can be successfully employed for the simultaneous purification and concentration of protein mixtures using silica-based stationary phase materials[1,8]. In this report, we extend this work to larger particle diameter polymer-based systems.

The separation of the proteins α-chymotrypsinogen, cytochrome *c* and lysozyme by displacement chromatography was first investigated using a 50 × 5 mm I.D. column packed with 10-μm Mono-S cation-exchange material. The resulting dis-

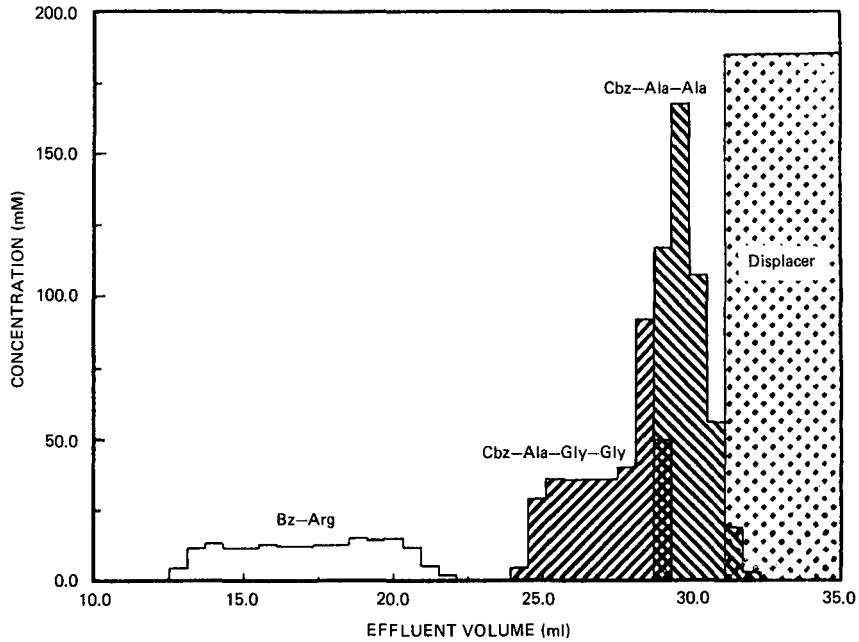

Fig. 3. Displacement chromatogram of a peptide mixture on a 20-μm particle diameter system. Chromatographic conditions as in Fig. 1 with the exception of: column, 300 × 7.8 mm I.D. μBondapak ODS (15–20 μm); feed, 27.8 mg Bz-Arg, 66.6 mg Cbz-Ala-Gly-Gly and 74.9 mg Cbz-Ala-Ala in 8 ml carrier; flow-rate, 0.4 ml/min; fraction volume, 600 μl.

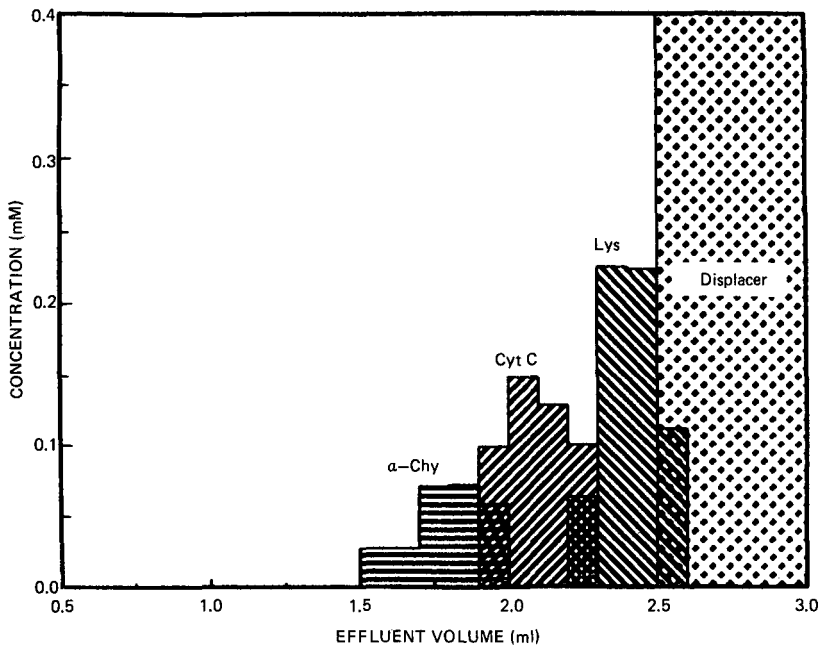

Fig. 4. Displacement chromatogram of a three-component protein mixture. Column, 50 × 5 mm I.D. Mono-S cation exchanger (10 μm); carrier, 0.1 *M* ammonium sulfate in 25 m*M* phosphate buffer, pH 7.5; displacer, 30 mg/ml Nalcolyte 7105 in carrier; flow-rate, 0.1 ml/min; temperature, 22°C; feed, 500 μl of 1.67 mg/ml each of α-chymotrypsinogen (α-Chy), cytochrome *c* (Cyt C) and lysozyme (Lys); fraction volume, 100 μl.

placement chromatogram, shown in Fig. 4, demonstrates that the proteins were well-separated during the displacement process. While the Nalcolyte displacer was readily removed from the column using standard regeneration techniques, these polymer-based materials have the distinct advantage of being able to withstand extremes of pH. In fact, column regeneration was also easily achieved by the perfusion of 6 ml of 2 *M* NaOH.

Scale-up of protein displacement

The purification of proteins by displacement chromatography was investigated with larger particle diameter materials. Fig. 5 shows the displacement chromatogram of the proteins α-chymotrypsinogen, cytochrome *c* and lysozyme using 75 mg/ml Nalcolyte 7105 to displace the proteins from a chromatographic column packed with 30-μm Sepharose S cation-exchange material. Under these conditions, the proteins were well separated and concentrated during the displacement process. These results are indeed dramatic in that they demonstrate that displacement chromatography of proteins is not limited to small particle diameter systems.

However, in ion-exchange displacement chromatography, the adsorption of the displacer not only results in the displacement of the feed components but can also result in desorption of the salt molecules in the system. This in turn can result in an effective "salt-gradient" moving down the column ahead of the displacer front. Thus,

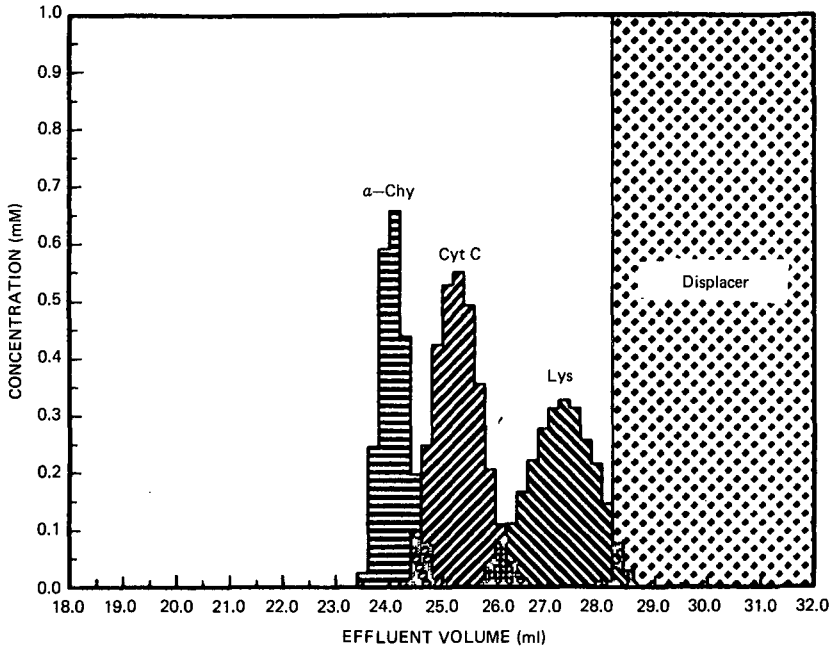

Fig. 5. Displacement chromatogram of a three-component protein mixture on a 30-μm particle diameter system. Column, 300 × 10 mm I.D. Sepharose S cation exchanger (30 μm); carrier, 0.1 *M* ammonium sulfate in 25 m*M* phosphate buffer, pH 7.5; displacer, 75 mg/ml Nalcolyte 7105 in carrier; flow-rate, 0.4 ml/min; temperature, 22°C; feed 6 ml of 1.67 mg/ml each of α-chymotrypsinogen, cytochrome *c* and lysozyme; fraction volume, 200 μl.

it is critical that the effect of the desorbed salt molecules on the feed components downstream of the displacer front be investigated.

In the above displacement purification, a carrier containing 0.1 *M* ammonium sulfate in 25 m*M* phosphate buffer, pH 7.5, was employed. In order to examine whether this separation was due primarily to the action of an effective "salt-gradient" induced by the displacer, the following idealized control experiment was carried out. After the introduction of the feed mixture, a step change in the salt concentration from 0.1 to 0.25 *M* ammonium sulfate was carried out at the column inlet. This step-gradient was selected such that the breakthrough times of the proteins in the two experiments were comparable. The profile obtained in this control experiment is shown in Fig. 6. While the proteins had comparable effluent concentrations and retention times under these conditions, there was more mixing and significant tailing of the feed components in the step gradient experiment. Although this does not represent an optimal step gradient for these components, it illustrates that the displacement separation is not solely due to the action of the induced salt gradient.

In order to examine the displacement behavior of this system in the absence of the ammonium sulfate salt, the displacement experiment was repeated with no salt present in the carrier. The resulting profile from this control experiment is shown in Fig. 7. Again, the three proteins were well separated and concentrated during the

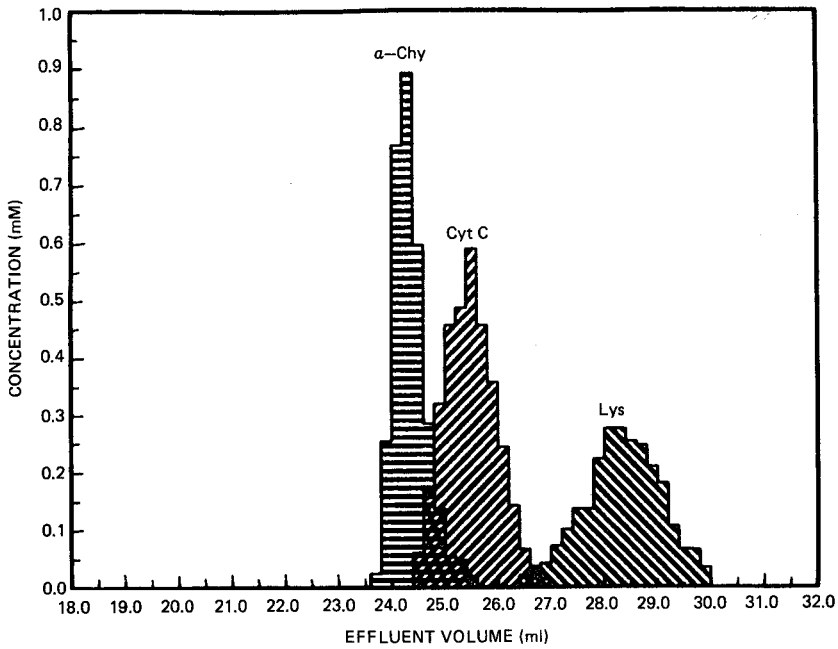

Fig. 6. Step-gradient separation of a three-component protein mixture on a 30-μm particle diameter system. Chromatographic conditions as in Fig. 5 with the displacer replaced by a solution of 0.25 *M* ammonium sulfate in 25 m*M* phosphate buffer, pH 7.5.

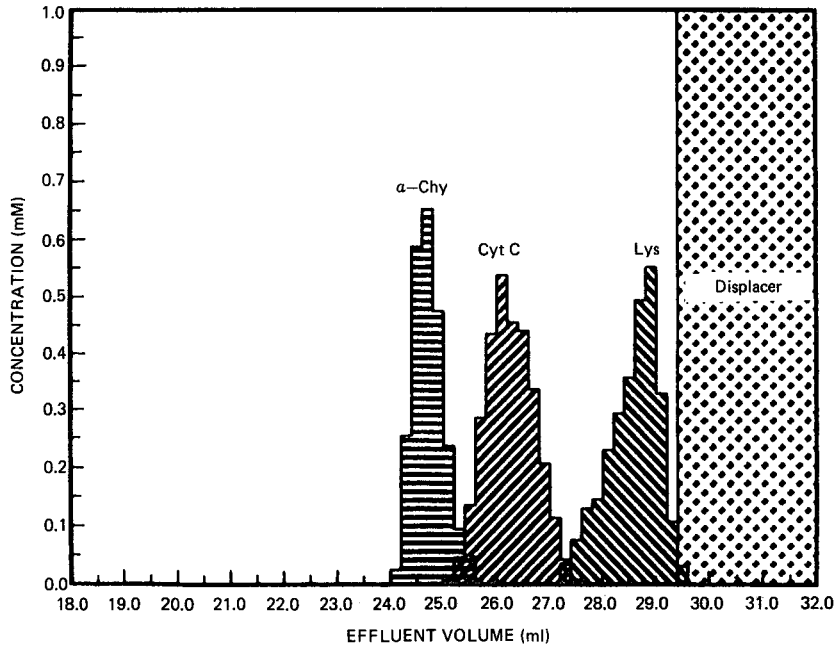

Fig. 7. Displacement chromatogram of a three-component protein mixture on a 30-μm diameter system. Chromatographic conditions as in Fig. 5 with the exception of: carrier, 25 m*M* phosphate buffer, pH 7.5.

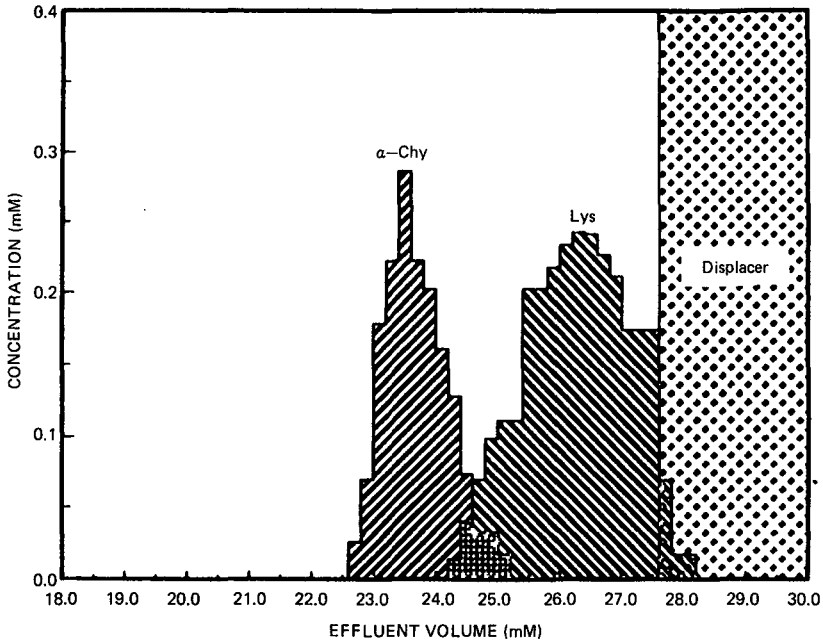

Fig. 8. Displacement chromatogram of a two-component protein mixture on a 90-μm particle diameter system. Chromatographic conditions as in Fig. 5 with the exception of: column, 300 × 10 mm I.D. Sepharose S cation exchanger (90 μm); feed, 6 ml of 1.67 mg/ml each of α-chymotrypsinogen and lysozyme.

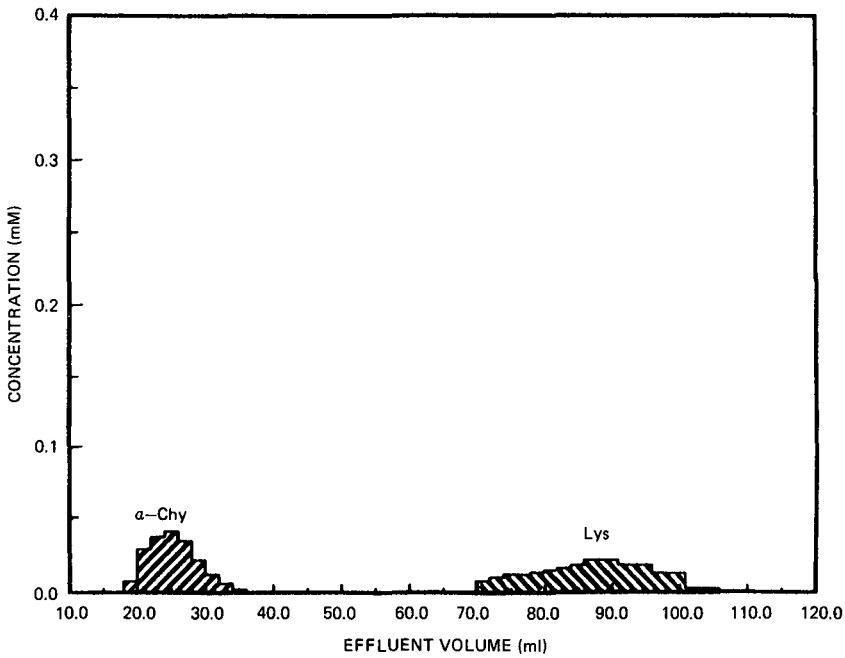

Fig. 9. Preparative elution chromatogram of a two-component protein mixture on a 90-μm particle diameter system. Column, 300 × 10 mm I.D. Sepharose S cation exchanger (90 μm). Chromatographic conditions as in Fig. 8 with the absence of the displacer.

displacement process. Thus, displacement chromatography of proteins can be readily carried out with or without the presence of salt in the carrier.

Displacement chromatography of proteins was further scaled-up to 90-μm agarose-based materials. The simultaneous concentration and purification of the proteins α-chymotrypsinogen and lysozyme on these materials is shown in Fig. 8. The displacement zones exhibited relatively sharp boundaries, which is quite remarkable for such large particle diameter systems. The separation was repeated in the absence of the displacer. Preparative non-linear elution chromatography under the same carrier conditions resulted in extremely long elution times with significant dilution of the feed proteins as shown in Fig. 9. While this preparative elution experiment was not optimized, it serves to dramatize the action of the displacer in these systems.

CONCLUSIONS

In this report we have demonstrated that the displacement purification of biomolecules can be readily scaled-up to larger particle and column diameter systems. Indeed, the ability to simultaneously concentrate and purify biomolecules by displacement chromatography using preparative columns packed with large particle diameter materials may have a significant impact on the economics of preparative chromatography.

ACKNOWLEDGEMENTS

The gifts of stationary phase materials from Waters Chromatography Division (Millipore, Milford, MA, U.S.A.), Pharmacia LKB Biotechnology (Piscataway, NJ, U.S.A.) and DuPont (Wilmington, DE, U.S.A.) are gratefully acknowledged. This work was supported by Grant No. CBT-8708799 from the National Science Foundation.

REFERENCES

1 G. Subramanian, M. W. Phillips and S. M. Cramer, *J. Chromatogr.*, 439 (1988) 341.
2 Cs. Horváth, in F. Bruner (Editor), *The Science of Chromatography*, Elsevier, Amsterdam, 1985, p. 179.
3 A. M. Katti and G. A. Guiochon, *J. Chromatogr.*, 449 (1988) 25.
4 J. H. Knox and H. M. Pyper, *J. Chromatogr.*, 363 (1986) 1.
5 S. M. Cramer and Cs. Horváth, *Prep. Chromatogr.*, 1 (1988) 29.
6 A. Tiselius, *Ark. Kemi Mineral. Geol.*, 16A, No. 18 (1943) 1.
7 J. Frenz and Cs. Horváth, *AIChE J.*, 31 (1985) 400.
8 G. Subramanian and S. M. Cramer, *Biotech. Progress*, 5(3) (1989) 92.
9 Cs. Horváth, J. Frenz and Z. El Rassi, *J. Chromatogr.*, 255 (1983) 273.
10 Cs. Horváth, A. Nahum and J. H. Frenz, *J. Chromatogr.*, 218 (1981) 365.
11 Z. El Rassi and Cs. Horváth, *J. Chromatogr.*, 266 (1983) 319.
12 J. Frenz, Ph. Van der Schrieck and Cs. Horváth, *J. Chromatogr.*, 330 (1985) 1.
13 G. Viscomi, S. Lande and Cs. Horváth, *J. Chromatogr.*, 440 (1988) 157.
14 S. M. Cramer, Z. El Rassi and Cs. Horváth, *J. Chromatogr.*, 394 (1987) 305.
15 E. A. Peterson, *Anal. Biochem.*, 90 (1978) 767.
16 E. A. Peterson and A. R. Torres, *Anal. Biochem.*, 130 (1983) 271.
17 A. R. Torres, B. E. Dunn, S. C. Edberg and E. A. Peterson, *J. Chromatogr.*, 316 (1984) 125.
18 A. R. Torres, G. G. Krueger and E. A. Peterson, *Anal. Biochem.*, 144 (1985) 469.
19 A. R. Torres, S. C. Edberg and E. A. Peterson, *J. Chromatogr.*, 389 (1987) 177.

20 A. W. Liao, Z. El Rassi, D. M. LeMaster and Cs. Horváth, *Chromatographia*, 24 (1987) 881.
21 G. Vigh, Z. Varga-Puchony, G. Szepesi and M. Gazdag, *J. Chromatogr.*, 386 (1987) 353.
22 A. L. Lee, A. W. Liao and Cs. Horváth, *J. Chromatogr.*, 443 (1988) 31.
23 T. W. Lorne Burke, C. T. Mant and R. S. Hodges, *J. Liq. Chromatogr.*, 11(6) (1988) 129.
24 D. J. Sawyer, J. E. Powell and H. R. Burkholder, *J. Chromatogr.*, 455 (1988) 193.
25 S. M. Cramer and G. Subramanian, in G. Keller and R. Yang (Editors), *New Directions in Adsorption Technology*, Butterworths, Stoneham, MA, 1988, p. 187.
26 M. W. Phillips, G. Subramanian and S. M. Cramer, *J. Chromatogr.*, 454 (1988) 1.

Journal of Chromatography, 484 (1989) 237–250
Elsevier Science Publishers B.V., Amsterdam — Printed in The Netherlands

CHROM. 21 799

DISPLACEMENT CHROMATOGRAPHY ON CYCLODEXTRIN–SILICAS

I. SEPARATION OF POSITIONAL AND GEOMETRICAL ISOMERS IN THE REVERSED-PHASE MODE

GYULA VIGH*, GILBERTO QUINTERO and GYULA FARKAS
Chemistry Department, Texas A & M University, College Station, TX 77843-3255 (U.S.A.)

SUMMARY

The retention behaviour of several charged and uncharged solutes on β-cyclodextrin–silica was studied as a function of the methanol concentration, ionic strength and pH of the eluent in order to develop efficient displacement chromatographic separations for positional and geometric isomers. These retention curves were used to predict the eluent (carrier solvent) compositions that result in solute retentions in excess of $k' = 10$. The adsorption isotherms of several cationic detergents were determined in these carrier solutions and were found to be convex. The adsorption isotherms of several positional isomers used as test solutes were also determined in these carrier solutions. The adsorption isotherms permitted the development of efficient displacement chromatographic separations for the isomers tested. Column loadings as high as 58 mg were achieved on a regular 4.6 mm I.D. analytical-scale cyclodextrin silica columns.

INTRODUCTION

Cyclodextrins have been increasingly used in liquid chromatography to effect the separation of positional isomers, geometric isomers and enantiomers. The toroidally shaped β-cyclodextrin molecule contains seven glucose units, which are connected through α-(1,4) linkages[1–3]. The inner surface of the cyclodextrin cavity is relatively hydrophobic and has a high electron density, whereas the exterior surface of cyclodextrin is hydrophilic owing to the presence of clockwise projecting 2-hydroxyl groups and counter-clockwise projecting 3-hydroxyl groups at the rim of the larger opening of the cavity, and primary 6-hydroxyl groups at the smaller opening of the cavity. Cyclodextrins readily form 1:1 and 1:2 guest–host complexes with molecules that penetrate into their cavities. The stability of the complex depends on the "snugness" of the fit and the subsequent stabilization of the complex via secondary intermolecular interactions[4].

In liquid chromatography, cyclodextrins are used either as mobile-phase additives[5] or as stationary phases[3,6–10]. With cyclodextrins as mobile-phase additives[5], separation is accomplished in the reversed-phase mode, and is based on the hydro-

0021-9673/89/$03.50

phobicity change of the solutes that is caused by inclusion complex formation. This approach works well in analytical separations, but it is impractical in preparative separations. Cyclodextrin stationary phases are either insoluble cyclodextrin polymers[11] or cyclodextrin units immobilized on a silica support[12–18]. Cyclodextrin polymers have high capacity, but lack chromatographic efficiency[11]. The first high-performance liquid chromatographic (HPLC)-grade cyclodextrin-silicas contained ethylenediamine[12] or diamide bridges[13], had low coverage (50 μmol/g immobilized cyclodextrin) and were hydrolytically unstable. Stable, higher capacity cyclodextrin–silicas, immobilized via alkyl spacers, have been developed[14] and are now commercially available from ASTEC (Whippany, NJ, U.S.A.)[16] with α-, β- or γ-cyclodextrin moieties. Derivatized bonded cyclodextrins, which posses different selectivities, have recently been synthetized by carbamoylation[17] and acetylation[16].

Owing to the special geometry of cyclodextrin and its inclusion complex formation, cyclodextrin–silicas can be used for the separation of positional isomers, geometric isomers and enantiomers. The positional isomers of polysubstituted benzenes[19–23], benzoic[22] and aminobenzoic acids, methylindoles, prostaglandins and steroids and the geometric isomers of polyaromatic hydrocarbons and derivatives have been separated successfully[20]. The separations of *cis–trans* isomers of stilbenes[20], prostaglandins[24], cyclic nitrosamines[25], acyclic nitrosamines[26], cyclohexane derivates[27] and tamoxifen[28] have been reported. Enantiomer separations are actively pursued aspects of cyclodextrin research and have been reviewed[7,8,10,29], but are not dealt with in this paper.

Chromatographic separations can be effected in the elution mode, frontal mode and displacement mode[30,31]. Elution is more suitable for analytical separations (dilute solutions, linear sorption isotherm); frontal and displacement modes (concentrated solutions, non-linear sorption isotherms) offer advantages (high throughput, yield and sample concentration) for preparative separations. Although displacement chromatography has been known for a long time[32], it was revived only when Horvath *et al.*[33] reported efficient separations using HPLC equipment. Recent reviews demonstrate its rapid growth[31–36].

In displacement chromatography, the column is first equilibrated with the carrier solution that has the least affinity for the column. Then the sample, whose components are adsorbed more strongly, is introduced, followed by the displacer, which has the strongest affinity for the stationary phase. As the front of the displacer moves down the column, it displaces the sample components which, in turn, displace each other according to their adsorption strength. If the adsorption strengths of the components are sufficiently different and the column has the necessary efficiency, the components occupy adjacent zones and move at the same velocity in the fully developed displacement train. Component concentrations in the isotachic train depend only on the respective adsorption isotherms and the concentration of the displacer.

Solute concentrations and column loadings that are orders of magnitude higher than in elution chromatography have been achieved in the displacement mode[33–36]. While much has been learned about the role of the operational parameters (column efficiency, capacity, dispersion, mass transfer rate, relative sample loading)[37–39], little is yet known about the rules of displacer selection and selectivity control. The factors that hamper most the wider acceptance of displacement chromatography include the lack of knowledge of solute adsorption isotherms and the lack of well characterized

displacers. Displacer selection is still done by trial-and-error methods. Most modern displacement chromatographic separations were carried out in the reversed-phase mode and dealt with small polar molecules, antibiotics, oligopeptides and small proteins[33–40].

However, displacement chromatographic separations with cyclodextrins, combining the unique selectivity of cyclodextrins and the preparative efficiency of displacement chromatography, as reported here, have not previously been described. This combination permits efficient and unique preparative separations hitherto unavailable, separations which are important in the field of chemical and biomedical sciences and technologies. In this paper, we discuss the displacement chromatographic separations of positional and geometric isomers in the reversed-phase mode. In forthcoming papers we shall describe the displacement chromatographic separations of positional and geometric isomers in the normal-phase mode[41] and the displacement chromatographic separations of enantiomers in the reversed-phase mode[42].

EXPERIMENTAL

A computer-controlled displacement chromatograph, shown in Fig. 1, was constructed from commercial components. It is based on designs described previously[38,40] and consists of two LC 2010 liquid chromatographic pumps (Varian, Walnut Creek, CA, U.S.A.), two computer-controlled, pneumatically activated Type 7001 switching valves (Rheodyne, Cotati, CA, U.S.A.), a computer-controlled, pneumatically activated Type 7125 injection valve (Rheodyne), an LC 2050 variable-wavelength UV detector (Varian), a Series RI-3 refractive index (RI) detector (Varian) and a Powermate II personal computer (NEC, Computer Access, College Station, TX, U.S.A.). Detector signals were recorded by a Maxima Workstation (Waters Assoc.,

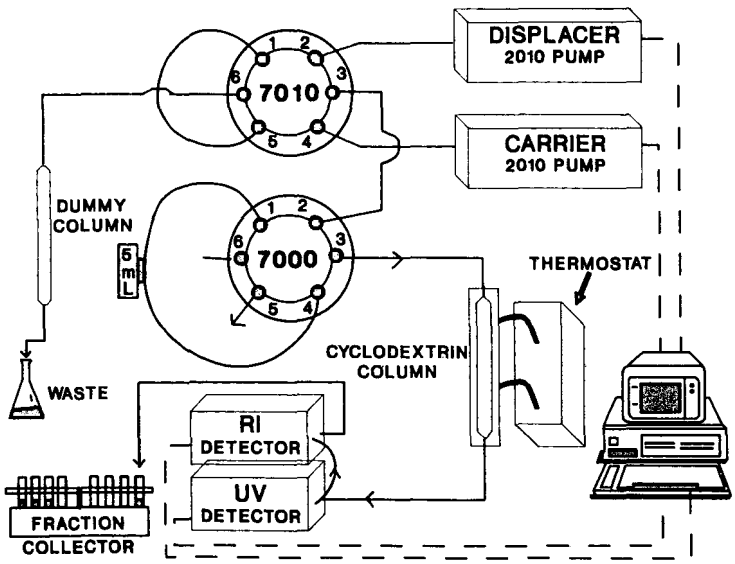

Fig. 1. Schematic diagram of the displacement chromatograph.

Dynamic Solutions, Milford, MA, U.S.A.). Retention volume measurements from elution experiments, individual excess surface adsorption isotherms from frontal chromatographic measurements and preparative-scale displacement chromatographic separations alike can be effected with this instrument. Consumption of chemicals during the isotherm determination steps was minimized by using small-bore columns, packed in our laboratory with commercially available α- and β-cyclodextrin–silicas (ASTEC, Whippany, NJ, U.S.A.). Columns of different length were used in the frontal chromatographic measurements in order to insure comparable adsorption isotherm accuracies for both the strongly and the slightly adsorbed components. The displacement chromatographic separations were completed using the same stationary phases, custom-packed into 250 mm × 46 mm I.D. stainless-steel columns. As retention varies sensitively with temperature, all measurements were carried out with water-jacketed columns thermostated at 30°C.

An integration-algorithm-based interactive graphics program, written in QUICKBASIC for the IBM AT-compatible NEC Powermate II personal computer, was developed to analyze the digitalized frontal chromatograms. Chromatograms measured by the Maxima system were transfered as ASCII files for post-run evaluation by this program. The SAS PC program package (SAS Institute, Cary, NC, U.S.A.) was used to determine the adsorption isotherm parameters.

All solutes were from Aldrich (Milwaukee, WI, U.S.A.) and used without further purification. The components used as displacers were from Sigma (St. Louis, MO, U.S.A.). Eluents were prepared from HPLC-grade methanol (Mallinckrodt, St. Louis, MO, U.S.A.) and water produced by a Milli-Q unit (Millipore, Bedford, MA, U.S.A.).

RESULTS

The parameters that influence elution-mode solute retention on cyclodextrin–silicas were investigated first, then the individual excess surface adsorption isotherms of a few displacers, both ionic and non-ionic, were determined, followed by the adsorption isotherms of selected solutes. Finally, displacement chromatographic separations of these solutes were carried out on cyclodextrin-silicas to demonstrate the feasibility of the proposed preparative separation method.

Retention as a function of the methanol concentration in the eluent

The retention curves (log capacity factor, k', *vs.* methanol concentration) of a few polar positional isomers (naphthols, nitroanilines, ethoxyanilines and chloroanilines) are shown in Figs. 2 and 3 for methanol–water eluents. As it was found with other solutes[41], these curves on β-cyclodextrin silica show poorer linearity, and the slopes for the different solute types vary more than on "regular" alkylsilicas. The common feature of these curves is that the solute retention is very low (and almost constant) when the eluents are rich in methanol (*i.e.*, above 60–70% methanol), and increases rapidly as the methanol concentration is decreased.

Retention as a function of the ionic strength and pH of the eluent

It has been stated that on cyclodextrin–silicas solute retention decreases as the ionic strength of the eluent increases, because the eluent cations occupy the cyclo-

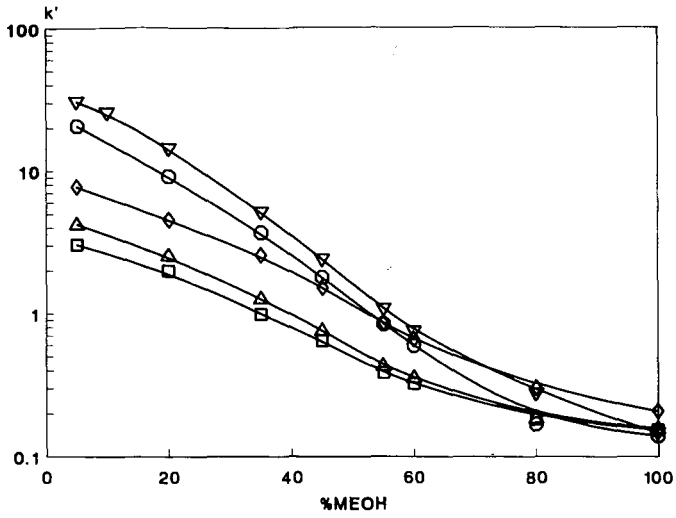

Fig. 2. Retention of the naphthol and nitroaniline isomers on β-cyclodextrin–silica as a function of the methanol (MEOH) concentration of the eluent. ◇ = *p*-Nitroaniline; △ = *o*-nitroaniline; □ = *m*-nitroaniline; ○ = 2-naphthol; ▽ = 1-naphthol.

dextrin cavities and exclude the solute molecules[16]. We found that the role of ionic strength is much more complex and that it depends on both the type of solute and the pH of the eluent. The log *k'* *vs.* ionic strength curves for quinine and quinidine at pH 3.66 (50 m*M* phosphate buffer, ionic strength adjusted with sodium bromide) are

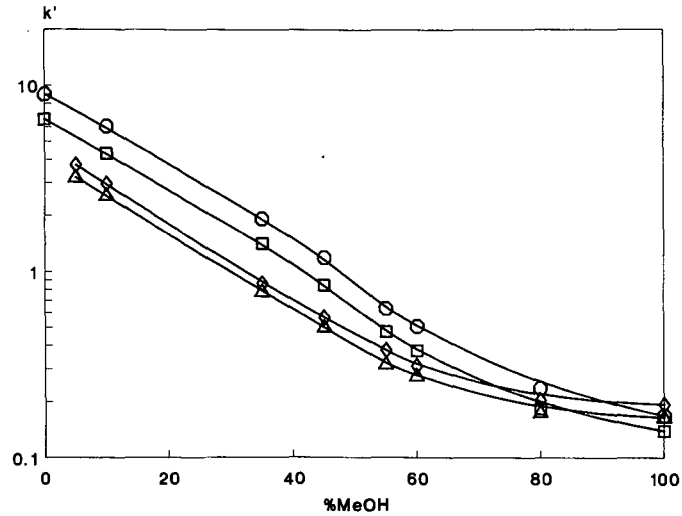

Fig. 3. Retention of ethoxyaniline and chloroaniline isomers on β-cyclodextrin–silica as a function of the methanol (MeOH) concentration of the eluent. ◇ = *p*-Ethoxyaniline; △ = *m*-ethoxyaniline; ○ = *p*-chloroaniline; □ = *m*-chloroaniline.

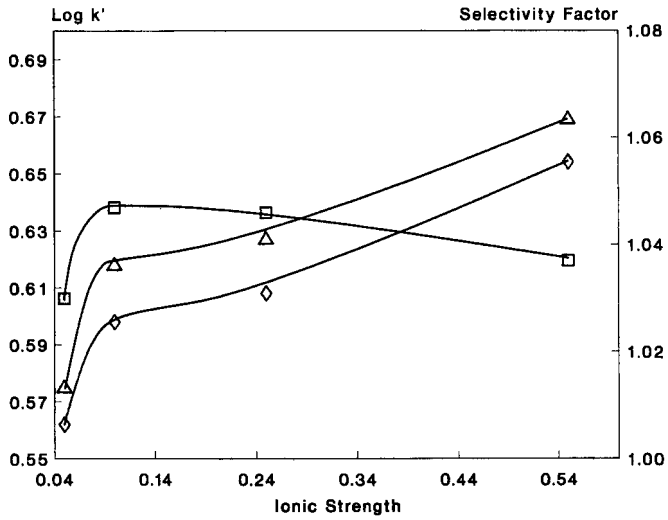

Fig. 4. Retention of (◇) quinine and (△) quinidine and (□) selectivity factor as a function of the ionic strength of the eluent at pH 3.66 (50 m*M* phosphate buffer and NaBr).

shown in Fig. 4. These positively charged components become more retained as the ionic strength increases. However, at higher pH, such as pH 5.55 (Fig. 5) and 6.55 (Fig. 6), their retention decreases with increasing ionic strength. As the pK_a value of the protonated quinine is 6.74, the solutes remain positively charged in the pH range 3.5–6.5. Hence there is no change in the extent of solute ionization to explain the increased (by an order of magnitude) retention. Instead, an ion-exchange mechanism,

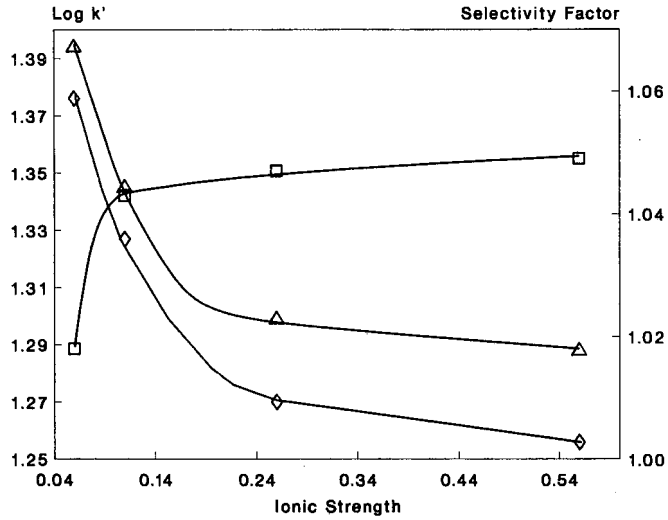

Fig. 5. Retention of (◇) quinine and (△) quinidine and (□) selectivity factor as a function of the ionic strength of the eluent at pH 5.55 (50 m*M* phosphate buffer and NaBr).

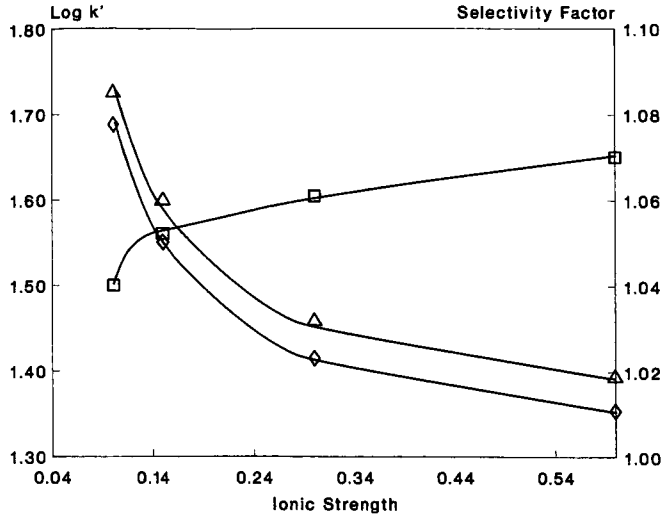

Fig. 6. Retention of (◇) quinine and (△) quinidine and (□) selectivity factor as a function of the ionic strength of the eluent at pH 6.55 (50 m*M* phosphate buffer and NaBr).

similar to that reported by Papp and Vigh[43,44] for alkylsilicas, is operative. At higher pH the silanol groups of the silica support are dissociated more completely, and ion exchange contributes to the retention of positively charged solutes more strongly than inclusion complex formation. Therefore, cation retention decreases in the eluents of higher ionic strength where more competition is present. Simultaneously, and importantly, as ion exchange is repressed by the salt, the chances of selective retention by the cyclodextrin moiety improve, *i.e.* the separation selectivity factor increases, as shown in Figs. 5 and 6.

When there is no such ion exchange, *i.e.*, when the silanol groups are not yet dissociated sufficiently (as in Fig. 4), or when the solute is negatively charged (as the dansylphenylalanine enantiomer pair in Fig. 7) or uncharged (as the naphthol isomers in Fig. 8), retention increases with increasing ionic strength, as in ordinary reversed-phase systems. Unfortunately, as the hydrophobic interaction becomes stronger, the differentiating ability of cyclodextrin–silica decreases and the selectivity factor decreases (Figs. 7 and 8).

Hence it can be seen that the effects of ionic strength and eluent pH are much more complex on cyclodextrin–silicas than is commonly perceived. The retention trends are different for the positively and negatively charged solutes and the uncharged solutes. The retention changes are large enough to necessitate a closer examination of these factors during the development of a preparative separation.

Individual excess adsorption isotherms of selected displacers

The success of any displacement chromatographic separation scheme depends critically on the finding of an appropriate displacer. Therefore, the individual excess surface adsorption isotherms of a few detergents were determined on cyclodextrins using frontal chromatographic measurements. The isotherms of several quaternary

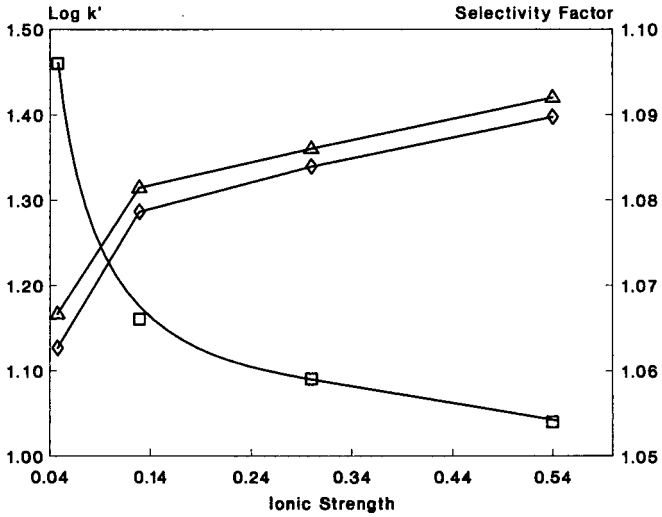

Fig. 7. Retention of the dansylphenylalanine enantiomers (◇ = D-; △ = L-) and (□) selectivity factor as a function of the ionic strength at pH 5.55 (50 m*M* phosphate buffer and NaBr).

ammonium salts are shown in Fig. 9 [β-cyclodextrin–silica, 13% (v/v) methanol–water solution, no pH or ionic strength control[45,46]].

The individual excess surface adsorption isotherms of the symmetrical tetraalkylammonium bromides (tetrabutyl and tetrapentyl) rise much more slowly than the isotherms of the detergents that have a single, long alkyl chain. When the detergents contain a cetyl chain, such as the cetylpyridinium, cetrimide and

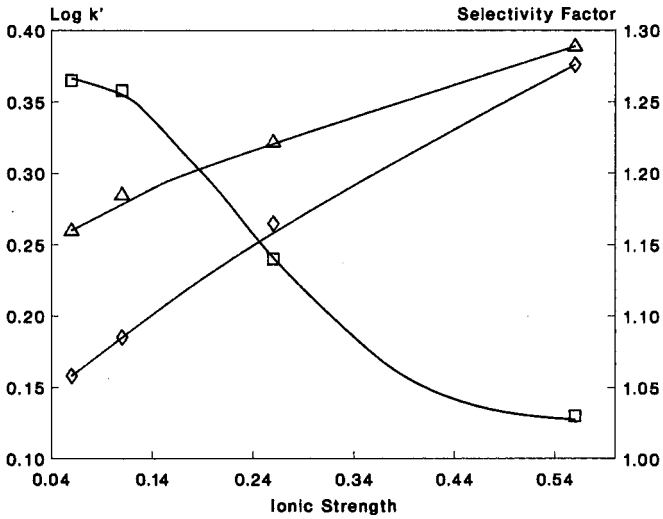

Fig. 8. Retention of the nitrophenol isomers (◇ = *m*-; △ = *p*-) and (□) selectivity factor as a function of the ionic strength at pH 5.55 (50 m*M* phosphate buffer and NaBr).

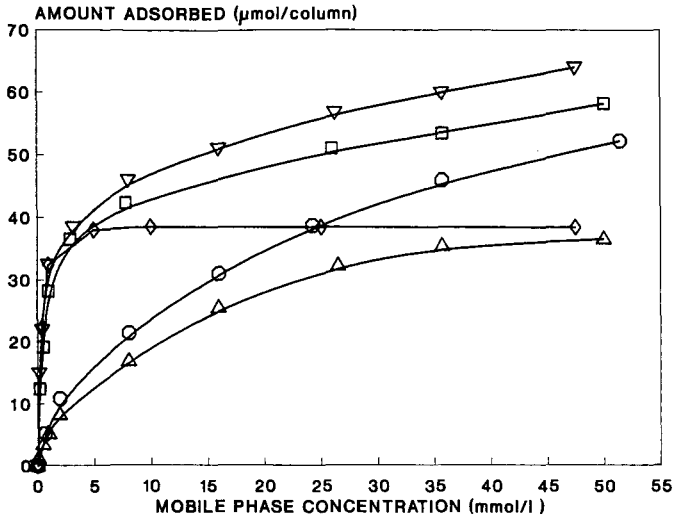

Fig. 9. Adsorption isotherms of the quaternary ammonium salts on β-cyclodextrin–silica from 13% (v/v) methanol–water. ◇ = Cetrimide; △ = tetrabutylammonium bromide; ○ = tetrapentylammonium bromide; ▽ = benzylcetyldimethylammonium chloride; □ = cetylpyridinium bromide.

benzylcetyldimethylammonium cations, there is a very steep initial rise in the isotherm. The isotherm of benzylcetyltrimethylammonium bromide soon levels off. However, the isotherms continue to rise if the detergents contain a bulky group (*e.g.*, a six-membered ring) in addition to the cetyl chain. None of the isotherms follows the simple Langmuir equation. The methanol concentration, pH and ionic strength of the solution also have an important effect on the extent of excess surfactant adsorption and the shape of the isotherm[45,46].

Displacement chromatographic separations on β-cyclodextrin silica

The naphthol and nitroaniline positional isomers were selected to demonstrate the feasibility of displacement chromatographic separations on β-cyclodextrin–silica. As their retention behaviour in methanol–water eluents was known (Fig. 2), a composition of the carrier in which the initial solute retention is sufficiently large ($k' > 10$),

TABLE I

INITIAL BREAKTHROUGH VOLUMES OF CATIONIC DETERGENT-TYPE DISPLACERS IN 13% (V/V) METHANOL–WATER CARRIER SOLUTION

Detergent	*Solution concentration (mM)*	*Breakthrough volume (ml)*
Tetrabutylammonium bromide	0.51	3.86
Tetrapentylammonium bromide	0.65	5.06
Cetyltrimethylammonium bromide	0.54	32.68
Cetylpyridinium bromide	0.50	44.57
Benzyldimethylcetylammonium chloride	0.43	47.84

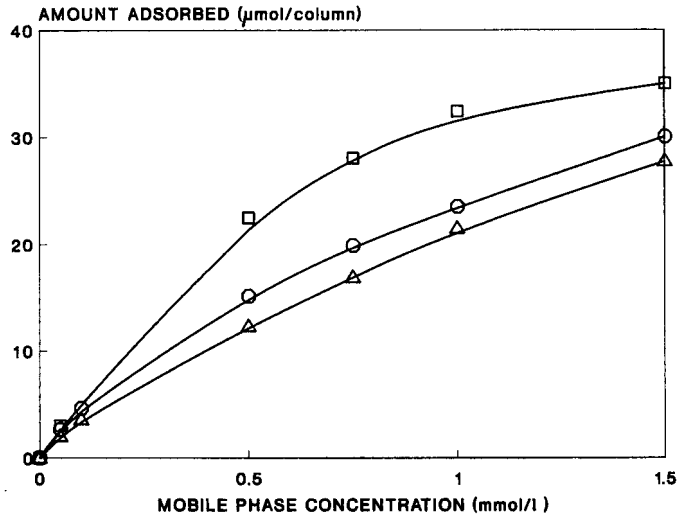

Fig. 10. Adsorption isotherms of (□) cetrimide and the (○) 1- and (△) 2-naphthol on β-cyclodextrin–silica from 13% (v/v) methanol–water.

could be selected *i.e.*, containing 13% (v/v) methanol. The adsorption isotherms of the displacers were also determined in this solution (Fig. 9). The initial breakthrough volumes belonging to the first measured point of the isotherms are shown in Table I. As the extrapolated retention volumes of the naphthol isotherms are larger than the breakthrough volume of tetrapentylammonium bromide, but smaller than that of cetrimide, the latter was considered as a possible displacer. The adsorption isotherms of the naphthol isomers and the cetrimide displacer in 13% (v/v) methanol are shown in Fig. 10. The isotherms of the naphthol isomers run below the isotherm of cetrimide, indicating that the contemplated displacement chromatographic separation may be feasible.

A sample of 8 μmol of 2-naphthol and 10 μmol of 1-naphthol was loaded (from a total volume of 1.8 ml) onto two 250 mm x 4.6 mm I.D. β-cyclodextrin-silica columns in series, pre-equilibrated with the 13% (v/v) methanol–water carrier. The 1.5 m*M* cetrimide displacer solution was introduced at a flow-rate of 0.5 ml/min. The displacement chromatogram, shown in Fig. 11, was recorded using a refractive index (RI) detector. Three individual steps can be observed in the chromatogram. Elution-mode HPLC analysis of the collected fractions showed that the first plateau corresponds to 2-naphthol, the second to 1-naphthol and the third to cetrimide. To our knowledge, this is the first displacement chromatogram ever obtained on β-cyclodextrin–silica columns.

The displacement chromatogram of the nitroaniline isomers was obtained to demonstrate that sometimes the approximate conditions of a first displacement chromatographic separation can be determined solely from the extrapolated retention volumes and the initial breakthrough volumes (adsorption isotherms) of the displacers, without a detailed knowledge of the actual adsorption isotherms of the pure solutes. The extrapolated retention volumes of the nitroaniline isomers with 13% (v/v) methanol–water eluent were calculated from the log k' *vs.* methanol concentra-

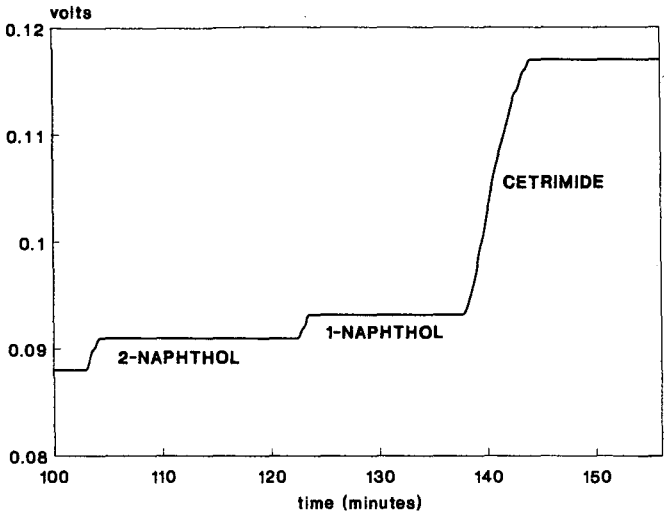

Fig. 11. Displacement chromatogram of the naphthol isomers on β-cyclodextrin–silica with 1.5 m*M* cetrimide [in 13% (v/v) methanol–water] as displacer. Flow-rate, 0.5 ml/min.

tion curves (Fig. 2) to be above $k' = 10$, the minimum retention value generally considered conducive to a successful displacement chromatographic separation. These retention volumes were compared with the initial displacer breakthrough volumes in Table I. Benzylcetyldimethylammonium chloride was found to have a much larger initial breakthrough volume than the retention volumes of the nitroanilines; consequently, its selection as a possible displacer can be considered a reasonably safe proposition.

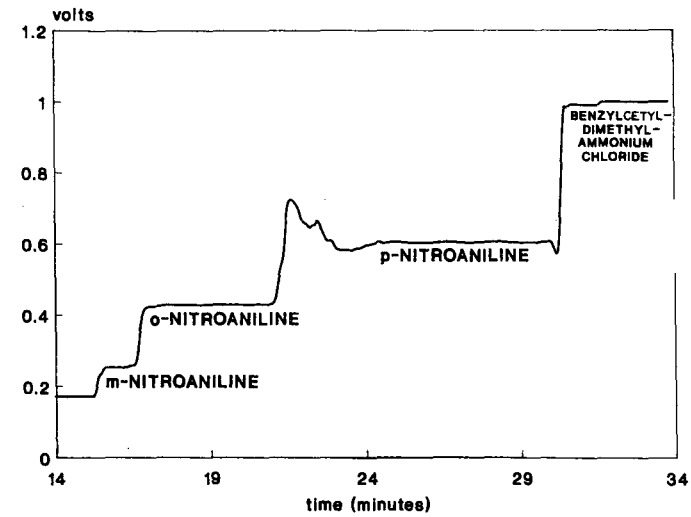

Fig. 12. Displacement chromatogram of the nitroaniline isomers on β-cyclodextrin–silica with 52.6 m*M* benzylcetyldimethylammonium chloride [in 13% (v/v) methanol–water] as displacer. Flow-rate, 0.5 ml/min.

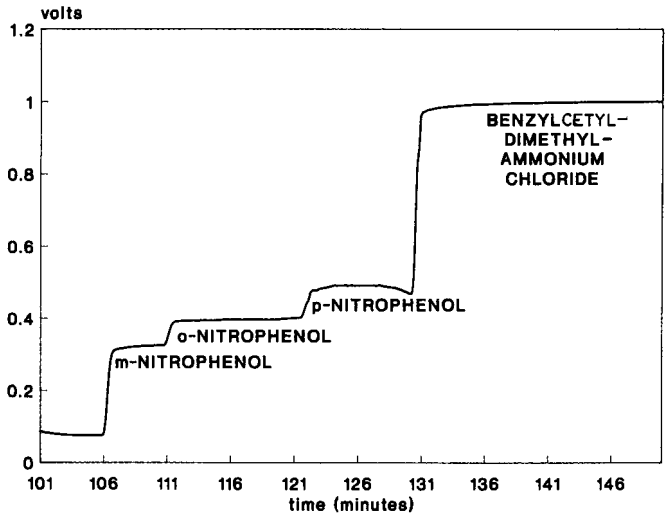

Fig. 13. Displacement chromatogram of the nitrophenol isomers (*m*-, 12 mg; *o*-, 25 mg; *p*-. 21 mg) on β-cyclodextrin–silica with 10% (v/v) methanol–water as carrier and 64 m*M* benzylcetyldimethylammonium chloride as displacer. Flow-rate, 0.5 ml/min.

A sample that contained 0.7 μmol of *m*-nitroaniline, 1.6 μmol of *o*-nitroaniline and 4.8 μmol of *p*-nitroaniline was injected, from 5 ml of 13% (v/v) methanol carrier solution, onto two 250 mm × 4.6 mm I.D. β-cyclodextrin–silica columns in series, then a 52.6 m*M* solution of benzylcetyldimethylammonium chloride was introduced at a flow-rate of 0.5 ml/min as displacer. The displacement chromatogram, shown in Fig. 12, was recorded with an RI detector. Four steps can be observed in the chromatogram. HPLC analysis of the collected fractions showed that the plateaus correspond to *m*-, *o*- and *p*-nitroaniline and benzylcetyldimethylammonium chloride. Some unknown contaminants were also found at the front section of the *p*-nitroaniline fraction. Their origin was traced back to the *o*-nitroaniline standard used, but the identity of the contaminants was not determined.

The displacement chromatogram of 12 mg of *m*-nitrophenol, 25 mg of *o*-nitrophenol and 21 mg of *p*-nitrophenol (a total of 58 mg of sample loaded onto a 4.6 mm I.D. analytical column!) is shown in Fig. 13. The carrier was 10% (v/v) methanol–water and the displacer 64 m*M* benzylcetyldimethylammonium chloride, at a flow-rate of 0.5 ml/min. The yields corresponding to the 99% purity level were calculated from the reconstructed chromatograms and turned out to be 89% for *m*-, 80% for *o*- and 75% for *p*-nitrophenol. Notwithstanding the high load excellent separation of the isomers was achieved.

CONCLUSIONS

It was shown that although the log *k'* *vs.* methanol concentration relationships for polar solutes, especially the positively charged type, are not as simple as on ordinary alkylsilica reversed-phase packings, they are regular enough to permit the

use of a reasonably small number of actual retention measurements to predict (by extrapolation) the carrier solvent compositions that result in sufficiently large initial solute retentions ($k' > 10$ or, preferably, $k' > 25$).

The adsorption isotherms of cationic detergents were found to be convex, although the simple Langmuir isotherm equation could not be used to describe the individual excess adsorption isotherms. The stationary-phase concentrations of the detergent-type displacers varied more sensitively with the methanol concentration of the carrier solution than is observed on regular alkylsilica-type reversed-phase stationary phases.

Using estimated solute retention volumes, predicted carrier compositions and actual displacer adsorption isotherms, succesful displacement chromatographic separations of up to 60-mg samples of positional isomers have been achieved on regular analytical-scale columns. Hence the unique separation selectivity of β-cyclodextrin–silicas, as known from elution chromatographic separations, was successfully combined with the efficient displacement chromatographic mode of operation and resulted in hitherto unavailable preparative separations.

Further work is in progress in our laboratory (and will be reported soon) to study in detail: (1) the retention behaviour of a large number of solutes, representing the three unique application fields of cyclodextrin–silicas (positional, geometric and optical isomers); (2) the adsorption isotherms of selected displacers, both ionic and non-ionic detergents, and "designer displacers" specifically synthesized to meet the requirements of cyclodextrin–silicas; (3) the general rules of displacer selection for cyclodextrin–silicas; and (4) the operating conditions that allow the separation of a large number of positional and geometric isomers and enantiomers of industrial significance.

ACKNOWLEDGEMENTS

Financial support by the Texas Coordination Board of Higher Education TATR Program (Grant Number 14956) and the Minority Access for Research Careers, National Institute of Health Program (Grant Number 5F31GM11689), is acknowledged. The authors are greatful to Dr. Thomas Beesley of ASTEC for the β-cyclodextrin-silica sample used in this study.

REFERENCES

1 M. L. Bender and M. Komiyama, *Cyclodextrin Chemistry*, Springer, Berlin, 1978.
2 J. Szejtli, *Cyclodextrins and Their Inclusion Complexes*, Akademiai Kiado, Budapest, 1982.
3 J. Szejtli, B. Zsadon and T. Cserhati, in W. L. Hinze and D. W. Armstrong (Editors), *Ordered Media in Chemical Separations* (*ACS Symposium Series*, No. 342), American Chemical Society, Washington, DC, 1987, p. 200.
4 H. J. Issaq, M. L. Glennon and S. P. Fox, in W. L. Hinze and D. W. Armstrong (Editors), *Ordered Media in Chemical Separations* (*ACS Symposium Series*, No. 342), American Chemical Society, Washington, DC, 1987, p. 235.
5 D. Sybilska, in W. L. Hinze and D. W. Armstrong (Editors), *Ordered Media in Chemical Separations*, (*ACS Symposium Series*, No. 342), American Chemical Society, Washington, DC, 1987, p. 218.
6 E. Smolkova-Keulemansova, *J. Chromatogr.*, 251 (1982) 15.
7 D. W. Armstrong, *J. Liq. Chromatogr.*, 7 (1984) 353.
8 T. J. Ward, D. W. Armstrong, *J. Liq. Chromatogr.*, 9 (1986) 407.

9 R. Dappen, H. Arm and V. R. Meyer, *J. Chromatogr.*, 373 (1986) 1.
10 W. H. Pirkle, in S. Ahuja (Editor), *Chromatography and Separation Chemistry, Advances and Developments*, American Chemical Society, Washington, DC, 1986, p. 101.
11 B. Zsadon, L. Decsi, M. Szilasi, F. Tudos, J. Szejtli, *J. Chromatogr.*, 270 (1983) 127.
12 K. Fujimura, T. Ueda and T. Ando, *Anal. Chem.*, 55 (1983) 446.
13 Y. Kawaguchi, M. Tanaka, M. Nakae. K. Funazo and T. Shono, *Anal. Chem.*, 55 (1983) 1852.
14 D. W. Armstrong, *U.S. Pat.* 4 539 399 (1985).
15 D. W. Armstrong and W. DeMond, *J. Chromatogr. Sci.*, 22 (1984) 411.
16 *Cyclobond Handbook*, Astec, Whippany, NJ, 1987.
17 M. Tanaka, H. Ikeda and T. Shono, *J. Chromatogr.*, 398 (1987) 165.
18 D. W. Armstrong, A. Alak, W. DeMond, W. L. Hinze and T. E. Riehl, *J. Liq. Chromatogr.*, 8 (1985) 261.
19 K. A. Connors and D. D. Pendergast, *J. Am. Chem. Soc.*, 106 (1984) 7607.
20 D. W. Armstrong, W. DeMond, A. Alak, W. L. Hinze, T. E. Riehl and K. H. Bui, *Anal. Chem.*, 57 (1985) 234.
21 C. A. Chang, Q. Wu and D. W. Armstrong, *J. Chromatogr.*, 354 (1986) 454.
22 C. A. Chang, Q. Wu and L. Tan, *J. Chromatogr.*, 361 (1986) 199.
23 C. A. Chang and Q. Wu, *J. Liq. Chromatogr.*, 10 (1987) 1359.
24 B. G. Snider, *J. Chromatogr.*, 351 (1986) 548.
25 H. J. Issaq, J. H. McConnell, D. E. Weiss, D. G. Williams and J. E. Saavedra, *J. Liq. Chromatogr.*, 9 (1986) 1783.
26 H. J. Issaq, Glennon, D. E. Weiss, G. N. Chmurny and J. E. Saavedra, *J. Liq. Chromatogr.*, 9 (1986) 2763.
27 G. W. Tindall, *J. Liq. Chromatogr.*, 10 (1987) 1077.
28 R. D. Armstrong, T. J. Ward, N. Pattabiraman, C. Benz and D. W. Armstrong, *J. Chromatogr.*, 414 (1987) 192.
29 D. W. Armstrong, *Anal. Chem.*, 59 (1987) 84A.
30 F. G. Hellferich and G. Klein, *Multicomponent Chromatography—Theory of Interference*, Marcel Decker, New York, 1970.
31 Cs. Horváth and W. R. Melander, in E. Heftmann (Editor), *Chromatography, Part A: Fundamentals and Techniques* (*Journal of Chromatography Library*, Vol. 22A), Elsevier, Amsterdam, 1983, p. A27.
32 A. Tiselius, *Ark. Kemi Mineral. Geol.*, 16A, No. 18 (1943) 1.
33 Cs. Horváth, A. Nahum and J. H. Frenz, *J. Chromatogr.*, 218 (1981) 365.
34 Cs. Horváth, J. Frenz and Z. El Rassi, *J. Chromatogr.*, 255 (1983) 273.
35 Cs. Horváth, in F. Bruner (Editor), *The Science of Chromatography* (*Journal of Chromatography Library*, Vol. 32), Elsevier, Amsterdam, 1985, p. 179.
36 H. Kalasz and Cs. Horváth, *J. Chromatogr.*, 215 (1981) 295.
37 F. G. Helfferich, *Ind. Eng. Chem., Fundam.*, 6 (1967) 362.
38 J. Jacobson, J. H. Frenz and Cs. Horváth, *J. Chromatogr.*, 316 (1984) 53.
39 J. H. Frenz and Cs. Horváth, *AIChE J.*, 31 (1985) 400.
40 Gy. Vigh, Z. Varga-Puchony, G. Szepesi and M. Gazdag, *J. Chromatogr.*, 386 (1986) 353.
41 Gy. Vigh, Gy. Farkas and G. Quintero, *J. Chromatogr.*, 484 (1989) 251.
42 Gy. Farkas and Gy Vigh, *J. Chromatogr.*, submitted for publication.
43 E. Papp and Gy. Vigh, *J. Chromatogr.*, 259 (1983) 49.
44 E. Papp and Gy. Vigh, *J. Chromatogr.*, 282 (1983) 59.
45 A. Bartha, Gy. Vigh, H. Billiet and L. de Galan, *J. Chromatogr.*, 291 (1984) 91.
46 A. Bartha, Gy. Vigh, H. Billiet and L. de Galan, *J. Chromatogr.*, 303 (1984) 29.

Journal of Chromatography, 484 (1989) 251–257
Elsevier Science Publishers B.V., Amsterdam — Printed in The Netherlands

CHROM. 21 926

DISPLACEMENT CHROMATOGRAPHY ON CYCLODEXTRIN–SILICAS

II. SEPARATION OF *cis–trans* ISOMERS IN THE REVERSED-PHASE MODE ON α-CYCLODEXTRIN–SILICA

GYULA VIGH*, GYULA FARKAS and GILBERTO QUINTERO
Department of Chemistry, Texas A&M University, College Station, TX 77843 (U.S.A.)

SUMMARY

The feasibility of preparative separations of *cis–trans* isomers by displacement chromatography on analytical-scale α-cyclodextrin–silica columns operated in the reversed-phase mode is demonstrated by using the isomers of 3-hexen-1-ol as model substrates and *n*-alkanols as displacers. The importance of matching the size of the cyclodextrin cavity and the solutes is shown. The crucial role of the displacer (both type and concentration) in the success of the displacement chromatographic separation is demonstrated.

INTRODUCTION

Cyclodextrins are capable of forming inclusion complexes with guest molecules[1–3]. As the cyclodextrin cavity has a well defined size and geometry, the stability of the inclusion complex depends on the snugness of the fit and the strength of the intermolecular interactions that develop between the polar functional groups of the guest solute and the secondary and primary hydroxyl groups of the cyclodextrin[2–4]. Cyclodextrins can be used to effect the separation of positional and geometric isomers, *cis–trans* isomers and ciral solutes provided that the solutes can penetrate the cyclodextrin cavity.

The analytical separations of positional and geometric isomers[4–9] and enantiomers[10–13] have been reviewed recently and are not dealt with in his paper. The *cis* and *trans* isomers of stilbene[14], six prostaglandins[15], cyclic nitrosamines[16], acyclic nitrosamines[17], cyclohexane derivatives[18] and tamoxifen[19] were successfully separated on β-cyclodextrin-silica columns using aqueous methanol and acetonitrile eluents. Generally, the *trans* isomers elute first. The bulkier and/or more hydrophobic substituents lead to longer solute retention and different separation selectivity.

Compared with other silica-based high-performance liquid chromatographic (HPLC) stationary phases, most cyclodextrin–silicas have low loading capacities and show relatively low selectivity factors. Hence they are more suited for analytical separations than for preparative work. However, in Part 1[20] we showed that the preparative chromatographic limitations of cyclodextrin–silicas can be circumvented if the columns are used in the self-focusing displacement chromatographic mode.

0021-9673/89/$03.50

Horváth *et al.*[21] used modern HPLC hardware to achieve efficient non-linear chromatographic separations by displacement chromatography[22,23]. Several good recent reviews discuss the principles and use of displacement chromatography in detail (*e.g.*, ref. 24). A number of research groups are actively pursuing the theoretical and practical aspects of displacement chromatography[25–28].

We showed in Part 1[20] that good preparative separations of positional and geometric isomers can be effected on analytical β-cyclodextrin–silica columns even when the elution-mode separation selectivities are as low as 1.05–1.09. Sample loadings as high 60 mg were achieved on 4.6 mm I.D. analytical columns. In this paper we show that the preparative displacement chromatographic separation of *cis* and *trans* isomers is also possible on cyclodextrin–silicas in the reversed-phase mode.

EXPERIMENTAL

A multifunctional displacement chromatograph, assembled from commercially available components as described in Part 1[20], was used. The instrument can be operated in (i) the elution mode to determine the capacity factors of the solutes and to analyse the fractions collected during the preparative separations, (ii) the frontal mode to determine the adsorption isotherms of the displacers and the solutes and (iii) the displacement mode to carry out the preparative separations. The experimental procedure was the same as described previously[20].

Both α-cyclodextrin–silica (Cyclobond III, 5 μm) and β-cyclodextrin–silica (Cyclobond I, 5 μm) were obtained from ASTEC (Whippany, NJ, U.S.A.) and slurry-packed in our laboratory into 4.6 mm I.D. stainless-steel analytical columns. The *cis* and *trans* isomers of 3-hexen-1-ol (Aldrich, Milwaukee, WI, U.S.A.) were used as test solutes and 1-hexanol and 1-heptanol (Aldrich) as displacers. All chemicals were used without further purification. All eluents, carrier solutions and displacer solutions were prepared from HPLC-grade methanol (Mallinckrodt, St. Louis, MO, U.S.A.) and Milli-Q water (Millipore, Bedford, MA, U.S.A.).

RESULTS

In order to develop a displacement chromatographic separation, the elution-mode retention behavior of the solutes has to be studied first. This information is then used to select the composition of the carrier solution. The log k' *vs.* methanol concentration curves of *cis*- and *trans*-3-hexen-1-ol are shown in Fig. 1. As in ordinary reversed-phase chromatography, an almost linear relationship is obtained. However, for a successful displacement chromatographic separation, the solutes have to be sufficiently retained in the carrier solution ($k' > 10$). It can be seen in Fig. 1 that the k' value of the less retained *cis* isomer is only 1.9, even in the weakest eluent, pure water. The weak retention probably results from the β-cyclodextrin cavity being too large for the 3-hexene-1-ol isomers and a tight fit cannot be achieved. Therefore, the retention studies were repeated on an α-cyclodextrin-silica column.

The log k' *vs.* methanol concentration curves for *cis*- and *trans*-3-hexen-1-ol are shown in Fig. 2. Again, good linear retention behavior can be observed. Sufficient (although by no means large) retention can be achieved with pure water as the carrier solvent.

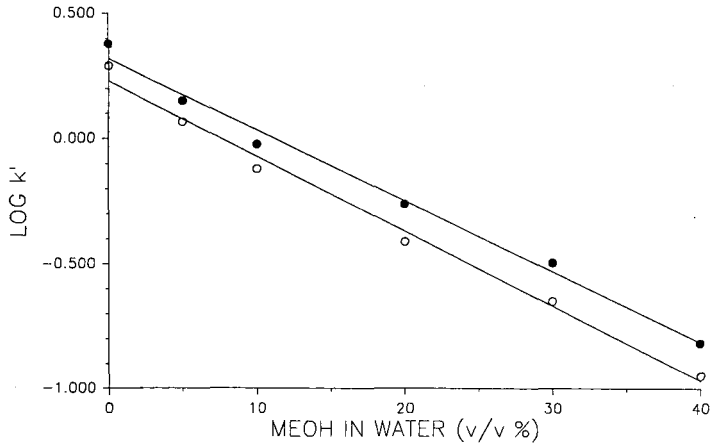

Fig. 1. Retention of (●) *cis*- and (○) *trans*-3-hexen-1-ol on β-cyclodextrin–silica as a function of the methanol (MEOH) concentration of the eluent.

Once the composition of the carrier solution has been determined, a suitable displacer has to be selected for the separation. Components that have a structure similar to that of the solute are generally good displacers on cyclodextrin–silicas, provided that they are slightly more hydrophobic than the solutes and/or have slightly stronger intermolecular interactions with cyclodextrin than do the solutes. Therefore, 1-hexanol and 1-heptanol were selected as potential displacers. Their retention curves are also shown in Fig. 2. Both *n*-alkanols are more retained than the *cis–trans* solute pair. The elution mode, infinite dilution separation selectivity factors for the *cis–trans* pair and the *n*-hexanol–*trans* isomer solute pair are approximately the same. Thus, at least in principle, both 1-hexanol and 1-heptanol are good displacers, because the *cis* and *trans* isomers can be separated from each other and then, owing to the identical

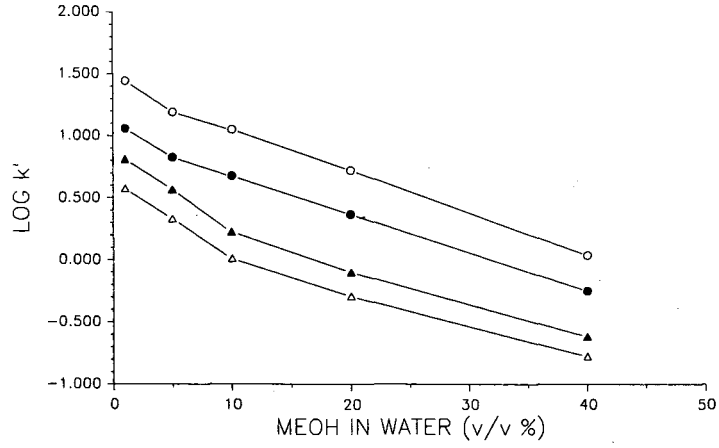

Fig. 2. Retention of (●) 1-hexanol, (○) 1-heptanol and (△) *cis*- and (▲) *trans*-3-hexen-1-ol on α-cyclodextrin–silica as a function of the methanol (MEOH) concentration of the eluent.

α values the *trans* isomer can also be separated from the displacer. To test the validity of this assumption, the adsorption isotherms of the solutes and of both potential displacers were determined.

The adsorption isotherms of the solutes, *cis*- and *trans*-3-hexen-1-ol and the potential *n*-alkanol displacers are show in Fig. 3. Both 1-hexanol and 1-heptanol are more strongly adsorbed than the *cis*–*trans* solute pair, indicating that either of them could be used as a displacer. The isotherms of 1-hexanol and *trans*-3-hexen-1-ol are much closer to each other than those of *cis*- and *trans*-3-hexen-1-ol. This shows that the selectivities of the separation at infinite dilution (Fig. 2) and at higher concentrations (Fig. 3) are different.

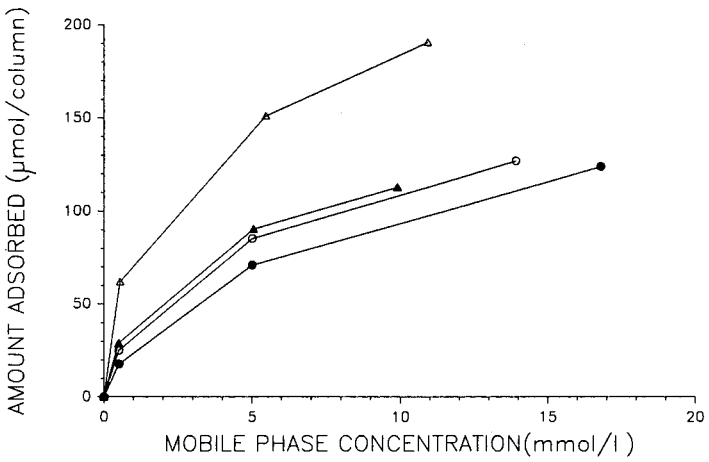

Fig. 3. Adsorption isotherms of (▲) 1-hexanol, (△) 1-heptanol and (●) *cis*- and (○) *trans*-3-hexen-1-ol on α-cyclodextrin–silica from pure water as carrier.

Once the adsorption isotherms are known, the actual displacement chromatographic separations can be designed. First, an 11.8 m*M* solution of 1-heptanol in water (saturated 1-heptanol solution) was tried as a displacer. The dispacement chromatogram of a sample containing 3 mg of the *cis* and 2.9 mg of the *trans* isomer is shown in Fig. 4. There are two steps and the plateau of the displacer in the chromatogram. Fractions of 300 μl were collected for further analysis. By analyzing the individual fractions, the reconstructed displacement chromatogram could be obtained. The reconstructed displacement chromatogram in Fig. 5 reveals that the first band is pure *cis* isomer and the second is pure *trans* isomer. When the yields corresponding to the 99% purity level are calculated they turn out to be 94.5% for the first component and 75.6% for the second. It is likely that, with smaller fraction sizes, an even higher yield could have been obtained, especially for the first component.

In order to obtain more concentrated fractions, a less steep displacer operational line has to be selected. However, as the displacer used in Fig. 4, 1-heptanol, is already at its saturation concentration, the less strongly adsorbed 1-hexanol has to be selected as the new displacer. An operational line 25% less steep than in Fig. 4 can be obtained by

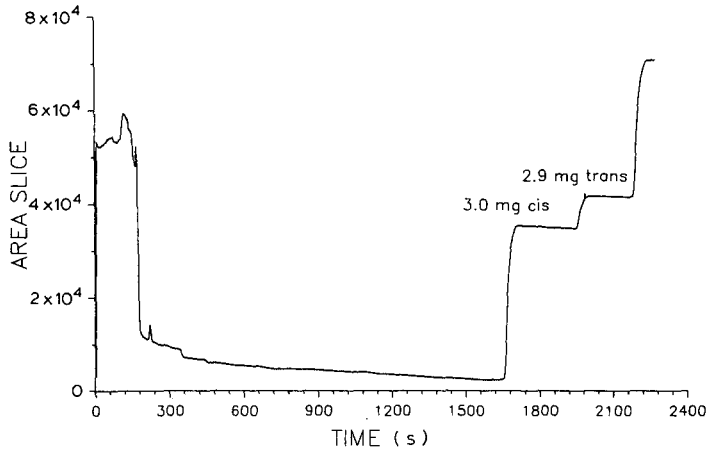

Fig. 4. Displacement chromatogram of a 6-mg sample of 3-hexen-1-ol on two 250 mm × 4.6 mm I.D. analytical α-cyclodextrin columns, with 11.9 m*M* 1-heptanol in pure water as displacer, at 1.0 ml/min and 30°C.

using 8.1 m*M* 1-hexanol solution as the displacer. The displacement chromatogram of 6 mg of a *cis–trans* isomer sample is shown in Fig. 6. There is a large elution-type peak at the beginning of the chromatogram, followed by three steps and the plateau of the displacer. The reconstructed displacement chromatogram derived from the analysis of the collected fraction is shown in Fig. 7. The first elution-type peak corresponds to pure *cis* isomer and so does the first plateau. The second plateau contains a mixture of the *cis* and *trans* isomers and their ratio is constant throughout the zone, indicating that the higher separation speed afforded by the new operational line cannot effect a complete separation of the same sample load that was well resolved in Fig. 4. The third plateau again contains the pure *trans* isomer.

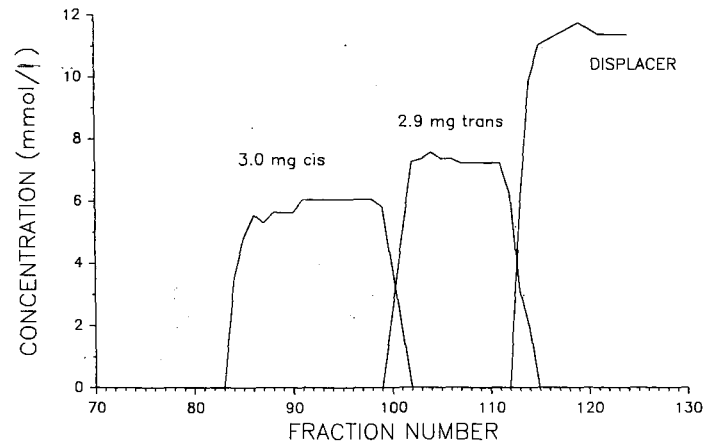

Fig. 5. Reconstructed displacement chromatogram of the separation shown in Fig. 4. Fraction size, 300 μl.

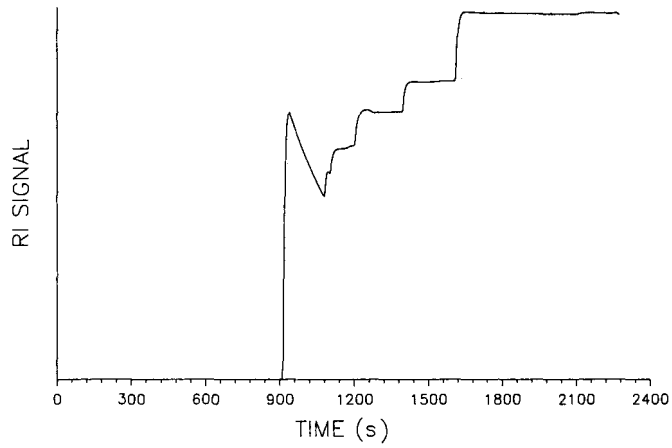

Fig. 6. Displacement chromatogram of a 6 mg sample of 3-hexen-1-ol on two 250 mm × 4.6 mm I.D. analytical α-cyclodextrin columns, with 8.1 m*M* 1-hexanol in pure water as displacer, at 1.0 ml/min and 30°C. RI = Refractive index.

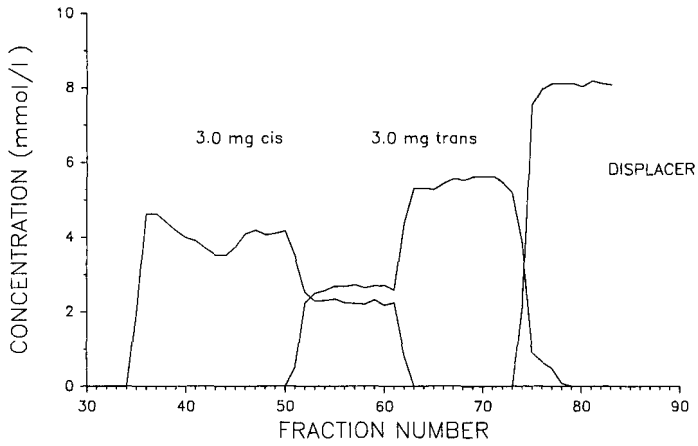

Fig. 7. Reconstructed displacement chromatogram of the separation shown in Fig. 6. Fraction size, 300 μl.

CONCLUSIONS

Based on elution-mode retention studies and adsorption isotherm measurements, a reversed-phase displacement chromatographic system has been developed for the separation of *cis*- and *trans*-3-hexen-1-ol. High purity and good yield could be achieved by using structurally related *n*-alkanols as displacers. The type and concentration of the displacer plays a major role in the success and quality of the displacement chromatographic separation.

ACKNOWLEDGEMENTS

Financial support by the Texas Coordination Board of Higher Education TATR Program (grant No. 3376) and the Minority Access for Research Careers, National Institute of Health program (grant No. 5F31GM11689) is acknowledged. The authors are grateful to Dr. Thomas Beesley of ASTEC for the cyclodextrin–silica samples.

REFERENCES

1 M. L. Bender and M. Komiyama, *Cyclodextrin Chemistry*, Springer, Berlin, 1978.
2 J. Szejtli, *Cyclodextrins and Their Inclusion Complexes*, Akademiai Kiado, Budapest, 1982.
3 J. Szejtli, B. Zsadon and T. Cserhati, in W. L. Hinze and D. W. Armstrong (Editor), *Ordered Media in Chemical Separations (ACS Symposium Series*, Vol. 342), American Chemical Society, Washington, DC, 1987, p. 200.
4 S. L. Abidi, *J. Chromatogr.*, 362 (1986) 33.
5 C. A. Chang, H. Abdel-Aziz, N. Melchor, Q. Wu, K. H. Pannell and D. W. Armstrong, *J. Chromatogr.*, 347 (1985) 51.
6 K. A. Connors and D. D. Pendergast, *J. Am. Chem. Soc.*, 106 (1984) 7607.
7 D. W. Armstrong, W. DeMonde, A. Alak, W. L. Hinze, T. E. Riehl and K. H. Bui, *Anal. Chem.*, 57 (1985) 234.
8 C. A. Chang, Q. Wu and D. W. Armstrong, *J. Chromatogr.*, 354 (1986) 454.
9 C. A. Chang, Q. Wu and L. Tan, *J. Chromatogr.*, 361 (1986) 199.
10 D. W. Armstrong, *J. Liq. Chromatogr.*, 7 (1984) 353.
11 T. J. Ward and D. W. Armstrong, *J. Liq. Chromatogr.*, 9 (1986) 407.
12 W. H. Pirkle, in S. Ahuja (Editor), *Chromatography and Separation Chemistry, Advances and Developments*, American Chemical Society, Washington, DC, 1986, p. 101.
13 D. W. Armstrong, *Anal. Chem.*, 59 (1987) 84A.
14 *Cyclobond Handbook*, Astec, Whippany, NJ, 1988.
15 B. G. Snider, *J. Chromatogr.*, 351 (1986) 548.
16 H. J. Issaq, J. H. McConnell, D. E. Weiss, D. G. Williams and J. E. Saavedra, *J. Liq. Chromatogr.*, 9 (1986) 1783.
17 H. J. Issaq, M. Glennon, D. E. Weiss, G. N. Chmurny, J. E. Saavedra, *J. Liq. Chromatogr.*, 9 (1986) 2763.
18 G. W. Tindall, *J. Liq. Chromatogr.*, 10 (1987) 1077.
19 R. D. Armstrong, T. J. Ward, N. Pattabiraman, C. Benz and D. W. Armstrong, *J. Chromatogr.*, 414 (1987) 192.
20 Gy. Vigh, G. Quintero and Gy. Farkas, *J. Chromatogr.*, 484 (1989) 237.
21 Cs. Horváth, A. Nahum and J. H. Frenz, *J. Chromatogr.*, 218 (1981) 365.
22 F. G. Hellferich and G. Klein, *Multicomponent Chromatography— Theory of Interference*, Marcel Dekker, New York, 1970.
23 Cs. Horváth and W. R. Melander, in E. Heftmann (Editor) *Chromatography, Part A: Fundamentals and Techniques (Journal of Chromatography Library*, Vol. 22A), Elsevier, Amsterdam, 1983, p. A27.
24 Cs. Horváth, in F. Bruner (Editor), *The Science of Chromatography, (Journal of Chromatography Libary*, Vol. 32), Elsevier, Amsterdam, 1985, p. 179.
25 Gy. Vigh, Z. Varga-Puchony, G. Szepesi and M. Gazdag, *J. Chromatogr.*, 386 (1986) 353.
26 G. Guiochon and A. Katti, *Chromatographia*, 24 (1987) 165.
27 S. M. Cramer and Cs. Horváth, *Prep. Chromatogr.*, 1 (1988) 29.
28 M. W. Phillips, G. Subramanian and S. M. Cramer, *J. Chromatogr.*, 454 (1988) 1.

Journal of Chromatography, 484 (1989) 259–265
Elsevier Science Publishers B.V., Amsterdam — Printed in The Netherlands

CHROM. 22 014

SOLID INJECTION, A NEW TECHNIQUE FOR APPLICATION OF INSOLUBLE SAMPLES IN PREPARATIVE LIQUID CHROMATOGRAPHY

LARRY MILLER*, HELGA BUSH and ELLEN M. DERRICO
G. D. Searle & Co., 4901 Searle Parkway, Skokie, IL 60077 (U.S.A.)

SUMMARY

A new technique for the application of insoluble samples in preparative liquid chromatography has been developed. This technique, solid injection, greatly reduces the time and inefficiencies associated with techniques previously developed for this problem. Examples of purifications accomplished with this technique are given for compounds of pharmaceutical interest.

INTRODUCTION

In preparative liquid chromatography one of the important steps in a purification is the application of the sample to the column. To obtain best results and to minimize potential problems the sample should be dissolved in a minimal volume of mobile phase[1]. Sometimes this is not possible due to extreme insolubility (< 10–100 mg/ml) of the sample in the mobile phase. Occasionally, this problem can be solved by dissolving the sample in a large volume of mobile phase, but this may reduce resolution and efficiency[2]. A stronger eluting solvent may also be used to increase solubility of the sample. This technique can be problematic and give undesired results[1]. Another way to apply insoluble samples to a preparative column involves pre-adsorbing the sample onto the stationary phase[3–6]. In this process, the sample is dissolved in any solvent, combined with stationary phase and the solvent evaporated producing a dry, powdered matrix of sample coated onto the stationary phase. The coated stationary phase is dry-packed into a column which is inserted in the preparative chromatography system prior to the main column. For this technique to work, it is important that all of the solvent is removed. A potential problem is the degradation of the sample during solvent removal. This process can give desirable results but is time consuming.

In this paper we will discuss a new technique we have developed for dealing with insoluble samples. This technique, which we have named solid injection, requires less time for sample preparation and eliminates any possibility of sample degradation during sample application. In addition, examples of purifications utilizing this technique will be described.

0021-9673/89/$03.50

EXPERIMENTAL

Equipment and materials

The large-scale preparative liquid chromatograph was either a Sep Tech Model ST/800A or ST/800C (Wakefield, RI, U.S.A.). The small-scale preparative liquid chromatography system was a modular system sold by Beckman (Berkeley, CA, U.S.A.). The preparative columns varied in size from 250 mm × 10 mm I.D. to 6 ft. × 6 in. I.D. and were obtained from a variety of sources. The bulk packings were ICN adsorbents 32–63 μm, 60 Å irregular silica gel from ICN Biomedicals (Cleveland, OH, U.S.A.), Merck silica gel 60, 40–63 μm, 60 Å irregular silica gel from EM Science (Cherry Hill, NJ, U.S.A.) or Partisil Prep 20 ODS-3 and Prep 40 ODS-3 from Whatman (Clifton, NJ, U.S.A.).

The analytical chromatograph consisted of a Waters Assoc. Model 590 solvent delivery system and a U6K injector or Waters Intelligent Sample Processor (Milford, MA, U.S.A.), a Kratos Model 783 variable-wavelength detector (Ramsey, NJ, U.S.A.), a Linear Model 585 recorder (Hackensack, NJ, U.S.A.), and a Digital Equipment Corporation VAX 11/785 computer with Searle chromatography data system.

All chemicals for purification were synthesized in the Chemical Development laboratories of G. D. Searle & Co. (Skokie, IL, U.S.A.). The solvents were reagent grade or better and obtained from a variety of sources.

Preparation of sample for solid injection

To achieve optimum results it is important that the chemical being purified is crushed to a fine powder. This is done to avoid slow dissolution of large particles. The crushed sample is thoroughly mixed with packing material to ensure homogeneity. The mixture is dry-packed into a sample column, and any remaining space is filled with packing material. As an alternative, packing material from the top of the main column can be removed and replaced with the packing and sample mixture. This is especially useful with axial compression columns.

The amount of packing to be mixed with the crushed sample is dependent on the relative solubility of the sample. For extremely insoluble samples (<5 mg/ml), between five and ten parts packing to one part sample is needed. This reduces the chance of crystallization of the chemical which could block the sample column. For samples with intermediate solubility (5 to 50 mg/ml), between two and five parts packing to one part sample should be sufficient.

RESULTS AND DISCUSSION

Solid injection is a technique which was developed to deal with the insoluble samples encountered during the purification of potential drug products. These samples become especially difficult to dissolve at the preparative loadings (50–100 mg sample per gram packing) used for these purifications. This technique is especially useful with samples exhibiting solubility of less than 100 mg/ml in the mobile phase. Solid injection has been used successfully with samples having solubilities of less than 1 mg/ml. It can be used with either silica gel, bonded normal-phase or bonded reversed-phase packings.

The column containing the packing and sample mixture should be inserted into the preparative system in a vertical position. This is necessary since a void will form in the column as the sample dissolves and enters the main column. If the column is in a horizontal position, a channel will form and most of the sample will never be dissolved. Initially, a lower flow-rate can be used to allow for efficient dissolution of the sample, although good results have been obtained using either a low or normal flow-rate of mobile phase.

To ensure that highly retained compounds enter the main column, the sample column should be kept in the preparative system throughout the run. Column switching has also been utilized to selectively dissolve and separate portions of a sample. For example, when purifying a sample containing early eluting impurities, the eluent from the sample column can be diverted to a collection vessel while these impurities dissolve and exit the sample column. Once they have been removed from the sample column, the eluent can be diverted to the main column. Conversely, with highly retained impurities, after the desired component of the mixture has dissolved and entered the main column, the sample column can be removed from the solvent stream.

If air is detrimental to the adsorbent bed in the main column, one can pump a known amount of solvent through the sample column so that the packing is wetted before connecting it to the main column. This should serve to displace a large percentage of the air present.

Examples

Purification of compound 1. Compound 1 (Fig. 1) needed to be purified to >99.5% for preparation of a highly pure standard. The only impurity present was compound 2 (Fig. 1) at *ca.* 1%. The analytical high-performance liquid chromatographic (HPLC) separation of compounds 1 and 2 is shown in Fig. 2. This method was scaled up for preparative purification. Sample preparation involved mixing the sample (88 g) with 200 g of packing. The sample was purified on 4900 g of Partisil Prep 40 ODS-3 (53 μm) at a loading of 18 mg sample per gram of packing. A mobile phase of acetonitrile–water (40:60, v/v) and a flow-rate of 800 ml/min was used. The results of this purification are summarized in Table I. Using this method we were able to isolate 88% of the available compound 1 at a purity of >99.8%. The amount of compound 2 was reduced from 1.05% to 0.15% during the purification.

Purification of compound 3. There were two objectives to be met during the purification of compound 3 (Fig. 3): (1) production of chemical (>99%) for a highly pure standard, and (2) enrichment of unknown impurities for further isolation and

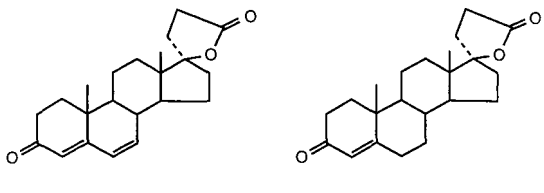

1 2

Fig. 1. Structure of compounds 1 and 2.

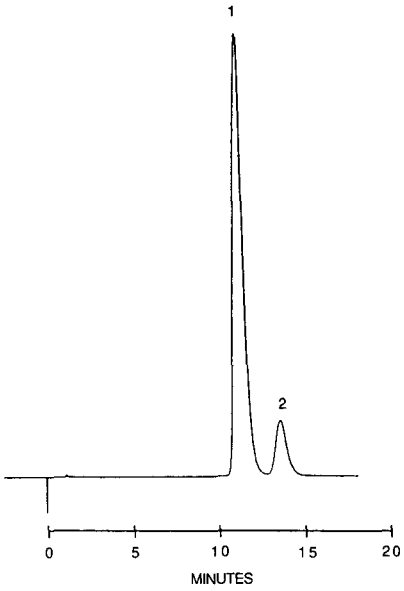

Fig. 2. Analytical HPLC separation of compounds 1 and 2. Analysis conducted on Partisil 10 ODS-3 (250 mm × 4.6 mm I.D.) with a mobile phase of acetonitrile–water (40:60). A flow-rate of 2 ml/min and detection at 254 nm, 0.1 a.u.f.s. was used. The sample shown was spiked with compound 2 for demonstration purposes and is not representative of the sample that was purified.

identification work. The analytical HPLC method and retention times of the desired components are summarized in Table II. Sample preparation for the preparative purification involved mixing the sample (94 g) with 700 g of Partisil Prep 40 ODS-3 (53 μm). The sample was purified on 4900 g of Partisil Prep 40 ODS-3 (53 μm) at a loading of 19 mg sample per gram of packing. A mobile phase of acetonitrile–water (50:50) and a flow-rate of 425 ml/min was used. The results of this purification are summarized in Table III. Although the main component eluted over a large volume, resulting in a long purification method, we were able to isolate 51% of the available compound 3 at a purity of >99.8%. In addition, another 23% of the chemical was

TABLE I

RESULTS OF PREPARATIVE PURIFICATION OF COMPOUND 1

Fraction	*k' (start)*[a]	*k' (end)*[b]	*Weight (g)*	*Compound 2 (%)*[c]	*Compound 1 (%)*[c]
S[d]	–	–	87.4	1.05	98.95
A	13	20	74.6	0.15	99.85
B	20	21	5.23	1.05	98.95
C	21	24	4.68	8.11	91.89

[a] Capacity factor for start of fraction.
[b] Capacity factor for end of fraction.
[c] HPLC area percent.
[d] Sample prior to purification.

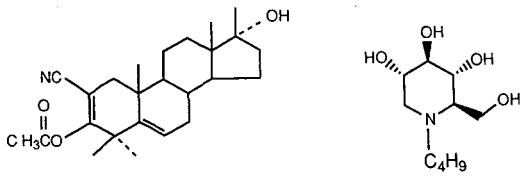

3 4

Fig. 3. Structure of compounds 3 and 4.

produced at a purity slightly less than 99%. The three impurities were greatly concentrated in the fractions not containing compound 3. This made the subsequent isolation of each of these three impurities (also done using solid injection) much less time consuming.

Purification of compound 4. Compound 4 (Fig. 3) needed to be purified to >99% for preparation of a highly pure standard. The purification method was scaled up from the thin-layer chromatography method described in Fig. 4. Sample preparation involved mixing the sample (14.6 g) with 74 g of Merck silica gel (40–63 μm). The sample was purified on 1000 g of silica gel at a loading of 14 mg sample per gram of packing. A step gradient of varying percentages of chloroform, methanol and ammonium hydroxide and a flow-rate of 500 ml/min were used. Thin-layer chromatographic analysis of the individual fractions from this purification is shown in Fig. 4. Using this method we were able to isolate 67% of the available chemical at a purity of >99.8%.

TABLE II

ANALYTICAL HPLC DATA FOR COMPOUND 3

HPLC conditions: Partisil 5 ODS-3 RAC II (100 mm × 4.6 mm I.D.); mobile phase, acetonitrile–water (60:40) adjusted to pH 3.0 with phosphoric acid; 2.0 ml/min; detection, 238 nm, 0.1 a.u.f.s.

Component	*Retention time (min)*	*HPLC area%*
Impurity 1	1.42	0.37
Compound 3	3.68	97.51
Impurity 2	4.85	0.36
Impurity 4	5.23	0.09

TABLE III

RESULTS OF PREPARATIVE PURIFICATION OF COMPOUND 3

Fraction	*k' (start)*	*k' (end)*	*Weight (g)*	*Purity (%)*[a]
S	–	–	98.4	97.51
A	21	22.5	22.1	98.42
B	22.5	31.5	49.2	99.86

[a] HPLC area%.

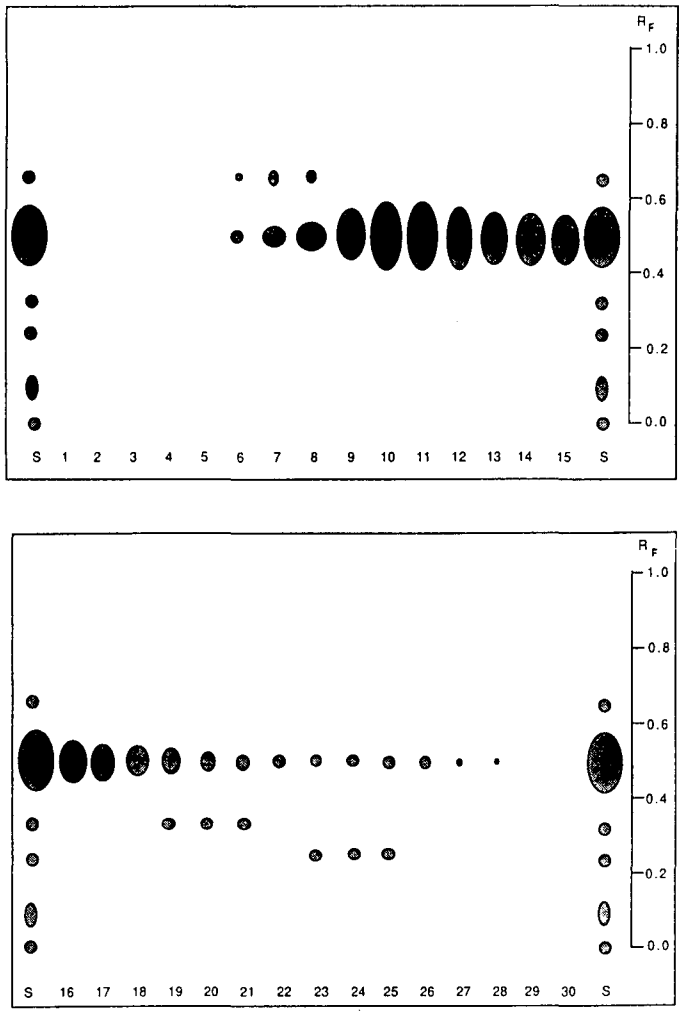

Fig. 4. Thin-layer chromatographic analysis of fractions from the preparative purification of compound 4. Solvent system, chloroform–methanol–ammonium hydroxide (40:58:2); detection, *tert.*-butyl hypochlorite–starch–potassium iodide; TLC adsorbent, Merck silica gel 60 F_{254}. S is sample prior to chromatography. Each fraction is one half of a column volume.

CONCLUSION

Since the development of this technique approximately four years ago, we have proven it to be extremely versatile and time saving. Good results have been obtained on more than fifty purifications using both silica gel and reversed-phase packing materials. Our purification objectives have always been met whenever we have used this solid injection technique. The compound types which have been used with this technique include steroids, di- and tripeptides, fatty acid derivatives, sugars, amino

sugars, quinolones, heterocyclics and prostaglandin precursors. This technique has proven useful for samples ranging from 0.1 g to 1900 g in weight. The majority of this work was done with low-molecular-weight (<600) compounds. Solid injection may also be useful with other types of compounds.

ACKNOWLEDGEMENTS

The authors wish to thank James Murphy, Kippert Welzel and Katie Wright for their technical support. The chemicals for purification were provided by chemists in the Synthesis Development Group at G. D. Searle & Co.

REFERENCES

1 P. D. McDonald and B. A. Bidlingmeyer, in B. A. Bidlingmeyer (Editor), *Preparative Liquid Chromatography*, Elsevier, Amsterdam, 1987, Ch. 1, p. 79.
2 M. Verzele and C. Dewaele, *Preparative High Performance Liquid Chromatography, A Practical Guideline*, TEC, Ghent, 1986, p. 119.
3 B. F. Bowden, J. C. Coll, S. J. Mitchell and G. J. Stokie, *Aust. J. Chem.*, 31 (1978) 1303.
4 D. E. Nettleton, Jr., *J. Liq. Chromatogr.*, 4 (Suppl. 1) (1981) 141.
5 J. Kriz, M. Brezina and I. Vodicka, *J. Chromatogr.*, 248 (1982) 303.
6 P. D. McDonald and B. A. Bidlingmeyer, in B. A. Bidlingmeyer (Editor), *Preparative Liquid Chromatography*, Elsevier, Amsterdam, 1987, Ch. 1, p. 80.

Journal of Chromatography, 484 (1989) 267–272
Elsevier Science Publishers B.V., Amsterdam — Printed in The Netherlands

CHROM. 21 801

PREPARATIVE PACKING UTILITY AS A FUNCTION OF PARTICLE SIZE

JOHN A. PERRY* and TED J. SZCZERBA
Regis Chemical Company, 8210 Austin Avenue, Morton Grove, IL 60053 (U.S.A.)

SUMMARY

The idea is still current, if not indeed prevalent, that more efficient packings overload more quickly than less efficient, and that therefore they are less useful in preparative liquid chromatography. In the light of new measurements made for this purpose, we have reassessed the terms such as overload, loadability, and dynamic capacity. These terms are self-referent, refer only to the ideal behavior of a given packing at zero load, and are not useful for comparing the relative preparative utilities of packings that differ merely in particle size. An "equal-cut-point" approach is proposed as a better method for this comparison.

Given an equal-cut-point approach, a 20-μm column is seen to be roughly 15 times more productive than an 80-μm column, roughly 4.5 times more productive than a 40-μm column, all of equal length. If the costs of the packings are taken into account, the 20-μm column is seen to be almost 10 times more valuable than an 80-μm column, that is, more productive per dollar paid for the packing; and about 3 times more valuable than a 40-μm column.

INTRODUCTION

Preparative liquid chromatography[1–6] continues to attract rapidly increasing interest. In the practice of preparative liquid chromatography (LC), among the more important parameters is the particle size of the preparative column. Although smaller particles produce more efficient columns at analytical loads, the use of smaller particles for preparative loads has been viewed skeptically on the grounds that smaller particles overload more quickly than larger. This view may have had its origin in a study by De Jong *et al.*[1], who in their conclusions reported finding "higher loadabilities ... for coarser particles".

Particle size was one of the parameters considered in a thorough review of and model for preparative LC methodology[7]. Combining this study with other recently preceding ones[8,9], Snyder *et al.*[10] proposed a comprehensive model to make it "possible to draw a number of general conclusions relating to optimum conditions for preparative HPLC". In the fourth and last of these conclusions, however, they stated, "... there is currently no single 'rule of thumb' to guide (the) choice (of particle size). ... the optimum particle size for any given case can best be determined only from a knowledge of the exact circumstances surrounding the separation"[10].

0021-9673/89/$03.50

As is proper in theory, each relevant parameter is varied over the full range of its pertinent continuum. However, most practitioners do not have the luxury of choosing the values of their parameters from a continuum in which, for instance, column length can take on any value. For most practitioners, parameter values refer not to a continuum but to components that can be purchased from catalogues. For many, preparative column length is 25 cm, perhaps extendable *in extremis* to 50 cm; and the range of available preparative pressures and flow-rates is set by the pumps at hand (and they, probably analytical). Our study refers to this limited laboratory in which a real question is, "In the preparative column I am about to order, what particle size should I specify?".

In this study, we have remeasured peak widths over a wide range of loadings, correlated the results, and rephrased the findings. We present here these findings from both the earlier, "overloading" point of view, and a new and simpler one that might be called, "equal-cut-point".

EXPERIMENTAL

Materials

For this study, dibutylphthalate (DBP), purchased from Aldrich (Milwaukee, WI, U.S.A.), was used as the solute. HPLC grade solvents were used throughout.

Columns and equipment

The four columns used were 25 cm × 4.6 mm I.D., and had been packed at Regis with irregular, 100-Å pore-diameter, ODS-bonded silica particles 10, 20, 40, and 80 μm in diameter.

Procedures

As mobile phase, methanol–water (80:20, v/v) was used at a flow-rate of 1.0 ml/min. Throughout, elution was isocratic. The amounts of DBP charged to each column in 50-μl volumes varied by a factor of over 7000, ranging from 2 to somewhat over 10 000 μg DBP/g of packing, specifically, 1.43, 14.3, 1430, 3570, 7140, 10 700, and 14 300.

Shown in Fig. 1 for each particle size is the variation of peak width (measured at half-height) as a function of solute loading.

RESULTS AND DISCUSSION

The term "overload" was early defined in gas chromatography as an increase in peak width 10% over that characteristic of zero load. One can also approach the problem by measuring the number of theoretical plates produced by a given column as a function of increasing load, then noting that load at which the number of theoretical plates decreases by a chosen fraction. If the loading is expressed in load/g of packing, one has the term, *specific loadability*[1]. We have been unable to find where the terms "capacity" and then "dynamic capacity" were introduced; here, for our isocratic elutions we use "specific dynamic capacity" to mean the load per gram of packing at which is observed a peak width 50% greater than that found at essentially zero load. All such terms express a certain increase in peak width caused by a corresponding

TABLE I

SPECIFIC DYNAMIC CAPACITY AS A FUNCTION OF PARTICLE DIAMETER

Particle diameter (μm)	*Specific dynamic capacity (μg DBP/g packing)*
10	2000
20	3400
40	5000
80	9600

increase in sample load, differ mutually only in degree, and are arbitrary in choice of degree of peak broadening.

In Table I, the *specific dynamic capacity* just defined is listed for each of the four particle sizes used. It can be seen that the specific dynamic capacity increases with increasing particle size, in agreement with the idea alluded to in the Introduction, that coarser particles show higher loadabilities. To show the relative magnitude of the increase, we can divide the capcities by the smallest one measured; the result is shown in Table II. The 80-μm particles show 4.8 times higher specific dynamic capacity, or loadability, than the 10-μm particles.

Nevertheless, we *are* talking about the chromatographic efficiencies of columns that differ mutually only in the sizes of the particle contained, and thus about the efficiencies of these particles. If the smaller particles are admittedly more efficient at loadings that approach zero, then if they overload more quickly, surely the curves must cross (an active concept: at the ASTM meeting in Baltimore, MD, U.S.A. as late as October 1988 and in the discussion following a paper on preparative LC, that the curves cross was given voice by a speaker). However, whether the curves cross can be seen in Fig. 1. Although theory may predict they would eventually coincide[1], the curves do not cross.

How is it, then, that as just shown in Tables I and II, more efficient packings *do* overload more quickly? It comes from entrapment in language. Terms such as overload, specific loadability, and dynamic capacity are self-referent, only; they refer to the ideal behavior of a given packing, its chromatographic efficiency at zero load. These terms are not useful for comparing the preparative utility of one packing with another that differs from the first only in particle size. A different approach is needed, one that actually compares such packings.

TABLE II

RELATIVE SPECIFIC DYNAMIC CAPACITIES

Particle diameter (μm)	*Restated dynamic capacity (μg DBP/g packing)*
10	Unit
20	1.7
40	2.5
80	4.8

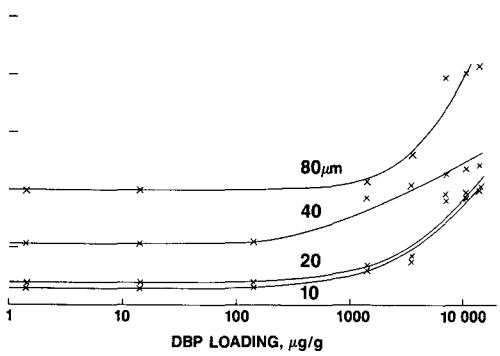

Fig. 1. Loading curves showing peak width as a function of sample loading for particles of diameters of 10, 20, 40 and 80 μm [Biochrom 100 Å (ODS)]. If a more efficient packing were to show a larger peak width for a given loading than a less efficient one, the curves would have to cross. Here the curves do not cross.

Let us suppose that we have two columns that differ only in the particle size of the packings. Let us set up our separation, cut points and all, on the column that contains the coarser particles. Then we replace the column with the coarser particles by the one with the finer particles. Now, using the larger charge required by the more efficient column to produce the peak width that corresponds to the cut points already established with the less efficient column, we repeat the separation. The operations with the two columns are shown in diagram in Fig. 2, wherein vertical lines indicate the cut points established with the coarser-particle column. In Fig. 2, the peaks are tracings from chromatograms produced for this paper; and the vertical lines indicate the loading corresponding to the specific dynamic capacity of the coarser-particle column. Let us call this the "equal-cut-point" approach.

Listed in Table III are the loadings determined by the two approaches: the specific dynamic capacity and the equal cut point. In Table IV are listed the

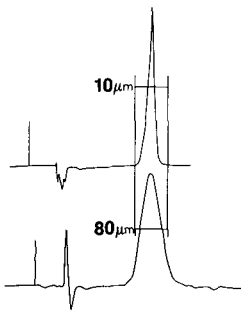

Fig. 2. Figure suggesting diagrammatically that a separation first be set up with a less efficient column that contains coarser particles, and then that the less efficient column be replaced by one that is more efficient. The vertical lines correspond to a 50% increase in peak width of the solute peak from the less efficient column. The vertical lines are taken as cut points. Let enough sample be charged to cause the peak from the more efficient column to have a width equal to those cut points. The data, obtainable from the loading curves in Fig. 1, listed in Table IV, show that under the conditions tested here, columns that contain 20-μm particles are more both productive and valuable than those that contain either 80- or 40-μm particles.

TABLE III
PREPARATIVE CAPACITY AS A FUNCTION OF METHOD OF EXPRESSION

Particle diameter (μm)	*Capacity (μg DBP/g packing)*	
	Specific dynamic	*Same cut point*
10	2000	23 000
20	3400	22 000
40	5000	5000
80	9600	1500

intra-column ratios of these loadings. The specific dynamic capacity ratios were shown earlier, in Table II. The equal-cut-point ratios show that, given the identical experimental operations, a 20-μm column is roughly 15 times more productive than an 80-μm column, roughly 4.5 times more productive than a 40-μm column. These measurements do not show much improvement in using 10-μm particles rather than 20-μm.

There is also the matter of packing costs. More efficient packings cost more. If we divide the ratios of Table IV by the costs of the respective packings, we produce ratios that express value. The value ratios (see Table V) show that a 20-μm column is almost 10 times more valuable than an 80-μm column, that is, more productive per dollar paid for the packing; and about 3 times more valuable than a 40-μm column. Again, the value ratios show no advantage in replacing a 20-μm column by a 10-μm.

TABLE IV
RELATIVE PACKING CAPACITIES

Particle diameter (μm)	*Capacity (μg DBP/g packing)*	
	Specific dynamic	*Same cut point*
10	Unit	15.3
20	1.7	14.7
40	2.5	3.3
80	4.8	Unit

TABLE V
RELATIVE PACKING VALUES

Particle diameter (μm)	*Value (capacity/dollar)*	
	Specific dynamic	*Same cut point*
10	Unit	4.1
20	4.1	9.5
40	8.7	3.1
80	18.	Unit

Note that the value ratios hold without regard to the cost or selling price of whatever product is being purified.

Pressure is simply not considered in the equal-cut-point approach, in which the packings to be compared are contained in columns of equal length. Columns, of course, need not be of equal length. In the Knox–Pyper review[7], pressures were held equal, columns could have any length and contain particles of any size. Performance (g/h of purified product) then does not depend on particle size. Consider these two points of view.

In columns of equal length and inner diameter, the pressure required for a given flow-rate and mobile phase varies inversely as the square of the particle diameter of the packing. Compared to the 80-μm column, the 20-μm column requires (80/20) squared times as much pressure per length: 16 times as much. Just let the 80-μm column be long enough to require that pressure, and it will do as well as the 20-μm. (Merely choose to use 16 80-μm columns or 4 40-μm and proportionately more pure solvent and column hardware, rather than one 20-μm.) In actual practice, the more efficient packing, easily accommodated by the pressure capabilities of current equipment, is the one of choice.

REFERENCES

1 A. W. J. de Jong, H. Poppe and J. C. Kraak, *J. Chromatogr.*, 209 (1981) 432–436.
2 A. W. J. de Jong, J. C. Kraak, H. Poppe and F. Nooitgedacht, *J. Chromatogr.*, 193 (1980) 181–195.
3 K. P. Hupe and H. H. Lauer, *J. Chromatogr.*, 203 (1981) 41–52.
4 G. Cretier and J. L. Rocca, *Chromatographia*, 16 (1982) 32–38.
5 R. W. Stout, J. J. de Stefano and L. R. Snyder, *J. Chromatogr.*, 261 (1983) 189–212.
6 M. Verzele and C. Dewaele, *LC · GC*, 3 (1985) 22–28.
7 J. H. Knox and H. M. Pyper, *J. Chromatogr.*, 363 (1986) 1–30.
8 J. E. Eble, R. L. Grob, P. E. Antle, G. B. Cox and L. R. Snyder, *J. Chromatogr.*, 405 (1987) 82–96.
9 A. Jaulmes, C. Vidal-Madjar, H. Colin and G. Guiochon, *J. Phys. Chem.*, 90 (1986) 207.
10 L. R. Snyder, G. B. Cox and P. E. Antle, *Chromatographia*, 24 (1987) 82–96.

Journal of Chromatography, 484 (1989) 273–291
Elsevier Science Publishers B.V., Amsterdam — Printed in The Netherlands

CHROM. 22 061

PREPARATION AND EVALUATION OF A POLYMER-COATED ZIRCONIA REVERSED-PHASE CHROMATOGRAPHIC SUPPORT

M. P. RIGNEY*[a], T. P. WEBER and P. W. CARR
Department of Chemistry, University of Minnesota, 207 Pleasant St. S.E., Minneapolis, MN 55455 (U.S.A.)

SUMMARY

The preparation of a reversed-phase high-performance liquid chromatographic support by deposition and cross-linking of polybutadiene on the surface of microporous zirconia is described. It is demonstrated that acidic solutes undergo very strong interactions with the zirconia surface even in the presence of a thick polymer layer. These interactions can be minimized by the use of phosphate in the mobile phase, in which case the small solute retention characteristics of the polymer coated zirconia are comparable to alkylsilane-derivatized silica-based reversed-phase supports. Most importantly, the polymer-coated zirconia was stable in alkaline solution. There was no evidence for degradation of the support even when it was exposed to a mobile phase of 1 *M* sodium hydroxide at 100°C. In contrast, polybutadiene-coated alumina was not stable under these conditions.

INTRODUCTION

Reversed-phase high-performance liquid chromatography (RP-HPLC) is the most common mode of HPLC for many reasons, including its applicability to the separation of solutes of very different polarity, molecular weight and chemical functionality. Another important factor in the widespread use of RP-HPLC is the convenience, versatility and high efficiency of silica-based, microparticulate, bonded-phase chromatographic supports. The popularity of silica as a chromatographic support results from the cumulative impact of its excellent mechanical strength, availability in a wide range of pore sizes, nearly ideal pore structure (and concomitant mass transfer properties) and the great versatility of silanization chemistry for altering the chemical properties of its surface. However, silica gel and derivatized bonded phases also have significant limitations, most notably their solubility in aqueous alkaline media and lack of tolerance to harsh treatments both chemical and thermal. The dissolution of silica in aqueous mobile phases is widely recognized and has been extensively documented[1–6]. The stability of silica-based bonded-phase supports is also limited in acidic mobile phases due to acid-catalyzed hydrolysis of the siloxane bonds (Si–O–Si) that anchor the bonded-phase to the silica surface[7–9]. As an example of their lack of

[a] Present address: Ecolab, Inc., Ecolab Center, St. Paul, MN 55102, U.S.A.

0021-9673/89/$03.50

robustness, routine sanitization measures used extensively in biochemistry, such as cleaning with hot alkali, cannot be applied to silica-based columns. The inherent instability of silica-based supports is a particularly significant limitation for preparative-scale work. The need for extreme stability, chemical and otherwise, in preparative-scale columns is inherent in the high cost of the columns and the expense involved in developing large scale separations. Clearly it is very desirable in preparative-scale work to be able to rejuvenate contaminated columns. This often requires the use of very harsh reagents and conditions which can damage silica-based columns.

Although the great majority of work in RP-HPLC has been done using modified silica, a variety of other support materials have been investigated in an effort to develop alternatives to silica and silane chemistry to circumvent the above mentioned limitations. Among these are rigid and semi-rigid organic polymer supports[10–12], graphitized carbon[13–15], and modified alumina[16–22].

Although hydrous zirconia and zirconium phosphate have been used as ion-exchange supports, there has been only one report on the use of spherical, microparticulate zirconia as a reversed-phase chromatographic support[23]. This work involved use of a low-surface-area zirconia (9 m^2/g even after hydrothermal treatment) that was dynamically modified with a hydrophobic quaternary amine. No attempt was made to characterize the chromatographic properties of the zirconia nor to develop a permanent means of surface modification. A reversed-phase zirconia support has also been preparated by direct precipitation of an organophosphate or organophosphonate with zirconium(IV)[24–26]. This latter approach was used to prepare layered crystalline reversed-phase chromatographic supports of the formula $Zr(O_3POR)_2$, where R = butyl, lauryl, octylphenyl or octadecyl[27,28]. Although these materials had reversed-phase characteristics, attempts to use particle sizes of less than 180 μm led to bed compaction and excessive back-pressures[25].

We have previously described the properties and alkaline stability of porous microparticulate zirconia[29]. The goal of the present work was to produce a polymer-coated zirconia reversed-phase material with alkaline stability comparable to that of the unmodified zirconia.

EXPERIMENTAL

Chromatographic supports

A variety of samples of porous zirconia were used during the course of this work. The identity and physical properties of these materials were described previously[29]. A 15 cm × 0.46 cm I.D. column packed with γ-RP1 polybutadiene-coated alumina was obtained from ES Industries (Marlton, NJ, U.S.A.). A sample of 5-μm Spherisorb 5AY alumina (Phase Separations, Norwalk, CT, U.S.A.) was also used.

Chemicals

All reagents used were obtained from commercial sources and were reagent grade or better, unless noted below. Polybutadiene (PBD), molecular weight 4500, 45% vinyl was obtained from Aldrich (Milwaukee, WI, U.S.A.). Polybutadiene standards of molecular weight 439, 982, 2760 and 22 000 were obtained from Polysciences (Warrington, PA, U.S.A.). Dicumyl peroxide (DCP) was obtained from Alfa (Danvers, MA, U.S.A.). Methanol, 2-propanol, acetonitrile and tetrahydrofuran (THF)

were CHROMAR grade obtained from Mallinckrodt (St. Louis, MO, U.S.A.). The water used in all experiments was from a Barnstead Nano-Pure system with a "Organic-Free" final cartridge. All chromatographic mobile phases were filtered through 0.45- or 0.22-μm filters prior to use. Water for use in the preparation of high pH mobile phases was boiled prior to use to remove carbon dioxide.

Apparatus

The chromatographic apparatus, column hardware and column packing procedures were described previously[29].

Modification procedure

The modification procedure used was based on that of Schomburg and coworkers[30,31]. In all cases, the support was boiled in carbon dioxide-free water to fully hydrate the surface, dried at 125°C under vacuum for 12 h and cooled in a desiccator over P_2O_5 prior to modification. Four different modification procedures were used and are described below.

Procedure A. Zirconia with a high carbon load was prepared by adding 50 ml of pentane containing 0.55 g of PBD to 3.5 g of the support. The slurry was then placed in an ultrasonic bath and a vacuum applied for approximately 5 min. DCP (0.01 g) was added and the slurry again placed in an ultrasonic bath and a vacuum applied. The pentane was removed by vacuum (aspirator) and the material dried at 70°C *in vacuo* for 12 h. The coated support was heated in a tube furnace at 200°C for 2 h with a constant nitrogen purge. After removing the coated/cross-linked support from the tube furnace and allowing it to cool, it was washed successively with 200 ml of pentane, toluene, methylene chloride, THF, methanol and methanol–water (50:50).

Procedure B. Zirconia with a low carbon load was prepared by adding 35 ml of pentane containing 0.09 g of PBD to 3.5 g of the support. The slurry was then placed in an ultrasonic bath and a vacuum applied for approximately 5 min. A 10-ml volume of pentane containing 0.002 g of DCP was added and the slurry again placed in an ultrasonic bath and a vacuum applied. The slurry was then placed in a shaker bath at room temperature for 1 h after which the supernatant was removed by filtration. The material was heated in a tube furnace at 200°C for 4 h under nitrogen, washed as described in Procedure A and dried at 70°C for 12 h.

Procedure C. Zirconia with an intermediate carbon load was prepared by adding 50 ml of pentane containing 0.27 g of PBD to 3.0 g of the support. The slurry was then placed in an ultrasonic bath and a vacuum applied for approximately 5 min. A 10-ml volume of pentane containing 5.2 mg of DCP was added. The methodology of Procedure A was then followed.

Procedure D. A 20-ml volume of pentane containing 0.2 g of PBD was added to 3.5 g of support. The slurry was placed in an ultrasonic bath and a vacuum applied for approximately 5 min. The pentane was removed by an aspirator and the material dried at 70°C *in vacuo* for 12 h. The PBD was cross-linked by irradiation with an ESI Research accelerated-electron beam at a dosage of 5 Mrad at 175 kV by the Process Research Laboratory of the 3M Company (St. Paul, MN, U.S.A.). The cross-linked PBD-coated support was then washed as described in Procedure A.

Stability tests

The stability of the modified supports was determined by monitoring the retention of a set of non-polar test solutes with time in a mobile phase of methanol–0.1 *M* sodium hydroxide (50:50) at a temperature of 50°C. The columns used were 5 cm × 0.46 cm I.D. and were packed as described previously[29]. A 5 cm × 0.46 cm I.D. column was also packed with PBD-coated alumina obtained by unpacking a 15 cm × 0.46 cm I.D. ES Industries γRP-1 column.

The stability of zirconia–PBD and alumina–PBD in 1 *M* sodium hydroxide at 100°C was determined as described previously[29].

Chromatographic evaluation

Retention data were obtained at a flow-rate of 1 ml/min and a column temperature of 40°C unless otherwise noted. The system dead volume used in the calculation of capacity factors was determined by injection of ^2H_2O, or by the method of Knox[32]. Volumes of 2, 5 or 10 μl of a 1 m*M* solute solution were injected.

Static phosphate adsorption

A 10-ml volume of 10 m*M* phosphoric acid was added to 0.1 g of support and the mixture ultrasonicated under vacuum for 20 min. After 12–24 h, an aliquot of the supernatant was withdrawn, filtered through a 0.45-μm filter and the phosphorous content determined by inductively coupled plasma emission spectrometry (ICP-ES). The amount of phosphate adsorbed was determined from the difference in this measurement and that of a phosphoric acid blank.

RESULTS AND DISCUSSION

Initial attempts to produce a zirconia-based reversed-phase were made by modifying the surface by reaction with organosilanes under a wide variety of conditions. Although reversed-phase supports of moderate coverages were obtained, silanized zirconia was not stable in aqueous mobile phases due to the susceptibility of the Zr–O–Si bond to hydrolysis. This instability is not surprising given the instability of Si–O–Si bonds and the fact that the replacement of a silicon atom in a siloxane bond by a heteroatom in general produces M–O–Si bonds which are less stable than the Si–O–Si bond[33].

Other attempts were made to produce monomeric zirconia-based reversed phases by reaction of zirconia with organizirconium compounds and by adsorption of organophosphonates, however, in all cases the resulting phases were not stable in alkaline media.

Preparation of polymer-coated zirconia

Stable zirconia-based reversed phases were prepared by depositing and cross-linking polymers on the zirconia surface. In addition to stability, another advantage of polymer-coated reversed phases is the ability to prepare materials with widely varying carbon loads, irrespective of the population of reactive sites on the surface or the stability of bonds to the surface. As shown by the data in Table I, the amount of carbon on the support surface is easily varied over an order of magnitude by adjusting the amount of polybutadiene offered to the support. It is important to take into

TABLE I

COATING OF ZIRCONIA WITH POLYBUTADIENE

%PBD[a]	Preparation method[b]	%C[c]	d_f[d]
0.88	C	1.2	0.22
2.7	C	2.1	0.39
2.9	B	0.84	0.19
4.0	B	2.9	0.60
5.0	D	2.3	0.43
5.0	C	4.6	0.85
5.0	C	4.5	0.83
5.0	C	4.3	0.79
15.7	A	7.7	1.7
15.7	A	7.5	1.7

[a] %PBD = %PBD (w/w) in solution, with respect to weight of zirconia.

[b] For details, see Experimental section.

[c] %C = %carbon (w/w) on coated support as determined by conventional C,H,N analysis.

[d] d_f = film thickness (nm), as determined from zirconia surface area and amount of immobilized PBD (assumes no change in PBD density as a result of immobilization and cross-linking).

account the surface area of the zirconia supports when considering the carbon analysis data in Table I. When normalized to the support surface area, these data cover a range which includes "typical" carbon loads of commercial silylated SiO_2 reversed-phase supports. Note that under the conditions given above the modification process is reproducible as reflected by the agreement among the carbon analysis data obtained on different supports prepared from the same lot of zirconia with the same amount of polybutadiene.

Clearly, the carbon load (or film thickness) of the coated supports increases upon increasing the amount of PBD added to zirconia, although this increase is not linear with the amount of PBD offered, as shown in Fig. 1. This is not surprising since results of static adsorption experiments indicate that approximately 30 mg PBD/g zirconia represents monolayer coverage on a zirconia support with 50 m^2/g of surface

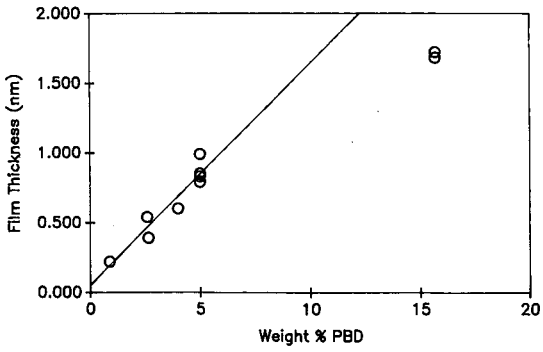

Fig. 1. Variation of PBD film thickness with %PBD. Zirconia–PBD prepared according to procedures A and C. Weight% PBD and film thickness have the same meaning as in Table I.

area. When the PBD coverage exceeds a monolayer, it is likely that washing with pentane prior to cross-linking removes a greater fraction of the PBD deposited on the zirconia surface than it does when coverages are lower. It is also quite possible that geometric considerations dictate less effective cross-linking as coverage exceeds a monolayer. Both of these factors lead to lower immobilization "efficiency" with increasing amounts of applied PBD.

It is, of course, unavoidable that as the amount of polymer on the surface is increased, there will be a concomitant decrease in the surface area of the support as the thickness of the polymer layer reduces the effective mean pore diameter of the support. This loss in surface area with increasing polymer film thickness is demonstrated by the data of Table II. This phenomenon is not limited to polymer-coated supports; it is well documented for silylated supports[30]. When zirconia–PBD was prepared as described in Procedure A, almost all of the surface area was lost. Microscopic inspection of the support particles showed a very irregular outer surface and a high degree of particle aggregation. By contrast, at carbon loads approximating monolayer coverage the loss in surface area is comparable to that encountered in silanization of silica with octadecylsilane. There is no evidence of an irregular polymer layer or particle aggregation.

As noted in the experimental section, the PBD cross-linking reaction was initiated by either a chemically generated free radical, or via electron-beam irradiation of the coated sample in the absence of a chemical initiator. The extent of cross-linking, as well as the course of the cross-linking reaction, was followed by monitoring the C=C stretching band at approximately 1640 cm^{-1} in the infra-red spectrum. Fig. 2 shows diffuse reflectance infrared Fourier transform (DRIFT) spectra of a sample cross-linked with DCP at avarious exposure times at 200°C. A 60% decrease in absorbance at 1640 cm^{-1} occurs during the first hour of treatment at 200°C and after 21.5 h the absorbance is decreased by more than 90%. We do not believe that this extremely low apparent degree of unsaturation is due solely to a high cross-linking efficiency, rather we think that some oxidative degradation may occur in addition to the cross-linking reaction. A spectrum of the sample cross-linked by irradiation with a high energy electron beam is shown in Fig. 3. The extent of cross-linking is comparable to that achieved with DCP-initiated cross-linking.

Column efficiency

One of the potential limitations of polymer-coated chromatographic supports is

TABLE II

VARIATION IN SURFACE AREA OF POLYBUTADIENE-COATED ZIRCONIA

%C[a]	Preparation method[b]	d_f[a]	SA_b[c]	SA_a[d]
2.9	B	0.19	50.4	38.9
5.0	C	0.85	60.6	29.3
7.7	A	1.7	50.4	4.0

[a] As defined in Table I.
[b] For details, see Experimental section.
[c] SA_b = surface area of zirconia before immobilization of PBD.
[d] SA_a = surface area of PBD-coated zirconia.

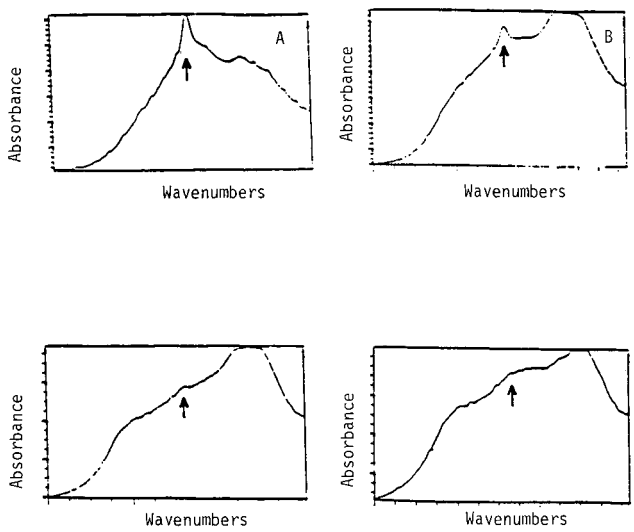

Fig. 2. DRIFT spectra of zirconia coated with 50 mg/g of PBD. A = 0 h at 200°C; B = 1 h at 200°C; C = 4 h at 200°C; D = 21.5 h at 200°C. C=C stretching bands at 1640 cm^{-1} are indicated by the arrows.

a loss in chromatographic efficiency that may result from restricted mass transfer of solutes in a polymer layer. We investigated the extent of this problem by determining the efficiency of supports coated with varying amounts of PBD. Plots of plate height, *h*, *vs.* linear velocity, *u*, for PBD–zirconia with two different PBD film thicknesses are shown in Fig. 4. Note that varying the film thickness by a factor of approximately three has an observable effect on the efficiency of the chromatographic support. This effect is evidenced by the fact that the support with a 0.43-μm PBD film reaches its minimum *h* of 2.9 at a mobile phase velocity of about 0.042 cm/s, whereas the support

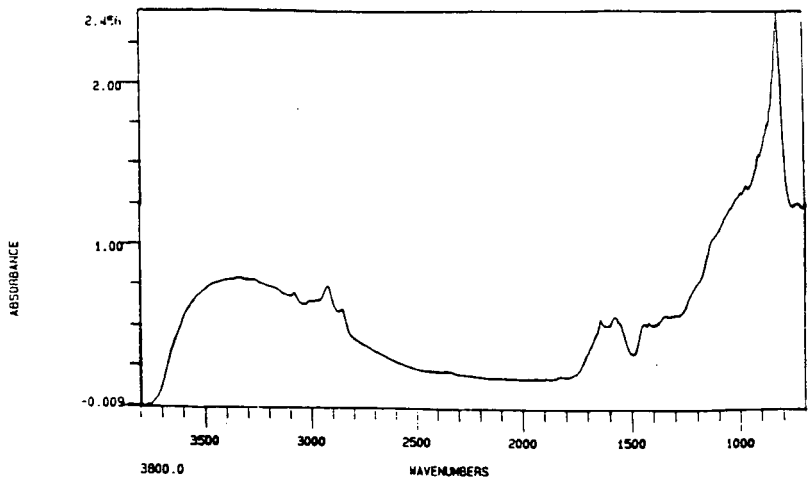

Fig. 3. DRIFT spectrum of zirconia coated with 50 mg/g PBD and crosslinked by high energy electron beam. Dosage = 5 Mrad at 175 kV.

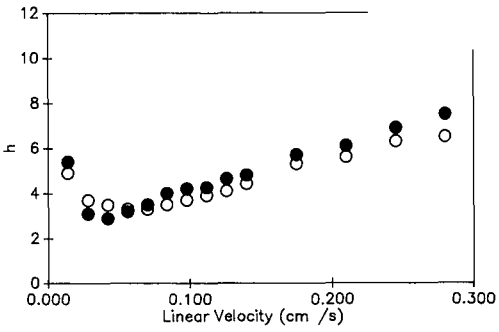

Fig. 4. Efficiency of PBD-coated zirconia. Solute octanophenone. Mobile phase methanol–water (60:40) Column temperature 25°C. PBD film thickness: ○ = 0.15 nm; ● = 0.43 nm.

with a 0.15-μm PBD film reaches its minimum h of 3.3 at a mobile phase velocity of 0.056–0.07 cm/s. Both of these effects would result if restricted mass transfer in the polymer film was a significant factor in determining the chromatographic efficiency. The smaller h_{opt} exhibited by the support with the 0.43-μm film is not consistent with this conclusion, however, this data was obtained on a lot of zirconia with a fairly broad particle size distribution and a high level of very small (<2 μm) particles such that the column beds were rather unstable. It is likely that the poorer optimum efficiency exhibited by the support with the 0.15-μm film is a consequence of the geometry of the packing bed and not related to the film thickness. Despite evidence of the adverse effect of the polymer layer on efficiency, it should be recognized that these supports do have an h_{opt} of about 3. Columns packed from lots of zirconia with a narrower particle size distribution routinely have h_{opt} of less than 3.

Stability of modified zirconia

The results of stability testing on PBD-coated supports prepared as described in Procedures A–D, and on a PBD-coated alumina support are shown in Fig. 5. For all of the zirconia–PBD columns there was an initial 2–5% decrease in the retention of ethylbenzene after which there was no further decrease. In the case of the alumina–PBD column, the stability test was terminated after 8000 column volumes of methanol–0.1 *M* sodium hydroxide (50:50) were passed through the column due to the appearance of double peaks and a 20% increase in column pressure. The alumina column was disassembled and the column bed examined. A void of approximately 2–3 mm had formed at the head of the column, and there was obvious channelling along the walls of the column. When the PBD-coated alumina column was unpacked, aggregated particles of diameter greater than 44 μm were observed. None of the zirconia columns exhibited any voids, nor any other indication of instability upon exposure to 30 000 column volumes of the alkaline mobile phase.

The data in Table III show that the carbon content of the supports decreased after treatment at high pH. Note that the carbon content of the aggregated >44-μm alumina–PBD particles was approximately 15% higher than that of the 5-μm alumina–PBD. Coupled with the results of the chromatographic evaluation, the carbon analysis indicates a loss of uncross-linked or partially cross-linked polymer in the initial stages of the stability test despite the preliminary washing. Sample C was

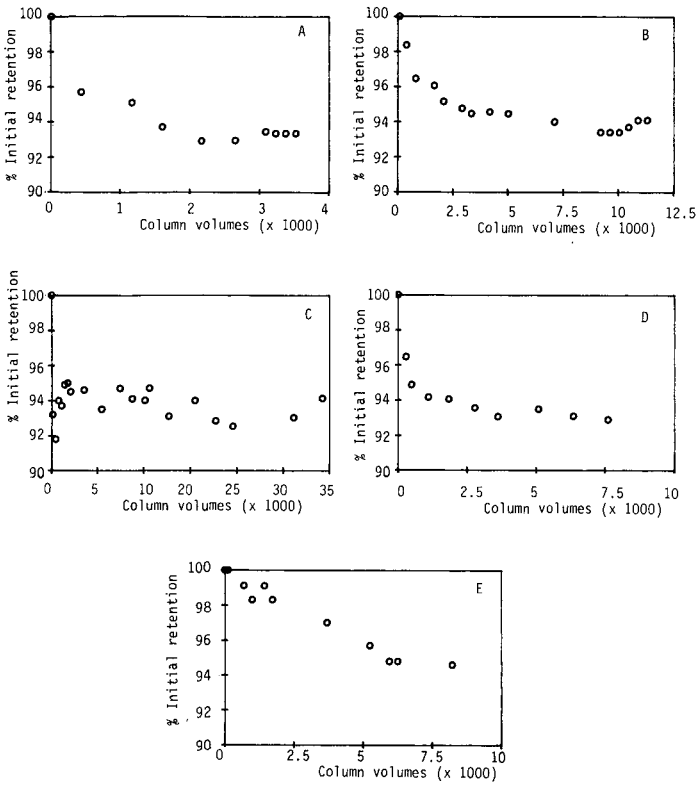

Fig. 5. Chromatographic evaluation of the alkaline stability of PBD-coated supports. A = zirconia–PBD prepared by Procedure A; B = zirconia–PBD prepared by Procedure B; C = zirconia–PBD prepared by Procedure C; D = zirconia–PBD prepared by Procedure D; E = Al_2O_3–PBD.

TABLE III

CARBON CONTENT OF POLYBUTADIENE-COATED SUPPORTS BEFORE AND AFTER TREATMENT WITH AN ALKALINE ELUENT

Sample	$\%C_b$ [a]	$\%C_a$ [b]
A	7.7	6.7
B	0.8	0.6
C	2.5	2.1
D	2.3	1.7
Al_2O_3	3.8	3.0
Al_2O_3 >44 μm		3.5

[a] Carbon content of support as determined by conventional C, H, N analysis.

[b] Carbon content of support after exposure to methanol–0.1 *M* sodiumhydroxide (50:50) at a flow-rate of 1 ml/min and a column temperature of 50°C. Volume of mobile phase passed through each column is shown in Fig. 5.

Soxhlet extracted with toluene for 24 h prior to testing its stability in an attempt to remove partially cross-linked oligomers, but this treatment had no apparent effect on the initial decrease in retention, nor on the loss of carbon.

A third measure of stability was to assay the column effluent for zirconium by ICP-ES. This evaluation was carried out for samples C and D in Table III. Zirconium was absent at the level of detectability of 0.03 μg/ml. Even if zirconium was present at the detection limit, this corresponds to a cumulative loss of less than 0.001% of the mass of zirconium originally present in the column. No determination of aluminum in the effluent of the PBD-coated alumina column was made, however, the peak dou-

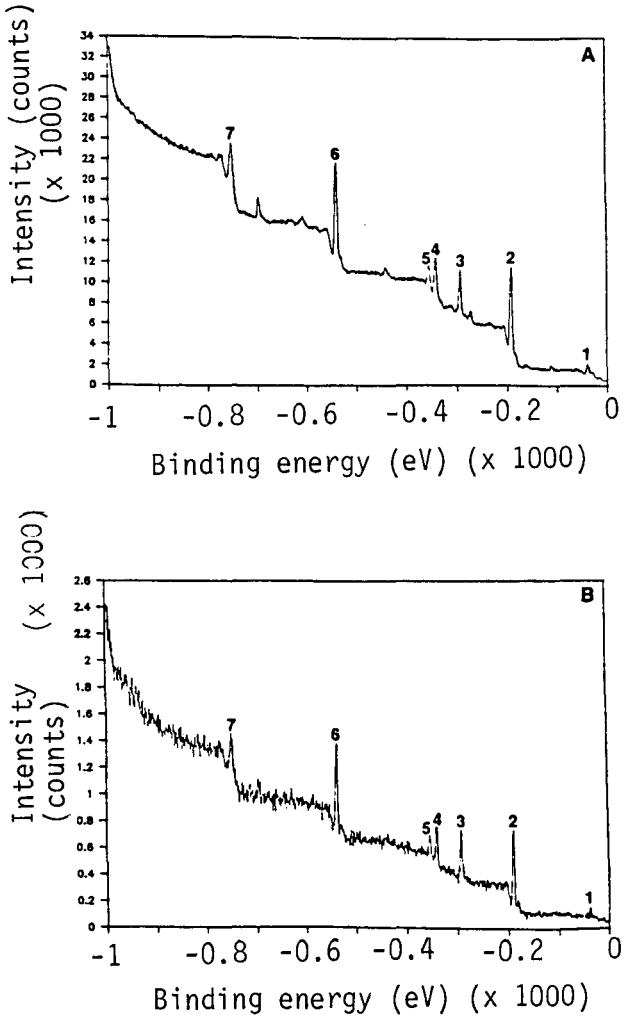

Fig. 6. ESCA spectra of zirconia–PBD. A = Spectrum of sample A before alkaline stability test; B = spectrum of sample A after 30 000 column volumes of methanol–0.1 *M* sodium hydroxide (50:50). Column temperature 50°C. Peaks: 1 = Zr 4p; 2 = Zr 3d; 3 = C ls; 4 = Zr 3p 5/2; 5 = Zr 3p 1/2; 6 = O ls; 7 = O Auger.

bling, increased column pressure and presence of a substantial void at the head of the column after the stability test all indicated that alumina dissolved during the course of the experiment.

Electron spectroscopy for chemical analysis (ESCA) spectra of a sample of zirconia–PBD before and after the stability test described above are shown in Fig. 6. Once again, there is no evidence for any gross changes in the zirconia–PBD after treatment at extreme pH.

In addition to the stability test described above, the stability of zirconia–PBD and alumina–PBD prepared by procedure C was evaluated by exposing columns packed with these supports to a mobile phase of 1 *M* sodium hydroxide at 100°C. The results of ICP analysis of the column effluents are given in Table IV. No zirconium was found in the column effluent. In contrast, it is obvious from the data in Table IV that alumina dissolves to a significant extent during the first hour of exposure to these conditions. In fact, after 3.25 h of exposure the amount of aluminum found in the effluent corresponded to loss of more than 10% of the alumina originally present in the column. The dissolution of alumina was confirmed by visual inspection of the column, which revealed a void of several mm as well as channeling along the column walls. Initially, it was surprising that the dissolution of such a large amount of alumina was not accompanied by a collapse of the column bed, but the alumina has a relatively low porosity (*ca.* 50%) so that a large amount of alumina would have to dissolve before the column bed would collapse.

The retention of a reversed-phase test probe, ethyl benzene, actually increased by approximately 15% on both columns after this treatment. Although this increase in retention is not understood, it does point out that, unlike a conventional monomeric bonded phase column in which dissolution of the inorganic support must be accompanied by loss of bonded phase, dissolution of the support of a polymer-coated column does not necessarily result in loss of stationary phase. Given the high degree of cross-linking of the polymer coating and its insolubility in typical reversed-phase eluents, it is likely that the polymer would remain in the column even as the inorganic column bed dissolves. This is a possible explanation for the existence of the large (aggregated >44 μm) particles in the alumina column after exposure to alkaline conditions. Exposure to alkaline conditions causes dissolution of alumina particularly from the more accessible outer surface of a bead. The relative amount of PBD on

TABLE IV

EXPOSURE OF POLYBUTADIENE-COATED SUPPORTS TO 'STERILIZING' CONDITIONS

Column	*Time (h)*[c]	*Al* (μg/ml)[a]	*Si* (μg/ml)[a]	*Zr* (μg/ml)[a]
Al_2O_3–PBD	1	680	13.6	–[b]
	3.25	243	3.3	–[b]
Zirconia–PBD	1	–[b]	1.6	–[b]
	3.25	–[b]	2.1	–[b]
Zirconia, unmodified	1	–[b]	2.4	–[b]
Blank (1 *M* NaOH)		–[b]	1.5	–[b]

[a] μg/ml in column effluent as determined by ICP-ES.

[b] Less than the detection limit by ICP-ES.

[c] Time of exposure to 1 *M* NaOH at a flow-rate of 1 ml/min; T = 100°C.

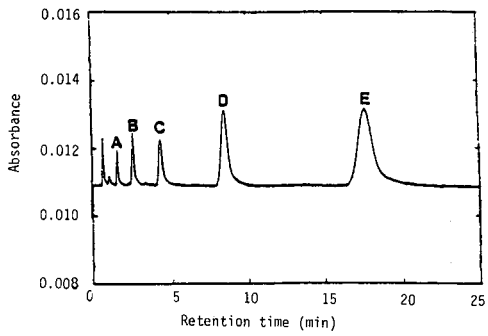

Fig. 7. Separation of alkyl aryl ketones on zirconia–PBD. Column = 5 cm × 0.46 cm I.D. packed with 3.5-μm zirconia with 0.39 nm PBD film. Column temperature 25°C. Mobile phase methanol–water (50:50). Flow-rate 1 ml/min. Peaks: A = propanophenone; B = butanophenone; C = pentanophenone; D = hexanophenone; E = heptanophenone.

the outer surface will thereby increase and particle aggregation occurs. This conclusion is supported by the high carbon content of these aggregates relative to the 5-μm particles recovered from the column as well as by the fact that a significant loss in reversed-phase retention is not observed despite the dissolution of a substantial amount of alumina.

The results described above strongly suggest that a meaningful evaluation of the alkaline stability of an inorganic-based polymer-coated chromatographic support must be based not only on the retention of non-polar test solutes, but also on analysis of the effluent for dissolved support.

Retention characteristics

A typical separation of several alkyl aryl ketones on a zirconia–PBD support is shown in Fig. 7. As expected for a reversed-phase support, the solutes elute in order of increasing alkyl carbon number. The hydrophobicity of the zirconia–PBD support is clearly indicated by the linearity of the plot of log capacity factor (k') *versus* alkyl carbon number for these solutes, shown in Fig. 8. Similar plots for alkylbenzenes and

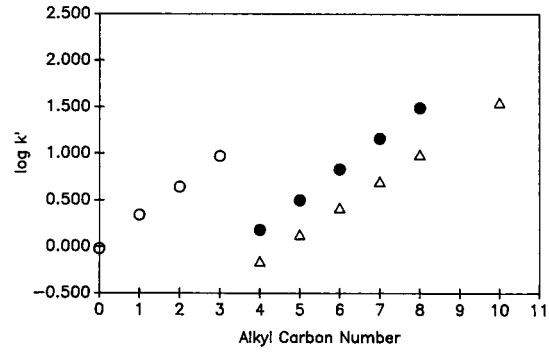

Fig. 8. Reversed-phase retention on zirconia–PBD. Mobile phases as indicated in figure; other chromatographic conditions as in Fig. 7. ○: Alkylbenzenes, methanol–water (50:50), slope = 0.33, intercept = −0.011, r = 0.9993; ●: alkylarylketones, methanol–water (50:50), slope = 0.33, intercept = −1.14, r = 0.9999; △: alkylarylketones, methanol–water (60:40), slope = 0.28, intercept = −1.30, r = 0.9999.

for the alkyl aryl ketones in a stronger mobile phase are shown in Fig. 8. In view of the more polar nature of the alkyl aryl ketones, the alkylbenzenes were more retained than the alkyl aryl ketones at any alkyl carbon number as expected for reversed-phase retention. Increasing the methanol content of the mobile phase decreased the retention of the alkyl aryl ketones and also led to a lower slope in the plot of log k' *vs.* carbon number; this is also consistent with a reversed-phase retention mechanism.

The general retention characteristics of zirconia–PBD relative to a monomeric octyl–silane support were further evaluated in a pH 3 phosphate-containing mobile phase using the solvatochromic comparison method[34] with a set of 18 solutes. The overall conclusion from the solvatochromic comparison experiment is that there are no dramatic qualitative differences in the retention characteristics of the zirconia–PBD column relative to a conventional RP-HPLC column. This is, at least in part, due to the fact that the conditions chosen for this comparison minimized the effect of solute interactions with the zirconia support. Under different chromatographic conditions the effect of these interactions becomes quite evident. This is demonstrated by the data in Table V which summarizes the retention of several test solutes on two different zirconia–PBD columns. These data show only slight differences in the retention of a variety of uncharged non-polar solutes on a given column in the three

TABLE V

CHROMATOGRAPHIC EVALUATION OF PBD-COATED ZIRCONIA COLUMNS

Capacity factors for a 5 μl injection of a 1 m*M* test solute solution determined at a flow-rate of 1 ml/min and a column temperature of 40°C.

Solute	*Capacity factors*					
	Column 1[a]			*Column 2*[b]		
	Mobile phase			*Mobile phase*		
	1[c]	*2*[d]	*3*[e]	*1*[c]	*2*[d]	*3*[e]
Benzene	1.03	1.02	0.93	0.16	0.16	0.05
Toluene	2.14	2.16	2.04	0.40	0.40	0.20
Ethylbenzene	4.24	4.15	4.02	0.78	0.76	0.70
Nitrobenzene	0.68	0.66	0.54	0.11	0.12	0
Fluorobenzene	1.09	1.10	1.00	0.19	0.18	0.13
Chlorobenzene	2.70	2.70	2.50	0.54	0.52	0.44
Bromobenzene	3.60	3.60	3.36	0.74	0.72	0.63
Iodobenzene	5.65	5.65	5.30	1.18	1.16	1.03
Benzoic acid	–[f]	–[f]	−0.23	–[f]	–[f]	−0.22
Cinnamic acid	–[f]	–[f]	−0.17	–[f]	–[f]	−0.21
Phthalic acid	–[f]	–[f]	−0.23	–[f]	–[f]	−0.19
Phenyl phosphonic acid	–[f]	–[f]	−0.22	–[f]	–[f]	−0.21

[a] 5 cm × 0.46 cm I.D. ZrO_2–PBD column with 0.43 nm PBD film.
[b] 5 cm × 0.46 cm I.D. ZrO_2 column with 0.15 nm PBD film.
[c] Mobile phase 1: methanol–water (40:60).
[d] Mobile phase 2: methanol–0.1 *M* NaCl (40:60).
[e] Mobile phase 3: methanol–0.1 *M* phosphate buffer pH 7 (40:60).
[f] No elution observed in 1 h at 0.0005 a.u.f.s.

different mobile phases, indicating that these solutes are retained by a reversed-phase retention mechanism.

In contrast, elution of benzoic acid, phthalic acid, cinnamic acid and phenyl phosphonate was not observed at all in methanol–water (40:60), even in the presence of 100 m*M* sodium chloride. This indicates that these solutes were either irreversibly adsorbed onto the zirconia support, or were so strongly retained that their retention times were too long and the peaks too broad to permit detection. When phosphate was added to the mobile phase, these solutes eluted with negative capacity factors. We previously reported that the presence of phosphate in the mobile phase converts microporous zirconia into a cation exchanger[29], and these data indicate that solute elution occurred prior to the dead volume as a result of electrostatic exclusion of the negatively charged solute from the pores of the negatively charged support.

Note that the data in Table V show no evidence that solute–zirconia interactions were diminished on the support with a thicker (0.43 nm) film. In fact, although the data are not given, this same effect was observed on supports with PBD films as thick as 1.5 nm. Clearly, there is a very strong interaction between these anionic solutes and the zirconia support which the PBD film does not completely inhibit, regardless of its thickness. This is consistent with the expectation that deactivation of surface sites does not necessarily accompany the deposition of a polymer film since in many cases no specific interaction or reaction with the surface sites occurs. By contrast, a substantial "deactivation" which was dependent on film thickness was reported with silica coated with PBD[31].

The apparent accessibility of anion-exchange sites on the zirconia surface even after deposition of a thick polymer film was confirmed by determining the static phosphate adsorption capacity of several supports with different PBD film thicknesses. The results of this experiment, which are summarized in Table VI, show that some reduction in phosphate adsorption accompanies the deposition of a PBD film on the zirconia surface. Fig. 9 shows that the amount of phosphate adsorbed decreases linearly with PBD film thickness for films of less than 0.58 nm. The amount of phosphate decreased from 3.9 μmoles/m^2 on bare zirconia to 2.3 μmoles/m^2 on zirconia–PBD with a 0.58 nm PBD film. Note that this data encompasses a PBD molecular

TABLE VI

STATIC PHOSPHATE ADSORPTION ON ZIRCONIA–PBD

Support	*PBD (mol. wt.)*	d_f[a]	*μmoles/m^2*[b]
Zirconia	No PBD	0	3.93
Zirconia	400	0.1	3.54
Zirconia	2700	0.43	3.42
Zirconia	900	0.24	3.22
Zirconia	4500	0.22	3.21
Zirconia	4500	0.45	2.74
Zirconia	4500	1.7	2.35
Zirconia	22 000	0.58	2.30

[a] d_f = PBD film thickness in nm.

[b] μmoles/m^2 = μmoles of phosphate adsorbed/m^2 zirconia.

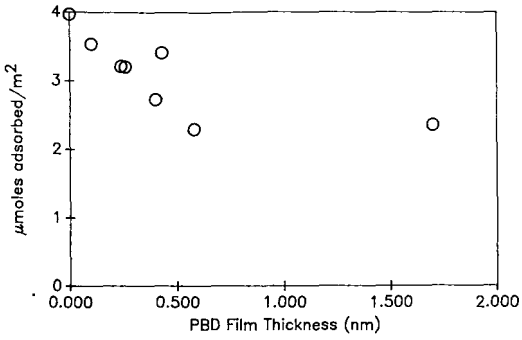

Fig. 9. Dependence of phosphate adsorption on PBD film thickness d_f and μmoles/m^2 as defined in Table VI.

weight range from 400 to 22 000 daltons. The value of 2.3 μmoles/m^2 appears to represent the lower limit of phosphate adsorption, as increasing the PBD film thickness by a factor of three did not result in any further reduction in the amount of phosphate adsorbed on the zirconia–PBD support. The significance of this lower limit is not clear. The independence of the amount of phosphate adsorbed on the molecular weight of PBD clearly indicates that the 2.3 μmoles/m^2 of "unblockable" anion-exchange sites are not a consequence of a simple size exclusion effect, that is, they are not sites which are located in micropores or other regions of the zirconia particle which are accessible to inorganic phosphate but inaccessible to PBD because of its larger size. These unblocked sites are analogous to the silanol groups which remain underivatized on silica after reaction with small organosilanes (*i.e.*, endcapping reagents). The resistance of these silanol sites to derivatization has been explained in terms of geometric effects related to the highly fractal nature of the silica surface[35]. Since the surface of zirconia is also highly fractal, it is likely that local geometric factors (as opposed to geometric factors such as exclusion from pores) are involved in the fact that a finite number of surface sites remain accessible even after deposition of an extremely thick PBD film. Another possible explanation for the adsorption of 2.3 μmoles/m^2 of phosphate even in the presence of a heavy PBD load is that a PBD monolayer covers a certain fraction of the zirconia surface leading to the initial decrease in phosphate adsorption and that additional PBD layers, which are not in intimate contact with the zirconia surface, do not further restrict access to the surface.

The chromatographic results and the results of the static phosphate adsorption experiment both clearly indicate that the zirconia–PBD support has substantial anion-exchange capacity. The presence of accessible anion-exchange sites leads to mixed-mode retention mechanisms which complicate the chromatography of acidic solutes such as carboxylic acids and organophosphonates. One possible strategy for inhibiting the interaction of these solutes with the zirconia surface is to use phosphate-containing mobile phases so that inorganic phosphate competes for anion-exchange sites with the solute molecules. This approach is analogous to the use of amine-containing mobile phases to improve the chromatography of amines on silica-based reversed phases.

The data in Table VII demonstrate the effect of various concentrations of inorganic phosphate on the chromatography of several test solutes. If the retention of

TABLE VII

EFFECT OF PHOSPHATE CONCENTRATION ON RETENTION ON PBD COATED ZIRCONIA[a]

Solute	*1 mM H_3PO_4*[b]		*10 mM H_3PO_4*[c]		*100 mM H_3PO_4*[d]	
	k'[e]	N[f]	k'	N	k'	N
Benzene	0.58	242	0.60	205	0.47	278
Benzoic acid	0.64	43	0.53	82	0.24	263
Toluene	1.0	179	1.1	159	0.84	216
Toluic acid	0.90	37	0.72	79	0.40	187
Benzylamine	0.32	196	0.36	211	0.23	273
Phenyl phosphonic acid	—[g]		—[g]		0.13	43

[a] Column, 5 cm × 0.46 cm I.D. packed with 10 μm–15 μm zirconia–PBD; flow-rate, 1 ml/min; column temperature, 40°C; injection volume, 5 μl; solute concentration, 1 m*M*.

[b] Mobile phase: methanol–1 m*M* H_3PO_4 (50:50) adjusted to pH 3.

[c] Mobile phase: methanol–10 m*M* H_3PO_4 (50:50) adjusted to pH 3.

[d] Mobile phase: methanol–100 m*M* H_3PO_4 (50:50) adjusted to pH 3.

[e] k' = capacity factor.

[f] $N = 5.54\,(t_r/W)^2$.

[g] No elution observed at $k' < 100$.

these solutes were due solely to a reversed-phase process, benzoic acid and *p*-toluic acid should elute before benzene and toluene, respectively, as a result of their greater polarity. In fact, in 1 m*M* phosphate at pH 3, benzoic acid is slightly more retained than benzene, while toluene is more retained than toluic acid. In 10 m*M* and 100 m*M* phosphate, benzoic acid and toluic acid elute before benzene and toluene, respectively. Clearly, in the presence of even a small amount of phosphate in the mobile phase, there are few anion-exchange sites present on the zirconia–PBD support. This finding is consistent with the reported conversion of zirconia from an anion exchanger to a cation exchanger upon treatment with inorganic phosphate[36]. In 1 m*M* phosphate, the benzoic acid and toluic acid peaks are tailed and broader than the benzene and toluene peaks as reflected in the number of theoretical plates. (It should be noted that the column used for this experiment was packed with a 10–15 μm zirconia-PBD support that had a non-uniform particle size distribution. As a result the column efficiency was low. The comparison of the benzoic acid and toluic acid peaks to the benzene and toluene peaks is still valid.)

The chromatography of benzoic acid and toluic acid improved upon increasing the phosphate concentration so that in the presence of 100 m*M* phosphate the plate counts determined from these peaks are comparable to those determined for benzene and toluene. Note that phenyl phosphonic acid is irreversibly adsorbed in both the 1 and 10 m*M* phosphate mobile phases, and elutes as a broad peak in 100 m*M* phosphate. The chromatography of benzylamine is comparable to that of benzene. It elutes sooner than benzene as is expected for a less hydrophobic solute and has a slightly wider peak, but there is no evidence that it exhibits the strong interactions with zirconia–PBD that acidic solutes do under these conditions. Other inorganic phosphate species, including pyrophosphate and tripolyphosphate, were also used as mobile phase modifiers without appreciably different results from those described above for orthophosphate. Mobile phase additives other than phosphate will most

likely be less effective in controlling the interaction of these solutes with the zirconia surface since their interaction with the surface is weaker than that of phosphate. Results obtained with acetic acid as a mobile phase modifier confirmed this expectation.

Clearly, a more desirable approach for controlling the interactions with the zirconia surface would be to deactivate the surface permanently by incorporation of a blocking agent in the modification procedure. An attempt was made to do so by adsorbing allylphosphonate onto the anion-exchange sites both before and after deposition of the PBD film and to then "anchor" the allylphosphonate by cross-linking it with the PBD. The initial attempt involved adsorbing the allylphosphonate onto unmodified zirconia from methanol and then depositing a PBD film according to Procedure C given above. The effectiveness of the allylphosphonate deactivation was determined by examining the chromatography of benzoic acid and other solutes in methanol–H_2O (50:50) mobile phase. Benzoic acid was irreversibly adsorbed on an untreated zirconia–PBD support under these conditions. The initial result on the allylphosphonate-deactivated support was encouraging in that elution of benzoic acid was observed, however, there was still strong anion-exchange retention as evidenced by a capacity factor of 6.2 for benzoic acid compared to a value of 0.3 for benzene. Additional injections of benzoic acid were made and the retention increased in a regular fashion upon each injection as shown in Fig. 10. The extent of increase in retention was dependent on the amount of injected benzoic acid. If no injections were made, there was essentially no increase in the retention of benzoic acid with time. These observations indicate that the benzoic acid displaced allylphosphonate from the zirconia surface thereby exposing more sites and causing an increase in anion-exchange retention with each subsequent injection. The same approach to deactivation was also attempted using octylphosphonic acid, but once again, deactivation was incomplete and the retention of benzoic acid increased upon repetitive injections.

Both of the supports prepared by adsorbing an organophosphonate and then depositing a PBD film had carbon loads which were much lower than expected based on the amount of PBD offered. This could be due to desorption of the adsorbed

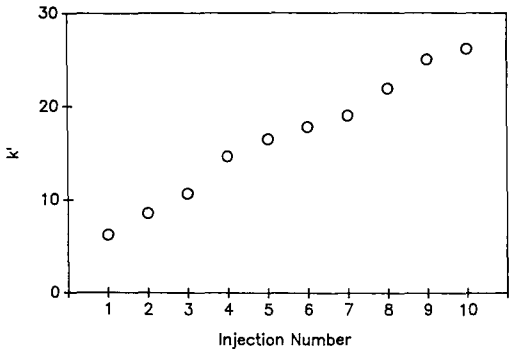

Fig. 10. Retention of benzoic acid on deactivated zirconia–PBD. Column, 5 cm × 0.46 cm I.D. packed with 10–15 μm zirconia coated with allylphosphonate and PBD; mobile phase, methanol–10 m*M* H_3PO_4 (50:50) adjusted to pH 3; flow-rate 1 ml/min; column temperature, 40°C; injection volume, 5 μl; solute concentration, 1 m*M*.

phosphonate into pentane during the wash step in the PBD deposition procedure, to less adsorption of PBD onto the non-polar zirconia–organophosphonate surface from pentane, or to the masking of specific sites on the zirconia surface onto which PBD adsorbs. To avoid any or all of these possible problems, the deactivation was attempted by depositing the PBD film and then adsorbing allylphosphonate onto the surface from methanol, however, this approach also gave low carbon loads and an unstable, incompletely deactivated surface.

Although a stable, completely deactivated zirconia–PBD support was not prepared, deactivation of the zirconia surface with an unsaturated organophosphonate, such as allylphosphonate, followed by deposition and cross-linking of a polymer film should be a viable approach to the preparation of a permanently deactivated zirconia–PBD. Experimental problems which need to be addressed are the appropriate organophosphonate to use and the appropriate solvents and conditions from which to adsorb the organophosphonate and PBD in order to maximize surface coverage and deactivation.

CONCLUSIONS

The preparation of a polymer-coated zirconia–based support has been described. Polybutadiene was immobilized on porous microparticulate zirconia and cross-linked chemically or by irradiation with high-energy electrons. The coated, cross-linked support has very high alkaline stability which we believe is superior to that of any inorganic-based chromatographic support previously reported, and probably adequate for any conceivable use.

Zirconia–PBD has very similar retention characteristics to alkyl–silica bonded phases with respect to the retention of small solutes in a phosphate buffer at pH 3. Under other conditions, particularly when phosphate is absent from the mobile phase, acidic solutes are very strongly retained due to interactions with (basic) anion-exchange sites on the surface of the zirconia support. These interactions can be controlled to some extent by the addition of phosphate to the mobile phase.

ACKNOWLEDGEMENTS

The authors gratefully acknowledge the contributions of E. F. Funknenbusch, D. A. Hanggi, Scott Culler and Paul Martin of the 3M Company. This work was supported in part by grants from the University of Minnesota Center for Biological Process Technology and the 3M Company.

REFERENCES

1 R. E. Iler, *The Chemistry of Silica*, Wiley-Interscience, New York, 1979.
2 K. K. Unger, *Porous Silica*, (*Journal of Chromatography Library*, Vol. 16), Elsevier, Amsterdam, 1979.
3 R. P. W. Scott, *Adv. Chromatogr.*, 20 (1982) 167.
4 C. T. Wehr and R. E. Majors, *LC·GC, Mag. Liq. Gas Chromatogr.*, 5 (1987) 942.
5 A. Wehrli, J. C. Hildenbrand, H. P. Keller, R. Stampeli and R. W. Frei, *J. Chromatogr.*, 149 (1978) 199.
6 K. Krummen and R. W. Frei, *J. Chromatogr.*, 132 (1977) 27.
7 J. J. Glajch, J. J. Kirkland and J. Köhler, *J. Chromatogr.*, 384 (1987) 81.
8 K. K. Unger, N. Becker and P. Roumeliotis, *J. Chromatogr.*, 125 (1976) 115.
9 C. Horváth, W. Melander and I. Molnar, *Anal. Chem.*, 49 (1977) 142.

10 J. R. Benson and D. J. Woo, *J. Chromatogr. Sci.*, 22 (1984) 386.
11 F. Nevejans and M. Verzele, *Chromatographia*, 20 (1985) 173.
12 L. D. Bowers and S. Pedigo, *J. Chromatogr.*, 371 (1986) 243.
13 H. Colin, C. Eon and G. Guiochon, *J. Chromatogr.*, 119 (1976).
14 J. H. Knox and M. T. Gilbert, *U.K. Pat.*, 7 939 449 (1979); *U.S. Pat.*, 4 263 268 (1979).
15 J. H. Knox and B. Kaur, *Eur. Chromatogr. News*, 1 (1987) 12.
16 A. Pryde and F. J. Darby, *J. Chromatogr.*, 115 (1975) 107.
17 J. H. Knox and A. Pryde, *J. Chromatogr.*, 112 (1975) 171.
18 Y. Hirata, M. Novotny, T. Tsuda and D. Ishii, *Anal. Chem.*, 51 (1979) 1807.
19 H. Billiet, C. Laurent and L. de Galan, *Chromatographia*, 17 (1983) 253.
20 P. Kolla, J. Köhler and G. Schomburg, *Chromatographia*, 23 (1987) 465.
21 U. Bien-Vogelsang, A. Deege, H. Figge, J. Köhler and G. Schomburg, *Chromatographia*, 19 (1984) 170.
22 R. M. Chicz, Z. Shi and F. E. Regnier, *J. Chromatogr.*, 359 (1986) 121.
23 Y. Ghaemi and R. A. Wall, *J. Chromatogr.*, 174 (1979) 51.
24 M. B. Dines and P. M. DiGiacomo, *Inorg. Chem.*, 20 (1981) 92.
25 M. B. Dines and P. C Griffith, *J. Phys. Chem.*, 86 (1982) 571.
26 G. Alberi, U. Constantino, S. Allulli and N. Tomassini, *J. Inorg. Nucl. Chem.*, 40 (1978) 1113.
27 L. Maya, *Inorg. Nucl. Chem. Lett.*, 15 (1979) 207.
28 L. Maya and P. O. Danis, *J. Chromatogr.*, 190 (1980) 145.
29 M. P. Rigney, E. F. Funkenbusch and P. W. Carr, *J. Chromatogr.*, in press.
30 H. Figge, A. Deege, J. Köhler and G. Schomburg, *J. Chromatogr.*, 351 (1986) 393.
31 G. Schomburg, J. Köhler, H. Figge, A. Deege and U. Bien-Vogelsang, *Chromatographia*, 18 (1984) 265.
32 J. H. Knox and R. Kaliszan, *J. Chromatogr.*, 349 (1985) 211.
33 W. Noll, *Chemistry and Technology of Silicones*, Academic Press, New York, 1968.
34 P. C. Sadek, P. W. Carr, R. M. Doherty, M. J. Kamlet, R. W. Taft and M. H. Abraham, *Anal. Chem.*, 57 (1985) 2971.
35 D. Farin and D. Avnir, *J. Chromatogr.*, 406 (1987) 317.
36 C. B. Amphlett, L. A. McDonald and M. J. Redman, *J. Inorg. Nucl. Chem.*, 6 (1958) 236.

Journal of Chromatography, 484 (1989) 293–298
Elsevier Science Publishers B.V., Amsterdam — Printed in The Netherlands

CHROM. 21 804

PREPARATIVE REVERSED-PHASE HIGH-PERFORMANCE LIQUID CHROMATOGRAPHY IN THE SYNTHESIS OF VISCOSIN, A CYCLIC DEPSIPEPTIDE

TERRENCE R. BURKE, Jr.* and BHASKAR CHANDRASEKHAR
Peptide Technologies Corporation, 125 Michigan Avenue N.E., Washington, DC 20017 (U.S.A.)

SUMMARY

The importance of peptides in biochemical research and the facility with which they can be prepared by solid-phase techniques highlights the need for continuing research in the chromatographic purification of these molecules on a preparative scale. In this regard, synthesis of the cyclic depsipeptide antibiotic, viscosin, has provided the opportunity to demonstrate the use of radial compression cartridge technology in the reversed-phase purification of three key peptide intermediates on a scale of several hundred milligrams. Superior resolution of linear and cyclic peptide mixtures on a Bondapak C_{18} radial compression cartridge by using an aqueous acetonitrile solvent system containing 0.1% trifluoroacetic acid contributed significantly to the first total synthesis of viscosin, and demonstrates the applicability of this system to the purification of peptide mixtures.

INTRODUCTION

Peptides play an ever more important role in many areas of scientific research. One reason for this rapid expansion is the relative ease with which a diversity of peptides and peptide analogues can be prepared by using solid-phase techniques[1]. While products of solid-phase peptide synthesis are often remarkably pure, even the best of synthesis can be contaminated by structurally similar side products. Chromatographic techniques such as counter-current distribution or the Ito coil planet centrifuge can give substantial purification of peptide mixtures[2,3]. However, these suffer from the disadvantage of lengthy separation times and an inability to resolve closely eluting species. High-performance liquid chromatography (HPLC), on the other hand, gives rapid resolution of very complex mixtures, and has established itself as a valuable method not only in the monitoring of the formation of side products during peptide synthesis[4] but also in the purification of synthetic peptide mixtures[5–7]. Various reversed-phase media have found successful application in this regard[5,6,8] and the utility of novel separation schemes has been demonstrated[9]. The commercial availability of high-flow pumps and new high-capacity columns continues to make the preparative HPLC purification of large-scale peptide synthesis an important area of investigation.

0021-9673/89/$03.50

Radial compression cartridges offer a less expensive alternative to stainless-steel columns while maintaining high capacity and resolution, and their use has been successfully demonstrated in the purification of hundreds of synthetic peptides[6]. Our research on peptide antibiotics afforded the opportunity to examine the efficacy of the Bondapak C_{18} radial compression cartridge, the PrepPak 1000 compression module and the Model 3000 pumping system in the purification of large amounts of peptide reaction products. Work centered on the peptide antibiotic viscosin which was discovered by Kochi in 1951 and was shown to have antimicrobial[10] and antiviral[11] properties. After an initial incorrect structural assignment[12], the revised structure had been postulated as **1** (Fig. 1), a cyclic peptide lactone composed of alternating D- and L-amino acids, with a D-β-hydroxydecanoyl peptide side chain[13]. The Waters Millipore cartridge system was used for the purification of three key peptide intermediates and served as a significant factor in our successful completion of the first total synthesis of viscosin[14].

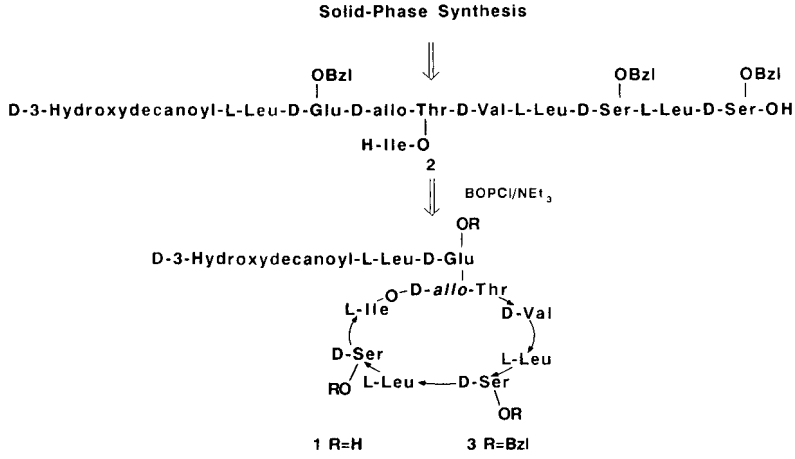

Fig. 1. Cyclization of precursor fragment **2** to peptide lactone **3**. Bzl = benzyl; Et = ethyl.

EXPERIMENTAL

Materials

Solvents were purchased from Fisher Scientific (Fairlawn, NJ, U.S.A.). Acetonitrile was HPLC grade and water was passed through a Barnstead Nanopure II cartridge purification system (Dubuque, IO, U.S.A.) with a 0.2-μm filter (>18 MΩ/cm). Peptides were obtained by synthetic procedures reported elsewhere[14] and lyophilized from reagent-grade tetrahydrofuran (dried over 4-Å sieves).

Methods

Chromatography was performed on a Waters Division of Millipore (Milford, MA, U.S.A.) LC 3000 solvent delivery system equipped with a Rheodyne 7010 injector (having a 7012 filler port and a 5.1-ml sample loop). Additional equipment consisted of a Waters Model 381 variable-wavelength detector and Model 740 data module. Solvent systems were (A) 0.1% trifluoracetic acid (TFA) in water and (B) 0.1% TFA in

acetonitrile with gradients as indicated in Figs. 2–6 (% B shown). Analytical chromatography was carried out on a μBondapak C_{18}, 10 μm, 15 × 0.39 cm I.D. column (Waters) with a flow-rate of 1 ml/min and detection at 214 nm. Samples were typically injected in a volume of 100 μl. Semipreparative chromatography was performed by using a Waters μBondapak C_{18}, 10 μm, 15 × 1.9 cm I.D. column at a flow-rate of 10 ml/min. Samples (75 mg) were injected in 3 ml of dioxane. Preparative chromatography was performed at a flow-rate of 60 ml/min by using a Waters PrepPak 1000 radial compression module equipped with a Waters Bondapak C_{18} prep cartridge, 15–20 μm, 30 × 4.7 cm I.D. maintained under 760 p.s.i. Samples were pumped on in 20–50 ml of dioxane. Both analytical and semipreparative runs utilized UV detection with an analytical cell (10 mm path length), while preparative runs utilized a semipreparative cell (2.1 mm path length). Prior to lyophilization, samples were taken to dryness under rotary evaporation at reduced pressure. Temperatures of 50–60°C were permissible for benzyl-protected peptides, while a temperature of 40°C was used for debenzylated material. Residues were lyophilized from dioxane, giving white solids. Assigned structures were confirmed by amino acid analysis and fast atom bombardment mass spectrometry.

RESULTS AND DISCUSSION

A central problem in the synthesis of cyclic depsipeptides is ring closure. This closure is traditionally achieved through amide bond formation rather than through ester bond formation[15]. For the synthesis of viscosin, a scheme was developed using solid-phase peptide techniques based on an acid-sensitive resin[16] and fluorenylmethyloxycarbonyl (Fmoc)/butyloxycarbonyl (Boc) amino protection, which produced a linear fragment **2** suitable for cyclization to the benzyl-protected viscosin (**3**) (Fig. 1). Crude linear **2** was examined by analytical HPLC and was shown to consist primarily of a faster-eluting pyroglutamic acid derivative (**2a**)[17] and product **2** with a side product of unknown composition (**2b**) (Fig. 2). Initial semipreparative HPLC

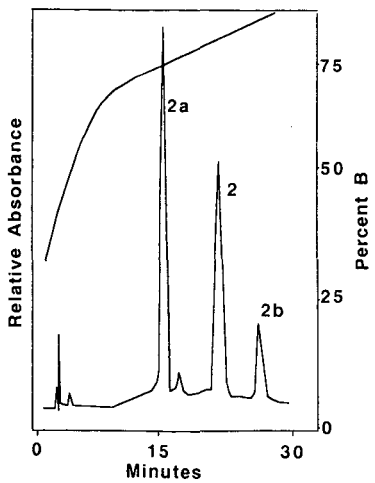

Fig. 2. Analytical HPLC of crude **2** resulting from the TFA cleavage of the solid-phase resin. Absorbance at 214 nm.

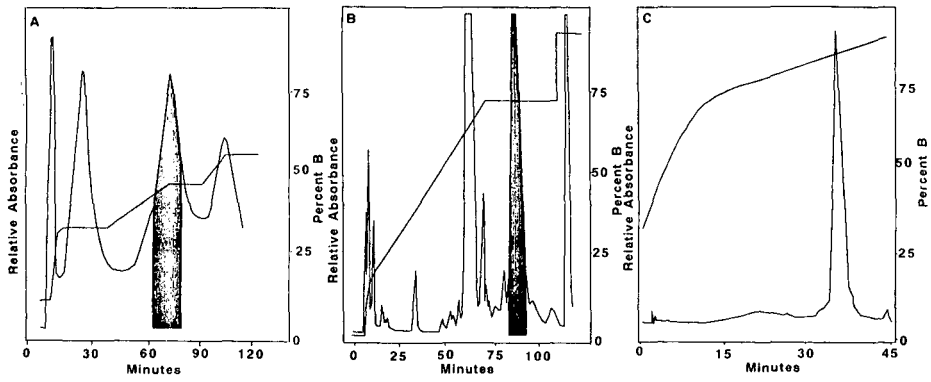

Fig. 3. Purification of crude **2**. Shaded areas indicate portions collected. (A) Semipreparative HPLC purification of a 75-mg sample; (B) preparative purification of an 800-mg sample; (C) analytical HPLC of purified **2** obtained from preparative purification indicated in (B). Absorbance at 220 nm (A) and (B) or 214 nm (C).

purification of a 75-mg sample of crude **2** failed to give baseline resolution (Fig. 3A), however, 21 mg (28% of crude) of pure linear **2** was obtained by this procedure. Superior resolution was achieved in the subsequent preparative HPLC purification of 800 mg of crude **2** (Fig. 3B), where baseline separation yielded 277 mg (35%, w/w) of pure **2** (Fig. 3C). The linear velocity of the preparative run (200 cm/h) was approximately one half that of the analytical scale (500 cm/h), and this in combination with a shallower gradient resulted in preparative retention times approximately three times longer than the analytical retention times. Qualitatively, chromatograms obtained preparatively were remarkably similar to analytical results.

After several hundred milligrams of pure linear **2** had successfully been obtained, cyclization of **2** was carried out under various conditions. Cyclization was finally achieved under high dilution by using the activating agent bis(2-oxo-3-oxazolidinyl)-phosphinic chloride (BOPCl)[18] in dioxane (Fig. 1). The resulting crude reaction mixture contained the desired cyclized product **3** and a faster eluting impurity **3a** (Fig. 4A). Preparative HPLC purification of the crude reaction mixture from a 250-μmol reaction (representing approximately 360 mg of peptide) (Fig. 4B) gave 82 mg of highly enriched benzyl-protected viscosin **3** (Fig. 4C), which was of sufficient purity to carry through the subsequent deprotection step.

Debenzylation of 82 mg of **3** was achieved by stirring with ammonium formate in methanol in the presence of 10% Pd · C[19]. The reaction was followed by analytical HPLC until the mixture of partially debenzylated products coalesced to one unchanging peak. The crude reaction product (Fig. 5A) was then subjected to preparative HPLC purification (Fig. 5B), yielding 52 mg (75%) of pure synthetic viscosin (**1**) (Fig. 5C), which was indistinguishable from natural material[a] both chromatographically (Fig. 6) and by NMR.

[a] A sample of natural viscosin was kindly obtained from Sumitomo Chemical Company, Osaka, Japan.

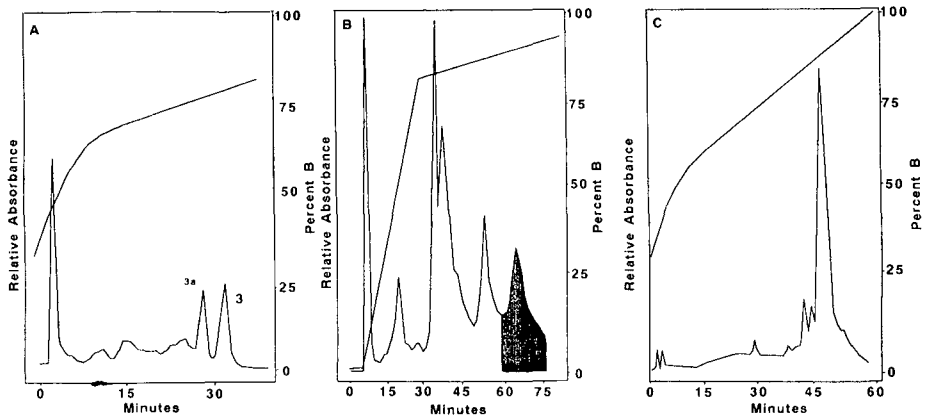

Fig. 4. Purification of benzyl-protected peptide lactone **3**. (A) Analytical HPLC of crude cyclized **3**; (B) preparative HPLC of approximately 360 mg of crude **3**; (C) analytical HPLC of purified **3** obtained from preparative HPLC (B). Absorbance at 214 nm.

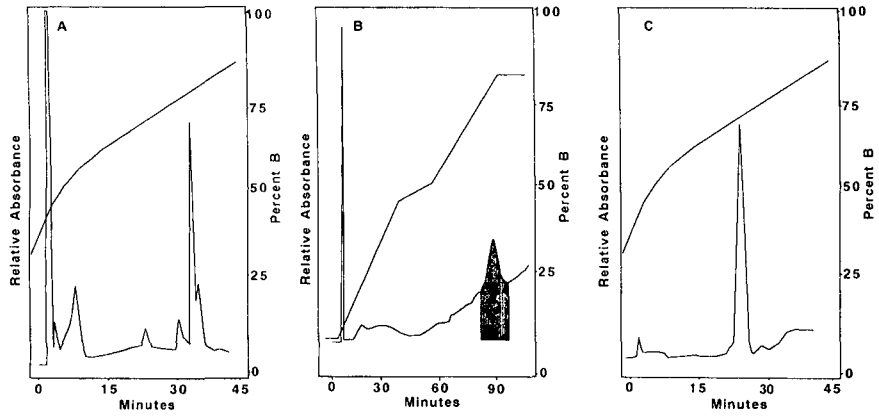

Fig. 5. Purification of synthetic viscosin **1**. (A) Analytical HPLC of crude synthetic viscosin resulting from debenzylation of **3**; (B) preparative HPLC of crude **1**; (C) analytical HPLC of purified viscosin obtained from (B). Absorbance at 214 nm.

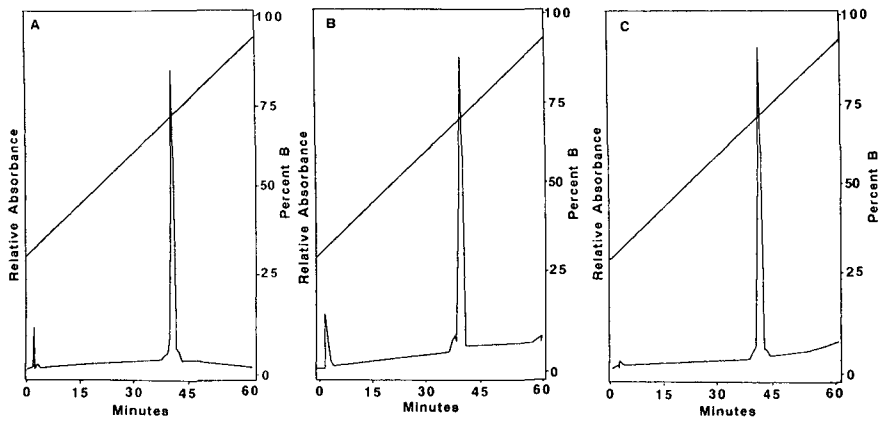

Fig. 6. Comparison of synthetic and natural viscosin by analytical HPLC. (A) Synthetic viscosin; (B) natural viscosin; (C) cochromatography of approximately equal amounts of natural and synthetic viscosin. Absorbance at 214 nm.

While preparative HPLC purification of linear **2** and final product **1** was conducted with good separation, the problematic purification of cyclized, benzyl-protected **3** needed to be re-examined. It was found that debenzylation of crude **3** directly without intermediate purification gave a reaction mixture the components of which could be more easily resolved, yielding the desired **1**. It was therefore found to be more expedient to bypass the intermediate purification of **3** and to debenzylate the crude reaction product directly. Preparative HPLC purification of the resulting crude debenzylated mixture was then achieved in yields (19% overall from linear **2**) comparable to that obtained by using an intermediate purification of benzylated precursor (18% overall yield).

In summary, the first total synthesis of viscosin has afforded the opportunity to examine the utility of the Bondapak C_{18} radial compression PrepPak 1000 system in the large-scale purification of peptide reaction products. The resulting purification of the benzyl-protected linear and cyclized peptides as well as deprotected cyclic viscosin enabled the achievement of the first total synthesis of viscosin.

ACKNOWLEDGEMENTS

Appreciation is expressed to Sumitomo Chemical Company, Osaka, Japan for providing a reference sample of viscosin and to Dr. Anthony Mauger for helpful discussions and Sara Gluch for amino acid analysis used in the verification of structures. Some of the fast atom bombardment mass spectral determinations utilized for structure determination were carried out at the Middle Atlantic Mass Spectrometry Laboratory, a National Science Foundation Shared Instrumentation Facility. Appreciation is also expressed to Dr. Martha Knight for critical reading of this manuscript. Funding for this work was provided by National Institutes of Health grant No. AI 23571.

REFERENCES

1 B. F. Gisin, R. B. Merrifield and D. C. Tosteson, *J. Am. Chem. Soc.*, 91 (1969) 2691–2695.
2 T. R. Burke, Jr. and M. Knight, *J. Chromatogr.*, 411 (1987) 431–435.
3 M. Knight, J. D. Pineda and T. R. Burke, Jr., *J. Liq. Chromatogr.*, 11 (1988) 119–131.
4 G. Szokan, A. Torok and B. Penke, *J. Chromatogr.*, 387 (1987) 267–280.
5 M. Knight, G. D. Mack, R. Perkins and T. R. Burke, *J. Chromatogr.*, 444 (1988) 345–348.
6 J. Rivier, R. McClintock, R. Galyean and H. Anderson, *J. Chromatogr.*, 288 (1984) 303–328.
7 J. X. Huang and G. Guiochon, *BioChromatogr.*, 3 (1988) 140, 143–148.
8 K. Larsson, W. Hermann, P. Moller and D. Sanchez, *J. Chromatogr.*, 450 (19888) 71–80.
9 T. W. L. Burke, C. T. Mant and R. S. Hodges, *J. Liq. Chromatogr.*, 11 (1988) 1229–1247.
10 M. Kochi, D. W. Weiss, L. H. Pugh and V. Groupe, *Bacteriol. Proc.*, (1951) 29–30.
11 V. Groupe, L. H. Pugh, D. Weiss and M. Koch, *Proc. Soc. Exp. Biol. Med.*, 78 (1951) 354–358.
12 T. Ohno, S. Tajima and K. Toki, *J. Agric. Chem. Soc. Jpn.*, 27 (1953) 665–669; *Chem. Abstr.*, 49 (1955) 3012d.
13 M. Hiramoto, K. Okada and S. Nagai, *Tetrahedron Lett.*, 13 (1970) 1087–1090.
14 T. R. Burke, Jr., M. Knight, B. Chandrasekhar and J. Ferretti, *Tetrahedron Lett.*, 30 (1989) 519–522.
15 K. L. Rinehart, V. Kishore, S. Nagarajan, R. J. Lake, J. B. Gloer, F. A. Bozich, K. M. Li, R. E. Maleczka, W. L. Todsen, M. H. G. Munro, D. W. Sullions and R. Sakai, *J. Am. Chem. Soc.*, 109 (1987) 6846–6848.
16 S. S. Wang, *J. Am. Chem. Soc.*, 92 (1970) 5748, 5749.
17 A. J. Hubert, R. Buyle and B. Hargitay, *Helv. Chim. Acta.*, 46 (1963) 1429–1445.
18 R. E. Shute, B. Dunlap and D. H. Rich, *J. Med. Chem.*, 30 (1987) 71–78.
19 M. K. Anwer and A. F. Spatola, *Synthesis*, (1980) 929–932.

Journal of Chromatography, 484 (1989) 299–305
Elsevier Science Publishers B.V., Amsterdam — Printed in The Netherlands

CHROM. 21 802

PURIFICATION OF SYNTHETIC PEPTIDES ON A HIGH-RESOLUTION PREPARATIVE REVERSED-PHASE COLUMN

MARTHA KNIGHT* and SARA GLUCH
Peptide Technologies Corporation, 125 Michigan Avenue N.E., Washington, DC 20017-1004 (U.S.A.)
and
RICHARD MEYER and ROBERT S. COOLEY
YMC, Inc., 51 Gibraltar Drive, Morris Plains, NJ 07950 (U.S.A.)

SUMMARY

A 2-in. I.D. column filled with 10-μm spherical C_{18} bonded silica with 120 Å pores was used for the preparative purification of various synthetic peptides in one step. The small-sized silica packing afforded high resolution and the spherical shape helped maintain a relatively low back-pressure during the chromatography. Conditions for performing the separations were derived from the analytical chromatography of samples on a column of similar 5-μm material. The same amount of organic modifier, but with the gradient duration increased, achieved very similar separations on the preparative column.

INTRODUCTION

The purification of solid-phase synthesized peptides has been performed using a recently available preparative column filled with small-diameter spherical C_{18} bonded silica support material. To achieve the one-step purification of laboratory-scale preparative amounts of peptides, a high-resolution column is advantageous over a column containing larger diameter particles (>20 μm) for the highly heterogeneous products of automatic or manual solid-phase synthesis. Although these columns are expensive, a one-step purification procedure effects significant cost savings as it is more rapid. Moreover, the use of precolumns can extend their lifetimes. The analytical chromatography was carried out on very high-resolution columns of 5-μm ODS silica with 120- or 200-Å pores, which are suitable for the size of peptides synthesized here. After some experience the conditions and results of analytical-scale chromatography suggested preparative-scale chromatographic conditions that were satisfactory without the need for extended chromatographic studies. We describe here the conditions and columns used for both analytical and preparative chromatography that achieved the preparative purification of many linear peptides. This strategy seems to be suitable for the peptides that we have studied, which are up to twenty residues in length.

EXPERIMENTAL

Solvents were of high-performance liquid chromatographic (HPLC) or analytical-reagent grade from Fisher Scientific (Pittsburgh, PA, U.S.A.) and trifluoroacetic acid (TFA) was obtained from Halocarbon (Hackensack, NJ, U.S.A.). Water was distilled and passed through a Nanopure cartridge filtration system (Barnstead, Boston, MA, U.S.A.). Peptides were synthesized by standard solid-phase techniques[1] using Boc-amino acid derivatives, either manually or in a Biosearch (Novato, CA, U.S.A.) 9500 AT peptide synthesizer. The syntheses were made on phenylacetamidomethyl (PAM) or chloromethyl resin. After the assembly of amino acids, the peptide–resin was treated with anhydrous hydrogen fluoride, which cleaved the peptides and removed side-chain protecting groups. After lyophilization, the product was analyzed by HPLC for the determination of impurities and the amino acid composition was determined by amino acid analysis of a 22-h mercaptoethanesulfonic acid hydrolysis using ion-exchange chromatography with post-column *o*-phthalaldehyde fluorescence detection[2] (St. Johns Assoc., Beltsville, MD, U.S.A.).

Analytical chromatography was carried out in Waters/Millipore equipment consisting of a U6K injector, two Model 510 pumps with extended flow heads, a Model 681 variable-wavelength UV detector, a Model 680 gradient controller and an SE120 recorder (all from Waters/Millipore, Milford, MA, U.S.A.). A YMC-Pack, 5-μm spherical ODS, 200 Å, 150 × 6 mm I.D. column was used (AMP-312-5; YMC, Morris Plains, NJ, U.S.A.). The solvent system was 0.1% aqueous phosphoric acid and acetonitrile gradients at a flow-rate of 1 ml/min. Preparative chromatography was conducted with a Waters/Millipore LC3000 solvent-delivery system with helium sparging of the mobile phase consisting of 0.1% aqueous TFA and gradients of 0.1% TFA in acetonitrile at 50 ml/min. A 300 × 50 mm I.D. column of spherical, 10-μm ODS, 120 Å, silica (R-354-S10; YMC) was used with a 50 × 50 mm I.D. guard column of 50 μm ODS, 120 Å, silica (YMC). The effluent was passed through a Model 680 UV detector equipped with a preparative flow cell. An SE120 recorder was used and fractions were collected manually.

The sample was dissolved in water at a concentration of 1–5 mg/ml and filtered through 0.45-μm filters. The sample was pumped at 25 ml/min onto the column, which had been equilibrated in 0.1% aqueous TFA. Subsequently, one column volume (600 ml) of 0.1% aqueous TFA was pumped at 50 ml/min, then the gradient was started. The peak fractions were analyzed by HPLC and those containing the peptide were directly lyophilized. The purified peptide was analyzed by analytical HPLC and amino acid analysis. These procedures were modified from previously published methods[3,4].

RESULTS AND DISCUSSION

An analog of kallidin, designed for radiolabeling, dehydrokallidin (Lys–Arg–ΔPro–ΔPro–Gly–Phe–Ser–ΔPro–Phe–Arg; ΔPro = dehydroproline), was synthesized manually on 4 g of Boc-tosyl-Arg-chloromethyl resin. After cleavage with hydrogen fluoride, 890 mg of powder resulted. Dehydrokallidin was initially separated on an analytical column to determine the complexity of the compound, optimize the separation and develop gradient conditions for the large-scale column. The lower

part of Fig. 1 shows the analytical separation with detection at 254 nm, indicating a major peak eluting at 24 min and an earlier eluting component well separated in the gradient to 20% acetonitrile. The peptide was purified in two batches of 400 and 490 mg on the 2-in. diameter column (300 × 50 mm I.D.) packed with 10-μm spherical ODS, 120 Å, silica (Fig. 2). The sample was loaded as described under Experimental. After passing 600 ml of 0.1% aqueous TFA, a gradient to 20% acetonitrile was run in 20 min, *i.e.*, the same final conditions as in the analytical chromatography. The first peak that was eluted contained very little mass (43 min, Fig. 2). The analytical chromatography of this material is shown in Fig. 1 (15-min peak, upper panel). This

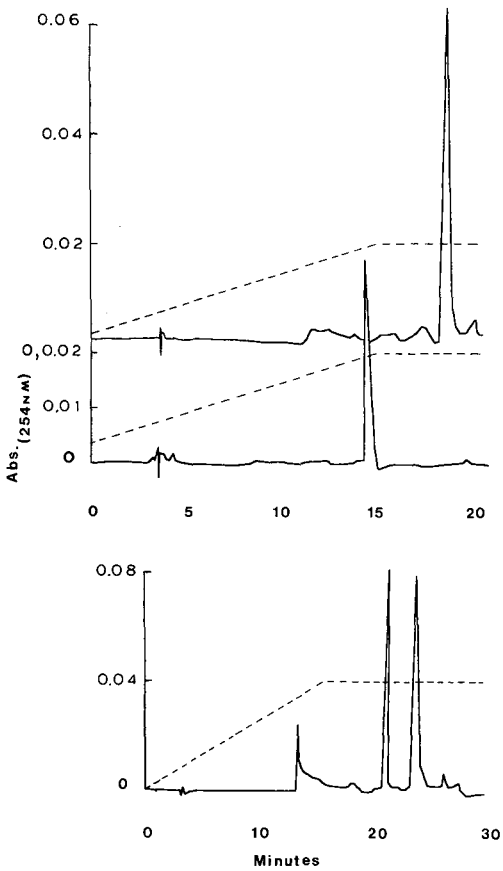

Fig. 1. Analytical chromatography of unpurified dehydrokallidin (lower chromatogram) and of the two peaks separated in the preparative chromatography (top two traces). The lower panel represents *ca.* 100 μg of the synthetic product chromatographed on the YMC 6-mm I.D. column as described under Experimental using 0.1% aqueous phosphoric acid as A and acetonitrile as B at a flow-rate of 1 ml/min; the gradient used was 0–20% B in 15 min. Peptide was eluted at 24 min and an impurity at 20.5 min. Upper panel: samples of 20 μl of the peak fractions from the preparative run in Fig. 2 were chromatographed with a gradient from 3 to 20% B in 15 min. Detection at 254 nm. The lower trace in the upper panel represents the 43-min preparative peak or side-fraction eluting at 14.5 min and the upper trace the peak fraction of the second peak containing the purified peptide which was eluted at 19 min under these conditions.

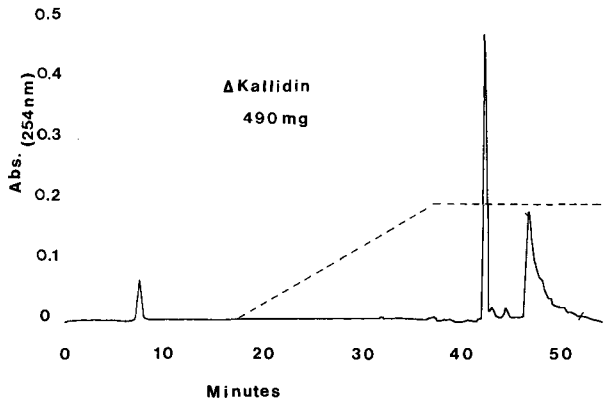

Fig. 2. Chromatogram of half of the dehydrokallidin synthesis product on the YMC 50-mm I.D. column as described under Experimental using 0.1% aqueous TFA as A and 0.1% TFA–acetonitrile as B at a flow-rate of 50 ml/min. The end of sample loading was 0 min and, because some material was eluted at the void volume, the gradient was started later and went from 0 to 20% B in 20 min. The peak at 43 min was collected as one fraction and the following peak (46.5 min) was collected in nine fractions and contained the pure peptide. The fractions between the marks on the peak trace were pure and were combined. Detection at 254 nm with 0.5 a.u.f.s.

corresponded to the first component in the crude peptide. The second peak was collected in many fractions. Analytical HPLC of these appeared as shown in Fig. 1 (18-min peak, uppermost trace). The fractions were dried and fractions 4–10 were pure, containing 276 mg of white crystals. The other run gave similar results, 219 mg

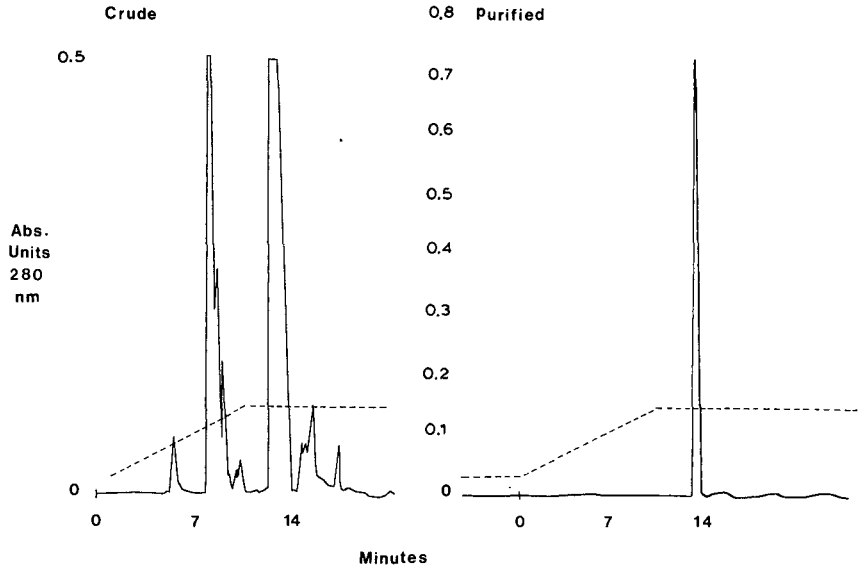

Fig. 3. Analytical chromatography of *ca.* 50 μg of crude (left) and 25 μg of final purified hexapeptide Lys–Ala–Met–Tyr–Ala–Pro (right). Conditions similar to those in Fig. 1 except that the gradient was from 3 to 15% B in 10 min and detection was at 280 nm. The peptide was eluted at *ca.* 14 min (both chromatograms) and an impurity was eluted at *ca.* 8 min (left).

of crystals being recovered. The amino acid analysis showed the expected molar ratios of the constituent amino acids. The chromatographic result on the 5-μm column was similar to that of the preparative chromatography. A gradient to the same percentage of acetonitrile with only a 5-min increase in the duration resulted in similar elution of the material. The back-pressure under these conditions was *ca.* 400 p.s.i.

A hexapeptide was synthesized on a Boc-Pro-PAM resin. On analytical chromatography a significant amount of earlier eluting impurities was evident (Fig. 3, left chromatogram). Originally we used a 5–10% lower acetonitrile concentration in the final conditions for preparative elution, but for a series of small hexapeptides elution did not occur until the level of acetonitrile was increased. Therefore, to maintain the maximum separation and establish the level of acetonitrile that would effect elution, we increased the gradient time so as to reach a percentage of organic modifier that would definitely elute the compound. Thus, for Lys–Ala–Met–Tyr–Ala–Pro, the analytical gradient conditions were 3–15% acetonitrile in 15 min and a large heterogeneous impurity was eluted before the major product, as seen in Fig. 3 (left chromatogram). The sample was chromatographed with a long gradient, the compound being expected to elute before the end of the gradient. However, as shown in Fig. 4, the components were eluted at about 15% acetonitrile. The appearance of the minor components is very similar to that in the analytical chromatography of the crude peptide (Fig. 3). The second peak in the chromatogram contained the major product that was purified, as seen in the chromatogram of Fig. 3, with a recovery of 65% of the total mass loaded. Hence long gradient times are advantageous for maximizing separations especially when there is uncertainty about the percentage of acetonitrile required to elute the sample. The earlier eluting impurities could be due to oxidized methionine or carbonates of lysine, which would create more polar structures. Nevertheless, pure peptide was obtained in one step.

Another peptide, Ala–His–Ser–Asn–Arg–Lys–Leu–Met–Glu–Ile–Ile, was synthesized on Boc-Ile-PAM resin. The tosyl protecting group on histidine was removed from the imidazole ring after the coupling by treatment with hydroxybenzotriazole.

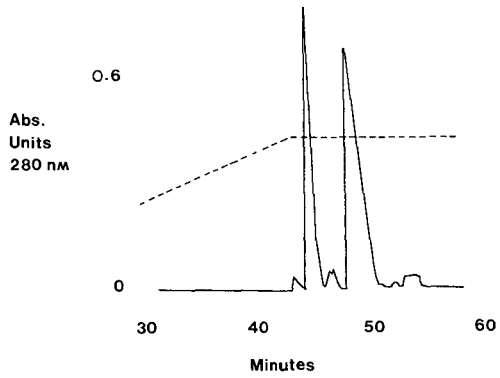

Fig. 4. Preparative chromatography of the hexapeptide Lys–Ala–Met–Tyr–Ala–Pro (158 mg) on the YMC 50-mm I.D. column in the solvent system as described in Fig. 2. The gradient was started 13 min after loading and went from 0 to 25% B in 30 min. The part of the run from 30 to 60 min is shown. The fractions across the whole of the second peak (48–50 min) were pure by analytical HPLC (not shown). The 45-min peak contained impurities.

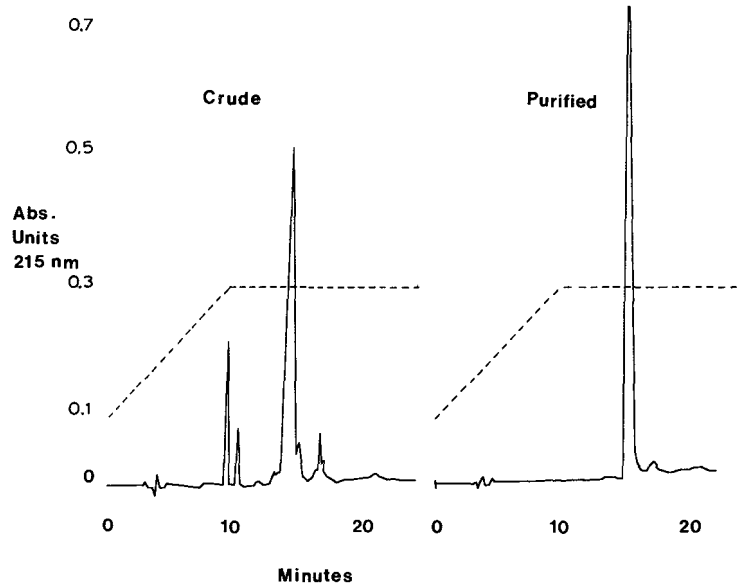

Fig. 5. Chromatographic analysis of the undecapeptide Ala–His–Ser–Asn–Arg–Lys–Leu–Met–Glu–Ile–Ile unpurified (left) and purified (right), 10 μg each, in a gradient from 10–30% B (same mobile phase as in Fig. 1) in 10 min with detection at 215 nm with 1 a.u.f.s. The peptide was eluted at *ca.* 15 min.

The resulting peptide had the expected molar ratios and the analytical chromatography showed the presence of multiple but minor impurities (Fig. 5). Most of the peptide (330 mg) was loaded and a gradient to 30% acetonitrile was run in 30 min. Fig. 6 shows the preparative chromatogram; the composition is similar to the analyt-

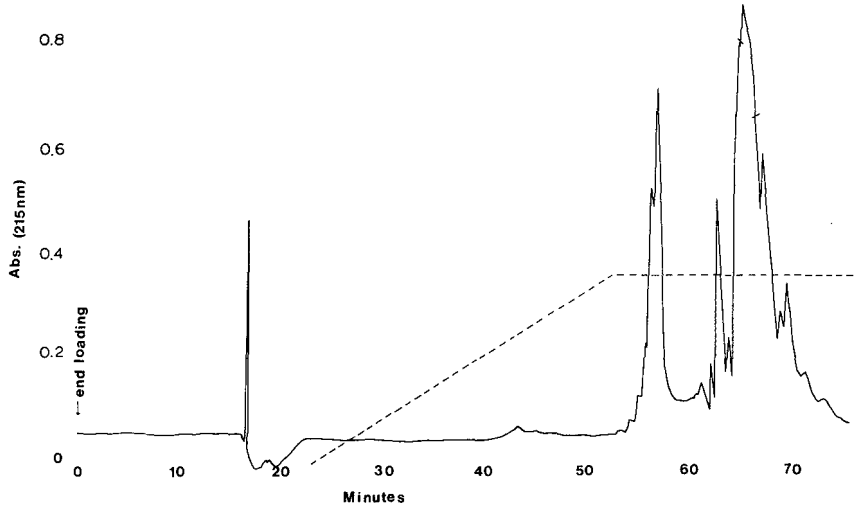

Fig. 6. Preparative chromatography of the undecapeptide Ala–His–Ser–Asn–Arg–Lys–Leu–Met–Glu–Ile–Ile (330 mg) on the YMC 50-mm I.D. column. The gradient was started after 20 min and was run from 0 to 30% B (same solvent system as in Fig. 2) in 30 min. The part of the major peak (65 min) between the marks was taken as the pure peptide. Detection was at 215 nm at 1 a.u.f.s.

ical separation. To increase the separation of the components, it was important to increase the duration of the gradient. The fractions collected between the marks on the large peak were pure and used for experiments. The fractions on either side were 80–90% pure and not pooled with the purest fractions. The recovery of the pure peptide was approximately 80 mg. The remainder of the mass in the whole peak was undetermined. To recover more pure peptide, it is possible to rechromatograph the impure fractions, but we derived sufficient material for the experiments.

The column of 10-μm spherical ODS bonded-phase particles gave results of high resolution for preparative-scale chromatography. The issue of whether the pore size should be larger, *i.e.*, 300 Å, at least for peptides of MW <2300, does not appear to be important with respect to capacity or resolution. We found the kind of elution that can be scaled up successfully is one in which the peak of interest is eluted 3–6 min following the completion of the gradient reaching the final solvent percentage. The gradient duration is usually 10–15 min. The same percentage of acetonitrile can be used as the final conditions in the 2-in. column, but always starting from 0% and making the gradient duration two to four times that in the analytical run, or 30–60 min. The longer gradient duration can be used to elute the more polar impurities. The linear velocities of the analytical and preparative columns are comparable but not identical, being 3.9 and 2.9 cm/min, respectively. Hence the final percentage of acetonitrile, which is reached *ca.* 5 min before the peptide elutes, can be used as the final conditions with appropriate lengthening of the time to reach that level, as was done in the examples of dehydrokallidin and the undecapeptide. For convenience in detection, phosphoric acid is used for the analytical chromatography owing to its transparency at low wavelengths. Although the elution may be different using TFA, especially for basic peptides, this has rarely occurred in our experience (unpublished results).

The examples shown here involve more heterogeneous synthetic products of relatively small peptides because of the presence of certain amino acids known to give more impurities owing to the methods of synthesis. However, these were removed expeditiously by these procedures. The large column used in these purifications has been used continuously for more than 6 months for the purification of over 25 different peptides.

ACKNOWLEDGEMENTS

We thank Truc T. Dang and Linda Kocak for help with the synthesis of the peptides. The compounds were prepared for the National Institutes of Health, Bethesda, MD, and the Nova Pharmaceutical Corporation, Baltimore, MD, U.S.A.

REFERENCES

1 J. M. Stewart and J. D. Young, *Solid Phase Peptide Synthesis*, Pierce, Rockford, IL, 2nd ed., 1984.
2 J. R. Benson and P. E. Hare, *Proc. Natl. Acad. Sci. U.S.A.*, 72 (1975) 619.
3 M. Knight, M. P. Strickler, M. J. Stone, L. Chiodetti, S. Gluch and T. Shinohara, *J. Chromatogr.*, 459 (1988) 361.
4 M. Knight, G. D. Mack, R. Perkins and T. R. Burke, Jr., *J. Chromatogr.*, 444 (1988) 345.

Journal of Chromatography, 484 (1989) 307–318
Elsevier Science Publishers B.V., Amsterdam — Printed in The Netherlands

CHROM. 21 815

PREPARATIVE-SCALE SYNTHESIS AND REVERSED-PHASE PURIFICATION OF A GONADOTROPIN-RELEASING HORMONE ANTAGONIST

CARL HOEGER, JOHN PORTER, JAROSLAV BOUBLIK and JEAN RIVIER*
Clayton Foundation Laboratories for Peptide Biology, Salk Institute, 10010 N. Torrey Pines Road, La Jolla, CA 92138 (U.S.A.)

SUMMARY

The preparation of "Nal–Glu" antagonist (Ac–D-Nal–D-Cpa–D-Pal–Ser–Arg–D-2-amino-5-oxo-5-(4-methoxyphenyl)pentanoic acid–Leu–Arg–Pro–D-Ala–NH_2) was accomplished in two steps: (i) preparation of [Ac–D-Nal[1], D-Cpa[2], D-Pal[3], Arg[5], D-Glu[6], D-Ala[10]]-GnRH via standard solid-phase synthetic techniques and (ii) acylation of anisole (Friedel–Crafts) by the glutamic acid residue in position 6. The preparative-scale, reversed-phase high-performance liquid chromatographic (HPLC) purification of the crude "Nal–Glu" antagonist employs first a triethylammonium phosphate (TEAP) (pH 2.25)–acetonitrile solvent system, followed by an HPLC-based desalting procedure, yielding the acetate salt of the peptide. This repetitive process of purification in TEAP–acetonitrile, followed by counter-ion exchange with 0.5% acetic acid–acetonitrile is highly reproducible and allows large amounts of a given peptide to be purified efficiently in a batchwise fashion. The procedure described for the synthesis, purification and characterization of the "Nal–Glu" antagonist is presented as a model for the multi-gram synthesis and purification of peptides to be used in clinical investigations.

INTRODUCTION

The role assumed by high-performance liquid chromatography (HPLC) in the isolation and purification of biologically significant peptides and proteins is well documented[1]. As new peptides were isolated and characterized and the need for their duplication by total synthesis became imperative, the usefulness and power of preparative reversed-phase (RP) HPLC was recognized[2]. The technological advances that have arisen in the synthesis and chromatographic handling of peptides have led to a situation where it is now recognized that selected (10- to 40-residue) peptides synthesized in the solid phase pioneered by Merrifield[3] can be purified to the point where the most sophisticated analytical techniques cannot detect significant amounts of impurities. Work in this laboratory has demonstrated that such peptides [in our case, the releasing factors gonadotropin-releasing hormone (GnRH)[4], somatostatin (SS)[5], corticotropin-releasing factor (CRF)[6,7] and growth hormone-releasing factor (GRF)[8]] can be successfully and safely used in a clinical setting. Since large (multi-

0021-9673/89/$03.50

gram) amounts of these peptides are needed for toxicological studies and clinical investigations *per se,* we have developed large-scale methodologies for both the synthesis and purification of these peptides.

One peptide of current clinical interest prepared in this laboratory is "Nal–Glu" antagonist: Ac–D-Nal–D-Cpa–D-Pal–Ser–Arg–D-2-amino-5-oxo-5-(4-methoxyphenyl)pentanoic acid–Leu–Arg–Pro–D-Ala–NH_2.[9] This peptide, a GnRH antagonist, is prepared via a hydrofluoric acid-mediated Friedel–Crafts acylation of the glutamic acid residue of [Ac–D-Nal[1], D-Cpa[2], D-Pal[3], Arg[5], D-Glu[6], D-Ala[10]]-GnRH by anisole. The purification of this compound employs a triethylammonium phosphate–acetonitrile solvent system, followed by an HPLC-based desalting procedure to obtain the acetate salt. We describe here the synthesis, purification and characterization of this unique GnRH antagonist, the procedure for which we offer as a model for the large-scale preparation of clinical peptides.

EXPERIMENTAL

Apparatus

The analytical chromatographic system consisted of a Perkin-Elmer Series 400 liquid chromatograph with quaternary gradient capabilities, a Houston Instruments Omniscribe strip-chart recorder, a Hewlett-Packard 3390A reporting integrator, a Rheodyne 7125 injector and a Kratos 757Z variable-wavelength UV detector.

The preparative chromatographic system consisted of a Waters Assoc. DeltaPrep Model 3000 instrument, a Houston Instruments Omniscribe strip-chart recorder and a Kratos Model 757 variable-wavelength UV detector.

Analytical columns

The analytical columns (25 × 0.46 cm I.D.) were packed with Vydac (5-μm, particle size and 300 Å pore size) C_{18} silica[10], obtained from the Separations Group (Hesperia, CA, U.S.A.).

Preparative cartridges

Empty polyethylene cartridges and frits (part numbers 50411 and 50421) obtained from Waters Assoc. were dry-packed in our laboratory with Vydac C_{18} derivatized silica (15–20-μm particle size and 300-Å pore size). For a discussion regarding packing materials for preparative chromatography, see ref. 10.

Solvent systems

Distilled, deionized, sterile water was used in all purification steps. The triethylammonium phosphate (pH 2.25) (TEAP) and the trifluoroacetic acid (TFA) solvent systems have been described earlier[11,12]. The TEAP system was prepared from 0.9% (v/v) phosphoric acid and 0.9% (v/v) triethylamine and the pH was adjusted to 2.25 by addition of either phosphoric acid or triethylamine. Ammonium acetate (puriss. p.a.) was obtained from Fluka (Buchs, Switzerland). Solvent A was always the aqueous buffer and solvent B was acetonitrile–buffer A (60:40) unless indicated otherwise. Analytical and preparative flow-rates were 2 and 85–100 ml/min, respectively. The wavelength at which the eluent was monitored and the absorbance scale used are shown on the left-hand ordinate of the figures, the gradient shape is indicated as an

overlay, with percentage of acetonitrile values indicated on the right-hand ordinate, and the abscissa indicates the time of elution.

Peptides

[Ac–D-Nal[1], D-Cpa[2], D-Pal[3], Arg[5], D-Glu[6], D-Ala[10]]-GnRH was synthesized manually by the solid-phase approach using classical solid-phase peptide synthesis techniques[13,14]. In brief, this peptide was assembled on 250 g of a methylbenzhydrylamine resin, as the ultimate desired final product had a C-terminal carboxamide (the substitution level was 0.92 mequiv. NH_2/g). Hydrogen fluoride cleavage and deprotection at 0°C for 1.5 h in the presence of anisole as a carbocation scavenger yielded, after extraction and lyophilization, the crude peptidic preparation, which was converted to "Nal–Glu" antagonist by subjecting this material in a batchwise fashion to an anhydrous hydrofluoric acid mediated Friedel–Crafts acylation reaction with anisole (see discussion below). After removal of the hydrofluoric acid and unreacted anisole under vacuum, the peptide was treated with anhydrous diethyl ether to remove residual hydrofluoric acid and anisole. The material thus obtained was filtered, dissolved in acetonitrile–water (10:90) and lyophilized.

Sample preparation and loading

Approximately 1–3 g of the crude, lyophilized material obtained after the Friedel–Crafts reaction was dissolved, just prior to chromatography, in a buffer (100–200 ml) whose concentration of organic modifier was equal to or below that used for the equilibration of the cartridge prior to the run and the pH of the solution was adjusted to *ca.* 7.0 with 6 *M* sodium-hydroxide. After stirring for 20–30 min the solution was acidified and filtered to remove particulates. This solution, often slightly opalescent, was then loaded onto the radially compressed column through the pumps and chromatographed using the gradient conditions given in the individual figure legends.

Sample composition analysis

The composition of the final purified product was determined by a number of methods, including mass spectral analysis (City of Hope, Duarte, CA, U.S.A.); C,H,N and ash determination (Galbraith Labs., Knoxville, TN, U.S.A.), Karl Fischer water determination (Bachem, Torrance, CA, U.S.A.), and analysis of counter ions (see Table I). Amino acid composition was determined by hydrolysis with 4 *M* methanesulfonic acid (Pierce, Rockford, IL, U.S.A.) at 110°C for 24 h, followed by amino acid analysis.

RESULTS AND DISCUSSION

The structure of "Nal–Glu" antagonist is shown in Fig. 1. It contains six substitutions of the native GnRH structure (pGlu–His–Trp–Ser–Tyr–Gly–Leu–Arg–Pro–Gly–NH_2), five of which are D-amino acids. The unusual amino acid present in the 6-position, D-2-amino-5-oxo-5-(4-methoxyphenyl)pentanoic acid (**I**), is prepared via a hydrofluoric acid-mediated Friedel–Crafts acylation and modification of D-glutamic acid with anisole[15,16]. With the exception of this modified glutamic acid, the remaining amino acids are either commercially available or readily prepared in sufficient amounts for the synthesis of this peptide[9]. The keto amino acid **I** must be

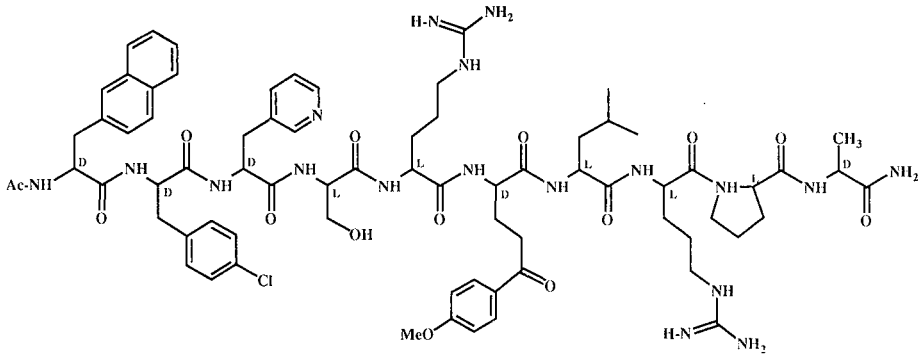

Fig. 1. Structure of "Nal–Glu" antagonist (Ac–D-Nal–D-Cpa–D-Pal–Ser–Arg–D-2-amino-5-oxo-5-(4-methoxyphenyl)pentanoic acid–Leu–Arg–Pro–D-Ala–NH_2). The chirality of the individual residues is represented by an appropriate stereochemical label on the C-α carbons.

prepared post-synthetically, as the free amino acid is known to undergo cyclization to form the dehydroproline derivative **II** (eqn. 1)[16].

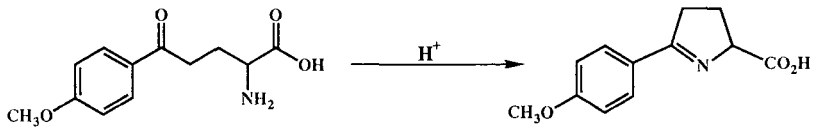

I II (1)

This reaction is also responsible for the inability of the modified Glu to be detected upon amino acid analysis of the hydrolyzed peptide. Although methods could undoubtedly be devised for the synthesis of **I**, we opted to prepare "Nal–Glu" antagonist via the Friedel–Crafts acylation reaction, as this reaction is generally a reliable method for its preparation.

Synthesis of "Nal–Glu" antagonist

The general procedure for the synthesis of "Nal–Glu" antagonist has been reported elsewhere[9]; it is based on a side reaction of glutamic acid first elucidated in 1975[15,16]. The first step in this reaction involves the preparation of [Ac-D-Nal^1, D-Cpa^2, D-Pal^3, Arg^5, D-Glu^6, D-Ala^{10}]-GnRH. This peptide is synthesized utilizing standard solid-phase peptide synthesis techniques[13,14]. Batchwise, concurrent deprotection and cleavage of the resin-bound peptide by hydrofluoric acid–anisole at 0°C provided, after extraction and lyophilization, 227 g of this crude "Nal–Glu" precursor. The analytical HPLC–UV trace of product run in 0.1% TFA–acetonitrile is presented in Fig. 2; very few impurities are seen in this crude peptide preparation. It has been determined in this laboratory that the crude [Ac-D-Nal^1, D-Cpa^2, D-Pal^3, Arg^5, D-Glu^6, D-Ala^{10}]-GnRH is sufficiently pure to carry on to the Friedel-Crafts acylation step, as neither the impurities nor the salts and non-peptidic materials interfere to a significant extent with the subsequent conversion to and purification of crude "Nal–Glu" antagonist.

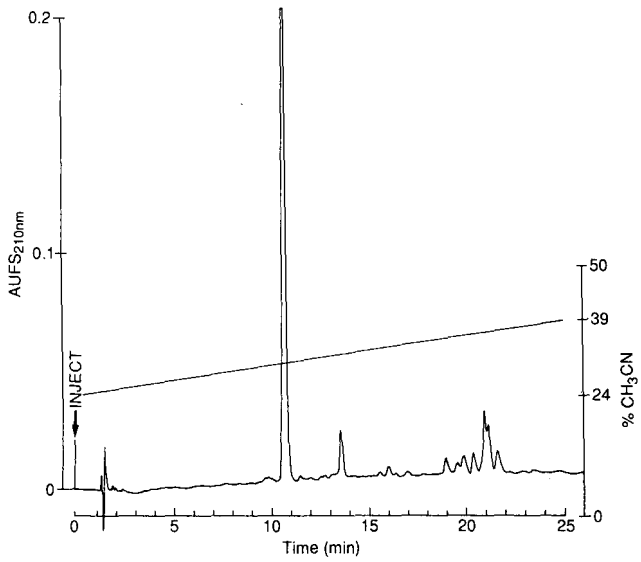

Fig. 2. Load: crude, lyophilized [Ac-D-Nal[1], D-Cpa[2], D-Pal[3], Arg[5], D-Glu[6], D-Ala[10]]-GnRH from HF cleavage (1.5 μl, *ca.* 5 μg). Column: Vydac (5 μm) C_{18}, 25 × 0.46 cm I.D. Solvent: 0.1% TFA in water–acetonitrile. Gradient: 24–39% acetonitrile in 25 min. Flow-rate: 2.0 ml/min, 2000 p.s.i. back-pressure.

The conversion of this crude peptide to "Nal–Glu" antagonist was accomplished in a batchwise fashion as follows: 5.0–24.0 g (average 20 g) of [Ac-D-Nal[1], D-Cpa[2], D-Pal[3], Arg[5], D-Glu[6], D-Ala[10]]-GnRH were placed in a graduated Kel-F HF cleavage vessel containing 20 ml of anisole and a magnetic stirring bar. After cooling the vessel for 5 min in a liquid nitrogen bath, it was evacuated and subsequently charged with 160–180 ml of anhydrous hydrofluoric acid. The mixture was then stirred in a hood at ambient temperature (22°C) overnight (16–18 h). This procedure, although potentially dangerous, is a convenient and facile method for the preparation of "Nal–Glu" antagonist. After the hydrofluoric acid treatment of all of the [Ac-D-Nal[1], D-Cpa[2], D-Pal[3], Arg[5], D-Glu[6], D-Ala[10]]-GnRH analog, the weight of crude "Nal–Glu" antagonist obtained was 210 g. The absorbance profile obtained for this crude material is presented in Fig. 3.

Purification of "Nal–Glu" antagonist

The crude material obtained directly after the acylation reaction contains an approximately 1:1 mixture of the desired "Nal-Glu" antagonist (starred peak) and a closely associated hydrophilic impurity (Fig. 3), in addition to a number of other hydrophobic and hydrophilic impurities. When one examines the mechanism and reaction conditions employed in the synthesis of "Nal–Glu" antagonist, two interesting facets to the reaction become apparent. The first arises out of the mechanism of the Friedel–Crafts reaction. The presumed intermediate in the conversion of the glutamic acid to the keto amino acid **I** is the acylium ion; this reactive species can add not only to anisole but also to other nucleophilic species in the reaction medium, the most prevalent being the amide nitrogens in the peptide backbone[15,16]. The peptides aris-

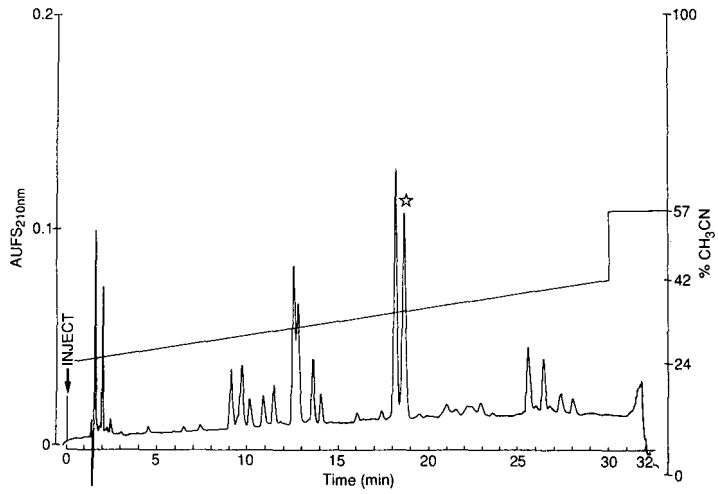

Fig. 3. Load: crude, lyophilized "Nal–Glu" antagonist (10 μl, 10 μg). Column: Vydac (5 μm) C_{18}, 25 × 0.46 cm I.D. Solvent: 0.1% TFA in water–acetonitrile. Gradient: 24–42% acetonitrile in 30 min. Flow-rate: 2.0 ml/min, 2000 p.s.i. back-pressure. The starred peak is the desired compound.

ing from this reaction account for the early-eluting hydrophilic impurities; the amounts of these materials formed can be minimized by optimization of concentrations of anisole (10%) and peptide–substrate (10 g of peptide per 100 ml of anhydrous hydrofluoric acid–anisole). Most important, however, is the observation that peptides containing serine, when treated under acidic conditions at elevated temperatures for

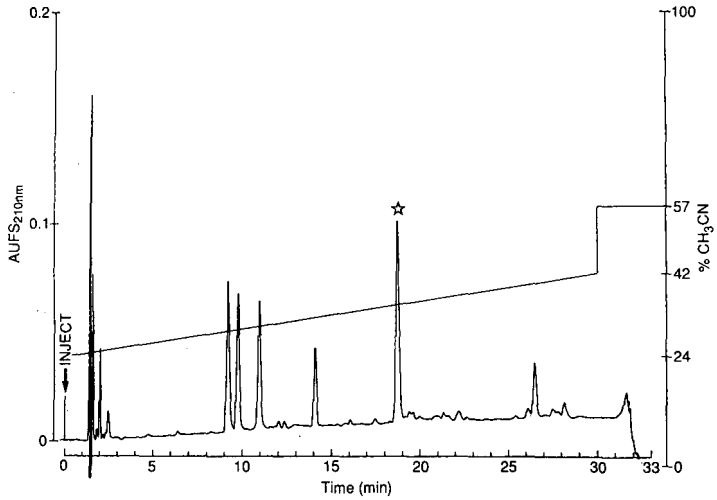

Fig. 4. Load: crude, lyophilized "Nal–Glu" antagonist (10 μl, 10 μg) after stirring at pH 6.5 for 30 min. Column: Vydac (5 μm) C_{18}, 25 × 0.46 cm I.D. Solvent: 0.1% TFA in water–acetonitrile. Gradient: 24–42% acetonitrile in 30 min. Flow-rate: 2.0 ml/min, 2000 p.s.i. back-pressure. The starred peak is the desired compound.

prolonged periods, can undergo an N-to-O acyl shift[17]. This side-reaction is not a serious problem, as adjustment of the pH of a solution of the crude peptide to 6.0–7.5 will result in a rapid reversal of this reaction (O-to-N acyl shift). In this instance, the closely associated hydrophilic "impurity" arises from just such an N-to-O acyl shift between the D-Pal[3] carboxamide nitrogen and the Ser[4] side-chain hydroxyl group (eqn. 2); stirring crude "Nal–Glu" antagonist at pH > 6 for 30 min reverses this shift and simplifies the analytical HPLC–UV trace considerably, as shown in Fig. 4 (compare with Figure 3; the starred peak is "Nal–Glu" antagonist). Thus, an understanding of the chemistry aids in the simplification of the purification of the desired peptide from the crude material and in an increase in yield.

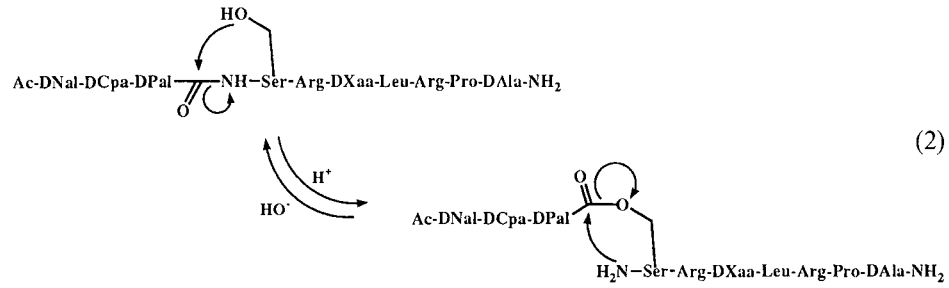

(2)

Purification of "Nal–Glu" antagonist from the crude material was accomplished through HPLC procedures as described elsewhere[18,19]. A typical HPLC profile of the preparative-scale purification is shown in Fig. 5. Analytical isocratic conditions that will yield maximum information on the composition of the mixture around the desired product were first determined; in general this is obtained when the desired product elutes with a solute capacity factor (k') between 4 and 8; in the present instance, the ideal conditions employ a flow-rate of 2 ml/min with an isocratic solvent composition of 36% acetonitrile in water + 0.1% TFA.

The analytical HPLC screening of various fractions obtained from the preparative HPLC run (depicted in Fig. 5) is presented in Fig. 6. A solvent system consisting of 0.1% TFA–acetonitrile is particularly convenient as the UV transparency of this solvent system at 210 nm allows for high sensitivity, in addition to providing an extended column life span, and reproducibly good separations, extremely important points when faced with purifications on the scale reported here. Determination of the isocratic analytical conditions allows the successive and rapid assessment of the identity and purity of the fractions obtained from the individual preparative HPLC purification runs. As we have found that the TEAP–acetonitrile solvent system generally gives higher resolution and different selectivity than the corresponding TFA system, preparative-scale purification is run first employing TEAP at pH 2.25 and acetonitrile, applying a gradient selected on the basis of the analytical chromatogram obtained for the crude material (see Figs. 3 and 4). Owing to the strong elutropic characteristics of the TEAP buffer, preparative gradient conditions are generally started at about 10% lower acetonitrile concentration than the isocratic analytical conditions in TFA with a slope of 1% increase in acetonitrile per 300 ml of solvent that is eluted.

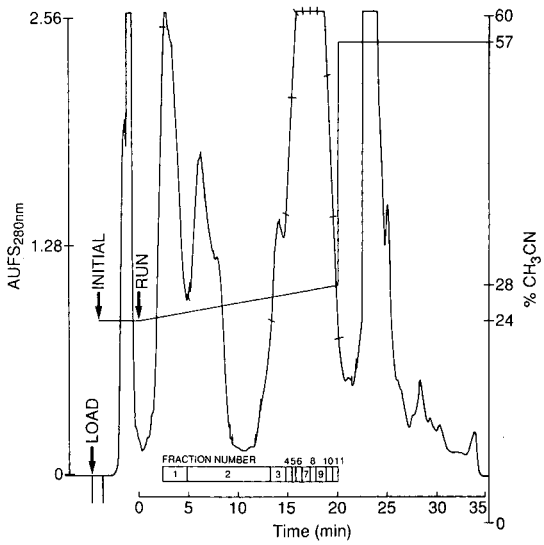

Fig. 5. Load: purified crude, lyophilized "Nal–Glu" antagonist after stirring at pH 6.5 for 30 min (3.0 g in 150 ml). Cartridge: 30 × 5 cm I.D., packed with Vydac (15–20 μm) C_{18}. Solvent: TEAP (pH 2.25)–acetonitrile. Gradient: 24–28% acetonitrile in 20 min. Flow-rate: 90 ml/min, 500 p.s.i. column back-pressure. Fractions taken are indicated by slash marks on the trace and boxes under the absorbing peak.

The fractions obtained from this purification step are screened analytically and pooled based on the composition as determined from analytical HPLC; in this fashion three pools are obtained: "good" (total impurities <1%) and "philic" and "phobic" (fractions containing hydrophilic or hydrophobic impurities, respectively,

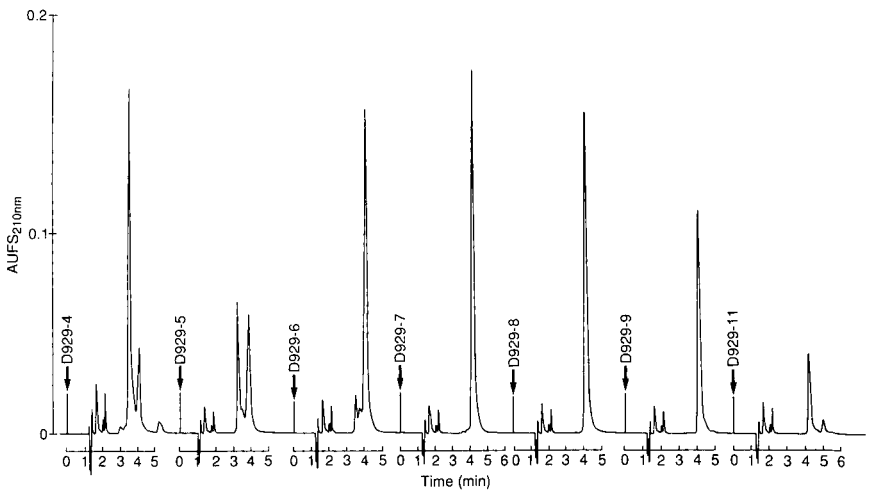

Fig. 6. Analytical screening of fractions 4–9 + 11 obtained from the TEAP purification shown in Fig. 5 (*ca.* 10 μl, 10 μg). Column: Vydac (5 μm), C_{18}, 25 × 0.46 cm I.D. Solvent: 0.1% TFA in water–acetonitrile; isocratic at 36% acetonitrile. Flow-rate: 2.0 ml/min, 2000 p.s.i. back-pressure.

of 1–30%). From the preparative run depicted in Fig. 5, the relative fates of the fractions obtained are as follows: 1–5, waste; 6, "philic"; 9–11, "phobic"; and 7–8, "good". The "phobic" and "philic" pools are then concentrated and separately re-purified to obtain additional pure material. This repurification, in the case of "Nal–Glu" antagonist, was accomplished using either a TEAP–acetonitrile solvent system and a different gradient or 0.5% acetic acid–acetonitrile. Although a high degree of purity can be achieved with the TEAP system, a desalting step utilizing 0.5% acetic acid–acetonitrile is required to free the peptide from any TEAP salt. Purification in two systems (TEAP followed by acetic acid) and analysis in another (TFA) was found in general to minimize the probability of missing any impurities and to maximize the probability of obtaining a pure final product while offering good recovery.

The conversion of the peptide from its TEAP salt to the corresponding acetate form is accomplished through HPLC procedures utilizing a 0.5% acetic acid–acetonitrile solvent system. This method of preparing acetate salts is based in part on an earlier procedure[19]. Briefly, this material was desalted and converted to the acetate salt form in the following manner: a pool of "acceptable" fractions containing approximately 3–6 g of peptide (as determined by analytical HPLC) was diluted with an equal volume of 0.07 *M* ammonium acetate (pH 4.5). This solution was then applied to the same preparative HPLC cartridge as used in the purification above. After loading the peptide, the cartridge was washed with 1.5 l of 6% acetonitrile in water containing 0.5% acetic acid, after which the peptide was eluted from the cartridge by

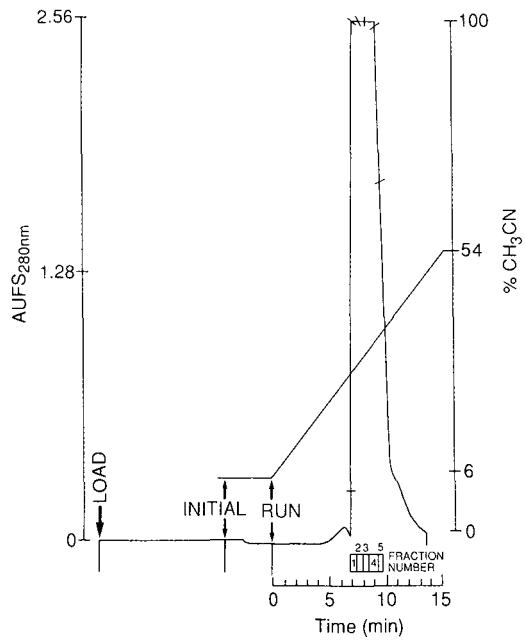

Fig. 7. Load: concentrated/desalted "good" "Nal–Glu" antagonist pool (*ca.* 3 g in 4 l). Cartridge: 30 × 5 cm I.D., packed with Vydac (15–20 μm) C_{18}. Solvent: 0.5% acetic acid–acetonitrile. Gradient: 6–54% acetonitrile in 15 min. Flow-rate: 95 ml/min, 500 p.s.i. column back-pressure. Fractions taken are indicated by slash marks on the trace and boxes under the absorbing peak.

application of a gradient running from 6 to 54% acetonitrile in water containing 0.5% acetic acid over 15 min at a flow-rate of 95 ml/min. The HPLC trace of this process is given in Fig. 7. This batch-wise procedure was repeated until all of the peptide had been converted to the corresponding acetate.

The fractions of the desired product that were deemed acceptable by analytical HPLC screening (data not shown) of the fractions obtained from these runs were collected and pooled for lyophilization. Each batch of lyophilized powder was re-lyophilized from 2.5 l of 0.5% acetic acid to ensure the complete removal of acetonitrile from the peptide. To ensure homogeneity of "Nal–Glu" antagonist, a final single-batch lyophilization was carried out. The purified peptide was dissolved in 2 l of deionized, distilled water and stirred until a clear solution was obtained (15 min). The solution was then filtered into clean, acid-washed lyophilizer bottles so that the resulting solution prior to lyophilization contained no visible particulate matter. After lyophilization at ambient temperature (20–22°C), 36.2 g of the "Nal–Glu" antagonist were obtained as a fluffy white powder. We find this result, and also the method, to be both general and reliable for a wide range of peptides, and an alternative to the pyridine–acetic acid–2-propanol–water method of Gabriel[20] or the use of classical anion-exchange supports based on cellulose, Sephadex or polystyrene[21].

Characterization of "Nal–Glu" antagonist

As the end usage of this preparation of "Nal–Glu" antagonist is for human clinical use and toxicological studies, it was subjected to a complete chemical and biological analysis. Table I gives a summary of some of the data obtained for this preparation of "Nal–Glu" antagonist. The homogeneity of this peptide in two analytical HPLC solvent systems (TEAP–acetonitrile and 0.1% TFA–acetonitrile) is given in Fig. 8a and b. Finally, this compound was shown to co-elute with authentic "Nal–Glu" antagonist and the analytical HPLC for this experiment is shown in Fig. 8c. Homogeneity in at least two solvent systems and coelution with a standard (if available) is a routine procedure in our laboratory for large batches of peptides; although it is not a final criterion of purity, it is always an important indicator. The amino acid analysis gave (with expected values in parentheses) Ser, 0.79 (1.00); Leu, 1.00 (1.00); Pro, 0.99 (1.00); Ala, 0.98 (1.00); Cpa, 1.03 (1.00); Nal, 1.02 (1.00); and Arg, 2.07 (2.00); neither the modified glutamic acid nor the pyridylalanine residues can be detected using currently available protocols; however, the presence of these two ami-

TABLE I

CHARACTERIZATION OF "NAL–GLU" ANTAGONIST

Parameter	*Value*
Mass spectrum	MH^+ = 1485.52 (calc., MH^+ = 1485.72)
C,H,N analysis	Found: C 54.96; H 6.88; N 15.11%
	Calc.: C 54.81; H 6.77; N 15.07%
Ash	<0.16%
Acetate content	6.33 ± 0.26% CH_3COOH
Water content	5.43% ± 0.13% H_2O
Optical rotation	−35.7° (*c* = 1.00; 50% CH_3COOH in H_2O)
Composition	$C_{73}H_{97}O_{18}Cl \cdot 1.67\ H_2O \cdot 4.7\ CH_3COOH$

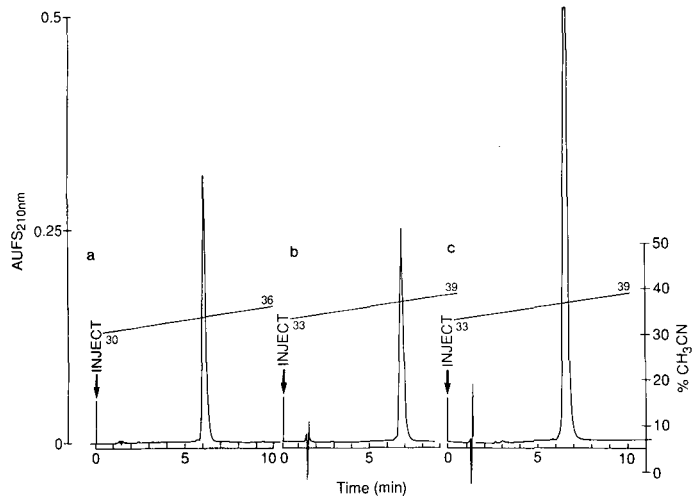

Fig. 8. Analytical HPLC traces of purified "Nal–Glu" antagonist, including coelution experiment. For all three runs the following parameters apply: column, Vydac (5 μm) C_{18}, 25 × 0.46 cm I.D.; flow-rate, 2.0 ml/min, 2000 p.s.i. back-pressure. (a) Load: purified "Nal–Glu" antagonist (5 μl, 5 μg). Solvent: TEAP–acetonitrile. Gradient: 30–36% acetonitrile in 10 min. (b) Load: purified "Nal–Glu" antagonist (5 μl, 5 μg). Solvent: 0.1% TFA in water–acetonitrile. Gradient: 33–39% acetonitrile in 10 min. (c) Load: co-injection of purified "Nal–Glu" antagonist (4 μl, 4 μg) with "Nal–Glu" antagonist standard (4 μl, 4 μg). Solvent: 0.1% TFA in water–acetonitrile. Gradient: 33–39% acetonitrile in 10 min.

no acids is confirmed by both mass spectral and C,H,N analysis (see Table I). For completeness, the water and acetate counter-ion contents of the peptide were also determined; based on these data, and the peptide composition as determined by amino acid analysis, this preparation of peptide is found to be *ca.* 90% peptide, with the remainder attributable to acetate counter ions and water of hydration.

CONCLUSION

Over the past few years, the methodology and technology for preparing and purifying synthetic peptides on a scale sufficiently large to allow toxicological and clinical studies to be carried out has progressed considerably. We have shown previously that clinical batches of peptides can be synthesized and obtained in a highly purified form and that this can be accomplished in the setting of an academic laboratory. This is satisfying in that it is seldom possible (or plausible) for an academic research laboratory to have the opportunity to undertake and complete such a task. We have demonstrated that we can make this extension in the case of "Nal–Glu" antagonist and hopefully have convinced the reader that, at least in some instances, an academic laboratory can successfully accomplish industrial-type development.

ACKNOWLEDGEMENTS

This research was supported by NIH contract NO1-HD-7-2907 and NIH Grant HD13527. We thank Drs. Terry Lee (City of Hope, Duarte, CA, U.S.A.) and

Mike Verlander (Bachem, Torrance, CA, U.S.A.) for the mass spectral and water content data, respectively. We are indebted to Duane Pantoja, Dean Kirby, Charleen Miller, Dr. Marilyn Perrin, Dr. William Hook (NIH) and Drs. Rehan Naqvi and Marjorie Lindberg (EG&G Mason Research Institute, Worcester, MA, U.S.A.) for their expert assistance in the purification and chemical and biological characterization of the peptide.

REFERENCES

1 J. Rivier and R. McClintock, in A. R. Kerlavage (Editor), *The Use of HPLC in Protein Purification and Characterization*, Alan R. Liss, New York, 1989, pp. 77–106.
2 R. Burgus and J. Rivier, in A. Loffet (Editor) *Peptides 1976*, Editions de l'Université, Brussels, 1976, p. 85.
3 R. B. Merrifield, *J. Am. Chem. Soc.*, 85 (1963) 2149.
4 S. Yen, R. Rebar, G. VandenBerg, F. Naftolin, H. Judd, Y. Ehara, K. Ryan, J. Rivier, M. Amoss and R. Guillemin, in C. Gual and E. Rosenberg (Editors), *Hypothalamic Hypophysiotropic Hormones*, Excerpta Medica, Amsterdam, 1973, p. 217.
5 S. Yen, T. Siler, G. DeVane, J. Rivier, W. Vale, P. Brazeau and R. Guillemin, in S. Raiti (Editor), *Advances in Human Growth Hormone Research*, U.S. Government Printing Office, Department of Health, Education and Welfare, Publ. No. (NIH) 74-612, 1973, p. 609.
6 J. H. Liu, K. Muse, P. Contreras, D. Gibbs, W. Vale, J. Rivier and S. S. C. Yen, *J. Clin. Endocrinol. Metab.*, 57 (1983) 1087.
7 D. N. Orth, C. R. DeBold, G. S. DeCherney, R. V. Jackson, W. R. Sheldon, W. E. Nicholson, H. Uderman, A. N. Alexander, D. P. Island, J. Rivier and W. W. Vale, *Clinical Studies with Synthetic Ovine Corticotropin-Releasing Factor*, Santa Barbara, CA, 1985, p. 197.
8 A. D. Rogol, R. M. Blizzard, A. J. Johanson, R. W. Furlanetto, W. S. Evans, J. Rivier, W. W. Vale and M. O. Thorner, *J. Clin. Endocrinol. Metab.*, 59 (1984) 580.
9 J. Rivier, J. Porter, C. Rivier, M. Perrin, A. Corrigan, W. A. Hook, R. P. Siraganian and W. W. Vale, *J. Med. Chem.*, 29 (1986) 1846.
10 J. Rivier and R. McClintock, *J. Chromatogr.*, 268 (1983) 112.
11 J. Rivier, *J. Liq. Chromatogr.*, 1 (1978) 343.
12 J. P. J. Bennett, A. M. Hudson, C. McMartin and G. E. Purdon, *Biochem. J.*, 168 (1977) 9.
13 R. B. Merrifield, *Angew. Chem., Int. Ed. Engl.*, 24 (1985) 799.
14 J. M. Stewart and J. D. Young, *Solid Phase Peptide Synthesis*, Pierce, Rockford, IL, 1984.
15 S. Sano and S. Kawanishi, *J. Am. Chem. Soc.*, 97 (1975) 3480.
16 R. S. Feinberg and R. B. Merrifield, *J. Am. Chem. Soc.*, 97 (1974) 3485.
17 R. Bergmann *et al.*, *Hoppe-Seyler's Z. Physiol. Chem.*, 131 (1923) 1.
18 C. A. Hoeger, R. Galyean, R. A. McClintock and J. E. Rivier, in *HPLC of Peptides and Proteins: Separation, Analysis, and Conformation*, CRC Press, Boca Raton, FL, 1989, in press.
19 C. Hoeger, R. Galyean, J. Boublik, R. McClintock and J. Rivier, *Biochromatography*, 2 (1987) 134.
20 T. F. Gabriel, *Int. J. Pept. Protein Res.*, 30 (1987) 40.
21 L. R. Snyder and J. J. Kirkland, *Introduction to Modern Liquid Chromatography*, Wiley, New York, 1979.

Journal of Chromatography, 484 (1989) 319–325
Elsevier Science Publishers B.V., Amsterdam — Printed in The Netherlands

CHROM. 21 800

CHROMATOGRAPHY OF PEPTIDES ON A MULTI-COIL COUNTER-CURRENT CHROMATOGRAPH

MARTHA KNIGHT*
Peptide Technologies Corporation, 125 Michigan Avenue N.E., Washington, DC 20017-1004 (U.S.A.)
and
YOICHIRO ITO
Laboratory of Technical Development, National Heart, Lung, and Blood Institute, National Institutes of Health, Bethesda, MD 20892 (U.S.A.)

SUMMARY

A modified horizontal flow-through coil planet centrifuge has been constructed that has the potential for preparative chromatography. The multi-coil counter-current chromatograph, equipped with a set of four multi-layer coils, has have improved performance with polar solvents suitable for peptide elution. Separations of a group of dipeptides and purification of a cholecystokinin fragment and an undecapeptide were achieved with *n*-butanol–acetic acid–water at high flow-rates with good resolution.

INTRODUCTION

Coil planet centrifuges[1] are modern instruments for counter-current chromatography, a preparative method in use prior to the development of high-performance liquid chromatography (HPLC). Although peptides can be chromatographed by reversed-phase and ion-exchange chromatography, the option of the many solvent systems possible with counter-current chromatography makes this method attractive. With a suitable two-phase solvent composition devised for a particular separation, high selectivity is possible.

Over the years we have used a horizontal flow-through coil planet centrifuge for the preparative purification of synthetic peptides[1], but the flow-rates and centrifugal rates were slower than on later designed instruments for counter-current chromatography[2]. However, as this instrument was able to utilize the more polar solvent systems useful for peptides, this instrument has been continuously applied for this purpose and is the design that can be used with all solvent systems at room temperature[3]. Previously reported was an apparatus with a narrower frame holding a column-coil with more layers of tubing, thus maintaining the volume of the older instrument but able to be centrifuged faster[4]. When various types of coils were tested on the column holder, a multi-layer coil was found to have the highest resolution in chromatography. More recently, to increase the capacity further, an instrument fitted with four multi-layer coils connected in series by the flow tubing has been built and found to operate at increased centrifugal speed and flow-rate[5]. The separation of enzymes in a poly-

0021-9673/89/$03.50

ethylene glycol solvent system was achieved using this instrument. This instrument has been assessed for its capability to chromatograph peptides under high-performance conditions.

The serial multi-layer coil planet centrifuge, which we shorten to multi-coil counter-current chromatograph, is a modification of the horizontal flow-through coil planet centrifuge equipped with a set of four counterbalancing multi-layer column-coils of tubing around a column holder. These are parallel and displaced from the center axis of rotation of the centrifuge. The open tubing throughout the system connects the coils in series for increased volume in which the solvent equilibration and solute partitioning take place. Fig. 1 is a photograph of the prototype at the Laboratory of Technical Development, National Institutes of Health. The rotary frame carries a column holder on one side and a counterbalance on the other. Both are at a distance of 10 cm from the central axis. Engagement of the planetary gear mounted on the holder shaft with the identical stationary sun gear on the central axis of the apparatus produces the desired planetary motion of the holder, *i.e.*, revolution of the holder around the central axis of the apparatus and simultaneous rotation of the holder about its own axis at the same angular velocity in the same direction. The mixing induced by the motion maintains an equilibration of the two phases in the coils. The force holds a stationary phase of a two-phase liquid with the other phase being pumped through. Thus, if one phase is continuously pumped through, the excess leaves at the other end, allowing a continuous-flow elution mode.

As models for the performance of earlier prototype instruments, dipeptides have been chromatographed in flow-through coils, toroidal coils, non-synchronous instruments and the multi-layer coil planet centrifuge[6]. Dipeptides containing aromatic

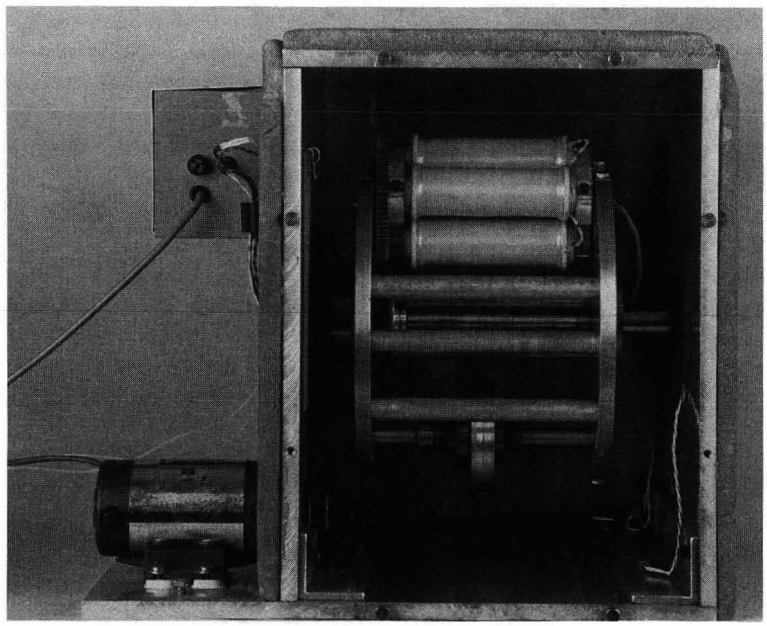

Fig. 1. Photograph of multi-coil counter-current chromatograph (from ref. 5).

amino acids for detection have been applied for the determination of the resolution and selectivity. Another peptide previously purified in the horizontal flow-through coil planet centrifuge is a cholecystokinin (CCK) fragment peptide CCK(26–30) amide[7], which when unsulfated is not soluble in water. This is an example of small, highly aromatic acidic peptides that contain substantial amounts of solid-phase synthesis side products, and the mixture is difficult to chromatograph on reversed-phase columns owing to solubility problems. Another peptide was chromatographed that had also been purified in the older instrument.

EXPERIMENTAL

Materials

The dipeptides were purchased from Sigma (St. Louis, MO, U.S.A.) and solvents from Burdick and Jackson (Muskegon, MI, U.S.A.). The peptides were synthesized manually in a table-top shaker (St. Johns Assoc., Beltsville, MD, U.S.A.) using methods described previously[8]. The identity and purity were established by amino acid analysis and HPLC.

Instrument

The apparatus has been described previously[5] (Fig. 1). The four coils around the holder are prepared from 1.6 mm I.D. polytetrafluoroethylene (PTFE) tubing (Zeus Industrial Products, Raritan, NJ, U.S.A.) wound on a spool 12.5 cm wide and 1.25 cm across in six layers. The entire coil and flanges are enclosed in a heat-shrunk poly(vinyl chloride) covering. The coils are equally spaced around the column holder shaft at a distance of 3.5 cm from the holder axis. Each coil has a volume of 50 ml, thus the total volume is 200 ml. The tubing is connected from the outside of the first column to the inside end of the next column and so on; the inlet and outlet tubing ends pass through the holder shaft and through the central stationary pipe. At the exit the flow tubes are clamped so they do not twist during the motion. The revolutional speed control unit regulates the speed up to 1200 rpm (Bodine Electric, Chicago, IL, U.S.A.). The unit is equipped with heating pads and a temperature-control unit (RFL Industries, Boonton, NJ, U.S.A.) that was not utilized in these experiments.

Procedure

The solvent system used for all the experiments was *n*-butanol–acetic acid–water (4:1:5, v/v/v), which was separated into two phases in a separatory funnel. The coil was filled with the upper phase, then the sample, dissolved in equal volumes of both phases, was loaded. The rotation was started and usually run at 800 rpm with the mobile phase or lower phase pumped through at 1 ml/min using a minipump (LDC/Milton Roy, Riviera Beach, FL, U.S.A.). The eluent was passed through an LKB Uvicord S flow cell detecting at 275 nm and recorded in an LKB six-channel chopper recorder (LKB, Gaithersburg, MD, U.S.A.) and collected in an LKB Ultrorac fraction collector in 3-ml fractions. For some experiments, aliquots of fractions were diluted with water or methanol and the absorbance was determined manually. After the run, the contents of the coil were flushed out with nitrogen and the volumes of the stationary and mobile phases were measured. The fractions from the undecapeptide chromatography were evaporated to dryness in a centrifugal evaporator (Savant Instruments, Farmingdale,

NY, U.S.A.). The fractions were analysed by HPLC as described previously[9] on a μBondapak C_{18} column (15 × 0.4 cm I.D.) (Waters/Millipore, Milford, MA, U.S.A.) in 0.1% aqueous phosphoric acid and acetonitrile gradients at 0.8 ml/min with detection at 280 nm using Waters/Millipore equipment consisting of a manual U6K injector, two Model 510 pumps with extended flow heads, a Model 680 gradient controller, a Model 681 variable-wavelength UV detector and an SE120 recorder.

RESULTS AND DISCUSSION

A sample load of 30 mg each of Tyr–Gly, Val–Tyr and Leu–Tyr and 10 mg of Tyr–Trp was dissolved in 6 ml of the solvent system and introduced into the coil (head end of first coil). The rotation was set at 850 rpm with the flow-rate at 1 ml/min in the head-to-tail direction and fractions of 3 ml were collected. The solvent front emerged at the 44th tube and all the components were eluted in 5 h. The run was stopped after 6 h. Samples of 0.1 ml were diluted with 1 ml of methanol and the absorbance was determined (Fig. 2). The retention of the stationary phase under these conditions was 33.8%. There was almost baseline separation of each dipeptide and the separation of Val-Tyr and Leu–Tyr showed good selectivity. The order of elution corresponds to increasing hydrophobicity.

CCK (26–30) amide, owing to the final extraction steps in the synthesis and the presence of Trp and Met, which can form many alkylation side-products, has a significant amount of extra mass. A load of 500 mg was chromatographed at 800 rpm and the chromatogram is shown in Fig. 3. Fractions 78–95 contained the purified peptide with a recovery of 67 mg. The large amount of impurities was easily removed with fractions 106–122 contaning a peptide side-product. The partition coefficient (K) calculated from the run as the concentration of the solute in the mobile phase divided by the concentration in the stationary phase[7,10], was 0.18. The retention of the stationary phase was 30.2% and the solvent front emerged at fraction 21. This was a high mass load for the 200-ml coil but examination of the mass recovered indicated that the peptide present was recovered. For a suitable solvent system for a compound, the capacity is limited by the solubility. The fractions with the pure peptide were flash

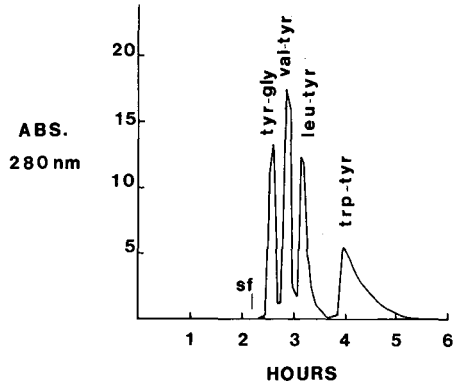

Fig. 2. Total absorbance units of the fractions from the chromatography of four dipeptides.

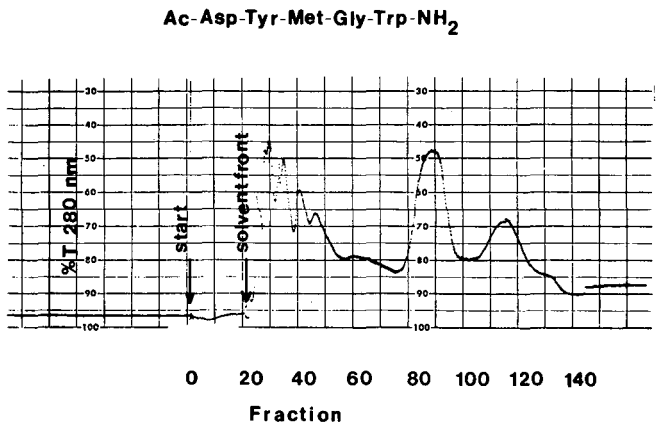

Fig. 3. Recording of chromatographic run of CCK (26–30) amide, 500 mg. Ac = Acetyl.

evaporated and lyophilized in a small volume of glacial acetic acid and the peptide was later sulfated.

The same conditions were used for the preparative purification of 225 mg of the undecapeptide acetyl–Glu–Glu–Trp–Asp–Pro–Ser–Asp–Gln–Glu–Pro–Cys–NH_2 at a centrifugal rate of 850 rpm (Fig. 4). The fractions across the peak were analysed by HPLC. The results are shown in Fig. 5. The peak tubes contained the most pure peptide. The fractions were combined in three pools with recoveries of (53–56) 27 mg, (57–59) (purest fraction) 54 mg and (60–67) 37 mg, with a total mass recovery of 52% in the peak. The K value for this compound was 1.6 in this solvent system and the stationary phase retention was 40%. The earlier and later eluting material was analysed by HPLC and appeared heterogeneous, as shown in Fig. 6, and the retention times corresponded to the order of elution from the counter-current coil.

These results indicate that the multi-coil counter-current chromatograph is useful for the preparative-scale chromatography of polar compounds such as peptides. The CCK fragment and the undecapeptide that had also been purified in the older horizontal flow-through instrument were chromatographed faster here. Specifically, the CCK peptide was eluted in 9 h compared with almost 40 h in the older instrument

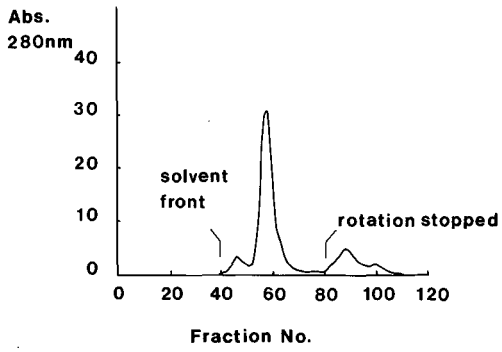

Fig. 4. Total absorbance of the fractions from the chromatography of the synthetic undecapeptide.

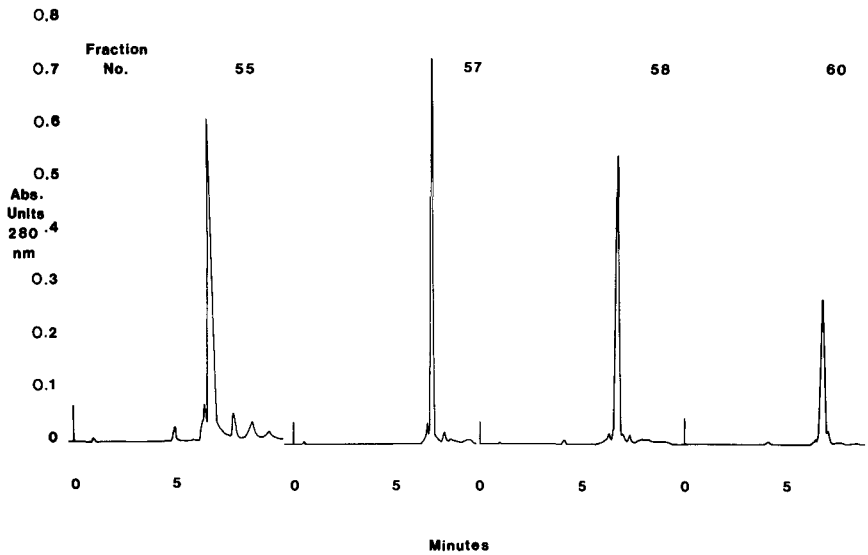

Fig. 5. Analytical HPLC of peak fractions on a μBondapak C_{18} column (15 × 0.4 cm I.D.) in 0.1% phosphoric acid with a gradient of 10–20% acetonitrile in 10 min at a flow-rate of 0.8 ml/min. Detection was at 280 nm (1 a.u.f.s.).

with the same solvent system and mobile phase[7]. The undecapeptide was eluted in 3 h whereas, using the upper mobile phase in the older instrument it was eluted in 13 h. For particular peptides that are not water soluble, this procedure can remove insoluble impurities easily without the requirement for elaborate procedures to clarify solutions

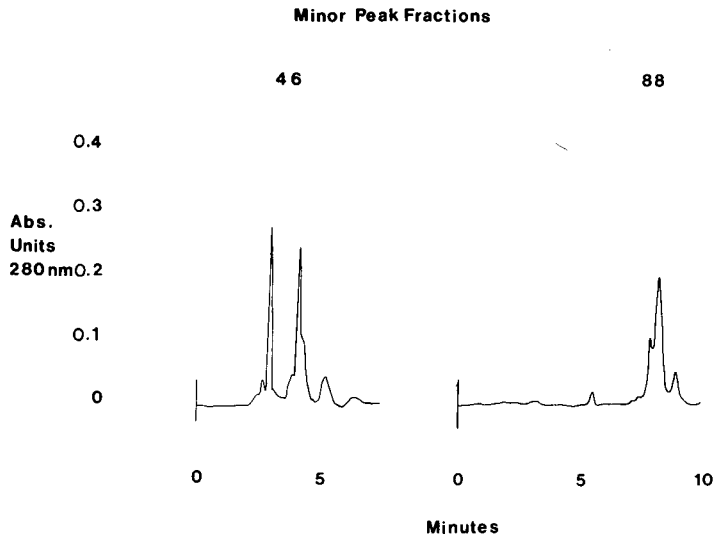

Fig. 6. Analytical HPLC of side-fractions of the undecapeptide separation under the same conditions as in Fig. 5.

for loading onto the chromatograph. We are currently assessing a new prototype (project with Varex, Burtonsville, MD, U.S.A.) with more coils for increased volume and sample capacity.

ACKNOWLEDGEMENTS

We thank Mark Rasevic and Sara Gluch for assistance.

REFERENCES

1 Y. Ito, *Methods Enzymol.*, 91 (1983) 335.
2 Y. Ito, J. L. Sandlin and W. G. Bowers, *J. Chromatogr.*, 244 (1982) 247.
3 M. Knight, Y. Ito, J. L. Sandlin and A. M. Kask, *J. Liq. Chromatogr.*, 9 (1986) 791.
4 J. L. Sandlin and Y. Ito, *J. Liq. Chromatogr.*, 11 (1988) 55.
5 Y. Ito and H. Oka, *J. Chromatogr.*, 457 (1988) 393.
6 Y. Ito, in N. B. Mandava and Y. Ito (Editors), *Countercurrent Chromatography— Theory and Practice*, Marcel Dekker, New York, 1988, pp. 79–438.
7 M. Knight, A. M. Kask and C. A. Tamminga, *J. Liq. Chromatogr.*, 7 (1984) 351.
8 M. Knight, Y. Ito, J. D. Gardner, C. A. Tamminga and T. N. Chase, *J. Chromatogr.*, 301 (1984) 277.
9 M. Knight, Y. Ito and T. N. Chase, *J. Chromatogr.*, 212 (1981) 356.
10 W. D. Conway, in N. B. Mandava and Y. Ito (Editors), *Countercurrent Chromatography— Theory and Practice*, Marcel Dekker, New York, 1988, pp. 443–461.

Journal of Chromatography, 484 (1989) 327–335
Elsevier Science Publishers B.V., Amsterdam — Printed in The Netherlands

CHROM. 21 816

PREPARATIVE ISOLATION OF GLYCOPROTEINS FROM PLASMA MEMBRANES OF DIFFERENT RAT ORGANS

DJURO JOSIĆ*, KATRIN ZEILINGER, YOW-PIN LIM, MICHAEL RAPS, WERNER HOFMANN and WERNER REUTTER

Institut für Molekularbiologie und Biochemie, Freie Universität Berlin, Arnimallee 22, 1000 Berlin 33 (Dahlem) (F.R.G.)

SUMMARY

By a combination of high-performance affinity chromatographic (HPAC) methods, several membrane proteins from liver, Morris hepatoma and kidney were isolated. The use of a tandem system, consisting of a concanavalin A (ConA) and a wheat germ agglutinin (WGA) high-performance liquid chromatographic (HPLC) column, as a first purification step allowed the isolation of proteins directly from organ homogenates. In a subsequent step, the membrane proteins can be isolated by simply using a combination of immunoaffinity HPLC and preparative sodium dodecyl sulphate polyacrylamide gel electrophoresis (SDS-PAGE). However, with these methods most proteins lose their biological activity. If native proteins are required, a combination of different HPAC methods has to be applied. Several membrane proteins were isolated in milligram amounts under non-denaturing conditions using either HPAC columns or Mem Sep membranes with immobilized lectins, collagen, amino acids, crown ethers or heparin.

INTRODUCTION

The isolation of plasma membranes from animal organs and the separation of membrane glycoproteins by different chromatographic methods has become a matter of routine in many laboratories[1–3]. The introduction of high-performance liquid chromatography (HPLC) and high-performance affinity chromatography (HPAC) has made isolation methods quicker, simpler and more reproducible. The yield of isolated proteins has been increased and the biological activity could be retained more often as a consequence of shorter isolation times[4–6]. However, the problem of low yields persists in the preparative isolation of membrane glycoproteins. The greatest loss of material does not occur in the chromatographic processes, but during plasma membrane isolation. In liver plasma membrane isolation, for example, the yield does not exceed 10%, regardless of whether zonal centrifugation is used according to the method of Neville[7] or isolation with a sucrose gradient[1]. In order to avoid these losses, we have tried to isolate the membrane proteins directly from the organ homogenates through a combination of preparative HPAC, HPLC and gel electrophoretic methods.

0021-9673/89/$03.50

EXPERIMENTAL

Animals and chemicals

Male Wistar or Buffalo rats, weighing about 180–200 g, were fed on a commercial diet (Altromin R, Altromin, Lage/Lippe, F.R.G.). The non-ionic detergents Triton X-100 and Triton X-114 were purchased from Aldrich (Milwaukee, WI, U.S.A.). All other chemicals, of analytical-reagent grade, were purchased from Merck (Darmstadt, F.R.G.), Serva (Heidelberg, F.R.G.) or Sigma (Munich, F.R.G.).

Production of plasma membranes and organ homogenates

Plasma membranes were isolated by zonal centrifugation using a Kontron (Munich, F.R.G.) centrifuge. Membrane purity was routinely checked by electron microscopy and by assays for marker enzymes, as described[1]. Plasma membranes were extracted selectively with detergents.[8] For the production of homogenates, the organs (liver, Morris hepatoma 7777 or kidney) were cut into small pieces after removal of connecting tissue. Each organ was then suspended in 100 ml of 5 m*M* Tris – HCl (pH 7.2) and 1 m*M* calcium chloride per 10 g of weight and homogenized (Ultra-Turrax homogenizer; Janke & Kunkel, Staufen, Breisgau, F.R.G.). The nuclei were removed by centrifugation at 1000 *g* for 10 min. The enriched membrane fraction was obtained through centrifugation at 40 000 *g* for 35 min (Kontron centrifuge). The supernatant after centrifugation was discarded. The pellet was suspended in 10 m*M* Tris–HCl (pH 7.4) containing 155 m*M* sodium chloride, 1 m*M* magnesium chloride, 1 m*M* calcium chloride and 1% (w/v) Triton X-100 and then homogenized in a Dounce homogenizer. It was subsequently solubilized for at least 2 h[2,8]. The protein content in the membrane fractions and in the homogenates was determined according to the method of Lowry *et al.*[9].

HPLC

The HPLC system consisted of two pumps, a programmer, a spectrophotometer with a deuterium lamp, a loop injection valve (all from Knauer, Berlin F.R.G.) and a Frac-100 fraction collector (Pharmacia–LKB, Freiburg, F.R.G.). The chromatographic conditions are given in the figure legends. Recovery was determined either by measuring the amount of protein or the activity of the membrane-bound enzyme dipeptidyl peptidase IV (DPP IV)[10].

Columns

The following column materials were used: Eupergit C 30N concanavalin A (ConA), particle size 30 μm, pore size 50 nm (Röhm Pharma, Weiterstadt, F.R.G.), Fractogel (Tosohaas, Yamaguchi, Japan) with wheat germ agglutinin (WGA), immobilized in our laboratory[11], Eupergit C 30N protein A (Röhm Pharma) and protein G Sepharose "Fast Flow" (Pharmacia–LKB). Ligands such as arginine, collagen and crown ethers were immobilized either on Eupergit C 30N or on Fractogel. Mem Sep 1.000, epoxy activated, "membrane" columns were obtained from Knauer. The ligands immobilized on this column were collagen, arginine, heparin and protein G. The procedures for ligand immobilization have been described elsewhere[4,11,12]. The dimensions of the HPLC columns were 250 × 20 mm I.D. unless stated otherwise in the figure legends.

Buffers

The buffers used for ConA and WGA HPAC were as follows. Buffer A was 10 m*M* Tris–HCl (pH 7.8), containing 155 m*M* sodium chloride and 1 m*M* each of Ca^{2+} and Mg^{2+}. An amount of 0.1% (w/v) of Triton X-100, reduced, was added to buffer A. For column rinsing the amount of Triton X-100, reduced, was 1%. The elution buffer for the ConA column was buffer A with 0.1% or 1% Triton X-100, reduced, to which 0.2 *M* methyl-α-D-mannopyranoside was added. The elution buffer for the WGA column was also buffer A with 0.1% or 1% Triton X-100, reduced with the addition of 0.2 *M* N-acetylglucosamine.

Buffer A for collagen and arginine HPAC was 5 m*M* Tris–HCl (pH 8.0) with 0.1% Triton X-100, reduced. Buffer B was buffer A containing 500 m*M* sodium chloride.

Buffer A for crown ether HPAC was 5 m*M* Tris–HCl (pH 7.5) containing 0.1% Triton X-100, reduced, and 10 m*M* potassium chloride. Buffer B was buffer A to which 500 m*M* sodium chloride was added.

Sodium dodecyl sulphate polyacrylamide gel electrophoresis (SDS-PAGE)

Samples of 10–25 μl were mixed with 3–7 μl of 300 m*M* Tris–HCl buffer (pH 6.8) containing 15% (w/v) SDS, 25% (v/v) mercaptoethanol, 30% (v/v) glycerol and 0.005% (w/v) bromophenol blue. SDS-PAGE was performed according to the method of Laemmli[13], using the Bio-Rad mini system (Bio-Rad Labs., Munich, F.R.G.). An amount of protein between 5 and 20 μg was applied to each track.

Preparative SDS-PAGE was carried out in a disk gel, 60 mm long and 12 mm diameter, with a system from Bethesda Research Labs. (Bethesda, MD, U.S.A.).

RESULTS AND DISCUSSION

ConA and WGA HPAC

Although a purification step consisting of centrifugation at 40 000 *g* (see Experimental) is carried out in the processing of the material in order to remove the soluble components from the cytosol, the homogenates are still cloudy and contain large amounts of serum albumin. This happens especially in liver processing. In the first step, lectin HPAC, the glycoproteins and eventually the glycolipids are bound. No other components bind to the column. If ConA HPAC is used as a first purification step, only between 60 and 70% of the membrane-bound enzyme DPP IV binds to the column. The remaining 30–40% runs through the column, even if applied several times. In these experiments, DPP IV is used as a marker enzyme in order to control the complete binding of membrane proteins. If the sample, which does not bind to the ConA column, is subsequently applied to a WGA column, between 20 and 30% of the DPP IV does bind, and the yield after the runs on two lectin columns will come to a total of 90%. We have also successfully operated the ConA and WGA columns in tandem. About 80–90% of the DPP IV activity was bound and could be eluted. Fig. 1 shows the SDS-PAGE of glycoproteins from liver and kidney homogenates bound to the ConA and WGA columns. They were eluted with α-methyl mannopyranoside and N-acetylglucosamine, respectively.

When organ homogenates are applied according to the method described here, some points require special attention. The extracted proteins have a tendency towards

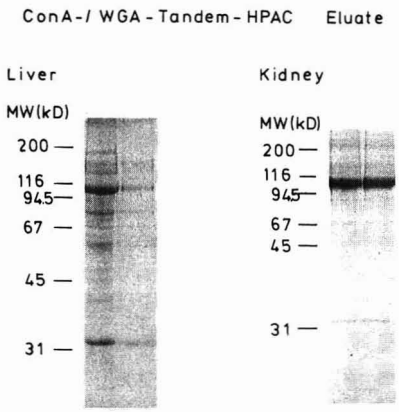

Fig. 1. SDS-PAGE of glycoproteins which were eluted from a tandem column system consisting of one ConA HPAC and one WGA HPAC column. The bound glycoproteins were eluted from the ConA column with 0.2 *M* α-D-methyl mannopyranoside and from the WGA column with 0.2 *M* N-acetylglucosamine. They were subsequently pooled. Recovery was controlled by measuring DPP IV activity; homogenate of the liver and/or kidney, containing 420 000 mU, were applied to a lectin affinity column. Of the kidney DPP IV, 400 000 mU (95%) bound to the column, of which 380 000 mU (90%) could be eluted. Of the liver DPP IV, the same amount was bound and 364 000 mU (87%) could be eluted. MW = Molecular weight; kD = kilodalton.

aggregation and precipitation. Therefore, the sample has to be newly centrifuged before being applied to the column, at at least 50 000 *g* for 30 min. The columns used must allow a quick and simple exchange of the frits. Apart from these risks, aggregation and precipitation lead to a loss of material. It is therefore recommended that the samples are used promptly after production.

Isolation of membrane glycoproteins under denaturing conditions with indirect immunoaffinity HPLC

The eluate from lectin HPAC can be used for the further isolation of membrane proteins. If the proteins are expected to retain their biological activity, as with the enzymatic activity of DPP IV, a number of successive purification steps have to be applied, as described below. If, however, the proteins are required for analytical purposes, such as sequencing or sugar analysis, the use of immunoaffinity HPLC is best.

Several monoclonal and polyclonal antibodies were raised against membrane glycoproteins in our laboratory and routinely used for different investigations[14,15]. We purified these antibodies and bound them to activated HPLC supports. In this way several membrane glycoproteins could be isolated by immunoaffinity (IA) HPLC[4,12]. A problem that arises when immobilized antibodies are used in IA-HPLC is the short life of the columns. Some monoclonal antibodies, including the monoclonal antibody No. 13.4 against DPP IV, lose almost 90% of their binding activity upon immobilization. This loss of activity could not be avoided, although different supports were tested. Therefore, we tried to bind the antibodies non-covalently to protein A or protein G supports, and to elute the antigen–antibody complex from the

column, after the binding of the antigen and extensive rinsing. The method has been described by Phillips *et al.*[16] We modified it and were able to use it successfully as an analytical method instead of immunoprecipitation[12,17]. "Indirect" IA-HPLC with protein G Sepharose "Fast Flow" as support has been sucessful also as a preparative method. A 3-mg amount of monoclonal antibody No. 13.4 against DPP IV was applied to a protein G column. The amount of bound antigen was about 5 mg. The antibody did not have to be purified previously. In the first step, 1 ml of ascites fluid was applied, from which only the antibody bound to the column. In contrast to the method suggested by Phillips *et al.*[15], the antibody is not chemically cross-linked. Instead, the antigen is applied in a subsequent step.

Fig. 2a shows the SDS-PAGE of the eluted antigen–antibody complex. Almost 90% of the antigen has bound. This was verified by measuring the enzymatic activity of DPP IV in the plasma membrane extract before and after the run on the immunoaffinity column. As the antigen against the light and the heavy chain of the immunoglobulin has an apparent molecular weight in SDS-PAGE of 110 000, it is much larger and can therefore be separated by preparative SDS-PAGE in another step. This is shown in Fig. 2b. When DPP IV is isolated with this combination of "indirect" IA-HPLC and preparative SDS-PAGE, a loss of its enzymatic activity has to be expected. For each chromatographic run, new antibody has to be used. It cannot be applied a second time, as it is inactivated in preparative SDS-PAGE and thereby lost. The advantage of this method is that pre-purification of ascites is unnecessary and that the protein G column has a long life. The columns in our laboratory have been in continuous use over a period of 6 months without showing any weakining in their binding activity for antibodies. Non-specific binding of other proteins was minimal with the use of the protein G Sepharose "Fast Flow". This applied to proteins from ascites fluid, from antiserum and from plasma membrane extract.

With the method shown here, several membrane proteins could be isolated in

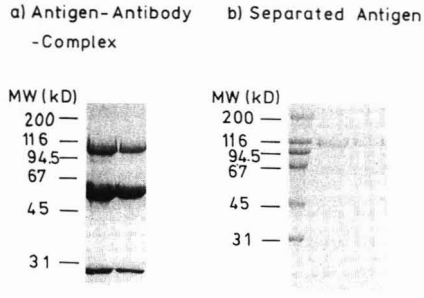

Fig. 2. Isolation of DPP IV of liver by a combination of "indirect" immunoaffinity HPLC and preparative SDS-PAGE. First 1 ml of ascites fluid with antibody No. 13.4 against DPP IV was applied to a protein G Sepharose "Fast Flow" column (30 × 8.0 mm I.D.). The column was then rinsed with 20 ml of Tris-buffered saline (pH 7.2) containing 1% Triton X-100. Then the ConA/WGA eluate of the liver homogenate with 300 000 mU DPP IV was applied, of which about 265 000 mU (about 5 mg of protein) bound to the column. The antigen–antibody complex was eluted with 0.1 *M* citrate buffer (pH 2.4). In a second step, the DPP IV with an apparent molecular weight of 110 000 was separated by preparative SDS-PAGE from the light and heavy immunoglobulin chains. (a) SDS-PAGE of the antigen–antibody complex, eluted from the protein G column; (b) SDS-PAGE of DPP IV after separation of the light and the heavy immunoglobulin chain by preparative SDS-PAGE.

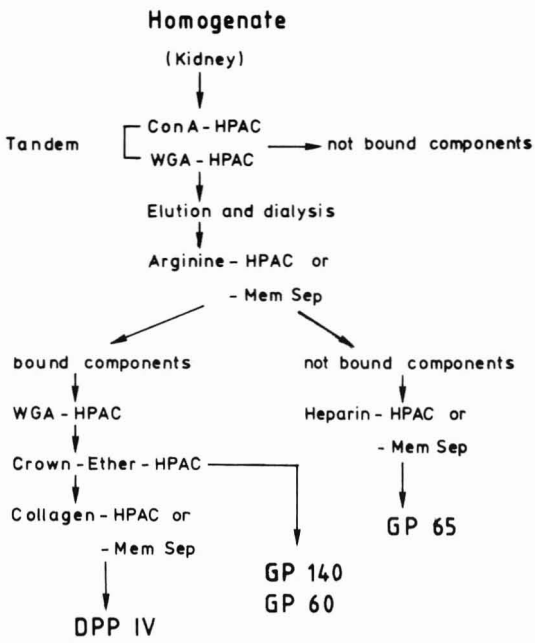

Fig. 3. Scheme for isolation of membrane proteins from kidney homogenate by a combination of different HPAC methods.

addition to DPP IV, such as cell–cell adhesion receptor Cell-CAM (apparent molecular weight in SDS-PAGE of 110 000) and the membrane proteins GP 120 and GP 190 (not shown here). The requirement for a successful separation of the proteins from immunoblogulin chains by preparative SDS-PAGE is a considerable difference in the apparent molecular weight. In our experiments we were able to separate from the immunoglobulin chains the proteins that had an apparent molecular weight of at least 80 000 in SDS-PAGE.

Isolation of membrane proteins under non-denaturing conditions

Many HPAC methods, especially IA-HPLC, have the disadvantage that the elution of the bound ligand from the column has to be carried out under conditions that inevitably lead to their denaturation and loss of biological activity. Lectin HPAC and HPAC with immobilized collagen with heparin and with immobilized low-molecular-weight ligands all have the advantage that elution is carried out under very mild conditions. In most instances a sugar or sodium chloride gradient is used. Fig. 3 shows a scheme for the isolation of different membrane proteins through a combination of HPAC methods. For these purification methods HPAC columns are used in addition to Mem Sep membranes with a bound ligand. The use of Mem Sep membranes was particularly successful when only a step gradient, not a linear gradient, was used for elution. In Fig. 3 these are the purification steps with arginine, heparin and collagen affinity chromatography.

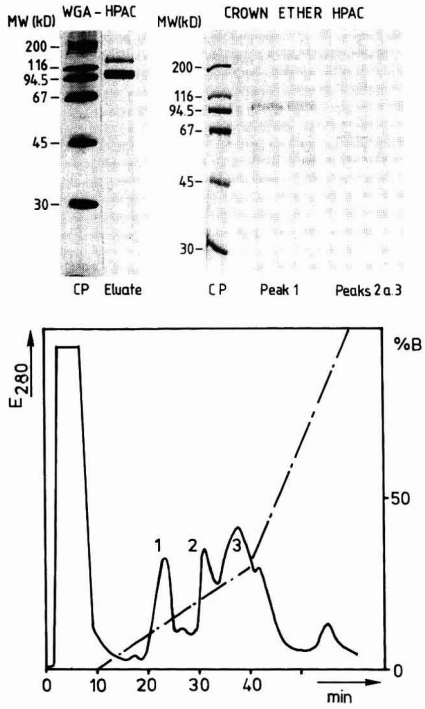

Fig. 4. Isolation of kidney membrane proteins by crown ether HPAC. A 20-ml volume of solution containing 20 mg of proteins that had bound to the arginine and WGA columns (see Fig. 3) was dialysed against a buffer with 5 m*M* Tris-HCl (pH 7.5) and applied to a Eupergit C 30N crown ether column. Elution was carried out with a sodium chloride gradient. In peak 1 the DPP IV was enriched. The glycoproteins with apparent molecular weights of 140 000 (GP 140) and 60 000 (GP 60) in SDS-PAGE were eluted later (peak 2). SDS-PAGE of the isolated proteins is shown in the upper part. Chromatographic conditions: buffer A, 5 m*M* Tris–HCl (pH 7.5) with 20 m*M* potassium chloride and 0.1% Triton X-100, reduced; buffer B, buffer A containing 1 *M* sodium chloride; column, 120 × 8.0 mm I.D.; flow-rate, 1 ml/min; pressure, 5 bar; room temperature. The gradient is shown.

In Figs. 4–6 some of the isolation steps are shown separately. With the combination of affinity chromatographic steps we isolated DPP IV and the glycoproteins with apparent molecular weights in SDS-PAGE of 140 000, 65 000 and 60 000 (GP 140, GP 65 and GP 60, respectively). Their activity was retained, as the elution of the bound proteins was carried out under mild conditions. This was controlled by measuring the DPP IV activity. The amounts of single proteins isolated through the combined affinity chromatographic methods were between 2 mg (GP 60 from kidney) and 50 mg (DPP IV from kidney).

The process as a whole can be scaled up. The answers that we have presented to the varions problems can serve as a model for the isolation of glycoproteins from complex mixtures, such as serum, cell supernatants and cell lysates.

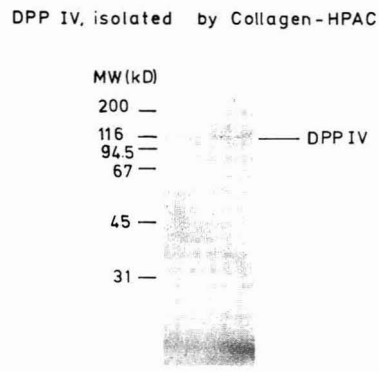

Fig. 5. SDS-PAGE of DPP IV after the last purification step, collagen HPAC. A 13-mg amount of protein in 5 ml after crown ether HPAC was dialysed against 5 m*M* Tris–HCl (pH 8.0) and applied to a Eupergit C 30 N collagen column. The column was rinsed with 10 ml of 5 m*M* Tris–HCl (pH 8.0) and 0.1% octylglucose, then elution was carried out with a step gradient with 0.2 *M* sodium chloride and 0.1% octylglucose. A similar result was obtained with the Mem Sep membrane, with immobilized collagen. A 1-mg amount of protein in 2 ml was applied to the Mem Sep collagen membrane. Rinsing and elution were carried out as above. Chromatographic conditions: HPAC column, 120 × 8.0 mm I.D.; flow-rate, 0.5 ml/min; pressure, 2 bar; temperature, 0°C; membrane, Mem Sep 1000 (Knauer); pressure, 1 bar; other conditions as above.

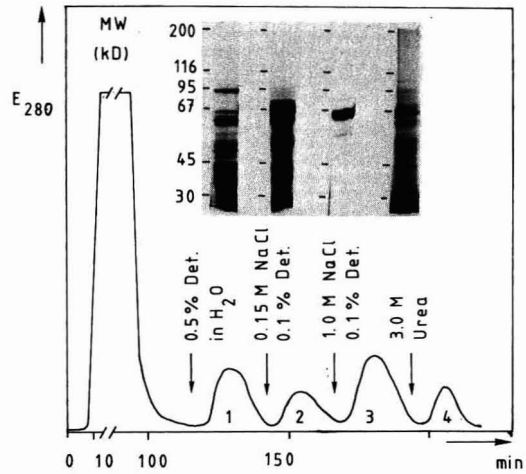

Fig. 6. Heparin HPAC of proteins that were not bound to the arginine column. A 30-mg amount of protein in 30 ml of 5 m*M* Tris–HCl (pH 8.0) was applied to a Eupergit C 30N heparin column and eluted in several steps as shown. SDS-PAGE of single eluted fractions is shown. The same result was obtained with the Mem Sep heparin membrane, but only one fifth of the material was applied and eluted. Chromatographic conditions; column, 120 × 8.0 mm I.D. (or Mem Sep heparin membrane); flow-rate, 0.5 ml/min; pressure, 2 bar; temperature, 0°C. Det = detergent Triton X-100, reduced.

ACKNOWLEDGEMENTS

We thank Knauer Säulentechnik for packing the columns and for providing the hardware for preparative HPAC columns. Thanks are also due to Mr. Oliver Baum for carrying out the lectin HPAC experiments. This work was supported by the Deutsche Forschungsgemeinschaft (DFG Re 523/3-3), the Trude Goerke-Stiftung and the Fonds der Chemischen Industrie.

REFERENCES

1 R. Tauber and W. Reutter, *Eur. J. Biochem.*, 83 (1978) 37.
2 W. Schütt, *M.D. Thesis*, Freie Universität Berlin, 1987.
3 J. R. Bartles, L. T. Braitermann and A. L. Hubbard, *J. Biol. Chem.*, 260 (1985) 12792.
4 Dj. Josić, W. Hofmann, R. Habermann and W. Reutter, *J. Chromatogr.*, 444 (1985) 29.
5 D. Renauer, F. Oesch, J. Kinkel, K. K. Unger and R. J. Wieser, *Anal. Biochem.*, 151 (1985) 424.
6 D. Corradini, Z. El Rassi, Cs. Horváth, G. Guerra and W. Horne, *J. Chromatogr.*, 458 (1988) 1.
7 D. M. Neville, *J. Biophys. Biochem. Cytol.*, 8 (1960) 413.
8 Dj. Josić, W. Schütt, R. Neumeier and W. Reutter, *FEBS Lett.*, 185 (1985) 182.
9 D. H. Lowry, N. J. Rosenbrough, A. L. Farr and R. J. Rendall, *J. Biol. Chem.*, 195 (1951) 265.
10 Dj. Josić, M. Raps, S. Hartel-Schenk, W. Hofmann and W. Reutter, in H. Höpker (Editor), *Proc. Würzburger Chromatographiegespräche*, Pharmacia–LKB, Vogel Verlag, Würzburg, 1989.
11 Dj. Josić, W. Hofmann, R. Habermann, A. Becker and W. Reutter, *J. Chromatogr.*, 397 (1987) 39.
12 Dj. Josić, W. Hofmann, R. Habermann, J.-D. Schulzke and W. Reutter, *J. Clin. Chem. Clin. Biochem.*, 26 (1988) 559.
13 U. K. Laemmli, *Nature (Londen)*, 227 (1970) 680.
14 A. Becker, R. Neumeier, C. Heidrich, N. Loch, S. Hartel and W. Reutter, *Biol. Chem. Hoppe-Seyler*, 367 (1986) 681.
15 Y.-P. Lim, *M.D. Thesis*, Freie Universität Berlin, in preparation.
16 T. M. Phillips, W. D. Queen, N. S. More and A. M. Thompson, *J. Chromatogr.*, 327 (1985) 213.
17 Dj. Josić, R. Tauber, W. Hofmann, J. Mauck and W. Reutter, *J. Clin. Chem. Clin. Biochem.*, 25 (1987) 869.

Journal of Chromatography, 484 (1989) 337–345
Elsevier Science Publishers B.V., Amsterdam — Printed in The Netherlands

CHROM. 21 798

PREPARATIVE RESOLUTION OF ENANTIOMERS OF PROSTAGLANDIN PRECURSORS BY LIQUID CHROMATOGRAPHY ON A CHIRAL STATIONARY PHASE

LARRY MILLER* and HELGA BUSH
Chemical Development Department, G.D. Searle and Co., 4901 Searle Parkway, Skokie, IL 60077 (U.S.A.)

SUMMARY

Preparative liquid chromatographic methods were developed for the chiral resolution of two different cyclopentenone precursors of a synthetic prostaglandin. Various solvent combinations of alcohols and alkanes were investigated to determine the method which has the greatest throughput. The effect of particle size on the chiral resolution was also investigated. In addition, the preparative system was automated to llow for unattended operation for up to 10 h.

INTRODUCTION

Cyclopentenones are important intermediates for numerous natural products including prostaglandins[1,2]. Since they contain a chiral carbon, various synthetic methods to produce optically pure cyclopentenones have been developed[3–5]. Only a limited amount of work on the resolution of the enantiomers of prostaglandin precursors using liquid chromatography (LC) has been published[2]. In 1987 a new synthetic prostaglandin E_1 analogue was synthesized at G. D. Searle and Co. To support the development activities of this compound, multigram quantities of a chiral cyclopentenone precursor were needed. There are two approaches to obtaining enantiomerically pure chemicals. These are (1) asymmetric synthesis of the desired isomer and (2) resolution of a racemic mixture into individual isomers. The methods of resolution can include recrystallization, formation of diastereomeric derivatives followed by chromatographic resolution on an achiral stationary phase, or direct chromatographic resolution of enantiomers using a chiral stationary phase or a chiral mobile phase additive. Direct resolution of the enantiomers using LC on a chiral stationary phase was used to isolate the desired enantiomer from a racemic mixture.

In this paper we will discuss the investigations and the method which was used to generate approximately 25 g of the desired enantiomer. We will also discuss the automation of the preparative system to allow for unattended operation and to reduce the manual labor required for this purification.

0021-9673/89/$03.50

EXPERIMENTAL

Materials

The chiral stationary phase, Chiralcel OC, used for these studies was obtained from Daicel (Tokyo, Japan) through J. T. Baker (Phillipsburgh, NJ, U.S.A.) as prepacked analytical (250 mm × 4.6 mm I.D.) and preparative (500 mm × 10 mm I.D. and 500 mm × 20 mm I.D.) columns.

The prostaglandin precursors were synthesized in the Chemical Development Labs. of G. D. Searle and Co. (Skokie, IL, U.S.A.). Prior to the separation of the enantiomers, all prostaglandin precursors were purified on 40-μm silica gel using a mobile phase of ethyl acetate–hexane (10:90 for compound 1, 50:50 for compound 2) to remove minor impurities. The solvents were reagent grade or better and obtained from a variety of sources.

Equipment

The analytical chromatograph consisted of a Spectra-Physics (San Jose, CA, U.S.A.) Model SP8100 pump, a Waters (Milford, MA, U.S.A.) intelligent sample processor Model 712, a Kratos (Ramsey, NJ, U.S.A.) Model 757 variable-wavelength UV detector, a Kipp and Zonen (Delft, The Netherlands) Model BD41 two-channel recorder and a Digital Equipment Corp. (Maynard, MA, U.S.A.) VAX 11/785 computer with a Searle chromatography data station.

The preparative chromatograph consisted of two Beckman (Berkeley, CA, U.S.A.) Model 101 pumps with preparative heads, a Model 165 variable-wavelength detector with a 5-mm semi-preparative flow cell, a Model 450 data system/controller and a Kipp and Zonen Model BD41 two-channel recorder. A Rheodyne (Cotati, CA, U.S.A.) Model 7125 syringe loading sample injector equipped with a 10-ml loop (Valco Instruments, Houston, TX, U.S.A.) or a Gilson Model (Middleton, WI, U.S.A.) 401 dilutor in combination with a Rheodyne electrically actuated Model 7010 injector equipped with a Valco 10-ml loop were used for sample injection. Effluent fractions were collected with either a Gilson Model FC220 or Model 201 fraction collector. A Valco electrically actuated six-port valve was used to allow effluent flow to different locations.

RESULTS AND DISCUSSION

Mobile phase selection

The analytical separation of the protected racemic cyclopentenone (compound 1, Fig. 1) is shown in Fig. 2. The elution order of the enantiomers is *R*, *S*. The capacity factor, k', is suitable for scale-up to a preparative separation and therefore was used as a starting point for preparative method development using a Chiralcel OC column

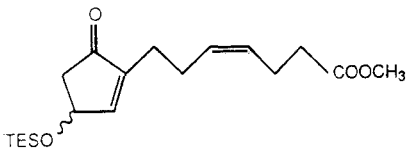

Fig. 1. Structure of triethylsilyl protected cyclopentenone, compound 1.

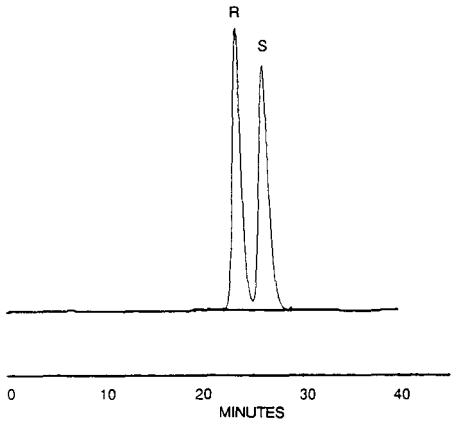

Fig. 2. Analytical HPLC separation of compound 1 on a Chiralcel OC column (250 mm × 4.6 mm I.D.), with a mobile phase of isopropanol–hexane (2:98). A flow-rate of 0.5 ml/min and detection at 215 nm, 0.1 a.u.f.s. were used.

packed with 10-μm particles. Chiralcel OC (Fig. 3) is the phenylcarbamate derivative of cellulose which is adsorbed onto silica gel. Cellulose-based phases have mobile phase restrictions since certain solvents can dissolve the cellulose. The manufacturer of these columns recommends the use of alkanes with low percentages (<40%) of alcohols as polar modifiers. For the solvent selection portion of our method development we investigated different alkanes such as hexane and 1,1,2-trimethylpentane (isooctane) with alcohols such as absolute ethanol, isopropanol and *tert.*-butanol. These experiments were all performed at a loading of 4 mg of sample per gram of packing and at a flow-rate of 20 ml/min. Analytical high-performance LC was used to determine the enantiomer content of the fractions from the preparative separation.

The results of these experiments are summarized in Table I. The object of these experiments was to determine the method that produced the largest amount of pure *R* enantiomer in the shortest time. Based on these criteria the ethanol–hexane system was chosen. The ethanol–isooctane system produced an equal amount of pure *R* enantiomer but had a slightly longer run time. An additional benefit was that the ethanol–hexane system produced more pure *S* enantiomer. A chromatogram of a preparative separation using ethanol–hexane as mobile phase is shown in Fig. 4.

Throughput studies

The throughput is the amount of purified chemical produced per hour.

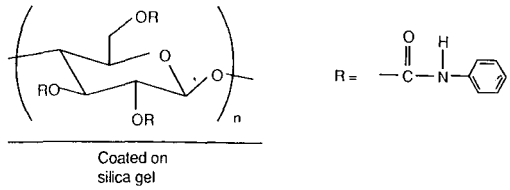

Fig. 3. Structure of the Chiralcel OC packing.

TABLE I
EFFECT OF MOBILE PHASE COMPOSITION ON THE SEPARATION OF COMPOUND 1

Mobile phase[a]	*R enantiomer isolated*[b]		*S enantiomer isolated*[c]		*Run time (min)*
	%	*Weight (mg)*	*%*	*Weight (mg)*	
Ethanol–hexane (1:99)	54	135	17	44	25
Ethanol–isooctane (1:99)	55	137	12	31	30
Isopropanol–hexane (2:98)	37	91	none		30
tert.-Butanol–hexane (2:98)	32	80	none		60

[a] Flow-rate, 20 ml/min; loading, 4 mg sample per g packing.
[b] Purity >99.5% (by high-performance LC).
[c] Purity > 99% (by high-performance LC).

Flow-rate and loading studies help to establish additional parameters required to maximize the throughput. The throughput can be increased by increasing the quantities produced per run and/or by decreasing the run time. For increased quantities, the loading must be increased and for decreased run time, the flow-rate must be increased. Flow-rates of 10, 20 and 40 ml/min and loadings of 2, 4, and 8 mg of sample per g of packing were investigated. The results of these experiments are summarized in Table II.

This table shows that as the loading increases, the amount of chemical produced per hour increases even though the percent of isolated enantiomer decreases. The same trend is seen with increasing flow-rate. Increasing the loading and the flow-rate increases the amount of pure chemical produced per hour and therefore results in a method with a higher throughput.

There are many factors which could influence the decision on which loading and

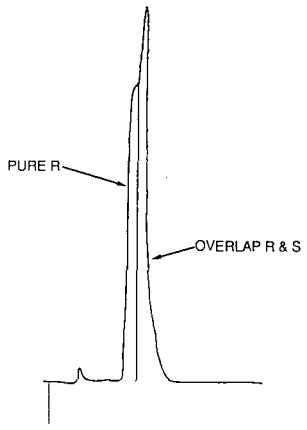

Fig. 4. Chromatogram of the preparative resolution of the enantiomers of compound 1. The purification was conducted on a Chiralcel OC column, 10-μm (500 mm × 20 mm I.D.), with a mobile phase of ethanol–hexane (1:99). A flow-rate of 20 ml/min, detection at 254 nm, 0.5 a.u.f.s. and a loading of 4 mg of sample per gram of packing were used.

TABLE II
FLOW-RATE AND LOADING STUDIES
Mobile phase, ethanol–hexane (1:99).

Flow-rate (ml/min)	*Loading (mg/g)*	*% R isolated*	*mg R/injection*	*mg R/h*
10	4	62	155	233
20	4	54	135	405
40	4	49	123	738
20	2	79	99	297
20	4	54	135	405
20	8	32	162	486

flow-rate to use for purifications. Some of these factors are: cost of the chemical prior to separation, the amount of chemical that must be produced, the added cost and effort of isolating additional chemical from the overlap portions, safety, and equipment capabilities. If the chemical being purified is expensive and relatively small quantities are required, the purification can be run at lower loadings, thus isolating the largest percentage of chemical possible while sacrificing the throughput. If the chemical is relatively inexpensive, higher loadings can be used, allowing larger quantities to be isolated.

Since our chemical was relatively expensive and only 40 g were required for initial development studies, we decided on a loading of 4 mg of sample per g of packing and a flow-rate of 20 ml/min. A flow-rate of 40 ml/min should have been used for greatest throughput. Due to equipment limitations and safety considerations the lower flow-rate of 20 ml/min was used.

Effect of particle size on separation

Packing of 20 μm is available as an alternative to the 10-μm packing for preparative separations. This 20-μm material is sold as prepacked columns or as bulk packing. If this material gave a comparable separation we would be able to pack larger columns, resulting in lower cost and greatly increasing the throughput. The results of these experiments are shown in Table III. This data shows that for compound 1, the separation was greatly reduced when using 20-μm packing. For our separation, use of this packing was not practical.

TABLE III
COMPARISON OF 10- AND 20-μm CHIRALCEL OC
Flow-rate, 20 ml/min; loading, 4 mg of sample per g packing.

Particle size (μm)	*R enantiomer isolated*		*S enantiomer isolated*	
	%	*Weight (mg)*	*%*	*Weight (mg)*
10	54	137	17	44
20	12	29	–	–

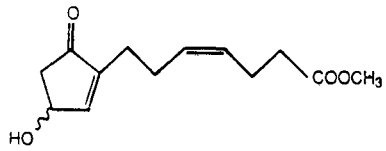

Fig. 5. Structure of unprotected hydroxycyclopentenone, compound 2.

Purification of unprotected hydroxycyclopentenone

In addition to the *R* enantiomer, the *S* enantiomer of compound 1 was required for product development activities. Table I shows that only small amounts of the second eluting *S* enantiomer were isolated during the isolation of the *R* enantiomer. To obtain the *S* enantiomer we took advantage of the fact that the elution order of the enantiomers for the unprotected hydroxycyclopentenone (compound 2, Fig. 5) is reversed from that of the protected hydroxycyclopentenone (compound 1). The elution order for compound 1 is *R*, *S*, and for compound 2 the order is *S*, *R*. During the separation of compound 2, the *S* enantiomer elutes first, allowing more of that enantiomer to be isolated than if it eluted second. The chemistry necessary to interconvert compound 1 and 2 is simple and does not result in racemization. Therefore we could isolate the *S* enantiomer of compound 1 through the isolation of the *S* enantiomer of compound 2 and then conversion to compound 1.

The analytical separation of compound 2 is shown in Fig. 6. Due to the small amounts of the *S* enantiomer needed, only three loadings and two different solvent compositions were investigated. The methods and the results are summarized in Table IV. The method used for purification was hexane–isopropanol (85:15) as mobile phase and a loading of 2 mg of sample per g of packing.

Automation of preparative LC equipment

Method development for the isolation of the *R* enantiomer of compound

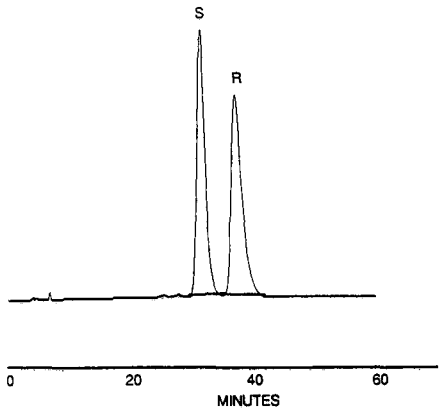

Fig. 6. Analytical HPLC separation of compound 2 on a Chiralcel OC column (250 mm × 4.6 mm), with a mobile phase of isopropanol–hexane (15:85). A flow-rate of 1.0 ml/min and detection at 215 nm, 0.1 a.u.f.s. were used.

TABLE IV
LOADING AND SOLVENT COMPOSITION STUDIES FOR COMPOUND 2
Chiralcel OC, 500 mm × 10 mm I.D., flow-rate 8 ml/min.

Mobile phase (hexane–isopropanol)	*Loading (mg sample/g packing)*	*% S enantiomer isolated*[a]
85:15	1	63
85:15	2	36
85:15	4	19
90:10	1	56
90:10	2	39
90:10	4	34

[a] No *R* enantiomer isolated.

1 showed that a 10-μm Chiralcel OC column was needed for the purification. Since the largest column commercially available was 500 mm × 20 mm I.D., a large number of repetitive injections would be necessary to produce the required amount of chemical. To help reduce the manhours necessary for this operation, automation of pump control, sample injection, and fraction collection is needed. This automation was accomplished with a pump controller, a programmable fraction collector and a 10-ml autosyringe to fill the loop of an electrically actuated injector. The complete preparative system consisted of pumps, an injector, detector, recorder and fraction collector. All were controlled though the use of flags and contact closures from the system controller.

The system controller is able to run programs up to 10 h in length. Multiple

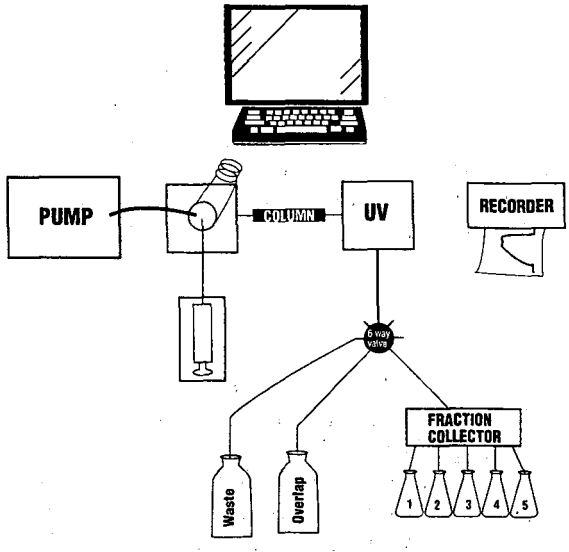

Fig. 7. Schematic of automated preparative system.

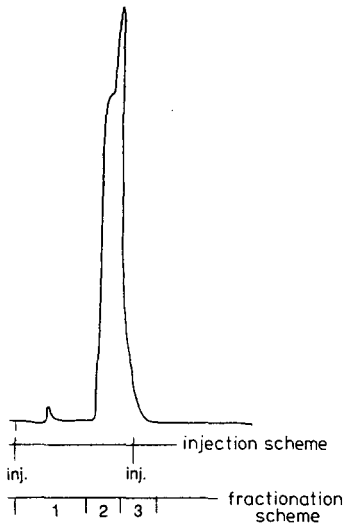

Fig. 8. Chromatogram of automated preparative run of compound 1. The purification was conducted on a Chiralcel OC column, 10-μm (500 mm × 20 mm I.D.), with a mobile phase of ethanol–hexane (1:99). A flow-rate of 20 ml/min, detection at 254 nm, 0.5 a.u.f.s. and a loading of 4 mg of sample per g of packing were used. 1 = waste fraction; 2 = fraction collector; 3 = overlap fraction.

fraction collectors were used because the fraction collectors could only collect 220 fractions for approximately 3.5 h. An electrically actuated six-port valve was installed after the detector allowing multiple fraction collectors to be used. While this allowed for unattended operation, it generated large numbers of fractions that needed analysis and workup.

To reduce the number of fractions, a different fraction collector was used that contained a funnel assembly, allowing for the collection of up to 27 fractions. In addition there was no limit on the fraction size. This allowed the effluent from repetitive injections to be collected into the same fraction vessels. Using this setup we were able to run unattended for up to 10 h and generate only 27 fractions which required analysis. The fractionation scheme was also adapted so that effluent containing impure or no chemical was diverted to a large container. A schematic of the automated system is shown in Fig. 7. A chromatogram from an automated run is shown in Fig. 8.

CONCLUSION

These studies demonstrate that preparative LC on a chiral stationary phase can be used to isolate multigram quantities of pure enantiomers. The separations are usually difficult but can be optimized through the investigation of solvent selectivities, loadings and flow-rate. It was also demonstrated that automation could be utilized to allow for unattended operation of the preparative LC system and greatly reduce the manual labor required for these purifications. We were able to isolate approximately 400 mg of *R* enantiomer per h and to produce a total of 25 g of *R* enantiomer.

ACKNOWLEDGEMENTS

The authors wish to thank Ellen Derrico, Rosemary DiMaggio, and Cara Weyker for their technical support and Todd Minske and Julie Garramore for graphics support. The chemicals were provided by chemists in the Synthesis Development group at G. D. Searle & Co.

REFERENCES

1 A. J. H. Klunder, W. B. Huizinga, P. J. M. Sessink and B. Zwanenburg, *Tetrahedron Lett.*, Vol. 28 (1987) 357.
2 Y. Okamoto, R. Aburatani, M. Kawashima, K. Hatada and N. Okamura, *Chem. Lett.*, (1986) 1767.
3 R. Noyori and M. Suzuki, *Angew. Chem. Int. Ed. Engl.*, 23 (1984) 847.
4 G. Stork and M. Isobe, *J. Am. Chem. Soc.*, 97 (1975) 6268.
5 M. Asami, *Tetrahedron Lett.*, 26 (1985) 5803.

Journal of Chromatography, 484 (1989) 347–359
Elsevier Science Publishers B.V., Amsterdam — Printed in The Netherlands

CHROM. 21 803

PURIFICATION OF RADIOLABELED PHARMACEUTICALS

CHRISTINE BAKER, CHRISTINE BOWLEN, DAVID KOHARSKI* and PAUL McNAMARA
Schering-Plough Research, 60 Orange Street, Bloomfield, NJ 07003 (U.S.A.)

SUMMARY

The chromatographic purification of radiolabeled compounds of diverse structural types, in milligram to gram amounts, is described. The compounds purified were a steroid, a D-1 receptor antagonist, an ACE inhibitor and a small peptide mimic. The purification methods used included isocratic normal-phase high-performance liquid chromatography (HPLC), gradient reversed-phase HPLC, counter-current chromatography and the use of a normal-phase gravity column with fraction monitoring by rapid analytical HPLC.

INTRODUCTION

Radiolabeled compounds are essential tools in modern drug research and development[1] and are particularly valuable in drug metabolism studies[2]. Radiolabeled compounds must be of high radiochemical and chemical purity[3] in order to conduct meaningful experiments. High purity is most effectively achieved using liquid chromatography. Pharmaceutical radiochemistry groups are called on to provide structurally diverse compounds, at high purity, in milligram to gram amounts. The rational development of efficient purification methods, using basic chromatography theory[4], is described below.

The steroid[^{3}H]mometasone furoate (**1a**) was purified by isocratic normal-phase high-performance liquid chromatography (HPLC). A solvent system was developed using thin-layer chromatography (TLC). The optimum column loading was established using analytical HPLC. The developed system was used on a semi-preparative column to purify 25-mg amounts of [^{3}H]mometasone furoate.

[^{3}H]Sch 39166 (**3**), a D-1 receptor antagonist, was purified by gradient reversed-phase HPLC. Using analytical HPLC, the capacity factor (k') and peak shape were optimized and a feasible loading was established. The separation was transferred to a semi-preparative column. Gradient elution allowed the loading of the relatively insoluble sample in a large solution volume with sample enrichment at the column head and subsequent elution of the compound in small volume.

[^{14}C]Sch 34826 (**4**) is a small peptide mimic which was purified on a gram scale using a gravity column packed with 12–25 μm silica gel. The separation was first run on a small column and scaled up by increasing the column diameter; all other parameters were held constant. Rapid analytical HPLC with both UV and radioactivity detection was used for fraction analysis.

0021-9673/89/$03.50

The ACE inhibitor [^{14}C]spiraprilat (**5**) is difficult to purify by column chromatographic methods because of its poor solubility properties and impurity profile. The compound was succesfully purified by counter-current chromatography on a coil planet centrifuge instrument. A suitable solvent system was chosen based on partition coefficients in two-phase systems of varying polarities and pH. [^{14}C]Spiraprilat was purified in 150–200-mg amounts using a 300-ml column.

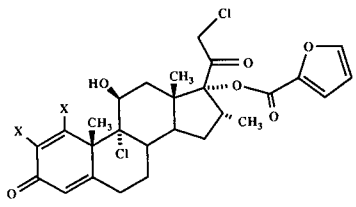

1a X=^{3}H
1b X=^{2}H

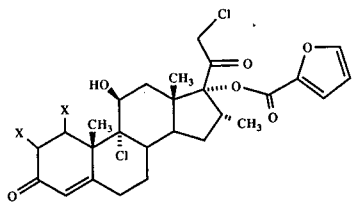

2a X=^{3}H
2b X=^{2}H

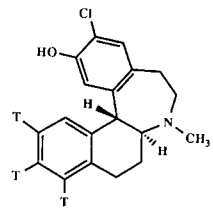

3

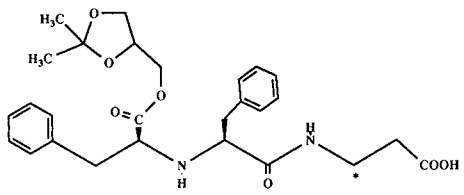

4

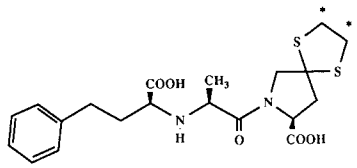

5

EXPERIMENTAL

*[^{3}H]Mometasone furoate (**1a**)*

The HPLC instrument consisted of a Model 6000A pump and a U6K injector (Waters Assoc., Milford, MA, U.S.A.), a 970A variable-wavelength UV–VIS detector (Tracor, Austin, TX, U.S.A.) set at 254 nm and a Recordall Series 5000 recorder (Fisher Scientific, Springfield, NJ, U.S.A.) and Model LB-5025 radioactivity detector (Berthold Analytical, Nashua, NH, U.S.A.).

Analytical reversed-phase HPLC was carried out on a 25 cm x 4.6 mm I.D. LC-8 column (Supelco, Bellefonte, PA, U.S.A.). The mobile phase was methanol–water (35:65) at a flow-rate of 1 ml/min. Aquassure liquid scintillation cocktail (DuPont/NEN, Boston, MA, U.S.A.) at a flow-rate of 2 ml/min was used in the radioactivity detector. Normal-phase chromatography was carried out on 25 cm × 4.6 mm I.D. and 50 cm × 9.4 mm I.D. Partisil 10 silica columns (Whatman, Clifton, NJ,

U.S.A.). The mobile phase was dichloromethane–methyl *tert.*-butyl ether (93:7) at flow-rates of 1 and 4 ml/min, respectively.

*[^{3}H]Sch 39166 (**3**)*

The preparative HPLC system consisted of an LC-85 UV spectrophotometer set at 280 nm (Perkin-Elmer, Norwalk, CT, U.S.A.), Model 6000A and 510 pumps and a Maxima 820 chromatography workstation (Waters Assoc.), a Model 7125 injector with a 1.0-ml loop (Rheodyne, Cotati, CA, U.S.A.) and an M9 Partisil 10 CCS/C_8 column (50 cm × 9.4 mm I.D.) (Whatman). The flow-rate was 4.0 ml/min.

The analytical HPLC system consisted of a Model 490 multiwavelength spectrophotometer set at 280 nm, a Model 600 multi-solvent delivery system, a Model 840 data and chromatography control station, a Model 712 WISP autoinjector (Waters Assoc.), a Flo-One Model CT radiochemical detector with a 500-μl flow cell, (Radiomatic, Tampa, FL, U.S.A. and a RAC II Partisil 5 CCS/C_8 column (10 cm × 4.6 mm I.D.) (Whatman). The mobile phase consisted of methanol (solvent A) and 0.1 *M* ammonium acetate adjusted to pH 5 with glacial acetic acid (solvent B). The flow-rate was 1.0 ml/min and the temperature was ambient. Aquassure liquid scintillation cocktail was used for analytical radioactivity flow monitoring at 2.0 ml/min. The isocratic mobile phase was A–B (50:50). The gradient program was as follows: segment 1, A–B (50:50) isocratic for 10 min; segment 2, A–B (50:50) to 100% A linear gradient over 5 min; segment 3, 100% A isocratic for 15 min.

*[^{14}C]Sch 34826 (**4**)*

Preparative chromatography was carried out in glass Chromaflex columns (Kontes, Vineland, NJ, U.S.A.). The columns were packed with 12–25-μm LPS-1 silica gel (Whatman), slurried in chloroform. The slurry was briefly sonicated before packing. Compounds were placed on the columns as chloroform solutions and eluted with chloroform–methanol–glacial acetic acid (100:3:0.5). Fractions were collected in a Frac 100 fraction collector (Pharmacia, Piscataway, NJ, U.S.A.) and analyzed by HPLC. The HPLC system consisted of a Model 8800 gradient controller, Model 834 automatic sampler, Model 870 pump and column compartment equipped with a 50-μl loop Valco A45 injector (DuPont, Wilmington, DE, U.S.A.), Model 490 programmable multi-wavelength detector (Waters Assoc.) set at 220 nm and Model LB 5025 radioactivity detector (Berthold Analytical). Data reduction was done on a Model 840 data and chromatography control station (Waters Assoc.). A 10 cm × 4.6 mm I.D. Partisil 5 RAC II ODS-3 column was used with a mobile phase composed of methanol–acetonitrile–0.05 *M* K_2HPO_4 (pH 7.4) (20:20:60) at 1 ml/min. Aquassure liquid scintillation cocktail at a flow-rate of 1.5 ml/min was used in the radioactivity detector.

*[^{14}C]Spiraprilat (**5**)*

Counter-current chromatography was carried out on an Ito Model 1 multilayer coil separator–extractor equipped with a 300-ml coil (P.C. Inc., Potomac, MD, U.S.A.), a Model 6000A HPLC pump (Waters Assoc.) and a Model 7125 injector with a 2-ml loop (Rheodyne). Fractions were collected by a Frac 100 (Pharmacia) fraction collector. The solvent system was chloroform–methanol–2% acetic acid at a flow-rate of 4 ml/min.

Fractions were analyzed by HPLC. The HPLC system consisted of a Model 490 multi-wavelength spectrophotometer set at 220 nm, a Model 600 multi-solvent delivery system, a 712 WISP autoinjector, a Model 840 data and chromatography control station (Waters Assoc.) and a Flo-One Model CT (Radiomatic) with a 500-μl flow cell. The column was a 5-μm Partisil 5 RAC III ODS-3 (10 cm x 4.6 mm I.D.) (Whatman). The liquid scintillation cocktail was Aquassure at a flow-rate of 1.5 ml/min. The mobile phase was methanol–acetonitrile–0.05 *M* K_2HPO_4 (pH 7.5) (20:20:75) at 1.0 ml/min.

RESULTS AND DISCUSSION

*[^{3}H]Mometasone furoate (**1a**)*

[^{3}H]Mometasone furoate (**1a**), after attempted purification by preparative TLC and recrystallization, contained the 1,2-dihydro derivative **2a** as the major contaminant. Compound **2a** co-chromatographed with an authentic sample of **2b** prepared by an unambiguous route and characterized spectroscopically. A radiochromatogram of **1a** is shown in Fig. 1.

Mometasone and its dihydro derivative **2a** were barely resolved by reversed-phase HPLC. Additionally, a 125-mg batch required purification. A normal-phase HPLC system giving adequate separation of the two components ($\alpha \geqslant 1.2$) and acceptable loading (25 mg per run) was needed. A synthetic mixture of **1b** and **2b** (97:3) in dichloromethane (20 mg/ml) was used to develop a preparative HPLC sys-

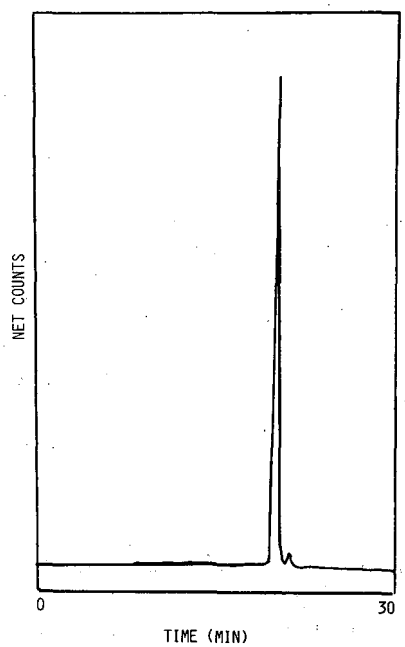

Fig. 1. Analytical reversed-phase radiochromatogram of crude [^{3}H]mometasone furoate (**1a, 2a**). Column, Supelco LC-8 (25 cm × 4.6 mm I.D.); mobile phase, methanol–water (35:65) at 1.0 ml/min; Aquassure liquid scintillation cocktail at 2.0 ml/min.

TABLE I

COLUMN LOADING RESULTS FOR A 25 cm × 4.6 mm I.D. COLUMN

Mass injected	*k'*	
	*Sch 32088 (**1a**)*	*Dideutero-Sch 32088 (**2a**)*
100 μg	5.7	4.4
500 μg	5.7	4.3
750 μg	5.6	4.4
1.0 mg	5.4	4.3
1.5 mg	5.6	4.3
2.0 mg	5.6	4.3
2.5 mg	5.7	4.4

tem. Solvent systems were screened on silica gel TLC plates. The solvent mixture dichloromethane–methyl *tert.*-butyl ether (93:7) was chosen because adequate separation was achieved (α = 1.3), the calculated retention (k' = 6) on a column was acceptable (approximate k' values were calculated from TLC mobility data using the relationship $k' = (1 - R_F)/R_F$ from ref. 5, the solvents were volatile and readily removed and **1a** was very soluble in this mixture. A loading study on a 25 cm × 4.6 mm I.D. silica gel column was carried out with the test mixture (Table I).

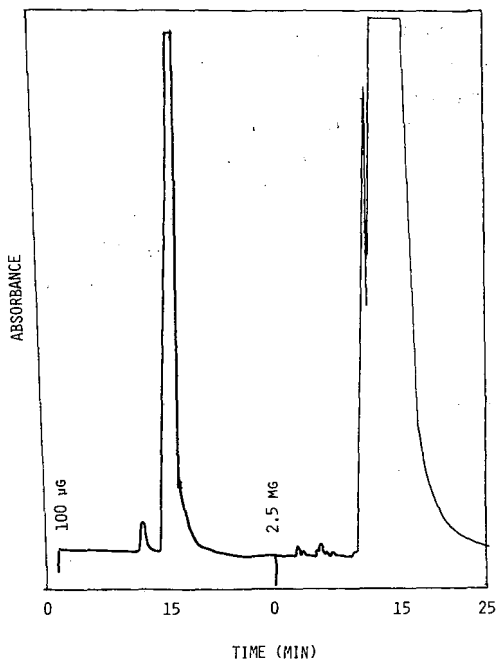

Fig. 2. Loading study of **1b–2b** synthetic test mixture. Column, Whatman Partisil 10 silica (25 cm × 4.6 mm I.D.); mobile phase dichloromethane–methyl *tert.*-butyl ether (93:7) at 1.0 ml/min.

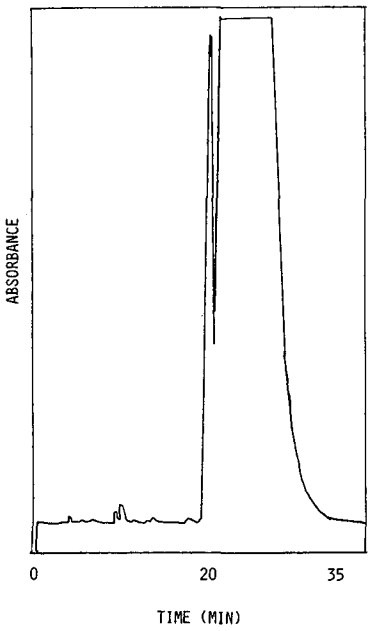

Fig. 3. Injection of 25 mg of **1a–1b** test mixture. Column, Whatman Partisil 10 silica Magnum 9 (50 cm × 9.4 mm I.D.); mobile phase, dichloromethane–methyl *tert.*-butyl ether (93:7) at 4.0 ml/min.

No change in k' was noted for a 2.5-mg compared with a 0.1-mg injection (Figure 2), although the bands had broadened. Thus the column had been loaded up to its "loading limit" for touching-band separation[6]. The separation was transferred directly to a 50 cm × 9.4 mm I.D. semi-preparative column and injections of 5 and 25 mg of the test mixture were made. The results, shown in Fig. 3, indicate that a 25-mg loading was acceptable, even though k' was slightly decreased.

[^{3}H]Mometasone furoate was purified in 25-mg portions. A typical preparative chromatogram is shown in Fig. 4. The yield of pure compound was 88% with a radiochemical purity of 98.9%. A radiochromatogram of the purified compound is shown in Fig. 5.

[^{3}H]Sch 39166 (3)

[^{3}H]Sch 39166 was prepared by platinum catalyzed exchange in tritiated water–trifluoroacetic acid[7] (labeling chemistry was carried out at the National Tritium Labeling Facility, Lawrence Berkeley Laboratory, U.C. Berkeley, Berkeley, CA, U.S.A.).

A radiochromatogram of the crude exchange product is shown in Fig. 6. Major radioactive impurities were tritiated water (11%) and strongly retained materials (4%) eluted when the reversed-phase column was stripped with methanol.

For purification of [^{3}H]Sch 39166, a 50 cm × 9.4 mm I.D. reversed-phase column was used in a gradient mode. This allowed the sparingly soluble [^{3}H]Sch 39166 to be loaded in a large volume with enrichment at the column head and subsequent elution in a small volume.

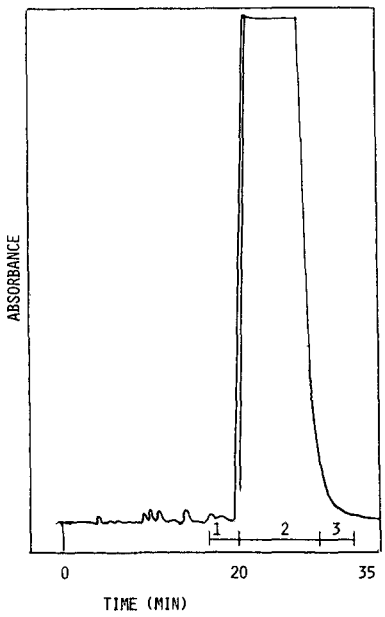

Fig. 4. Injection of 25 mg of crude [^{3}H]mometasone furoate (**1a, 2a**). Column, Whatman Partisil 10 silica Magnum 9 (50 cm × 9.4 mm I.D.); mobile phase, dichloromethane–methyl *tert.*-butyl ether (93:7) at 4.0 ml/min.

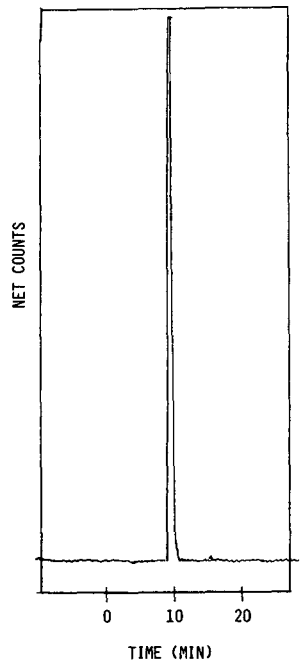

Fig. 5. Analytical reversed-phase radiochromatogram of purified [^{3}H]mometasone furoate (**1a**). Column, Supelco LC-8 (25 cm × 4.6 mm I.D.); mobile phase methanol–water (35:65) at 1.0 ml/min; Aquassure liquid scintillation cocktail at 2.0 ml/min.

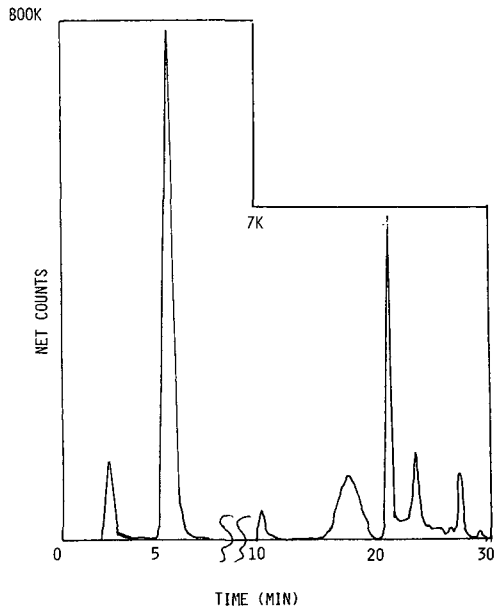

Fig. 6. Composite analytical radiochromatogram of crude [^{3}H]Sch 39166 (**3**). Column, Whatman Partisil 5 CCS/C_8 RAC II (10 cm × 4.6 mm I.D.); mobile phase, methanol–0.1 *M* ammonium acetate at 1.0 ml/min; 10-min isocratic (50:50) separation of tritiated water from [^{3}H]Sch 39166; detector sensitivity was then increased for the detection of strongly retained impurities during a 5-min linear gradient to 100% methanol and a 15-min isocratic column strip.

The column was equilibrated in 100% buffer at 4 ml/min. A 400-ml volume of sample was loaded into the injector loop and injected onto the column, followed by a 1-min (4-ml) buffer rinse. The process was repeated a further five times for a total sample load of 3.8 mg in 2.4 ml of methanol. A 15-min linear gradient to methanol followed by a 15-min isocratic elution was then run. Fractions were collected as shown on the preparative chromatogram in Fig. 7. Fractions 3 and 4 are [^{3}H]Sch

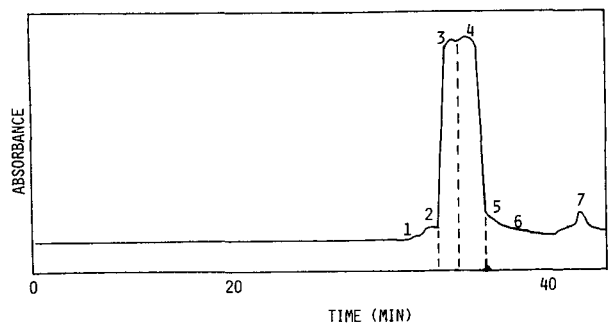

Fig. 7. Semi-preparative column injection of crude [^{3}H]Sch 39166 (**3**). Column, Whatman Partisil 10 CCS/C_8 Magnum 9 (50 cm × 9.4 mm I.D.); mobile phase, (1) 0.1 *M* ammonium acetate isocratic for 15 min (2) 15-min linear gradient to methanol, (3) 15-min methanol isocratic; flow-rate, 4.0 ml/min.

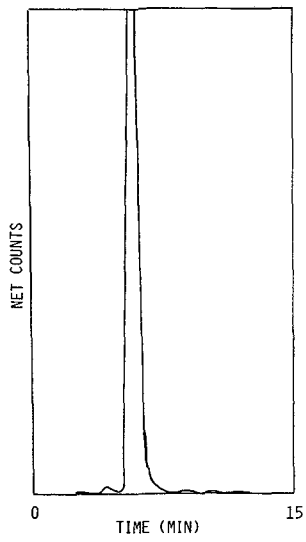

Fig. 8. Analytical reversed-phase radiochromatogram of purified [^{3}H]Sch 39166 (**3**). Column, Whatman Partisil 5 CCS/C_8 RAC II (10 cm × 4.6 mm I.D.); mobile phase, methanol–0.1 *M* ammonium acetate (50:50) at 1.0 ml/min; Aquassure liquid scintillation cocktail at 2.0 ml/min.

39166; cut-points are indicated by dotted lines in Fig. 7. These fractions represent a 94.7% recovery of the [^{3}H]Sch 39166 radioactivity applied to the column. Fractions were combined based on rapid analytical HPLC with radiochemical flow monitoring. After purification and pooling of all the tritium-exchanged reaction batches, a final batch purity of 97.5% was obtained. Fig. 8 shows a representative [A–B (50:50) isocratic] analytical radiochromatogram.

*[^{3}H]Sch 34826 (**4**)*

Chromatographic columns used for the purification of radioactive materials frequently become contaminated and cannot be used for other projects. Therefore, expensive preparative HPLC columns capable of handling gram amounts of material are rarely used in radiochemical purifications. Gravity liquid chromatography is a viable alternative. Crude [^{14}C]Sch 34826 contained several chemical and radiochemical impurities, as shown in Fig. 9. A 212-mg portion was purified on a 30 cm × 2.5 cm I.D. silica gel column using the solvent system chloroform–methanol–glacial acetic acid (100:3:0.5). Silica gel with a small particle size (12–25 μm) was slurried in chloroform and briefly sonicated, then poured into the column. One column volume of chloroform was passed through the column to stabilize the bed. The compound was dissolved in 1 ml of chloroform, carefully applied to the column and eluted with mobile phase. Fractions were collected and those with significant radioactivity were examined by HPLC. Pure fractions were pooled and evaporated. The purification was scaled up by chromatographing 925 mg of crude [^{14}C]Sch 38426 on a 30 cm × 4.8 cm I.D. column. The preparative chromatogram is shown in Fig. 10. HPLC analyses of the fractions are shown in Table I. It can be seen that purity across the main peak in the preparative chromatogram was not uniform. Fractions were com-

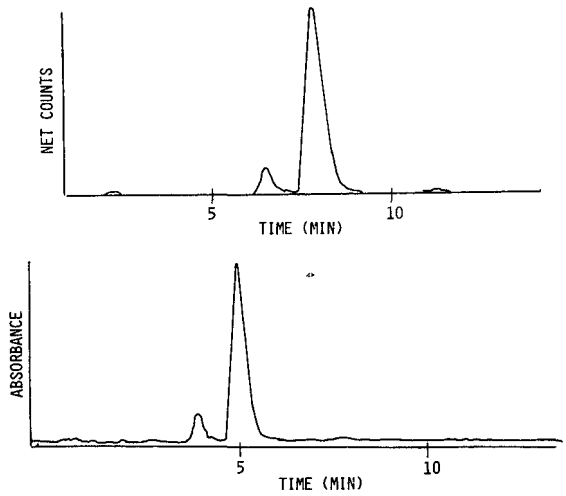

Fig. 9. Analytical UV (bottom) and radiochromatograms (top) of crude [^{14}C]Sch 34826 (**4**). Column Whatman Partisil 5 ODS-3 RAC II (10 cm × 4.6 mm I.D.); mobile phase, methanol–acetonitrile–0.05 *M* K_2HPO_4 (pH 7.4) (20:20:60) at 1.0 ml/min; Aquassure liquid scintillation cocktail at 1.5 ml/min.

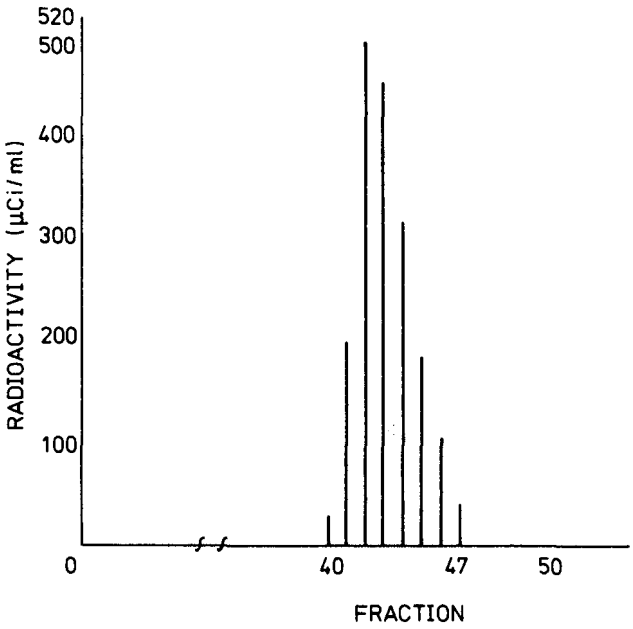

Fig. 10. Bar graph of liquid scintillation counting results for [^{14}C] 34826 (**4**) gravity column fraction aliquots. Column, 30 cm × 4.8 cm, packed with 12–25-μm Whatman LPS-1 silica gel; mobile phase, chloroform–methanol–glacial acetic acid (100:3:0.5).

TABLE II

REVERSED-PHASE HPLC FRACTION ANALYSIS

Fraction	*Radioactivity (μCi/ml)*	*Sch 34826*	
		Radiochemical purity (%)	*Chemical purity (%)*
40	33	90.8	90.9
41	203	98.5	99.0
42	512	100	100
43	470	97.7	97.3
44	324	95.7	94.2
45	192	94.8	93.5
46	111	94.3	93.1
47	39	93.8	92.9

bined based on analytical HPLC data. The yield of applied radioactivity in pure fractions from both columns was 64%.

A radiochromatogram of the purified material is shown in Fig. 11. Difficult separations may be effected by gravity LC by using silica gel of small particle size and careful fraction monitoring by rapid HPLC analysis.

*[^{14}C]Spiraprilat (**5**)*

[^{14}C]Spiraprilat has previously been purified by recrystallization or gravity LC with only marginal success; the highest radiochemical purity achieved was 96%. The poor solubility of spiraprilat in most solvents inhibited the development of alternative purification methods such as ion-exchange chromatography. Counter-current chromatography[8] proved to be an excellent method for purifying this compound. Potential solvent systems were chosen by literature analogy[9].A partition coefficient of 0.2–5

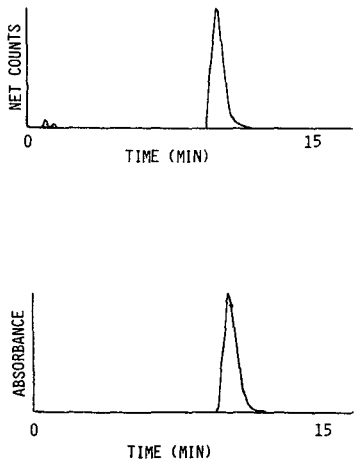

Fig. 11. Analytical UV (bottom) and radiochromatograms (top) of purified [^{14}C]Sch 34826 (**4**). Column, Whatman Partisil 5 ODS-3 RAC II (10 cm × 4.6 mm I.D.); mobile phase, methanol–acetonitrile–0.05 *M* K_2HPO_4 (pH 7.4) (20:20:60) at 1.0 ml/min; Aquassure liquid scintillation cocktail at 1.5 ml/min.

TABLE III

SOLVENT SYSTEMS FOR COUNTER-CURRENT CHROMATOGRAPHY

Solvent system	*Partition coefficient*	*pH of upper phase*
Methanol–chloroform–2% acetic acid (1:1:1)	1.5	3.3
Methanol–chloroform–water (1:1:1)	0.14	4.5

is recommended[10]. Crude [^{14}C]Spiraprilat was partitioned between equal volumes of upper and lower phases of the solvent systems shown in Table III. The relative radioactivity in both layers was determined by liquid scintillation counting. As can be seen in Table III, manipulation of partition coefficients by manipulation of pH is very effective for an ionizable compound such as spiraprilat. The solvent system chloroform–methanol–2% acetic acid (1:1:1) was chosen because of its desirable partition coefficient and its ability to dissolve large amounts (50 mg/ml) of spiraprilat.

The 300-ml coil was first loaded with stationary upper phase and the sample [70 mg in 1.5 ml of methanol–chloroform–2% acetic acid (1:1:1)] was injected. The mobile lower phase was pumped through the coil at 4 ml/min and 8-ml fractions were collected. An aliquot of each fraction was mixed with liquid scintillation cocktail for radioactivity measurements. Fig. 12 shows a typical histogram. Fractions 24–34 were pooled and the solvent was removed.

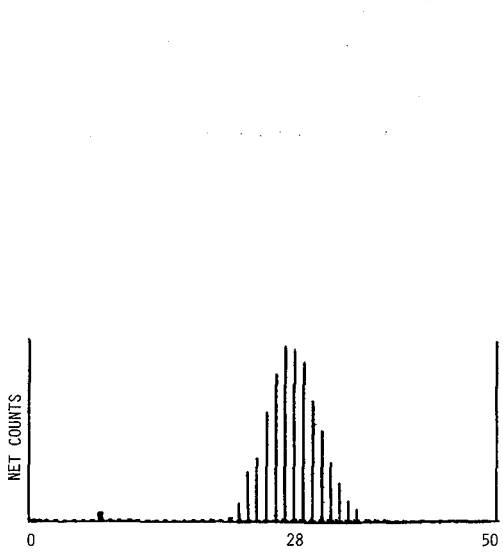

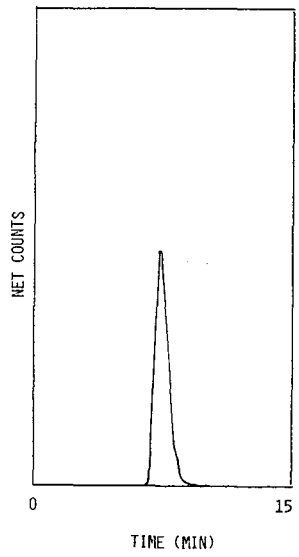

Fig. 12. Histogram of liquid scintillation counting analysis of [^{14}C]Spiraprilat (**5**) preparative counter-current chromatographic fraction aliquots. Ito multi-layer coil separator–extractor, 300-ml coil; mobile phase, chloroform–methanol–2% acetic acid (1:1:1) at 4.0 ml/min.

Fig. 13. Analytical reversed-phase radiochromatogram of purified [^{14}C]Spiraprilat (**5**). Column, Whatman Partisil 5 ODS-3 RAC II (10 cm × 4.6 mm I.D.); mobile phase, methanol–acetonitrile–0.05 *M* K_2HPO (pH 7.5) (20:20:75) at 1.0 ml/min; Aquassure liquid scintillation cocktail at 1.5 ml/min.

Purification of 300 mg of crude reaction product was performed in several 70-mg runs, with an overall 67% mass recovery. Analytical HPLC with radioactivity flow monitoring gave a final batch radiochemical purity of 99.0% (Fig. 13). This is a significant increase over the best value (96%) previously achieved by recrystallization.

REFERENCES

1 D. R. Hawkins, in E. A. Evans and K. G. Oldham (Editors)), *Radiochemicals in Biomedical Research*, Wiley, Chichester, 1988, p. 14.
2 A. Benakis, in W. P. Duncan and A. B. Susan (Editors), *Synthesis and Applications of Isotopically Labeled Compounds—Proceedings of an International Symposium, Kansas City, MO, June 6–11, 1982*, Elsevier, Amsterdam, 1983, p. 45.
3 E. A. Evans, in J. A. Elvidge and J. R. Jones (Editors), *Isotopes: Essential Chemistry and Applications*, Chemical Society, London, 1980, p. 67.
4 L. R. Snyder and J. J. Kirkland, *Introduction to Modern Liquid Chromatography*, Wiley, New York, 2nd ed., 1979.
5 L. R. Snyder and J. J. Kirkland, *Introduction to Modern Liquid Chromatography*, Wiley, New York, 2nd ed., 1979, p. 383.
6 G. B. Cox and L. R. Snyder, *LC · GC, Mag. Liq. Gas Chromatogr.*, (1988) 894.
7 J. L. Garnett and M. A. Long, in E. Buncel and J. R. Jones (Editors), *Isotopes in the Physical and Biomedical Sciences, Vol. 1, Labelled Compounds (Part A)*, Elsevier, Amsterdam, 1987, p. 89.
8 I. A. Sutherland, D. Haywood-Waddington and Y. Ito, *J. Chromatogr.*, 384 (1987) 197.
9 Y. Ito, *CRC Crit. Rev. Anal. Chem.*, 17 (1986) 65.
10 *Instrument Manual for Ito Multi-layer Coil Separator–Extractor*, P.C. Inc., Potomac, MD.

Journal of Chromatography, 484 (1989) 361–368
Elsevier Science Publishers B.V., Amsterdam — Printed in The Netherlands

CHROM. 21 795

PREPARATIVE LIQUID CHROMATOGRAPHY OF HOP AND BEER BITTER ACIDS

M. VERZELE* and G. STEENBEKE
Laboratory of Organic Chemistry, Rijksuniversiteit Ghent, Krijgslaan 281(S4), B-9000 Gent (Belgium)
and
L. C. VERHAGEN and J. STRATING
Heineken Technisch Beheer, Zoeterwoude (The Netherlands)

SUMMARY

Methods and liquid chromatographic (LC) systems for the separation on a preparative scale (Prep-LC) of hop alpha acids and of beer iso-alpha acids were developed. The optimization of the selectivity factor for the *cis–trans* pairs of the iso-alpha acids was particularly studied. The highest values were achieved on reversed-phase packing materials with acetonitrile–water mixtures containing a relatively high proportion of water, to which magnesium salts are added, as eluent. Up to 400 mg of isomerized hop extract could be treated in one run on a laboratory Prep-LC column of dimensions 25 × 2.2 cm I.D. This application illustrates some critical points of Prep-LC, *viz.*, the need for a high selectivity value, the problem of detection at high concentrations and the difficulties of obtaining the separated compounds undegraded from the collected Prep-LC fractions.

INTRODUCTION

In the beer brewing process, the three major hop alpha acids (humulone, cohumulone and adhumulone) are converted into six major beer-bittering iso-alpha acids (three *cis* forms and three *trans* forms). The large-scale separation of these six intensely bitter compounds is of interest for the evaluation of their individual contributions to the bitter taste of beer. We have used counter current distribution to isolate large amounts of the most prominent iso-alpha acids, but this is a very lengthy and costly procedure. Today, it is obvious to turn to liquid chromatography (LC) on a preparative scale (Prep-LC) for this purpose. Several LC systems for separating the iso-alpha acids have been described[1], but they are useless for preparative purposes because the selectivities are too low. Analytical LC of the iso-alpha acids does not aim at the highest possible selectivity between the indiviual compounds, but rather tries to obtain them separated from the matrix, preferably all together in a single peak[2]. This simplifies quantification, which is the major aim of the analytical LC of iso-alpha acids of beer and of isomerized hop extracts. Most analytical LC systems for determining iso-alpha acids use a reversed-phase octadecylated silica gel with a water–

0021-9673/89/$03.50

acetonitrile or methanol–phosphoric acid mixture as solvent. Such systems do not separate the *cis* and *trans* forms of the iso-alpha acids, or insufficiently so. They also do not separate *cis*- and *trans*-isohumulone from *cis*- and *trans*-isoadhumulone. They do separate *cis*- and *trans*-isocohumulone (as a single peak) from the other four iso-alpha acids, but for preparative LC purposes this is not sufficient.

We have evaluated many LC systems for the larger scale separation of beer bitter acids, initially with little success. Buffered silica gel as used by Schwarzenbach[3] and ourselves[1] gave problems with the recovery of the compounds from the column. Silica gel, derivatized with a wide variety of silanes, did not markedly improve the selectivity obtainable on octadecylated silica gel reversed-phase column packing materials. Increasing the selectivity value of the intended separation is, however, of such great importance for Prep-LC[4] that the search was continued, but now directed at the composition of the solvent. This was rewarded with a decisive improvement, obtained by adding magnesium salts to the reversed-phase eluent and by using a relatively large proportion of water.

EXPERIMENTAL

The chromatograph was a Varian 5000 Series instrument with a Varian UV-50 detector (Varian, Walnut Creek, CA, U.S.A.). The injector was a Valco 7000 p.s.i. sample loop injector (Vici, Houston, TX, U.S.A) fitted with external loops of the required volume (10 μl to 2 ml). The columns (RSL, Eke, Belgium) were packed with 5-μm RoSil-C_{18} (RSL) for analytical LC (25 × 0.46 cm I.D.) and with the same material of 10-μm size for Prep-LC (25 × 2.2 cm I.D.). The solvents were of LC quality. The amounts indicated are in millilitres. The phosphoric acid used had a content of 85%.

Optimization of selectivity by eluent and pH adjustment

The iso-alpha acids are known to give chelated salts with bivalent cations. The influence of magnesium cations on their chromatographic separation, as revealed in this work, is therefore not surprising. We also evaluated other divalent cations such as beryllium, calcium, strontium and barium, but without much success. The last three cations have a similar effect to magnesium, but not so pronounced. Beryllium salts have the curious effect of causing extreme broadening of the iso-alpha acid peaks while leaving the alpha acid peaks unaffected. This was verified with pure *trans*-isohumulone. The reason for this effect of beryllium is not clear. Magnesium bromide, which is readily soluble in the eluents in question, poses the problem that the stainless-steel parts of the LC instrument are sensitive to bromide, and these parts have to be washed carefully after each series of chromatographic runs in which this salt was used. Magnesium sulphate is better in this respect, but it needs at least 45% water in the eluent system because of solubility problems. Magnesium acetate is also not acceptable for solubility reasons.

Optimization of the chromatographic conditions was achieved on analytical columns with *trans*- and *cis*-isohumulone as the probe pair of diastereoisomers to be separated. These are readily available by isomerization of pure humulone in brewing conditions. Without adding magnesium salts, with methanol in the usual concentration (10–30%) in the reversed-phase eluent, the *cis* isomer elutes first (α = 1.03),

whereas the opposite occurs with acetonitrile (α = 1.07). Therefore, we use a mixture of methanol and acetonitrile in the procedure for the determination of iso-alpha acids[2]. In this way the isomers are compressed together in a single peak. Chromatograms for the separation of *cis*- and *trans*-isohumulone with methanol or acetonitrile as the organic component in the eluent mixture and in proportions that are usual for reversed-phase LC are shown in Fig. 1. The selectivity factor of these separations is insufficient for Prep-LC. It can be increased significantly with acetonitrile by using a large proportion of water in the eluent. With a 50:50 composition of acetonitrile and water the selectivity factor increases to 1.13 but the retention times then become very long. The latter can be shortened again, while the selectivity factor is further increased, by lowering the pH and by adding magnesium salts to the eluent. This is partly illustrated in Fig. 2.

The best results are obtained at about pH 2 with 50% water in the eluent and with 0.1 *M* magnesium sulphate added. The chromatograms further show that the retention time of humulone (some residual humulone is always present in the isomerization mixtures) does not change on adding magnesium salts to the eluent, whereas it does for the *cis* and *trans* isomers (decreasing with higher magnesium salt concentration). The selectivity factor attained can be as high as 1.3, which indicates good Prep-LC possibilities. A preparative separation is shown in Fig. 3. Although the detection wavelength was 320 nm or far from the absorption maximum, the chromatogram shows that a still longer wavelength is indicated for the larger samples that the system obviously can handle.

In the same way, a mixture of *cis*- and *trans*-isocohumulone can be separated. This mixture can be obtained by isomerization of pure cohumulone. While humulone

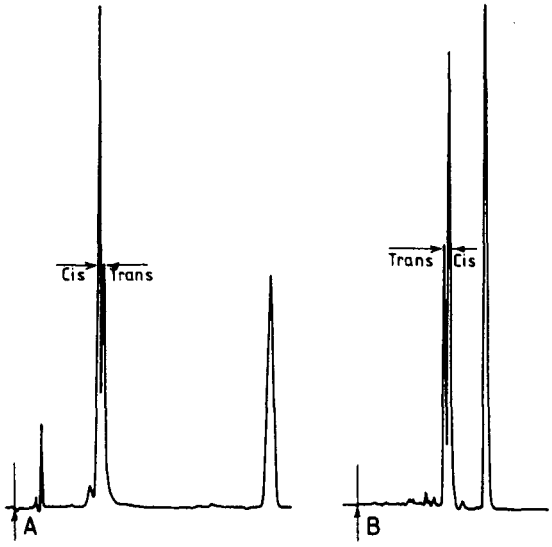

Fig. 1. LC of *cis*- and *trans*-isohumulone. Column, 25 × 0.46 cm I.D. packed with 5-μm RoSil-C_{18}. Reversed-phase eluent: (A) methanol–water (85:15)–0.25% phosphoric acid (selectivity factor, α = 1.03); (B) acetonitrile–water (70:30)–0.25% phosphoric acid (α = 1.07). Detection at 270 nm. Flow-rate, 1 ml/min. Note the reversal of elution order and the higher selectivity with the acetonitrile system. The third peak is unchanged humulone still present in the isomerization mixture.

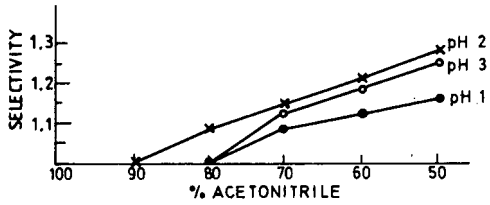

Fig. 2. Influence of pH and acetonitrile concentration on the selectivity factor for the *cis–trans*-isohumulone pair. Column, 25 × 0.46 cm I.D. packed with 5-μm RoSil-C_{18}. Detection at 270 nm. Flow-rate, 1 ml/min.

can be prepared by repeated crystallization of an alpha acid–*o*-phenylenediamine complex, pure cohumulone cannot be isolated in this way and is therefore much more difficult to obtain. A Prep-LC system for the separation of cohumulone from an alpha acids mixture was therefore first developed. Fig. 4 shows the separation of 400 mg of alpha acids on a 25 × 2.2 cm I.D. preparative LC column. This chromatography afforded 140 mg of cohumulone at each pass. This was repeated, sometimes more than ten times, until the desired amount of cohumulone was obtained. After isomerization, as explained above for humulone, the *cis*- and *trans*-isocohumulone were separated under identical conditions to those in Fig. 3. The retention times of these isocohumulones are shorter than those of the humulone-based analogues.

Optimization of magnesium ion concentration

A desirable possibility would be to separate the iso-alpha acids from a pre-isomerized hop extract, rather than to have to isolate pure humulone or pure cohumulone first. However, with the solvent system is Fig. 3 the peaks of *cis*-isocohumulone and *trans*-isohumulone coelute. This problem is solved by lowering the pH to 1

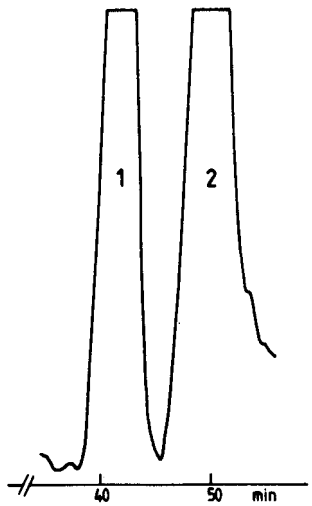

Fig. 3. Prep-LC of 40 mg of a mixture of *cis*- and *trans*-isohumulone. Column, 25 × 2.2 cm I.D. packed with 10-μm RoSil-C_{18}. Eluent: acetonitrile–water (50:50)-0.1 *M* $MgSO_4$ with phosphoric acid to pH 2. Flow-rate, 10 ml/min. Detection at 320 nm. Sample loop, 1 ml. With this acetonitrile-based solvent system, the first peak is *trans*-isohumulone and the second peak is *cis*-isohumulone.

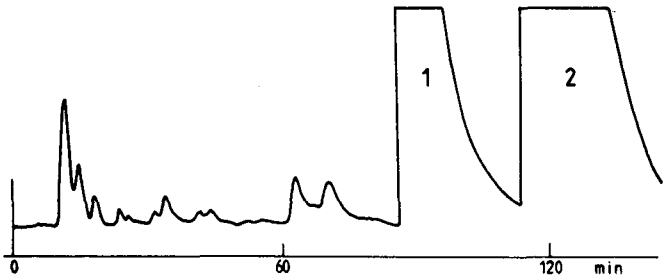

Fig. 4. Prep-LC of alpha acids for the isolation of cohumulone. Column, 25 × 2.2 cm I.D. packed with 10-μm RoSil-C_{18}. Eluent: acetonitrile–water–phosphoric acid (50:50:1). Flow-rate, 10 ml/min. Detection at 340 nm. Sample loop 1 ml. Sample size, 400 mg of alpha acids (hop extract) dissolved in the eluent. Elution sequence as in Fig. 3.

by adding more phosphoric acid. The selectivity for the *cis–trans* pairs is then lower, but the above-mentioned coelution is avoided. The phosphoric acid concentration must always be high, because at lower concentrations the peaks begin to tail and even disappear because of interaction with residual trace iron (iron traces are present in the column packing material and come from the whole LC system). The further problem of long retention times can be solved by adjusting the magnesium salt concentration. The retention times for the four most prominent iso-alpha acids as a function of the magnesium salt concentration are given in Table I.

The chromatograms in Table I are shown in Fig. 5. As a compromise, taking also the time element into consideration, the optimum concentration of magnesium salt was calculated to be 6 g/l. A chromatogram obtained under these conditions on a preparative column with an analytical sample size is shown in Fig. 6. For preparative purposes, a sample of 400 mg of isomerized hop extract, dissolved in 1 ml of eluent and containing about 70% iso-alpha acids, gave the chromatogram in Fig. 7. Fractions of 10 ml were collected and analysed on the analytical column in Fig. 5. From

TABLE I

RETENTION TIMES OF FOUR ISO-ALPHA ACIDS AS A FUNCTION OF MAGNESIUM SALT CONCENTRATION

Column, 15 × 0.46 cm I.D. packed with 5-μm RoSil-C_{18}. Eluent: acetonitrile- water-phosphoric acid (50:50:2). The magnesium salt, in this instance the sulphate, was added to the water; 12 g in 500 ml of water corresponds to 12 g/l in the LC eluent or to 0.1 *M*.

$MgSO_4$ (g)	*Retention time (min)*				*P (atm)*
	trans-Isocohumulone	*cis-Isocohumulone*	*trans-Isohumulone*	*cis-Isohumulone*	
0	16.42	19.17	24.34	28.64	233
0.6	16.86	19.82	25.00	28.79	235
1.2	16.01	19.06	23.56	27.38	235
2.4	14.44	17.43	21.03	24.77	236
4.8	12.55	15.50	18.08	21.76	240
7.2	11.35	14.23	16.19	19.75	246
12	9.92	12.61	13.96	17.25	261

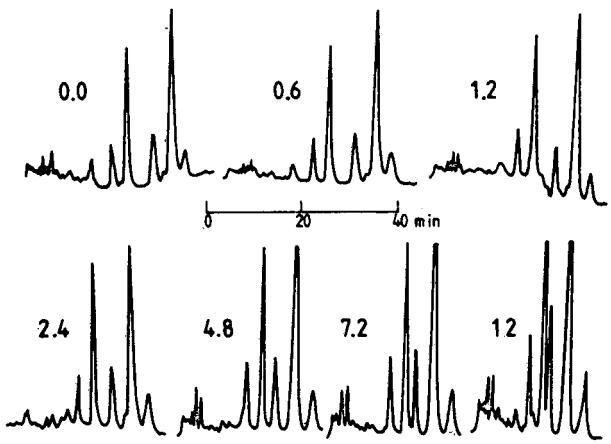

Fig. 5. Analytical separations of isomerized hop extract as a function of the amount magnesium sulphate (g/l) added. Column, 15 × 0.46 cm I.D. packed with 5-μm RoSil-C_{18}. Eluent: acetonitrile–water–phosphoric acid (50:50:2). Sequence of major peaks: *trans*-isocohumulone, *cis*-isocohumulone, *trans*-isohumulone, *cis*-isohumulone + *trans*-isoadhumulone, *cis*-isoadhumulone.

the marked parts in Fig. 7, iso-alpha acids with over 95% purity could be isolated. These results illustrate that the separation in Fig. 7 is better than the chromatographic trace indicates. UV detection is obviously not optimal for Prep-LC, as has been reported previously[5]. An insensitive linear detector seems to be desirable for Prep-LC. Results of the determination of the individual iso-alpha acids content of the sample and of the actual amounts obtained from Fig. 7 are given in Table II.

A problem with working with iso-alpha acids is their instability. They cannot be kept unchanged for more than a few days, even in a freezer. This is a most frustrating situation, as it implies that reference iso-alpha acids (*e.g.*, *trans*-isohumulone) have to be repurified every time they are needed.

One purpose of this work was to isolate pure iso-alpha acids for organoleptic studies. This was achieved for the *cis*- and *trans*-isohumulones and -isocohumulones. The concentration of *cis*- and *trans*-isoadhumulones in the mixtures was too low for successful isolation.

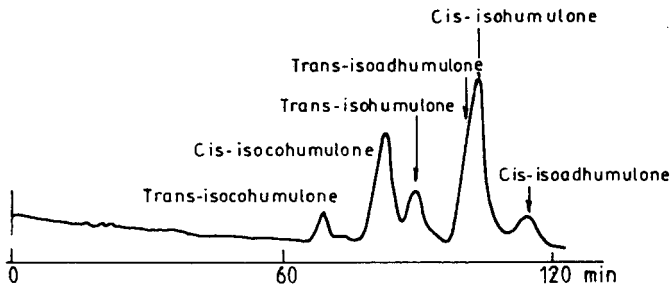

Fig. 6. Prep-LC of isomerized hop extract. Column, 25 × 2.2 cm I.D. Eluent: acetonitrile–water–phosphoric acid (50:50:2) + 6 g/l $MgSO_4$. Flow-rate, 10 ml/min. Sample size, 1 mg of isomerized extract in 10 μl of eluent. Detection at 270 nm. Elution sequence as in Fig. 5.

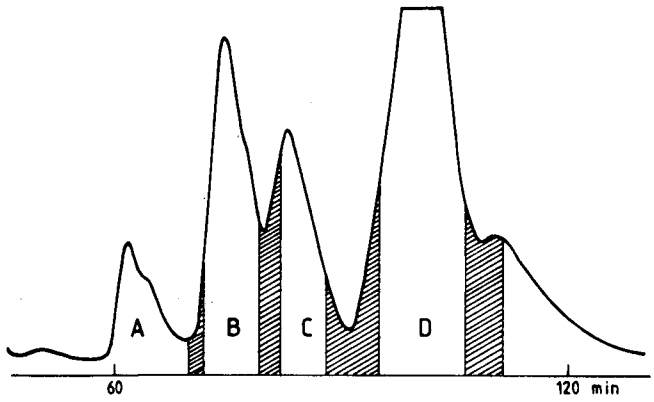

Fig. 7. Prep-LC of isomerized hop extract. Conditions as in Fig. 6 except the sample size, which was about 400 mg of isomerized hop extract in 1 ml of eluent. Detection at 320 nm. The areas marked A, B, C and D gave the amounts as indicated in Table II in each run.

Preliminary results indicate that the *cis* compounds are slightly more bitter than the *trans* compounds. There are also slight taste differences. It was very difficult to obtain the separated compounds unchanged and uncontaminated for a taste panel. Oxidation, degradation and contamination on working up collected Prep-LC fractions are major concerns. Fractions from several Prep-LC runs, collected over several days, are worked up together. Rechromatography at the end is always necessary. The finally collected solution, which is a reversed-phase solvent mixture containing salts and phosphoric acid, can obviously not be evaporated as such to obtain the desired iso-alpha acid. To remove the inorganic involatile chemicals, the final chromatographic solution has to be extracted with, *e.g.*, hexane. Removing this hexane completely without damaging the compounds is not easy. Work on these aspects and problems is continuing.

TABLE II

RECOVERY OF INDIVIDUAL ISO-ALPHA ACIDS OBTAINED FROM ONE PREP-LC SEPARATION IN FIG. 7

Iso-alpha acid	*Amount injected (mg)*	*Amount obtained (mg)*
trans-Isocohumulone (A)	21	12
cis-Isocohumulone (B)	75	33
trans-Isohumulone (C)	40	7
cis-Isohumulone (D)	120	33

CONCLUSION

Optimized chromatographic systems have been described for the preparative separation of some hop and beer bitter acids on an octadecylated silica gel reversed-phase column. For hop alpha acids this packing material can handle about 6 mg of alpha acid mixture per gram. For beer iso-alpha acids, a relatively high water content and magnesium ions in the reversed-phase eluent lead to a selectivity factor that can be as high as 1.3 for *cis*- and *trans*-isohumulone. The column capacity is lower for mixtures of the iso-alpha acids (up to 4 mg/g).

Working up the collected fractions from a Prep-LC run without degrading the compounds is an underestimated aspect of Prep-LC.

ACKNOWLEDGEMENTS

G. S. thanks Heineken Breweries for a grant enabling him to prepare a Dr.Sc. degree. L. C. V. and J. S. thank the Board of Heineken Technisch Beheer for permission to publish this work.

REFERENCES

1 C. Dewaele and M. Verzele, *J. Chromatogr.*, 197 (1980) 189.
2 M. Verzele, C. Dewaele, M. Van Kerrebroeck, J. Strating and L. Verhagen, *Proc. Am. Soc. Brew. Chem.*, 41 (1983) 36; 42 (1984) 94.
3 R. Schwarzenbach, *Proc. Am. Soc. Brew. Chem.*, 37 (1979) 180.
4 M. Verzele, C. Dewaele, J. Van Dijck and D. Van Haver, *J. Chromatogr.*, 249 (1982) 231.
5 M. Verzele, M. De Coninck, J. Vindevogel and C. Dewaele, *J. Chromatogr.*, 450 (1988) 47.

Journal of Chromatography, 484 (1989) 369–379
Elsevier Science Publishers B.V., Amsterdam — Printed in The Netherlands

CHROM. 21 993

STRATEGY FOR THE PREPARATIVE-SCALE HIGH-PERFORMANCE LIQUID CHROMATOGRAPHIC ISOLATION OF KADSURENONE AND FUTOQUINOL FROM THE MEDICINAL PLANT *PIPER FUTOKADSURA*

M. P. STRICKLER* and M. J. STONE
Waters Chromatography Division of Millipore, Fairfax, VA 22030 (U.S.A.)
and
A. S. KENNINGTON and D. M. GOLDSTEIN
Department of Chemistry, University of Virginia, Charlottesville, VA 22904 (U.S.A.)

SUMMARY

The chemical constituents of a Chinese herbal plant, haifenteng (*Piper futokadsura*), have been investigated. In addition to terpenes and lignans of diverse chemical structure, a potent receptor antagonist of platelet activating factor (PAF), kadsurenone, has been isolated and identified. PAF is a highly potent lipid mediator of acute inflammation, allergy and anaphylaxis. Its receptor antagonists are potential therapeutic agents for asthma and various cardiovascular and inflammatory disorders. More recently, a plant sample from Taiwan was re-examined in detail by normal-phase open column and high-performance liquid chromatography. The co-elution of sigificant amounts of futoquinol, a known lignan previously isolated from *P. futokadsura*, hampered the isolation of kadsurenone. To facilitate the isolation of kadsurenone a separation of futoquinol and kadsurenone from a methylene chloride extract of plant was developed on 10-μm silica using gradient chromatography with hexane–methylene chloride–ethyl acetate–acetonitrile. Silica packings of 10, 15 and 37–55 μm were evaluated with this gradient and the 15-μm silica was selected for the initial fractionaton of plant extract. The kadsurenone-containing fractions from the normal-phase separation were re-chromatographed using reversed-phase chromatography. A 15-μm C_{18} column using water–methanol and water–acetonitrile mobile phases yielded pure kadsurenone.

INTRODUCTION

The chemical constituents in the stems of *Piper futokadsura* (haifenteng), a medicinal plant found in southeast China, have been examined with numerous terpenes and lignans described[1–4]. The isolation of a novel receptor antagonist of platelet activating factor (PAF), kadsurenone (I, Fig. 1), has generated renewed interest in this medicinal plant[5]. PAF is a highly potent mediator of acute inflammation, allergic reactions, anaphylaxis and ischemia[6,7]. PAF receptor antagonists are potential therapeutic agents for the treatment of asthma and various cardiovascular and inflammatory disorders. Kadsurenone has been isolated from

0021-9673/89/$03.50

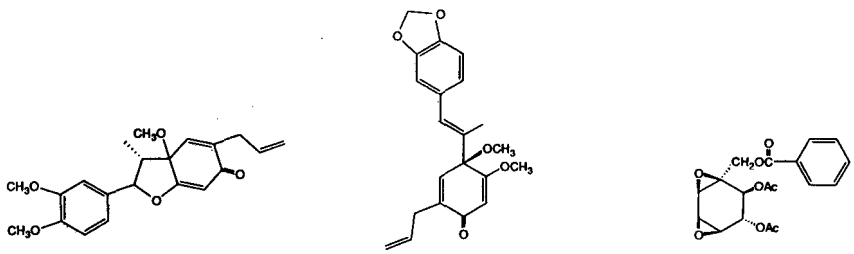

I II III

Fig. 1. Structures of kadsurenone (I), futoquinol (II) and futoxide (III). Ac = Acetyl.

methylene chloride extracts of haifenteng by open column chromatography on silica gel using hexane with increasing amounts of ethyl acetate. Fractions containing kadsurenone were further purified on 55–100-μm particle silica with a mobile phase of hexane–ethyl acetate (3:1, v/v)[5].

Recent attempts to obtain kadsurenone from a haifenteng sample collected in Taiwan, using this separation scheme, have been hampered by the presence of significant amounts of two lignans identified as futoquinol (II, Fig. 1) and futoxide (III, Fig. 1)[8]. Both lignans have been prevously isolated from *P. futokadsura*[9,10]. Additionally, kadsurenone can only be crystallized from very concentrated solutions and the amount of kadsurenone in this recent extract is low compared to previous plant extracts examined. To facilitate the isolation of kadsurenone from this extract for further chemical and biological studies, a more practical and effective preparative high-performance liquid chromatographic (HPLC) procedure was developed.

EXPERIMENTAL

Materials

Solvents and reagents used were of HPLC or reagent grade (Fisher Scientific, Pittsburgh, PA, U.S.A.). Water was purified through the Millipore reverse-osmosis and cartridge filtration system (Millipore, Bedford, MA, U.S.A.).

A Taiwan specimen of *Piper futokadsura* was a gift from the Merck, Sharp and Dohme Research Labs. (Rahway, NJ, U.S.A.). A 1-kg amount of the stems of *P. futokadsura* was extracted with 2 l of methylene chloride for 3 days. After removal of the methylene chloride 20 g of extract were obtained; 12 g were used in this study. The crude methylene chloride extract was prepared in the laboratories of Dr. T. Y. Shen, Department of Chemistry, University of Virginia (Charlottesville, VA, U.S.A.).

Normal-phase chromatography

Analytical and preparative normal-phase chromatography was performed on the Delta-Prep instrument equipped with a Model 481 variable-wavelength UV detector set at 290 nm with a semi-preparative flow cell (Waters Chromatography Division of Millipore, Milford, MA, U.S.A.). For analytical chromatography 10 mg of crude extract, dissolved in 150 μl of methylene chloride, were separated on a 30 cm $\times$ 0.39 cm I.D. column packed with 10-, 15- or 37–55-μm silica (Waters). Eluents, (A) hexane, (B) methylene chloride, (C) ethyl acetate and (D) acetonitrile, were used at

a flow-rate of 1 ml/min to generate the following gradient: A–B (25:75) for 5 min, a 5-min linear gradient to 100% B followed by a 5-min hold, a 20-min linear gradient to B–C–D (59:37:4), and a 10-min gradient to C–D (96:4) to wash the column. The same gradient was used to separate 1, 5 and 6.5 g of crude extract, dissolved in 30, 150 and 200 ml of hexane–methylene chloride (25:75) on a 30 cm × 4.7 cm I.D. Prep Pak cartridge packed with 15-μm silica (Waters). The flow-rate was 80 ml/min and the samples were applied to the column through a port on the solvent delivery system. Fractions (1 min) were collected from all separations. Fractions from the preparative separations were brought to dryness and weighed. Futoquinol in fractions 28 and 29 from the 5- and 6.5-g preparative separations (2 g) was crystallized using cold methanol.

Reversed-phase chromatography

The equipment used for the analytical reversed-phase (RP) HPLC was two Model 510 pumps, a WISP multiple sample injector and a Model 440 UV detector set at 254 nm. Data analysis and system control were provided by a Model 840 chromatography work station (Waters). Aliquots (1 ml) of the fractions from the normal-phase separations were dried and re-dissolved in 1 ml of methanol. Volumes of 5 or 10 μl were analyzed on a 15 cm × 0.39 cm I.D., 5-μm Delta Pak C_{18} column with isocratic elution of water–methanol (35:65) at a flow-rate of 0.5 ml/min. The analyses and spectral comparison of the isolated futoquinol and kadsurenone to standards were made on the same system equipped with a Model 990 photodiode-array UV detector set to scan from 240 to 400 nm.

Preparative RP-HPLC of the kadsurenone-containing fractions from the normal-phase separation was performed on a Model 600 HPLC instrument, with a Model 490 multi-wavelength detector, set at 340 and 290 nm, and a Model 840 chromatography work station (Waters). Fractions 30 (1.2 g), from the 5- and 6.5-g normal-phase separations, were each dissolved in 3 ml of methanol. A white crystalline precipitate, futoxide, was removed and 1.0 or 1.5 ml (approximately 300 mg) of supernatant, containing kadsurenone, was injected on a 30 cm × 1.9 cm I.D., 15-μm Delta Pak C_{18} column. The kadsurenone was isolated using isocratic elution with water–acetonitrile (55:45) at a flow-rate of 5 ml/min. Six preparative separations were required to process all the material. Fractions 31 (0.6 g), from the 5- and 6.5-g normal-phase separations, were each dissolved in 1.5 ml of methanol, and the precipitate was removed. Six 1-ml injections of the supernatant (approximately 70 mg) were applied to the 15-μm Delta Pak C_{18} column and eluted with water–methanol (40:60) at a flow-rate of 5 ml/min.

RESULTS AND DISCUSSION

Since standards of both futoquinol and kadsurenone were available, a number of separation techniques were explored. Futoquinol and kadsurenone were easily separated on RP-HPLC C_{18} columns using either water–acetonitrile or water–methanol gradients. Resolution of these two compounds from the crude extract was identical to the standards. In addition RP-HPLC separated kadsurenone from the other plant constituents. RP-HPLC isolation of kadsurenone directly from extract, however, proved impractical for large-scale separations, because many of the

compounds present in the crude extract had limited solubility in the aqueous methanol or acetonitrile mobile phases. Attempts to put even moderate amounts of extract (mg loads) caused a substantial increase in the operating pressure of the column. The column could be cleaned and returned to normal operating pressures only after extensive washing with acetonitrile, which would be impractical for preparative-scale chromatography. The removal of insoluble and low-solubility components from the crude extract by selective precipitation always resulted in co-precipitation of kadsurenone.

Due to the limited solubility of futoquinol and other plant constituents in reversed-phase eluents, the development of a normal-phase HPLC method to separate futoquinol and kadsurenone was undertaken. Analytical-scale RP-HPLC was effective in assessing the purity of fractions collected from subsequent normal-phase separations. Isocratic elution with water–methanol (35:65) on a 5-μm, 15 cm × 0.39 cm I.D. Delta Pak C_{18} column resolved many of the plant constituents. Since kadsurenone was soluble in reversed-phase eluents, preparative HPLC was used for its purification from fractions collected from normal-phase chromatography.

Normal-phase chromatography on a 30 cm × 0.39 cm I.D., 10-μm silica column showed that using any combination of hexane–ethyl acetate mobile phases co-eluted futoquinol and kadsurenone. Methylene chloride–ethyl acetate gradients resolved the two compounds; however, the limited resolution of futoquinol and kadsurenone restricted the amount of extract that could be injected. Separation of futoquinol and kadsurenone was greatly improved by holding the initial conditions, hexane–methylene chloride (25:75), for 5 min followed by a 5-min gradient to 100% methylene chloride. These conditions were held for 5 min to elute the futoquinol and then kadsurenone was eluted by a 5-min gradient to methylene chloride–ethyl acetate (80:20). The resolution of kadsurenone from the other plant constituents was maximized as shown in Fig. 2A, by replacing the gradient to methylene chloride–ethyl acetate (80:20) with a 20-min gradient to methylene chloride–ethyl acetate–acetonitrile (59:37:4).

Using the gradient conditions presented in Fig. 2, 10 mg of extract, dissolved in methylene chloride, were injected on 30 cm × 0.39 cm I.D. columns packed with 10-, 15- and 37–55-μm silica as shown in Fig. 2. Analyses of these fractions using the reversed-phase method, described previously, showed the futoquinol to be well separated from kadsurenone (not shown). RP-HPLC analyses of the kadsurenone isolated from both the 10-μm (not shown) and 15-μm silica columns eluted relatively free of other plant constituents as shown in Fig. 3. However, RP-HPLC analysis of kadsurenone isolated from the 37–55-μm silica showed the presence of contaminants (Fig. 4); therefore, 15-μm silica was chosen as the packing for the preparative-scale separations.

A loading study was carried out to determine the maximum amount of extract that could be applied to the 15-μm column. More than 65 mg of crude extract showed loss of resolution between futoquinol and kadsurenone, while 10 to 45 mg of extract yielded 75–80% of the kadsurenone, contaminated with one major component. The sample mass for a fixed resolution applied to a preparative column is a function of the cross-sectional area and can be increased as the squares of the diameters of the columns[11]. Using a scale factor of 145 increases the preparative sample load to between 1.45 and 6.5 g of crude extract.

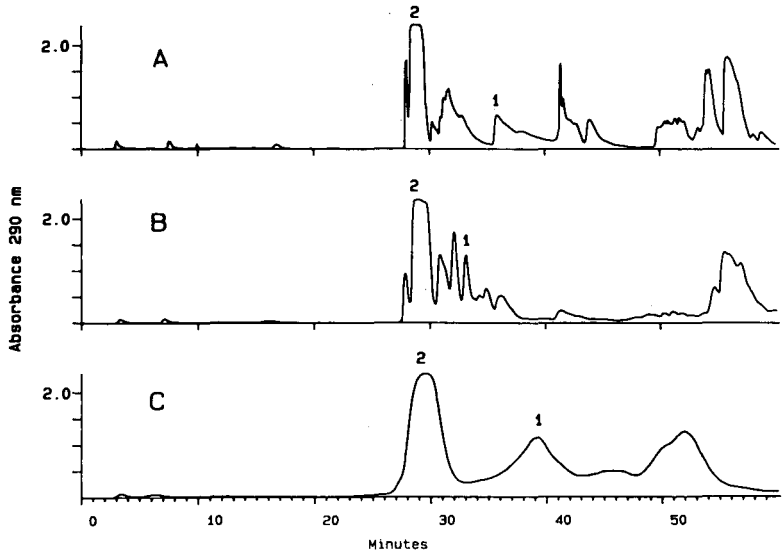

Fig. 2. Effect of silica particle size on the resolution of kadsurenone (1) and futoquinol (2). A 10-mg amount of extract per 150 μl methylene chloride was separated on 30 cm × 0.39 cm I.D. columns packed with 10-μm (A), 15-μm (B) and 37–55-μm (C) silica. Eluents, (A) hexane, (B) methylene chloride, (C) ethyl acetate and (D) acetonitrile, were combined as follows: 0–5 min A–B (25:75), 5–10 min linear gradient to 100% B, 10–15 min hold at 100% B, 15–35 min gradient to B–C–D (59:37:4), 35–45 min gradient to C–D (96:4) at a flow-rate of 1 ml/min. Detection, 290 nm, 2.0 a.u.f.s.

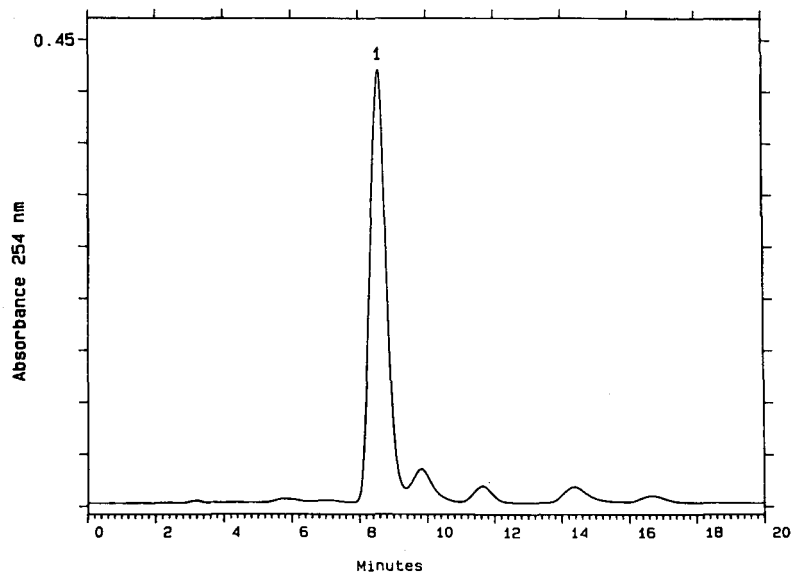

Fig. 3. RP-HPLC analysis of kadsurenone (1) in 20 μl of fraction 33, from the 15-μm silica separation, on a 15 cm × 0.39 cm I.D., 5-μm Delta Pak C_{18} column, using water–methanol (35:65) at a flow-rate of 0.5 ml/min. Detection, 254 nm, 0.45 a.u.f.s.

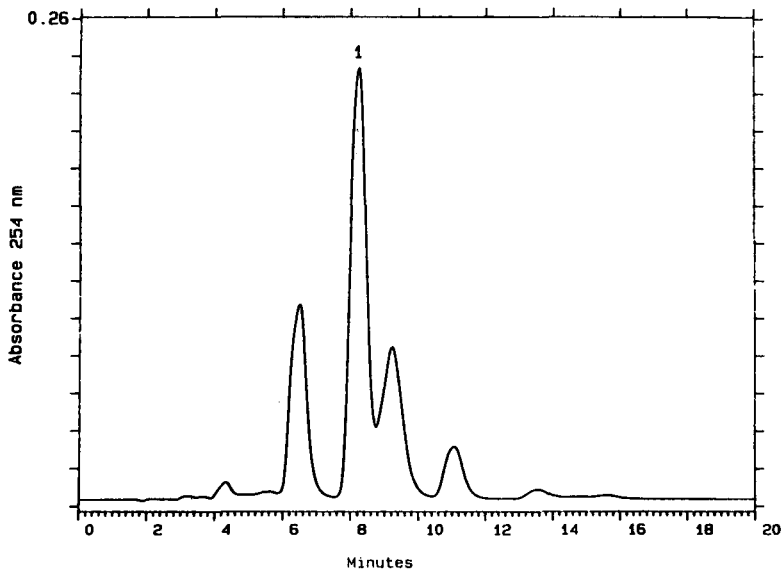

Fig. 4. RP-HPLC analysis of kadsurenone (1) in 20 μl of fraction 40 from the 37–55-μm silica separation. Conditions as in Fig. 3, 0.26 a.u.f.s.

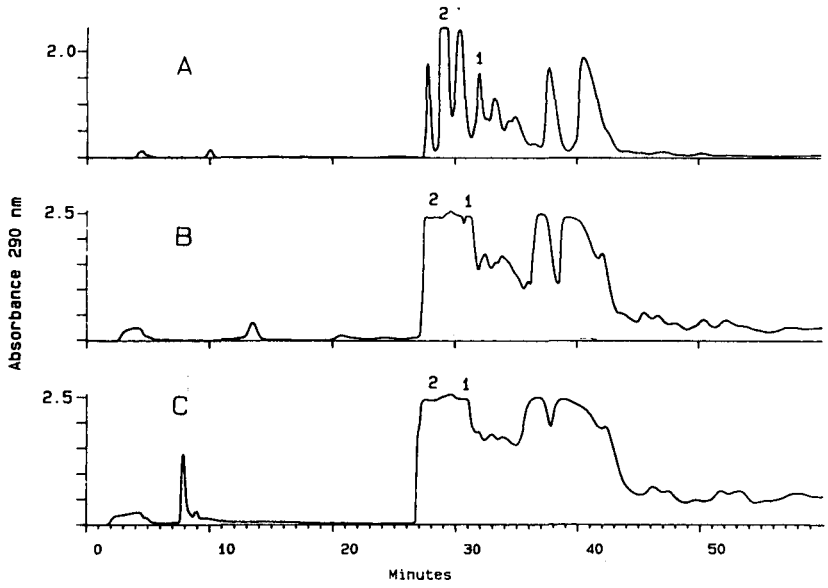

Fig. 5. Preparative-scale separation of 1 g/30 ml (A) 5 g/150 ml (B) and 6.5 g/200 ml (C) of crude extract in hexane–methylene chloride (25:75) on a 30 cm × 4.7 cm I.D. Prep Pak 15-μm silica cartridge. Eluents and conditions as in Fig. 2. Flow-rate was 80 ml/min. Detection was at 290 nm, 2.0 a.u.f.s. (A) and 2.5 a.u.f.s. (B and C). Peaks: 1 = kadsurenone; 2 = futoquinol.

Aliquots of crude extract dissolved in hexane–methylene chloride (25:75), containing 1, 5 and 6.5 g, were fractionated on a 30 cm × 4.7 cm I.D. Prep Pak cartridge packed with 15-μm silica. The chromatographic conditions were identical to those run on the 30 cm × 0.39 cm I.D. column, but at a flow-rate of 80 ml/min as shown in Fig. 5. Fractions (1 min) were collected, a 1-ml aliquot was reserved and the remainder dried and weighed. More than 80% of the total mass applied to the preparative column was recovered for each separation.

The 1-ml aliquots were dried and re-dissolved in methanol for analyses on the reversed-phase column. Fig. 6 shows the RP-HPLC of the futoquinol- and kadsurenone-containing fractions from the 6.5-g separation. The futoquinol elutes in fractions 28 (Fig. 6A) and 29 (Fig. 6B) with most of the kadsurenone in fraction 30 (Fig. 6C). The amount of kadsurenone (277 mg) present in fractions 30 and 31 from the 5- and 6.5-g separations was calculated by comparison of the peak areas to that of kadsurenone standard. The elution profiles of these fractions from the other normal-phase separations are very similar (results not shown).

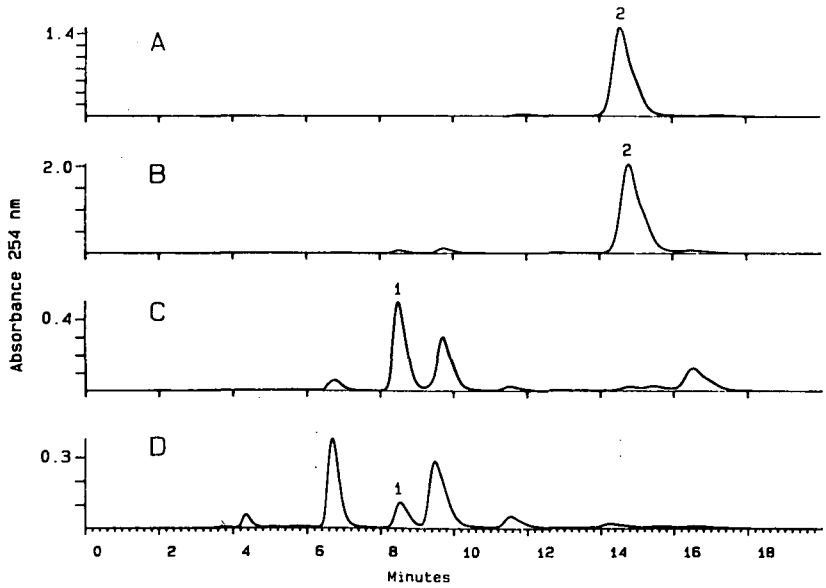

Fig. 6. RP-HPLC analyses of kadsurenone (1) and futoquinol (2) in 5 μl of 1-ml aliquots of fractions 29–32 (A–D) from the 6.5-g normal-phase separation. Conditions as in Fig. 3. Detection was at 254 nm, 1.0 a.u.f.s. (A), 1.4 a.u.f.s (B), 0.4 a.u.f.s. (C) and 0.15 a.u.f.s. (D).

Futoquinol (720 mg) was crystallized from these fractions using cold methanol. Fig. 7A shows the reversed-phase analysis of crystallized futoquinol and Fig. 7B shows the comparison of the UV spectrum of the isolated material to that of the standard.

Fractions 30 (1.2 g), containing kadsurenone, from the 5- and 6.5-g separations were dissolved in methanol, and a white crystalline precipitate, futoxide, was removed. The kadsurenone in the supernatant was then purified by reversed-phase HPLC on a 30 cm × 1.9 cm I.D., 15-μm Delta Pak C_{18} column using isocratic elution with

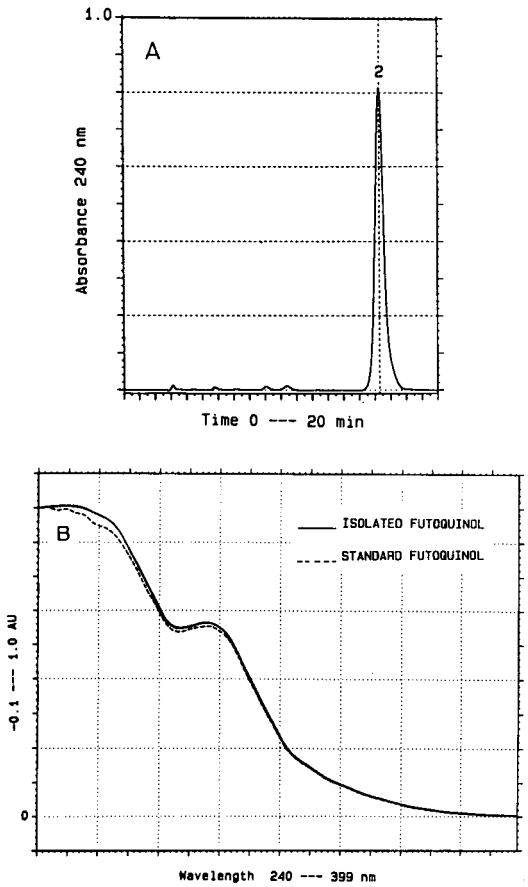

Fig. 7. RP-HPLC analysis of isolated futoquinol (2). Conditions as in Fig. 3. The chromatogram was monitored at 240 nm (A) and the spectra (B) of both the standard and isolated futoquinol scanned from 240 to 399 nm.

water–acetonitrile (55:45) at a flow-rate of 5 ml/min as shown in Fig. 8. Six injections of approximately 300 mg of supernatant were required to process all of the material. Kadsurenone has UV absorbance at 340 nm whereas the contaminants are best detected at lower wavelengths (290 nm). Dual-wavelength monitoring at 340 and 290 nm was used to distinguish the kadsurenone from contaminants facilitating the isolation of kadsurenone at overload conditions. Fractions 31 (0.6 g), containing kadsurenone, from the 5- and 6.5-g separations were similarly dissolved in methanol, and the futoxide was removed. The kadsurenone was purified on the 15-μm Delta Pak C_{18} column, but using water–methanol (40:60) as the mobile phase shown in Fig. 9. Six injections of approximately 70 mg of supernatant were required to process all the material. The water–methanol gave a better separation of the kadsurenone from the contaminants in this more complex fraction. A total of 266 mg of kadsurenone was recovered from these fractions, a 96% recovery. RP-HPLC analysis of this material is

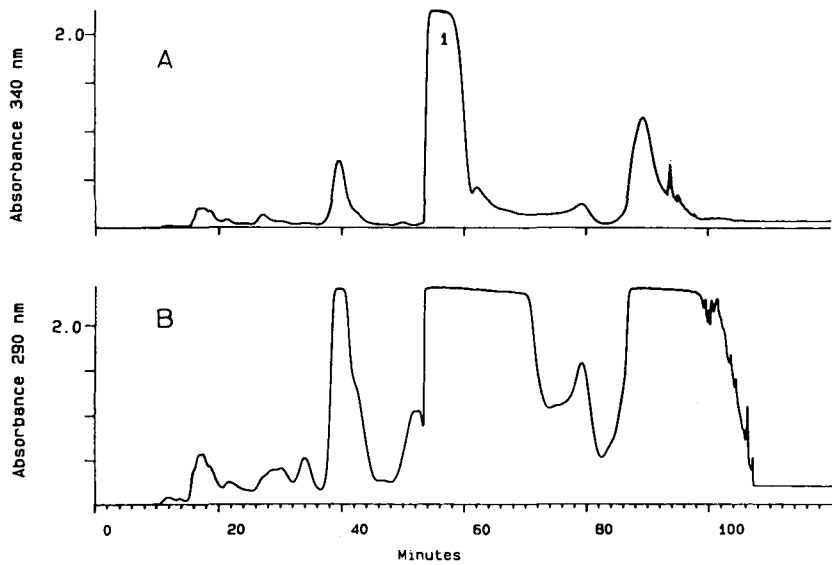

Fig. 8. Preparative RP-HPLC of kadsurenone (1) in 330 mg of fractions 30 from the 5- and 6.5-g normal-phase separation (Fig. 5C), on a 30 cm × 1.9 cm I.D., 15-μm Delta Pak C_{18} column. Isocratic elution at 5 ml/min with water–acetonitrile (55:45) was used. Detection was at 340 nm, 2.0 a.u.f.s. (A) and 290 nm, 2.0 a.u.f.s. (B).

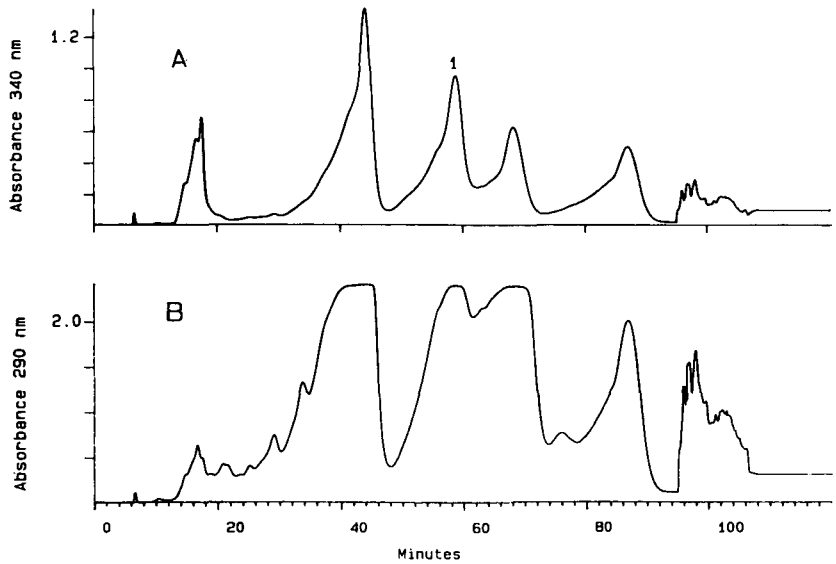

Fig. 9. Preparative RP-HPLC of kadsurenone (1) in 70 mg of fractions 31 from the 5- and 6.5-g normal-phase separation (Fig. 5B), on a 30 cm × 1.9 cm I.D., 15-μm Delta Pak C_{18} column. Isocratic elution at 5 ml/min with water–methanol (40:60) was used. Detection was at 340 nm, 1.2 a.u.f.s. (A) and 290 nm, 2.0 a.u.f.s. (B).

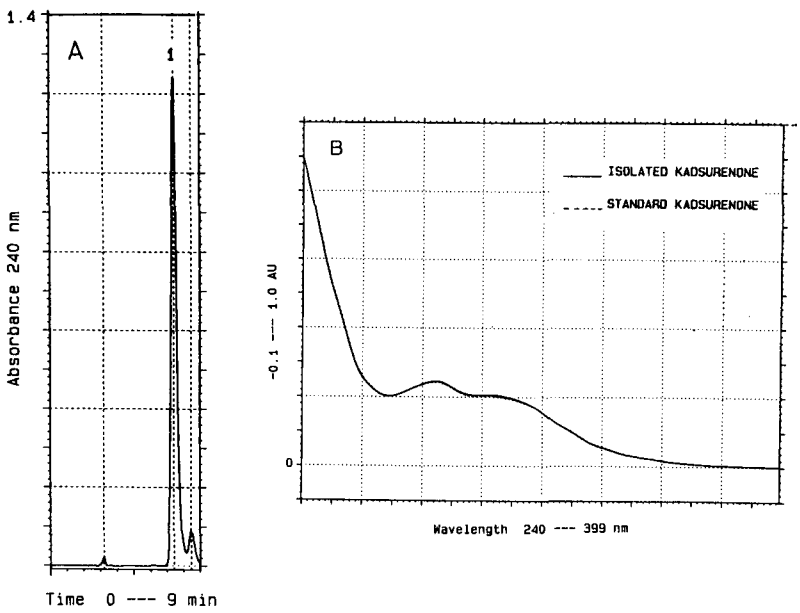

Fig. 10. RP-HPLC analysis of isolated kadsurenone (1). Conditions as in Fig. 3. The chromatogram was monitored at 240 nm (A) and the spectra (B) of both the standard and isolated kadsurenone scanned from 240 to 399 nm.

presented in Fig. 10A, while Fig. 10B shows the comparison of the UV spectra of the isolated kadsurenone to the standard.

In conclusion, the use of analytical HPLC simplified the task of methods development. The normal-phase separation of futoquinol and kadsurenone was developed on a 10-μm silica column by changing the selectivity of the mobile phase from hexane–ethyl acetate to methylene chloride–ethyl acetate. The introduction of two additional solvents, hexane and acetonitrile, into the gradient separation maximized both the amount of extract that was injected on to the column, as well as the resolution of kadsurenone from other plant constituents. Using this gradient, the resolution of the 10-, 15- and 37–55-μm columns was compared and the 15-μm silica selected for the preparative separation. The preparative normal-phase separation was carried out and futoquinol was crystallized from the fractions. Methods development on the reversed-phase column showed this technique useful, not only as an analytical technique for assessing the purity of fractions collected from the normal-phase separation, but as a preparative method for the final purification of kadsurenone.

ACKNOWLEDGEMENT

The research of A. S. K. and D. M. G. was supported in part by Grant CIT BIO-87-010 from the center for Innovative Technology, State of Virginia.

REFERENCES

1 K. Matsui and K. Munakata, *Tetrahedron Lett.*, 24 (1975) 1905.
2 K. Matsui, K. Wada and K. Munakata, *Agric. Biol. Chem.*, 40 (1976) 1045.
3 K. Matsui and K. Munakata, *Agric. Biol. Chem.*, 40 (1976) 1113.
4 K. Matsui and K. Munakata, *Tetrahedron Lett.*, 48 (1976) 4371.
5 T. Y. Shen, S. Hwang, M. N. Chang, T. W. Doebber, M. T. Lam, M. S. Wu, X. Wang, G. Q. Han and R. Z. Li, *Proc. Natl. Acad. Sci. U.S.A.*, 82 (1985) 672.
6 P. Braquet, L. Touqui, T. Y. Shen and B. B. Vargaftig, *Pharmacol. Rev.*, 39 (1987) 97.
7 P. Braquet, M. Paubert-Braquet, M. Koltai, R. Bourgain, F. Bussolino and D. Hosford, *Trends Pharmacol. Sci.*, 10 (1989) 23.
8 T. Y. Shen, J. T. Loper and B. A. Outten, Department of Chemistry, University of Virginia, Charlottesville, VA, unpublished results.
9 S. Takahashi and A. Ogiso, *Chem. Pharm. Bull.*, 18 (1970) 100.
10 S. Takahashi, *Phytochemistry*, 8 (1969) 321.
11 C. Stacey, R. Brooks and M. Merion, *J. Anal. Purif.*, 2 (1987) 52.

Journal of Chromatography, 484 (1989) 381–390
Elsevier Science Publishers B.V., Amsterdam — Printed in The Netherlands

CHROM. 21 938

PROCESS-SCALE REVERSED-PHASE HIGH-PERFORMANCE LIQUID CHROMATOGRAPHY PURIFICATION OF LL-E19020α, A GROWTH PROMOTING ANTIBIOTIC PRODUCED BY *STREPTOMYCES LYDICUS* SSP. *TANZANIUS*

D. R. WILLIAMS, G. T. CARTER, F. PINHO and D. B. BORDERS
American Cyanamid Company, Medical Research Division, Lederle Laboratories, Pearl River, NY 10965 (U.S.A.)

SUMMARY

LL-E19020α is a novel antibiotic produced by fermentation of the soil microorganism *Streptomyces lydicus* ssp. *tanzanius*. The compound is highly effective in inducing increases in weight gain and feed conversion efficiency in livestock. In order to obtain kilogram quantities of the material for field trials, pilot plant scale fermentations (up to 7500 l) were carried out. The antibiotic was recovered from the fermentation broth by solvent extraction. The resultant crude extract was subjected to reversed-phase (C_{18}) chromatography on a process-scale high-performance liquid chromatography (HPLC) unit. The heart of the instrumentation is the Millipore Kiloprep® chromatograph with the standard 12-l cartridge column. The laboratory housing the chromatograph has been specifically designed for this work. Tanks for mobile phase preparation are mounted on load cells for precise measurement of components. In this explosion-proof laboratory, all solvent handling areas are well ventilated and a separate breathing air system is provided for the operators. For the purification of the LL-E19020 antibiotics, the mobile phase consisted of a gradient of acetonitrile in 0.1 *M* ammonium acetate at pH 4.5. The effluent was monitored by UV absorbance at 325 nm. Fractions were collected across the peaks of interest and these were analyzed by analytical HPLC. The maximum yield of LL-E19020α obtained in a single run was approximately 100 g. The antibiotic was recovered from the mobile phase by extraction with methylene chloride. The methylene chloride phase was concentrated under reduced pressure to yield a gummy residue which was finally freeze-dried from tertiary butanol to yield an off-white solid suitable for blending with various feed components.

INTRODUCTION

Two recently discovered antibiotics designated LL-E19020α and LL-E19020β (Fig. 1)[1] are highly modified versions of the aurodox family[2]. The LL-E19020 antibiotics have an exceptionally narrow antimicrobial spectrum against human pathogens, showing meaningful activity *versus Streptococcus* species and certain anaerobes (minimum inhibitory concentration, MIC 0.1–1 μg/ml). These compounds

0021-9673/89/$03.50

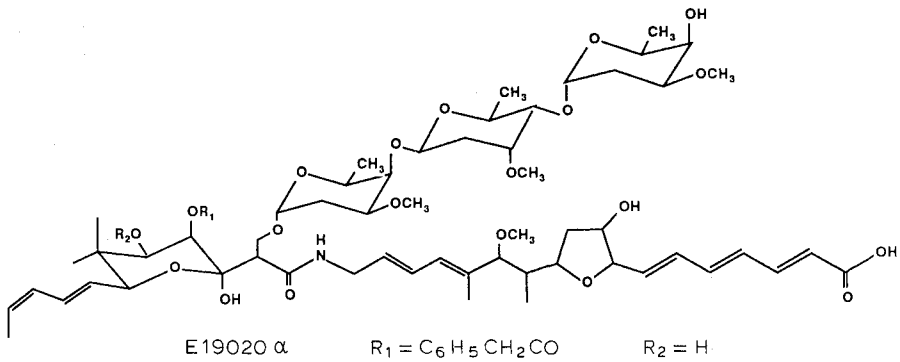

Fig. 1. Structures of the LL-E19020 antibiotics.

are highly effective as growth promoting agents in animals, producing superior performance in chicks during comparison trials with bacitracin and virginiamycin. The unique structural features of these compounds, including the hydroxymethyl-linked trisaccharide and shortened carbon skeleton ending in a carboxylic acid, may explain their greatly enhanced growth promoting activity relative to aurodox. After our initial structure reports[3,4], the structures of phenelfamycins E and F were revised[5] indicating that they were identical to E19020α and β, respectively.

The compounds are isomers of molecular weight 1225 with very similar physico-chemical properties (Table I). The only difference between the two is that LL-E19020α has the phenyl acetate ester linked at C-23, whereas LL-E19020β has this ester group at C-24 (see Fig. 1).

Interest in providing relatively pure kilogram quantities of each antibiotic for field trials in a short period of time necessitated an evaluation of resources and possible methods for achieving this goal. Development of a new chemical isolation process at

TABLE I
CHARACTERIZATION DATA FOR LL-E19020α AND β

	α	β
Molecular formula	$C_{65}H_{95}NO_{21}$	$C_{65}H_{95}NO_{21}$
Molecular weight	1225	1225
Molecular ion $[M+Na]^+$ [a]	1248.6187	1248.6193
	(Calc. 1248.6270)	
$[\alpha]_{26}^{D}$ (methanol)	−8° (1.0%)	−17° (0.46%)
UV absorbance (nm) methanol	233 (ε 49 800)	233 (ε 47 000)
	290 (ε 36 600)	290 (ε 34 100)
IR absorbance (cm^{-1}) (KBr)	3420 1617	3430 1543
	2970 1525	2970 1454
	2925 1445	2930 1367
	1717 1365	1712 1265
	1695 1092	1648 1098
	1647 1018	1620 1020

[a] Determined with high-resolution fast atom bombardment mass spectrometry.

this stage of the project was rejected as being too lengthy and labor intensive. The Millipore Kiloprep® had recently been installed and was operational. Laboratory experience suggested that direct scale-up of purification of the crude LL-E19020 mixture by preparative high-performance liquid chromatography (HPLC) should work. The decision to implement preparative HPLC, therefore, was made and proved to be the most efficacious method of meeting our goal.

EXPERIMENTAL

Fermentation

Isolation of LL-E19020α and LL-E19020β (Fig. 2) begins with the fermentation of the soil microorganism *Streptomyces lydicus* ssp. *tanzanius*[6] in a complex medium containing dextrin, a soy product, corn steep liquor and calcium carbonate for pH control. Inoculum build-up proceeded through three stages beginning with a shaker flask (100 ml culture) and culminating in a 300-l stirred fermentor. After inoculation,

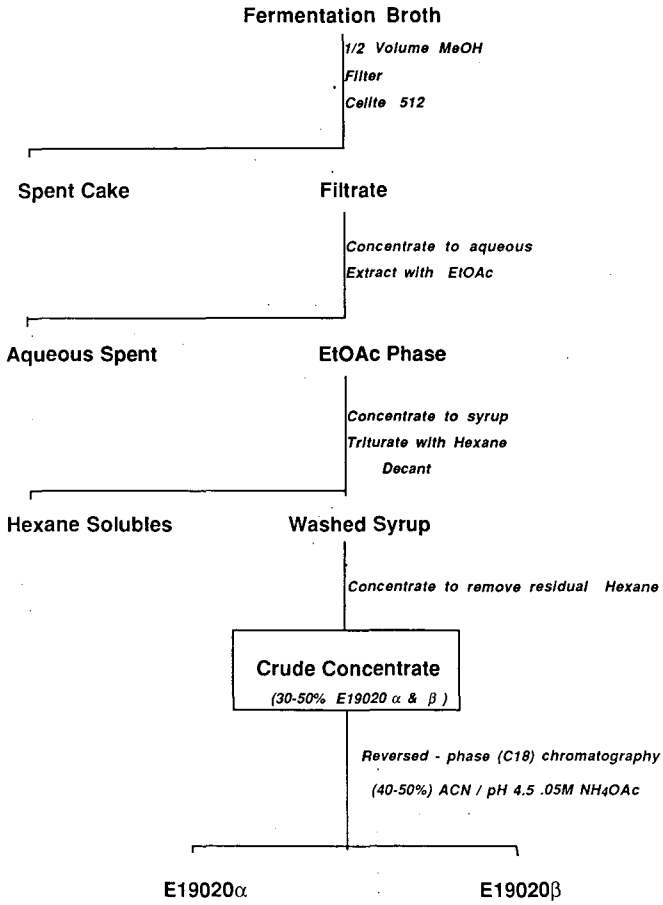

Fig. 2. Isolation and purification of LL-E19020α and β. MeOH = Methanol; EtOAc = ethylacetate; ACN = acetonitrile; NH_4OAc = ammonium acetate.

the large-scale fermentation was carried out at 28–30°C in 1500 and/or 3000-l fermentor(s) for five to six days. Aeration was set at 0.67 VVM (= volume of air per volume of fermentation broth per minute) and agitation was sufficient to maintain dissolved oxygen levels above critical levels at all times. The fermentors were then harvested for refining. Harvest potencies for LL-E19020α averaged approximately 300 μg/ml and approximately 100 μg/ml for LL-E19020β as determined by analytical HPLC.

Fermentation processing

The initial processes in the purification of this fermentation product were recovery of the material from the broth and concentration to a workable volume. In this example, recovery and concentration were achieved through solvent extraction and evaporation as follows. The harvested fermentation mash (3200 l) was mixed with toluene (45 l) for 30 min. Methanol (1600 l) was added and the suspension was stirred for 1 h. Celite 512 filter aid (150 lbs) was then added and mixing was continued for 15 min. The suspension was filtered through a filter press and washed with 320 l of water. The press cake was discarded. The combined filtrate and wash were concentrated under reduced pressure from 5000 to 2950 l. Ethyl acetate (1500 l) was added to the concentrate and the mixture was stirred for 2 h. Separation of the aqueous phase left approximately 900 l of ethyl acetate phase containing the antibiotics, which was concentrated under reduced pressure to 80 l. To this concentrate was added ethyl acetate (190 l) and the mixture was stirred for 1 h. The aqueous phase (20 l) was removed and the ethyl acetate phase concentrated under reduced pressure to 1–2 l. In the lab, this concentrate was allowed to further evaporate in the hood to a thick black syrup. The syrup was washed repeatedly with a equal volumes of hexane, which was decanted and discarded, to remove fats, oils and antifoam agent prior to reversed-phase chromatography. The final preparation, 2 l of thick black syrup, contained 0.385 g/ml E19020α and 0.136 g/ml E19020β. A typical analytical chromatogram of LL-E19020 crude extract is shown in Fig. 3. The ratio of α and β components varies in individual fermentations from about 1:1 to 9:1, depending upon the conditions selected.

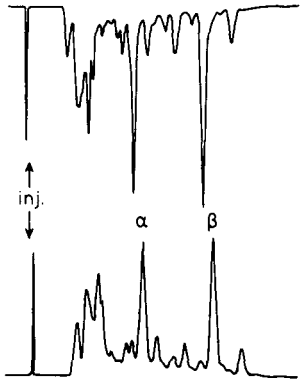

Fig. 3. Analytical HPLC of defatted crude LL-E19020; system A (chart speed 0.25 cm/min).

PROCESS-SCALE CHROMATOGRAPHY

General

Operations in the analytical laboratory which are routine and taken for granted become significant problems to be overcome in process-scale chromatography. The building housing the Millipore Kiloprep is designated as an explosion-proof area (class I, division 1, group D), wich means that all equipment must meet explosion proof standards. Even the hand tools used to open the various 55-gallon solvent drums must be made of non-sparking material. Electrical power is run in sealed conduit, enclosures, and fixtures. Pneumatically operated pumps and agitators are also in use. Instrumentation is either intrinsically safe or is housed in explosion-proof enclosures. All equipment is grounded and portable grounds are available for movable equipment and solvent drums to prevent an explosion due to a static spark. A fire alarm, emergency lighting, and sprinkler system are installed.

The building has an extensive ventilation system from which the airflow inwards is ballanced. The ventilator system to the walk-in hood, the laboratory bench, and the sink area is equipped with high-efficiency particulate air (HEPA) filters to prevent the release of toxic material (if any) to the environment. Portable ventilator trunks are strategically located wherever open solvent containers could be in use. The ventilation system is also monitored and controlled by the fire alarm system.

A breathing air system is available for use, not only in the process chromatography building, but throughout the entire pilot plant complex. An oil-free air compressor linked with an air purification and alarm system provides breathable air to conveniently located 3M filter regulator panels (W-2806). The operator plugs in his or her air hose and is supplied cooled or heated (as needed) breathable air to the 3M white cap helmet.

Other services provided to the building include compressed air to operate the pumps and agitators and nitrogen to inert the process tanks when pumping flamable solvents. The process tanks are vented to the atmosphere and use the appropriate flame arresters. Nitrogen is also used to inert the detector enclosure on the chromatograph. High-pressure steam is used to operate the two-stage steam ejector system (Kinema) which provides vacuum for routine use and to operate two Buchi 20-l rotary evaporators. The steam condensate is removed by an automatically pumped condensate system. For the storage of process samples and product, *etc.*, a roof-mounted refrigeration unit is used to provide cooling ($5 \pm 2°C$) for an explosion-proof chill room. A Millipore Super-Q system coupled with the Millipore Continental Water system de-ionized water system delivers high-quality de-ionized water for chromatographic buffer system preparation. The de-ionized water is piped to the process tanks in the process chromatography building and also the main pilot plant.

System preparation

There are three process tanks (640 l each) associated with the chromatograph. They are identical with the exception that the "prep tank" has an agitator. All tanks are mounted on load cells and therefore can only have flexible couplings to the tanks. The load cells effectively weigh each tank and shows each reading on individual explosion-proof light-emitting diode (LED) displays. It is therefore important to make the necessary corrections for the density of solvents different from water. The aqueous

buffer system (0.1 *M* ammonium acetate at pH 4.5) is prepared in the prep tank as follows: 519 l of de-ionized water are drawn in and 4 kg of reagent-grade ammonium acetate are dissolved with mixing. The pH is adjusted to 4.5 with HPLC-grade acetic acid. The buffer system is then pumped through a Millipore Rogard® cartridge filter to tank A, which feeds one inlet of the Kiloprep unit. ACS reagent-grade acetonitrile is then pumped either directly or through the filter system into the other tank, tank B, which feeds a separate inlet to the chromatograph. The valving, piping, pumping, and filtration system have been designed so that it is possible to transfer and/or filter from any tank to any tank. In addition, the dual Rogard cartridge filter assembly is set up in parallel so one cartridge can be changed while the other is in use.

Operation of the process chromatograph

The A and B tank inlets to the unit are each connected to recycle pumps and back-pressure valves on the unit, which continuously recycle the solvent or buffer system to its respective tank. This provides a constant-pressure feed for the solvent/buffer delivery system regardless of the tank volumes. As the A and B tanks are recycling their respective contents, a microprocessor-controlled system of check and solenoid valves sample the two liquid streams to give the desired composition of acetonitrile–0.1 *M* ammonium acetate of pH 4.5 (45:55), initially. This mixture is pumped using the Bran & Lubbe pump (variable from 0 to 5 l/min) through the 3-l guard column and the standard Millipore 12-l cartridge, each packed with 55–105-μm μBondapak C_{18}. A system of valves and tubing allows flow to be directed to waste or to fraction collection bottles. Also, a small portion of the flow (30 ml/min) is diverted to the detector to aid in fraction collection. The column was equillibrated for 0.5 h before the charge (400 ml of defatted syrup described above dissolved in 700 ml methanol) was injected. The initial mobile phase consisted of acetonitrile–0.1 *M* ammonium acetate of pH 4.5 (45:55) flowing at 1.6 l/min. Following elution of the LL-E19020α, a linear gradient was run, increasing the acetonitrile content from 45 to 65% in 60 min. During this gradient elution, the flow-rate was maintained at 2.0 l/min. The chromatographic effluent was monitored with a UV absorbance detector set at 325 nm at 2.0 a.u.f.s. deflection. Throughout the chromatography, fractions were collected at 10-min intervals as noted on the chart in Fig. 4. These fractions were assayed by the analytical HPLC method described below. Based upon these measurements for the run shown in Fig. 4, fractions 8–11 were combined as LL-E19020α and 17–20 were combined as LL-E19020β.

Fraction processing

These antibiotics were recovered from the mobile phase by first concentrating the respective fractions to half their original volume under reduced pressure by using the 20-l Buchi rotary evaporators. The antibiotic was then partitioned into one half volume of reagent-grade methylene chloride. The methylene chloride extracts of the individual antibiotics were evaporated and the residues redissolved in warm *tert.*-butyl alcohol. The solvent was removed by lyophilization to yield light tan to light yellow solids. Analytical results for three separate finished batches of the α component, representing 20 chromatographic runs, are presented in Table II. Typical overall recoveries of LL-E19020α through processing and chromatography are summarized in Table III. Analytical HPLC chromatograms of typical LL-E19020α and β material obtained in this manner are shown in Fig. 5.

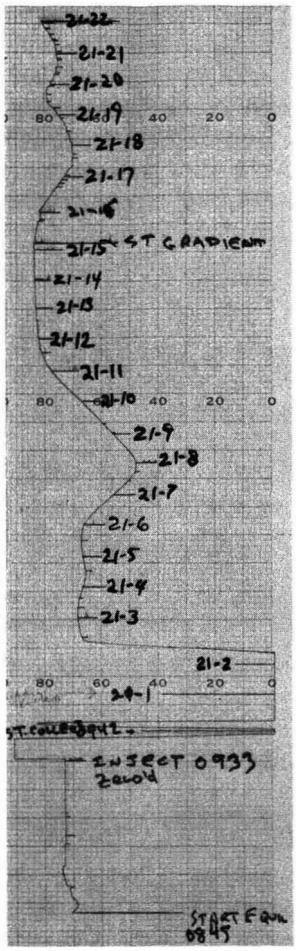

Fig. 4. Typical chromatogram from Kiloprep run. Fractions (21-1 to 22) were collected at 10-min intervals.

Analytical HPLC system

Analytical chromatography was performed with a C_{18} column (μBondapak 10 μm, 100 × 8 mm I.D.) eluted with either mobile phase A [acetonitrile–0.1 *M* ammonium acetate of pH 4.5 (60:40)] at 0.5 ml/min, or B [acetonitrile–0.1 *M* ammonium acetate of pH 4.5 (45:55)] at 1.5 ml/min. Detection was by UV absorbance at 254 nm (lower trace in the figures) and 280 nm (upper trace in the figures). Retention times for α and β in system A were 6.0 and 9.9 min, respectively, and in B 8.0 and 19.3 min, respectively.

RESULTS AND DISCUSSION

The solvent extraction process outlined in the flow-chart of Fig. 2 results in recovery of approximately 80% of the antibiotics as a syrupy concentrate (Table III).

TABLE II
ANALYTICAL FINDINGS FOR LL-E19020α

	Batch 1	*Batch 2*	*Batch 3*
Description	Tan powder	Light yellow powder	Light yellow powder
Batch size (g)	400	356	800
Purity (%), as is	86.3	79.3	84.0
anhydrous	87.4	81.4	85.0
Identification confirmed by UV, IR, ^{1}H-NMR, ^{13}C-NMR, Mass spectrometry	yes	yes	yes
Composition (%)			
LL-E19020α	86.3	79.3	85.0
Impurities	8.2	16.0	11.7
Volatiles	2.8	2.5	1.4
Water (Karl Fischer)	1.09	2.09	0.96
Ash	0.1	0.08	0.02
$[\alpha]_{26}^{D}$ (1% in methanol)	−10°		−8°

Trituration of this viscous material with hexane removes the non-polar by-products of the fermentation as well as any silicone oil antifoam agent added during the fermentation process. This step was included to prolong the useful lifetime of the

TABLE III
TYPICAL YIELDS OF LL-E19020α AND β

	Yield			
	Grams			*%*
	α	β	*Total*	
Fermentation				
6000 l Broth (3 fermentors)	1020	889	1909	100
Crude refining				
Filtration step (9531 l methanol filtrate and wash)	1005	717	1722	90.2
Solvent extraction steps (3.64 l of syrup)	929	606	1535	80.4
Process-scale chromatography (1 run)				
Charge derived from similar runs (after defatting)	62	40.3	102.3	
Chromatographic fraction processing and lyophilization				
Weight solids (approx. 80% pure)	(39.3)	(36.3)	(75.7)	
weight × 80% purity	31.5	29.6	60.5	
Overall chromatographic yield (Chromatography to LL-E19020)	50.8%	72.1%	59.2%	
Estimated overall yield (fermentation to LL-E19020)			47.6%	

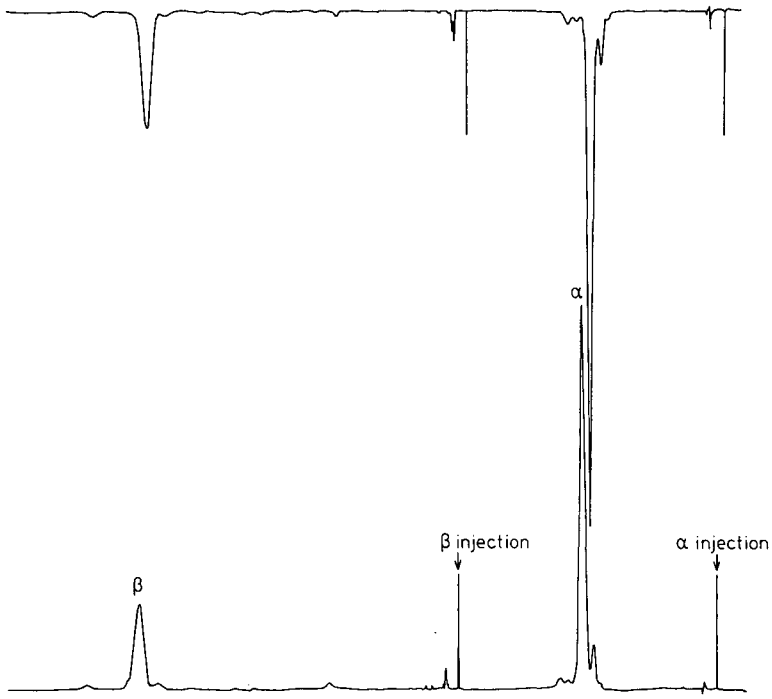

Fig. 5. Analytical HPLC of lyophilized LL-E19020α and LL-E19020β; system B (α retention time 80 min; β retention time 19.3 min).

reversed-phase columns. The defatted crude material contained between 30 and 50% (w/w) antibiotic (α + β), depending on the productivity of a particular fermentation, medium constituents used and by-products produced. The ratio of α to β was also higly dependent on the fermentation conditions employed and was found to vary between about 1:1 and 9:1.

The preparative HPLC procedure represents a nearly direct scale-up from the analytical system developed to monitor titers of the antibiotics during the fermentation. Attempts were made to replace acetonitrile with methanol as the organic modifier in the mobile phase to reduce the cost of the process, however no alternative system was found to produce equivalent chromatographic results. Buffering the mobile phase at pH 4.5 was essential for good resolution and also enhanced the stability of the material. At significantly lower pH's decomposition is evident and at pH greater than 8 equilibration of the α and β forms occurs as well as decomposition. Loadings for the preparative separation were determined empirically by gradual increases in the amount of crude extract charged onto the column and monitoring the effect of each successive increment on the quality of the separation achieved. In order to obtain material consistently with 85% purity, no more than about 500 g of the crude syrup (containing up to 150 g of α and a lower variable amount of β) could be used. Owing to solubility constraints, the crude had to be dissolved in methanol. To obtain the required resolution, no more than 1200 ml of solution could be used for an injection. Flow-rates were maintained between 1 and 2 l/min primarily to minimize

back pressure. Within this range, variations in the flow-rate had little effect on the chromatographic resolution.

The analytical profiles of the 3 batches of LL-E19020α presented in Table II show that 80–85% material was routinely obtained. Overall recovery from broth to final product approached 50% (Table III). The most common volatile impurities found in the batches were acetic acid from the mobile phase and *tert.*-butanol from incomplete lyophilization. The impurities listed in Table II ranged from 8.2 to 16.0% between batches. These are evidently related components, since their UV spectra show very similar chromophores to LL-E19020α and β. The identities of these minor components are still under investigation.

In general, preparative HPLC provides a method of obtaining relatively pure material in a timely fashion. Once the operating parameters were defined there was very little fine-tuning required from run to run. The availability of a chromatograph with this capacity, which conformed so closely with the analytical separation, made it possible to achieve the production goals for these experimental compounds within a short and predictable timeframe.

In terms of chromatographic hardware, we are continuing to upgrade the preparative HPLC operation for increased control and safety. The electrically operated transfer pumps have been replaced with safer air-operated pumps. The determination of mobile phase concentration will be facilitated with the installation of a mass flow meter. Currently the difference in weight *versus* time of the load cell readings corrected for density is used. The mass flow meter should give "instantaneous" readings. It is hoped to install a new UV detector with a variable-path flow cell so that "on stream" detection will alleviate some of the need for analytical HPLC support from the laboratory.

ACKNOWLEDGEMENTS

The skillful assistance of Ms. J. A. Nietsche and Mr. J. L. Baker for providing chromatographic support is gratefully acknowledged. Mr. J. D. Korshalla and Mr. K. A. Cote are thaked for providing additional chromatographic support. They also provided microbiological testing and maintained the fermentation processes. The staff of both the Fermentation and Refining Pilot Plants are thanked for their assistance. In addition, Drs. J. C. James and L. Gehrlein are acknowledged for providing analytical services on the lyophilized LL-E19020α.

REFERENCES

1 G. T. Carter, D. W. Phillipson, J. J. Goodman, T. S. Dunne and D. B. Borders, *J. Antibiot.*, 41 (1988) 1511–1514.
2 H. Maehr, M. Leach, T. H. Williams and J. F. Blount, *Can. J. Chem.*, 58 (1980) 501–526.
3 G. T. Carter, in A. L. Demain, G. A. Somkuti, J. C. Hunter-Cevera and H. W. Rossmoore (Editors), *Novel Microbial Products for Medicine and Agriculture*, Society for Industrial Microbiology, Amsterdam 1989, Ch. 26, pp. 233–237.
4 G. T. Carter, D. W. Phillipson, T. S. Dunne, D. R. Williams, F. Pinho, J. A. Nietsche, J. J. Goodman, M. J. Torrey and D. B. Borders, *presented at the 28th Interscience Conference on Antimicrobial Agents and Chemotherapy, Los Angeles, CA, 1988*, abstract 312.
5 J. E. Hochlowski, M. H. Buytendorp, D. N. Whittern, A. M. Buko, R. H. Chen and J. B. McAlpine, *J. Antibiot.*, 41 (1988) 1300–1315.
6 W. M. Maiese, M. P. Lechevalier, H. A. Lechevalier, J. D. Korshalla, J. J. Goodman, M. J. Wildey, N. A. Kuck, S. D. Conner and M. Greenstein, *J. Antibiot.*, in press.

Journal of Chromatography, 484 (1989) 391–397
Elsevier Science Publishers B.V., Amsterdam — Printed in The Netherlands

CHROM. 21 796

PURIFICATION OF NITROPHENYLVALERIC ACID REACTION MIXTURES BY COUNTER-CURRENT CHROMATOGRAPHY

WALTER D. CONWAY*
School of Pharmacy, State University of New York at Buffalo, 565 Hochstetter Hall, Amherst, NY 14260 (U.S.A.)
JACK D. KLINGMAN
Department of Biochemistry, School of Medicine, State University of New York at Buffalo, G7 Farber Hall, 3435 Main Street, Buffalo, NY 14214 (U.S.A.)
and
DAVID GRECO and KYONGSANG HUH
School of Pharmacy, State University of New York at Buffalo, 565 Hochstetter Hall, Amherst, NY 14260 (U.S.A.)

SUMMARY

Failure of purification of nitrated phenylvaleric acid reaction mixtures by conventional recrystallization and column chromatographic methods using silica gel, led to a trial of counter-current chromatography. Poor solubility of the nitration products precluded the use for aqueous systems and led to the examination of systems using ethylene glycol or formamide as the stationary phase, with chloroform and other solvents as mobile phases. Prospective solvent pairs were first screened by a micro-partitioning method and then by counter-current chromatography in an analytical micro counter-current chromatograph. Partition coefficients derived from these methods facilitated optimization of the solvent system and scale-up to a preparative counter-current chromatography range. Using the system chloroform–ethylene glycol, crude product was readily purified and then identified as 5-(2,4-dinitrophenyl)valeric acid. Purification using a 292-ml column provided high resolution and required 6 h. Purification with lower resolution on a 56-ml column required 2 h.

INTRODUCTION

Counter-current chromatography (CCC) has been used extensively for separation of water soluble natural products[1,2] and antibiotics[3,4] derived from fermentation. Application to lipophilic materials has been limited by their insolubility in water and lack of information on the physiochemical characteristics of various applicable nonaqueous solvent systems, which provide greater solubility.

The majority of non-aqueous solvent systems employed in CCC have been derived by mixing one or more additional solvents (such as methylene dichloride, ethyl acetate or nitromethane, with the immiscible pairs formed by alkyl hydrocarbons plus

0021-9673/89/$03.50

methanol or acetonitrile[5,6]. While applicable to essential oils and other very lipophilic materials, these provide insufficient solubility for preparative purification of substances with intermediate polarity, which class includes the majority of synthetic organic chemicals.

Many water-insoluble organic chemicals are quite soluble in ethylene glycol (EG) or formamide (FA), each of which forms two-phase systems with organic solvents ranging in polarity from hexane through ethyl acetate[7,8]. The present study applies these systems, particularly $CHCl_3$–EG, to the purification of the products obtained by nitration of phenylvaleric acid.

CCC symbols and nomenclature

In discussing non-aqueous solvent systems for CCC, the common, though not universal, practice of writing components of solvent systems from left to right, in order of increasing polarity (as in $CHCl_3$–CH_3OH–H_2O) will be followed. Thus the polar EG and FA components will be written to the right of the less polar CH_2Cl_2 or $CHCl_3$ as CH_2Cl_2–EG, $CHCl_3$–EG or $CHCl_3$–FA.

The retention volume, V_R, in CCC is given by the equation common to all forms of chromatography, $V_R = V_m + KV_s$, where V_m and V_s are the respective volumes of mobile and stationary phase and K is the partition coefficient defined as the ratio of solute concentrations in stationary and mobile phase, $K = C_s/C_m$. Either the normal-phase or reversed-phase mode can be employed in CCC. The generally accepted meanings of these terms, the normal-phase mode having the more polar phase stationary and the reversed-phase mode having the less polar phase stationary, can be equally applied to aqueous and nonaqueous solvent systems.

In surveying solvent systems for CCC, it is convenient to express solute partition coefficients as either $K_N = C_{\text{non-polar phase}}/C_{\text{polar phase}}$ or as $K_P = C_{\text{polar phase}}/C_{\text{non-polar phase}} = 1/K_N$. In aqueous systems the subscript N can be interpreted as either non-polar or non-aqueous, which are synomymous in aqueous systems. Since there is no adsorption in CCC, solute retention volumes, V_R, can be readily calculated from partition coefficients determined by non-chromatographic methods. One need only employ the appropriate partition coefficient as K in the above equation, $K = K_P$ for the normal-phase mode, or $K = K_N$ for the reversed-phase mode. Since only the normal-phase mode is employed in this paper, partition coefficients will be expressed as K_P.

Because of the resulting simplicity, it is always desirable to index counter-current chromatograms with the expected retention volumes, or the corresponding retention times, for solutes with $K = 0$, 1, 2, etc. Unretained solutes, $K = 0$, are eluted at the apparent solvent front, $V_R = V_m$. The retention volume for a solute with $K = 1$ is a focal point on the counter-current chromatogram and always occurs at one column volume, V_c, of eluent, $V_{R,K=1} = V_m + V_s = V_c$. Solutes with integrally higher K values are eluted with corrected retention volumes, $V'_R = V_R - V_m$, which are directly proportional to the solute partition coefficients, $V'_R = KV_s$.

To describe the counter-current chromatogram in terms of partition coefficients, it is convenient to rewrite the retention volume equation as $V_K = V_0 + K(V_1 - V_0)$ and the corresponding retention time equation as $t_K = t_0 + K(t_1 - t_0)$, in which V_K is the retention volume for a solute with partition coefficient K, V_0 is V_R for a solute with $K = 0$ and $V_1 = V_c + V_d$ is the column volume. As index points on a counter-current

chromatogram, V_0, V_1, V_2, etc., or the corresponding times t_0, t_1, t_2 etc., indicate the retention volumes, or times, for solutes with partition coefficients signified by the subscripts. The point of injection is indicated by V_i or t_i and any dead volume by V_d or t_d. The chromatograms in Figs. 1–3 are indexed in this way. Partition coefficients of chromatographic peaks can then be calculated by linear interpolation between these reference points.

MATERIALS AND METHODS

Solvents and chemicals employed were HPLC or reagent grade (Fisher Scientific, Rochester, NY, U.S.A.).

Nitration of phenylvaleric acid

To 1 g of a stirred mixture of 5-phenylvaleric acid (Alrich, Milwaukee, WI, U.S.A.) in 4 ml of conc. sulfuric acid, was added, dropwise, 4 ml of conc. nitric acid. The temperature was not allowed to rise above 60°C and was maintained at 45°C for 10 min following nitric acid addition. The reaction mixture was poured onto 25 g of crushed ice. The precipitate was collected by centrifugation and dried in air. The crude yield was 470 mg. The product was purified by CCC.

Partition coefficients

Partition coefficients were estimated for the crude nitrated phenylvaleric acid, in the solvent systems CH_2Cl_2–EG, $CHCl_3$–EG and $CHCl_3$–FA, by partitioning a small quantity of solute between 1 ml of each phase and determining the concentrations spectrophotometrically[9,10]. Results were expressed as K_P = concentration in polar phase/concentration in non-polar phase. This ratio corresponds to the K values employed in the CCC purification here, since the more polar EG phase was employed as the stationary phase. K_P values were 1.7, 2.8 and 3.1 for CH_2Cl_2–EG, $CHCl_3$–EG and $CHCl_3$–FA systems respectively.

Analytical counter-current chromatography

Preliminary examination of solvent systems was done using a micro multilayer coil planet centrifuge (P.C. Inc., Potomac, MD, U.S.A.). The orbital radius was 5 cm and the coil was a multilayer winding of 12.6 m of 0.86 mm I.D. PTFE tubing with a volume, V_c, of 7.8 ml. It was used with a Valco C6U injection valve, an SSI No. 350-60 chromatography pump, and an ISCO UA-5 detector with a Type 9 optical unit operated at 254 nm with a 2-mm preparative flow cell. Injected samples were 0.2 ml volume, containing 5 mg/ml of phenylvaleric acid or 1 mg/ml of crude nitrated product dissolved in mobile phase. The system dead volume sensed by the detector, V_d, was 0.6 ml, including half the injection volume. After saturation with the appropriate mobile phase (CH_2Cl_2 or $CHCl_3$), EG was loaded into the stationary CCC column manually, with a syringe. Rotation was then adjusted to 1500 rpm and mobile phase was pumped at 40 ml/h from a central head to a peripheral tail, (H) → T. After initial displacement of some stationary phase, the system remained stable for several hours, allowing repeated injection of samples.

The dead time, t_d, was calculated as $t_d = V_d/f$, where f = flow-rate in ml/min. The time, t_1, for emergence of a solute with $K = 1$, was calculated as $t_1 = (V_d + V_c)/f$.

Emergence of an initial impurity peak was taken as an estimate of the time t_0, for emergence of the solute with $K = 0$. The fraction of column volume filled with stationary phase, S_F, was then estimated as $S_F = (t_1 - t_0)/(t_1 - t_d)$. The expected elution times, t_K, of solutes with higher partition coefficients were calculated as $t_K = t_0 + K(t_1 - t_0)$. All times are measured from the time of injection, t_i. The subscript 0 signifies a partition coefficient of zero. The partition coefficient is $K = K_P$ = solute concentration in stationary phase/solute concentration in mobile phase.

Preparative counter-current chromatography

Preparative CCC was done using an Ito multilayer coil separator extractor (P.C. Inc.) with a No. 14 (1.68 mm I.D.) coil, V_c 292 ml, a Milton Roy No. 196-31 pump and an ISCO V-4 monitor with a 2-mm preparative flow cell. Effluent was monitored at 270 nm. Samples were loaded using a Rheodyne No. 50410 four-way valve and a loop of No. 14 PTFE tubing. Fractions were changed manually. The dead volume, V_d, of 1.3 ml in the preparative system was neglected in calculating t_K values. Preparative CCC was also done using a No. 14 coil with a 56-ml volume, monitored at 254 nm using a 3-mm cell in a Glenco 5480 monitor.

After mutual saturation of $CHCl_3$–EG in a separatory funnel, the stationary column was filled with EG using the pump. The column was then rotated at 800 rpm and $CHCl_3$ pumped in at a rate of 120 ml/h in the (H) → T direction, where (H) signifies a central head. Pumping was continued for about 1 h, to establish a steady baseline, prior to injection of a 470 mg sample dissolved in 5 ml of the $CHCl_3$ phase. Fractions comprising the peak eluted at 4.8 h were combined and washed three times with one-tenth volumes of water to remove traces of EG. The $CHCl_3$ solution was dried with anhydrous Na_2SO_4 and evaporated to dryness to yield 123 mg of white crystals. Washing the product with 2 ml of water and drying over KOH, *in vacuo*, gave 117 mg white crystals, m.p. 86–89°C. Recrystallization of a 27-mg sample gave 26 mg of m.p. 88–89°C, which on analysis gave C, 49.37; H, 4.53; N, 10.40%. Theory for $C_{11}H_{12}N_2O_6$ is C, 49.26; H, 4.51; N, 10.44%.

A ^1H NMR spectrum was obtained on a Varian EM-390 spectrometer in C^2HCl_3 (1% tetramethylsilane) gave: δ 1.58–1.8 (m, four H, H_3 and H_4), 2.24–2.50 (m, two H, H_5), 2.80–3.14 (m, two H, H_2), 7.55 (d, one H, $J = 9$ Hz, Hm, m), 8.35 (dd, one H, $J = 9.3$ Hz, Ho, p), 8.73 (d, one H, $J = 3$ Hz, Ho, o) corresponding to 5-(2,4-dinitrophenyl)valeric aid (I).

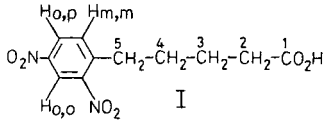

I

RESULTS AND DISCUSSION

Analytical CCC

Preliminary assessment of CCC for the purification of nitrated phenylvaleric acid using the P.C. Inc. micro multilayer CCC with EG as stationary phase and CH_2Cl_2 or $CHCl_3$ as mobile phases is summarized in Fig. 1. Each provided a stable

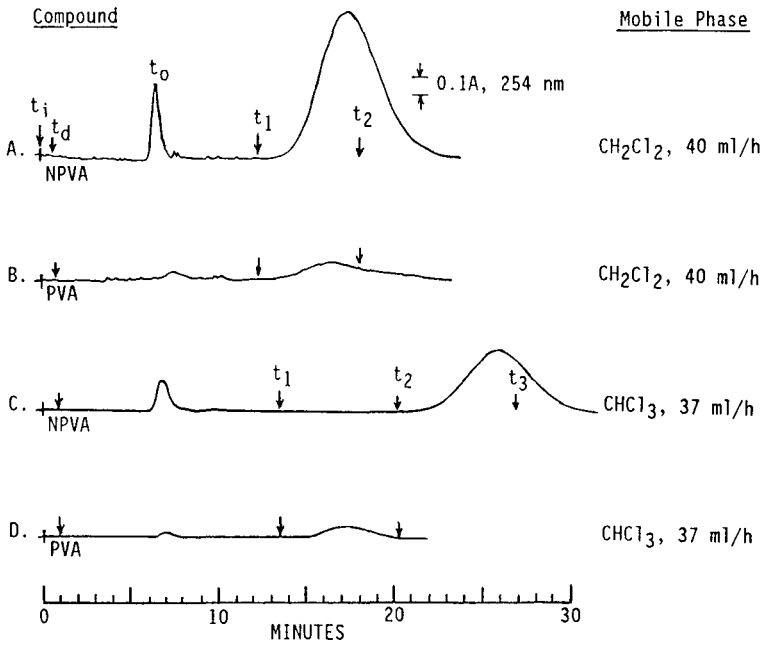

Fig. 1. Preliminary CCC of nitrated phenylvaleric acid (NPVA) and phenylvaleric acid (PVA) with P.C. Inc. micro CCC using a 12.6 m × 0.86 mm I.D. column at 1500 rpm. Stationary phase is ethylene glycol. A and B, mobile phase CH_2Cl_2 phase, 40 ml/h, (H) → T, S_F 0.50. C and D, mobile phase $CHCl_3$ phase, 37 ml/h, (H) → T, $S_F = 0.53$. Positions of column dead time, t_d and elution times, t_K, for $K = 1, 2$ etc., are indicated. The stationary phase fraction, S_F and t_K times were estimated by assuming that the first peak signified emergence of $K = 0$. Column volume, V_c, was 7.8 ml.

chromatographic system, retaining a stationary phase volume 50% or more of the column volume and permitted repetitive sample injection, with elution of solutes with partition coefficients up to 3 in less than 30 min. In both systems the synthetic product exhibited a small early impurity peak and a later major peak. Partition coefficients for the major chromatographic peaks are approximately 1.9 and 2.8 for the CH_2Cl_2 and $CHCl_3$ systems respectively, in good agreement with the values of 1.7 and 2.8 determined independently by a micropartitioning method. Comparison of the retention times for the starting material, phenylvaleric acid, indicates that a better separation would be obtained with the $CHCl_3$–EG system.

When subjected to CCC separation using the $CHCl_3$–FA system, in the microchromatograph, a retention time of 67 min was observed. This corresponds to a K_P value of about 8, compared to 3.1 estimated by micropartitioning. The reason for the discrepancy is not presently known but, because of the excessive retention time, the $CHCl_3$–FA system was not further investigated.

Preparative CCC

Preparative purification of a 470-mg sample of crude product, using a 292-ml column of 1.68 mm I.D. PTFE tubing, is summarized in Fig. 2. Evaporation of the $CHCl_3$ fractions comprising the major peak (after removal of EG by extraction with

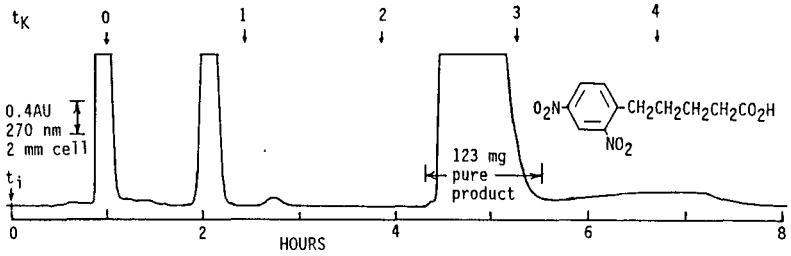

Fig. 2. Preparative purification of nitrated phenylvaleric acid in the P.C. Inc. Ito multilayer separator extractor. Conditions: 800 rpm, No. 14 (1.68 mm I.D.) coil, V_c = 292 ml, $CHCl_3$–EG, normal-phase mode, mobile phase $CHCl_3$, (H) → T, 120 ml/h. Sample was 470 mg crude product in 5 ml $CHCl_3$ phase. S_F = 0.52 from recovered column contents.

water) yielded 123 mg of crystalline product, which was shown by elemental analysis and NMR spectrometry to be 5-(2,4-dinitrophenyl)valeric acid. The partition coefficient of 2.8, calculated by interpolation of the t_K scale on the chromatogram, is in excellent agreement with values determined by micropartitioning and micro CCC methods. No crystalline material was recovered from the impurity peaks at 1.0, 2.1, 2.7 and 6.6 h. The crude product contained more polar materials which are retained in the ethylene glycol. A 26% yield of pure product was obtained from the heterogeneous reaction mixture.

CCC purification of crude material from a second synthesis is summarized in Fig. 3. Chromatographic conditions were identical except that a smaller column, with a volume of 56 ml was used. This permitted much faster chromatography, but with less than half the resolution of the 292-ml column. This 56-ml column has been shown to provide better resolution than can be achieved by "flash chromatography"[11]. Selection of a central cut of the major peak, between 40 and 60 min, washing the combined fractions with water and evaporation as above, yielded 66 mg of 5-(2,4-dinitrophenyl)valeric acid, identical to the product identified above. Note that the partition coefficient estimated from the chromatogram is also in good agreement with the values obtained in the other CCC runs and by micropartitioning. No crystalline material was recovered by processing fractions corresponding to the impurity peaks. Negligible additional material was also recovered by processing the

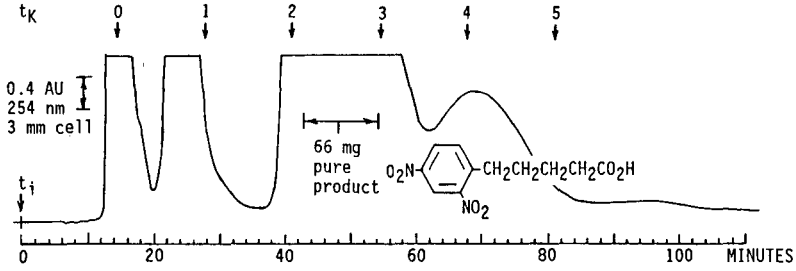

Fig. 3. Preparative purification of nitrated phenylvaleric acid by CCC. Conditions as in Fig. 2 except that a smaller volume No. 14 (1.68 mm I.D.) coil, V_c = 56 ml, was used. Sample was 180 mg crude product in 4 ml $CHCl_3$ phase. S_F = 0.48.

leading and trailing edges of the major peak. The chromatographic recovery of 37% of pure product from crude material again reflects degradation during the non-specific synthesis. The recovery of some *p*-nitrophenylbutyric acid from another comparable nitration of phenylvaleric acid is a further indication of the extent to which starting material is oxidized. The presence of more polar constituents in the crude material was also indicated by the observation of peaks eluting early in analytical CCC chromatograms using heptane–25% aqueous 2-propanol (1:1) in the reversed-phase mode.

CONCLUSIONS

Aqueous solvent systems, which are widely used in CCC, provide limited capacity to dissolve a wide range of compounds encountered in organic synthesis. The polar organic solvents, ethylene glycol and formamide, are excellent solvents for organic compounds, are immiscible with less polar solvents ranging from hexane to ethyl acetate and serve well as stationary phases for CCC purification of synthetic organic compounds.

REFERENCES

1 K. Hostettmann, M. Hostettmann and A. Marston, *Nat. Prod. Rep.*, 1 (1984) 471.
2 K. Hostettmann, M. Hostettmann and A. Marston, *Preparative Chromatography Techniques, Applications in Natural Product Isolation*, Springer, Berlin, 1986.
3 G. M. Brill, J. M. McAlpine and J. E. Hochlowski, *J. Liq. Chromatogr.*, 8 (1985) 2259.
4 D. B. Martin, C. Biles and R. E. Peltonen, *Am. Lab. (Fairfield, Conn.)*, 18, Oct. (1986) 21.
5 B. Domon, M. Hostettmann and K. Hostettmann, *J. Chromatogr.*, 246 (1982) 133.
6 K. Hostettmann, C. Appolonia, B. Domon and M. Hostettmann, *J. Liq. Chromatogr.*, 7 (1984) 231.
7 W. D. Conway and Y. Ito, *J. Liq. Chromatogr.*, 7 (1984) 291.
8 H. S. Freeman and C. S. Willard, *Dyes Pigments*, 7 (1986) 407.
9 W. D. Conway and Y. Ito, *J. Liq. Chromatogr.*, 7 (1984) 275.
10 W. D. Conway, *Countercurrent Chromatography*, VCH, New York, 1990, in press.
11 W. D. Conway, E. L. Bachert, A. M. Sarlo and C. W. Chan, *Northeast Regional Meeting of the American Chemical Society, Rochester, NY, November, 1987*, Abstract No. 111.

Journal of Chromatography, 484 (1989) 399–408
Elsevier Science Publishers B.V., Amsterdam — Printed in The Netherlands

CHROM. 21 797

PREPARATIVE AND AUTOMATED COUMPOUND CLASS SEPARATION OF VENEZUELAN VACUUM RESIDUA BY HIGH-PERFORMANCE LIQUID CHROMATOGRAPHY

LANTE CARBOGNANI* and ALEJANDRO IZQUIERDO
INTEVEP S.A., P.O. Box 76343, Caracas 1070A (Venezuela)

SUMMARY

Deasphalted vacuum residua of heavy and medium Venezuelan crude oils were separated into saturates, aromatics and two types of resins with a preparative high-performance liquid chromatographic system. The separation was achieved with a combination of silica and cyano-bonded silica columns and cyclopentane, chloroform–methanol and chloroform as eluents. The maximum sample load was 250 mg. Automated repetitive injection allowed the unattended separation of 3 g of sample in 8 h. Fractions were totally recovered from the columns (100.1 ± 1.3%) and the efficiency of the separation was determined by elemental analysis of whole samples and collected fractions.

INTRODUCTION

Compositional changes taking place during upgrading of heavy crudes and residua have been monitored with group-type separation procedures such as the API-60[1], the clay-gel adsorption chromatographic ASTM Standard[2] and the saturates aromatics, resins and asphaltenes (SARA) method[3]. Faster analytical procedures have been proposed employing either liquid chromatography[4–6] or thin-layer chromatography[7–11]. Unfortunatly, these techniques do not provide sufficient material for further characterization or are destructive.

Rapid preparative separations employing liquid chromatographic columns packed with silica gel[5,12,13] have been described. However, several workers have reported irreversible adsorption of polar compounds associated with the use of polar column packings such as silica, alumina and clay[14–16]. Resins constitute the polar fraction in deasphalted oils, and their abundance[17], their associations with asphaltenes[18–20] and their geochemical importance in heavy oils[21] are the main reasons for their isolation and characterization.

Derivatized polar packing materials have been developed in order to overcome the retention problems posed by the mentioned adsorbents. Analytical high-performance liquid chromatographic (HPLC) SARA analyses have been described, using amino[5], alkylamine and alkylnitrile[16], alkynitrile-substituted secondary alkylamine[22] and cyano- and aminocyano-bonded silica[23].

An automated semipreparative method for SAR separations of deasphalted

0021-9673/89/$03.50

samples using an amino-bonded silica packing and showing excellent recoveries has been published[14]. However, other workers[24] suggested the use of cyano-bonded phases in order to avoid the reactivity of the amino moiety towards acidic and carbonylic coumpounds.

This paper describes an automated preparative system assembled with common HPLC components that allows the unattended separation of 3 g of deasphalted samples in 8 h. The fractions obtained are saturates, aromatics and two types of resins, and the separation was achieved with a combination of silica and cyano-bonded silica columns, employing cyclopentane, chloroform–methanol and chloroform as eluents.

The maximum sample load was estimated for the described system and repetitive injections were carried out. The sample was totally recovered (100 ± 1.3%). Elemental analyses were included and showed the efficiency of the separation.

EXPERIMENTAL

Samples and solvents

Vacuum residua were provided by the Department of Process Development, INTEVEP. Solvents were obtained from Burdick & Jackson, Fisher and Merck and were used as received. The chloroform employed was free from alcoholic preservatives.

HPLC system

The HPLC system (Fig. 1) consisted of the following components: a Waters Assoc. 590 EF programmable pump (1) that controlled two pneumatic actuated valves (Waters Assoc.), *viz.*, a solvent select valve (2) and a six-port switching valve (3); a DVSP-4 digital valve sequence programmer from Valco (4) that commanded the operation of three pneumatic valves, *viz.*, a Rheodyne 7010 injection valve provided with a 1.043-ml loop (5), a Valco backflush valve (6)and a Valco six-port switching valve (7); a Glenco 410 programmable fraction collector (8), provided with a 6 + 1-port Rheodyne 7060 valve; a Knauer 98:00 refractive index (RI) detector (9) and a Glenco 5840 UV–VIS detector operated at 254 nm (10); an Altex gas-tight glass column (11) operated as sampling reservoir, filling the sampling loop of the injection

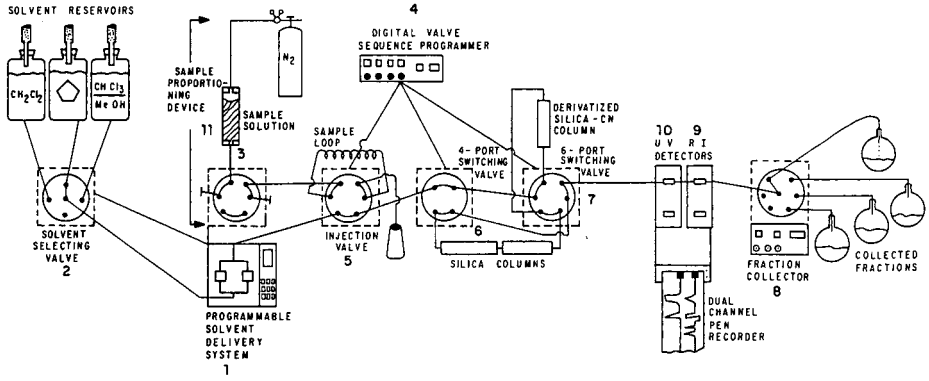

Fig. 1. Automated preparative liquid chromatograph for separation of saturates, aromatics and resins. MeOH = Methanol.

valve (5) under an small nitrogen pressure (*ca.* 3 ml/min); and columns (Valco, 25 cm × 1 cm I.D.) slurry-packed by means of a Haskell air-driven fluid pump. The packing materials were Adsorbosil LC (10 μm), irregular (Alltech) and Polygosil 60-10CN (10 μm), irregular (Macherey Nagel). The former material was dried for 1 h at 120°C before packing. The cyano column was end-capped with trimethylchlorosilane (Pierce) according to a previously described procedure[25].

Sample preparation

Asphaltenes were precipitated by refluxing the sample for 1 h with *n*-heptane in a ratio of 100:1. The suspension was cooled to room temperature and filtered through a cellulose extraction thimble. The precipitate was extrated with *n*-heptane until no colour was observed in a Soxhlet apparatus and the extract was combined with the filtrate. Asphaltenes were dissolved with benzene. The solutions were filtered (Whatman No. 41) and the solvents removed in a rotary evaporator under a stream of nitrogen. Maltenes and asphaltenes were brought to constant weight in a vacuum oven at 70°C.

Maltenes solutions of known concentration (*ca.* 240 mg/ml) were prepared in cyclopentane and charged to the glass column (11).

Events programme

Table I shows the command sequence used in each of the three controllers employed. For preparative purposes, the 38-min cycle is repeated several times and weak resins are eluted manually with a final chloroform backflush. For analytical purposes, the 52-min run affords all the fractions with a single injection.

RESULTS AND DISCUSSION

Group-type separation of deasphalted crude oil residua into saturates, aromatics and two types of resins was achieved with a combination of a deactivated cyano-bonded silica column and two bare silica columns. This was performed on a semi-preparative scale (milligram amounts) and repetitive and automated cycles, employing the HPLC system shown in Fig. 1, resulted in the unattended separation of 3 g of sample in 8 h.

The sample is dissolved in cyclopentane rather than in the deasphalting solvent (*n*-C_7), because cycloalkanes cause fewer reprecipitation problems than *n*-alkanes[16]. The sample solution concentration (*ca.* 25%, w/v) and the injection volume (*ca.* 3% of the system) were chosen so as to avoid excessive viscosity and sample dilution on injection.

The sample is injected and initially eluted with cyclopentane through the cyano column, where the most polar coumpounds (strong resins) are retained. The other components proceed to the silica columns and the less retained (saturates) are eluted and observed with the refractive index detector (Fig. 2).

Aromatics and weak resins are held on the polar silica surface. Once the saturates have been eluted, the flow is inverted through the cyano column and, by changing the eluent to the more polar chloroform–methanol (80:20, v/v) strong resins are recovered. At this stage no eluent flows through the silica columns, and the resins eluting are monitored with the UV detector. In order to recover the aromatics, cyclopentane is

TABLE I
EVENTS PROGRAMME FOR SAR SEPARATION

Time (min)	*590 EF pump (1)*	*Digital valve sequence programmer (4)*	*Fraction collector (8)*
0.00	Flow-rate: 4.9 ml/min Solvent: cyclopentane	Actuate injection valve 5	Stream 1 to saturates vessel
11.00		Return valve 5 to load position Actuate 6-port valve 7 to backflush the CN column	
11.25			Stream 2 to strong resins vessel
13.50	Flow-rate: 16.5 ml/min Solvent: chloroform–methanol		
21.00	Flow-rate: 16.5 ml/min Solvent: cyclopentane		
25.00		Actuate 4-port valve 6 to backflush silica columns	Stream 3 to aromatics vessel
35.00	Flow-rate: 4.9 ml/min Solvent: cyclopentane		
36.00	Actuate sample proportioning valve 3		
36.50	Return sample proportioning valve 3		
37.00		Return backflush valves 6 and 7 to initial positions	Stream 1 to saturates vessel
38.00		Start a new run	

Weak resins are eluted by backflusing all the system with chloroform after repetitive injections allow all the sample to go through. Complete elution of the four fractions in a single run requires the following steps in the program, following the 25.00 min instructions.

35.00	Flow-rate: 14.0 ml/min Solvent: chloroform		Stream 4 to weak resins vessel
43.00	Flow-rate: 14.0 ml/min Solvent: cyclopentane		
47.00	Flow-rate: 16.5 ml/min Solvent: cyclopentane		
50.00	Flow-rate: 4.9 ml/min Solvent: cyclopentane		
50.50	Flow-rate: 0.1 ml/min Solvent: cyclopentane		
51.00		Return backflush valves 6 and 7 to initial positions	Stream 1 to saturates vessel
52.00		End of run	

again employed, initially to remove the previous eluent from the system (methanol affects the performance of the silica columns), and then to backflush the aromatics when the flow is inverted through the whole system. Aromatics are detected with both detectors. This cycle is repeated until all the sample has been injected into the columns. To recover the weak resins held in the silica columns through the repetitive injections, chloroform was used to backflush the whole system. Dichloromethane was employed in the initial experiments to recover weak resins, but it was found that the silica

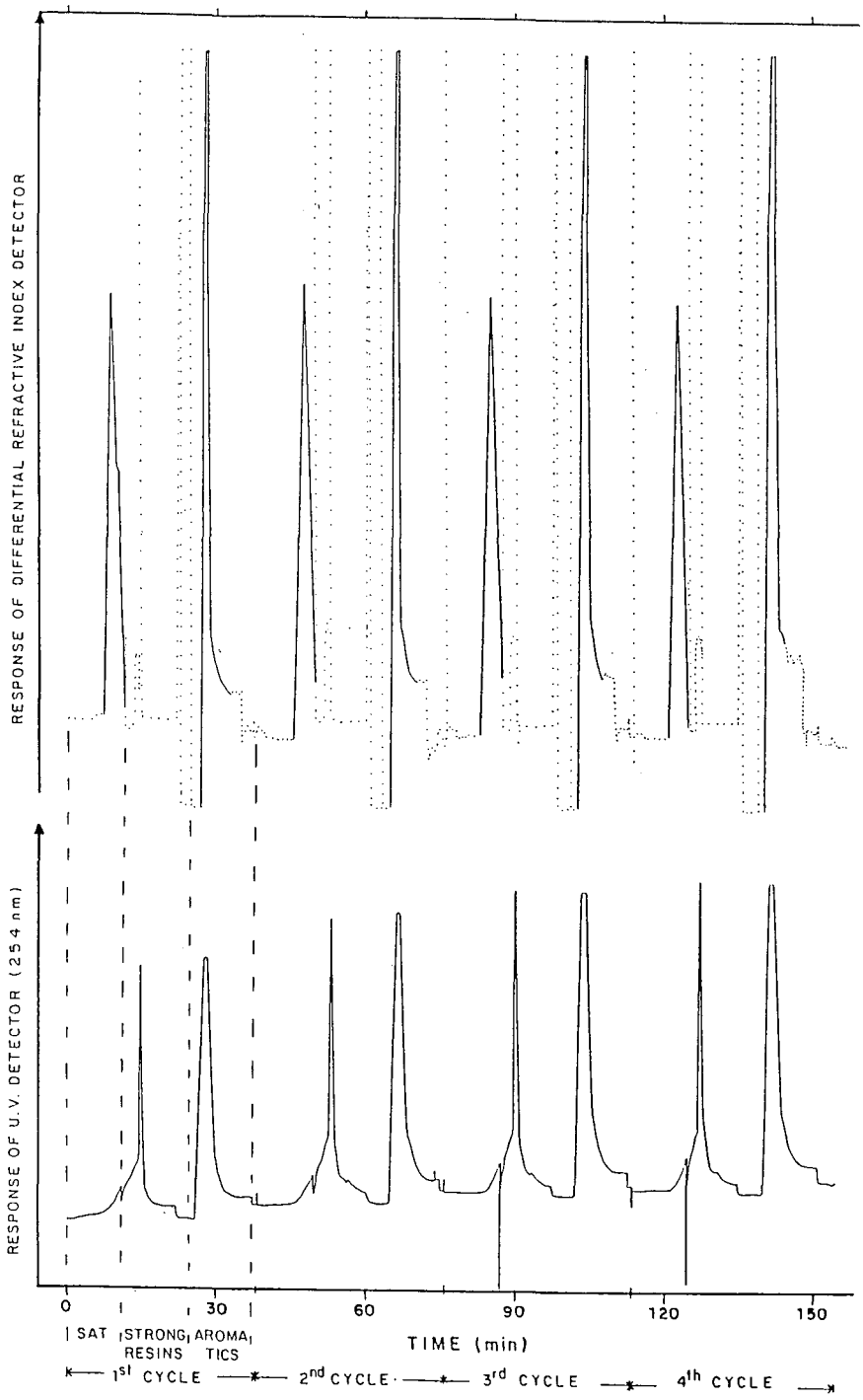

Fig. 2. Typical SAR separation of a deasphalted oil vacuum residua. Dotted lines correspond to variations of pressure or solvent composition.

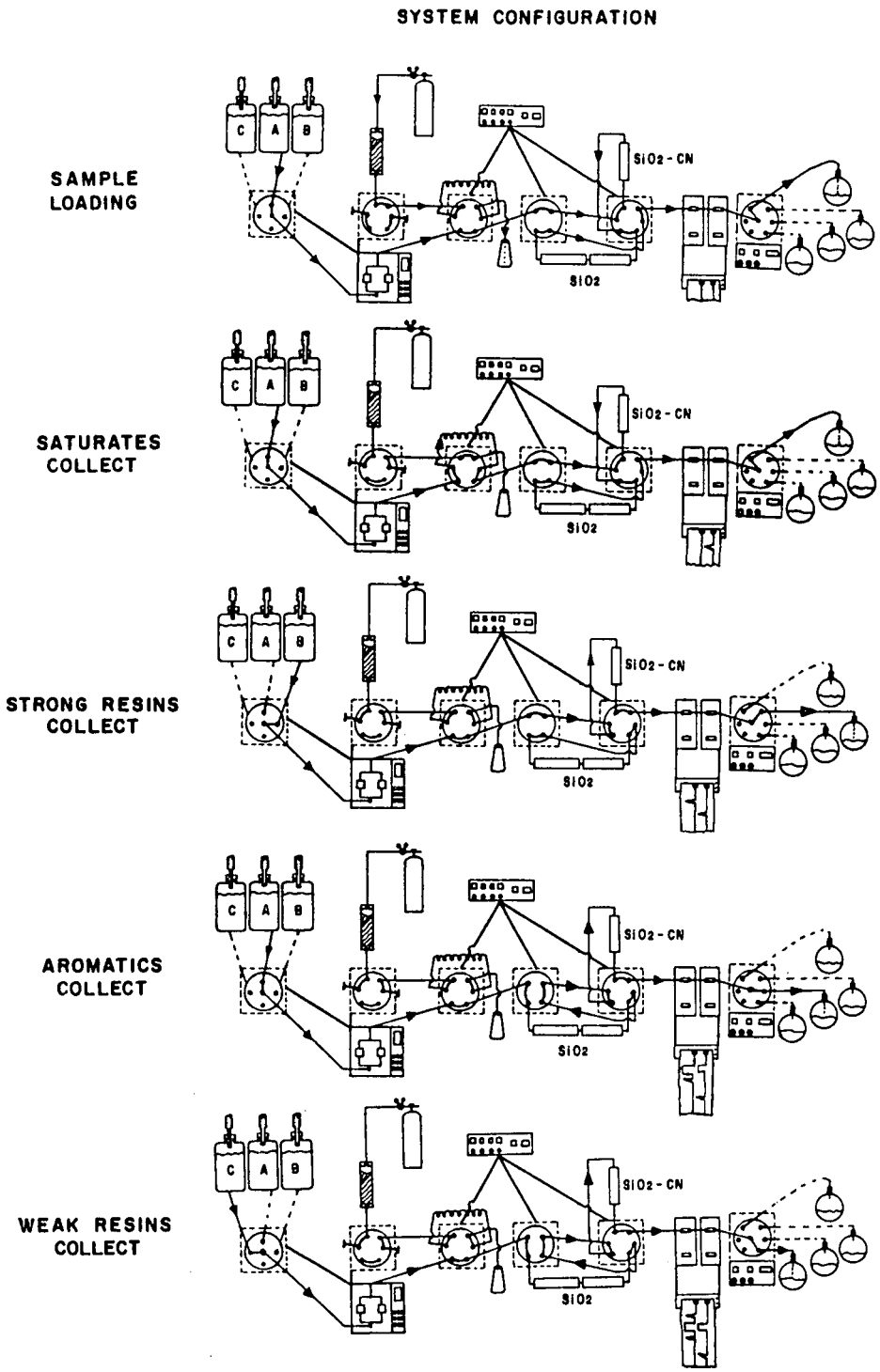

Fig. 3. System configuration during each step. A = Cyclopentane; B = chloroform–methanol; C = chloroform.

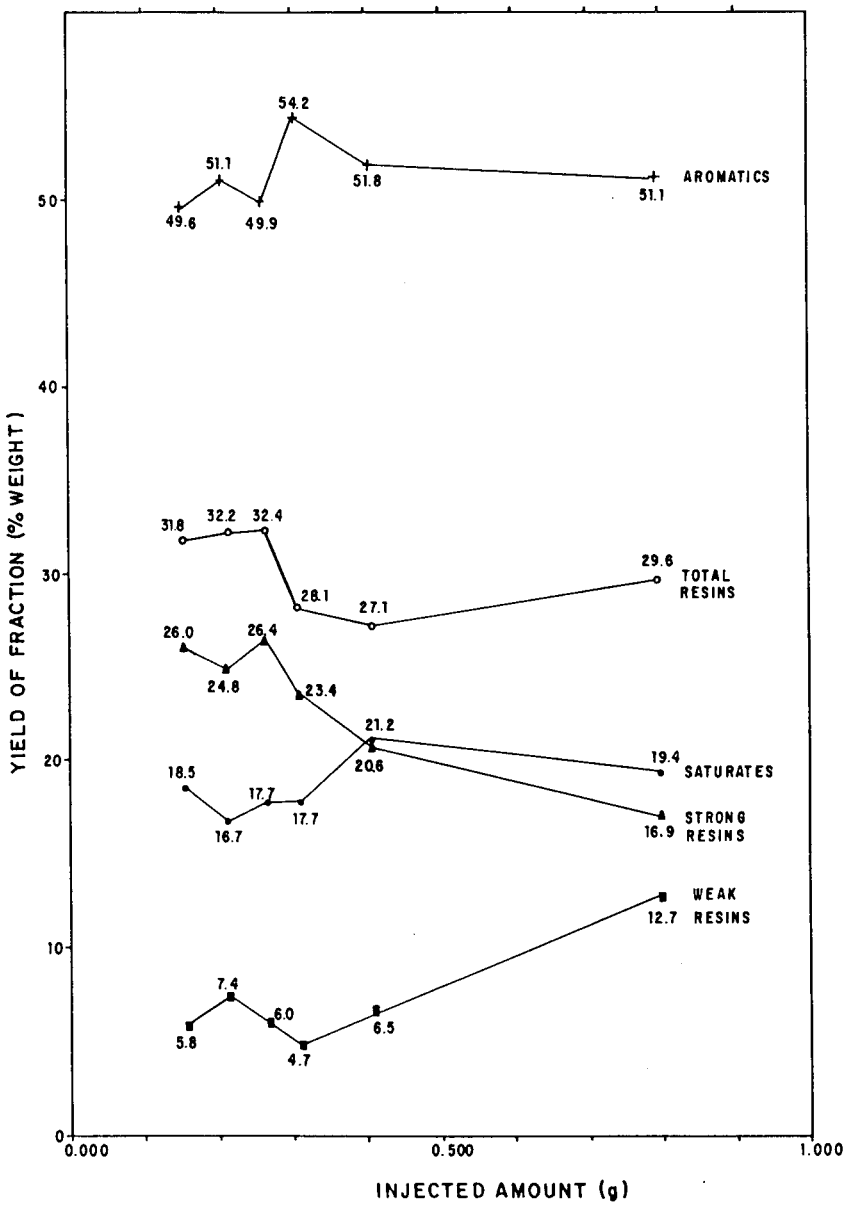

Fig. 4. Fraction yields *vs.* amount of sample injected in typical SAR separations.

columns were deactivated rapidly as consequence of humidity, so this solvent was replaced.

The chromatographic conditions and column dimensions were chosen such that the saturates had not completely eluted before all the compounds that were unretained by the cyano column entered the silica columns. The eluent flow-rate was initially selected to permit an adequate resolution of saturates; after this group had been

TABLE II
REPETIBILITY AND MASS RECOVERY DATA FOR SAR SEPARATION OF DEASPHALTED VACUUM RESIDUA

Origin of crude oil	*Sample*[a]	*Saturates*	*Aromatics*	*Weak resins*	*Strong resins*	*Total recovery (%, w/w)*	*No. of injectons*	*Sample amount per injection (mg)*
Orinoco	I	9.0	48.2	8.5	34.2	99.9	6	129.4
Basin		9.3	50.4	9.4	30.8	99.9	6	143.3
	II	13.9	51.4	6.2	26.5	98.0	7	130.7
	III	5.7	56.1	8.2	29.1	99.1	6	301.6
Barinas-	IV	18.6	52.3	4.9	24.2	100.0	6	143.5
Apure		18.0	54.2	4.1	24.1	100.4	3	226.0
Basin	V	17.2	51.5	4.5	26.1	99.3	7	139.3
		18.1	51.1	6.2	27.1	102.5	3	266.3
Experi-	VI	21.6	54.3	3.1	21.1	101.1	13	98.0
mental		22.6	57.6	3.5	17.9	101.6	10	232.4
blend								

[a] Samples included were 510°C vacuum residua, excluding sample III, which was a 540°C vacuum residua.

collected the flow-rate was set at a value that permitted a rapid elution without exceeding a pressure of 5500 p.s.i., as the pump was designed to operate at a maximum of 6000 p.s.i. Fig. 3 shows the system configuration during each of the steps.

Fig. 4 shows the yields of the different fractions depending on the amount of sample injected in a single run. This was done in order to establish the maximum amount of sample that could be analysed, which is important considering that the aim is a preparative separation of different compound classes for further characterization. A 250-mg amount of sample proved to be the maximum that could be chromatographed without affecting the quality of the separation. Above this level, a slight increase in the percentage of saturates is observed. This is due to overloading of the silica columns, as a result of which some aromatics coelute. It was also found that the amount of weak resins increased and that of strong resins decreased as a result of overloading of the cyano column. Part of the strong resins were not retained and appeared as weak resins. The aromatics remained relatively constant, probably because of overloading of resins that are not held by the silica and elute as the former.

Mass recovery data for some deasphalted vacuum residua are presented in Table II. The overall recoveries were 100.1 $\pm$ 1.3%, showing that no material was retained in the columns and also that the chosen columns performed well even with complex samples containing between 23 and 43% of resins. Recoveries greater than 100% were partially explained by solvent occlusion, which is a common source of error with this type of heavy fractions.

Elemental analysis was initially performed on the separated fractions in order to verify the effectiveness of the separation. Table III gives the results for some of the residua studied, showing differences in the nature of the fractions obtained. Note that although the H/C ratios for aromatics and weak resins are fairly similar, there are significant variations in the heteroatom content. Detailed information on the characterization of the fractions has been reported elsewhere[26].

TABLE III
ELEMENTAL ANALYSIS OF VACUUM RESIDUA AND THEIR SEPARATED FRACTIONS

Sample[a]	*Fraction*	*Concentration (%)*	*C (%)*	*H (%)*	*H/C*	*S (%)*	*Ni (ppm)*	*V (ppm)*
V	Vacuum residua		86.29	10.22	1.42	1.11	193	62
	Saturates	15.0	85.77	13.71	1.92			
	Aromatics	43.3	86.32	10.76	1.50	1.14	43	<10
	Weak resins	5.1	86.51	10.52	1.46	1.87	136	107
	Strong resins	22.1	86.54	9.32	1.29	1.40	285	119
	Asphaltenes	16.3	87.77	7.68	1.05	1.41	615	247
I	Vacuum residua		83.20	9.86	1.42	3.84	150	633
	Saturates	7.1	85.91	13.38	1.87			
	Aromatics	38.3	83.76	10.33	1.48	4.11	50	<10
	Weak resins	7.0	81.74	10.19	1.59	4.39	106	209
	Strong resins	25.3	79.82	9.07	1.36	4.35		835
	Asphaltenes	22.3	82.25	7.90	1.14	4.72	442	1747

[a] For identification, see Table II.

CONCLUSIONS

An automated preparative method for the separation of deasphalted heavy ends into saturates, aromatics and two types of resins has been developed. Unattended operation permitted to collect 3 g of fractions in 8 h for further characterization. Adoption of a cyano-derivatized silica column resulted in sample recoveries of nearly 100%.

ACKNOWLEDGEMENTS

This work was carried out under the project "New Methods of Chemical Analysis of Crudes, Residua and Products". Thanks are due to INTEVEP and Petróleos de Venezuela for permission to publish this paper.

REFERENCES

1 D. E. Hirsch, J. E. Dooley and H. J. Coleman, *Correlations of Basic Gel Permeation Chromatography Data and their Applications to High-Boiling Petroleum Fractions,* API-RP-60 Published Report No. 28, U.S. Bureau of Mines, Report on Investigations No. 787 S, 1974.
2 *Annual Book of ASTM Standards,* Vol. 05.02, ASTM, Philadelphia, PA, 1988, p. 15, standard D-2007.
3 D. M. Jewell, E. W. Albaugh, B. E. Davis and R. G. Ruberto, *Ind. Eng. Chem. Fundam.*, 13 (1974) 278.
4 H. V. Drushell, *Adv. Chem. Ser.*, 170 (1978) 295.
5 L. G. Galya and J. C. Suatoni, *J. Liq. Chromatogr.*, 3 (1980) 229.
6 J. M. Colin and G. Vion, in *Caracterisation des Huiles Lourdes et des Residus Pétroliers*, Technip, Paris, 1984, p. 292.
7 B. Sol, E. Romero, L. Carbognani, V. Sanchez and L. Sucre, *Rev. Téc. INTEVEP*, 4 (1985) 127.
8 B. Sol, E. Romero, L. Carbognani, V. Sanchez and L. Sucre, *Rev. Téc. INTEVEP*, 5 (1985) 39.
9 B. J. Fuhr, L. R. Holloway and C. Reichert, *J. Can. Pet. Technol.*, 25 (1986) 28.
10 Y. Yamamoto, *Sekiyu Gakkai Shi,* 29 (1986) 15.
11 M. L. Selucky, *Anal. Chem.*, 55 (1983) 141.
12 J. C. Suatoni and R. E. Swab. *J. Chromatogr. Sci.*, 14 (1976) 535.
13 M. Radke, H. Willsch and D. H. Welte, *Anal. Chem.*, 52 (1980) 406.

14 P. Grizzle and D. M. Sablotny, *Anal. Chem.*, 58 (1986) 2389.
15 M. Farcasiu, *Fuel*, 56 (1977) 9.
16 C. Bollet, J. C. Escalier, C. Souteyrand, M. Caude and R. Rosset, *J. Chromatogr.*, 206 (1981) 289.
17 B. Tissot, *Rev. Inst. Fr. Pet.*, 36 (1981) 429.
18 J. A. Koots and J. G. Speight, *Fuel*, 54 (1975) 179.
19 S. E. Moschopedis and J. G. Speight, *Fuel*, 55 (1976) 187.
20 J. G. Speight and S. E. Moschopedis, *Prepr., Div. Pet. Chem., Am. Chem. Soc.*,24 (1979) 910.
21 R. Pelet, F. Behar and J. C. Monin, *Org. Geochem.*, 10 (1986) 481.
22 R. Miller, *Anal. Chem.*, 54 (1982) 1742.
23 C. D. Pearson and S. G. Garfeh, *Anal. Chem.*, 58 (1986) 307.
24 E. Lundanes and T. Greibrokk, *J. Liq. Chromatogr.*, 8 (1985) 1035.
25 M. Verzele, M. de Coninck, C. Dewaele and E. Geeraert, *Chromatographia*, 19 (1984) 443.
26 A. Izquierdo, L. Carbognani, V. Leon and A. Parisi, *Prepr., Div. Pet. Chem., Am. Chem. Soc.*, 33 (1988) 292.

Journal of Chromatography, 484 (1989) 409–423
Elsevier Science Publishers B.V., Amsterdam — Printed in The Netherlands

CHROM. 21 891

PREPARATIVE HIGH-PERFORMANCE LIQUID CHROMATOGRAPHY UNDER GRADIENT CONDITIONS

I. BAND BROADENING IN GRADIENT ELUTION AS A FUNCTION OF SAMPLE SIZE

G. B. COX
Medical Products Department, E. I. du Pont de Nemours Inc., Glasgow, DE 19701 (U.S.A.)
and
L. R. SNYDER* and J. W. DOLAN
LC Resources Inc., 3182C Old Tunnel Road, Lafayette, CA 94549 (U.S.A.)

SUMMARY

Previous studies of gradient elution under mass-overload conditions are continued. Use of the Craig distribution model shows that there is a simple relationship between bandwidth, sample size and gradient conditions for single-solute samples. This allows the use of two or three experimental measurements to determine the saturation capacity of a column by a given sample. Several (reversed-phase) experimental studies with small-molecule samples provide quantitative confirmation of this model.

For the case of protein samples the model works equally well, but it appears that only 20–44% of the column capacity (as measured by saturation uptake) is available under separation conditions. The column capacity for lysozyme was measured as a function of pore diameter and the accessibility of the surface under separation conditions was found to increase with increasing pore size.

INTRODUCTION

It has been shown for the case of analytical (small-sample) separations that isocratic and gradient elution can be related in a straightforward fashion[1,2]; that is, well known relationships developed for isocratic high-performance liquid chromatography (HPLC) can be applied to "corresponding" gradient separations. This simple picture of gradient elution has since been extended[3–5] to include mass-overloaded separation. For "corresponding" separations (*i.e.*, similar conditions) of a mixture of two xanthines[3], it was shown that the same separation (resolution) resulted with either isocratic or gradient elution, as long as sample size was the same in the two runs being compared.

Computer simulations based on the Craig distribution process were also used to study band broadening in gradient elution as a function of sample size and gradient

0021-9673/89/$03.50

steepness[4]; however, some puzzling differences between isocratic and gradient separation were observed. In addition, experimental studies on band broadening *vs.* sample size and gradient conditions were reported for several protein samples[5]. Significant differences between observed and predicted results were found and attributed (incorrectly, as will be seen) to non-Langmuir sorption.

This paper describes additional work aimed at a better understanding of gradient elution separation under touching-band conditions. In Part II[6] these findings are applied to the design of a computer-simulation program for facilitating method development for the touching-band separation of peptide and protein samples by means of reversed-phase gradient elution.

THEORY

For the case of isocratic separation[7,8], it has been shown that band broadening in single-band separations can be described by

$$W^2 = W_o^2 + W_{th}^2 \tag{1}$$

where W is the baseline width of a mass-overloaded band, W_o is the corresponding width of a small-sample band and W_{th} is the contribution to band broadening from a large sample. Values of W_o and W_{th} can be expressed further as

$$\text{(isocratic)} \quad W_o = (16/N_o)^{\frac{1}{2}} t_o(1 + k_o) \tag{2}$$

and

$$\text{(isocratic)} \quad W_{th} = (6)^{\frac{1}{2}} t_o k_o (w/w_s)^{\frac{1}{2}} \tag{3}$$

(see Appendix). Here, the various terms have their usual meaning; see the list of symbols at the end of this paper.

Corresponding expressions for W_o and W_{th} hav been derived for gradient elution[4]. However, these relationships are complex, and they exhibit only partial agreement with Craig simulations and experimental data (for small molecules) to be reported here. If we assume that the isocratic–gradient analogy holds, however, it is straightforward to derive (new) corresponding expressions for eqns. 2 and 3. In eqn. 2, the isocratic parameter k_o can be replaced by the k' value at elution in gradient elution[1,2]:

$$k_e = 1/2.3b \tag{4}$$

where

$$b = V_m \Delta\varphi S / t_G F \tag{5}$$

The parameter b measures the steepness of the gradient, t_G is gradient time, F is flow-rate, V_m is column dead volume, $\Delta\varphi$ is the change in the volume fraction, φ, of

organic solvent during the gradient ($\Delta\%B/100$) and S is an isocratic property of the solute:

$$S = \mathrm{d}(\log k')/\mathrm{d}\varphi$$

$$\approx 0.48M^{0.44} \tag{6}$$

where M is the molecular weight of the solute.

Replacing k_o in eqn. 2 by k_e from eqn. 4 then gives

$$\text{(gradient)} \quad W_o = (16/N_o)^{\frac{1}{2}} t_o G J[1+(1/2.3\ b)] \tag{7}$$

The factor G is included to account for the compression of the band by the gradient[1]. The factor J ($1 < J < 1.8$) represents an anomalous band broadening as b increases[a]; for Craig simulations, J can be assumed to be equal to 1. In most prepatative separations, a small-scale separation will be carried out initially, so that values of W_o will be known or calculable.

A similar substitution of k_e for k_o in eqn. 3 gives[b]

$$\text{(gradient)} \quad W_{th} = (6)^{\frac{1}{2}}\ t_o k_e G(w/w_s)^{\frac{1}{2}}.$$

$$= 1.06 t_o G(w/w_s)^{\frac{1}{2}}/b \tag{8}$$

The mass-related band broadening, W_{th}, is of primary concern here. Previously it had been suggested[4,5] that W_{th} can be approximated by an expression of the form

$$W_{th} \approx \text{constant} \cdot (t_o/b)w^z \tag{9}$$

where $z \approx 0.85$ for a Langmuir isotherm (Craig simulations).

Experimental data for proteins showed good agreement with eqn. 9, except that $0.4 < z < 0.6$. In this paper it will be argued that Langmuir sorption should actually result in $z \approx 0.5$–0.6, suggesting that data previously reported[5] for the mass-overload gradient separation of proteins are in agreement with eqn. 8, and by inference those samples exhibit Langmuir sorption.

EXPERIMENTAL

Instrumentation

Chromatography was performed using either (1) a Hewlett-Packard (Avondale, PA, U.S.A.) 1090 liquid chromatograph fitted with a preparative injection accessory, (2) a DuPont (Wilmington, DE, U.S.A.) 8800 LC system using a Rheodyne septumless injection valve (fitted with a variety of loop sizes) plus a DuPont spectrophotometer

---

[a] In experimental systems, the product $JG \approx 1.1$ for different values of b. This simplifies the estimation of values of W_o as a function of gradient conditions.

[b] It is not yet known whether the effect represented by J for experimental small-sample separations (W_o, eqn. 7) will also apply to W_{th}; we assume not, until data to the contrary are reported.

TABLE I

PHYSICAL PROPERTIES AND SATURATION CAPACITIES OF DIFFERENT COLUMN PACKINGS WITH LYSOZYME SOLUTE

Packing[a]	*Pore diameter (nm)*	*Surface area (m^2/g)*	w_s[b] *(mg)*	w_s/SA[c] *(mg/m^2)*
C_8	7	300	70	0.13
PRO-10 C_8	13	160	112	0.39
PSM 120 C_8	12	98	70	0.39
PSM 300 C_8	30	50	50	0.55
PSM 500 C_8	50	30	34	0.63
PSM 1000 C_8	100	20	25	0.69

[a] Zorbax.
[b] Determined by breakthrough method.
[c] Column capacity w_s divided by column surface area SA; column contains 1.8 g of packing.

detector (fitted with a preparative flow cell) or (3) an LKB (Gaithersburg, MD, U.S.A.) gradient system using a DuPont spectrophotometer detector.

Columns

All columns were stainless steel (15 × 0.46 cm I.D.) and were loaded by a downward high-pressure slurry technique. The packing materials used are shown in Table I, together with their pore sizes, surface areas and particle sizes. All were Zorbax PSM silica (DuPont) which had been bonded with octadecyldimethylchlorosilane and capped with trimethylchlorosilane (Petrarch, Bristol, PA, U.S.A.) by conventional bonding techniques similar to those described by Kinkel and Unger[9].

Chemicals and protein standards

Solvents were of HPLC grade (J. T. Baker, Phillipsburg, NJ, U.S.A.) and were degassed with helium during use. Trifluoroacetic acid and sodium dihydrogen phosphate were of Baker Analyzed grade.

Protein standards were obtained from Sigma (St. Louis, MO, U.S.A.). All chemicals and standards were used without further purification.

Craig simulations

The model and software used in the present Craig simulations (CRAIG4) are similar to those reported earlier[4,10] and are described in detail in ref. 11. CRAIG4 was written for rapid calculations on an IBM-AT personal computer. Separations involving 1000–2000 plates can be carried out in 0.5–4 h running time, in either an isocratic or gradient mode, and for either one-component or two-component samples.

Verification of the present Craig simulations. The CRAIG4 program was used to calculate retention times and bandwidths for several small-sample isocratic and gradient elution separations, which can be compared with exact calculations as in ref. 4; all such comparisons showed excellent agreement (within a few tenths of a per cent for retention, within a few per cent for bandwidth). Similar comparisons were made for isocratic 1-solute mass-overloaded runs between previously reported computer-simulation results[12] and the same simulations via CRAIG4. These showed good

agreement (Fig. 1), confirming at least the consistency of the present approach. Comparisons in this paper of Craig with experimental gradient separations provide additional verification of the CRAIG4 software.

RESULTS AND DISCUSSION

Craig simulations

Isocratic data. In an effort to resolve certain anomalies in our previous Craig simulation treatment of mass-overloaded gradient elution[4,5] ($z \approx 0.85$ in eqn. 9), we first examined the case of isocratic separation; see also the discussion in ref. 11. Some representative data are shown in Fig. 1 for the sample-mass contribution to band broadening (W_{th}) as a function of sample size. The open points are from a previous study[a] and the closed triangles are new data from the use of CRAIG4. Three different data sets are plotted, for different values of k_o. The solid curves for these data points are a best fit to eqn. 3, assuming a single value of w_s for these simulations. For sample sizes $w/w_s > 0.1$, these initially linear plots are seen to curve downwards, as is predicted for heavily overloaded separations[4,7,13,14].

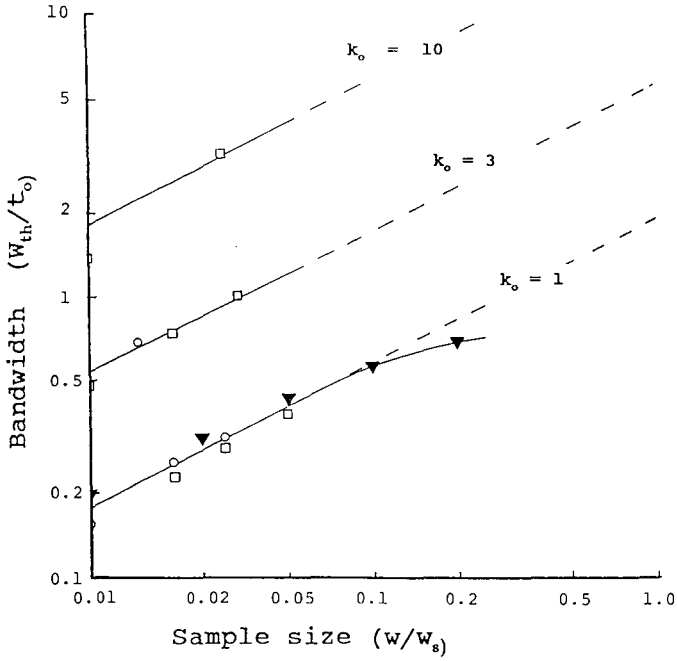

Fig. 1. Craig simulations of band broadening in isocratic separation as a function of sample size (cf., eqn. 3). Straight-line plots through these data are a best fit to eqn. 3 (see text). □, ○ = Data from ref. 12 for $n_c = 600$ and 1000, respectively; ▼ = data using CRAIG4.

[a] The open points in Fig. 1 are from ref. 12. The isotherm algorithms (polynomial fit) used in that study (for a single solute, fixed values of k_o and small values of w/w_s) are presumed to be slightly more accurate than the corresponding algorithms[12] of CRAIG4.

For moderate overloading of the column ($w/w_s < 0.10$), we have shown previously that values of W_{th} appear to increase more rapidly than predicted by theory[13] or Craig simulation[11,15]. That is, the sample sizes used in Craig simulation give W_{th} values that are too small. This can be corrected by increasing the sample sizes used in Craig simulation 1.8-fold[11], in which case Craig and experimental predictions of bandwidth are brought into agreement.

The data in Fig. 1 when fitted to eqn. 3 can be used to verify this correction factor (1.8-fold) for Craig simulation *vs.* the case of experimental data. This yields a value of 2.1-fold, which is reasonably close to the the above factor of 1.8. That is, any conclusions we obtain from isocratic Craig simulation must be modified for application to experimental separations; the value of w/w_s assumed in Craig simulations should be about 1.8-fold higher than for corresponding experimental systems if good agreement between experimental and Craig simulation results is to be obtained.

Gradient elution. Eqns. 8 and 9. Fig. 2 illustrates some CRAIG4 simulations for a single band as a function of sample size (other conditions remaining the same). A similar pattern was observed[4] in previous Craig simulations of gradient elution: overlapping ("nested") bands having a "shark-fin" shape. Values of W_{th} can be obtained for these various bands (eqn. 1); Fig. 3 shows a log–log plot of W_{th} *vs* sample size (w/w_s).

The data in Fig. 3 lie on a straight line, in agreement with eqn. 9. The slope of this straight-line plot is $z = 0.6$, in contrast to previous studies[4] which gave $z = 0.85$. There are several reasons for this difference between the present and previous Craig-

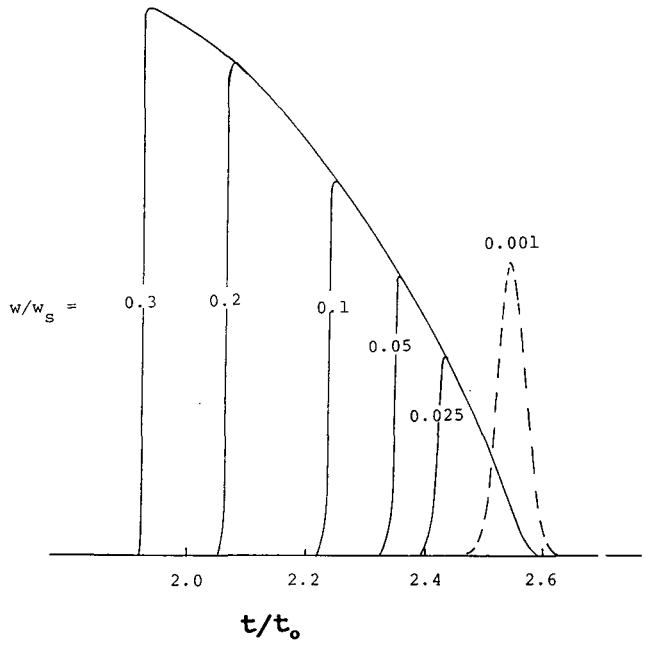

Fig. 2. Craig simulations (CRAIG4) for the gradient elution separation of a single band as a function of sample size. Conditions: $N_o = 1600$ ($n_c = 800$), $b = 1$, k_o at the start of the gradient (k_{og}) = 10.

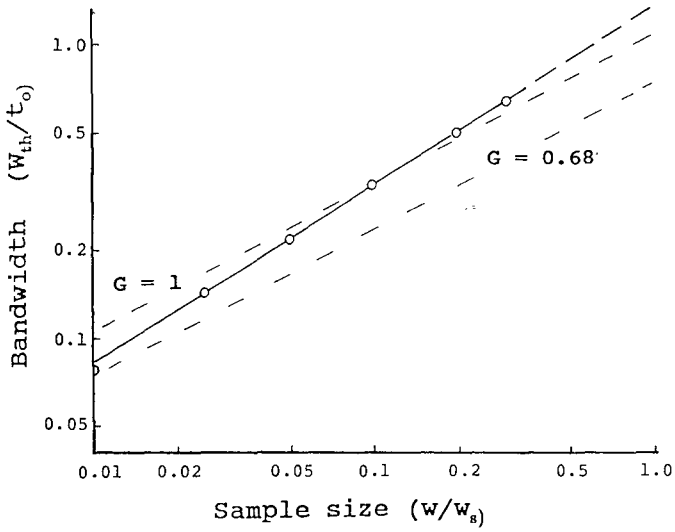

Fig. 3. Craig simulations of band broadening in gradient separation as a function of sample size (cf., eqn. 8). Dashed straight-line plots are predicted by eqn. 8 for different values of G (see tect). Data points (○) correspond to separations in Fig. 2 (same conditions).

simulation studies. First, we now know that the way in which bandwidths are measured for mass-overloaded bands can significantly affect values of W_{th} when w/w_s is small. It is relatively easy to determine the beginning of the band by the tangent method (see the examples in Fig. 2), but the end of the band is often ambiguous. We now feel that the best approximation to the end of the band is given by $t_R^o + (w_o/2)$, where t_R^o is the small-sample retention time. Second, Craig simulations are more reliable for larger values of N_o (larger values of n_c, the number of Craig stages)[12]. The data in Fig. 3 ($n_c = 800$) are based on twice the number of plates used in our previous study[4]. Finally, the algorithms used in CRAIG4 were more thoroughly tested than in the previous study[4], and may therefore be more reliable.

The dashed curves in Fig. 3 are from eqn. 8, assuming either the value of G for a small-sample separation ($G = 0.68$) or negligible band compression by the gradient ($G = 1$). For small samples ($w/w_s < 0.01$), there is no reason to believe that gradient compression should not affect the entire band (values of both W_o and W_{th}). For larger samples, however, the front of the band moves in a mobile phase that is much weaker (larger k_0). This corresponds to a smaller value of b (eqn. 4), for which the value of G then approaches 1, *i.e.*, there is negligible gradient compression for a small-sample band as the gradient becomes flatter (and approaches isocratic separation[a]). We therefore expect that plots as in Fig. 3 will approach the curve predicted by eqn. 8 ($G = 0.68$ in this case, for $b = 1$) for smaller samples, then trend toward the corresponding curve for $G = 1$ with larger samples. This is observed for the example in Fig. 3.

[a] This effect applies only to the front of the band, which is traveling through the column in a much weaker solvent. Therefore, the lack of gradient compression at the band front does not have much effect on the "shark fin" shape of the band (see Fig. 2).

In addition to demonstrating the agreement of eqn. 8 with these Craig simulations[a], Fig. 3 also shows that values of z should vary between roughly 0.5 and 0.6. For smaller values of b ($b = 1$ in Fig. 3), corresponding to more common gradient conditions, the lower dashed curve in Fig. 3 will approach the upper curve, so that then $z \approx 0.5$. For steeper gradients as in Fig. 3, z will tend toward a value of about 0.6. We shall see that this corresponds fairly well to experimental gradient elution separations.

EXPERIMENTAL

Small solute molecules

Two small-molecule solutes, caffeine and benzyl alcohol, were chosen for an experimental study of bandwidth *vs.* sample size in reversed-phase gradient elution. Previous studies[15] have shown that these solutes exhibit Langmuir-isotherm behaviour under reversed-phase conditions.

Caffeine as solute. Chromatography for caffeine was performed on a 15 × 0.46 cm I.D. column packed with Zorbax PSM 500 C8 (500 Å pore diameter, 8 μm particle size) with methanol and 0.05 *M* sodium phosphate (pH 5) as mobile phase components. This large-pore silica was chosen because its low surface area (and small value of w_s) allow the observation of mass-related band broadening for reasonably small samples, thus avoiding problems with sample solubility.

As we intended to compare our findings with the theoretical predictions of eqn. 8, values of the gradient-steepness parameter b were required. This in turn requires a value for the solute parameter S (eqn. 5). Exact values of S for a particular solute and HPLC system can be obtained using either isocratic or gradient data. For isocratic retention,

$$\log k_0 = \log k_w - S\varphi \tag{10}$$

Therefore, measurement of values of k' as a function of mobile phase composition φ serve to determine a value of S. Alternatively, two gradient runs with different values of b (different gradient steepness) can also be used[16]. For the HPLC system in Table II, values of S and k_w for caffeine were $S = 8.2$ (isocratic) and 7.9 (gradient) and $k_w = 26.0$ (isocratic) and 25.7 (gradient). Average values of $S = 8.0$ and $k_w = 25.8$ were assumed in further work.

The saturation capacity of the column for caffeine was next determined as described earlier[8] (based on eqns. 2 and 3 in ref. 11). Isocratic chromatograms were obtained using methanol–0.05 *M* sodium phosphate (10:90) as the mobile phase for a low (0.01 mg) and a high (0.1 mg) load of caffeine. Calculation of the saturation capacity (w_s) gave a value of 20 mg (equal to 0.33 mg/m^2 for this packing).

Gradient elution with sample sizes from 0.01 to 10.0 mg of caffeine were carried out under two sets of gradient conditions (corresponding to $b = 0.33$ and 0.165), *i.e.*, gradients from 0 to 50% B in 30 or 60 min (A is 0.05 *M* phosphate, B is methanol). Bandwidths W were measured, and mass-related bandwidths W_{th} were calculated for

[a] Note that the Craig simulations in Fig. 3 are uncorrected for the 1.8-fold discrepancy found in ref. 11; that is, these Craig simulations for gradient elution are in much closer agreement with theory as expressed by eqn. 8. The reason for this difference between isocratic and gradient separations is not yet clear.

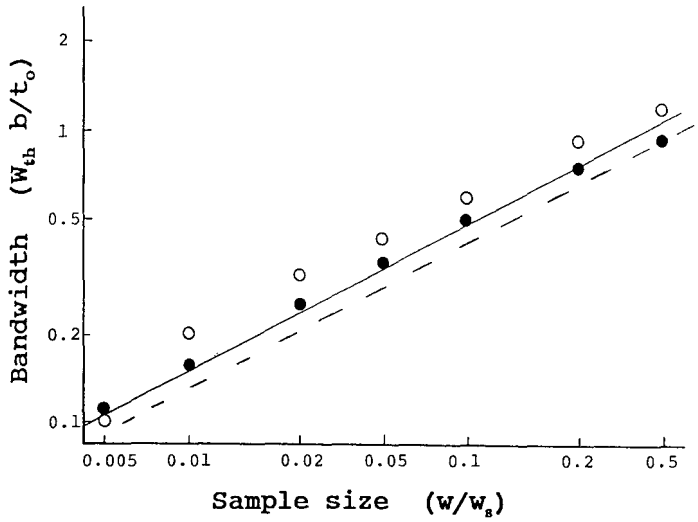

Fig. 4. Sample size-dependent band broadening for gradient elution runs with caffeine as solute. Conditions: 15 × 0.46 cm I.D. Zorbax PSM 500 C_8 column; 0–50% B gradient (A, 0.05 *M* sodium phosphate, pH 5; B, methanol); 1 ml/min. ○ = Gradient time 30 min; ● = gradient time 60 min. Solid line, $G = 1$; dashed line, $G = 0.85$.

each gradient run from eqn. 1 (using an experimental value of W_0). Fig. 4 shows resulting plots of $W_{th}b/t_0$ *vs.* w/w_s for both gradient conditions. The solid line is from eqn. 8, with $G = 1$, and the dashed line is for the small-sample G value of 0.85. The agreement between the experimental and calculated values is fairly good, although the bandwidths for the steeper gradient are slightly higher than expected. If the data of Fig. 4 are fitted to eqn. 9, a best value of $z = 0.46$ is obtained.

Benzyl alcohol as solute. Chromatography for benzyl alcohol was performed on a 15 × 0.46 cm I.D. Zorbax ODS column with methanol–water mixtures as the mobile phase. Values of S and k_w for this solute were determined as above: $S = 2.4$ (isocratic) and 2.2 (gradient) and $k_w = 32$ (isocratic) and 25 (gradient). Average values of these parameters were assumed in further work. The value of w_s for this packing and benzyl alcohol as solute was reported in ref. 15 as 64 mg for a 5-cm column; we have assumed $w_s = 192$ mg for the present 15-cm column. Fig. 5 shows a plot of W_{th} *vs.* w/w_s in the same manner as in Fig. 4 for caffeine. The best fit of these data to eqn. 9 gives $z = 0.54$. Again, there is reasonable agreement between observed and predicted results.

3-Hydroxypropyltheophylline (HPT) as solute. The gradient separation of this xanthine in admixture with hydroxyethyltheophylline (HET) has been reported[3] as a function of sample size. Plots of W_{th} *vs.* sample size can be derived, as in Figs. 4 and 5. These data are plotted in Fig. 6. The comparison of experimental values (○) with calculated curves (dashed lines) as in Figs. 4 and 5 gives a similar result, although the experimental values are now slightly lower than predicted. In this instance, the data for HTP may be affected by the presence of HET in the sample (the experiments in Figs. 4 and 5 involved single-solute samples). The value of z is 0.61.

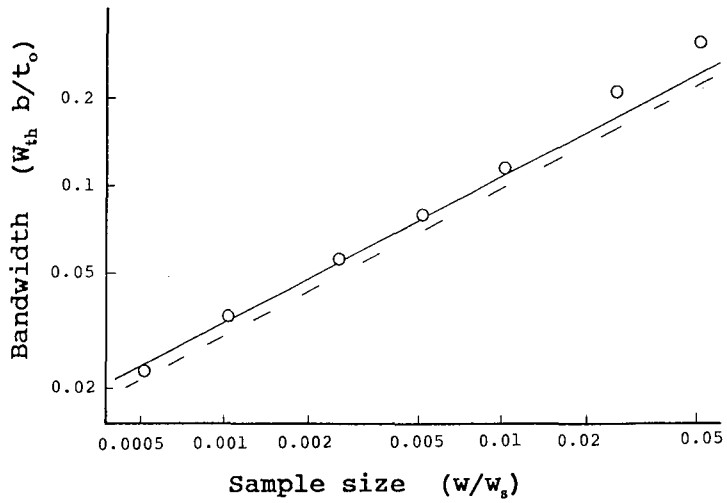

Fig. 5. Sample size-dependent band broadening for gradient elution runs with benzyl alcohol as solute. Conditions: 15 × 0.46 cm I.D. Zorbax ODS column; 0–50% methanol–water gradient in 30 min; 1 ml/min. Solid line, $G = 1$; dashed line, $G = 0.90$.

Protein solutes

Twelve plots of W_{th} *vs.* w (similar to those in Figs. 4–6) for various proteins and different reversed-phase columns were reported previously[5]. The observed value of z for all systems was found to be 0.54 ± 0.08 (S.D.), which is in good agreement with eqn. 8 and the discussion in Fig. 4. Therefore the conclusion in ref. 4 that reversed-phase protein separations appear not to follow Langmuir adsorption (which

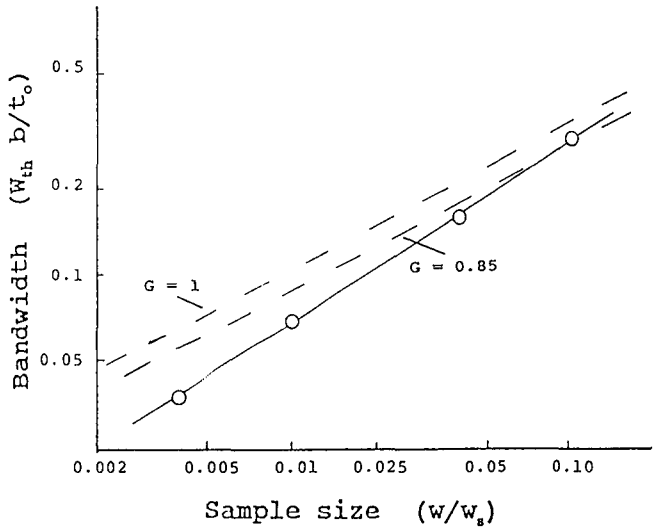

Fig. 6. Sample size-dependent band broadening for gradient elution runs with 3-hydroxypropyltheophylline as solute. Conditions: 15 × 0.46 cm I.D. Zorbax C_8 column; 5–100% B in 14.8 min [A = 0.1 *M* phosphate, pH = 2.2; B = acetonitrile–methanol (20:80, v/v)]; 1 ml/min. Solid line, $G = 1$; dashed line, $G = 0.85$.

is implicit in the derivation of eqn. 8) is incorrect. These HPLC systems may in fact exhibit non-Langmuir behavior in other respects, but the dependence of W_{th} on sample size (value of z) is consistent with Langmuir adsorption.

Column capacity w_s for protein samples as a function of column-packing pore diameter. The possibility that Langmuir adsorption is able to explain the separation of proteins as solutes for reversed-phase gradient elution can be tested further by making independent measurements of the column capacity, w_s (w_s values were not determined in the studies in ref. 5). The column capacity for a protein sample can be measured in various ways. We used successive injections of small amounts of protein with a weak mobile phase[a] until breakthrough is observed. The retained protein can then be eluted in a gradient run, as a check on the amount taken up. This approach was tried with lysozyme as a test solute and a 15 × 0.46 cm I.D. PSM 300 C_8 column. Within the limits imposed by the linearity of detector response (*i.e.*, high lysozyme concentrations plus a varying mobile phase composition), the amount of eluted protein (52 mg) agreed well with the amount measured in the breakthrough experiment (47 mg).

The column capacity of lysozyme was determined for a number of (otherwise identical) columns filled with packings of different pore size and surface areas. The results are given in Table I. As the pore diameter is increased from 7 to 100 nm, the column capacity first increases to a maximum of 112 mg for the packing of 13-nm pore diameter, then decreases continuously with further increase in pore diameter. Further insight into these column-capacity data are afforded by the surface areas (Table I) and column capacities per square meter of surface (last column of Table I).

In general, the surface area (m^2/g) of a packing decreases as the pore diameter increases. However, large solute molecules do not have access to all the pores of the packing, because of possible steric exclusion. Therefore, for a protein of intermediate size (lysozyme in the present example) the column capacity per square meter will increase with increasing pore diameter, but eventually approach a limiting value (about 0.7 mg/m^2) for the data in Table I. The latter dependence, combined with a continuous decrease in surface area with increasing pore diameter, then results in a maximum column capacity (for columns of given size, as in Table I) for an intermediate pore diameter (10–15 nm for lysozyme and reversed-phase columns). A similar situation has been described by Rounds *et al.*[17] for the ion-exchange separation of different proteins.

Column capacities inferred from eqn. 8. We have previously reported[5] values of W_{th} *vs.* sample size for the gradient elution separation of lysozyme and carbonic anhydrase, using columns similar to those in Table I. Eqn. 8 can be used to infer values of w_s for these various systems, for comparison with the saturation uptake values in Table I. The results are summarized in Table II.

It is seen that the w_s values from eqn. 8 are generally lower than the saturation-uptake values in Table II. Further, the fractional utilization of the total surface (as measured by saturation uptake) increases with increasing pore diameter. This suggests that under actual separation conditions (gradient elution as in ref. 5), protein samples can utilize only a fraction of the total surface available to the sample at

[a] We recommend 5–10% acetonitrile in water, rather than water alone, to allow adequate wetting of the packing by the mobile phase and avoid incomplete uptake of protein.

TABLE II

DYNAMIC COLUMN CAPACITIES INFERRED FROM DATA IN REF. 5 BY MEANS OF EQN. 8

Lysozyme solute, 15 × 0.46 cm I.D., 5-μm C_8 columns, 5–70% acetonitrile in 0.1%TFA–water gradients in 20 min, 1 ml/min.

Pore diameter of packing (nm)	w_s *(mg)*		*% surface utilization*[c]
	Table I[a]	*Eqn. 8*[b]	
15	80[d]	18	23
30	50	10	20
50	34	10	29
100	25	11	44

[a] Data from Table I except where noted otherwise.
[b] Eqn. 8 applied to data in ref. 5 (Figs. 8–11 in that paper).
[c] Eqn. 8 values divided by Table I values.
[d] Different packing to that shown in Table I; interpolated value from plot of w_s *vs.* pore diameter.

equilibrium. This fractional utilization apparently increases with more facile mass transfer (larger pores), as suggested also by the work of Kopaciewicz *et al.*[18].

The data in Table II suggest that actual column capacities (which determine the column loadability in gradient elution) for protein samples vary with column pore diameter in a complex fashion. This has obvious practical implications, which we will explore further elsewhere. Returning to the question of whether protein samples obey the Langmuir isotherm, it should be obvious that no final conclusions regarding this point can be drawn from the present study. The fact that the apparent column capacity for protein samples (in gradient elution) is less than the saturation uptake value suggests that both equilibrium (isotherm) and kinetic (mass transfer) effects contribute to the dependence of W_{th} on sample size. Under these circumstances, the observed agreement between Eqn. 8 and experimental data for proteins could be fortuitous.

Velayudhan and Horváth[19] argued against a Langmuir isotherm for the ion-exchange separation of proteins, in view of the fact that a single protein molecule will displace several salt ions (the Langmuir equation assumes a one-to-one displacement process). Similar logic can be used against a Langmuir isotherm for protein samples in reversed-phase systems, because of the evidence that reversed-phase retention also involves a displacement process[20]. Previously we have considered[15] the consequences of a non-stoichiometric displacement process as this affects Langmuir-type sorption processes. An extension of that treatment suggests that the sorption of protein molecules, with the resulting displacement of many solvent molecules by each sorbing protein molecule, can be approximated fairly well by the Langmuir equation (for $w/w_s < 0.5$), if the actual column capacity w_s is reduced by about half. This observation is suggestive in the light of the data in Table II, *i.e.*, the percentage surface utilization values shown there should actually be doubled.

CONCLUSIONS

The dependence of band broadening and separation in gradient elution has been further studied by both theoretical and experimental means. For the case of small

molecules, bandwidth as a function of sample size and gradient conditions can be described by a simple equation (eqn. 8). This relationship predicts that the mass-related contribution to bandwidth (W_{th}) will be proportional to (sample weight)^z, where z will normally vary between 0.5 and 0.6. Computer simulations based on the Craig distribution process confirm this relationship. Experimental data for several small-molecule samples are also in quantitative agreement with eqn. 8. It therefore appears that we have a reasonably good understanding of band broadening for a one-component sample as a function of sample size and separation conditions.

The gradient elution separation of protein samples by reversed-phase HPLC appears more complex. The same general relationship (eqn. 8 with $0.5 < z < 0.6$) also describes band broadening *vs.* sample size for these samples, but the apparent column capacities (w_s) inferred from band-broadening data are generally smaller than values measured by saturation uptake. This suggests that the mass-related contribution to band broadening (W_{th}) is a function of both equilibrium and kinetic properties of the system, unlike the case for small-molecule solutes. Nevertheless, a broad range of protein systems have been shown to exhibit a predictable increase in bandwidth with increasing sample size, as discussed further in Part II.

APPENDIX

Derivation of eqn. 3

This relationship has been reported previously[8] but not actually derived. We start with previous expressions for experimental values of N (for a large sample) and N_o (see ref. 11):

$$N_o = 16(t_R^o/W_o)^2 \tag{A1}$$

$$N = 16(t_R^o/W)^2 \tag{A1a}$$

$$N/N_o = 1/[1 + (3/8)w_{xn}] \tag{A2}^a$$

$$w_{xn} = N_o[k_o/(1+k_o)]^2(w/w_s) \tag{A3}$$

$$t_R^o = t_o(1+k_o) \tag{A4}$$

Eqns. 1, A2 and A4 combine to give

$$1/N = (w_o^2 + W_{th}^2)/16[t_o(1+k_o)]^2 \tag{A5}$$

Likewise, eqn. A2 can be written as

$$1/N = 1/N_o + [(3/8)w_{xn}/N_o] \tag{A6}$$

---

[a] This equation[7] is a best fit to experimental values of N; the corresponding *theoretical* expression[7,13] is $N/N_0 = 1/[1+(1/4)w_{xn})]$, which leads to the replacement of the factor $(6)^{\frac{1}{2}}$ in eqn. 3 by the factor 2.

Eqns. 1, A1 and A1a give

$$(1/N) - (1/N_o) = (W^2/16t_R^{o2}) - (W_o^2/16t_R^{o2})$$

$$= W_{th}^2/16t_R^2 \qquad \text{(A7)}$$

Eqn. A6 can be rewritten as

$$(1/N) - (1/N_o) = (3/8)w_{xn}/N_o \qquad \text{(A8)}$$

Eqns. A7 and A8 then give

$$W_{th}^2/16t_R^2 = (3/8)w_{xn}/N_o \qquad \text{(A9)}$$

Eqns. A3, A4 and A9 then give eqn. 3.

SYMBOLS (PARTS I–III)

Reference to equations or figures in the various papers in this series is identified by use of I-, II- or III-, *e.g.*, eqn. III-3 refers to eqn. 3 in Part III.

b	gradient steepness parameter; equal to $[1/(1.15\bar{k})]$ (eqn. I-5)
B	strong solvent in the mobile phase
F	flow-rate (ml/min)
G	gradient compression factor (eqn. I-7)
J	anomalous band-broadening factor in gradient elution (eqn. I-7)
k'	solute capacity factor
$\bar{k}$	average value of k' during gradient elution; equal to $[1/(1.15b)]$
k_e	value of k' in gradient elution when the band leaves the column (eqn. I-4)
k_o	value of k' for a small sample
k_w	value of k' for water as mobile phase
k_{wx}, k_{wy}	values of k_w for X and Y
M	solute molecular weight
n_c	number of Craig stages in a computer simulation; $n_c = [k'/(1+k')]N_o$
N_o	value of N for a small sample; in computer simulations, $N_o = [(1+k')/k']n_c$
P_R	production rate; mg/h of purified product
R_s	resolution
R_s'	value of R_s in an initial run (eqn. II-6)
$R_{s\ opt}$	optimum value of R_s (in a small-sample separation) to maximize resolution in a preparative run (eqn. II-6)
S	parameter that measures change in isocratic k' values with change in φ (eqn. 6)
SA	stationary phase surface area (m^2 for entire column)
S_x, S_y	values of S for X and Y
t_D	dwell time of gradient equipment (min)
t_g	retention time in gradient elution (min)
t_G	gradient time (min)
t_o	column dead time (min)

t_x, t_y	retention times in gradient elution for bands X and Y (min, small sample)
V_m	column dead volume (ml)
w	total weight of injected sample; usually combined weights of X and Y (mg)
W	baseline bandwidth (min); see Figs. 2 and 3
W_o	value of W for a small sample (min) (eqn. I-1)
w_s	column saturation capacity (mg)
W_{th}	sample-size contibution to W (min) (eqn. I-1)
w_x, w_y	weight of solutes X or Y injected on the column (mg)
x, y	subscripts referring to bands X and Y
X, Y	adjacent sample bands; Y corresponds to the desired product and X is the preceding band
z	slope of plot of W_{th} *vs.* w (I-9)
α	separation factor for two solutes
$\Delta\varphi$	change in φ during a gradient
φ	mobile phase composition; volume fraction of strong solvent B in the mobile phase
φ_i, φ_f	initial (i) and final (f) values of φ in a gradient

REFERENCES

1 L. R. Snyder, in Cs. Horváth (Editor), *High-Performance Liquid Chromatography —Advances and Perspectives*, Vol. 1, Academic Press, New York, 1986, p. 207.
2 L. R. Snyder and M. A. Stadalius, in Cs. Horváth (Editor), *High-Performance Liquid Chromatography —Advances and Perspectives*, Vol. 4, Academic Press, New York, 1986, p. 195.
3 J. E. Eble, R. L. Grob, P. E. Antle and L. R. Snyder, *J. Chromatogr.*, 405 (1987) 51.
4 L. R. Snyder, G. B. Cox and P. E. Antle, *J. Chromatogr.*, 444 (1988) 303.
5 G. B. Cox, P. E. Antle and L. R. Snyder, *J. Chromatogr.*, 444 (1988) 325.
6 L. R. Snyder, J. W. Dolan, D. C. Lommen and G. B. Cox, *J. Chromatogr.*, 484 (1989) 425.
7 L. R. Snyder, G. B. Cox and P. E. Antle, *Chromatographia*, 24 (1987) 82.
8 L. R. Snyder and G. B. Cox, *LC · GC, Mag. Liq. Gas Chromatogr.*, 6 (1988) 894.
9 J. N. Kinkel and K. K. Unger, *J. Chromatogr.*, 316 (1984) 193.
10 J. E. Eble, R. L. Grob, P. E. Antle and L. R. Snyder, *J. Chromatogr.*, 405 (1987) 1.
11 L. R. Snyder, J. W. Dolan and G. B. Cox, *J. Chromatogr.*, 483 (1989) 63.
12 J. E. Eble, R. L. Grob, P. E. Antle and L. R. Snyder, *J. Chromatogr.*, 384 (1987) 25.
13 J. H. Knox and H. M. Pyper, *J. Chromatogr.*, 363 (1986) 3.
14 S. Goshan-Shirazi and G. Guiochon, *Anal. Chem.*, 60 (1988) 2364.
15 J. E. Eble, R. L. Grob, P. E. Antle and L. R. Snyder, *J. Chromatogr.*, 384 (1987) 45.
16 M. A. Quarry, R. L. Grob and L. R. Snyder, *Anal. Chem.*, 58 (1986) 907.
17 M. A. Rounds, W. Kopaciewicz and F. E. Regnier, *J. Chromatogr.*, 362 (1986) 187.
18 W. Kopaciewicz, S. Fulton and S. Y. Lee, *J. Chromatogr.*, 409 (1987) 111.
19 A. Velayudhan and Cs. Horváth, *J. Chromatogr.*, 443 (1988) 13.
20 X. Geng and F. E. Regnier, *J. Chromatogr.*, 296 (1984) 15.

Journal of Chromatography, 484 (1989) 425–435
Elsevier Science Publishers B.V., Amsterdam — Printed in The Netherlands

CHROM. 21 887

PREPARATIVE HIGH-PERFORMANCE LIQUID CHROMATOGRAPHY UNDER GRADIENT CONDITIONS

II. A COMPUTER PROGRAM FOR THE DESIGN OF REVERSED-PHASE GRADIENT-ELUTION SEPARATIONS OF PEPTIDE AND PROTEIN SAMPLES

L. R. SNYDER*, J. W. DOLAN and D. C. LOMMEN
LC Resources Inc., 3182C Old Tunnel Road, Lafayette, CA 94549 (U.S.A.)
and
G. B. COX
Medical Products Department, E. I. du Pont de Nemours Inc., Glasgow, DE 19701 (U.S.A.)

SUMMARY

A commercially available computer program (BIOPREP) is described as an aid for developing preparative separations of peptide or protein samples using reversed-phase gradient elution. On the basis of four small-scale runs in the laboratory (with advice offered by the computer), experimental conditions for "touching-band" separations can be predicted. This in turn allows comparisons of the production rate of a purified product as a function of the gradient conditions and column dimensions. In this way, conditions can be selected that either maximize the production rate or provide an otherwise satisfactory separation.

INTRODUCTION

Currently reversed-phase gradient elution is widely used for the preparative purification of peptide and protein samples on either a laboratory[1] or a manufacturing[2] scale. The usual objective, especially at the R&D or pilot-plant stage, is to obtain a certain amount of purified product with the expenditure of minimum time and effort. Because of the complexity of these separations, and the strong dependence of production rate (g/h of purified material) on the separation conditions, the chromatographer is faced with the question of how much time should be spent on method development in order to minimize the time spent later in actually separating the sample.

The results described in Part I[3] can be used to guide the method development process, at least for the design of "touching-band"[a] separations. We can proceed

[a] "Touching-band" separations refer to the case where the sample is just large enough that the product band begins to overlap adjacent peaks (*e.g.*, yielding a 99.8% recovery of 99% pure product as in ref. 4); see the related discussion of touching-band separations in an isocratic mode[5,6].

0021-9673/89/$03.50

qualitatively (trial and error), or we can make use of accurate quantitative relationships for the selection of the best experimental conditions. In the latter instance, we can minimize the total number of experiments by using experimental data to calculate preferred conditions more precisely. However, this is tedious if carried out manually. A better approach is the use of a computer program to (a) execute the necessary calculations, (b) draw conclusions from prior experiments and (c) make recommendations and alert the user to potential problems as method development proceeds.

In this paper we describe an efficient approach to method development for the reversed-phase gradient-elution high-performance liquid chromatographic (HPLC) separation of peptide and protein samples. We also illustrate how this procedure can be simplified by the use of an appropriate computer program, BIOPREP. The resulting touching-band separations are suitable for the purification of multi-gram amounts of final product. Additional increases in production rate by the use of heavily overloaded (<99.8% recovery of product) separation are possible by the further trial-and-error adjustment of separation conditions. This will be examined in the future, but guidelines can be inferred in part from the results in ref. 4.

THEORY[a]

Our proposed method-development strategy can be summarized as follows:

(1) Carry out one or more initial runs with a small sample, varying the mobile phase composition (organic solvent, pH, additives) and column packing in order to maximize the selectivity. The objective is to achieve the largest possible value of the separation factor, α, between the product band and the adjacent earlier-eluting impurity.

(2) Use the initial run(s), typically carried out with wide-range gradients, to estimate favorable values of (a) the initial and final %B in the gradient, (b) gradient times for two additional exploratory runs and (c) flow-rate.

(3) Carry out two additional small-sample runs with the recommended gradient range from step 2, varying only the gradient time; these two runs can be used to define separation as a function of gradient conditions and column dimensions.

(4) Carry out a fourth run, using the same conditions as in step 3, but with a sample that is large enough to increase the bandwidth appreciably; this run can be used to estimate the column capacity w_s and loadability for the sample in question.

(5) With the data and conditions from steps 3 and 4, calculate the sample size and production rate for touching bands as a function of gradient time and column dimensions.

(6) Verify the predicted (best) separation from step 5 experimentally; fine-tune the conditions if necessary.

Step 1: maximizing α

The choice of preferred mobile and stationary phase conditions for a given sample is usually a matter of experience plus trial-and-error experimentation. In the absence of advance information, many workers will begin with a 5–70% water–

[a] A list of all symbols used in Parts I–III is included in ref. 3.

acetonitrile [0.1% trifluoroacetic acid (TFA)] gradient. In many instances[7–10], it will be possible to improve the initial separation considerably with these conditions (TFA–water–acetonitrile) by adjusting the gradient steepness. Alternatively, changes in the mobile phase pH, buffer or buffer concentration may be required to provide further improvements in band spacing.

Step 2: selecting favorable conditions for the next two runs

Gradient range. Experienced chromatographers will usually adjust the gradient range (select the best values of the initial and final %B) on the basis of an initial wide-range gradient. This is illustrated in Fig. 1 by a computer-simulated chromatogram[9] for a representative sample: interleukin-2 (IL-2), a 14 000-Da protein, plus three impurities that correspond to oxidation or reduction products of the parent molecule. In order to minimize separation time, it is desired to select a gradient range that just brackets the compounds of interest, *i.e.*, the product (IL-2) and the immediately preceding impurity band (marked with an asterisk in Fig. 1).

Theory[11,12] plus experience gained through the use of computer simulation[8] (DryLab G; LC Resources, Lafayette, CA, U.S.A.) suggests the following equations for estimating best values of the initial and final values of %B (φ_i and φ_f) from an exploratory gradient run such as in Fig. 1:

$$\varphi_i = (\Delta\varphi/t_G)\,(t_g - t_0 - t_D) + \varphi_i^0 - 2/S \tag{1}$$

and

$$\varphi_f = (\Delta\varphi/t_G)\,(t_g - t_0 - t_D) + \varphi_i^0 + 0.01 \tag{2}$$

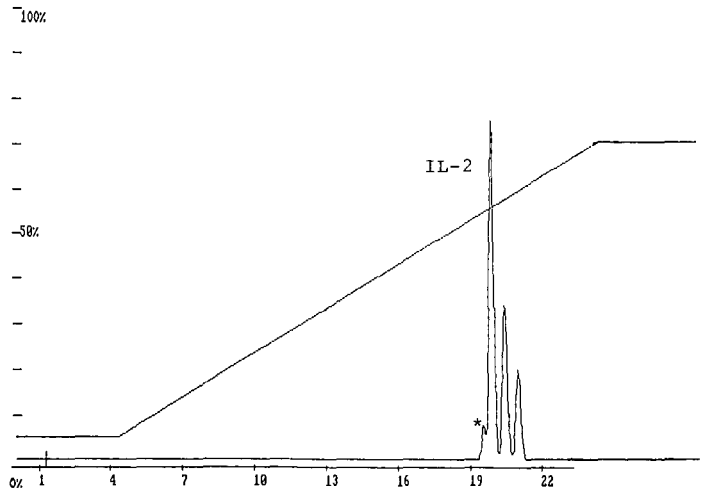

Fig. 1. Recreated chromatogram (using experimental data[9] plus DryLab G software[10]) for the separation of a mixture of desAla^{1}Ser^{125} IL-2 plus three oxidized/reduced impurities. Conditions: 25 × 0.46 cm I.D. C_3 column; 5–70% gradient of acetonitrile in water (0.1% TFA added in 20 min); flow-rate, 2 ml/min.

where t_g is the retention time of the product band, t_D is the dwell time of the HPLC equipment and φ_i^0 is the value of φ_i in the initial gradient run. The other symbols are standard terminology defined in the list of symbols in ref. 3.

Returning to the example in Fig. 1, the initial gradient is 5–70% B in a time of 20 min, the dead time t_0 is 1.28 min and the dwell time is 3.1 min. From the molecular weight of the product band (14 000 Da), $S \approx 32$ (eqn. 6 in Part I[3]). Eqns. 1 and 2 then give $\varphi_i = (0.65/20)(19.93 - 1.28 - 3.10) + 0.05 - (2/32) = 0.493$ and $\varphi_f = (0.65/20)(19.93 - 1.28 - 3.10) + 0.05 + 0.01 = 0.565$, *i.e.*, a 49.3–56.5% B gradient range is recommended.

Gradient times. For the next two experimental runs, it is desirable to adjust the gradient time t_G so as to yield effective values of k' ($\bar{k}$) in the range 3–9, corresponding to a gradient steepness $b = 0.1$–0.3. Eqn. 5 in Part I[3] then permits estimates of appropriate values of t_G for the two runs:

$$\text{(run 1)} \quad t_G = 3.5 V_m \Delta\varphi \; S/F \tag{3}$$

$$\text{(run 2)} \quad t_G = 10.5 V_m \Delta\varphi \; S/F \tag{4}$$

Thus, the gradient time for run 1 is $3.5 \cdot 2.56 \cdot (0.565 - 0.493) \cdot 32/2 = 10.3$ min. Similarly, the gradient time for run 2 is three times this value (30.9 min). Again, the symbols in eqns. 3 and 4 are given in ref. 3.

The resulting chromatograms for these recommended conditions for the next two experimental runs are shown in Fig. 2 for (A) run 1 and (B) run 2. Reasonable resolution of the sample is observed (the result of favorable $\bar{k}$ values), and the gradient now brackets the product band IL-2 and the preceding impurity peak (marked with an asterisk). Similar tests of eqns. 1–4 for other peptide and protein samples gave comparable results to those in Figs. 1 and 2 (if there are later bands in the chromatogram that would not be eluted by the recommended gradient range, a steep gradient segment can be added to the end of the recommended gradient).

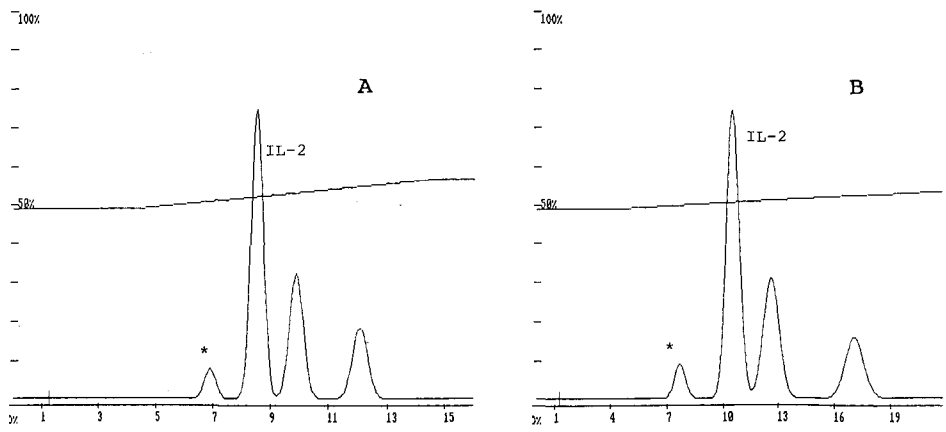

Fig. 2. Recreated chromatogram (using experimental data[9] plus DryLab G software[10]) for the separation of a mixture of desAla[1]Ser[125] IL-2 plus three oxidized/reduced impurities. Conditions as in Fig. 1, except: (A) 49.3–56.5% B gradient in 10.3 min; (B) the same in 30.9 min.

Flow-rate. In earlier papers[4,13] it was concluded that the column plate number in touching-band separations has a significant effect on production rate. That is, if the column length and/or flow-rate are varied while holding the column pressure below some upper limit (*e.g.*, 2000 p.s.i.), the best choice of flow-rate is one that will give a small-sample resolution of $R_s \approx 1.7$.

At this point we wish to select a flow-rate that is roughly optimum in terms of production rate. Resolution in gradient elution (for a small sample) is given by[11,12]

$$R_s = (1/4)\,(\alpha-1)N_0^{1/2}[\bar{k}/(\bar{k}+1)] \tag{5}$$

If we ignore the possible variation of α with gradient steepness b, the optimum value of $\bar{k}$ will be about 3[a]. The sample resolution for this value of $\bar{k}$ ($R_{s\,\mathrm{opt}}$) can then be related to the resolution R_s' of our initial run (as in Fig. 3) as

$$R_{s\,\mathrm{opt}} = 0.75[\bar{k}+1)/\bar{k}]\; R_s' \tag{6}$$

Likewise, N_0 can be assumed to vary with flow-rate F as

$$N_0 \approx \text{constant}/F \tag{7}$$

for conditions typical of preparative HPLC[b]. The optimum flow-rate F_2 relative to the initial flow-rate F_1 (as in Fig. 1) is then

$$F_2 = (R_{s\,\mathrm{opt}}/1.7)^2\; F_1 \tag{8}$$

Eqn. 8 follows from eqns. 5–7, with the preferred value of R_s (for a small sample) being 1.7, *i.e.*, the same as for isocratic runs[4]. The optimum flow-rate F_2 in subsequent runs is also limited by the maximum column pressure that we are willing to accept. For the moment it is assumed that we are not going to change the column length.

If the flow-rate for the next two runs (as in Fig. 2) is changed, the gradient time must be varied inversely, in order to maintain optimum values of $\bar{k}$ ($3 < \bar{k} < 9$). At this point we have chosen the most favorable conditions for further separation as in Fig. 2: initial and final %B, flow-rate, gradient times (differing by a factor of 3) for the next two (small sample) runs.

Step 3: second and third small-sample runs

Having established favorable conditions for further separations, two small-sample runs under these conditions are carried out (as in Fig. 2). From these two runs we can determine the separation characteristics of our sample as defined by the sample parameters S and k_w for both the product band and the adjacent, early-eluting impurity (see discussion in refs. 10 and 12). It is thus possible to estimate small-sample retention times (t_g) and bandwidths (W_0) as a function of gradient time. When values of S are different for the two bands, α will vary with gradient time, in turn leading to

---

[a] Unreported data.

[b] For example, mol. wt. = 1000–30 000, 10–20-μm particles, 25-cm columns, pressures of 1000–2000 p.s.i. These conditions correspond to $n \approx 1$; see ref. 13.

a marked increase in resolution (and production rate) for some value of t_G. This can be of critical importance in maximizing the production rate for a given sample (see Part III).

Steps 4 and 5: fourth run with a large sample; estimation of production rate and sample size vs. gradient time and column dimensions

One of the latter small-sample runs (as in Fig. 2) with optimum gradient conditions is now repeated with a larger sample[a]. If the width W of the product band is measured, a value of W_{th} can be determined from eqn. 1 in Part I[3]. Eqn. 9 in Part I[3] (assume $z \approx 0.6$) can then be used to determine values of W_{th} for other sample sizes and gradient times (which determine a value of b). This in turn permits the estimation for a given gradient time of (a) the sample size that will result in touching bands and (b) the production rate corresponding to that gradient time. The production rate can then be mapped against gradient time and a "best" gradient time can be selected.

This treatment can be extended to the case of longer or wider columns, using various relationships from preceding papers[3,4,13].

Step 6: verification of optimum run

The best conditions arrived at in the above fashion can be evaluated in a final experimental run. The predicted separation should be close to that observed, although small adjustments in sample size may be needed at this point.

EXPERIMENTAL

Equipment

The HPLC system was a Beckman System Gold liquid chromatograph equipped with a Model 126 programmable solvent module, a Model 166 programmable UV detector module (Beckman Instruments, San Ramon, CA, U.S.A.), a Rheodyne (Cotati, CA, U.S.A.) Model 7125 injector and a Model A-318 precolumn filter (Upchurch Scientific, Oak Harbor, WA, U.S.A.).

Reagents

Solvents were HPLC-grade acetonitrile (ACN) (American Burdick & Jackson, Muskegon, MI, U.S.A.), triethylamine (TEA) (J. T. Baker, Phillipsburg, NJ, U.S.A.) and HPLC/spectro grade trifluoroacetic acid (TFA) (Pierce, Rockford, IL, U.S.A.). A Milli-Q Plus system (Millipore, Bedford, MA, U.S.A.) was used for water purification and filtration. Solvents were degassed by helium sparging prior to and during use. Cytochrome *c* type V from bovine heart, type XVIII from dog heart and type III from horse heart were obtained from Sigma (St. Louis, MO, U.S.A.) and used without further purification.

Column

A 25 × 0.46 cm I.D. Zorbax BioSeries Protein PLUS column was used, packed

[a] It is possible to estimate a convenient sample size based on the approximate constancy of w_s values for proteins (10–20 mg for a 15 × 0.46 cm I.D. column) (eqn. 8 values from Table II in ref. 3).

with nominal 6-μm particles bonded with dimethylpropylchlorosilane (C_3) (DuPont, Wilmington, DE, U.S.A.).

Chromatographic conditions

Mobile phase A was prepared by combining 50 ml of ACN, 950 ml of water, 1.392 ml of TEA and 1.742 ml of TFA. Mobile phase B was prepared by combining 200 ml of water, 800 ml of ACN, 1.392 ml of TEA and 1.892 ml of TFA. Because each mobile phase contained a certain percentage of both ACN and water, actual gradient programs were designed to give the acetonitrile (%B) compositions indicated in the various figure captions, *i.e.*, a 30–38% B gradient begins at 30% (v/v) acetonitrile and ends at 38% (v/v) acetonitrile (with all other mobile phase components in proportion). The temperature of the column was maintained at 30°C with an oven. The detection wavelength was 220–240 nm for small samples and 254 nm for large samples.

Software

The BIOPREP program is available from the Medical Products Department of DuPont or from LC Resources.

RESULTS AND DISCUSSION

Development of a method for the purification of a cytochrome c sample using the BIOPREP program as a guide

The BIOPREP program is based on the preceding discussion under Theory, and the following example parallels that general treatment. Thus, when it is stated that "BIOPREP recommends ...", the recommendation is based on the Theory section; that is, there are no "black-box" features in the BIOPREP program; for further details, see ref. 14.

As an illustration of our computer-assisted approach, we shall describe the development of a preparative HPLC procedure for the purification of a sample of crude bovine cytochrome *c* (BCc; mol. wt. 13 300 Da). The sample was formulated as a mixture of BCc with smaller amounts of two "impurities", horse cytochrome *c* (HCc) and dog cytochrome *c* (DCc). The separation of this mixture by reversed-phase isocratic HPLC was previously reported by Terabe *et al.*[15].

For an unknown sample, the usual approach is to begin with an exploratory separation using a broad-range gradient. BIOPREP can be requested to suggest conditions for this initial run, *e.g.*, 5–60% acetonitrile–water (0.1% TFA) for a peptide or protein sample (this will elute most peptides and proteins). The resulting separation for the cytochrome *c* sample is shown in Fig. 3. The column packing was DuPont Zorbax BioSeries Protein PLUS as 5-μm particles in a 25 × 0.46 cm I.D. column. BIOPREP allows the user to enter data from this exploratory separation (Fig. 3) for an estimate of the optimum run conditions for later runs required by BIOPREP. These data from Fig. 3 are summarized in Table I.

On continuing computer simulation with the aid of BIOPREP, we are advised (eqn. 6) that there is potentially excess resolution for a maximum production rate. That is, a higher flow-rate (eqn. 8) or a shorter column is advisable. At this point we are asked to define a maximum column pressure; 2000 p.s.i. is our choice for the present example. The larger the allowable column pressure, the greater is the potential

Fig. 3. Initial separation of cytochrome *c* mixture (85% BCc, 10% HCc and 5% DCc) by reversed-phase gradient elution. Conditions: column, 25 × 0.46 cm I.D. 5-μm DuPont Zorbax Bioseries Protein PLUS; 5–60% acetonitrile in water (plus TEA and TFA) gradient in 20 min; flow-rate, 1 ml/min; ambient temperature; 5 μg injected (small sample).

production rate. Given this maximum pressure, BIOPREP next recommends conditions for two more small-sample runs on the starting (small-diameter) column: gradients of 30 to 38% B in 10 and 30 min, at 2.5 ml/min (all other conditions remaining the same as those used for the run in Fig. 3). These latter runs will allow BIOPREP to map retention as a function of gradient steepness, which is a parameter of major importance in the maximization of production rate.

TABLE I

SEPARATION DATA FROM INITIAL EXPLORATORY RUN IN FIG. 3 (CYCTOCHROME *c* SAMPLE) FOR ENTRY INTO BIOPREP

Parameter	*Value*	*Parameter*	*Value*
System dwell volume	2.3 ml		
Column length	25 cm	Gradient time	20 min
Column I.D.	0.46 cm	Bandwidth Y^a	0.24 min
Flow-rate	1.0 ml/min	Sample mol. wt.	14000 Da
Initial B concentration	5.0%		
Final B concentration	60.0%		
Retention times	First impurity 16.43 min, product band 16.92 min		

[a] Baseline bandwidth W_b.

The two runs recommended by BIOPREP are shown in Fig. 4. On entering the retention data for these two runs into BIOPREP, the computer recommends[a] a fourth experimental run with a larger sample, *i.e.*, 0.5 mg, with the same conditions as in Fig. 4A. This experimental run is shown in Fig. 5. The sample weight and width of the product band (BCc) are entered into BIOPREP, and the program is now able to

[a] Based on an estimated w_s value for the column; 10–20 mg of a protein sample for a 15 × 0.46 cm I.D. column. This fourth run should give a significant increase in W but maintain $R_s > 1$.

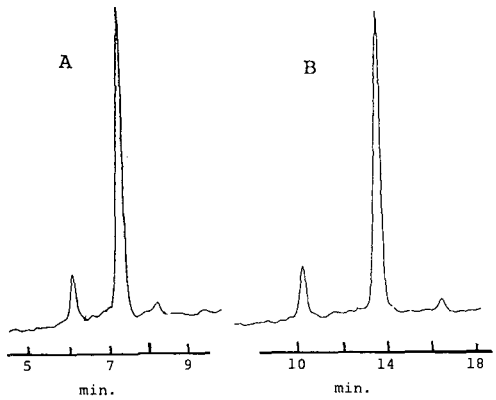

Fig. 4. The subsequent two small-sample runs for cytochrome *c* sample. Conditions: column as in Fig. 3; 30–38% acetonitrile in water in (A) 10 min and (B) 30 min; flow-rate 2.5 ml/min; pressure, 2000 p.s.i.; 5-μg sample.

predict the sample size and production rate for touching-band separation as a function of gradient time. This information, summarized in Table II, includes a 1-min column equilibration with 30% acetonitrile–water (recommended by BIOPREP[a]).

According to Table II, the maximum production rate is predicted for a gradient time of about 2 min. We arbitrarily chose a 2.5-min gradient with our 25-cm column (production rate 14 mg/h for a 25 × 0.46 cm I.D. column).

The conditions that we have selected allow for injection of a 0.8-mg sample. Assuming that we need to purify a larger amount of the product (BCc), we can automate the separation for repetitive injections as described in ref. 17. The resulting separation (three injections in series) is shown in Fig. 6. Touching-band separation is observed, confirming the predictions of the BIOPREP software. Continuous sample

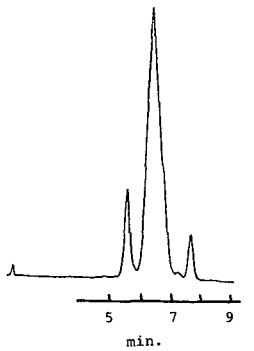

Fig. 5. Separation of a large sample (0.53 mg) of cytochrome *c* sample under conditions of the 10-min run of Fig. 4A.

[a] The recommended column equilibration time is based on 15 column volumes for a full-range (5–100% B) gradient, and proportionately less for a narrow-range gradient[16].

TABLE II
SAMPLE SIZE AND PRODUCTION RATE AS A FUNCTION OF GRADIENT TIME AND COLUMN LENGTH FOR SEPARATION OF CYTOCHROME *c* SAMPLE

Gradient time (mm)	*Sample size (mg)*	*Production rate (mg/h)*[a]
1.6	0.66	15
2.3	0.76	14
3.2	0.79	11
6.6	0.73	5.8
13.5	0.62	2.6
27.5	0.50	1.1

[a] Includes 1 min of column-regeneration time.

injections would be expected to result in the purification of 14 mg/h of BCc (taking column equilibration into account).

For an increased production rate, columns of larger diameter can be used. BIOPREP provided estimates of the optimum sample size and flow-rate for columns of other dimensions, based on constant values of w/w_s and mobile phase velocity u. Thus, a 2-in. I.D. column with a flow-rate of 300 ml/min is predicted to yield 2 g/h of purified product. These scale-up predictions are easy to calculate manually, but BIOPREP offers a more convenient alternative.

CONCLUSIONS

On the basis of the preceding discussions of touching-band separation, it is possible to develop systematically a reversed-phase gradient elution procedure for maximum production (g/h) of purified peptide or protein products. This requires attention to several aspects of the separation: (a) optimum values of α and $\bar{k}$, which can

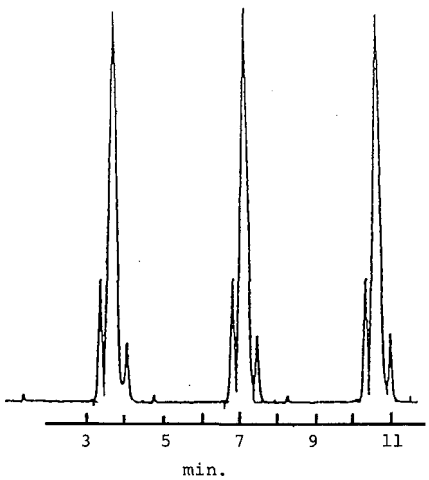

Fig. 6. Repetitive separations of cytochrome *c* sample with touching bands (conditions predicted by BIOPREP). Conditions as in Fig. 4, except 2.5-min gradient, 1-min re-equilibration with 30% B and 0.8-mg sample.

be varied by changing the gradient steepness; (b) an optimum value of N, which can be varied by changing the flow-rate (or column length and particle size, in some instances); (c) column dimensions, which allow a small-column separation to be scaled up.

This approach forms the basis of a commercially available computer program (BIOPREP) that is described here. Its application to the separation of a mixture of cytochrome *c* variants is shown as one example. BIOPREP allows the user to take advantage of our present knowledge of gradient-elution preparative HPLC so as to arrive quickly at reversed-phase conditions that are roughly optimum for the touching-band separation of a given peptide or protein sample. Further adjustment of the conditions can then be used to fine-tune the final separation and/or increase the production rate at the expense of product recovery.

REFERENCES

1 J. Rivier, R. McClintock, R. Galyean and H. Anderson, *J. Chromatogr.*, 288 (1984) 303.
2 E. P. Kroeff, R. A. Owens, E. L. Campbell, R. D. Johnson and H. I. Marks, *J. Chromatogr.*, 461 (1989) 45.
3 G. B. Cox, L. R. Snyder and J. W. Dolan, *J. Chromatogr.*, 484 (1989) 409.
4 L. R. Snyder, J. W. Dolan and G. B. Cox, *J. Chromatogr.*, 483 (1989) 63.
5 L. R. Snyder, G. B. Cox and P. E. Antle, *Chromatographia*, 24 (1987) 82.
6 L. R. Snyder and G. B. Cox, *LC · GC, Mag. Liq. Gas Chromatogr.*, 6 (1988) 894.
7 J. L. Glajch, M. A. Quarry, J. F. Vasta and L. R. Snyder, *Anal. Chem.*, 58 (1986) 280.
8 B. F. D. Ghrist, B. S. Silverman and L. R. Snyder, *J. Chromatogr.*, 459 (1989) 1, 25 and 43.
9 M. Kunitani, D. Johnson and L. Snyder, *J. Chromatogr.*, 371 (1986) 313.
10 J. W. Dolan, L. R. Snyder and M. A. Quarry, *Chromatographia*, 24 (1987) 261.
11 L. R. Snyder, in Cs. Horváth (Editor), *High-Performance Liquid Chromatography —Advances and Perspectives*, Vol. 1, Academic Press, New York, 1980, p. 207.
12 L. R. Snyder and M. A. Stadalius, in Cs. Horváth (Editor), *High-Performance Liquid Chromatography —Advances and Perspectives*, Vol. 4, Academic Press, New York, 1986, p. 195.
13 L. R. Snyder and G. B. Cox, *J. Chromatogr.*, 483 (1989) 85.
14 *BIOPREP Users' Manual*, Medical Products Department, E. I. DuPont de Nemours & Co., Wilmington, DE, 1989.
15 S. Terabe, H. Nishi and T. Ando, *J. Chromatogr.*, 212 (1981) 295.
16 J. W. Dolan and L. R. Snyder, *LC · GC, Mag. Liq. Gas Chromatogr.*, 5 (1987) 971.
17 G. Franke and F. Verillon, *J. Chromatogr.*, 450 (1988) 81.

Journal of Chromatography, 484 (1989) 437–450
Elsevier Science Publishers B.V., Amsterdam — Printed in The Netherlands

CHROM. 21 892

PREPARATIVE HIGH-PERFORMANCE LIQUID CHROMATOGRAPHY UNDER GRADIENT CONDITIONS

III. CRAIG SIMULATIONS FOR HEAVILY OVERLOADED SEPARATIONS

L. R. SNYDER* and J. W. DOLAN
LC Resources Inc., 3182C Old Tunnel Road, Lafayette, CA 94549 (U.S.A.)
and
G. B. COX
Medical Products Department, E. I. du Pont de Nemours & Co., Glasgow, DE 19702 (U.S.A.)

SUMMARY

Computer simulations for heavily overloaded gradient elution are reported for a limited range of conditions. These simulations show a dependence of separation on sample size and experimental conditions that is similar to that for heavily overloaded isocratic separation. When $\alpha > 1.5$, it appears that relatively large samples ($w/w_s \approx 0.5$ or greater) can often be injected with high recovery (>95%) of purified product. These predictions are corroborated by independent experimental data from peptide and protein samples separated by reversed-phase gradient elution.

Separation in gradient elution as a function of sample size can vary considerably with the nature of the sample. Specifically, the relative dependence of retention [$S = \mathrm{d}(\log k')/\mathrm{d}\varphi$] on mobile phase composition (%B) can have a major effect on overlapping-band separations. For this reason, it is important to measure values of S for the sample of interest prior to completing method development for overlapping-band separations by gradient elution.

INTRODUCTION

Previous papers in this volume[1–5] have presented a comprehensive picture that describes key aspects of preparative high-performance liquid chromatography (HPLC) carried out in either an isocratic or a gradient mode, under conditions of either lightly overloaded (touching-band) or heavily overloaded (overlapping-band) separation. On the basis of this and other work from our group, it appears that there is a general parallelism among all of these separation modes and the corresponding small-sample separations, as summarized in Fig. 1 and Table I. Thus, information from small-sample isocratic separations can be used directly to design corresponding gradient separations (and *vice versa*). Similarly, data from small-sample runs can be used to help infer optimum conditions for touching-band separations. One or two additional runs under lightly overloaded conditions are required (in either an isocrat-

0021-9673/89/$03.50

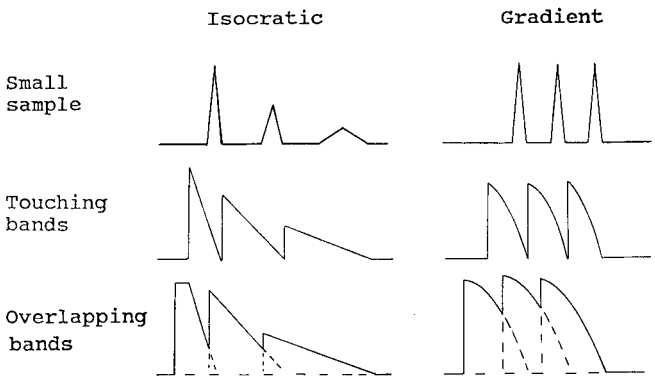

Fig. 1. Different separation modes of interest in preparative HPLC.

ic or a gradient mode), in order to measure the column capacity, w_s, and optimize conditions for touching-band separation. Finally, overlapping-band separations can be developed, using information from preceding small-sample and lightly overloaded runs to guide this process.

TABLE I

SUMMARY OF BASIC PARAMETERS FOR THE DESIGN OF A PREPARATIVE HPLC SEPARATION

Parameters	*Comment*
Small sample, isocratic:	
k_w, S, and N_o for X and Y	Two runs needed with different mobile phases (different %B); isocratic retention and bandwidth can then be predicted as a function of φ; gradient retention and bandwidth can be predicted as a function of gradient steepness (b)
Small sample, gradient:	
k_{og}, S and N_o for X and Y	Two runs needed with different gradient steepness[a]; isocratic retention and bandwidth can then be predicted as a function of φ, and gradient retention and bandwidth can be predicted as a function of gradient steepness (b)
Touching bands, isocratic:	
w_s for X and Y	One additional run needed with a larger sample, *e.g.*, w/w_s = 0.01–0.10. Bandwidth and position can then be calculated as a function of sample weight; the sample weight for touching-band separation can also be predicted (for either isocratic or gradient elution)
Touching bands, gradient:	
w_s for X and Y	Same comment as for the preceding case
Overlapping bands, isocratic:	
–	No additional information (parameters) required for computer simulation; exact predictions (without computer) not currently feasible, but general rules exist[1] to estimate preferred sample size and plate number N_o when the w_o values of X and Y are similar. General trends can be anticipated for case of unequal w_s values[3]
Overlapping bands, gradient:	
–	Similar to the previous case; also, S values of X and Y are very important

[a] Different value of b, usually involving different values of t_G.

The only case that we have not examined in detail is that of overlapping-band gradient elution. In this paper we report preliminary results from the use of computer simulation (CRAIG4) for the study of overlapping-band separation by gradient elution. We also present findings that are relevant to separations by touching-band gradient elution, and which provide additional insight into the use of a previously described[5] computer program (BIOPREP) for the preparative separation of peptide and protein samples by gradient elution.

EXPERIMENTAL

Equipment, materials and procedures were described in Part II[5]. The CRAIG4 software is described in ref. 1.

THEORY[a]

A theory of touching-band gradient separations can be inferred from the discussion in refs. 4 and 6; this background applies equally for separation in an overlapping-band mode. However, an important aspect of preparative gradient elution was ignored in this treatment, *viz.*, changes in band spacing (α) with change in gradient steepness (b), that is, isocratic values of α for various band pairs in a sample often vary when the mobile-phase strength (%B) is changed in reversed-phase HPLC[7]. These changes in α in isocratic elution lead to corresponding changes in α with b in gradient elution, which is also well documented[6,8–10]. The result is that gradients of intermediate steepness are often optimum for a given sample.

Retention (k') in reversed-phase isocratic elution can be represented by

$$\log k' = \log k_w - S\varphi \tag{1}$$

where k_w is the value of k' (small sample) for water as mobile phase (0%B), φ is the volume fraction of organic component (B) in the mobile phase and S is a constant that is characteristic of the solute and other experimental conditions. If eqn. 1 is written for solutes X and Y, having k_w values of k_{wx} and k_{wy} and S values of S_x and S_y, we can then derive[11]

$$\log \alpha = \log (k_{wy}/k_{wx}) + (S_x - S_y)\varphi \tag{2}$$

That is, α (and the band spacing) will remain constant for changes in φ when the S values of two adjacent bands are equal. This has been discussed in some detail in ref. 7. This is illustrated in Fig. 2, where $\log k'$ is plotted against %B (or φ) for two compounds having equal S values. The difference in $\log k'$ for these two compounds at a given value of %B is equal to $\log \alpha$, and the latter quantity is seen to remain constant for any value of %B.

Previous papers[8,9,11,12] have shown that gradient retention and separation can be inferred from isocratic plots of $\log k'$ *vs.* %B as in Fig. 2. Thus, in gradient elution

[a] A list of all symbols used in Parts I–III is included in ref. 4.

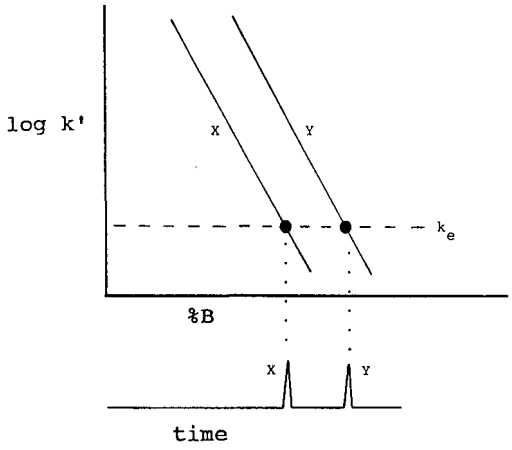

Fig. 2. Dependence of retention on mobile-phase composition in reversed-phase isocratic elution (top). Corresponding gradient elution separation (bottom); see text.

each band leaves the column with a final k' value (k_e) which is constant (for $S_x = S_y$), corresponding to the intersection of horizontal lines (equal k') with the plots for each solute (see dashed line in Fig. 2). Since %B is assumed to change linearly with time in gradient elution (linear gradient), a corresponding chromatogram can be aligned with the plots of log k' *vs.* %B as shown in Figure 2; the vertical dotted lines in Fig. 2 relate the %B at elution for each band with its retention time.

For the corresponding case of gradient elution, eqn. 2 can be written as[11]

$$t_y - t_x = (t_o/b)(\log \alpha) \tag{3}$$

where t_x and t_y are small-sample retention times in gradient elution. We can therefore see that α affects the band spacing in gradient elution in a similar fashion as for isocratic elution. Plots of log k' *vs.* %B (or φ) are shown in Fig. 3 for three different cases: $S_x = S_y$, $S_x < S_y$ and $S_x > S_y$. The small-sample resolution, R_s, is assumed to

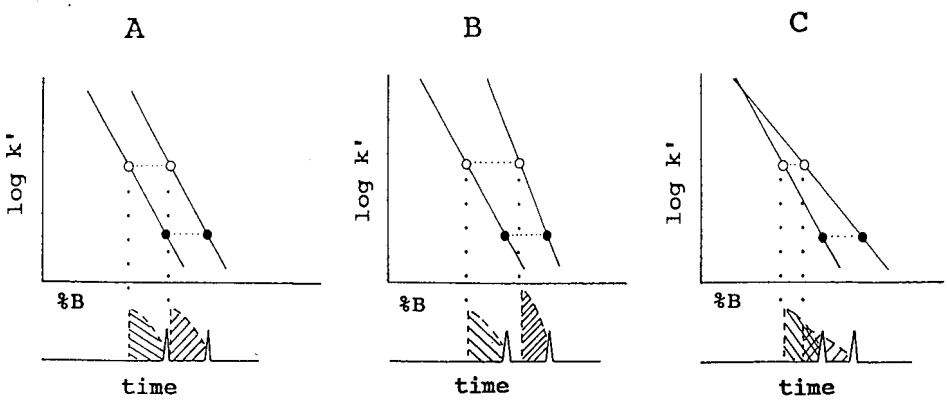

Fig. 3. Effect of relative values of S for two compounds on their preparative separation. (*A*) $S_x = S_y$; (B) $S_x < S_y$; (C) $S_x > S_y$.

be equal for each of these three examples owing to the equal values of α and k_e at elution.

According to eqn. 2, α will be constant as %B changes when $S_x = S_y$, α will decrease with %B when $S_x < S_y$ and α will increase with %B when $S_x > S_y$. Now consider the case of a touching-band separation, as illustrated in Fig. 3A for the cross-hatched bands at the bottom. The band maxima elute at %B values indicated by the vertical dotted lines in Fig. 3A. The small-sample separation (closed circles and triangular bands) in Fig. 3B is identical with that in Fig. 3A, but when a sample of similar size is injected the band maxima (dotted lines) leave the column with a larger value of α owing to their elution in a weaker solvent and the fact that $S_x > S_y$ (*cf.*, eqn. 3). The result is a better separation of the sample in Fig. 3B than in Fig. 3A. Finally, in Fig. 3C the opposite result is seen, *i.e.*, a poorer separation owing to the convergence of the log k' *vs.* %B plots.

The conclusions from Fig. 3 can also be stated in another way. When $S_x < S_y$, a larger sample can be separated with touching bands than in the case of equal S values and an equivalent small-sample separation. Similarly, a smaller sample will give touching bands when $S_x > S_y$. These conclusions appear to be correct in a qualitative sense, but a more detailed analysis (to be presented later) will show that unequal values of S for two compounds may imply unequal values of w_s (see the discussion in the Appendix I in ref. 3). This requires a more complex expression for the two-component retention isotherm than is currently used in CRAIG4.

In a previous paper[1] it was noted that large values of α are very important in overlapping-band separations. This suggests that unequal S values for two adjacent sample bands will lead to large differences in column loadability compared with the case of equal S values. We shall test this conclusion in the following section.

RESULTS AND DISCUSSION

Computer simulations ($S_x = S_y$)

Sample size effects. Fig. 4 illustrates the effect of increasing sample size in gradient elution, from small-sample to touching-band to overlapping-band separation. Here the gradient steepness $b = 1.0$, the initial k_0 values are $k_x = 10$ and $k_y = 15$ ($\alpha = 1.5$) and $N_0 = 1800$[a]. The numbers above each band pair correspond to the recovery of 99% pure product; thus 94/78 (for $w/w_s = 0.20$) indicates that 94% of compound X can be recovered in 99% purity and 78% of compound Y can be recovered in 99% purity. Several observations can be made concerning the simulations in Fig. 4. First, with increasing band overlap ($w/w_s > 0.16$), a fairly sharp boundary appears between the two bands, followed by a tail of X into Y. This can be compared with the simulated and experimental chromatograms shown in Fig. 2 in ref. 1; it confirms the essential similarity of overlapping-band separations in isocratic or gradient elution, which was observed also for small-sample[1,2] and touching-band[4] separations.

Second, consider the total *weight* of compounds X and Y that can be recovered

---

[a] Values of N_0 are reported for the first band; $N_0 = [(k' + 1)/k']n_c$, where n_c is the number of Craig stages (see ref. 1); the value of k' assumed is equal to $1/1.15b$. Sample sizes (w/w_s) have not been adjusted (see discussion of Fig. 3 in Part I[4]).

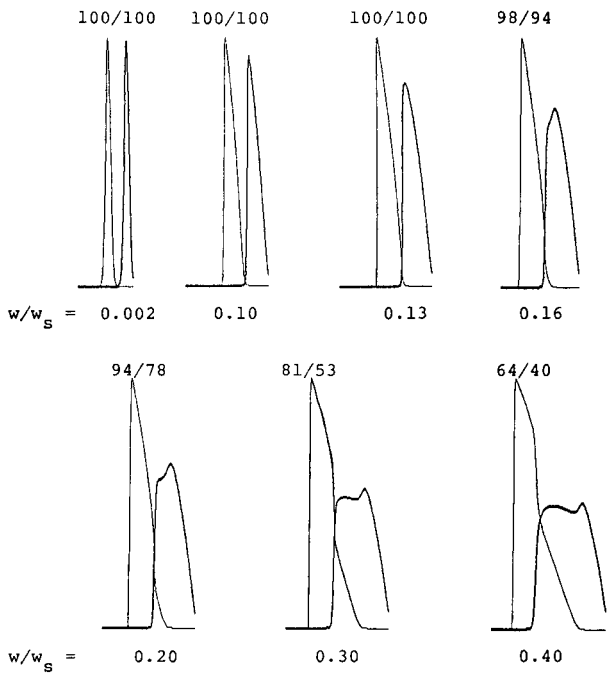

Fig. 4. CRAIG4 simulations of the separation of two compounds (X and Y) by gradient elution with sample size (w/w_s) varying. Conditions: $N_o = 1800$, $b = 1$, $k_x = 10$ and $k_y = 15$ at beginning of gradient (values of k_{og}). Equal amounts of X and Y in sample.

as a function of the injected sample size. This relationship is shown in Fig. 5 for each band, together with the recoveries. For both X and Y, the weight of pure product recovered increases with increasing sample size, well beyond the sample weight for

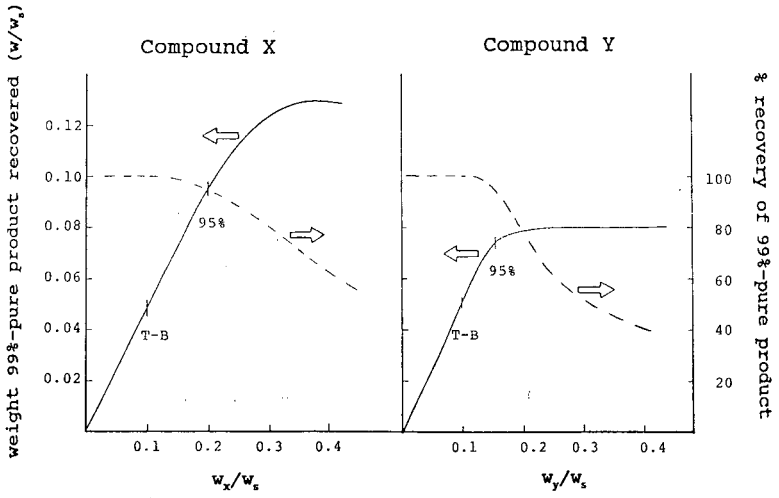

Fig. 5. Dependence of yield and recovery of pure product as a function of sample size. Data from Fig. 4.

touching bands (T-B in Fig. 5). For compound X it is possible to recover about twice as much pure X, with a recovery of 95% (noted in Fig. 5), as for the touching-band case. A similar situation is observed for compound Y, although the advantage with respect to touching bands is not as great. These observations parallel those found for the case of isocratic overlapping-band separation[1] (but note that the separations in Fig. 5 are not optimized in terms of N_o for maximum production rate).

Finally, it is seen that fairly large samples can be charged when α is as large as 1.5 (the value assumed in Fig. 5). Thus, a total sample weight $w/w_s = 0.15$ is possible for 95% recovery of 99% pure Y.

Effect of initial %B in gradient. This is illustrated for one set of conditions in Fig. 6. When there is substantial overlap for a gradient that begins with a higher %B (and smaller values of k' at the beginning of the gradient), a decrease in %B (with increase in the initial k' values) appears to give increased recovery (%) and yield (mg) of pure product. This effect levels off for initial k' values >100, and there is no advantage in beginning the gradient with a weaker mobile phase ($k_x > 100$), since the run time increases much faster than the recovery of pure product.

Effect of N_o. This is illustrated in Fig. 7 for conditions similar to those in Figs. 4 and 6: the initial k' values are 10 (X) and 15 (Y), $w/w_s = 0.40$ and $b = 1$. Separation as measured by the recovery of pure X and Y initially increases rapidly as N_o increases from 100 to about 800, but then levels off. This pattern is essentially similar to what we have seen for the other preparative HPLC modes in Fig. 1. As a result, there will

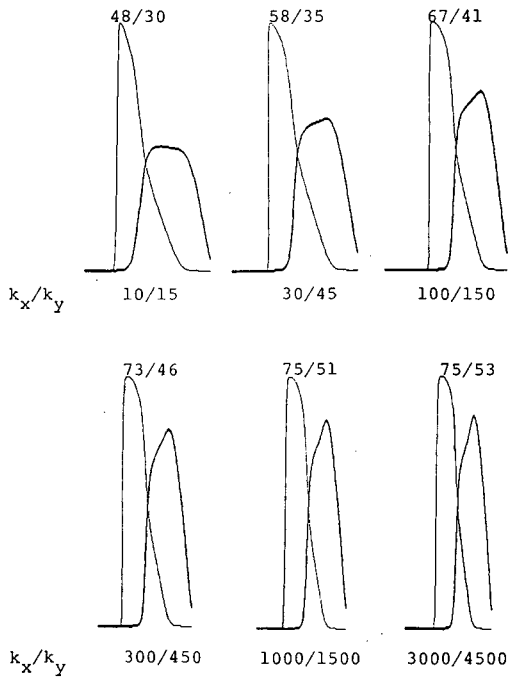

Fig. 6. CRAIG4 simulations of the separation of two compounds (X and Y) by gradient elution as a function of initial mobile phase composition (which determines initial values of k_{og}: k_x and k_y). Conditions: $N_o = 400$, $b = 1$, $w/w_s = 0.40$ and $\alpha = 1.5$. Equal amounts of X and Y in sample.

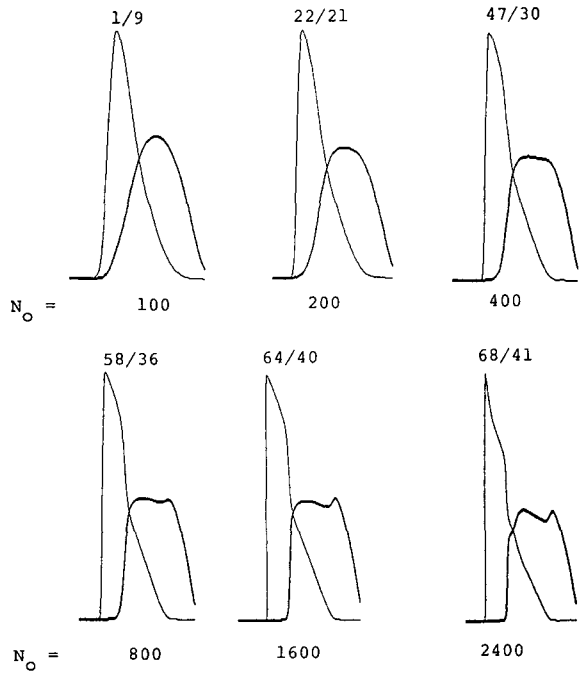

Fig. 7. CRAIG4 simulations of the separation of two compounds (X and Y) by gradient elution as a function of column plate number N_o. Conditions: $b = 1$, $k_x = 10$ and $k_y = 15$ at beginning of gradient (values of k_{og}), $w/w_s = 0.40$. Equal amounts of X and Y in sample.

be an optimum plate number for a given separation, one that yields a maximum production rate.

Effect of gradient steepness b. Separation generally improves as the gradient steepness is reduced and $\bar{k}$ increases, as illustrated in the simulations in Fig. 8. This is again similar to isocratic elution under overload conditions[1], where there is generally an optimum combination of N_o and k_o for maximum production rate. We have carried out a number of simulations where gradient steepness and plate number were changed together, with the general conclusion that separation (as measured by the recovery of pure X and Y) is similar when the product $N_0[k/(1+k)]^2$ is constant.

Computer simulations ($S_x \neq S_y$)

The preceding conclusions apply to the case where the S values of the two bands are equal, which should be approximately the case for most "real" samples, *i.e.*, samples having similar structures and molecular weights. However, the contrary ($S_x \neq S_y$) is often observed in practice[6–10,13,14]. Differences in solute S values can have a profound effect on preparative separations by gradient elution, as illustrated by the example in Fig. 9. Here, experimental conditions are assumed to be the same for two different samples (A and B), and the resolution for small-sample injections is seen to be identical in each instance. On the basis of our previous discussions, it would be expected that the separation of these two samples would also be similar for the injection of large samples of the same size. As seen, however, this is not so. Sample A

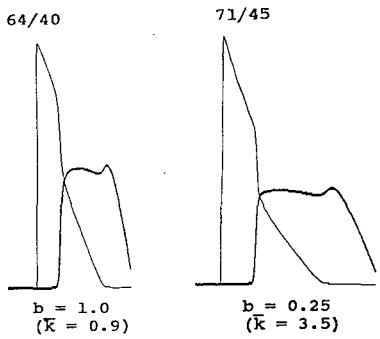

Fig. 8. CRAIG4 simulations of the separation of two compounds (X and Y) by gradient elution as a function of gradient steepness. Conditions as in Fig. 7, except N_o = 1600 and b varies.

shows almost total overlap of the two bands for a large sample (w/w_s = 0.8), whereas sample B is totally resolved. The only difference in the two samples is their values of S; $S_x < S_y$ for sample A and $S_x > S_y$ for sample B.

Effect of sample size. Preceding computer simulations (Figs. 4–8) have assumed $S_x = S_y = 10$. Fig. 10 shows simulations for similar conditions to those in the preceding examples, but for samples where X and Y have different values of S. In series A in Fig. 10, $S_x = 10$ and $S_y = 8$ (the unfavorable case). It is seen that extensive band overlap occurs for samples larger than $w/w_s > 0.15$. In series B, $S_x = 10$ and $S_y = 12$ (the favorable case). Here, it is possible to saturate the column almost

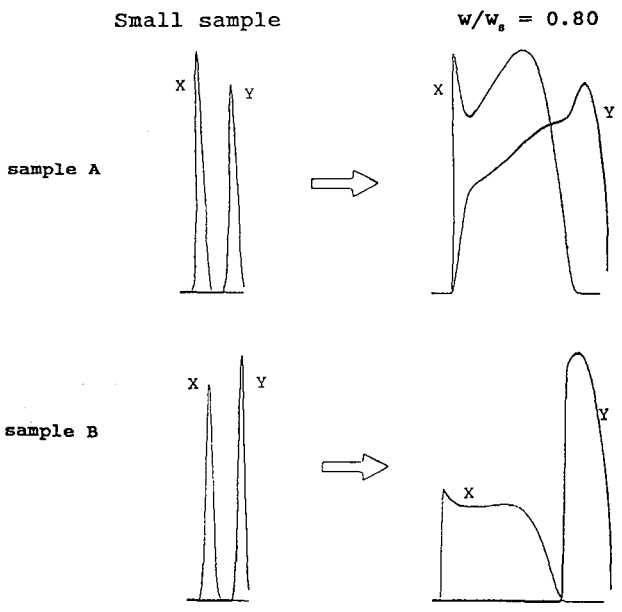

Fig. 9. CRAIG4 simulations of the separation of two compounds (X and Y) by gradient elution as a function of the sample and sample size. Examples taken from Fig. 10.

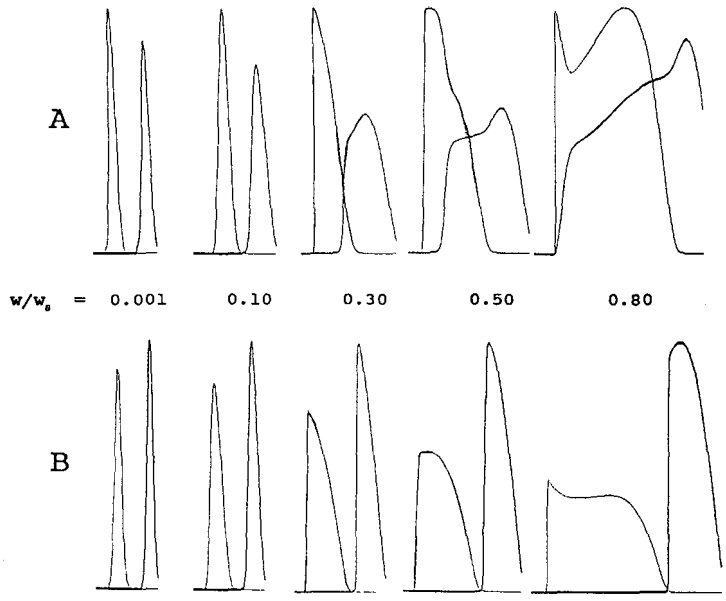

Fig. 10. CRAIG4 simulations of the separation of two compounds (X and Y) by gradient elution as a function of the sample and sample size. Conditions: $b \approx 1.0$, $N_0 = 400$; (A) initial $k' = 100$ (X) and 101 (Y), $S_x = 10$, $S_y = 8$; (B) initial $k' = 100$ (X) and 840 (Y), $S_x = 10$ and $S_y = 12$.

completely with sample ($w/w_s = 0.80$) without seeing significant band overlap. The reason for this differing behavior should be clear from the examples in Fig. 3, but it is nevertheless impressive.

Effect of initial mobile phase composition. When the S values for two compounds are equal, there is not a very large effect of the starting mobile phase composition on the resulting overlapping-band separation, as seen in Fig. 6 for initial k' values >100. The reason is that under conditions of large k' the bands (even under heavy-overload conditions) do not migrate very rapidly through the column, and therefore little separation occurs during this phase of the separation. However, when the S values for the two compounds differ appreciably, the situation can be completely different. This is illustrated in Fig. 11 for the (unfavorable) case where $S_x > S_y$. Simulated separations are shown for different sample weights and different initial mobile phases. As the initial mobile phase is made weaker (the initial k' value, k_x, increases from 10 to 1000), there is little effect on the separation of a small sample ($w/w_s = 0.002$). This is also the case when S values for the two compounds are equal, as discussed above. However, for larger samples ($w/w_s = 0.30, 0.50$), it is seen that an increase in the initial k' values of the sample results in a pronounced degradation of the separation. This reflects the fact (see Fig. 3C) that the initial α value is much smaller for a smaller %B and larger value of k_x, combined with the fact that a large sample migrates more rapidly in a given mobile phase than does a small sample. Consequently, the choice of the best starting mobile phase appears to be important.

When $S_x < S_y$ (favorable case), an opposite trend of separation *vs.* starting mobile phase composition (and k_x) will be observed. In this case, the separation can

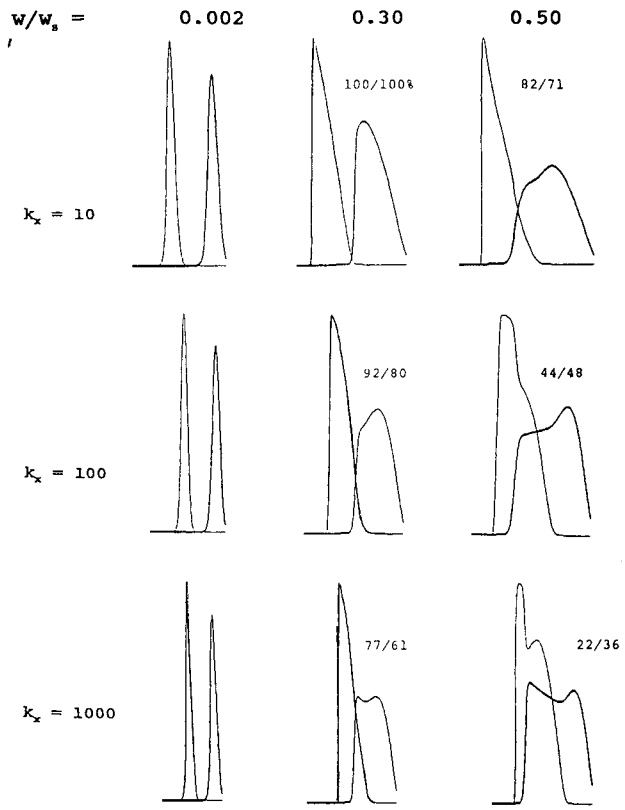

Fig. 11. CRAIG4 simulations of the separation of two compounds (X and Y) by gradient elution as a function of the starting mobile phase composition and sample size. Conditions: $b \approx 1.0$, $N_o = 400$; initial $k' = 10$ (X) and 12.8 (Y), 100 (X) and 101 (Y) and 1000 (X) and 780 (Y); $S_x = 10$, $S_y = 8$.

improve dramatically if the starting mobile phase is made weaker. We carried out further modeling studies in which separation was studied during migration on the column. It appears that the choice of mobile phase composition for the initial injection of the sample is not very important to the final separation. Rather, it is the migration on the column *following* injection that most affects the final separation. We shall report further on this in a later paper.

Experimental gradient separations under overlapping-band conditions

The previous examples (Figs. 4–11) suggest that under certain conditions it is possible to apply fairly large samples ($w/w_s > 0.5$) in gradient elution and obtain almost complete recovery of highly pure product. In some instances this is possible even when the α values for a comparable small-sample separation are fairly small ($\alpha < 1.5$). This observation must seem surprising to most workers (it was surprising to us!), but previous reports from the literature tend to support this possibility.

Literature examples. Using displacement chromatography, Horvath *et al.*[15] reported almost complete recoveries of pure product ($\alpha = 1.07$) from the reversed-

phase separation of 110 mg of a mixture of phenylacetic acids on a 25 × 46 cm I.D. column ($w_s \approx 400$ mg). Even more striking is the separation reported by Mant *et al.*[16] for a decapeptide sample ($\alpha \approx 1.7$) by reversed-phase gradient elution. In this example, reproduced in Fig. 12, the column capacity w_s can be estimated to be about 50 mg. Touching-band separation occurs for a sample of 1 mg, but a 20-mg sample yielded 99% of pure *X* and 98% of pure *Y*. Injecting a sample equal to the column capacity (50 mg) gave 87% pure *X* and 61% pure *Y*. It is hoped that these results are now easier to understand on the basis of the preceding discussion.

Protein separations. We carried out some preliminary gradient elution separations under overlapping-band conditions, using various proteins as samples. Fig. 13 shows a series of such separations for the proteins cytochrome *c* (*X*) and lysozyme (*Y*), where $N_o = 1750$, $S_x = 29.6$ and $S_y = 30.5$ (favorable values of *S*) and $\alpha = 2.3$ in these separations. The numbers (*e.g.*, 0.5/10.0) refer to the weight (mg) of *X* and *Y* in

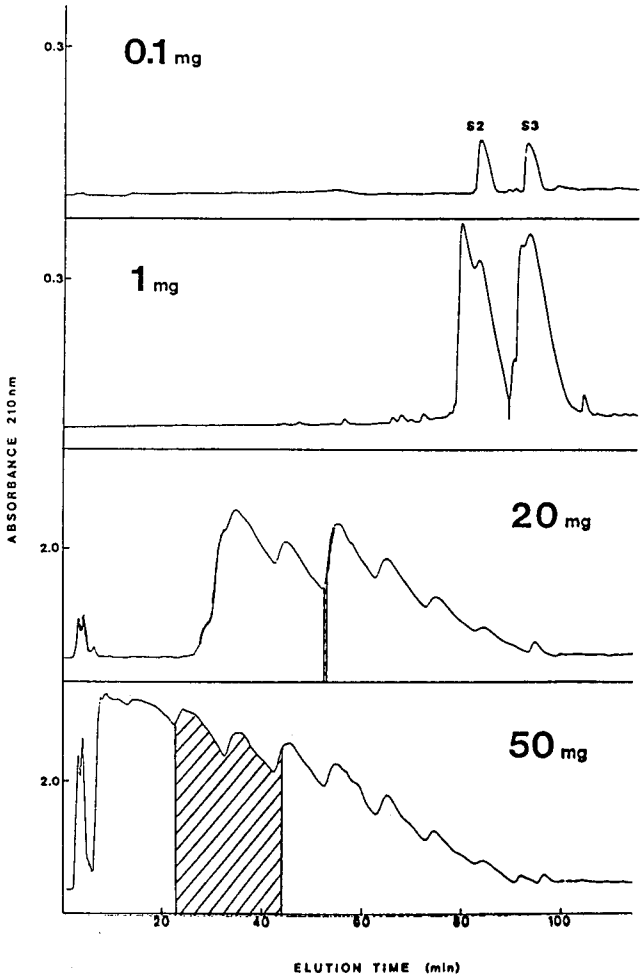

Fig. 12. Separation of decapeptide sample by reversed-phase gradient elution[16].

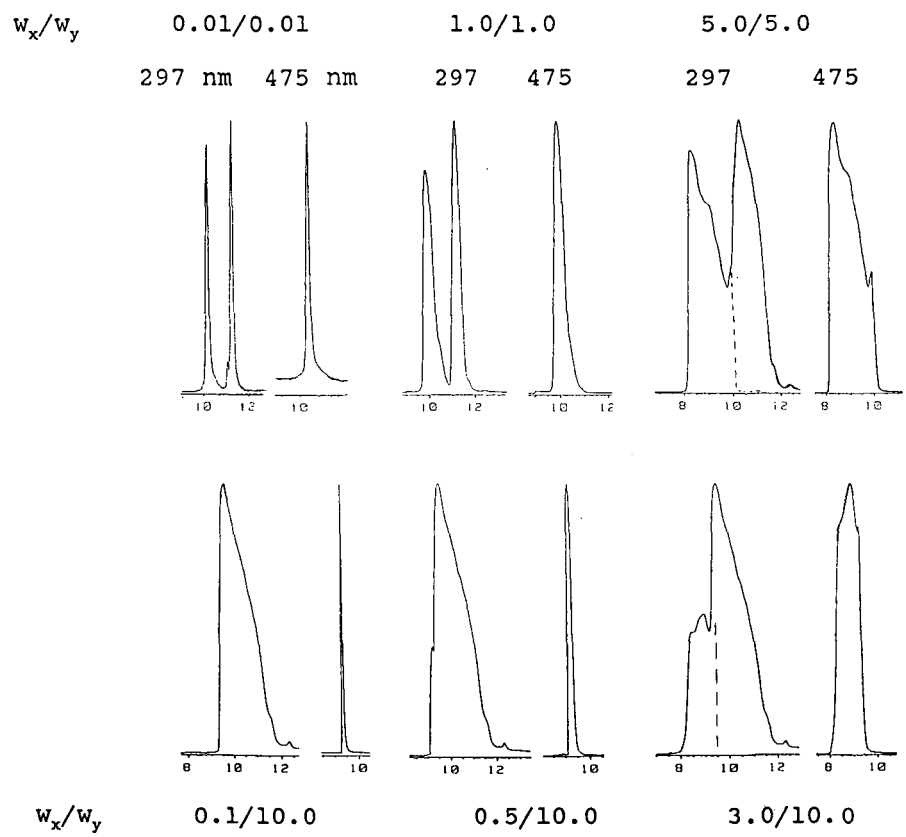

Fig. 13. Experimental separations of cytochrome *c*–lysozyme mixture by reversed-phase gradient elution. Sample size varies as indicated (*e.g.*, 0.1/10.0 signifies 0.1 mg of cytochrome *c* plus 10 mg of lysozyme in the injected sample). Conditions: 15 × 0.46 cm I.D. column of 100-nm pore-size C_8 packing (w_s = 11–20 mg, see Table II in ref. 4); flow-rate, 1 ml/min; gradient, 5–70% acetonitrile–water (plus 0.1% TFA) in 20 min; detection at either 297 or 475 nm.

the injected sample (*e.g.*, 0.5 mg of *X* and 10 mg of *Y*). Detection was carried out at two wavelengths (297 and 475 nm); cytochrome *c* absorbs at both wavelengths, but lysozyme absorbs only at 297 nm. Therefore, the 475-nm chromatograms show the cytochrome *c* band, whereas the 297-nm tracings track both bands. The dashed lines in some of these chromatograms (5.0/5.0 and 3.0/10.0 runs) indicate the superimposed plot of the cytochrome *c* band.

We note first that there is a sharp boundary between the two bands when they overlap appreciably, as a result of sample displacement. This is reminiscent of the computer simulations in Figs. 4 and 6, but is much more pronounced. Presumably this is due to the larger value of α for this sample (α = 2.3) compared with the smaller value of α (α = 1.5) assumed in the various simulations. As a result, we see again (Fig. 13) that fairly large samples can be separated with good recovery of purified product when the sample characteristics and separation conditions are favorable.

We have observed similar results to those in Fig. 13 for the separation of a

mixture of cytochrome *c* and ribonuclease A (results not shown). Later we shall report on the agreement between these experimental results and computer simulations based on CRAIG4. One complication in these comparisons, which requires further study, is the difference in the values of w_s determined by column saturation and chromatographic data under conditions of partial overload (for protein samples see Table II in Part I[4]).

CONCLUSIONS

This preliminary study reports computer simulations for the overlapping-band separation of various hypothetical samples by gradient elution. When the S values [$S = \mathrm{d}(\log k')/\mathrm{d}\varphi$] of two compounds are similar, the resulting separations parallel those obtained by corresponding isocratic separations. When the S values of two adjacent bands differ appreciably, this can have a profound affect on the separation. For the favorable case (S for the first band less than S for the second band), very large samples can be separated, even when α (and resolution) is fairly small for the small-sample separation. The optimum sample size can then be an order of magnitude greater than for touching-band separation. For the unfavourable case (S for the first band larger than S for the second), sample sizes larger than those which give touching bands lead to extensive band overlap and low recoveries of purified product. For this reason, it is important to know the values of S for compounds that are to be separated by gradient elution (both touching-band and overlapping-band sample sizes). Values of S can be readily determined from two experimental small-sample runs[6,17].

REFERENCES

1 L. R. Snyder, J. W. Dolan and G. B. Cox, *J. Chromatogr.*, 483 (1989) 63.
2 L. R. Snyder and G. B. Cox, *J. Chromatogr.*,483 (1989) 85.
3 G. B. Cox and L. R. Snyder, *J. Chromatogr.*,483 (1989) 95.
4 G. B. Cox, L. R. Snyder and J. W. Dolan, *J. Chromatogr.*, 484 (1989) 409.
5 L. R. Snyder, J. W. Dolan, D. C. Lommen and G. B. Cox, *J. Chromatogr.*, 484 (1989) 425.
6 J. W. Dolan, L. R. Snyder and M. A. Quarry, *Chromatographia,* 24 (1987) 261.
7 L. R. Snyder, M. A. Quarry and J. L. Glajch, *Chromatographia,* 24 (1987) 33.
8 B. F. D. Ghrist and L. R. Snyder, *J. Chromatogr.*, 459 (1988) 25.
9 B. F. D. Ghrist and L. R. Snyder, *J. Chromatogr.*, 459 (1988) 43.
10 J. L. Glajch, M. A. Quarry, J. F. Vasta and L. R. Snyder, *Anal. Chem.*, 58 (1986) 280.
11 J. E. Eble, R. L. Grob and L. R. Snyder, *J. Chromatogr.*, 405 (1987) 51.
12 L. R. Snyder, in Cs. Horváth (Editor) *High-performance Liquid Chromatography–Advances and Perspectives,* Vol. 1, Academic Press, New York, 1980, p. 207.
13 M. Kunitani, D. Johnson and L. Snyder, *J. Chromatogr.*, 371 (1986) 313.
14 J. W. Dolan and L. R. Snyder, *Chromatogr. Mag.*, 2 (1987) 49.
15 Cs. Horváth, A. Nahum and Frenz, *J. Chromatogr.*, 218 (1981) 365.
16 C. T. Mant, T. W. L. Burke and R. S. Hodges, *Chromatographia,* 24 (1987) 565.
17 M. A. Quarry, R. L. Grob and L. R. Snyder, *Anal. Chem.*, 58 (1986) 907.

Author Index

PUBLICATION SCHEDULE FOR 1989

Journal of Chromatography and Journal of Chromatography, Biomedical Applications

MONTH	J	F	M	A	M	J	J	A	S	O	N	D
Journal of Chromatography	461 462 463/1	463/2 464/1	464/2 465/1 465/2	466 467/1 467/2	468 469 470/1 470/2	471 472/1 472/2 473/1	473/2 474/1 474/2 475	476 477/1 477/2	478/1 478/2 479/1	479/2 480	481 482/1	482/2 483 484 485
Bibliography Section		486/1		486/2		486/3		486/4		486/5		486/6
Biomedical Applications	487/1	487/2	488/1 488/2	489/1 489/2	490/1 490/2	491/1	491/2	492 493/1	493/2 494	495	496/1 496/2	497

INFORMATION FOR AUTHORS

(Detailed *Instructions to Authors* were published in Vol. 478, pp. 453–456. A free reprint can be obtained by application to the publisher, Elsevier Science Publishers B.V., P.O. Box 330, 1000 AH Amsterdam, The Netherlands.)

Types of Contributions. The following types of papers are published in the *Journal of Chromatography* and the section on *Biomedical Applications:* Regular research papers (Full-length papers), Notes, Review articles and Letters to the Editor. Notes are usually descriptions of short investigations and reflect the same quality of research as Full-length papers, but should preferably not exceed six printed pages. Letters to the Editor can comment on (parts of) previously published articles, or they can report minor technical improvements of previously published procedures; they should preferably not exceed two printed pages. For review articles, see inside front cover under Submission of Papers.

Submission. Every paper must be accompanied by a letter from the senior author, stating that he is submitting the paper for publication in the *Journal of Chromatography*. Please do not send a letter signed by the director of the institute or the professor unless he is one of the authors.

Manuscripts. Manuscripts should be typed in double spacing on consecutively numbered pages of uniform size. The manuscript should be preceded by a sheet of manuscript paper carrying the title of the paper and the name and full postal address of the person to whom the proofs are to be sent. Authors of papers in French or German are requested to supply an English translation of the title of the paper. As a rule, papers should be divided into sections, headed by a caption (*e.g.*, Summary, Introduction, Experimental, Results, Discussion, etc.). All illustrations, photographs, tables, etc., should be on separate sheets.

Introduction. Every paper must have a concise introduction mentioning what has been done before on the topic described, and stating clearly what is new in the paper now submitted.

Summary. Full-length papers and Review articles should have a summary of 50–100 words which clearly and briefly indicates what is new, different and significant. In the case of French or German articles an additional summary in English, headed by an English translation of the title, should also be provided. (Notes and Letters to the Editor are published without a summary.)

Illustrations. The figures should be submitted in a form suitable for reproduction, drawn in Indian ink on drawing or tracing paper. Each illustration should have a legend, all the *legends* being typed (with double spacing) together on a *separate sheet*. If structures are given in the text, the original drawings should be supplied. Coloured illustrations are reproduced at the author's expense, the cost being determined by the number of pages and by the number of colours needed. The written permission of the author and publisher must be obtained for the use of any figure already published. Its source must be indicated in the legend.

References. References should be numbered in the order in which they are cited in the text, and listed in numerical sequence on a separate sheet at the end of the article. Please check a recent issue for the layout of the reference list. Abbreviations for the titles of journals should follow the system used by *Chemical Abstracts*. Articles not yet published should be given as "in press" (journal should be specified), "submitted for publication" (journal should be specified), "in preparation" or "personal communication".

Dispatch. Before sending the manuscript to the Editor please check that the envelope contains three copies of the paper complete with references, legends and figures. One of the sets of figures must be the originals suitable for direct reproduction. Please also ensure that permission to publish has been obtained from your institute.

Proofs. One set of proofs will be sent to the author to be carefully checked for printer's errors. Corrections must be restricted to instances in which the proof is at variance with the manuscript. "Extra corrections" will be inserted at the author's expense.

Reprints. Fifty reprints of Full-length papers, Notes and Letters to the Editor will be supplied free of charge. Additional reprints can be ordered by the authors. An order form containing price quotations will be sent to the authors together with the proofs of their article.

Advertisements. Advertisement rates are available from the publisher on request. The Editors of the journal accept no responsibility for the contents of the advertisements.

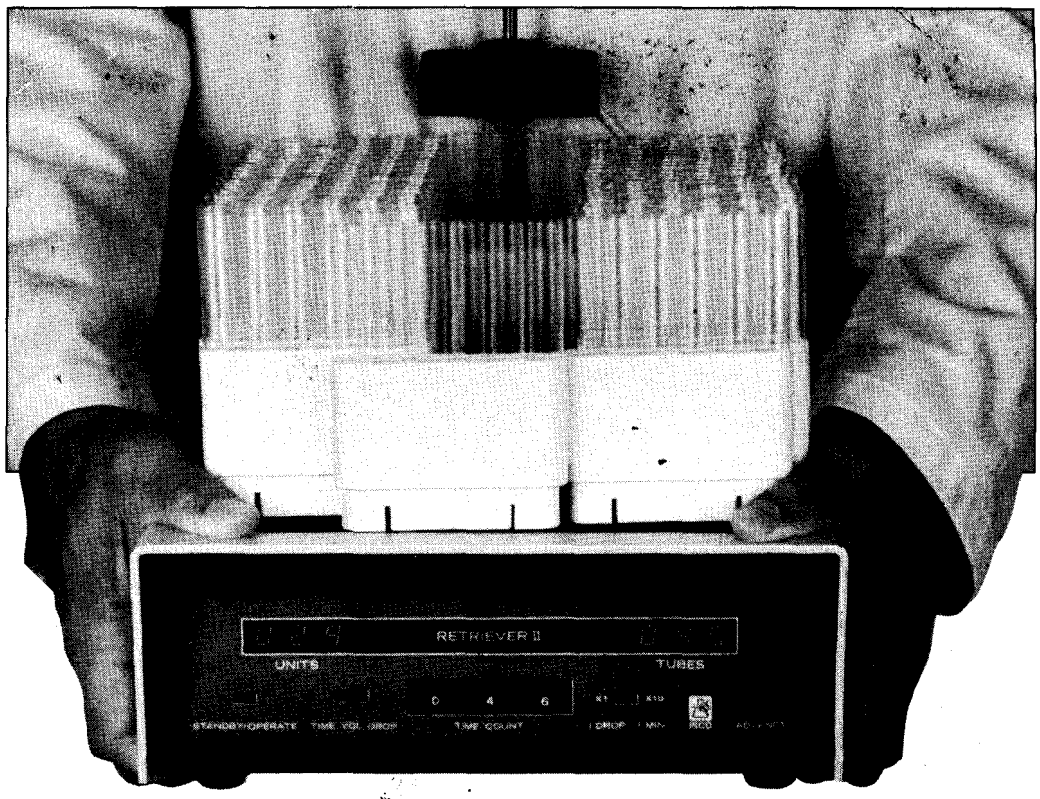

Compact fraction collector packs 174 tubes into a square foot.

Here's a fraction collector that combines small size with the capacity, versatility, and reliability you need for virtually any LC or HPLC job. It's Isco's Retriever II®.

It's compact. Retriever II needs just one square foot of your bench space, yet it holds up to 174 tubes of 12 or 13 mm diameter. Racks are also available to hold 10 to 18 mm tubes or 28 mm scintillation vials.

It's versatile. Retriever II's fast movement means it is as useful for HPLC as it is for open columns.

It can handle up to four columns at once and collect by time, drops, or pulses from a pump. You can even set volume directly in 0.1 or 1 ml increments, if you're using it with an Isco Wiz pump.

It's reliable. Retriever II's unique mechanism has been proven over many years in 20,000 similar fraction collectors and autosamplers. Its tough, metal construction, plus great chemical and humidity resistance means it will stand up to practically any job or environment. And the price including drop counter is actually lower than competing round collectors!

In the U.S.A., call **(800)228-4250** for a complete catalog. In Europe, fax Isco Europe AG at **(41-1)920 62 08.**

Isco, Inc.
P.O. Box 5347
Lincoln NE 68505, U.S.A.

Isco Europe AG
Brüschstr. 17
CH8708 Männedorf, Switzerland

ISCO

Distributors • **Austria:** INULA • **Belgium:** SA HVL NV • **Denmark:** Mikrolab Aarhus • **Finland:** ETEK OY • **France:** Ets. Roucaire, S.A. • **Germany:** Colora Messtechnik GmbH • **Hungary:** Lasis Handelsges. mbH • **Italy:** Gio. de Vita e C. s.r.l. • **The Netherlands:** Beun-de Ronde B.V. • **Norway:** Dipl. Ing. Houm A.S. • **Spain:** CHEMICONTROL, S.L. • **Sweden:** SAVEN AB • **Switzerland:** IG Instrumenten-Gesellschaft AG •**U.K.:** Life Science Laboratories, Ltc